

Doctoral thesis

Analysis of behaviour and residual capacity  
of fire-exposed concrete-filled tubular columns

**Author:**

mgr inż. Wojciech Szymkuć

**Supervisors:**

dr hab inż. Adam Glema, prof. uczelni

dr inż. Michał Malendowski

Poznań 2023



POZNAN UNIVERSITY OF TECHNOLOGY



FACULTY  
OF CIVIL AND TRANSPORT  
ENGINEERING

(this page is intentionally left blank)

## Table of contents

Abbreviations .....	9
Abstract .....	11
Streszczenie .....	13
Acknowledgements .....	15
1. Introduction .....	17
1.1. Concrete-filled steel tubular (CFST) columns.....	17
1.2. Early CFST design rules.....	20
1.3. Performance-based design approaches.....	21
1.4. Motivation.....	22
1.5. Goal and layout of the thesis.....	23
1.6. Hypothesis.....	25
2. History of fire resistance testing.....	27
2.1. Pre-standardised fire resistance .....	27
2.2. Standard temperature-time curves – ASTM E119, ISO 834.....	31
2.3. Burnout resistance and cooling.....	35
2.3.1. Burnout resistance.....	35
2.3.2. Cooling rates .....	37
3. Thermal actions on structures in fire .....	39
3.1. Heat flux .....	39
3.1.1. Convective heat flux.....	39
3.1.2. Radiative heat flux.....	41
3.1.3. Convective heat transfer coefficient and emissivity employed by other researchers.....	43
3.2. The measure of exposure (AST) .....	44
3.3. Controlling the furnace conditions.....	48
3.4. Summary .....	49
4. Properties of concrete and steel at ambient and elevated temperatures .....	51
4.1. Thermal properties of concrete at elevated temperatures.....	51
4.1.1. Density at elevated temperatures .....	53
4.1.2. Specific heat at elevated temperatures.....	53
4.1.3. Thermal conductivity at elevated temperatures.....	54
4.2. The effect of elevated temperatures on the mechanical response of concrete.....	57
4.2.1. Thermal expansion of concrete at elevated temperatures.....	57

4.2.2.	Concrete at temperatures from 20 °C to 105 °C.....	58
4.2.3.	Concrete at temperatures from 105 °C to 300 °C.....	60
4.2.4.	Concrete at high temperatures above 300 °C.....	61
4.2.5.	Models of mechanical properties of concrete at elevated temperatures.....	61
4.2.6.	Concrete after cooling.....	66
4.2.7.	The effect of simultaneous load and temperature on concrete.....	67
4.3.	Thermal properties of steel at elevated temperatures.....	70
4.3.1.	Thermal conductivity of steel.....	70
4.3.2.	Specific heat of steel.....	71
4.3.3.	Density of steel.....	71
4.4.	The effect of elevated temperatures on the mechanical properties of steel.....	71
4.4.1.	Relative thermal elongation and coefficient of thermal expansion of steel.....	72
4.4.2.	Steel at elevated temperatures.....	72
4.4.3.	Steel after exposure to elevated temperatures.....	74
5.	Experimental and theoretical investigations of CFST columns.....	81
5.1.	Historical experimental investigations of CFST columns.....	81
5.1.1.	Bauschinger (1884-1886).....	81
5.1.2.	Möller & Lüthmann (1886-1888).....	81
5.1.3.	Hamburg tests (1893-1895).....	82
5.1.4.	Other tests essential for the understanding of fire effects on columns.....	83
5.1.5.	Ingberg et al. (1921).....	83
5.1.6.	Developments between 1921 and 1980s.....	84
5.1.7.	Summary of the historical test data.....	85
5.2.	Modern fire resistance tests of CFST columns.....	85
5.2.1.	NRC Canada (1982-1994).....	85
5.2.2.	British Steel (1991-1992).....	86
5.2.3.	Han et al. (2003).....	87
5.2.4.	Universitat Politècnica de València (UPV, 2009-2013).....	88
5.2.5.	Description of tests not included in the validation domain.....	89
5.2.6.	Summary.....	90
5.3.	Reliability of temperature measurement.....	91
5.4.	Recommendations for future experimental research.....	97
5.5.	Design methods at ambient conditions.....	98
5.6.	Design methods in fire conditions.....	98

5.6.1.	Prescriptive design .....	98
5.6.2.	Tabulated data and simplified calculation methods .....	99
5.7.	Numerical modelling.....	100
6.	Analysis of structural behaviour of CFST columns in standard fire conditions .....	103
6.1.	Structural fire behaviour of CFST columns .....	103
6.2.	Analysis of influencing factors based on experimental data.....	105
6.2.1.	The role of the interaction between steel tube and concrete core.....	105
6.2.2.	Effect boundary conditions, eccentricity and length.....	108
6.2.3.	Effect of load level (20, 40, 60 %).....	113
6.2.4.	The effect of infill .....	116
6.2.5.	Local buckling .....	117
6.2.6.	Effect of steel fibre .....	118
6.2.7.	The moisture content of concrete .....	118
6.2.8.	Thermal gap conductance.....	119
6.2.9.	Concrete aggregate type .....	120
6.3.	Summary.....	120
7.	Numerical model of CFST column in fire conditions.....	121
7.1.	Description of the numerical model .....	121
7.1.1.	Modelling of concrete and steel.....	126
7.1.2.	Steel-concrete interface .....	128
7.1.3.	Finite elements and finite element mesh .....	129
7.2.	Validation of the numerical model.....	131
7.2.1.	What is fire resistance? .....	131
7.2.2.	Validation domain .....	133
7.2.3.	Validation results .....	137
7.2.4.	Conclusions .....	140
7.3.	Improving the convergence .....	140
7.3.1.	Friction .....	140
7.3.2.	Convergence criteria .....	142
7.4.	Analysis of the behaviour of fire-exposed CFST columns.....	142
7.4.1.	Contribution of core and tube to FRT .....	143
7.4.2.	Contact pressure.....	148
7.5.	The effect of boundary conditions and partial restraint .....	148
7.5.1.	The effect of rotational restraint.....	148

7.5.2.	The effect of axial restraint .....	150
7.6.	Parametric study.....	152
7.6.1.	The diameter and thickness of the steel tube.....	156
7.6.2.	The moisture content of concrete (sets 1, 2, 3, 4) .....	156
7.6.3.	Thermal conductivity of concrete (sets 1, 5, 6, 7) .....	158
7.6.4.	Thermal gap conductance (sets 1, 8, 9, 10).....	158
7.6.5.	The emissivity of the steel surface (sets 1, 11) .....	159
7.6.6.	Thermal expansion of concrete (sets 1, 12) .....	159
7.6.7.	Friction between concrete and steel (sets 1, 13).....	159
7.6.8.	Engulfed and insulated length .....	159
7.7.	Conclusions .....	161
8.	Burnout resistance of CFST columns.....	163
8.1.	The concept of burnout resistance and PDB analyses.....	163
8.2.	Numerical model.....	165
8.2.1.	Accounting for non-reversibility in numerical analysis.....	165
8.2.2.	Temperature within cross-section during heating and cooling.....	166
8.3.	Case study (car park) .....	170
8.3.1.	Geometry of the building.....	171
8.3.2.	Fire scenario and the design fire .....	171
8.3.3.	Fire .....	173
8.3.4.	CFD-FE coupling .....	174
8.3.5.	Results of the thermal analysis.....	176
8.3.6.	Results of the mechanical analysis.....	178
8.3.7.	Conclusions .....	182
9.	CFST with lightweight cementitious composites.....	183
9.1.	Materials and methods .....	187
9.1.1.	Mixing procedure.....	189
9.1.2.	Conditioning.....	189
9.1.3.	Heating regime for mechanical tests .....	189
9.1.4.	Density.....	189
9.1.5.	Flexural and compressive strength.....	189
9.1.6.	Scanning electron microscopy (SEM).....	190
9.2.	Results and discussion of material tests.....	190
9.2.1.	Density under ambient conditions and mass loss after heating .....	190

9.2.2.	Flexural and compressive strength.....	191
9.2.3.	Thermal analysis .....	193
9.2.4.	Microstructure analysis.....	195
9.2.5.	Conclusions of the experimental research on LCCC.....	200
9.3.	Determination of LCCC properties for the numerical model.....	201
9.3.1.	Specific heat .....	201
9.3.2.	Density.....	202
9.3.3.	Thermal conductivity .....	202
9.3.4.	Thermal diffusivity .....	203
9.3.5.	Strength reduction factors at elevated temperatures.....	205
9.3.6.	Stress-strain relationship for cylindrical specimens .....	205
9.3.7.	Behaviour of cylindrical specimens .....	211
9.4.	Fire performance of LCCC-filled steel tubular columns .....	219
9.5.	Conclusions and future work .....	228
10.	Summary .....	229
10.1.	General .....	229
10.2.	Specific conclusions and recommendations .....	229
10.3.	Future work.....	231
	Bibliography .....	233



## **Abbreviations**

AST – adiabatic surface temperature

CFST – concrete-filled steel tubular columns

FAC – fly ash cenosphere

FDS – Fire Dynamics Simulator

FRC – fibre reinforced concrete

FRT – fire resistance time

HSC – high strength concrete

LCCC -lightweight cementitious composite with cenosphere

NSC – normal strength concrete

NWC – normal weight concrete

PT – plate thermometer

RC – reinforced concrete

RLBC – residual load-bearing capacity

TC – thermocouple

UHPC – ultra high performance concrete

ULCC – ultra-lightweight cement composite



## **Abstract**

Analysis of behaviour and residual capacity  
of fire-exposed concrete-filled tubular columns

In this dissertation, the structural fire behaviour of concrete-filled steel tubular (CFST) columns is studied. The research focuses on circular CFST columns, and various aspects of their structural fire behaviour were studied. The study includes a historical background and its connection to the current state-of-the-art. The available experimental data were analysed thoroughly, which helped to identify areas that need improvement in the future.

A fully parametrized, nonlinear, three-dimensional finite element model was formulated in Abaqus. The parametrization helped to build a validation domain consisting of 50 unique full-scale columns tested in fire resistance furnaces in the past. The numerical model simulated the structural behaviour of CFST columns during standard fire exposure. The fire resistance time obtained in the test and the model predictions were in good agreement.

A detailed analysis of the state-of-the-art identified research gaps and highlighted possible areas of future improvement regarding the recording of test conditions. With the validated model, it was possible to identify several factors influencing the fire resistance of CFST columns.

The validated numerical model was then further developed to account for the non-reversibility of material properties during cooling. Concrete does not regain its strength upon cooling, and this characteristic was implemented in the form of user subroutines. A reasonable fire scenario with several design fires was investigated in Fire Dynamics Simulator. The investigation provided a realistic fire scenario, including heating, decay, and cooling stages. This allowed for studies on the burnout resistance of CFST columns, showing their fire performance and Residual Load-Bearing Capacity (RLBC) is influenced by both the design fire, and initial load.

Finally, the study explored the possibilities of improving the structural fire performance of CFST columns by filling them with a material that is less prone to the adverse effects of high temperature. To that end, a literature study was conducted, and several stages of experimental research were carried out. Several lightweight cementitious composites with cenospheres (LCCC) were developed and tested. The LCCC exhibited remarkable strength properties after exposure to temperatures up to 1200°C.

Then, a numerical feasibility study was performed. The available information from the tests on LCCC were implemented into numerical models to explore, how the new filling might influence the fire resistance time of LCCC-filled steel tubular columns. In conclusion, the test results on the material, supported by a numerical modelling of LCCC-filled steel tubular columns, showed that it is feasible to attain higher fire resistance, though there are areas worth improving in the future.



## Streszczenie

Analiza zachowania i nośność resztkowa zespolonych słupów  
z rur wypełnionych betonem poddanych działaniu ognia

W niniejszej rozprawie doktorskiej badane jest zachowanie słupów z rur stalowych wypełnionych betonem (CFST) w warunkach pożaru. Badania koncentrują się na okrągłych słupach CFST i różnych aspektach ich zachowania podczas pożaru. Badania obejmują tło historyczne i jego związek z aktualnym stanem wiedzy. Dostępne dane eksperymentalne zostały dokładnie przeanalizowane, co pomogło zidentyfikować obszary wymagające poprawy.

W pełni sparametryzowany, nieliniowy, trójwymiarowy model wykorzystujący metodę elementów skończonych został sformułowany w programie Abaqus. Parametryzacja pomogła zbudować domenę walidacyjną składającą się z 50 unikalnych pełnowymiarowych słupów testowanych w przeszłości w piecach ogniowych. Model numeryczny symulował zachowanie słupów CFST podczas oddziaływanie zgodnego ze standardową krzywą temperatura-czas. Czas odporności ogniowej uzyskany w badaniach i przewidywania modelu były zgodne.

Szczegółowa analiza aktualnego stanu wiedzy pozwoliła zidentyfikować luki badawcze i wskazała możliwe obszary przyszłej poprawy w zakresie rejestrowania warunków testowych. Model, po przeprowadzeniu procesu walidacji, umożliwił zidentyfikowanie czynników wpływających na odporność ogniową słupów CFST.

Model numeryczny został następnie rozwinięty w celu uwzględnienia nieodwracalności właściwości materiału podczas chłodzenia. Beton nie odzyskuje wytrzymałości po schłodzeniu, a cecha ta została zaimplementowana w postaci subrutyn użytkownika.

Program Fire Dynamics Simulator został wykorzystany do modelowania realistycznych scenariuszy pożaru z kilkoma pożarami projektowymi. Takie podejście zapewniło realistyczne oddziaływania termiczne, w tym fazy rozwoju, zaniku i chłodzenia. Pozwoliło to na zbadanie trwałości pożarowej (burnout) słupów CFST, pokazując, że na ich właściwości pożarowe i nośność resztkową (RLBC) ma wpływ zarówno pożar projektowy, jak i obciążenie początkowe.

Zbadano również możliwości poprawy odporności ogniowej słupów CFST poprzez wypełnienie ich materiałem, który jest mniej podatny na niekorzystne oddziaływanie wysokiej temperatury. W tym celu przeprowadzono badania literaturowe i kilka etapów badań eksperymentalnych. Opracowano i przetestowano kilka lekkich kompozytów cementowych z cenosferą (LCCC). Opracowanie kompozyty wykazały wyróżniające się właściwości wytrzymałościowe po oddziaływaniu temperatury do 1200 °C.

Następnie przeprowadzono numeryczne studium wykonalności. Dostępne informacje z badań własnych zostały zaimplementowane do modeli numerycznych w celu zbadania, w jaki sposób nowe wypełnienie może wpłynąć na czas odporności ogniowej stalowych słupów z rur wypełnionych LCCC. Podsumowując, wyniki badań materiałowych, poparte modelowaniem numerycznym stalowych słupów z rur wypełnionych LCCC, wykazały, że możliwe jest osiągnięcie wyższej odporności ogniowej, choć istnieją obszary warte poprawy w przyszłości.



## Acknowledgements

I wish to express my gratitude to everyone who helped me during the research.

I want to thank my supervisors, Professor Adam Glema and Dr Michał Malendowski.

The list of individuals I am grateful for their help or support in difficult times includes my friends Piotr and Joanna Tokłowicz, Dr Justyna Grzymisławska, Dr Maria Ratajczak, and my family Dorota Szymkuć, Kazimierz Szymkuć, Teresa Zgolińska and Jarosław Zgoliński.

I would like to thank the people who shaped the early stage of my career: Professor Aldona Łowińska-Kluge, Professor Tomasz Garbowski, Professor Peter Schaumann and Dr.-Ing. Inka Pehrs (ehem. Kleibömer).

Piotr Smardz, Adrian Poteralski, and Aleksandra Bczyk from INBEPO developed the initial CFD model described in Chapter 8. The results were presented in our paper Szymkuć et al. (2018b), and the subject was further researched in Szymkuć et al. (2023a).

Chapters 9.1 and 9.2 are based on a paper by Szymkuć et al. (2023b), co-authored by Piotr Tokłowicz and Dr Maria Ratajczak.

Several material manufacturers were kind enough to provide the materials (Cenospheres Trade & Engineering, Góraźdże, Eko Export, Astra, Sika, Stachema, Huta Łaziska) or equipment (Poznań branch of the General Directorate for National Roads and Motorways). This research was supported in part by PL-Grid and PCSS infrastructure.

I want to thank the people who kindly accepted me for my research stays, Dr Paweł Sulik, Professor Venkatesh Kodur, Professor Aldina Santiago, and Professor Helder Craveiro. Helder ran the first thermal tests on properties of the composite developed in Chapter 9.

I also want to thank my wonderful colleagues from RILEM, who showed me more people speak the concrete language than I expected.

I want to acknowledge the help and discussions with our expert technician, Dariusz Jezierski, and I wish we had more time to do the experiments.

There is one person whom I cannot thank anymore, therefore,

I dedicate this dissertation  
to the memory of my wife,  
Paulina Szymkuć.



# 1. Introduction

## 1.1. Concrete-filled steel tubular (CFST) columns

**Concrete-Filled Steel Tubular (CFST)** members, when used in a structural assembly, allow for reaching high standards of functional performance and aesthetics (Fig. 1.1). They combine several advantages, such as reduced erection time, durability in harsh conditions and no need for external fire protection (Wang & Kodur 2000).



*Fig. 1.1 CFST columns (<https://www.peikko.com/products/deltabeam-frame/atlant/>).*

Recently, CFST members gained more exposure through several European-level projects, such as UCoSiF or FRISCC (Schaumann et al. 2013, Romero et al. 2016). However, the rise of CFST columns took place much earlier than in recent years. Circular shapes are common in

nature, which makes them appealing to humans. The classical orders of architecture involved circular shapes, and they were used to form defensive structures such as towers. [Vitruvius \(27 BC\)](#) discussed the advantages of this shape compared to square towers, making an example of resistance against battering rams: *"The towers themselves must be either round or polygonal. Square towers are sooner shattered by military engines, for the battering rams pound their angles to pieces; but in the case of round towers they can do no harm"*.

The history of steel tubular members can be found in [Eekhout \(2011\)](#), who attributes the earliest scientific investigations of iron tubular shapes to Edmé Mariotte in 1660. As discussed in another chapter of this thesis, iron was considered fireproof at that time. Due to several fires and studies initiated by [Fairbairn \(1837\)](#), by the year 1860, it was widely recognised that iron itself could not provide enough fire resistance to the structural members. That led to the invention of double tube cast iron columns, with space between them filled with a *"solid mass of fire-proof composition"*, patented by Cornell in 1860. Two years later, in 1862, Reeves patented the Phoenix Column consisting of four or more wrought iron segments connected with rivets or bolts that formed a hollow cylinder. The riveting technique was used to construct the landmark Forth Bridge in Scotland, completed in 1890, which might be the most prominent use of hollow tubular shapes (Fig. 1.2).

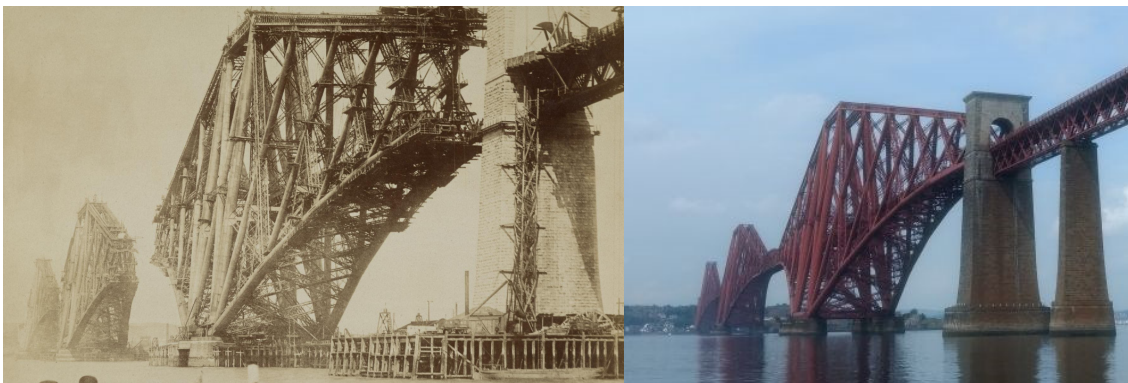


*Fig. 1.2 Forth Bridge during construction (left, National Galleries Scotland, CC license) and now (right, photo by the author).*

CFST members in bridges are discussed by, e.g. [Siekierski \(2018\)](#). Discussion on the development of tubular shapes should acknowledge the skew piercing process (the Mannesmann brothers 1886) and Pilger Process (tube drawing) developed several years later ([Wardenier et al. 2011](#)). Wide use of tubular shapes was made possible by the advancements in the fields of welding and connections between the 1930s and 1950s ([Wardenier et al. 2011](#)).

Among several advantages of using Concrete-Filled Steel Tubular Columns, the most frequently named are the aesthetic appearance, cost-effectiveness, and erection speed ([Morino et al. 2001](#)). Moreover, CFST columns can offer high fire resistance without the need for external fire protection. This is because the steel tube acts as a framework during concrete casting, while the concrete core, with or without reinforcement, has a significant role during a fire. On one hand, concrete acts as a heat sink, absorbing heat from the outer tube. On the other hand, steel lowers the temperature gradient in concrete, protecting it partially against spalling and falling-off. With the same external geometry, CFST columns may offer a wide range of fire resistance times, depending on the amount of reinforcement or compressive strength of concrete.

The aesthetic appearance and high slenderness (Fig. 1.1, Fig. 1.3) are important in many buildings, including lecture theatres, offices, and cultural centres.



Fig. 1.3 Column in the middle of a lecture theatre, Poznań (photo: Wojciech Szymkuć).

Higher compressive strength in RC columns means an increased risk of spalling. In CFST columns, the steel tube acts as a partial shielding. Therefore, temperature exposure of the concrete surface is less severe, and the thermal gradient in concrete is lower. Furthermore, despite the higher moisture content of sealed concrete, steel tube prevents larger chunks of concrete from spalling and falling off. The spalled concrete is usually in place, with its position secured by the steel tube, still fulfilling its insulation purpose (Han et al. 2013). Moreover, CFST columns are less prone to the effects of concrete peeling after exposure to high temperatures, in comparison with RC columns, as can be seen in Fig. 1.4, depicting several columns after fire resistance tests.



Fig. 1.4 CFST and RC columns after fire resistance tests. Extensive damage to concrete cover in RC columns is visible. BAM, Berlin (photo: Wojciech Szymkuć).

There are other areas where the use of CFST might be beneficial. For example, [Su et al. \(2016\)](#) performed a Life Cycle Assessment of columns and pointed out several advantages of CFST over reinforced concrete columns. Cost analysis by [Tailor et al. \(2017\)](#) indicates that CFST columns are more cost-efficient than steel columns. Several other features, such as favourable structural performance and high deformability, were discussed by Polish researchers, e.g. [Flaga & Furtak \(2015\)](#), [Szopa \(2007\)](#), [Kupina \(2015\)](#), and [Abramski \(2018\)](#).

[Moliner et al. \(2013\)](#) proposed a metric called Fire Concrete Contribution Ratio (FCCR), which is a ratio between the fire resistance time of CFST columns and steel (unfilled) tubular columns. They investigated several slender CFST columns and found that the average FCCR values were 2.30 and 3.42 for axially and eccentrically loaded columns, respectively. Moreover, the FCCR was at least 1.50 in all investigated cases. CFST columns facilitate achieving long fire resistance time without additional fire protection ([Wang & Kodur 2000](#)), which is costly, might have durability issues and might be visually unappealing. **Thus, it is clear that any effort to improve the structural fire performance of CFST columns should focus on improving the fire response of the material inside the tube - concrete.**

Many materials are used to fill tubular columns ([Romero et al. 2020](#)), including concretes with different strength, geopolymer concrete, foam concrete or embedding massive steel cores ([Schaumann & Kleibömer 2018](#)). [Szymkuć et al. \(2018a\)](#) proposed filling steel tubular columns with ultra-lightweight cement composites (ULCC) instead of ordinary concrete. Recently, [Li et al. \(2021a\)](#) tested several double-skin tubular columns filled with ULCCs at ambient conditions. [Lopes & Rodrigues \(2020\)](#) investigated tubular composite columns filled with lightweight concrete in fire conditions. [Espinosa et al. \(2015\)](#) hypothesised about using filling with enhanced thermal resistance and low thermal conductivity, possibly in conjunction with modern advanced steels. On the other hand, [Xiong & Liew \(2016\)](#) investigated the potential of using UHPC filling to improve the fire resistance of CFST columns.

The materials used to form the external tubing are available on the market. However, it is virtually impossible to manufacture them in the in-house laboratory. On the contrary, concrete and its final properties can be designed, tested and tailored to the specific use. Since virtually anybody can make concrete, it encourages further development of filling types. For this reason, other chapters of this thesis focus more on concrete than steel.

## 1.2. Early CFST design rules

The earliest known advice on the design of CFST columns can be found in early test reports from Bauschinger (reported by [Möller 1885](#)). However, the first qualitative guidance was set by [Ingberg et al. \(1921\)](#), who assigned a 25-minute fire resistance period to CFST columns ("*pipe columns filled with concrete*"), which could be further increased to a 45-minute fire resistance period if the concrete was reinforced (Fig. 1.5). [Ingberg et al. \(1921\)](#), who tested more than a hundred columns, provided more guidance, for example, stating that a 4-hour fire resistance period can be provided to reinforced concrete columns by using a cover of 1.5 inches (3.8 cm) of calcareous concrete or a cover of 2 inches (5.1 cm) of siliceous concrete. Interestingly, using a wire mesh to avoid concrete falling off was also addressed in the report.

**TABLE 46.—FIRE RESISTANCE PERIODS DERIVED FROM THE TEST RESULTS—Concluded**

Type of Column	PROTECTION		Minimum Area of Solid Material, Sq. In.	Nominal Thickness of Protection, In.	Fire Resistance Period
	Material	Details			
Steel pipe	Unprotected. Filled with concrete	Concrete mixture, 1:1½:3	35	.....	25 min.
Reinforced steel pipe	Unprotected. Filled with concrete and reinforced in the fill with structural shapes	Concrete mixture, 1:1½:3	45	.....	¾ hr.

Fig. 1.5 CFST columns and their "fire resistance periods" (Ingberg et al. 1921).

In Poland, the fire resistance of structural members was first prescribed by law by Warunki techniczne (1961). However, no mention of CFST columns was made at that time. In the 1960s, the performance CFST columns at ambient conditions was a subject of interest to many Polish researchers. Czarniawski (2016) cites four PhD theses defended at the Warsaw University of Technology between 1962 and 1970 (S. Domański, W. Merunowicz, M. Sandowicz and S. Matyaszewski). While not connected to fire resistance, this might have been why Safuta (1975) included CFST columns in his work (Fig. 1.6), even though the available test results on the fire performance of CFST columns were scarce at that time. Four years later, the Polish Building Research Institute (Instytut Techniki Budowlanej, ITB) issued its guidelines (Wróblewski & Pogorzelski 1979), which did not contain information on the fire resistance of CFST columns.

2.4.	Słupy z rur stalowych lub żeliwnych bez okładziny, wypełnione betonem (a — grubość ścianki)		$\phi 30 \quad a=0,8$ $\phi 25 \quad a=0,6$ $\phi 20 \quad a=0,7$	1 0,75 0,40	C D E
------	---	---	---	-------------------	-------------

Fig. 1.6 CFST columns in Polish regulations (Safuta 1975).

### 1.3. Performance-based design approaches

Two general frameworks of building design can be distinguished: prescriptive (traditional) and performance-based design (PBD). The difference between the two can be expressed as the difference between two approaches: (i) how a building is to be constructed (traditional) and (ii) how a building is to perform under fire conditions (Meacham & Custer 1995, Johann et al. 2006, Buchanan & Abu 2017).

For typical problems in the design of buildings, the prescriptive codes provide the designer with sufficient guidance. Tabulated data and closed-form solutions speed up the design process and often provide an adequate safety level. However, the designer might not be aware of this level. For example, simple fire design methods for columns in Eurocodes 2, 3 and 4 were calibrated in such a way that 60 %, 50 % or 80 % of the results were conservative compared to test results, respectively, for each method (Franssen 2000, Franssen et al. 1996, Albero et al. 2018). An example of prescriptive guidance for mitigating concrete spalling is to add polypropylene fibre. In most cases, it is a sufficient countermeasure. It is fast and cheap to apply compared

to a performance-based approach, which relies on detailed thermo-mechanical analyses or testing.

Several documents are related to the performance-based fire design of structures, as summarised in, e.g. ISO 24679-1 standard and technical reports ISO 24679 parts 2 to 8. Formally, in the European Union, performance-based design is referenced in the design standards. However, both EN 1991-1-2 and the classification standard EN 13501-2 (and their revised versions, prEN 1991-1-2:2021 and prEN 13501-2:2022) refer to the Interpretative Document ID2 (1994), which laid out a philosophy regarding the so-called essential requirements, for example, that in fire the "*load-bearing capacity of the construction is adequate for a specific period of time*" (ID2 1994).

Performance-based design is about asking the right questions, while prescriptive design is often about the formal criteria<sup>1</sup>. Moreover, to successfully use advanced and performance-based design methods, it is crucial to understand where our current knowledge comes from. The two approaches complement each other, as the "*Today's advanced PBD informs tomorrow's 'prescriptively' known solutions*"<sup>2</sup>. That is why several guidance documents try to lay out the philosophy and methods of advanced fire design, such as V4 guidelines co-authored by the author of this thesis (Figuli et al. 2021).

#### 1.4. Motivation

The work presented in this thesis was motivated by the desire to understand better the structural fire response of CFST columns and their constituents (steel and concrete). Such an understanding enables the search for new materials and design methods elaborated later in this thesis.

The reason for researching fire resistance of CFST columns was the author's work on a master's thesis in this area during a stay at the University of Hannover, while the RFCS project 'FRISCC' was carried out (Fire Resistance of Innovative and Slender Concrete Filled Tubular Composite Columns). Around that time, the existing method of fire resistance calculation described in Eurocode 4 was found to give results on the unsafe side for slender columns. This finding led CEN to start an SC4.T4 project '*Develop new rules for composite columns (concrete-filled tubes) in fire*'. The project aimed to develop a safe method of designing CFST columns in fire, regardless of their slenderness.

The direction of performance-based design and post-fire performance was forged through interactions with prof. Venkatesh Kodur, during the stay at the Michigan State University (Fig. 1.7). Further interactions with other researchers, such as Prof. Aldina Santiago and Prof. Hélder Craveiro from the University of Coimbra reinforced the idea of considering effects such as cooling and influence of the surrounding structure.

---

<sup>1</sup> As expressed by Prof. Oliver Vassart in 'Fire Engineering Explained With Prof. Dr. Olivier Vassart', <https://www.youtube.com/watch?v=u4g5YuFMdFg>

<sup>2</sup> Prof. Ruben van Coile, in the description of the ERC grant : <https://www.ugent.be/ea/structural-engineering/en/news-events/news/erc-starting-grant-for-ruben-van-coile>



Fig. 1.7 A sketch by Prof. Venkatesh Kodur, drawn during our discussion regarding the future direction of this PhD thesis. PBD stands for Performance-Based Design, and the graph depicts temperature varying in time and space, with a heating period followed by cooling.

With the growing interest in modelling the physically based fire exposure on structures, the knowledge of the material properties and behaviour of structural members during and after fire is essential. The effect of cooling is not described in EN 1992-1-2. However, it has been drawing considerable attention recently. That is why some provisions are introduced in the newest draft of prEN 1992-1-2. However, their applicability has not been extensively studied (Gernay 2019). For this reason, the work toward a better understanding of post-fire behaviour is currently carried out in organisations such as fib (TG2.3 Fire design of concrete structures, WP2.3.4 – Post-fire assessment) and RILEM (306-CFR Concrete during Fire - Reassessment of the framework). The author is participating in the efforts of the latter group.

### 1.5. Goal and layout of the thesis

The goal of this thesis is to analyse the structural fire and post-fire behaviour of CFST columns. Such an analysis can be carried out in two ways: using the experimental data and numerical models. In this thesis, both approaches are used. Furthermore, in this thesis, the physically-based approach is used to both fire and structural behaviour.

The purpose of developing a numerical model is not only to calculate fire resistance time or residual load-bearing capacity but also to identify factors that influence the behaviour of the column during and after exposure to elevated temperature. Through detailed examination of experimental data and results of numerical analyses, it was possible to determine crucial aspects governing the structural fire behaviour of CFST columns. This allowed to design a successful experimental campaign to develop and test a possible filling material that could improve the fire resistance of CFST columns.

The thesis consists of the following chapters:

### **Chapter 1: Introduction**

The Introduction presents the reasons for conducting the research on CFST columns in fire conditions.

### **Chapter 2: History of fire resistance testing**

Our current knowledge of structural fire behaviour is primarily based on observations made during and after real fires and fire resistance tests. Therefore, chapter 2 presents the history related to fire resistance testing and standard temperature/time curve development.

### **Chapter 3: Thermal actions on structures in fire**

The knowledge of thermal actions (thermal boundary conditions) during a fire is essential for structural analyses of fire performance. Therefore, in chapter 3, fire actions are presented in terms of convective and radiative heat flux. The issues of temperature measurement and furnace control are also discussed.

### **Chapter 4: Properties of concrete and steel at ambient and elevated temperatures**

Since CFST columns consist of steel and concrete, knowledge of the effect of fire on both materials is a prerequisite for any analysis. Therefore, chapter 4 discusses thermal and mechanical properties during and after exposure to elevated temperature.

### **Chapter 5: Experimental and theoretical investigations of CFST columns**

This chapter provides a state-of-the-art analysis of experimental data and findings from historical and modern fire resistance tests. This chapter also explains how we got to the current level of understanding. Several design methods of CFST columns exist in the literature, and are summarised in this chapter.

### **Chapter 6: Analysis of structural behaviour of CFST columns in standard fire conditions**

In this chapter, the author analyses phenomena discovered and reported by various researchers. Factors influencing the structural fire response of CFST columns and factors that might be neglected in further investigations are discussed. Such analysis is crucial for determining what is important in the numerical analysis in chapter 7.

### **Chapter 7: Numerical model of CFST column in fire conditions**

In this chapter, a numerical model of CFST columns is developed, described, and validated. Then, a validated model is used to quantitatively assess how several factors influence the CFST column's structural fire response.

### **Chapter 8: Burnout resistance of CFST columns**

In this chapter, the post-fire response and burnout resistance of CFST columns are discussed. The presented analysis connects the available and new data on CFST performance,

performance-based design, and knowledge on post-fire material properties and structural response of CFST columns.

### **Chapter 9: CFST with lightweight cementitious composites**

With the validated model and results of parametric studies presented in chapter 7, it is possible to determine promising directions for future research. In this chapter, a new type of filling of CFST columns is developed and tested in the laboratory. The feasibility for filling of steel tubular columns is assessed using numerical analyses.

### **Chapter 10: Summary**

In this chapter, a summary and directions for future research are presented.

## **1.6. Hypothesis**

The structural fire behaviour of Concrete-Filled Steel Tubular columns can be successfully modelled, and fire resistance can be improved by tailored core composites.



## 2. History of fire resistance testing

### 2.1. Pre-standardised fire resistance

The concept of fire resistance has been a core idea in structural engineering since the foundations for the first buildings were laid. For the context of this thesis, it is important to present the history related to fire resistance testing, particularly tubular structures filled with concrete or concrete-like materials.

Among the known societies tackling the issues related to fire, one could list ancient Babylon with its Code of Hammurabi inscribed on a basalt stele, Rome with its infamous fires, Militia Vigilium and works of Vitruvius, and lastly, fires of major cities, such as the Great Fire of London in 1666. In the Renaissance Poland one of its most brilliant minds set the first fire safety objectives in Poland. Andrzej Frycz-Modrzewski (1551), the father of Polish democracy, in *De Republica emendanda (On the Improvement of the Polish Republic; O poprawie Rzeczypospolitej)*: "*Ne quod detrimentum accipiant aedificia ab igne*" ("buildings shall not take damage from fire", in Bazylik's translation to Polish: "*Aby budowanie nie podejmowało szkody od ognia*"). While such an objective might seem straightforward, the means to arrive at this goal were only prescriptive, probably transferred from generation to generation. At that time, the situation was similar in other countries. However, with the birth and development of the scientific method, with the discovery of oxygen and the first theories of combustion, fireproof materials and buildings became a subject of study in the XVIII century. The most known is perhaps the Himmelwright's fireproof 'Model Fireproof Farm House', known as 'the Stone House'. Notably, Himmelwright underlined the need for sustainability and studied the environmental consequences of an infinite build-burn-rebuild loop.

Years later, in the XXI century, people recognised there was no such thing as a 'fireproof' building. However, new materials, new theories, and new calculation methods are constantly being developed, bringing us to a better understanding of both the fire phenomenon and the structural fire behaviour of buildings. The following sections give an overview that allows understanding the assumptions upon which today's knowledge and approach are based.

In the XVII century, the building walls were required to be made of brick or stone in cities such as London and Boston (Wermiel 1993). Charles Sylvester (1819), author of the *The Philosophy of Domestic Economy* wrote that before introducing the iron and brick, "*ceilings and roofs of stone*" were used. He criticised the fire proof ceilings of stone, calling them "*uncommon*", "*expensive*", and "*not at all adapted for the common purposes of life*". Langley (1749) advocated a solid masonry building system and stone staircases.

In the XVIII-century and early XIX-century understanding, fireproof buildings were made of incombustible materials. They did burn, but it was acknowledged they could be destroyed by fire. As time passed, most buildings were made of incombustible materials such as iron, steel, concrete or bricks, and the term 'fireproof' no longer bore any meaning that would allow to differentiate buildings.

Among other inventors of that time, the work of Hartley (1773) and Mahon (1778) should be acknowledged. The former used metal plates to encapsulate timber floors, and the latter developed a new type of plaster and claimed it was fire resistant. In the upcoming years, those

claims were challenged by Henry Holland, who authored the first comparative fire resistance tests and drafted a document that is recognised as the first report on fire resistance. In this document, Hartley's iron plates and Mahon's plaster were compared ([Associated Architects 1793](#)). The late XVIII century witnessed the development of the first fireproof lightweight systems, notably the one by William Strutt & Charles Bage developed in the 1790s, however similar systems, known as 'poteries et fer', can be tracked to at least 1780s in France ([Addis 2007](#)).

In the 1820's James Beaumont Neilson introduced the hot blast into the ironmaking, which quickly replaced the cold blast because it increased the iron production capacity. It was, however, openly debated whether the new process deteriorated the quality of iron. Recognizing the problem, the British Association for the Advancement of Science asked William Fairbairn and Eaton Hodginson to investigate it (as reminisced by [Fairbairn & Pole 1877](#)). In consequence, scientific curiosity led [Fairbairn \(1837\)](#) to become the first to perform experiments on the strength of materials at elevated temperatures.

In the 1830s, Farrow patented a floor consisting of wrought rather than cast iron reverse 'T' sections, with stones between them. At around the same time, also in the 1830s, Henry Fox built the first concrete floor, patented around 1844 and known later as the Fox & Barrett system. The system utilised inverted 'T' sections, laths and mortar. In the second half of the XIX century, systems with concrete arches between joists attracted significant attention ([Freitag 1899](#)). Some combustible materials could be encapsulated to protect them from fire. One such idea was conceived by Theodore Hyatt, brother of Thaddeus Hyatt, the contributor to the first theories on reinforced concrete. Theodore [Hyatt \(1873\)](#) patented a column made of timber encapsulated in asbestos, perhaps seeding the idea that was later transformed into CFST columns. Since then, keeping track of new solutions has become burdensome due to their large numbers. This coincides with the mass-scale adoption of a new material - concrete.

With the adoption of concrete, more and more construction became 'fireproof', and the term started to become irrelevant. As it was pointed out in [The Building News \(1861\)](#), "*Fireproof construction (...) nor does it imply that the buildings so called fireproof are absolutely safe from destruction or damage by fire*". Since the half of the XIX century, James Braidwood, the "Father of the British Fire Service", argued that "*large buildings, containing considerable quantities of combustible goods, with floors of brick-arches, supported by cast-iron beams and columns, are not, practically speaking, fire-proof*", and the only fire-proof construction would be of pillars with brick columns ([Braidwood 1866](#)).

Braidwood's view was confirmed with tragic consequences after the fire of Chicago in 1871. The intensified discussion on both sides of the Atlantic Ocean diverged into two trends: limiting the size of buildings or innovating fireproof solutions. The first approach was adopted in Britain, and the second in the U.S. ([Wermiel 1993](#)). The innovative approach was encouraged by [Reed \(1896\)](#) in words that could be repeated today: "*Such structures are already thronging our cities and, although we may eventually regulate and restrain many of their eccentricities, we must adapt ourselves to them*". The U.S. approach was viewed from Europe with jealousy and respect ([Stewart 1902](#)). In the words of the Superintendent Stewart, the materials that were not tested or did not pass a test were prohibited by the U.S. Bureau of Buildings (parts

of this approach remain to this date). The resulting competition between manufacturers stimulated "a constant study on the part of builders to better their materials, to make them stronger and more nearly fireproof, while at the same time seeking a minimum cost" (Stewart 1902).

On the other hand, there was a growing demand for knowledge - especially obtained with impartial tests. In 1871, Bauschinger established the first university-run material testing laboratory that would suit the needs of both scholars and the industry (Timoshenko 1953). In 1878, Wight, known for many patents, expressed the need to protect all iron-work (Wermiel 1993). At the same time, hollow tile floors got more and more attention, and the amount of Portland cement production increased. At the turn of the XIX and XX centuries, steel was getting more and more attention, partially due to tailored production methods and its price getting progressively more affordable. The need for providing external protection to iron columns was recognized very early. A comprehensive design guide is given by Hagn (1904) for different types of structural elements, such as columns, decks or walls. Hutton (1876) recognised that at that time, it was impossible to construct a fireproof building that would attain the magnitude of tragedies such as Chicago 1871 and Boston 1872 fires. Iron, wrote Hutton, "in the form of thin sheets, and all the various forms of corrugated iron for floors and roofs, as a fire-proof material, it is utterly useless". However, the analysis of those two fires showed that there were only two materials that, to some extent, were capable of resisting the fire: "An investigation of the most trustworthy accounts of the Chicago and Boston fires shows that in both cases there were two (and only two) materials that to any extent resisted the disintegrating action of the furious heats; and that these were brick and mortar" Hutton (1876). Moreover, after the San Francisco 1906 earthquake and fire, the concrete structures were found to perform relatively well, which significantly influenced their further development.

A good example of organised, comparative, and well-described fire resistance tests are the Denver tests. They were made to ensure that the Equitable Building in Denver is "absolutely fireproof". The Denver tests were not the first organised fire resistance tests, as they were predated by, e.g., Bauschinger's tests on columns. However, due to their scale and practical importance, the Denver tests need to be mentioned here. Floor-arches (Fig. 2.1) from three manufacturers were constructed and tested using fire and water tests (Andrews et al. 1891).

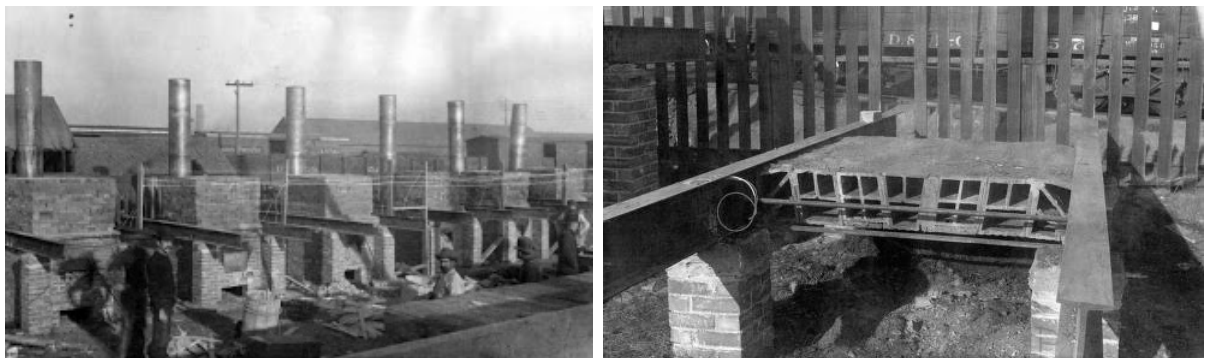


Fig. 2.1 Photos of the first organised structural fire resistance testing. Retrieved from: <https://digital.denverlibrary.org/digital/collection/p15330coll22/search/searchterm/fire%20proof%20arches/field/all/mode/all/conn/and/order/dated/ad/asc>

However, ad hoc tests, such as those in Denver, were criticised for the lack of conditions that would be easily comparable. Calls for standardised fire resistance tests were made by, e.g. [Reed \(1896\)](#):

- *"Steel or iron columns, girders, and beams, must be made on a full working scale and under the actual conditions, as far as possible, which would be obtained in a fire"*.
- *"To be a standard it must contemplate all fire possibilities, even the most remote, pertaining to those conditions..."*.

Similar calls were made earlier in Germany after the devastating Speicherbrand in Hamburg, which created a lengthy debate ([Müller 1891a](#), [Hagn 1891](#), [Deutsche Bauzeitung 1891](#), [Müller 1891b](#)). The German debate was not only a call towards standardised fire resistance testing but also performance-based design. Likely Mühlke ([Deutsche Bauzeitung 1891](#)) advocated for answering the following question during the design process: whether protection of columns is needed in certain spaces, and what kind of fires can be expected. This explicit call, together with problem recognition by Braidwood, and further contribution from Reed, may be viewed as the birth of the performance-based structural fire design.

After the Cripplegate fire in London in 1897, Edwin Sachs reported significant consequences of fire due to the lack of fire protection measures. As expressed in the introduction to [Sachs \(1902a\)](#), *"only in the event of some great catastrophe such as that of the Cripplegate or the Barbican fire do we find the "Man of the Street" impressed by the extent of the destruction wrought on a specific occasion"*. It was soon discovered that limiting buildings' allowable height or size (British approach) was no longer sufficient. Sachs was one of the founders of the British Fire Prevention Committee (Fig. 2.2). The Committee played a significant role during the early stage of the organised fire resistance tests ([Sachs 1902a](#), [Sachs 1902b](#)). Edwin Sachs is attributed to the 'classes' of fire resistance expressed as 'temporary', 'partial', and 'full', with the corresponding minimum temperatures of 1500 °F (816 °C), 1800 °F (982 °C), and 1800 °F (982 °C) maintained for a period between 45 to 240 minutes ([Sachs 1903](#)). The early ASTM standards from 1908 and 1909 for fire-proof floor construction and fire-proof partition construction required a constant 1700 °F (927 °C) temperature for four hours. Eventually, activities aimed at unifying test conditions led to adopting the standard temperature-time curve in 1918 ([Gales et al. 2020](#), [Law & Bisby 2020](#), [Sachs 1903](#)).



Fig. 2.2 British Fire Prevention Committee testing station ([Sachs 1902a](#)).

## 2.2. Standard temperature-time curves – ASTM E119, ISO 834

This section presents the background and early efforts that led to developing standard temperature-time curves – first ASTM E119 then ISO 834.

The development of standard temperature-time curves dates back to experiments made in the late XIX and early XX century. The origins of the standard temperature-time curve can be found in several papers (Babrauskas & Williamson 1978a, Babrauskas & Williamson 1978b, Gales et al. 2020, Gales et al. 2021, Law & Bisby 2020). Notably, the early XX-century knowledge of fire, and fire dynamics was rather limited. It was common to describe fire temperature as the "average fire temperature of 1500 °F" (816 °C) or "temperature of a coal fire equal to 2400 °F" (1316 °C) (US Geological Survey 1907). The bias towards rounded numbers was also present when efforts towards the standard temperature-time curve were undertaken in several countries, including early versions of NEN 1076 and DIN 4102.

In the XIX and early XX century, there was a discussion on the requirements for fire resistance of buildings and structural members. As it was previously mentioned, people recognised that there is no such thing as a fire-proof construction (the term was criticised several times). Braidwood (1866) stated that some structural members might be fire-proof when used in houses and non-fire-proof when used in an industrial building with high fire load density. A recurring theme in the design of fireproof buildings were cotton mills. Considering their size (Fig. 2.3), the machinery and the high fire load density provided by combustible cotton, it becomes obvious that changes in the building design were necessary.



Fig. 2.3 Cotton mill in Manchester (September 2023, photo by the author).

The efforts to standardise the fire resistance testing were preceded by acknowledging that the so-called 'fire-proof' materials were not 'fire-resistant', leading to a series of tests in Europe and the U.S. The introduction of standards was extensively discussed during the International Fire Prevention Congress in London ([Sachs 1903](#)). The discussions eventually led to classes of fire protection, which at some point were defined as 'Full', 'Partial', and 'Temporary Protection', later changed to 'Four-Hour Protection', 'Two-Hour Protection', 'One-Hour Protection' ([ASTM 1918](#)), sometimes expressed with letters, such as A, B, C, etc.

Eventually, ASTM E119 was adopted in 1918. The standard contained the first standard temperature-time curve (the first occurrence of the curve in known documents is presented in Fig. 2.4). The curve resulted from a joint effort by ten major U.S. organisations, among them NFPA and ASTM.

When considering standard fires or standard temperature-time curves, it is necessary to emphasize that the fire resistance periods or standard fire resistance (whatever they are called) are not the duration of a real fire. The adoption of the standard temperature-time curve, often viewed as representing fires in buildings, is, in fact, an "*arbitrary curve*", as described by Ira H. Woolson himself:

*"When you say it is a partition which will give two-hours' protection, it means it will resist a fire two hours according to the standard control curve given. That curve, which was presented last year **purely as an arbitrary curve**"*

*Ira H. Woolson, [NFPA \(1918\)](#)*

Ira H. Woolson, who was the Chairman of the NFPA's Committee on Fire-Resistive Construction and ASTM's Committee on Fireproofing ([Schulte 2013](#)), was responsible for the work of the ASTM E119 committee.

As foreseen by Woolson ([NFPA 1917](#)):

*"We want to get it as nearly right as possible before it is finally adopted , because , after it is adopted by these various associations, it will be pretty hard to change it"*

*Ira H. Woolson, [NFPA \(1917\)](#)*

Several authors extensively criticised the curve:

*"it always must be borne in mind that in a strict sense standard fire endurance (testing) is not a measure of the actual performance of an element in fire, and, furthermore, that it is not even a perfect measure for comparison"*

*"the results of standard fire tests do not represent either the times for which building elements actually withstand building fires"*

*Harmathy & Lie (1970)*

*"It should also be noted that the fire resistance relates to the test duration and not to the duration of a real fire"*

*Malhotra & Pearce (1987)*

"A 60 minute fire does not imply that a construction is expected to withstand a fire of 60 minutes duration but will withstand a fire of a longer or a shorter duration whose severity corresponds to the 60 minute furnace test"

Khoury et al. (2007)

"The performance of a building (not just structurally but functionally) should stay within acceptable limits under a range of conditions, and that these limits should be set largely on the basis of the severity of the perceived outcomes (...)

A true limit state philosophy should be applied, so that partial safety factors are applied to the loadings and fire conditions (fire load etc..) on the basis of the occurrence statistics and the uncertainty of prediction.

These should be combined with a "natural fire" prediction so that we can get rid of most of the witchcraft (the ISO834 Standard Fire, time-equivalence, fire resistance times ...) that currently muddies the waters".

Ian Burgess<sup>3</sup>

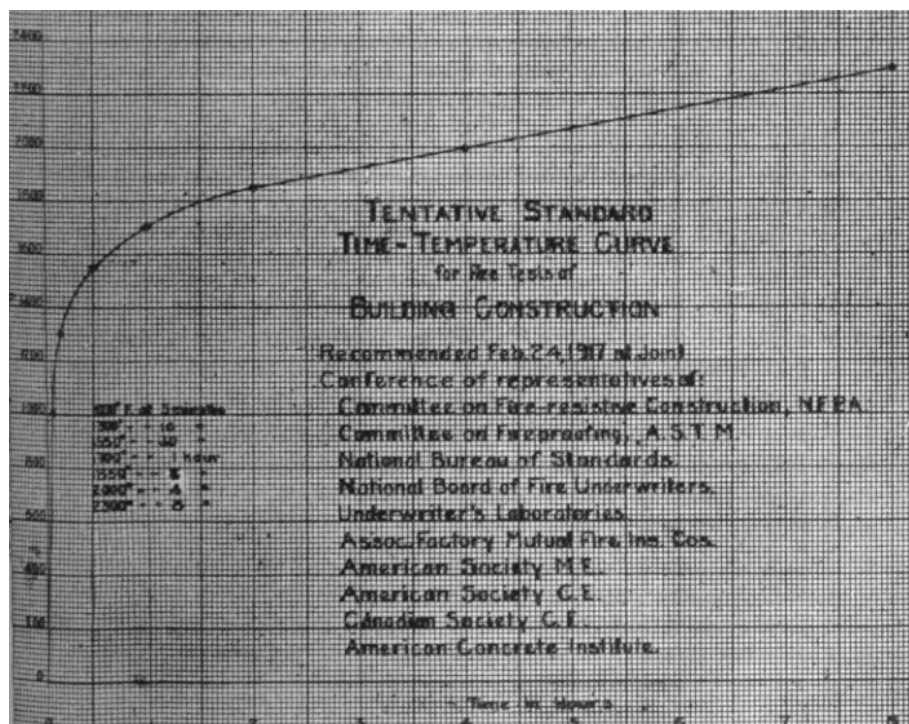


Fig. 2.4 The first known occurrence of the final version of the standard temperature-time curve in public documents (ASTM 1917). Defined for 8 hours, with temperatures in the left part and a list of contributing organisations in the right, below the curve. A slightly different curve appeared in the documents a year earlier.

Similar temperature-time curves were developed in various countries. As a response, CEN started the efforts to unify the standard temperature-time curves, leading to the adoption of national codes such as PN-B 02851 (1964), DIN 4102 (1965) and an international ISO 834

<sup>3</sup> Failure of Structures Under Fire: <http://fire-research.group.shef.ac.uk/steelinfire/discussion.html> [accessed 17.03.2019]

(1975). Ultimately, in testing and classification standards, the standard temperature-time curve took the form of:

$$T = 20 + 345 \cdot \log_{10}(8t + 1) \quad (2.1)$$

where T represents the furnace temperature (ISO 834), also called the average or mean furnace temperature (EN 1363-1, EN 13501-2).

The same relationship is present in the design standards, such as EN 1991-1-2:

$$\theta_g = 20 + 345 \cdot \log_{10}(8t + 1) \quad (2.2)$$

where  $\theta_g$  is the gas temperature in the fire compartment (EN 1991-1-2), in °C, and t is the time (in minutes).

There is a discrepancy in using the terms to describe the standardised fire exposure. On the one hand, the test and classification standards (such as EN 1363-1 or EN 13501-2) consistently use the term "standard temperature/time curve". On the other hand, structural Eurocodes use multiple words for standardised thermal exposure, such as standard fire conditions, exposure, exposure conditions, resistance, or simply standard fire.

Similar curves (such as the ASTM E119 curve and KSF 2257-1) were used in fire resistance tests of CFST columns. Other, such as hydrocarbon or external fire curves (Cooper & Steckler 1996), are used for specific applications. Fig. 2.5 illustrates the most common (nominal) temperature-time curves (also referred to as fire curves): standard temperature-time curve, external fire exposure curve, hydrocarbon fire curve, and slow heating curve. Confusing naming: *temperature-time*, *fire exposure*, *fire*, and *heating* curve was left deliberately as it appears in EN 1991-1-2, or EN 1363-2. Two other curves used in experimental programmes relevant to this thesis are also presented in Fig. 2.5.

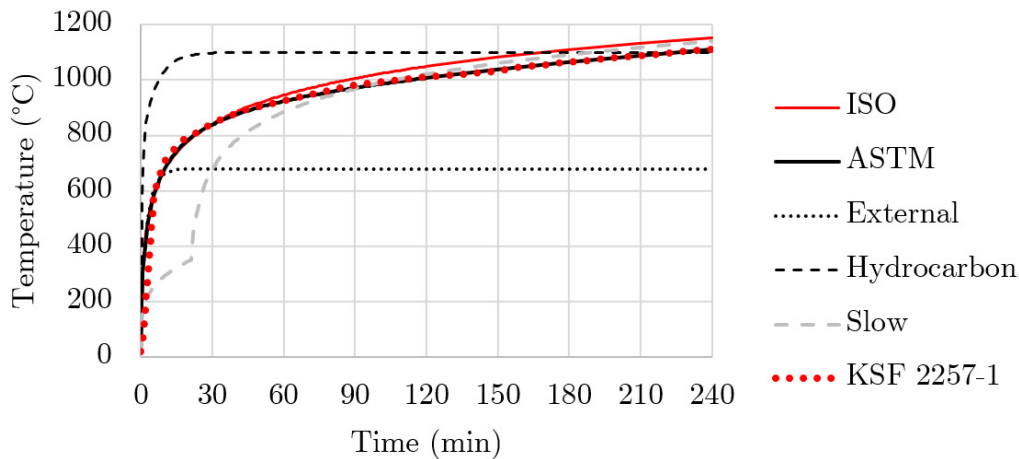


Fig. 2.5 Standard temperature-time curves

Fig. 2.6 presents a timeline of selected events related to fire resistance tests and CFST columns.

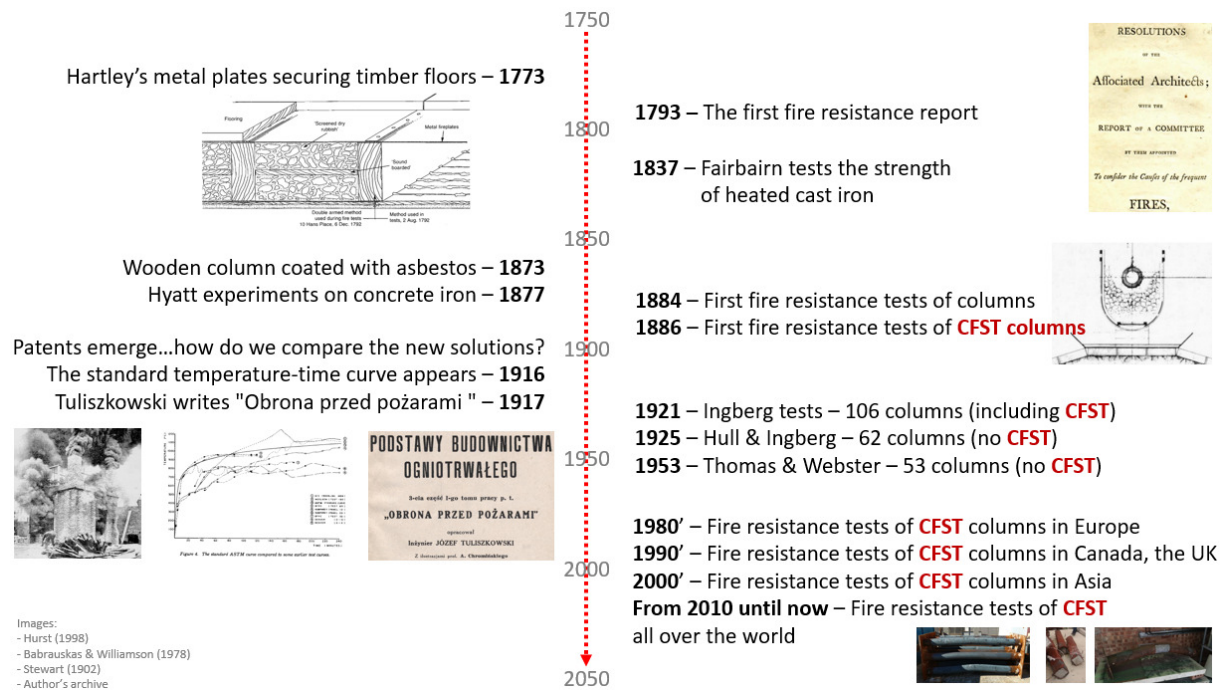


Fig. 2.6 Timeline of selected events related to fire resistance tests and CFST columns.

Using standard temperature-time curves has many advantages and disadvantages, but it certainly excels in comparing different materials and structural solutions (unless combustible materials are involved). In this thesis, data from standard tests are used to validate the numerical models. A validated model enables predictions regarding the fire and post-fire structural behaviour of CFST columns. Such an analysis can be considered a response to an early appeal by Reed (1896), who stated that for structural members we should consider "actual conditions, as far as possible, which would be obtained in a fire". The post-fire predictions require the definition of cooling rates, which are strongly connected to the concept of burnout.

## 2.3. Burnout resistance and cooling

### 2.3.1. Burnout resistance

Burnout resistance is the ability of a structural member to withstand a fire exposure, including heating, cooling and the period after cooling. The term burnout is connected to the previously mentioned 'full', 'partial', and 'temporary' protection. Originally, the 'full' protection was supposed to provide resistance for a whole fire duration - until all combustible material burns out and further during and after cooling. The period after cooling is important due to the risk of delayed failure, which is especially important for reinforced concrete or timber members (Gernay et al. 2022).

The concept of burnout is not new. It was already present during the first standardisation efforts in the early XX century. It is visible in, e.g. the requirements for a 'Standard building', which were established in 1913 by the NFPA, where:

- occupants would be protected against fire and panic,
- fire damage would be reduced to a minimum,

- structural members would be capable of surviving a burn out of all combustible contents (NFPA 1918).

In the first versions of ASTM E119, for a member to be classified, it was required to withstand:

- the test conditions for a period equal to 1.25 times of desired classification times,
- a fire and water test, where water was applied after a certain time.

Similar requirements were also present in the first version of BS 476-1. However, the water test was later abandoned as it was "*found to destroy much useful evidence of the behaviour of a structure and was rarely a deciding issue*" (BS 476-1:1953). In both ASTM E119 and BS 476-1:1953, selected members were loaded several hours after the test was concluded to observe whether they could support the load after cooling.

The discrepancy between standardised testing conditions and real fires was known, and it was a subject of research by Ingberg starting from the 1920s. The quantitative research was carried out to establish reliable relationships between the temperature, time, fire load, and compartment characteristics in Japan (Kawagoe 1958), the UK (Webster et al. 1959), and Sweden (Magnusson & Thelandersson 1970). More information can be found in, e.g., Byström (2017) or Karlsson & Quintiere (2022). Based on the relevant factors, fire scenarios can be deduced (ISO 24679-1:2019) and used in simulations to obtain probable temperature-time relationships inside a compartment. Often, multisimulations are used (Krasuski 2019).

Another problem related to burnout resistance is the time-related degradation of some materials, e.g. presented in Fig. 2.7.

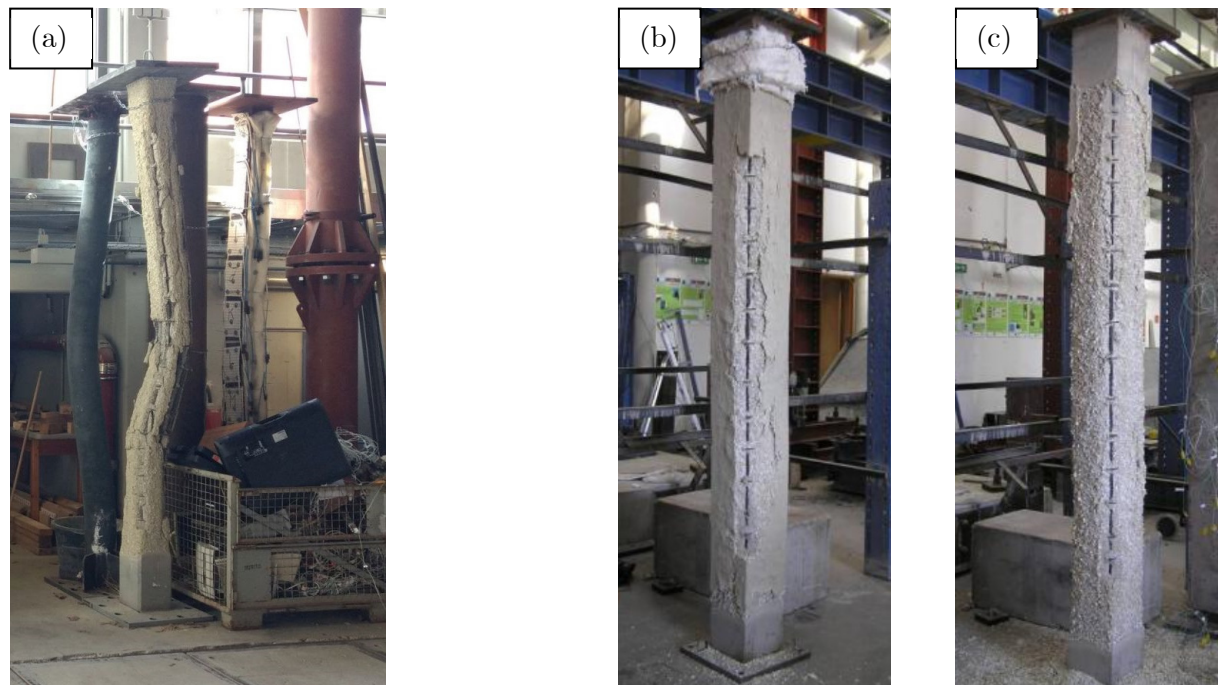


Fig. 2.7 (a) CFST and RC column after fire resistance tests. Extensive damage to the concrete cover in RC columns is visible. BAM, Berlin (photo: Wojciech Szymkuć), (b) RC column on the day of testing, (c) the same RC column one day after testing (Rodrigues et al. 2012).

### 2.3.2. Cooling rates

With the development of research on compartment fires and enclosure fire dynamics, it was possible to address the heating and cooling stage of fires in compartments. The companion document to the first issue of ISO-834:1975 standard – ISO TR-3956 (1975) – points to (Magnusson & Thelandersson 1970) as the source of assumed cooling rates. The cooling rates were later adapted by EN 1991-1-2 with changes proposed in (CEN 2001). The cooling was later elaborated by Lucherini et al. (2021). When the parameters related to the compartment are neglected, the cooling stage can be expressed by:

$\theta_g = \theta_{max} - 625(t - t_{max})$ $\theta_g = \theta_{max} - 250(3 - t_{max})(t - t_{max})$ $\theta_g = \theta_{max} - 250(t - t_{max})$	for $t_{max} \leq 0.5$ for $0.5 < t_{max} < 2$ for $t_{max} \geq 2$	(2.3)
---	---	-------

The formulas above result in cooling rates of about 10 °C/min for fire duration up to 30 minutes to about 4 °C/min for fires that are longer than 120 minutes (625 °C and 250 °C per hour, respectively). They are presented in Fig. 2.8 and Fig. 2.9.

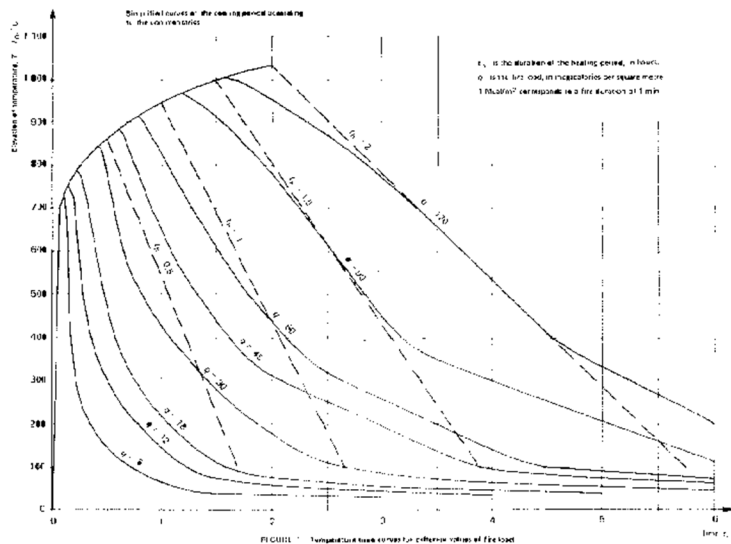


Fig. 2.8 ISO curve with cooling rates, reprinted from ISO TR-3956 (1975).

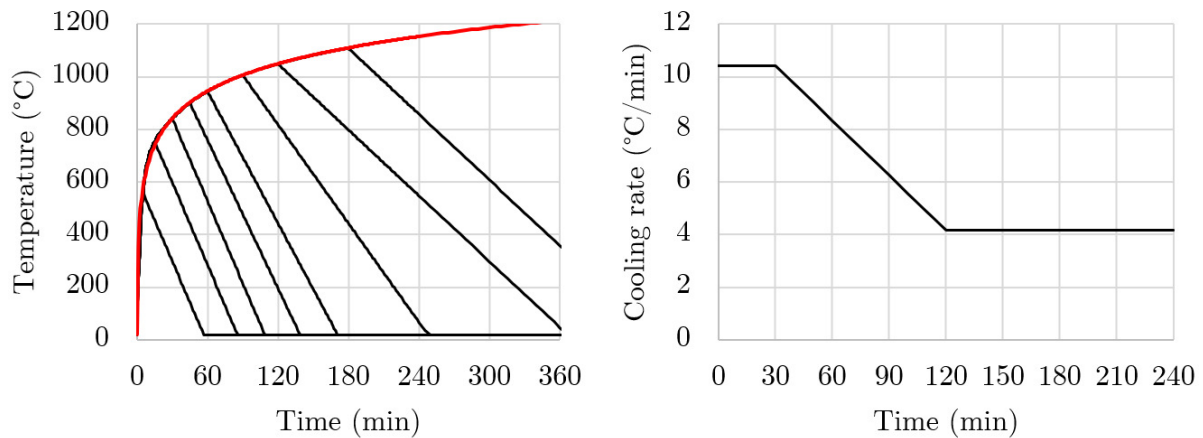


Fig. 2.9 (a) ISO curve with cooling, and (b) cooling rates after heating.

Having established heating and cooling conditions, the next task is to define how the heat is transferred between fire and structural members.



### 3. Thermal actions on structures in fire

This chapter discusses the convective and radiative heat fluxes, and selected issues regarding the control of furnace conditions. The provided information is used to define how the heat is transferred between fire environment and structural members.

#### 3.1. Heat flux

Thermal actions on building members can be represented by the net heat flux  $\dot{h}_{net}$ . Traditionally, different symbols are used in the heat transfer handbooks (for example  $\dot{q}$  for heat flux and  $h_c$  for the convective heat transfer coefficient). However, because  $q$  is traditionally related to quantities representing mechanical load or fire load in structural engineering, the Eurocode symbols are adopted here. The net heat flux  $\dot{h}_{net}$  is a sum of two components:

$$\dot{h}_{net} = \dot{h}_{net,c} + \dot{h}_{net,r} \quad (3.1)$$

where  $\dot{h}_{net,c}$  is the net convective heat flux and  $\dot{h}_{net,r}$  is the net radiative heat flux.

##### 3.1.1. Convective heat flux

The net convective heat flux is proportional to the difference between adjacent gas (fluid) temperature ( $\theta_g$ ) and surface temperature ( $\theta_m$ ). Moreover, it is proportional to the convective heat transfer coefficient  $\alpha_c$ , as expressed by the equation (Newton's law):

$$\dot{h}_{net,c} = \alpha_c(\theta_g - \theta_m) \quad (3.2)$$

The value of the convective heat transfer coefficient  $\alpha_c$  depends on the geometry of the analysed body (surface) and gas velocities (Wickström 2018). In simplified models, the convective heat transfer coefficient can be calculated based on the combination of free (natural) and forced convection. Free convection is a situation when there is no forced fluid flow, but free convection currents exist within the fluid (Bergman & Lavine 2017). Such currents are caused by density gradients, which are usually caused by temperature gradients. The forced convection can be caused by an external source (e.g. fan) or pressure gradient within the fire compartment.

The value of  $\alpha_c$  can be calculated or assumed constant. For example, in the Fire Dynamics Simulator (FDS), the heat transfer coefficient is calculated based on the combination of natural and free convection correlations:

$$\alpha_c = \max \left\{ \begin{array}{l} C|\theta_g - \theta_m|^{\frac{1}{3}} \\ \frac{k}{L} \text{Nu} \\ \frac{k}{0.5\delta n} \end{array} \right. \quad (3.3)$$

Where  $C$  is an empirical coefficient for free convection (different for horizontal and vertical planes or cylinders),  $k$  is gas thermal conductivity,  $L$  is a characteristic length,  $\text{Nu}$  is the Nusselt number, and  $\delta n$  is the gas phase cell size. The value of the convective heat transfer coefficient depends on the boundary layer in the vicinity of a body. Its precise calculation would require a fine mesh, detailed geometry and surface roughness. As a simplification, software such as FDS assumes a logarithmic velocity profile near a surface. The Nusselt number is a function of geometrical and flow characteristics. The correlations for the Nusselt number can be found in handbooks focusing on heat transfer, such as Holman (2010), Wickström (2016a), Atreya (2016) or Bergman & Lavine (2017).

The described correlations are simplified even further for practical structural fire engineering purposes. The SFPE Handbook (Lattimer 2016) estimates the heat transfer coefficient between 10 W/(m<sup>2</sup>·K) and 20 W/(m<sup>2</sup>·K), and up to 50 W/(m<sup>2</sup>·K) for fires where diffusion flame impinges on a ceiling. Table 3.1 lists values for different types of heating recommended by Eurocode 1 (EN 1991-1-2 and prEN 1991-1-2).

Table 3.1 Convective heat transfer coefficients.

Eurocode fire curve or model		$\alpha_c$ (W/(m <sup>2</sup> ·K))
<b>Nominal fire curves</b>	Standard temperature-time curve	25
	External fire curve	25
	Hydrocarbon curve	50
<b>Natural fire models (Physically based models)</b>	Simplified fire models: compartment fires, localised fires (such as Heskestad, Hasemi)	35
	Advanced fire models: one-zone models two-zone models CFD codels	35, unless more detailed information is available

The recommended coefficient for an unexposed surface (free convection) is  $\alpha_c = 4 \text{ W}/(\text{m}^2\cdot\text{K})$ . This value is valid when the radiative heat flux is modelled separately. Alternatively,  $\alpha_c = 9 \text{ W}/(\text{m}^2\cdot\text{K})$ , when it is intended to include the effect of radiation (in consequence, the surface emissivity  $\epsilon_m$  is assumed to be 0).

As given by Kay et al. (1996), the constant value of 25 W/(m<sup>2</sup>·K) for standard fire resistance tests was suggested by Both & Twilt (1990). They argued that in standard fire resistance tests, the surface temperature becomes closer and closer to the gas temperature. Consequently, the contribution of the net convective heat flux to the net heat flux becomes less relevant and a refined model is unnecessary. Fig. 3.1 presents the contribution of the convective and radiative heat flux according to Eurocode's model utilised for the HEA 360 steel section.

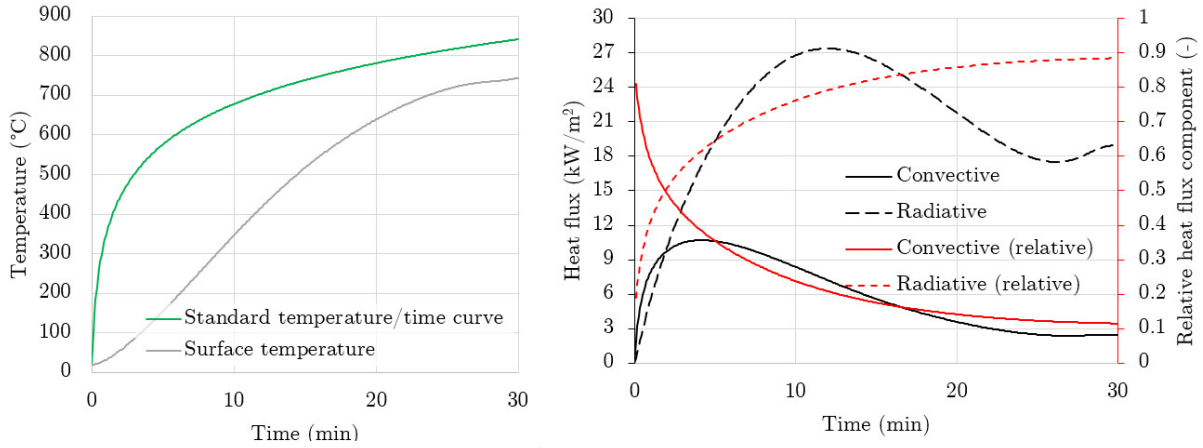


Fig. 3.1 Temperature and heat fluxes for HEA 360 cross-section during a 30-minute exposure to standard temperature-time conditions.

### 3.1.2. Radiative heat flux

With the increase in temperature, the net radiative heat flux grows in importance (see Fig. 3.1), as it is expressed by:

$$\dot{h}_{net,r} = \Phi \varepsilon_m \varepsilon_f \sigma (\theta_r^4 - \theta_m^4) \quad (3.4)$$

\* temperature in Klevin,

where  $\Phi$  is the configuration factor,  $\varepsilon_m$  and  $\varepsilon_r$  are surface emissivity and fire (furnace) emissivity,  $\sigma$  is the Stefan-Boltzmann constant ( $5.67 \cdot 10^{-8} \text{ W}/(\text{m}^2 \cdot \text{K}^4)$ ), and the  $\theta_r$  is the effective radiation temperature of the fire environment.

It is important to explain the term "effective radiation temperature of the fire environment". A definition of  $\theta_r$  is given by Wickström (2016b), who explains it as follows: "the temperature of a surface in equilibrium with the incident radiation, i.e., the absorbed heat by radiation is equal to the emitted heat". A different definition was used by Stefan (1879), who addressed the effective temperature of the Sun; see also Howell et al. (2013) and Prša et al. (2016).

According to the Eurocode, in case of members fully engulfed with fire, the  $\theta_r$  may be represented by the gas temperature  $\theta_g$  around the member. It is important to stress here that 'fully engulfed' usually does not cover the localised fire (unless the member is located inside the fire and the soot is optically thick). For the considerations regarding optically thick and thin environments, see, e.g. McGrattan et al. (2020).

The equation (3.4) describing the net radiative heat flux can also be written as:

$$\dot{h}_{net,r} = \varepsilon_m (\dot{h}_{inc,rad} - \sigma \theta_m^4) \quad (3.5)$$

where  $\dot{h}_{inc,rad}$  is the incident radiative heat flux.

One can already note that the thermal boundary conditions used in engineering are based on several simplifications, and the exposure conditions are 'averaged'. In standard fire resistance tests, which are the basis for most structural fire design methods (Franssen et al. 1996, Franssen 2000), gas temperature and effective radiation temperature are assumed equal. In Europe, furnaces used to be controlled with bare thermocouples, and after introducing the EN 1363-1:1999 and ISO 834-1:1999 standards, the exposure was measured by plate thermometers, as

elaborated in section 3.2. Hence, it is questionable to use the concept of gas temperature when, in fact, the furnace is controlled based on plate temperature output.

Knowing the emissivity of a surface is important for thermal calculations. The emissivity of a member's surface depends on the material of the surface, its roughness and the temperature. In particular, the above dependencies physically influence a wavelength and an angle of emission, which varies with temperature (Gale & Totemeier 2004). Though directional and hemispherical emissivities vary (Lautenberger et al. 2016), single values are used in structural fire engineering problems. This simplification is referred to as grey body radiation. Grey bodies are assumed to have equivalent absorptivity and emissivity. Moreover, it is assumed that grey bodies absorb a fixed fraction (from 0 to 1) of incident radiation, irrespective of the wavelength. The same behaviour is assumed for emission – the grey bodies emit a fixed fraction of blackbody radiation in all directions, and the wavelength range is not considered (FABIG 2014).

EN 1991-1-2 and prEN 1991-1-2 recommend taking the surface emissivity as 0.8, while EN 1993-1-2 and prEN 1993-1-2 recommend the constant value of 0.7. Other sources indicate that the steel emissivity is temperature dependent, summarised in Table 3.2.

Table 3.2 The values of emissivity recommended by other sources.

Source	Concrete	Carbon Steel	Stainless steel	HDG steel
EN 1991-1-2 prEN 1991-1-2		0.8		
EN 1992-1-2 prEN 1992-1-2:2021	0.7	-	-	-
EN 1993-1-2	-	0.7	0.4	-
prEN 1993-1-2	-	0.7	0.4	0.35 for $\vartheta_m \leq 500$ °C 0.7 for $\vartheta_m > 500$ °C
EN 1994-1-2	0.7	0.7	-	-
ISO/FDIS 24679-1:2018	-	0.8-1.0	-	-
Bergman et al. (2017)	0.88-0.93	-	0.17-0.90 <sup>a b</sup>	-
Sadiq et al. (2013)	-	0.28-0.69 <sup>a</sup>	-	-
Paloposki & Liedquist (2006)	-	0.2-0.65 <sup>a</sup>	0.2-0.35 <sup>a c</sup>	-
Fang et al. (2017)	-	0.2-0.7 <sup>a</sup>	-	-

<sup>a</sup> temperature-dependent

<sup>b</sup> steel grade dependent

<sup>c</sup> surface preparation dependent

<sup>d</sup> value valid for any material unless specified otherwise by relevant Eurocode

According to ISO/FDIS 24679-1:2018, the emissivity of steel changes from about 0.8 to 1.0 due to oxidation. Oxidation increases the surface roughness (Kay et al. 1996, Howell et al. 2013), which partially explains the difference between the emissivities of carbon and stainless steel.

According to [Howell et al. 2013](#), material is optically smooth when the "*surface imperfections are much smaller than the dominant radiation wavelength*". That is one of the reasons why the [EN 1363-1](#) recommends plate thermometers made of "*austenitic nickel-based superalloy for high temperature oxidation resistance*". Plate thermometers are aged at 1000 °C before their first use ([EN 1361-1](#)) because the Inconel – material PTs are made of – changes its emissivity during the heating ([Howell et al. 2013](#)) due to the oxidation. On the other hand, one could argue that PTs made of alloys with high oxidation resistance in a furnace atmosphere (limited amount of soot due to the fuel type used) may not be representative of carbon steel in a soot-rich environment ([Sultan et al. 1986](#), [Kay et al. 1996](#)), for example in furnaces fuelled with oil or when testing combustible elements, such as timber.

It can be concluded that establishing a precise emissivity value is not possible due to the number of factors upon which the emissivity depends. Hence, heat transfer models in the Eurocodes were calibrated so that simple, constant values could be used. The calibration was thoroughly and fiercely discussed by [Wickström \(2005\)](#), [Franssen \(2006\)](#) and [Wickström \(2006\)](#).

Let us briefly focus on the term 'net heat flux' so it is established without ambiguity. In both the convective and radiative net heat fluxes, there is a dependence on the surface temperature. The surface temperature depends on the properties of a body and the interactions between different layers of fluid adjacent to the surface. For example, in the case of CFST columns, the surface temperature of steel will be affected by the properties of steel, its surface (e.g., oxidation), the properties of concrete and the thermal gap conductance (air gap conductance) between steel and concrete. Naturally, the properties of concrete depend on the properties of its constituents.

This formulation of the 'net heat flux' is different from the 'heat flux to a surface at ambient temperature', which is used in standard fire resistance testing of, e.g., glazed partitions that need to satisfy the W criterion ([EN 13501-2](#)), where the water-cooled heat flux meter is used, and the measured heat flux is the "*net heat flux to a surface at ambient temperature*" ([Wickström 2016b](#)).

### **3.1.3. Convective heat transfer coefficient and emissivity employed by other researchers**

The previous section gave an overview of the convective heat transfer coefficient and emissivity values, as given by codes, handbooks, or measurements. As previously explained, the constant values are a simplification and result from fitting to the experimental data. Table 3.3 gives an overview of values assumed by different researchers, where some of them modelled the standard fire resistance tests, and others focused on different types of fires.

Table 3.3 The values of emissivity assumed by other researchers.

Source	Fire type	$\varepsilon_f^*$	$\varepsilon_s$	$\varepsilon_f \cdot \varepsilon_s$	$h_c$ (W/(m <sup>2</sup> K))
Ding & Wang (2008)	Furnace (CFST columns)	-	-	0.5	25
Hu et al. (2016)	Furnace (CFST columns)	1, 0.75, 0.38**	0.7, Bentz**, Sadiq	-	10, 25, 40
Hua et al. (2022)	Furnace (RC slabs)	NDA	0.7	-	10
Lange, Sjostrom, (2014)	Localized (CHS inside a pool fire)	1	0.8	-	10
Silva et al. (2016)	Localized (fire next to an I-section column)	NDA	NDA	-	Based on CFD: 9-11.4 for exposed 5-7 for unexposed surfaces
Byström et al. (2015)	Localized (CHS inside a pool fire)	NDA	0.9	-	25
Sandström (2008)	Localized (SHS beam under a slab)	NDA	NDA	-	10
Wickström (2016a)	Localized (SHS beam under a slab)	1	0.8	-	25
Yan & Gernay (2021)	Localized (Kamikawa test)	NDA	0.9	-	9
Yang et al. (2020)	Furnace (CFST columns)	-	-	0.5	25
FABIG (2014)	Pool fires, jet fires	0.25-0.92	0.1-0.9	-	20-95

\*Furnace emissivity was criticised by Wickström & Hermodsson (1997) as a 'fudge factor'.

\*\*Value recommended by the authors of Hu et al. (2016).

### 3.2. The measure of exposure (AST)

Measuring temperature, heat fluxes, or thermal exposure is not trivial. In fact, it is still often ambiguous what quantities are being measured and what quantities are useful for structural designers. In this chapter, a way to measure the furnace temperature is described.

In the first known iron test at elevated temperature (Fairbairn 1837), the temperature was expressed as, e.g. boiling water (100 °C), melted lead (315 °C), or red in the dark (480 °C). The history of temperature measurement is strongly related to combustion studies and can be found elsewhere (Webster & Eren 2014). It is, however, noteworthy that alloys with known melting temperature were used as a proxy for temperature in the Bauschinger's test and Hamburg tests (both are mentioned later in the text due to their connection with columns and the development of standardised fire resistance testing). Some of the problems that were challenging over 100

years ago still carry their burden up to this day, even though the issues had been solved years ago. One such problem is the criterion assumed for the insulation (I), based on the rather limited measurement abilities that existed in the early XX century (Prince 1915, Babrauskas 2009).

In all collected test data, it is assumed that the heating conditions inside the furnace were uniform, irrespective of the position and orientation inside the furnace. The 'average' furnace temperature rise is expressed with only one variable – time, Eq.(2.1).

However, from the physical point of view, the term 'average furnace temperature' is confusing. The control of the environment in the furnace has been a problem since the earliest standardised fire resistance tests (Sachs 1903, Ingberg et al. 1921, Gales et al. 2020). The furnace control was improved due to harmonised conditions that required controlling pressure (McGuire 1978) and, later, the thermal exposure. This exposure can be defined in terms of convective and radiative heat fluxes. The difference between temperature and thermal exposure was explained in detail by Wickström et al. (2018a, 2018b). However, the measurement of such quantities inside the furnace is troublesome. Hence, the exposure was for a long time measured with ordinary bare thermocouples or shielded thermocouples.

However, as argued in a series of papers in the 1970s and 1980s (Maluk et al. 2012), the measured temperature values depend on the lining and shape of the furnace (shallow vs deep) and the type of fuel, which is related to the amount of soot it produces during combustion, that further affect the optical density. For this reason, for over 30 years, achieving the necessary degree of exposure uniformity requires plate thermometers (PT, Fig. 3.2). In 1986, Wickström proposed plate thermometers to harmonise the test conditions between laboratories and furnaces of varying construction (Wickström 1986, Wickström & Hermodsson 1997). To the standard fire resistance testing, PTs were introduced in ISO 834-1 and EN 1363-1 in 1999. A detailed description of the influencing factors, heat transfer mechanisms inside furnaces and the influence of the furnace's depth can be found in Sultan et al. (1986), Van De Leur & Twiit (2000), Wickström & Hermodsson (1997). For a test in a standard 3 m x 3 m furnace, a wall specimen would require at least 1 PTs per 1.5 m<sup>2</sup> (EN 1365-1), while tests on columns (EN 1365-4) would require at least 6 PTs, located in pairs at 1/4, 1/2 and 3/4 of the heated length, and on the opposite sides of the columns.

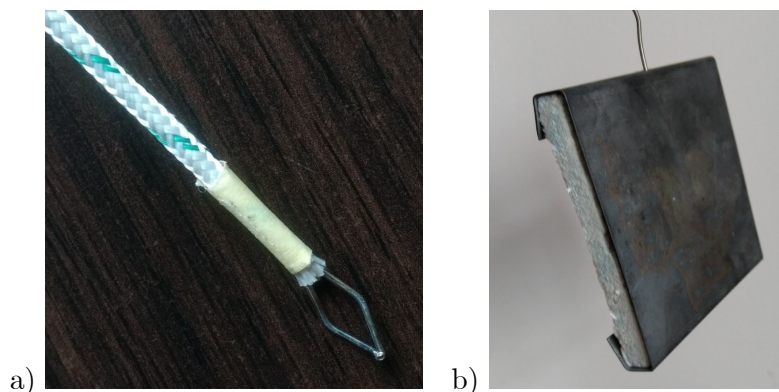


Fig. 3.2 (a) Thermocouple; (b) plate thermometer.

The **Adiabatic Surface Temperature (AST, or  $T_{AST}$ )** is the measure of heat exposure and the background of furnace heating according to [EN 1363-1](#). The AST is the effective temperature that is in equilibrium with the surroundings (net heat flux is zero), as expressed by:

$$\varepsilon_s(\dot{q}_{inc} - \sigma T_{AST}^4) + \alpha_c(\theta_g - T_{AST}) = 0 \quad (3.6)$$

The derivation of the above formula was presented and discussed by [Malendowski \(2018\)](#).

Until the 1990's furnaces were controlled with thermocouples (Fig. 3.2 a). Thermocouples are made of two connected dissimilar wires, a voltmeter, and compensation cables. Due to the Seebeck effect, two dissimilar wires connected at the tip of the thermocouple induce an electromotive force ([Childs 2013](#)). The small tip is insensitive to radiation; hence, the idea of building a device called a Plate Thermometer arose. A PT is essentially a thermocouple measuring the temperature of an isolated thin Inconel sheet. The AST is between the gas and effective radiation temperature. The higher the  $\varepsilon/\alpha_c$  ratio, the closer the AST is to the effective radiation temperature ([Malendowski 2017](#), [Wickström et al. 2018b](#)). One important feature of PT, as opposed to bare thermocouple, is that PT is measuring the heat exposure in a certain area in space related to a certain direction (or, more precisely, a hemisphere, Fig. 3.3). The 100 mm x 100 mm face of PT allows to capture the radiative heat flux. The lower the heat capacity of steel sheet, the better the agreement between PT and AST. Essentially, AST is the temperature of an ideal PT. Some adjustments were later proposed to enhance PT to address the issue related to the heat capacity of steel sheet ([Wickström et al. 2018b](#), [Yun et al. 2020](#), [Liu et al. 2021](#)). However, knowing the thermal properties of PT, and the properties of thermocouple (lags), AST can be calculated based on PT readings using the method developed by [Malendowski \(2018\)](#) and refined in [Malendowski et al. \(2023\)](#).

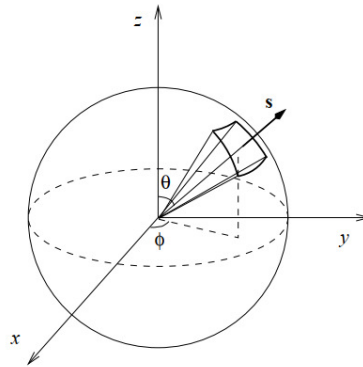


*Fig. 3.3 Coordinate system of the angular discretization ([McGrattan et al. 2023](#)).*

In testing and in engineering applications, it is assumed that the gas and the radiation temperature are equal. The temperature of the ideal PT (perfect back insulation, zero heat capacity of steel sheet) would be equal to  $T_{AST}$ . The values recorded by the PT and  $T_{AST}$  diverge at the beginning of the standard fire resistance test. The discrepancy between the PT reading and  $T_{AST}$  is high only at the beginning of the furnace operation. AST at a given position in space is associated with a vector normal to the PT surface. Hence, varying values can be associated with a single point, depending on the PT orientation, due to captured radiation. The difference between gas and PT temperature is obvious when considering everyday examples

of car body temperature higher than ambient air on a sunny day, facing a flame during a cold night, or when measured with both devices, as presented in Fig. 3.4.

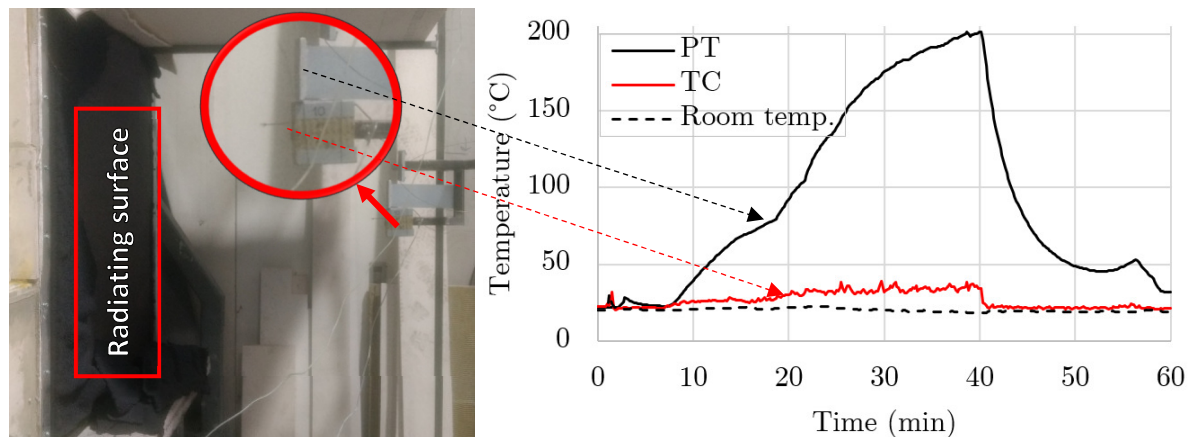


Fig. 3.4 Temperature of a plate thermometer (PT) and gas temperature (TC) during a test of an operable fabric curtain. Measuring points were located one meter from the fabric's unexposed face (own experiment).

Byström et al. (2011) did a similar experiment and measured the gas temperature with two thermocouples (0.25 mm, and 3 mm in diameter). Data in Fig. 3.5 shows the discrepancy that can arise due to the radiation captured by plate thermometer and thermocouples. Notably, there is a difference between values measured with 0.25 mm and 3 mm thermocouples – this is the effect of the thermocouple size, as the smaller thermocouple is less affected by the radiation. Moreover, the response of smaller TC is faster than, due to the difference in their heat capacities.

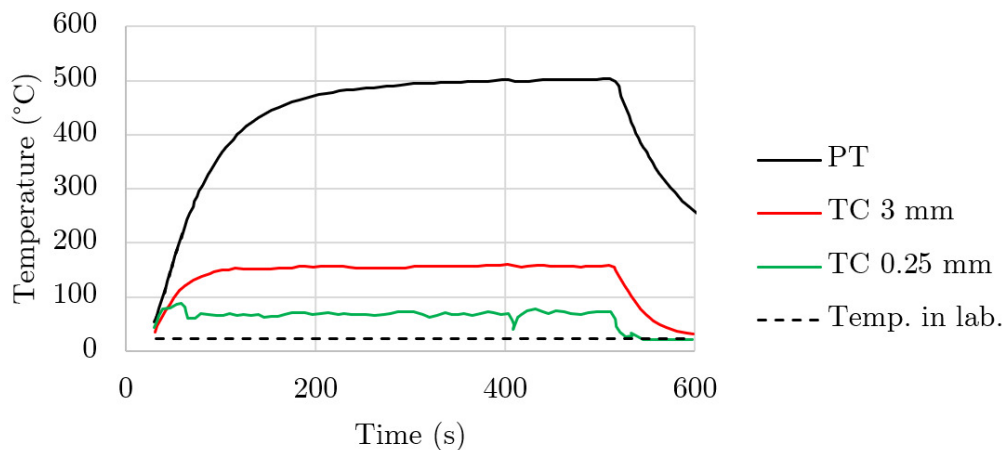


Fig. 3.5 Temperature of a plate thermometer (PT) and gas temperature (TC) during a cone calorimeter test. Adopted from: Byström et al. (2011).

The AST approach was validated numerous times (Wickström et al. 2018b, Malendowski et al. 2021). A quote from Kevin McGrattan will serve as a summary of the AST section:

*"The AST is the cleanest way I know of to transfer info between a fire model and a finite-element structural model"<sup>4</sup>.*

<sup>4</sup> Kavin McGrattan, <https://groups.google.com/g/fds-smv/c/X0jiO3ByIkg/m/OR8gFexBBwAJ?pli=1>

### 3.3. Controlling the furnace conditions

Most modern furnaces are gas-supplied (Turkowski & Węgrzyński 2022). Gas allows precise temperature and pressure control without problems related to the emissivity of furnace gases, that were present in furnaces operating with liquid fuel (Sultan et al. 1986). In some laboratories, electric furnaces are used (Ogrodnik & Szulej 2017, Rodrigues & Laím 2017b). Consequentially, the amount of combustion products is limited. Without the ventilation control, the temperature uniformity along the height of the electric furnace is hard to control. Electric furnaces without forced ventilation are also not very well suited for low temperatures, as it is challenging to maintain a steady temperature growth rate (Fig. 3.6).

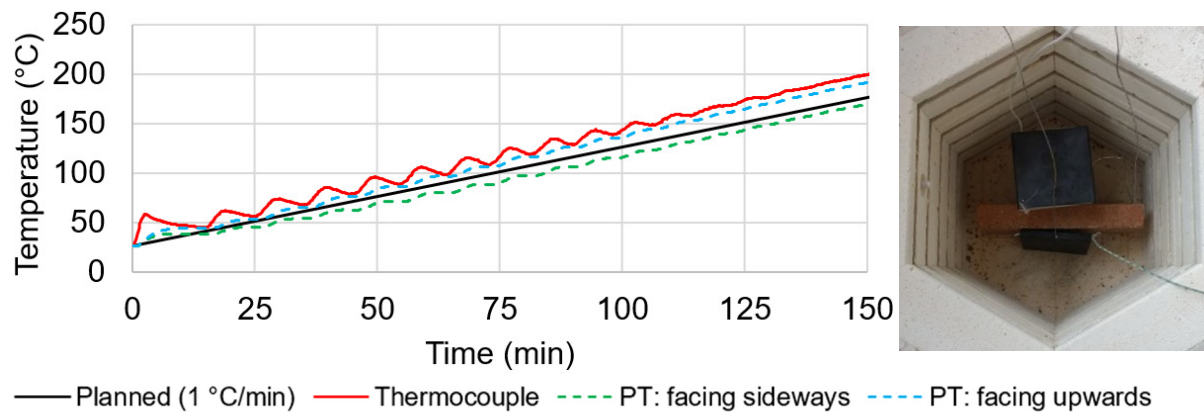


Fig. 3.6 Planned and measured temperature in an electric furnace (own data).

With the furnace control harmonisation achieved through the adoption of PT, the exposure of members inside the furnace can be considered the same, independent of the furnace characteristics, as long as it is PT-controlled. Most of the available fire resistance tests of CFST columns were carried out before PTs were adopted. The lack of PTs adds a layer of uncertainty. However, due to the lack of additional data, the exposure in each test was taken as the authors of the original study measured it. According to a study by Sultan (2004), the difference in exposure is most severe during the first 10-15 minutes of testing.

The lack of PTs is not the only problem related to the uncertainty of the results. Other challenges are associated with the proper (designed vs constructed) boundary conditions, the thermocouple layout inside the steel tube, column positioning relative to the flames, and last but not least – the quality of concrete, concrete casting and its mix design. Those factors will be addressed later.

Harmathy et al. (1987) noted that due to the furnace control (shielded vs. bare thermocouples), the ASTM test was slightly more severe than the ISO test. However, the differences would diminish after approximately 1-1.5 hours of the test. Even though the difference in temperatures seems to indicate that ISO fire in later stages is more severe (Fig. 2.5), they are, in fact, close to each other. According to a study by Harmathy & Sultan (1988), the ISO curve was slightly less severe than the ASTM curve. However, they concluded that the difference in the fire resistance assessed with ISO and ASTM standards was less than 5 minutes. This conclusion, while counterintuitive when analysing Fig. 2.5, can be explained by the differences in the test setup and caveats of the measured values.

### 3.4. Summary

This chapter described how humankind came from the interest in the response of buildings to fire to standardised fire exposure, followed by elements of performance-based (or physically-based) considerations. It also explained what factors are important when discussing how the fire acts on structure and how we can measure and model this action.

With many references to the standardisation efforts made throughout this chapter, let the quote from the creator of the standard for screw threads end this chapter:

*You can only make as well as you can measure.*

Joseph Whitworth, 1803-1887

Having established this, the next chapter will focus on materials – steel and concrete – and the effects of elevated temperature on their properties.



## 4. Properties of concrete and steel at ambient and elevated temperatures

Both steel and concrete experience thermally-induced change (or degradation) of their thermal and mechanical properties. Some of those changes are reversible during cooling, while others are permanent. The remainder of this chapter is focused on the effect of elevated temperature on the thermal and mechanical properties of concrete and steel.

### 4.1. Thermal properties of concrete at elevated temperatures

This section discusses the various factors that affect temperature distribution in heated concrete. The transfer of heat in nonporous and nontransparent materials occurs through conduction. However, for porous materials, heat is transmitted through conduction, radiation, and convection. Separating these three methods of heat transfer for practical purposes is not feasible. Furthermore, the measured thermal conductivity differs depending on the test conditions and methods employed, such as transient and steady-state methods. According to Kodur & Harmathy (2016), the thermal conductivity obtained through a particular method only applies to heat flow patterns similar to those utilized in the measurement process.

Those problems highlight the usefulness of the ‘*effective properties*’. Effective means that they were not directly determined using common methods such as guarded hot plate, heat flow meter, or transient plane source. Instead, they resulted from inverse techniques applied to the data obtained from full-scale furnace test results. Eventually, such properties are calibrated to provide accurate temperature prediction inside the cross-section and to allow for using the classical heat diffusion equation in concrete.

The effective properties offer a significant advantage, as they can be used in conjunction with the Fourier-Biot equation (Holman et al. 2010). This equation, when not considering the heat generation inside a solid body, and assuming isotropic thermal behaviour, is referred to as the diffusion equation and can be written as:

$$\frac{\partial}{\partial x}\left(\lambda \frac{\partial \theta}{\partial x}\right) + \frac{\partial}{\partial y}\left(\lambda \frac{\partial \theta}{\partial y}\right) + \frac{\partial}{\partial z}\left(\lambda \frac{\partial \theta}{\partial z}\right) = \rho c_p \frac{\partial \theta}{\partial t} \quad (4.1)$$

The calibration of effective thermal properties was primarily based on 1-D cases, where the diffusion equation can be expressed as follows:

$$\frac{\partial^2 \theta}{\partial x^2} = \frac{\rho c_p}{\lambda} \frac{\partial \theta}{\partial t} \quad (4.2)$$

The combination of  $\lambda/(\rho c_p)$  the thermal diffusivity and can be determined using simplified techniques (Felicetti et al. 2012, Ablaoui et al. 2023). These material properties – density, thermal conductivity, and specific heat are mostly temperature-dependent, and are essential in calculating the thermal field within structural members in fire. Steel has a thermal diffusivity that in fire conditions is approximately 15 to 20 times higher than that of concrete. Consequentially, steel conducts heat more efficiently, and its temperature can be conveniently approximated by a single value. Conversely, due to its low thermal diffusivity and big cross-sectional size, concrete experiences significant thermal gradients.

As already mentioned, the thermal properties in the Eurocodes are referred to as *effective properties*, and they are suited for a specific application. Even though Eurocode 2 and Eurocode 4 describe the same material, their approaches to modelling specific heat and thermal conductivity differ. Concrete is a porous material comprising aggregate, cement paste, and pores that are partially filled with air and water. As a result, establishing a set of general thermal properties can be challenging. Using the heat diffusion equation for a porous material is a simplification; however, it is generally acceptable. The thermal properties adopted for concrete in the first generation of Eurocodes were based on studies of concrete slabs (Anderberg et al. 2004). These *effective properties* were calibrated so that they can be used to calculate the correct temperature field in most cases, without explicitly considering the phenomena related to the porous nature of concrete and the effects of moisture transport. Notably, between the first and second generation of Eurocodes, the harmonization of relationships for thermal conductivity was the only change made to concrete's thermal properties. This confirms that there is an agreement on the applicability of Eurocode models for studying temperature distribution in concrete.

In order to model the structural response of columns, which is the aim of this dissertation, it is preferable to use effective thermal properties rather than attempting to model other complex phenomena, such as moisture transport. However, even with this simplification, some calibration is still necessary. Unfortunately, for large-scale fire resistance tests, the necessary level of detail of experimental data is not available. And even if it was, accurate modelling would not be feasible with current computational capabilities. Even the refined thermomechanical models are often limited to 2-dimensional problems, and they require high effort related to their calibration to individual tests and require several simplifications (Gawin et al. 2011). According to Scrivener et al. (2019), to model transport phenomena accurately, it would be necessary to capture pores below 10 nm in size, which is beyond the current computational capabilities of structural engineering. Moreover, the usual mesh size used in structural engineering problems is of the order of one cm or 10s of cm.

In addition, the movement of moisture impacts thermal properties, which is why it's important to have simple models that don't require complicated calculations (Anderberg et al. 1978). The Eurocode EN 1992-1-2 provides such a model. The details of the calibration approach can be found in Anderberg et al. (2004), Pimienta et al. (2017), Zehfuß et al. (2020). The new approach in the revision of the Eurocode is based on test results from 21 full-scale slabs, as described in CEN (2019). Two criteria were implemented there, the accuracy criterion ( $C_{NED}$ ) and the safety criterion ( $C_{Safety}$ ):

$$C_{NED} = \frac{\sqrt{\sum_{i=1}^n (Y_{exp,i} - Y_{calc,i})^2}}{\sqrt{\sum_{i=1}^n (Y_{exp,i})^2}} \quad (4.3)$$

$$C_{Safety} = \frac{\sum_{i=1}^n (Y_{calc,i} - Y_{exp,i})}{\sum_{i=1}^n \sqrt{(Y_{calc,i} - Y_{exp,i})^2}} \quad (4.4)$$

where  $Y_{exp}$  is the measured temperature, and  $Y_{calc}$  is the calculated temperature. The objective was to minimize the  $C_{NED}$ , which can be defined as the area between the experimental and

calculated curve, normalised to the area between the time axis (x) and experimental curve. The value of  $C_{safety}$  is between -1 and +1, where -1 means all predicted (calculated) temperatures are lower than measured, and +1 means all predicted temperatures are higher than measured (CEN 2019, Zehfuß et al. 2020).

#### 4.1.1. Density at elevated temperatures

The density of concrete changes with temperature due to the evaporation of water. The Eurocode model assumes a relationship between density and temperature in a range of 100 °C and 1200 °C, shown in Fig. 4.1. According to this model, the density change in this range is approximately 12%. However, it is important to note that the model is simplified and does not explicitly consider water evaporation or phase decompositions. The dehydration processes reduce the volume of hydration products, which leads to an increased porosity of cementitious materials. The density change is mainly a result of cement paste dehydration; however, carbonate aggregates might also contribute to the process.

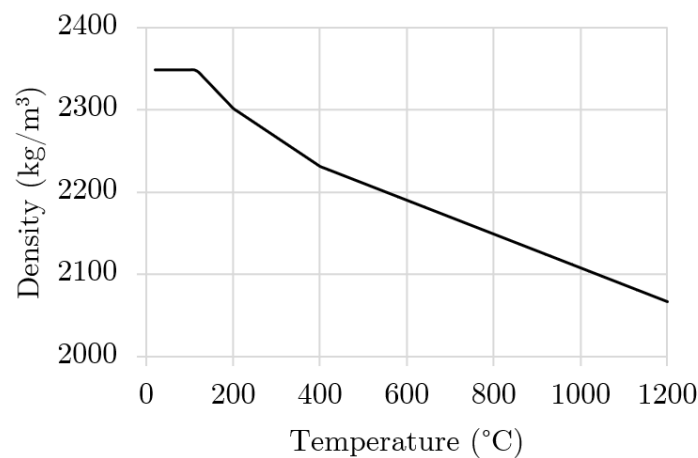


Fig. 4.1 Eurocode model of the concrete density at elevated temperatures.

#### 4.1.2. Specific heat at elevated temperatures

The specific heat of concrete changes with temperature, and its variability is governed mainly by the moisture content (water that would be evaporated if a specimen was dried at 105 °C to constant mass). The specific heat and the dynamics of water evaporation are influenced by the pressure inside concrete pores, which means that the specific heat will be different for sealed and unsealed concrete. These terms can refer to concrete that is literally sealed, such as inside a steel tube, or to concrete where water transport is hindered by dense microstructure. According to Khoury et al. (2007), a similar distinction can be made between external parts of the cross-section (unsealed) and parts that are deeper inside the cross-section (sealed). In such cases, the outer layers of the concrete remain unsealed while the deeper layers are sealed, leading to varying properties. The specific heat capacity of different types of aggregates used in concrete may vary slightly. Therefore, it is not a significant factor in determining the overall heat absorption capacity of concrete (Lucio-Martin et al. 2021). Hence, when it comes to determining the thermal properties of concrete, it is more crucial to consider the drying conditions rather than the specific type of aggregate used.

Fig. 4.2 presents the Eurocode models of specific heat of concrete according to Eurocode 2 and Eurocode 4 for two moisture contents: 3 % and 6 %. Eurocode 2 model, calibrated for concrete structures, illustrates the heat of water evaporation as a plateau between 100 °C and 115 °C.

On the other hand, the Eurocode 4 model, calibrated for composite structures, illustrates the heat of water evaporation as a single peak anywhere between 100 °C and 200 °C.

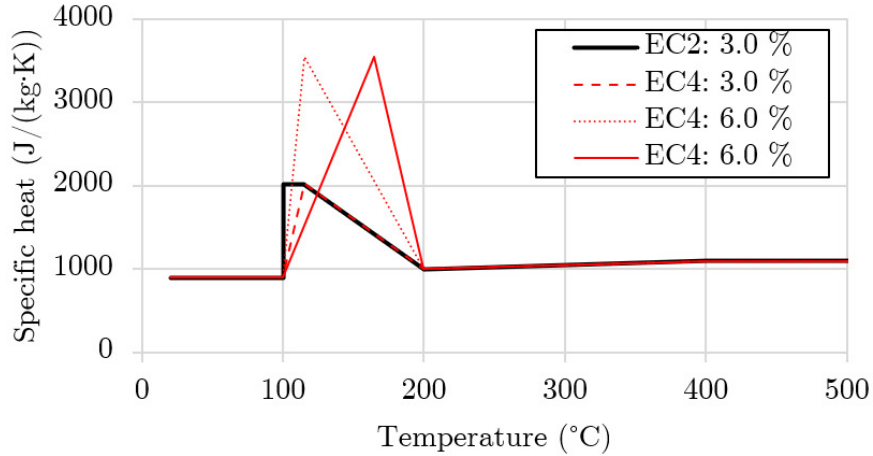


Fig. 4.2 Eurocode models of specific heat of concrete at elevated temperature. Peaks represent water evaporation for moisture content of 3 % and 6 % according to two models (EN 1992-1-2 and EN 1994-1-2).

The specific heat model from Eurocode 4 is more robust. It allows to consider the 'sealing' effects present in concretes with dense microstructure, which exhibit the moisture vaporisation plateau at temperatures higher than 100 or 115 °C. This effect can be represented by a 'shift' of the peak value, illustrated in Fig. 4.2.

#### 4.1.3. Thermal conductivity at elevated temperatures

Several factors responsible for the variability of concrete density and specific heat were given in the previous subsection. However, the variability of those two properties was not as highly influenced by the mix design as in the case of the thermal conductivity. The effective thermal conductivity of concrete is described in the EN 1992-1-2:2004 in the form of lower and upper limits:

The upper limit:

$$\lambda_c = 2 - 0.2451 \frac{\theta_c}{100} + 0.0107 \left( \frac{\theta_c}{100} \right)^2 \quad (4.5)$$

The lower limit:

$$\lambda_c = 1.36 - 0.136 \frac{\theta_c}{100} + 0.0057 \left( \frac{\theta_c}{100} \right)^2$$

According to the background documents to Eurocode 2, the lower limit of the thermal conductivity was calibrated to temperatures measured in concrete structures, while the upper limit was calibrated to temperatures measured in composite structures (Anderberg et al. 2004). Such an approach caused several problems, as the national annexes were allowed to specify the thermal conductivity used in each country. Table 4.1 shows how the national recommendations varied between countries.

Table 4.1 Recommendations of selected national annexes to EN 1992-1-2 regarding thermal conductivity for normal and high strength concrete.

National Annex	NSC (EN 1992-1-2, 3.3.3)	HSC (EN 1992-1-2, 6.3)
Finland	Lower	Lower
Sweden	Lower	Upper
United Kingdom	Lower	Upper
Germany	Upper	Upper
Luxembourg	Upper	Upper
France	Mix of upper and lower	Mix of upper and lower
Cyprus, Denmark, Poland	None	None

Due to these problems, the thermal conductivity in the prEN 1992-1-2:2021 was unified, following the recommendations provided by the French National Annex in 2009 (Fig. 4.3). A linear connection between former upper and lower limits was introduced between 140 °C and 160 °C; thus the thermal conductivity became:

$$\begin{aligned}
 \lambda_c &= 2 - 0.2451 \frac{\theta_c}{100} + 0.0107 \left(\frac{\theta_c}{100}\right)^2 && \text{for } \theta_c \leq 140 \text{ }^\circ\text{C} \\
 \lambda_c &= -0.02604 \theta_c + 5.324 && \text{for } 140 < \theta_c \leq 160 \text{ }^\circ\text{C} \\
 \lambda_c &= 1.36 - 0.136 \frac{\theta_c}{100} + 0.0057 \left(\frac{\theta_c}{100}\right)^2 && \text{for } 160 < \theta_c \leq 1200 \text{ }^\circ\text{C}
 \end{aligned} \tag{4.6}$$

Moreover, in the absence of more detailed data, the thermal conductivity of lightweight aggregate concrete was given as:

$$\begin{aligned}
 \lambda_c &= 1 - \left(\frac{\theta_c}{160}\right) && \text{for } \theta_c \leq 800 \text{ }^\circ\text{C} \\
 \lambda_c &= 0.5 && \text{for } \theta_c > 800 \text{ }^\circ\text{C}
 \end{aligned} \tag{4.7}$$

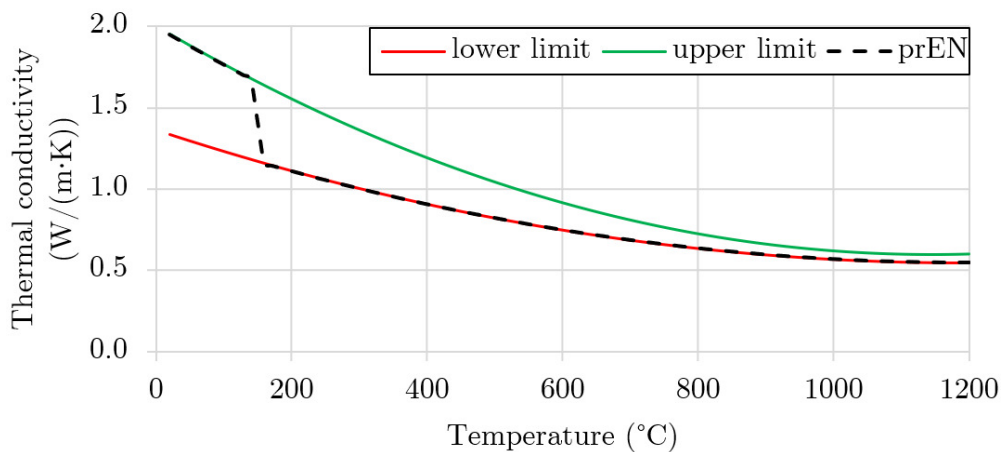


Fig. 4.3 Thermal conductivity of concrete according to Eurocode 2004 (upper and lower limit) and Eurocode 2021 (prEN curve).

One of the reasons behind the variability of thermal conductivity of concrete is the thermal conductivity of aggregates. Research has shown that concrete made with siliceous aggregate has a higher thermal conductivity compared to that made with calcareous aggregate (Tatro 2006, Lucio-Martin et al. 2021). Table 4.2 presents the thermal conductivity of different constituents of concrete, with air being the least conductive (0.026 W/(m·K)), followed by water (0.6 W/(m·K)) and cement paste. The thermal conductivity of cement paste depends on the water-to-cement ratio, with higher ratios leading to more pores in the paste. The range is from 0.356 W/(m·K) for high water to cement ratio (w/c=0.84), to 0.754 W/(m·K) for w/c equal to 0.36. The table also shows the thermal conductivity of selected aggregates, which significantly affect the thermal conductivity of concrete as the aggregate occupies most of the concrete's volume.

Table 4.2 Thermal conductivity of concrete and its constituents.

Constituents	Thermal conductivity (W/(m·K))	Source
Air	0.026	Bergman & Lavine (2017)
Water	0.6	Bergman & Lavine (2017)
Cement paste (dried)	0.66 (w/c=0.43) 0.356 (w/c=0.84) to 0.754 (w/c=0.36)	Brooks et al. (2018) Hajmohammadian Baghban et al. (2013)
Silica sand	4.0	Zhou & Brooks (2019)
Limestone	3.0 2.66 – 3.23	Zhou & Brooks (2019) Kim et al. (2003)
Basalt	2.87	Kim et al. (2003)
Granite	2.91 – 3.08	Kim et al. (2003)
Fly ash cenosphere	0.065 – 0.11	Losiewicz et al. (1996), Wang et al. (2011), Pichór (2009)
Concrete (dried)	1.3 – 2.4	Tao & Ghannam (2013)
Concrete (not dried)	1.75-3.3	Tao & Ghannam (2013)

Tao & Ghannam (2013) proposed the following relationship based on measured values of thermal conductivity (data obtained on oven-dried specimens at temperatures lower than 400 °C were excluded):

$$\lambda_c = 2.34 - 0.272 \frac{\theta_c}{100} + 0.0112 \left( \frac{\theta_c}{100} \right)^2 \quad (4.8)$$

This relationship is presented in Fig. 4.4, along with the raw data collected by Tao & Ghannam (2013) and limits of the effective thermal conductivity from EN 1992-1-2:2004.

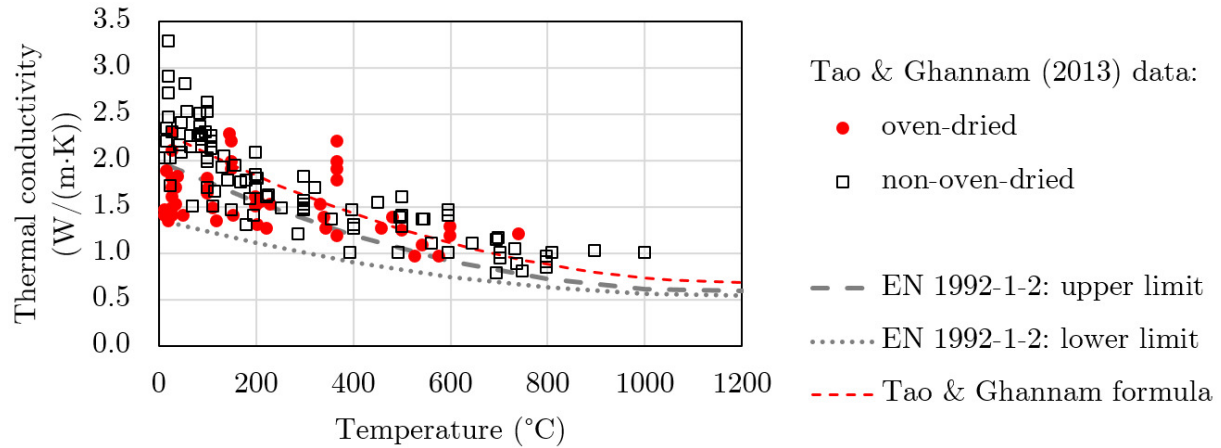


Fig. 4.4 Measured thermal conductivity of concrete, best fit equation (Tao & Ghannam 2013) and two limits of the effective thermal conductivity from Eurocode.

Based on Fig. 4.4, it can be concluded that the limits given by the Eurocode are quite low compared to the experimentally measured data. The concept of effective thermal properties is one of the reasons for such discrepancy.

## 4.2. The effect of elevated temperatures on the mechanical response of concrete

Elevated temperatures have a detrimental impact on the strength and physical properties of concrete. This is due to a range of physio-chemical processes that occur within concrete, affecting its components, such as cement paste, aggregates, and the interfacial transition zone (ITZ) between them. These processes include:

- the dehydration of calcium hydroxide,  $\text{Ca}(\text{OH})_2$ , and calcium silicate hydrate, C-S-H,
- weakening of the ITZ,
- growth of microcracks and the formation of larger cracks due to the thermal incompatibility of aggregate and cement paste.

When exposed to heat, the properties of cement paste undergo changes mainly attributed to decomposition. Water is gradually removed from concrete in a specific order dictated by the removal energy that binds water with solid (Hager 2013). First, free water evaporates, followed by capillary water, and lastly, physically bound water. Chemically bound water present in  $\text{Ca}(\text{OH})_2$  or C-S-H is removed at higher temperatures. This is important, as  $\text{Ca}(\text{OH})_2$  and C-S-H are the main phases of the hardened cement paste, contributing to the compressive strength of concrete. Both these phases decompose when exposed to elevated temperatures, leading to either fully or partially non-reversible mechanisms. This is a crucial factor when discussing the hot and residual compressive strength of concrete.

### 4.2.1. Thermal expansion of concrete at elevated temperatures

The thermal expansion of concrete is an outcome of the thermal expansion of its constituents. Specifically, the aggregate expands at elevated temperatures, while cement paste first expands and then contracts due to dehydration (Fig. 4.5). The most important factor for thermal expansion is the aggregate type. Ghannam (2019) collected the available data and proposed models to consider this factor. Under load, the initial stress level is also a contributing factor to the resulting elongation of concrete (Le et al. 2019). Interestingly, cement type and w/c

ratio do not influence elongation, according to Kakae et al. (2017). Additionally, Li et al. (2022a) observed that the initial moisture content only slightly affects thermal expansion up to 300 °C. Fig. 4.5 presents the thermal expansion of two types of concretes (siliceous and calcareous), a simplified model form Eurocode 4, an experimental data regarding the cement paste. Additionally, the Eurocode model for the thermal expansion of steel is presented for an easier comparison.

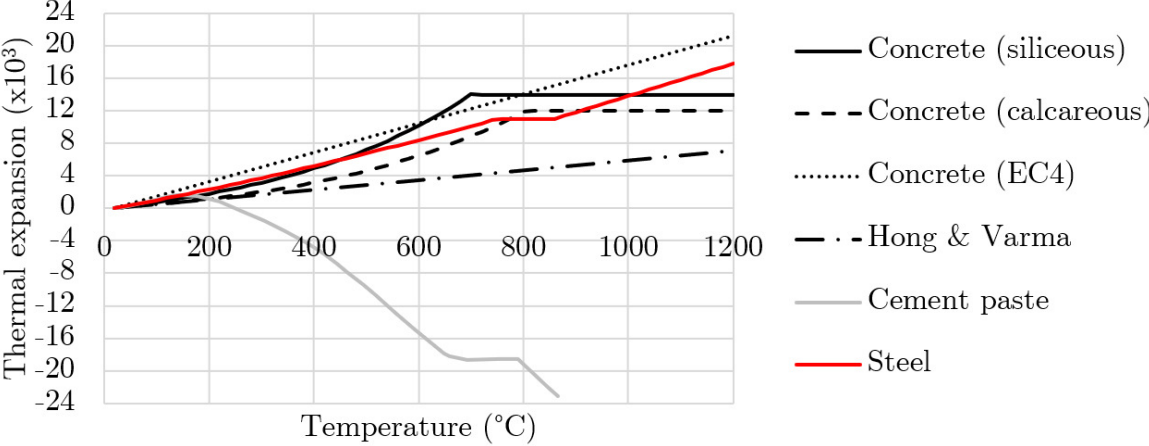


Fig. 4.5 Thermal expansion: siliceous and calcareous concrete (Eurocode 2), simplified relation (Eurocode 4); relationship used for CFST columns proposed by Hong & Varma (2009); thermal expansion of cement paste (Cruz & Gillen 1980); Eurocode model for thermal expansion of steel.

The difference between the thermal expansion of cement paste and concrete can be clearly observed in Fig. 4.5. This incompatibility causes the growth of microcracks and the formation of larger cracks, as explained earlier.

**4.2.2. Concrete at temperatures from 20 °C to 105 °C**

Water inside concrete pores affects the compressive strength of concrete. The effect of pore saturation level on compressive strength is presented in Fig. 4.6, where it can be seen that concrete might show the highest compressive strength when saturation levels are either 0 or 100 %.

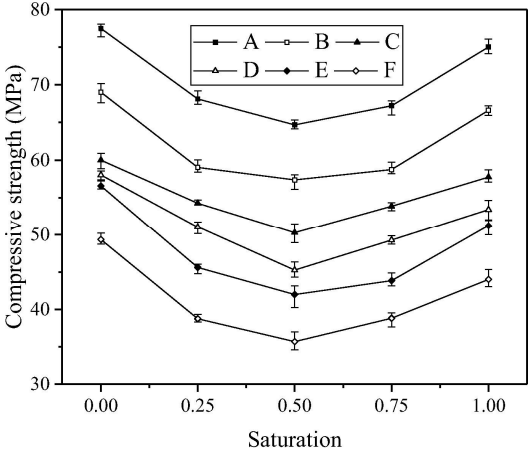


Fig. 4.6 Effect of pore saturation level on compressive strength. Data for six different concretes, each at five different moisture states. Reprinted from Shen & Xu (2019), with permission from Elsevier.

The influence of water saturation becomes more complex when the concrete is heated. It is widely acknowledged that cement paste remains chemically unchanged up to 80 °C, when ettringite (AFt) begins to decompose (Khoury et al. 2007). However, when the temperature exceeds 80 °C, the strength of concrete is affected not only by temperature, but also by water migration. Direct modelling of this complex interplay, however, would necessitate the use of sophisticated thermo-hygro-mechanical models to accurately describe the concrete behaviour at elevated temperatures (Gawin et al. 2011).

As the water is heated, the apparent strength of concrete decreases, as reported by Rostásy & Budelmann (1986) and Ehm (1986). The presence of water and vapour at temperatures close to 100 °C and above reduces the strength of concrete even more. Moreover, the lower the ability to quickly transport the water, the lower the compressive strength. Jansson & Boström (2013) conducted experiments on concrete specimens at different hygral and thermal states and found that:

1. after specimens were dried to equilibrium at 105 °C, the temperature during test (20 °C or 105 °C) had no effect on strength,
2. moist specimens had lower strength than dried (about 10 %), and
3. specimens boiled in water had the lowest strength (about 35 % lower than dried).

The difference between hot strength when moisture is allowed to escape, or when the water transport is hindered, is especially pronounced when normal and high strength concretes are compared. The possible reasons can be found in Ehm (1986), Khoury (1992), Castillo & Durrani (1990). Fig. 4.7 presents the results reported by Ehm (1986) for ordinary concrete.

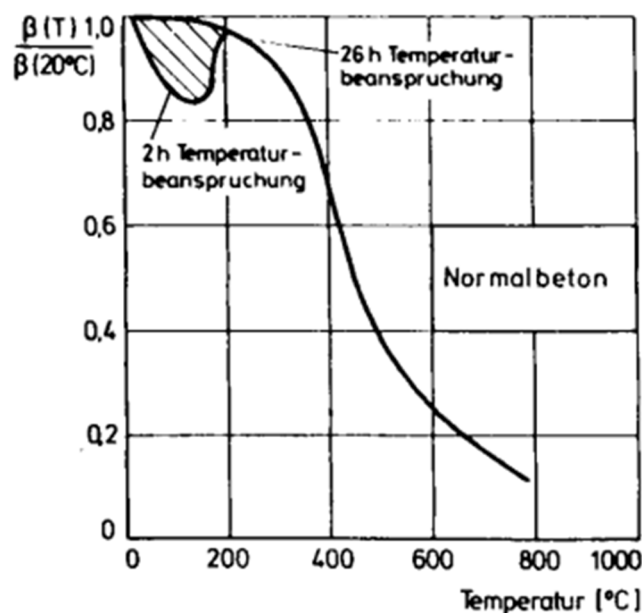


Fig. 4.7 Relative strength of concrete when exposed to elevated temperatures for 2 hours or 26 hours (reprinted from Ehm 1986).

Essentially, the difference observed in Fig. 4.7 is related to microstructure, permeability of concrete, and water behaviour. However, after the free water is removed, the hot strength of cement paste returns to its original value (Khoury et al. 2007) or even increases. Researchers (Khoury 1992, Hager 2013) attribute the temporary loss of strength between 80 and 100 °C of hot concrete to the behaviour of less viscous and dilated evaporable water and its effect of reducing van der Waals cohesive forces between C-S-H layers. According to Hager (2013),

cohesion forces between layers of C-S-H gel sheets contribute to a significant portion of cement paste strength. Hence, the movement and evaporation of water influences the strength, even before C-S-H decomposition starts. In a dense microstructure (sealed conditions), reverse behaviour can be noticed - as used for internal autoclaving. In this case, water might be forced to react with unhydrated cement grains due to additional internal pressure. The phenomenon of internal autoclaving is usually not observed in lightweight concrete - because there is no additional pressure build-up that could influence strength (Holan et al. 2020). As noted before, up to 80 °C cement paste remains chemically unaltered. This temperature marks the start of AFt decomposition, which disappears completely at around 100 °C. The C-S-H, which is in demand for high strength concrete, decomposes gradually, starting from about 100 °C.

#### 4.2.3. Concrete at temperatures from 105 °C to 300 °C

Up to 300 °C, strength loss is usually attributed to a combination of several inter-related factors, including water movement and vaporisation (Hager et al. 2021a), the start of dehydration of C-S-H (Jiang et al. 2020), and microcracking (Pimienta et al. 2017). Microcracks are present in concrete even before any load is applied (Shah et al. 1995, Litewka et al. 2003). The existing microcracks expand due to temperature gradients and thermal incompatibility, and the new cracks form. Cement paste under high temperature expands up to about 150 °C (Fig. 4.5), but is later counteracted by the shrinkage caused by water evaporation. From that point, cement paste starts to shrink (Cruz & Gillen 1980). In the range of temperatures described in this section (105 °C to 300 °C), the porosity, pore structures, and expulsion of water affect the apparent hot strength of concrete. This is especially noticeable in high strength concrete, as illustrated in Fig. 4.8.

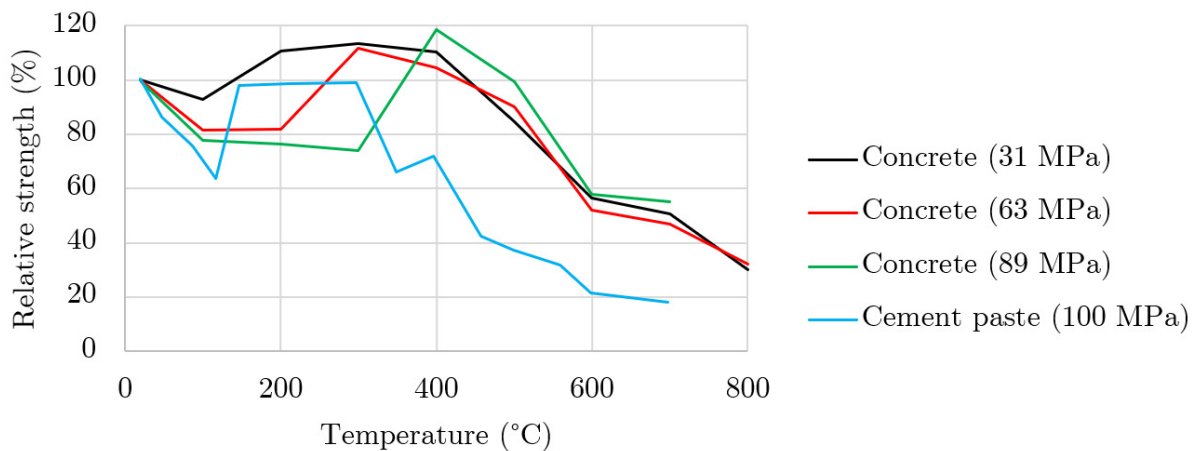
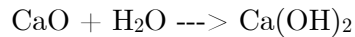


Fig. 4.8 Compressive strength of concrete and cement paste at elevated temperature (tested in hot conditions). Concrete with three compressive strengths tested by Castillo & Durrani (1990), cement paste (Dias et al. 1990).

At moderate temperatures (up to 300 °C), the change of concrete strength is strongly affected by C/S ratio (mols of lime to mol of silica ratio  $\text{CaO}/\text{SiO}_2$ ). This ratio plays a crucial role for the forms of C-S-H that are produced, as evidenced by research conducted by (Khoury et al. 2007, L'Hôpital et al. 2016, Tajuelo Rodriguez et al. 2017). Several studies explored the effect of high temperatures on dehydration, such as (Castellote et al. 2004), which details the decomposition or formation of Aft, CH,  $\text{CaCO}_3$ , C-S-H. Nevertheless, the dehydration of the main products of cement hydration deserves a description, as a deeper comprehension of the dehydration process is essential for understanding the effect of elevated temperatures on the properties of concrete.

#### 4.2.4. Concrete at high temperatures above 300 °C

Above 300 °C, concrete loses its compressive strength. At a temperature of approximately 400 °C, the decomposition of portlandite reaches its peak, producing lime (CaO) and water. The role of CaO is significant, since it might react with CO<sub>2</sub> during a fire to produce CaCO<sub>3</sub> (Iwama & Maekawa, 2022). However, more importantly, after cooling, lime reacts with moisture from the ambient environment:



If this reaction is not accommodated, it can lead to the degradation of cement paste or concrete, as seen by several researchers in the case of small specimens (Bahr et al. 2013, Dias et al. 1990, Halicka et al. 2013, Neuenschwander et al. 2016), full scale specimens (Rodrigues et al. 2012), and whole structures (Gambarova 2005). The delayed failure might also occur due to the thermal inertia of concrete, as seen in studies by Zhang et al. (2016) or Gernay et al. (2022).

The decomposition of C-S-H continues until it is decomposed, mainly to  $\beta$ -C<sub>2</sub>S ( $\beta$ -dicalcium silicate). The temperature at which C-S-H decomposition ends varies between studies. According to the fib bulletin (Khoury et al. 2007), it is completed at 898 °C; however, some XRD studies indicate faster decomposition (Huang et al. 2017). The decomposition was also studied using nuclear magnetic resonance (NMR) by, e.g. Li et al. (2021b). The peaks of C-S-H decomposition can be distinctly observed using Thermogravimetric Analysis (TGA), where two or three peaks can be noticed. The C-S-H decomposition causes further loss of concrete strength.

#### 4.2.5. Models of mechanical properties of concrete at elevated temperatures

So far, factors that help answer the question, "Why does concrete lose strength due to the elevated temperature?" were introduced. While some factors are beyond our control, others can be managed for better results. Within this controllable space, several factors can be distinguished, as concrete strength at elevated temperature depends on the following:

- aggregate type,
- concrete strength,
- supplementary cementitious materials (SCMs),
- presence of fibre,
- the effect of pre-load.

Some of these factors are mirrored in the structural codes. For example, the ACI 216 distinguishes between siliceous, carbonate (calcareous) and lightweight aggregate. Furthermore, it contains data for hot and residual strength. However, the relationships for concrete in ACI 216 are based on a single study by Abrams (1971). Conversely, the properties upon which Eurocode is based on are far more extensive (Anderberg et al. 2004). The Eurocode models are meant to be general and robust. That is why they do not take into account (at least not explicitly) factors such as the influence of SCMs, heating rate or pre-load (taken into account implicitly). More detailed data can be found in the literature. Some of the factors influencing concrete strength at elevated temperature will be discussed later.

Eurocode distinguishes several types of concrete:

- NWC (normal weight concrete, up to C50/60) with two subcategories:
  - siliceous aggregate concrete,
  - calcareous aggregate concrete (at least 80 % of calcareous aggregate).
- HSC (high strength concrete, C55/67 and above) with three subcategories:
  - class 1,
  - class 2,
  - class 3.
- Lightweight aggerate concrete (EC4).

In the [prEN 1992-1-2:2021](#) such multi-level distinction is simplified, and concrete is grouped into the following categories:

- concrete up to  $f_{ck} = 70$  MPa:
  - siliceous aggregate concrete,
  - calcareous aggregate concrete,
- concrete with  $f_{ck} = 70$  MPa and above,
- lightweight aggerate concrete, for which properties should be based on testing.

*Table 4.3 Strength reduction factors for concrete and strains at an elevated temperature according to EN 1992-1-2:2004 and prEN 1992-1-2:2021.*

Concrete temperature (°C)	EN 1992-1-2:2004					prEN 1992-1-2:2021		Both codes	
	NSC		HSC			$f_{ck} < 70$ MPa	$f_{ck} \geq 70$ MPa	Strain	
	Aggregate		Class 1 C55/67 C60/75	Class 2 C70/85 C80/95	Class 3 C90/105			$\varepsilon_{c1,\theta}$	$\varepsilon_{cu1,\theta}$
	Siliceous	Calcareous				%	%		
20	1	1	1	1	1	1	2.5	20.0	
50	1	1	1	1	1	1	3.3	21.3	
100	1	1	0.90	0.75	0.75	1	4.0	22.5	
200	0.95	0.97	0.90	0.75	0.70	0.75	5.5	25.0	
250	0.90	0.94	0.90	0.75	0.675	0.75	6.3	26.3	
300	0.85	0.91	0.85	0.75	0.65	0.75	7.0	27.5	
400	0.75	0.85	0.75	0.75	0.45	0.75	10.0	30.0	
500	0.60	0.74	0.60	0.60	0.30	0.60	15.0	32.5	
600	0.45	0.6	0.45	0.45	0.25	0.45	25.0	35.0	
700	0.30	0.43	0.30	0.30	0.20	0.30	25.0	37.5	
800	0.15	0.27	0.15	0.15	0.15	0.15	25.0	40.0	
900	0.08	0.15	0.08	0.1125	0.08	0.08	25.0	42.5	
1000	0.04	0.06	0.04	0.075	0.04	0.04	25.0	45.0	
1100	0.01	0.02	0.01	0.0375	0.01	0.01	25.0	47.5	
1200	0	0	0	0	0	0	-	-	

The stress-strain relationship for concrete is approximately linear until reaching 30 to 40 % of the peak stress. The initial damage is concentrated on the existing micro cracks and the ITZ ([Pacheco et al. 2019](#)). The orientation of cracks is related to the direction of maximum principal

stress. As the microcracks propagate towards cement paste, the stiffness of concrete decreases, resulting in a non-linear stress-strain response, as noted in (Litewka & Dębiński 2002). Near the peak stress, cracks start to merge, leading to further degradation of stiffness. In numerical models, providing a post-peak response is important. In displacement-controlled uniaxial tests, the post-peak response depends on factors such as the length of the specimen (Jansen & Shah 1997) and the friction between the specimen and loading plates (Kumar et al. 2016).

In order to discuss the differences between stress-strain relationships at ambient and elevated temperatures, a typical C30/37 grade concrete was selected. The stress-strain relationships were plotted at ambient conditions (Fig. 4.9) and at elevated temperature (Fig. 4.10). Simplified bi-linear or parabola-rectangle models are commonly used for concrete in ambient conditions. However, elevated temperatures cause the change of the initial slope (elasticity modulus) and strain corresponding to the compressive strength. In other words, concrete becomes more ductile. Opposite to NWC at ambient conditions, where simple linear models are available in the literature (Fig. 4.9), due to variation of both strength ( $f_{c,\theta}$ ) and strain ( $\epsilon_{c1,\theta}$ ), there are no simplified linear models for concrete at high temperatures, which leads to significant challenges. Workarounds are commonly used, such as ignoring rim zones and using the reduced cross-sectional dimensions, as seen in simplified calculation methods like isotherm 500 or the zone method (Jaszczak et al. 2021, Głowacki & Kowalski 2022).

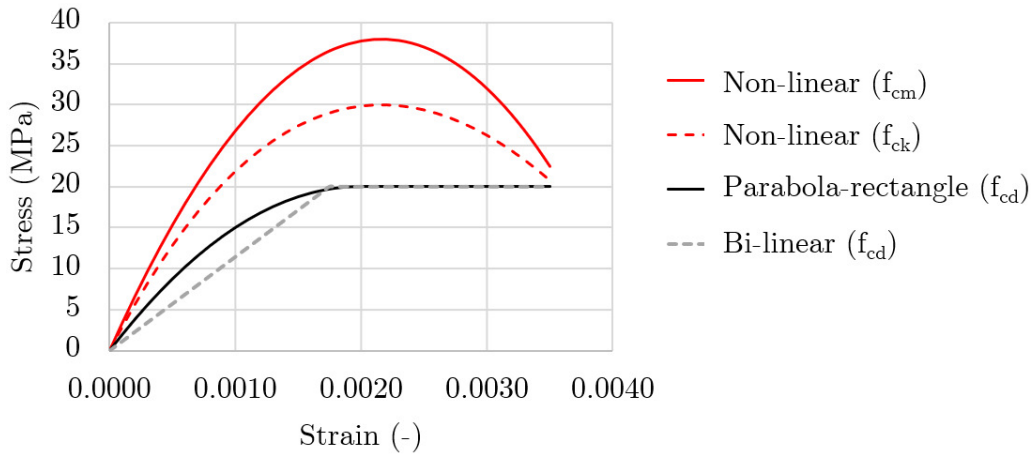


Fig. 4.9 Models of the stress-strain relationships for concrete in compression at ambient conditions, according to EN 1992-1-1.

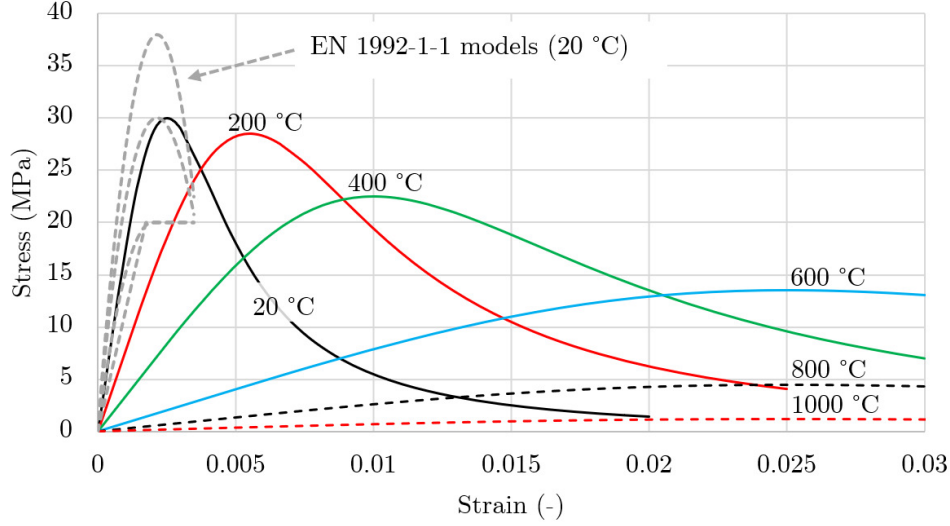


Fig. 4.10 Stress-strain models for concrete in compression at elevated temperatures, according to EN 1992-1-2.

Researchers have proposed various stress-strain models for concrete at elevated temperatures, including those by (Anderberg & Thelandersson 1976, Lie 1994, Li & Purkiss 2005, Han et al. 2005, Yin et al. 2006). However, the Eurocode model is the most commonly used. This model defines the stress-strain relationships using three parameters: compressive strength at elevated temperature ( $f_{c,\theta} = k_{c,\theta} \cdot f_c$ ), the strain corresponding to  $f_{c,\theta}$ :  $\varepsilon_{c1,\theta}$ , and the ultimate strain, when concrete strength is assumed to be zero ( $\varepsilon_{cu1,\theta}$ ). The stress-strain relationship is expressed by the following equation:

$$\sigma_c(\theta) = \frac{3\varepsilon_c \cdot f_{c,\theta}}{\varepsilon_{c1,\theta} \left(2 + \frac{\varepsilon_c}{\varepsilon_{c1,\theta}}\right)^3} \quad (4.9)$$

This temperature-dependent stress-strain relationship was based on the work of Popovics (1973). In 1985, the RILEM Committee PHT 44 recommended implementing this model, and to keep it simple, it was suggested to include the effect of transient thermal strain (TTS) implicitly, by adopting higher values of  $\varepsilon_{c1,\theta}$ . To this day, TTS remains one of the most complex strain components. Including TTS explicitly would result in decomposing concrete strain under load at high temperatures into four separate components:

$$\varepsilon = \varepsilon_{th} + \varepsilon_{\sigma} + \varepsilon_{creep} + \varepsilon_{tr} \quad (4.10)$$

where  $\varepsilon_{th}$  is the thermal strain (free thermal strain),  $\varepsilon_{\sigma}$  is the instantaneous stress-dependent strain,  $\varepsilon_{creep}$  is the creep strain, and  $\varepsilon_{tr}$  is the transient state strain. When compared to the ENV 1992-1-2:1996, only minor adjustments were made in the range between 20 and 300 °C for  $k_{c,\theta}$ . More importantly, in the final version of the Eurocode, TTS was implicitly embedded in the stress-strain relations by adopting increased values of  $\varepsilon_{c1,\theta}$ . The formula proposed by Popovics is robust enough, that it can be used and calibrated for other types of cementitious composites, as shown by e.g. Jelčić Rukavina et al. (2022).

TTS is considered crucial in the modelling of reinforced concrete columns. However, CFST columns display three distinct stages of vertical displacement (explained later); therefore, concrete filling usually remains unloaded for the first 20-40 minutes. Consequently, it is uncertain if existing TTS models, based on specimens loaded for an entire test duration, can help accurately describe the fire behaviour of CFST columns.

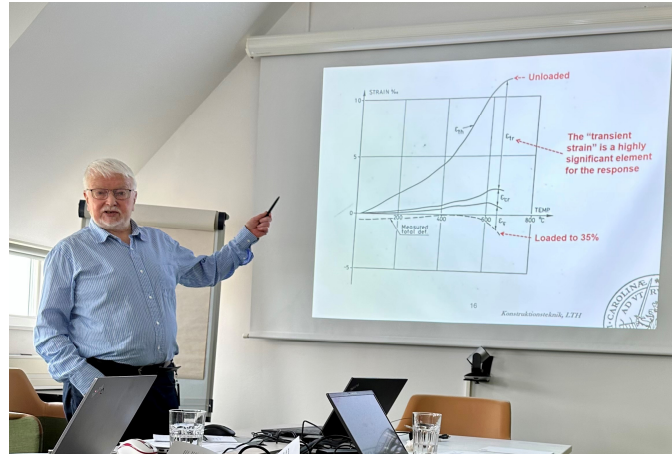


Fig. 4.11 Prof. Emeritus Sven Thelandersson, presenting "Fire resistance design of structures – research in Lund 50 years ago". RILEM 306-CFR meeting in Lund, March 2023.

Moreover, the Eurocode stress-strain model is valid for heating rates ranging from 2 °C/min to 50 °C/min. Part of the data is based on the testing protocol developed by former RILEM committees, which prepared the recommendations in 1995 and 2007 (Schneider et al. 2007). How well-suited are those relationships for members under physically-based fire exposure is a key focus of the current RILEM Committee 306-CFR: *Concrete during Fire – Reassessment of the framework*. In the prEN revision of the Eurocode, the heating rate limit was waived.

The current model has its drawbacks, as it is sensitive to the values of  $\epsilon_{c1,\theta}$  strain. Using the Eurocode stress-strain relationships results in an elasticity modulus of C20/25 concrete equal to 40 % of its initial value at 20 °C (see Fig. 4.12). For C50/60 concrete, the elasticity modulus at the same temperature is 80 % (Fig. 4.12). The per cent values are compared to the values used for ambient design (EN 1992-1-1), with  $E_{cm}$  modulus of 30 GPa, and 37 GPa, for C20/25 and C50/60, respectively.

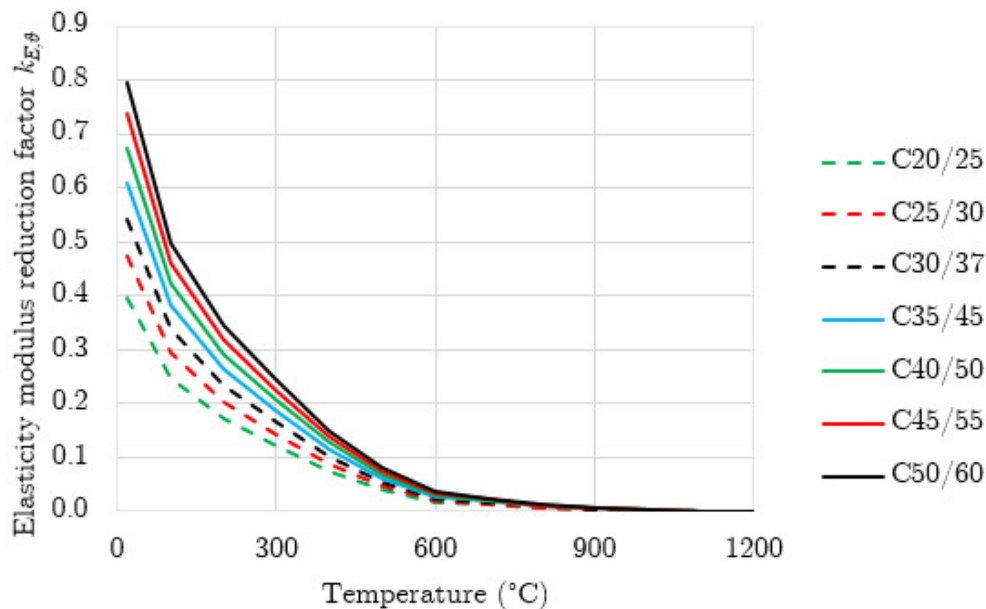


Fig. 4.12 The reduction factor for elasticity modulus of various grades of concrete.

Data on the effect of high temperature on the tensile strength of concrete is scarce. Only a handful of researchers tested specimens during or after high temperature exposure (Merwe, van der 2022). The Eurocode (EN and prEN) recommends assuming a linear decrease between 100 °C and 600 °C, while van der Merwe review suggests that the zero strength could be assumed at 800 °C. Van der Merwe underlined that steel fibres may positively impact tensile strength at elevated temperatures.

#### 4.2.6. Concrete after cooling

Testing hot properties of concrete requires expensive equipment and is time-consuming. Hence, most of the data available in the literature concerns the residual compressive strength. Residual tests are usually reliable due to the following reasons:

- concrete hot strength is higher than residual,
- in the design for burnout, it is not only important to achieve the desired fire resistance time, but also to maintain the load-bearing function after fire - including the cooling phase. Since concrete reaches its minimum compressive strength after cooling, such data are of great importance.

The Eurocode does not include any data on residual strength. However, ACI 216 does, based on the experiments by Abrams (1971). The prEN1992-1-2 formula for residual properties is taken from EN 1994-1-2, which suggests an additional 10 % strength loss during cooling, when compared to the strength at elevated temperature. For example, for concrete heated to 500 °C, the hot strength is  $f_{c,500,hot} = k_{c,500} f_{ck} = 0.6 f_{ck}$  and after cooling it becomes  $f_{c,500,residual} = 0.9 f_{c,500,hot} = 0.54 f_{ck}$ . The residual strength being lower than the hot strength is associated with the following mechanisms:

- the formation of additional micro- and macrocracks during cooling,
- rehydration of CaO due to the moisture in the atmosphere, which was explained earlier in this section.

The cracks in the ITZ and cement paste can be observed in Fig. 4.17. Fig. 4.13 illustrates the residual concrete strength based on data collected by Shahraki et al. (2022).

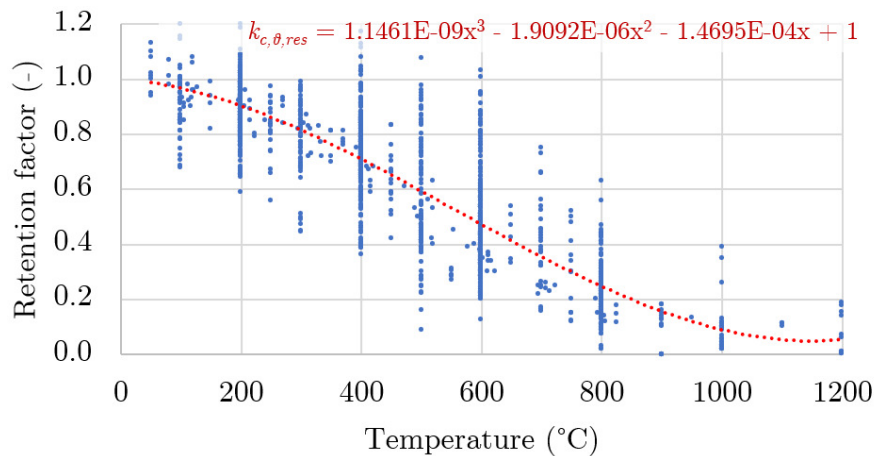


Fig. 4.13 Retention factors for the residual concrete strength, based on data collected by Shahraki et al. (2022).

After exposure to elevated temperatures and cooling, concrete might be exposed to various conditions, such as re-curing in air or water. Various researchers have studied the impact of re-curing, but the findings are inconclusive. The compressive strength may experience further loss after heating or a loss followed by partial recovery. Researchers highlight the significance of factors such as re-curing conditions or testing time after heating (Dias et al. 1990, Li et al. 2020). Cooling methods can significantly affect the results (Abramowicz & Kowalski 2005). In some cases, cement paste can degrade to an extent where compression tests are no longer possible several days after heating (Dias et al. 1990, Mendes et al. 2008). Such behaviour for a standard mortar is illustrated in Fig. 4.14.



*Fig. 4.14 Degradation of standard mortar after heating to 1000 °C (a) one day after heating, (b) one month after heating (own research).*

The available research shows the importance of controlling the post-heating time regime and re-curing conditions.

#### **4.2.7. The effect of simultaneous load and temperature on concrete**

In 1956, Malhotra (1956) conducted the first study on how the sustained load during heating influences the behaviour of concrete specimens (Fig. 4.15). Due to the time and cost involved in testing the mechanical properties of concrete at elevated temperatures, only a few researchers did similar studies in the following years (Abrams 1971, Phan & Carino 2002, Hager & Pimienta 2004, Bamonte & Gambarova 2010, Bamonte & Gambarova 2012, Rios et al. 2018).

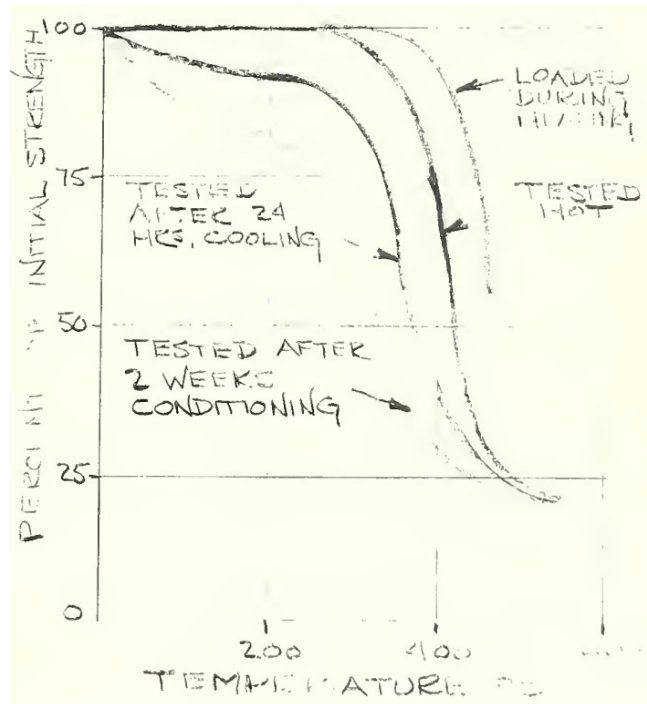


Fig. 4.15 The first published data indicating the strength of specimens stressed during heating is higher than the unstressed strength and residual strength. A sketch by A.F. Robertson, after visiting the laboratory of H.L. Malhotra (Robertson 1955).

In general, the strength remaining after exposure to high temperatures (residual strength) is lower than the strength measured at high temperatures (hot strength), as presented in Fig. 4.16. In addition, stressed specimens have a higher hot strength compared to unstressed ones.

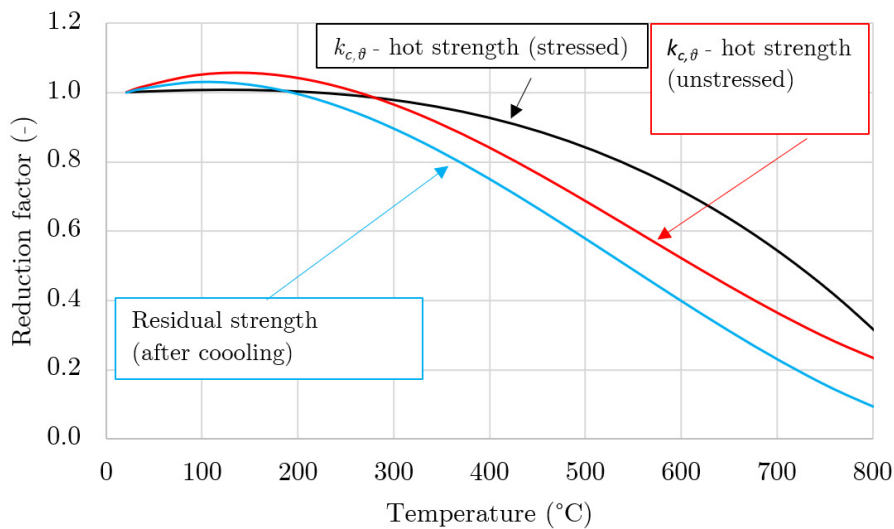
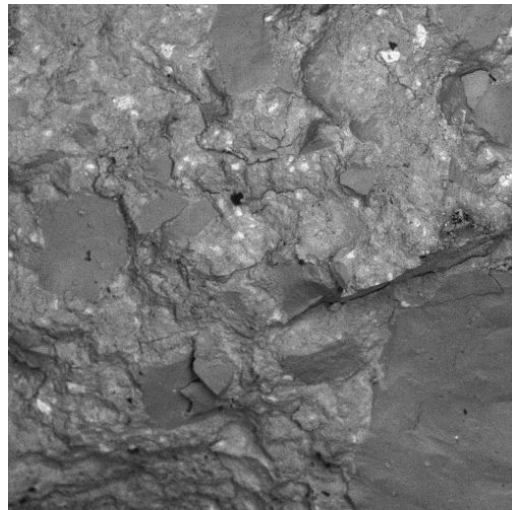
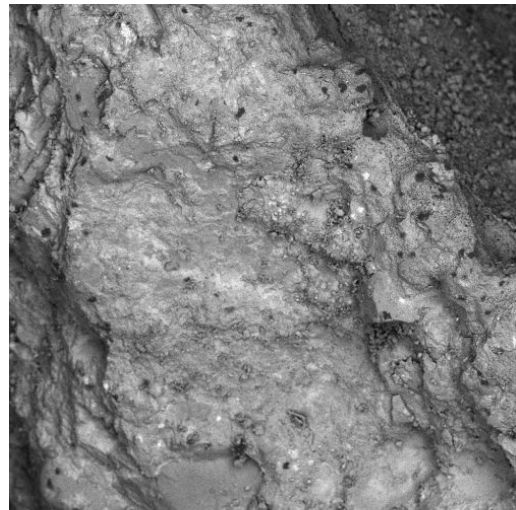


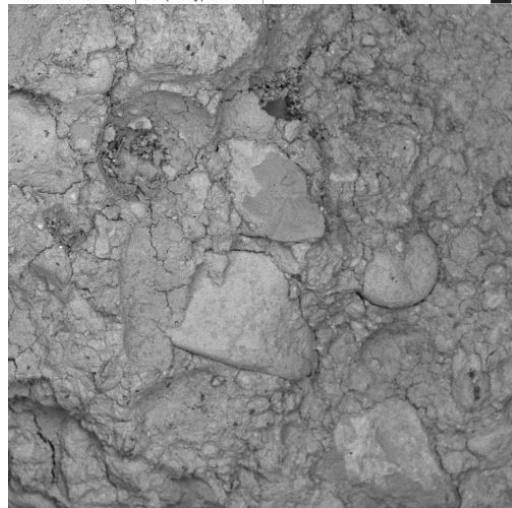
Fig. 4.16 Hot, hot stressed and residual strength of concrete (based on data in Knaack et al. 2010).



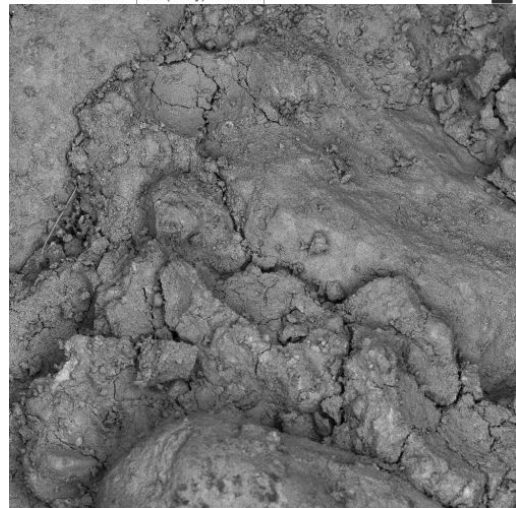
SEM MAG: 200 x	View field: 1.38 mm		VEGA3 TESCAN
WD: 15.00 mm	Det: BSE	200 µm	
SEM HV: 10.0 kV	Date(m/d/y): 12/28/22		



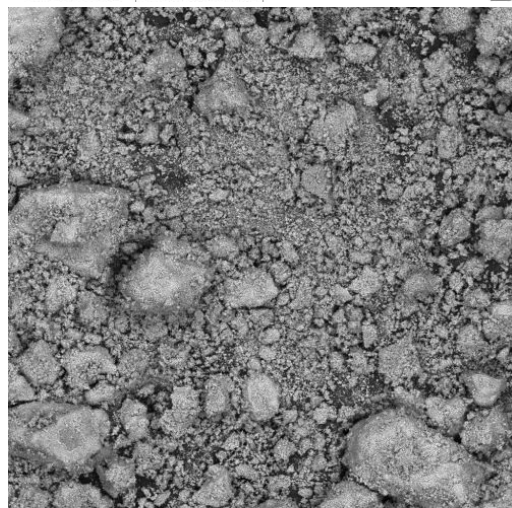
SEM MAG: 200 x	View field: 1.38 mm		VEGA3 TESCAN
WD: 14.99 mm	Det: BSE	200 µm	
SEM HV: 10.0 kV	Date(m/d/y): 12/30/22		



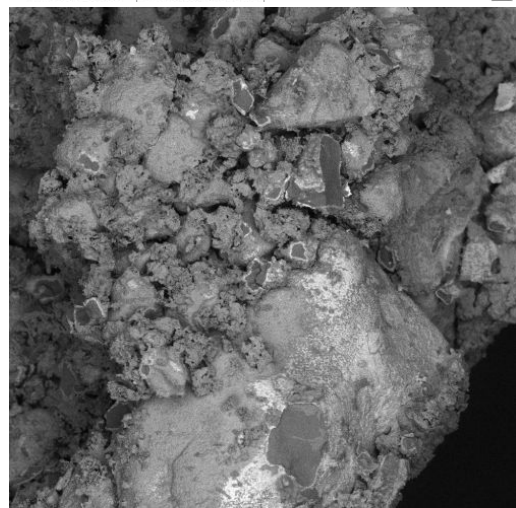
SEM MAG: 100 x	View field: 2.77 mm		VEGA3 TESCAN
WD: 15.00 mm	Det: BSE	500 µm	
SEM HV: 10.0 kV	Date(m/d/y): 12/28/22		



SEM MAG: 200 x	View field: 1.38 mm		VEGA3 TESCAN
WD: 15.06 mm	Det: BSE	200 µm	
SEM HV: 10.0 kV	Date(m/d/y): 12/28/22		



SEM MAG: 200 x	View field: 1.38 mm		VEGA3 TESCAN
WD: 15.00 mm	Det: BSE	200 µm	
SEM HV: 20.0 kV	Date(m/d/y): 12/29/22		



SEM MAG: 200 x	View field: 1.38 mm		VEGA3 TESCAN
WD: 15.00 mm	Det: BSE	200 µm	
SEM HV: 10.0 kV	Date(m/d/y): 12/29/22		

Fig. 4.17 SEM of standard mortar after exposure to (a) 20 °C, (b) 400 °C, (c) 600 °C, (d) 800 °C, (e) 1000 °C, and (f) 1200 °C. Images by Maria Ratajczak ([Szymkuć et al. 2023](#)).

### 4.3. Thermal properties of steel at elevated temperatures

#### 4.3.1. Thermal conductivity of steel

Metals have a higher thermal conductivity compared to most non-metals. The thermal conductivity of metals is mainly related to the motion of free electrons. The ability of electrons to move increases the thermal conductivity. Furthermore, lattice distortions in alloys affect the thermal conductivity, as can be seen in the difference between the thermal conductivity of iron and steel, i.e. at 293 K, the thermal conductivity of iron is about 80 W/(m·K) (Bergman & Lavine 2017). For steel, it is 53 W/(m·K) (Eurocode 3).

It is important to note that the thermal conductivity of metals changes with temperature. Above the Debye temperature<sup>5</sup>, the wavelengths of phonons become similar to the lattice spacing. The increase in molecular vibration hinders electron movement and ultimately affects the ability to conduct heat (thermal conductivity). At some point, this effect saturates, and thermal conductivity becomes constant (Peet et al. 2011), as shown in Fig. 4.18 (a), in which the saturation is observed at about 800 °C. In non-metals, the lack of free electrons makes the molecular vibrations the main factor influencing the thermal conductivity (Peet et al. 2011), which is then expected to increase with rising temperature. For materials such as concrete, where water evaporates, the resultant thermal conductivity also depends on the dehydration-induced porosity. Unlike concrete, in steel, the change in thermal conductivity is not related to the increased porosity but rather to the interactions within the metal lattice.

The engineering relationship between temperature and thermal conductivity of steel given by the EN 1993-1-2 is irrespective of the carbon content and is given by the following equations:

$$\begin{aligned} \lambda_a &= 54 - 0.0333\theta_a && \text{for } 20 \text{ }^\circ\text{C} \leq \theta_a < 800 \text{ }^\circ\text{C} \\ \lambda_a &= 27.3 && \text{for } 800 \text{ }^\circ\text{C} \leq \theta_a < 1200 \text{ }^\circ\text{C} \end{aligned} \quad (4.11)$$

where  $\theta_a$  is the steel temperature and  $\lambda_a$  is expressed in W/(m·K). This relationship is illustrated in Fig. 4.18.

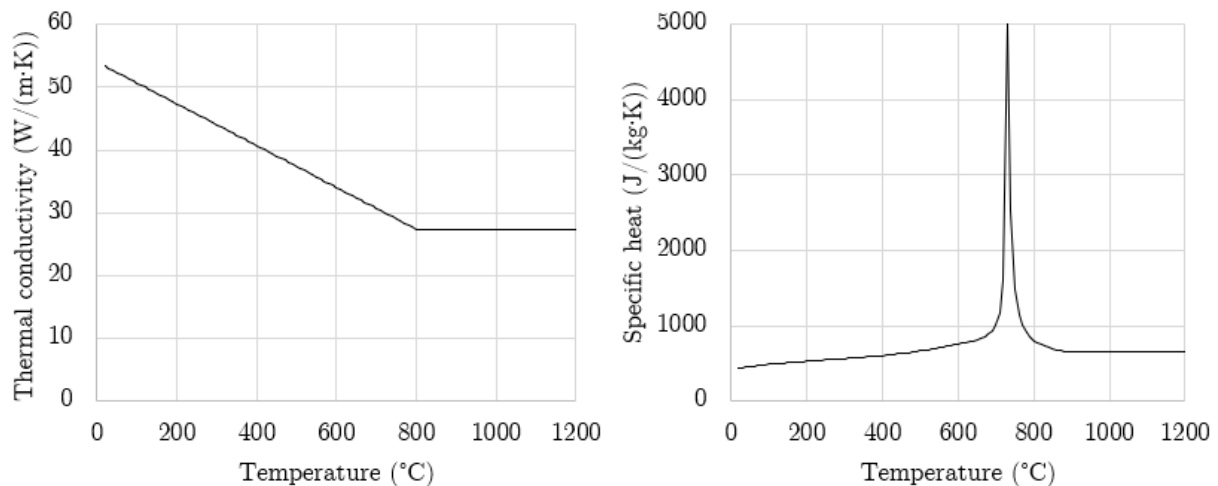


Fig. 4.18 Thermal conductivity (right) and specific heat (left) of carbon steel, according to Eurocode 3.

<sup>5</sup> Debye temperature, according to Luo & Wang (2008) is “the temperature of a crystal’s highest normal mode of vibration, and it correlates the elastic properties with the thermodynamic properties such as phonons, thermal expansion, thermal conductivity, specific heat, and lattice enthalpy”.

### 4.3.2. Specific heat of steel

The specific heat of steel is generally in the range between 440 and 650 J/(kg·K), with a peak representing the austenitizing temperature. This peak, clearly identified in Fig. 4.18 (b) is related to a phase change (Fig. 4.19) when heated atoms transition from a body-centred cubic (BCC) to face-centered cubic (FCC) structure.

### 4.3.3. Density of steel

The density of steel at ambient conditions is 7850 kg/m<sup>3</sup>, and for structural fire engineering, it is considered to be constant during heating. This is not true during the phase change, when atoms transition from BCC to FCC structure. However, this change can be ignored for practical purposes.

## 4.4. The effect of elevated temperatures on the mechanical properties of steel

The mechanical properties of steel degrade due to elevated temperature. However, the underlying mechanisms are distinct from those for concrete. The properties of steel during and after exposure to elevated temperatures are related to the manufacturing processes used to create steel with desired features. Many terms used in this chapter are elaborated in, e.g. metallurgy textbooks. Additionally, when discussing the effects of fire on steel, it is important to consider the Fe-C phase diagram, shown for further reference in Fig. 4.19.

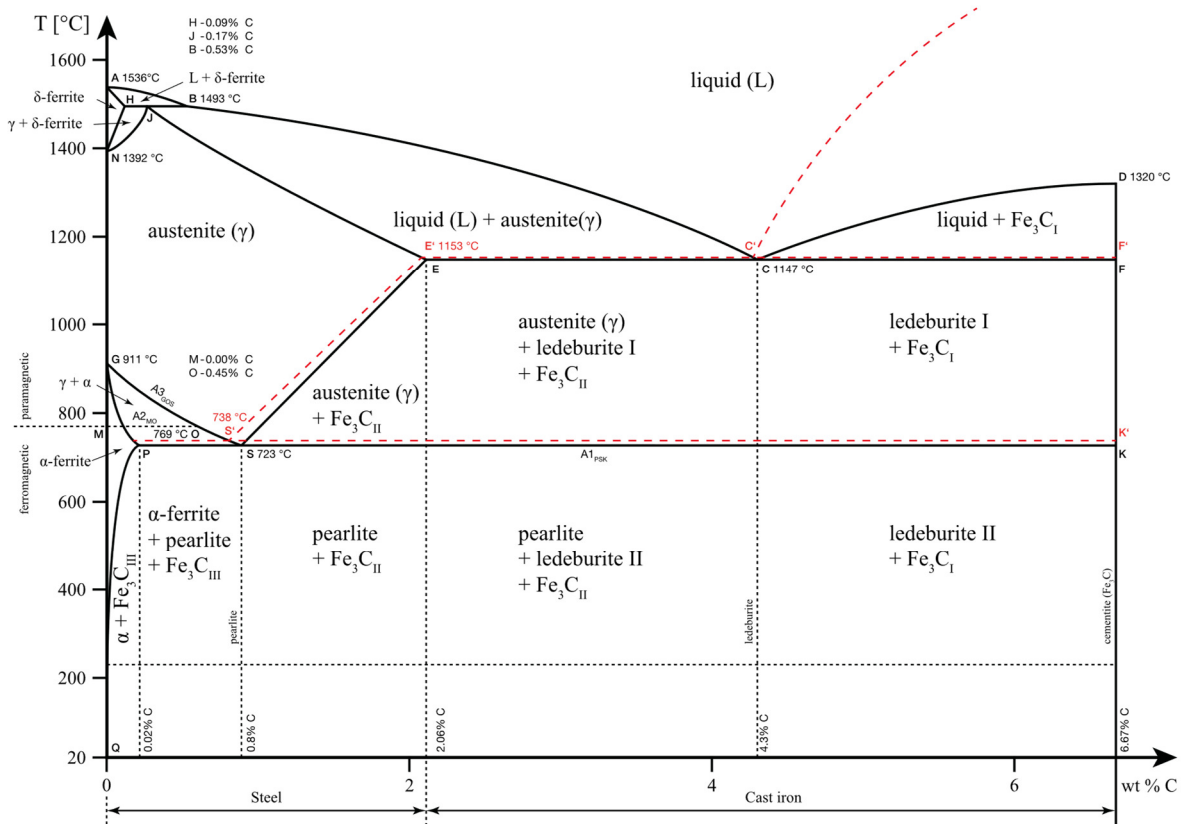


Fig. 4.19 Iron-carbon (Fe-C) phase diagram under atmospheric pressure. CC BY-SA 4.0 License. Source: [https://commons.wikimedia.org/wiki/File:Iron\\_carbon\\_phase\\_diagram.svg](https://commons.wikimedia.org/wiki/File:Iron_carbon_phase_diagram.svg)

#### 4.4.1. Relative thermal elongation and coefficient of thermal expansion of steel

The relative thermal elongation of carbon steel at elevated temperatures is expressed by the following equations (depicted in Fig. 4.20 (a)):

$$\begin{aligned} \Delta l/l &= 1.2 \cdot 10^{-5} \theta_a + 0.4 \cdot 10^{-8} \theta_a^2 - 2.416 \cdot 10^{-4} && \text{for } 20 \text{ }^\circ\text{C} \leq \theta_a < 750 \text{ }^\circ\text{C} \\ \Delta l/l &= 1.1 \cdot 10^{-2} && \text{for } 750 \text{ }^\circ\text{C} \leq \theta_a \leq 860 \text{ }^\circ\text{C} \\ \Delta l/l &= 2 \cdot 10^{-5} \theta_a - 6.2 \cdot 10^{-3} && \text{for } 860 \text{ }^\circ\text{C} < \theta_a \leq 1200 \text{ }^\circ\text{C} \end{aligned} \quad (4.12)$$

where  $l$  is the length at reference temperature  $\theta_0$  (20 °C), and the  $\Delta l$  is the temperature-induced elongation. For numerical purposes, the above relationships are recalculated to give the thermal expansion coefficient:

$$\frac{\Delta l}{l} = \alpha_T \cdot (\theta_a - \theta_0) \quad (4.13)$$

Hence, the temperature-dependent thermal expansion coefficient  $\alpha_T$  can be expressed as (depicted in Fig. 4.20 (b)):

$$\alpha_T = \frac{\Delta l}{l \cdot (\theta_a - \theta_0)} \quad (4.14)$$

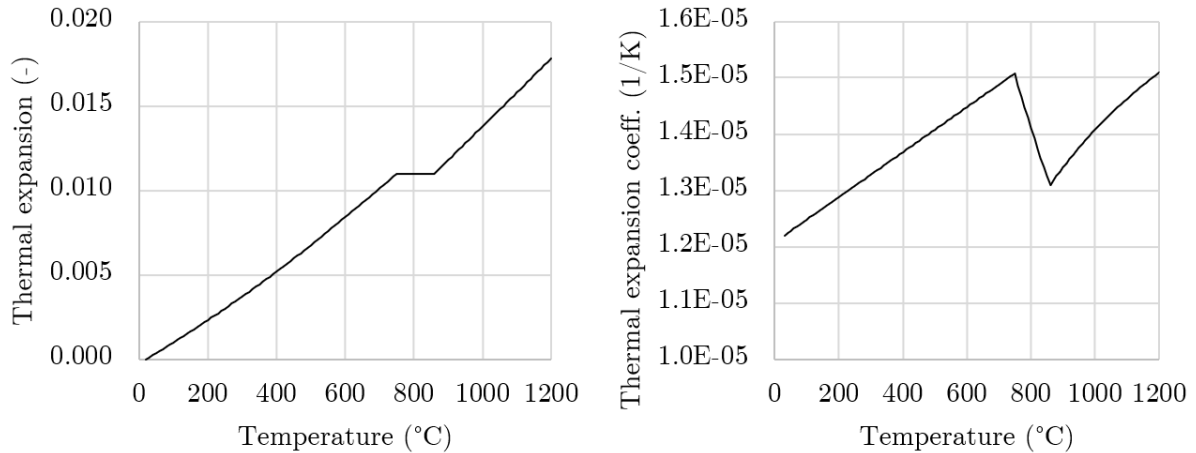


Fig. 4.20 Relative thermal elongation and thermal expansion coefficient of carbon steel.

The range in Fig. 4.20 (a), when relative thermal elongation is assumed constant, is related to the transition from BCC to FCC structure, with the respective packing factors of 68 % and 74 %. While, in fact, there is a density change and shrinkage related to the abovementioned packing factors, this effect is not modelled for practical purposes.

An important distinction between steel and concrete is that the thermally-induced changes to specific heat, thermal conductivity, and thermal elongation of steel are reversible during cooling.

#### 4.4.2. Steel at elevated temperatures

When evaluating the properties of steel at high temperatures, two procedures are commonly utilized: steady-state (isothermal) and transient-state (anisothermal). In the steady-state procedure, a specimen is first heated to the desired temperature, and then loaded until it fails.

Conversely, during the transient test, the specimen is first loaded, and then the temperature is increased, while maintaining the load and steady heating rate. It is important to note that material's sensitivity to initial stress level is one of the sources of uncertainty in the assessment of fire resistance of steel structures (Maślak 2008, Król 2015). Several reviews concentrating on the effects of using steady-state and transient-state procedures were published, e.g. Morovat & Engelhardt (2020), Li et al. (2021c), Molken & Rossi (2022). Performing transient tests has revealed that steel is sensitive to the heating rate, and the underlying mechanism is the high temperature creep.

In the 1970s, it was discovered that the Ramberg-Osgood (1943) model needed adjustments to account for the effects of elevated temperature and creep on steel behaviour. In response, several models were developed to describe the behaviour of steel at elevated temperatures, including those presented by Anderberg (1976), Anderberg (1988) or Poh (2001, 2014). Ultimately, the model proposed by Rubert & Schaumann (1985, 1986) was implemented in the Eurocode (Fig. 4.21). This model divides the stress-strain curve into four distinct regions: (i) a linear elastic, (ii) an elliptical hardening, and (iii) a linear yield plateau, followed by (iv) a linear decrease (Fig. 4.21). The initial slope is defined by elasticity modulus with the reduction factor  $k_{E,\theta}$ . The elliptical part is defined by a set of equations that can be found in (EN 1993-1-2). At 2 % strain, the curve transitions into an effective yield strength, which is a result of truncating the stress-strain relationship (EN 1993-1-2). Another factor that had been a subject of considerable debate, was the strain limit at which the steel strength is determined, e.g., 0.2 %, 1.0 %, or 2.0 % (Kirby & Preston 1988). Given the difficulty in resolving the issue of creep at high temperatures, the Eurocode's mechanical properties for steel were calibrated based on the results of transient tests conducted at various heating rates.

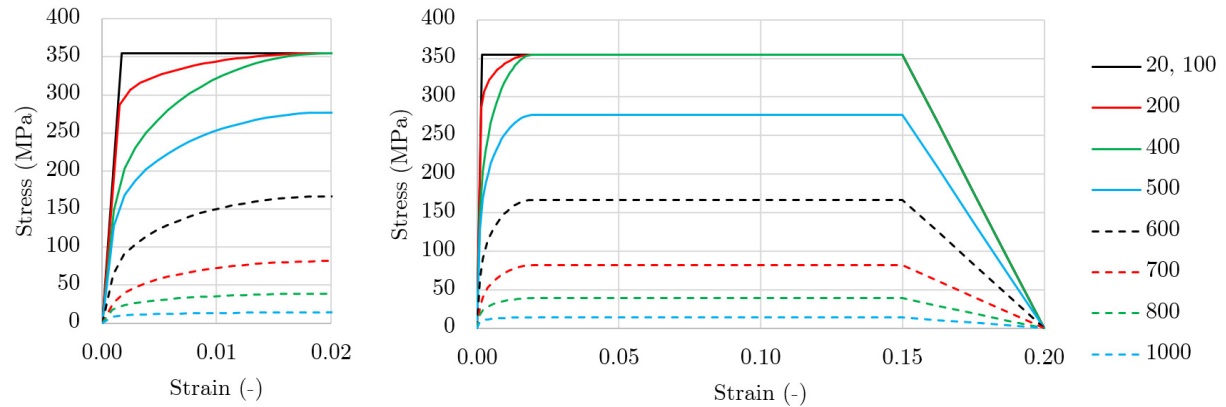


Fig. 4.21 Stress-strain relationship model for S355 steel at elevated temperatures.

The relationships given by the Eurocode are based on several transient-state tests with varying heating rates. For instance, Rubert & Schaumann (1986) conducted tests with heating rates ranging from 2.67 °C/min to 32 °C/min. Their findings revealed that the difference in critical temperature of steel specimens subjected to similar loads but different heating rates resulted from transient thermal creep. Nowadays, Eurocode's equations for the stress-strain relationships at elevated temperatures implicitly incorporate the phenomenon of transient thermal creep. That is also why the strength and stiffness properties of steel given by the Eurocode are valid for heating rates between 2 and 50 °C/min. According to Hanus et al. (2017), such a simplification was made to enable the use of simplified, closed-form design equations, such as those commonly found in structural design codes.

Other models are employed, such as the one-stage or two-stage Ramberg-Osgood model (Knobloch et al. 2013), or a modified Johnson-Cook (Zhu et al. 2022). These models rely on sets of temperature-dependent coefficients to fit stress-strain curves to the experimental data. Knobloch et al. (2013) demonstrated, through several loading and unloading cycles (Fig. 4.22), that the steel behaviour may be considered elastic up to the proportional limit, and plastic in the non-linear range, which in EC3 is modelled with an elliptical curve, followed by a linear yield plateau. Fig. 4.22 clearly illustrates that the slope of the unloading stage changes with the increase in temperature.

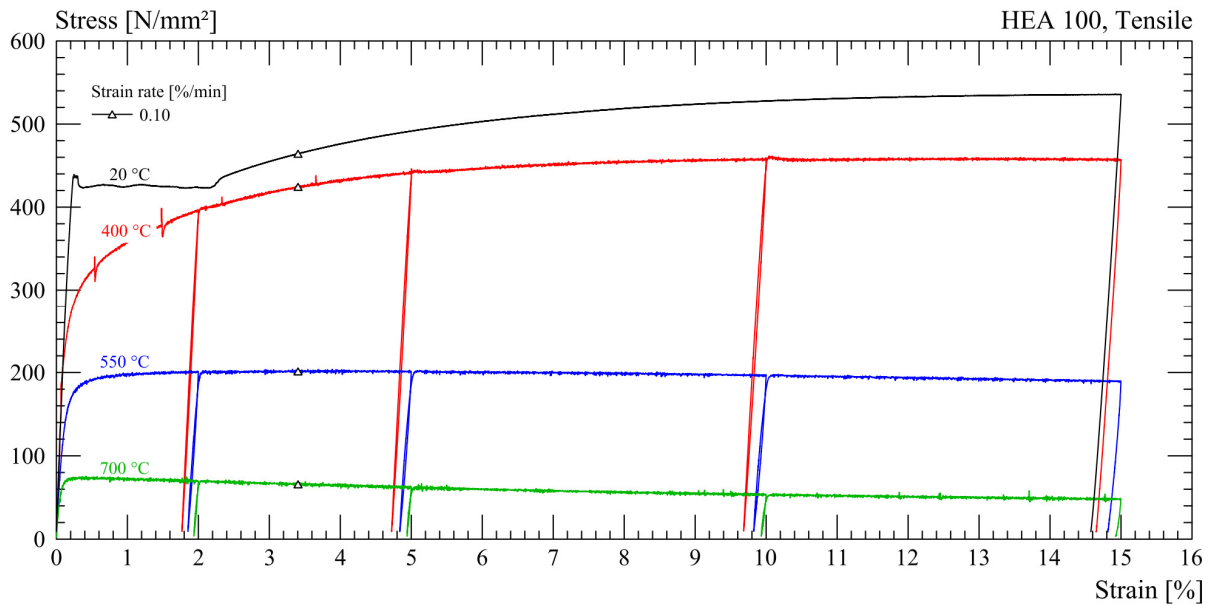


Fig. 4.22 Experimental stress-strain curves for coupons cut from hot-rolled HEA 100 section. Several unloading cycles are visible. Reprinted from Knobloch et al. (2013), with permission from Elsevier.

Skowroński (1988 & 1993) analysed the fire performance of steel beams and columns, explicitly considering creep. Refined models, explicitly taking creep into account, were also proposed by, e.g. Torić et al. (2013), Torić & Burgess (2016). Venkatachari & Kodur (2021) used a numerical model that explicitly accounted for transient creep to evaluate the performance of steel framed structure under a parametric fire. Kodur & Venkatachari (2020) suggested that the effects of transient creep become increasingly important in the evaluation of insulated steel members.

Although models with an explicit formulation of transient creep might be valuable in the future analyses of structures under physically-based fire exposure, there is currently insufficient experimental data to validate them under various strain rates, initial (or changing) stress levels, as well as heating rates, including cooling. Hence, more common relationships are investigated in this thesis. In relation to CFST columns, Wang & Young (2013) evaluated three models: Eurocode 1993-1-2, Lie & Irwin (1995) and Poh (2001), and found that the stress-strain relationships given by the Eurocodes provided the best agreement between the modelled and observed fire behaviour of CFST columns.

#### 4.4.3. Steel after exposure to elevated temperatures

Besides the two main procedures: steady-state (isothermal) and transient-state, the determination of residual mechanical properties of steel has also been a centre of attention. Different steel grades were investigated, with the focus on the differences in strength and

stiffness properties due to cooling in (i) air, (ii) water, e.g. through water immersion, jet, or spraying, or (iii) cooling with firefighting foam. The performance of steel after fire is highly influenced not only by the highest temperature reached, but also by the cooling process (see, e.g. Fig. 4.25). A great body of knowledge can be found in textbooks concerning steel manufacturing, where processes such as annealing, normalising, or quenching are of uttermost importance. The existing research shows that for steel cooled in air, the yield strength begins to be permanently reduced once steel has reached the austenitization temperature, which is typically 727 °C.

It shall be stressed, that the descriptions provided in this section are valid for carbon steel. Such a distinction is made, as e.g. Wang et al. (2020) showed differences in behaviour of High Strength Steel (HSS) after elevated temperature, when they tested steels with nominal yield strengths of 690 and 1090 MPa. The development of high strength (690 MPa) quenched and tempered steel dates to 1960s (Wang et al. 2020), however, it is not economically justified to use HSS as an external steel tube in CFST columns due to fast temperature rise. Furthermore, the high strength of quenched and tempered steel results from tempered martensitic microstructure, which is sensitive to elevated temperatures. Hence, the description of HSS is not provided here. Similarly, the relationships for high strength bolts, or cold-formed steel should be obtained elsewhere (Maraveas et al. 2017, Molken et al. 2021).

The heat treatment of steel is a science itself. Therefore, it would be burdensome to describe all the relevant processes that may occur during cooling. For a detailed explanation of different forms of heat treatment, one may refer to, e.g. EN 10052, classical textbooks on material science (Askeland & Wright 2016) or textbooks that focus on steel (Bhadeshia & Honeycombe 2017). That is why, the research on steel properties after exposure to fire temperatures is usually focused on the difference between water and air cooling (Ding et al. 2021, Sajid & Kiran 2018, Shi et al. 2022, Ren et al. 2020, or Zhang et al. 2020). The recently renewed interest in post-fire properties of steel has several reasons, one of them being the planned focus of Eurocode 1 on the physically based fire exposure. Steel structures can significantly benefit from using PBD methods with reasonable fire scenarios, instead of standard temperature-time curve. However, the Eurocode requires such analysis to cover the entire fire duration, **including cooling**, with the following clause:

*"With a physically based model, the temperature analysis of the structural members is made for the full duration of the fire, including the cooling phase".*

Followed by:

*"The mechanical analysis shall be performed for the same duration as used in the temperature analysis".*

The analysis required by the Eurocode requires taking cooling into account (not extinguishing). However, when conducting a post-fire analysis, it may be necessary to explicitly address the effects of water cooling. The duration of water cooling also plays a role, as stressed by Hager et al. (2021b) in relation to the process known as quenching and self-tempering (QST, or Tempcore), which creates self-tempered martensite, bainite and ferrite-pearlite structure in the outer, intermediate, and inner areas, respectively. Research by Kowalski & Kisielinski (2019) showed that the hot strength properties of reinforcing steel produced with Tempcore method are in line with the relationships given by the Eurocode up to 600 °C. However, when higher temperatures are reached and cooling is involved, the engineered heterogeneous microstructure is likely to be altered.

Fig. 4.23 depicts the microstructure of ASTM A36 steel (yield strength 384 MPa) before and after cooling in air and in water. This process is similar to quenching. In the last picture, a large amount of martensite is visible, which is responsible for brittle behaviour, shown in Fig. 4.24 (right).

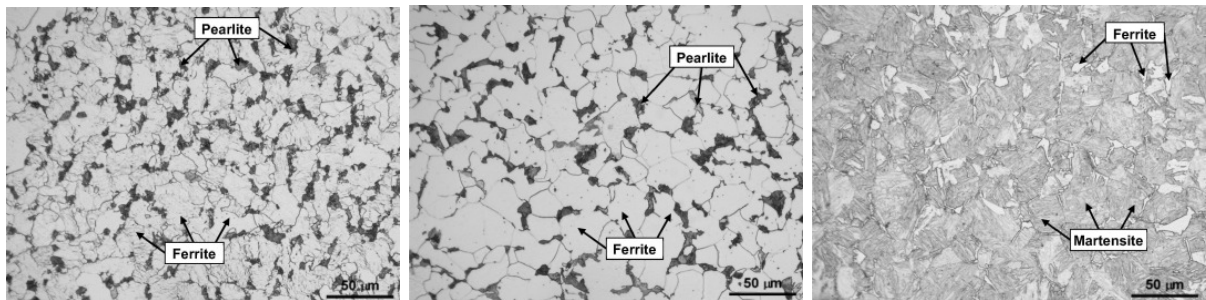


Fig. 4.23 Microstructure of ASTM A36 steel (a) before heating, (b) after air-cooling from 900 °C, (c) after water-cooling from 900 °C. Reprinted from *Sajid & Kiran (2018)*, with permission from Elsevier.

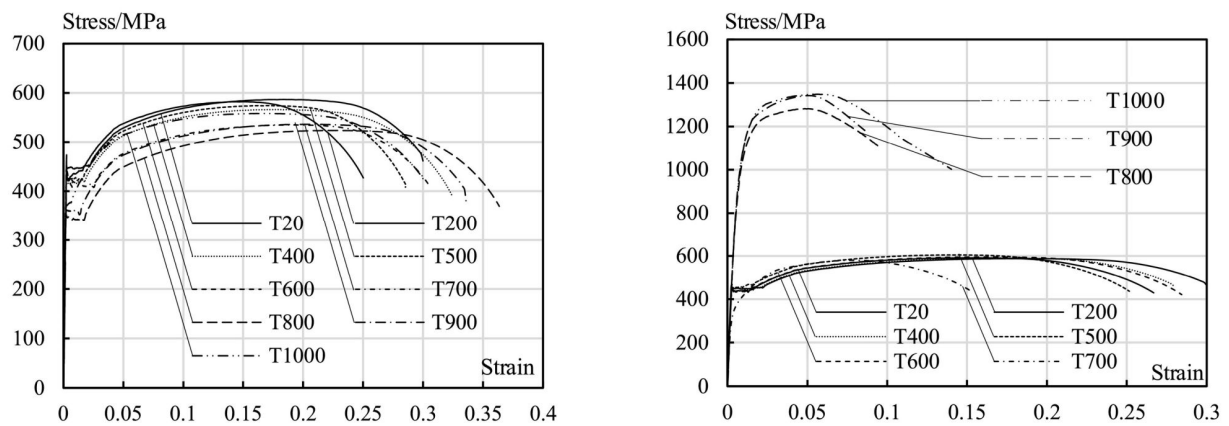


Fig. 4.24 Experimental stress-strain relationships for Q345 steel after exposure to elevated temperatures and two types of cooling (left) in air; (right) in water.  $T_{xxx}$  represents the temperature (°C) the specimen was heated to, hence T20 is a reference curve. Reprinted from *Shi et al. (2022)*, with permission from Elsevier.

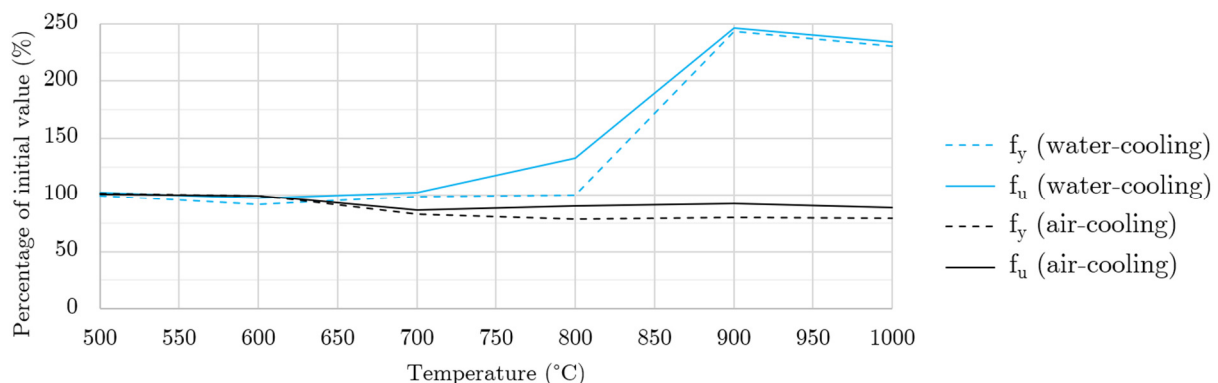


Fig. 4.25 The influence of air and water cooling on residual yield and ultimate strength (*Sajid & Kiran 2018*).

According to *Kirby et al. (1986)*, for the low grade 43A steel ( $f_y=255$  MPa), they concluded that in the absence of visual deformations, the strength properties are unlikely to fall below 90 % of the minimum specification values. This conclusion was later supported by *Outinen (2007)*. One of the reasons for the favourable 90 % of nominal strength, is the so-called overstrength. As explained by *Molkens et al. (2021)*, when a particular steel fails to meet the requirements for a particular grade, it is assigned a lower grade, which results in overstrength. Moreover, it is important to note that the conclusion given by *Kirby et al. (1986)* relates only

to the steel strength properties, not the load-bearing capacity of any structure. This is underlined, as the misinterpretation of the work by Kirby et al. (1986) led to many misconceptions, not supported by facts. In cases where a post-fire evaluation is necessary, the use of metallurgical analysis can help to determine not only the maximum temperature, but also the temperature history (Casaroli et al. 2022). Recently, Molken et al. (2021) proposed a set of safety factors to be considered when analysing structures after fire. However, even though they accounted for several uncertainties in material testing, there is a large number of unpredictable factors, such as the exact temperature, oxygen content, or cooling regime in real fires.

One of the commonly used formulations for the post-fire properties of carbon steel was proposed by Tao et al. (2013). They proposed different formulas for structural hot rolled steel, reinforcing steel and cold-worked steel. They proposed the following relationships for the residual yield strength of constructional steel:

$$\begin{aligned}
 &\text{for } \theta_{max} \leq 500^\circ\text{C:} \\
 &f_{y,\theta,post} = f_y \\
 &\text{for } \theta_{max} > 500^\circ\text{C:} \\
 &f_{y,\theta,post} = f_y(1 - 2.33 \cdot 10^{-4}(\theta_{max} - 500) - 3.88 \cdot 10^{-7}(\theta_{max} - 500)^2)
 \end{aligned} \tag{4.15}$$

and the following relationships for establishing the ultimate strength:

$$\begin{aligned}
 &f_{u,\theta,post} = f_u && \text{for } \theta_{max} \leq 500^\circ\text{C} \\
 &f_{u,\theta,post} = f_u(1 - 1.95 \cdot 10^{-4}(\theta_{max} - 500)) && \text{for } \theta_{max} > 500^\circ\text{C}
 \end{aligned} \tag{4.16}$$

In the absence of data regarding the ultimate strength, Tao et al. (2013) proposed to link the ultimate strength value to the yield strength:

$$\begin{aligned}
 &f_u = f_y(1.6 - 2.00 \cdot 10^{-3}(f_y - 200)) && \text{for } 200 \text{ MPa} \leq f_y \leq 400 \text{ MPa} \\
 &f_u = f_y(1.2 - 3.75 \cdot 10^{-4}(f_y - 400)) && \text{for } 400 \text{ MPa} < f_y \leq 800 \text{ MPa}
 \end{aligned} \tag{4.17}$$

Furthermore, they proposed to reduce the residual Young's modulus if steel temperature surpassed 500 °C:

$$\begin{aligned}
 &E_{s,\theta,post} = E_s && \text{for } \theta_{max} \leq 500^\circ\text{C} \\
 &E_{s,\theta,post} = E_s(1 - 1.30 \cdot 10^{-4}(\theta_{max} - 500)) && \text{for } \theta_{max} > 500^\circ\text{C}
 \end{aligned} \tag{4.18}$$

Fig. 4.26 depicts the stress-strain relationships for S355 steel after exposure to elevated temperatures according to the Tao et al. (2013) model.

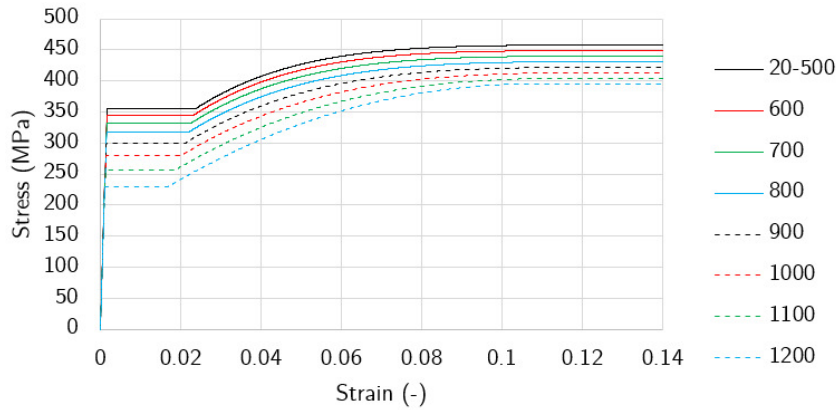


Fig. 4.26 Stress-strain relationships for S355 steel after exposure to elevated temperatures according to the [Tao et al. \(2013\)](#) model.

A comprehensive stress-strain model for steel after exposure to fire was proposed by [Han et al. \(2002\)](#). Recently, [Zhu et al. \(2022\)](#) proposed a modified Johnson-Cook model to describe the behaviour of steel after cooling. In a simplified approach proposed by [Gernay & Franssen \(2015\)](#), steel is assumed to lose 0.3 MPa per °C above 600 °C. As this ratio was implemented in SAFIR, it has been widely used in numerical modelling of structures.

There are, however, significant gaps in the research regarding the performance during and after cooling. Only a handful of researchers ([Mushahary et al. 2021](#), [Uszball & Knobloch 2022](#)) investigated the steel strength during cooling, by e.g., heating it to desired temperature, cooling down to intermediate temperature and then conducting tensile test. What is more surprising, is the data on the effect of preload on post-fire behaviour of steel is scarce. Most of the existing studies focused on specimens cut from steel members after fire test, where the stress or strain levels could not be controlled. Four exceptions in this regard are the studies by [Cao \(1998\)](#), [Crook \(1980\)](#), [Pons et al. \(2022\)](#) and [Lapuebla-Ferri et al. \(2021\)](#).

According to [Tao et al. \(2013\)](#), the research by [Cao \(1998\)](#) showed that the effect of preload on stress-strain response after fire is negligible. However, [Cao \(1998\)](#) considered only moderate temperatures up to 600 °C. Furthermore, as [Cao \(1998\)](#) allegedly did not test the residual strength of unloaded specimens, the conclusion might be prone to the overstrength effect ([Molkens et al. 2021](#)), as the reference level was not clear. The data reported for reinforcing steel by [Crook \(1980\)](#) did not reveal an effect of preload on yield and ultimate strength and Young's modulus (compared to unstressed specimens). However, those conclusions are in contradiction to the recent research by [Pons et al. \(2022\)](#) and [Lapuebla-Ferri et al. \(2021\)](#), who investigated the influence of existing preload on the steel performance after heating and cooling cycle for reinforcing and structural steel in the respective papers. According to their research, the lower the stress level before heating, the higher the recovery of the material properties after fire. This subject requires additional research, and in the absence of data, it is assumed for the purpose of this thesis, that the preload effect is negligible. Furthermore, decarburization, which occurs at temperatures above 700 °C in the presence of oxygen, is another effect that is not only difficult to predict or analyse, but also creates a divergence between material tests and reality. This is because the amount of oxygen in real fires (as opposed to material testing in electrical furnaces) is limited due to combustion.

**The review of data on the post-fire strength properties of steels reveals that:**

- The steel grade or type is an important factor: carbon, HSS, cold-formed, or stainless steels behave differently after exposure to elevated temperature (Molkens et al. 2021).
- For structural carbon steels, reduction of post-fire mechanical properties has been reported to start from 500 °C (Tao et al. 2013), 600 °C (Kirby et al. 1986, Gernay & Franssen 2015, Molkens et al. 2021), or 700 °C (Zhu 2022). All researchers agree, that passing the austenitizing temperature inevitably influences the steel microstructure, and above 700 °C this influence is always noticed. However, the magnitude of its degradation depends on other factors.
- The initial yield strength up to 400-500 MPa (the exact values vary with the source) does not influence the post-fire retention factors (Tao et al. 2013, Molkens et al. 2021, Naser & Uppala 2020). Steel that has a higher yield strength is impacted to a greater extent.
- The type of cooling (in air or water) influences the post-fire properties (Yu et al. 2019a, Ding et al. 2019, Shi et al. 2022), especially above 700 °C.

Since, in this thesis, post-fire material properties are used to assess the burnout resistance of CFST columns made of ordinary steel, several factors indicated in the review will not be investigated further, such as the effect of water cooling. This is because the burnout resistance does not consider the intervention of the fire service. Furthermore, in CFST columns, water cooling and possible heat transfer from the concrete core to the outside might cause effects similar to self-tempering in the cooling stage.

Due to the gaps in existing research, it might seem impossible to accurately predict the residual load-bearing capacity of structural members. Nevertheless, the analyses based on the currently available data can help quantify the effects of several factors. Consequentially, such analyses can help answer the question: which solution can better serve its purpose? After all, citing Henry Petroski in *The Essential Engineer*:

*"Medical doctors and engineers both welcome all the relevant science they can muster, but neither can wait for complete scientific understanding before acting to save life or create a new life-saving machine"*.

This quote summarises the role of the state-of-the-art regarding fire exposure and material behaviour. In the next chapter, the ultimate subject of this thesis will be of interest: **COLUMNS**.



## 5. Experimental and theoretical investigations of CFST columns

### 5.1. Historical experimental investigations of CFST columns

#### 5.1.1. Bauschinger (1884-1886)

The first tests on building columns date back to 1884, when Prof. Johann Bauschinger conducted fire tests on loaded columns in Munich, Germany. The first test series consisted of six cast iron columns, three wrought iron columns and fifteen columns made of mortar, brick or several kinds of building stone. Since the applied loads were later considered too small, in 1886, Bauschinger performed a second series of tests, consisting of two cast iron and five wrought iron columns. All columns were between 4 and 6 meters long.

**SUMMARY:** Bauschinger's tests were the first fire resistance tests of columns (Martens 1888, Ingberg et al. 1921); however, they did not include CFST columns.

#### 5.1.2. Möller & Lühmann (1886-1888)

The second research programme was conducted by Möller and Lühmann in 1886 in Hamburg (Möller & Lühmann 1888). The columns were one, two or four meters long, mainly cast or wrought iron. Several cross-sectional shapes were studied: (i) solid and (ii) hollow cylinders ( $d \approx 9$  cm or 15 cm,  $t \approx 1.5$  cm), (iii) an ornamental fluted cross-section and (iv) a column made of four angles connected with plates and lattice bars. From the perspective of this thesis, it is notable that three specimens were filled with mortar, and a few columns were protected by mortar cover. It is remarkable that shortly after the Bauschinger tests, columns filled with cementitious material were tested. In total, 40 tests were made, two-thirds of them being fire resistance tests. Metal alloys were used as temperature indicators. Furthermore, the explosive nature of pressure build-up inside the tube was recognised when a rupture of the tube hurled pieces of the column 17 meters away from the test stand during one of the tests. Columns were tested with an eccentricity of about 10 mm. The test setup used by Möller & Lühmann is presented in Fig. 5.1.

**SUMMARY:** Möller & Lühmann identified the potential problem of pressure build-up, when concrete is sealed by the tube. Furthermore, according to Ingberg et al. (1921), this test series identified the influence of boundary conditions on the load-bearing capacity of columns.

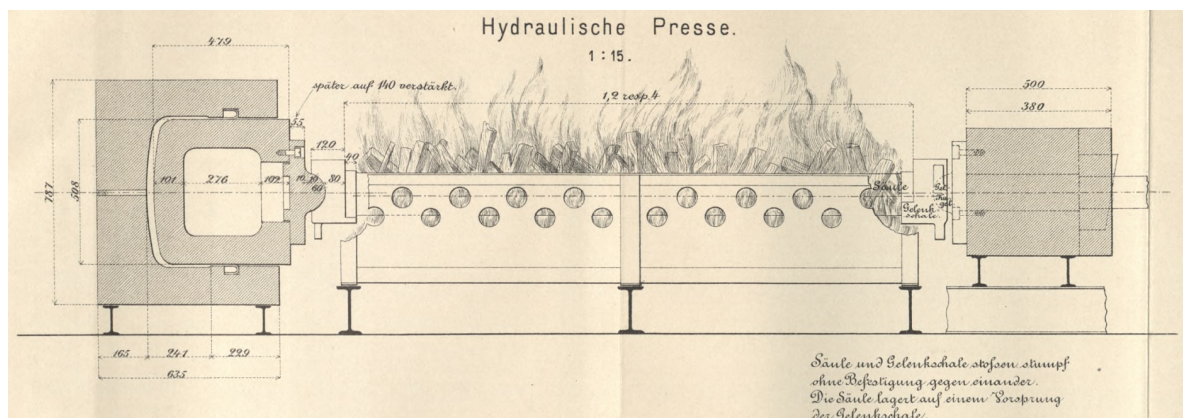


Fig. 5.1 Möller and Lühmann test setup. Tests performed in 1886 (Möller & Lühmann 1888).

### 5.1.3. Hamburg tests (1893-1895)

Between 1893 and 1895, two test series were undertaken in Hamburg, Germany. Two columns were filled with cinder concrete. It was concluded that cinder concrete infill gave little to the resistance of columns. Contrary to the previously reported experiments, where columns were tested horizontally above the wood or coke fires, Hamburg tests were the first to apply symmetrical heating. However, only one-third of the column length was heated. This was likely the first time a gas-fuelled furnace (shown in Fig. 5.2) was used in the fire resistance test, predating the efforts of Sylvanus Reed, who built the gas-fuelled furnace in the spring of 1896 (Reed 1896, Gales et al. 2020). According to Babrauskas & Williamson (1978a), the Hamburg test was the first time thermocouples were used in a fire resistance test.

The Hamburg tests are known not only because of their focus on columns but also on concrete in fire. In a seminal work on the strength of engineering materials, Johnson (1898) referred to Hamburg tests as "*The most elaborate investigations ever made into these [auth: fire-resisting] qualities of various concrete*".

**SUMMARY:** Hamburg tests (i) were the first to use a vertical gas-fuelled furnace and thermocouples, (ii) were the first to report vertical displacement-time relationship during the exposure, (iii) showed a minor positive effect of cinder concrete infill on fire resistance of columns.

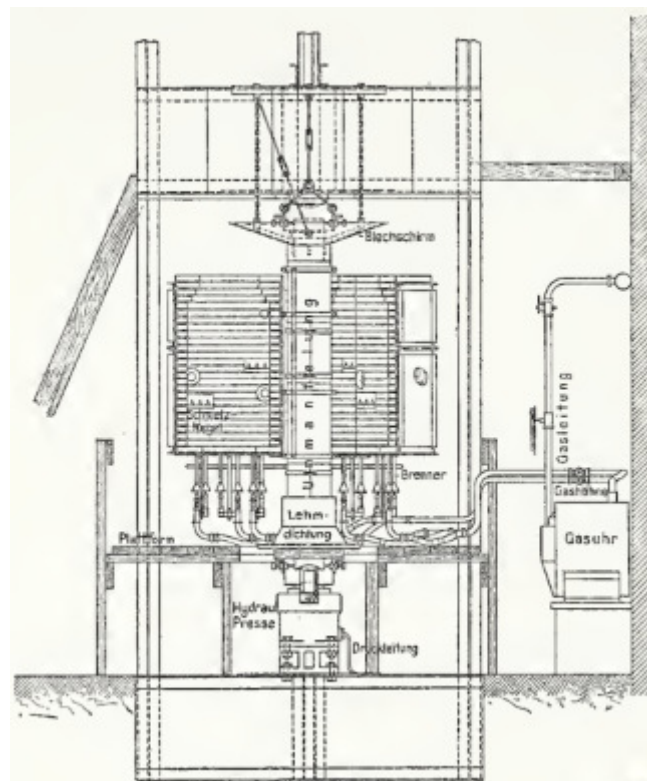


Fig. 5.2 Gas furnace used in Hamburg tests (1893-1895), as presented by Schüler (1897).

#### 5.1.4. Other tests essential for the understanding of fire effects on columns

Columns other than CFST were also tested. The turn of the century witnessed a raising interest in columns in the United States. Reed (1896) tested several cast-iron columns (the so-called New York tests). The first tests of reinforced concrete columns were probably made in 1903 (Guy B. Waite Co. of New York, Fig. 5.3) and later in 1906 (H. B. McFarland and E. V. Johnson at the Chicago laboratory of the National Fireproofing Company). The fire performance of concrete structures was also investigated in Britain by Sachs (1902) and in Germany by Gary (1911). The latter investigated spalling, which became an increasing concern due to the rising popularity of concrete in construction.

**SUMMARY:** Even though the tests mentioned in this section did not concern CFST columns, they are relevant as they helped better understand the effect of fire on columns on the material and structural level. Eventually, they led to the most extensive fire resistance test programme in history, described in the next paragraph.



FIG. 1.— CINDER CONCRETE TEST HOUSE. AFTER FOURTH FIRE

*Fig. 5.3 Guy B. Waite Co. of New York fire resistance tests performed in 1903 (Waite & Goodrich 1908).*

#### 5.1.5. Ingberg et al. (1921)

In the first two decades of the XX century, it was recognised that a unified way of testing would be beneficial; hence, works started on developing a standard-temperature curve, finalised in ASTM E119 in 1917-1918. Shortly thereafter, one of the most extensive research programmes was published by Ingberg et al. (1921), where 106 columns were tested. According to Ingberg, the average compressive strength of concrete at that time was about 12 MPa. Those tests were among the first to utilise the ASTM E119 standard temperature-time curve. During the investigation, columns were loaded and exposed to fire. Some columns were loaded, exposed to fire, and cooled with water to investigate heating and cooling effects. Ingberg et al. (1921) tested: (i) three hollow iron columns, (ii) one concrete-filled tubular iron column, (iii) one CFST column, and (iv) one CFST column reinforced with four angles (Fig. 5.4). The results for columns filled with concrete were not satisfying; hence, the subsequent research programme (Hull & Ingberg 1925) focused on RC columns, and CFST columns were not tested. The tests

in the 1920s served as a basis for prescriptive design in several countries, including the U.S.A. (NBS 1942) and Canada (NBC 1953).

**SUMMARY:** Due to Ingberg’s study, CFST columns were prescriptively assigned a fire resistance of 25 minutes for plain concrete filling and 45 minutes for reinforced concrete filling.

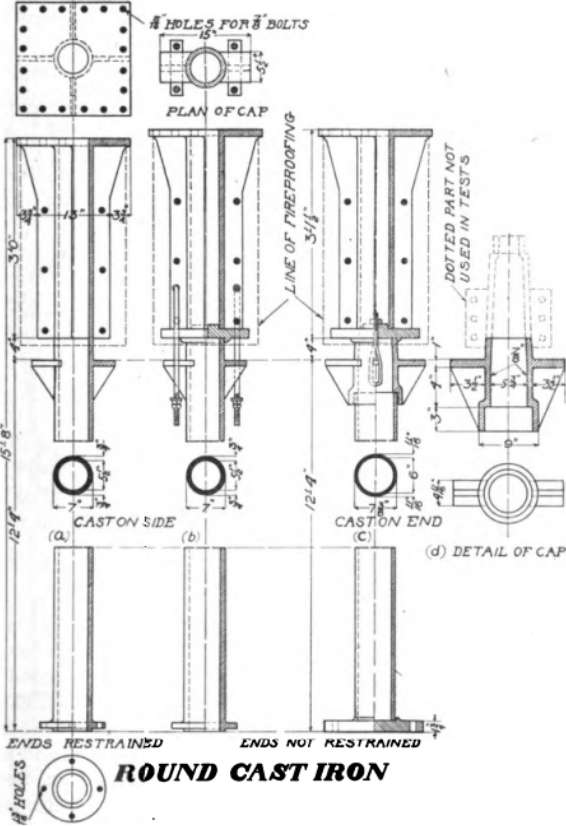


Fig. 6.—Details of cast iron columns.

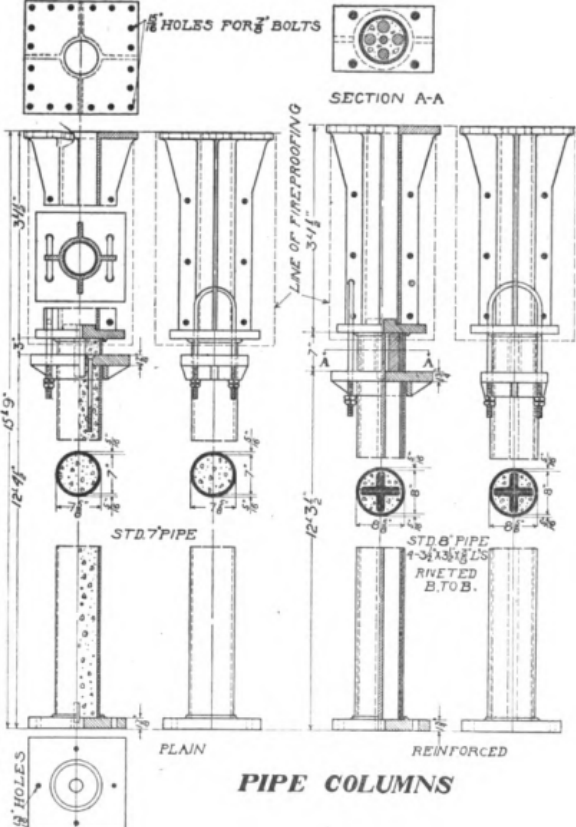


Fig. 7.—Details of pipe columns.

Fig. 5.4 Tubular columns investigated by Ingberg et al. (1921).

**5.1.6. Developments between 1921 and 1980s**

After 1921, there was a significant gap in the development and testing of CFST columns. Large testing programmes were conducted in Germany (Schulze & Wedler 1939) and the UK (Thomas & Webster 1953), yet they did not concern CFST columns. However, post-war conditions caused a dynamic development of composite structures in the 1950s and 1960s (Eggemann 2003). Consequentially, a growing interest in composite structures at ambient conditions stimulated questions regarding their fire resistance.

In the 1970s CFST columns received significant attention in the CIDECT program (Grandjean et al. 1980). 86 CFST columns were tested, mostly with square or rectangular cross-sections. Moreover, the first theoretical calculation method for CFST columns was proposed and validated. Widely known tests on RC columns carried out in the TU Braunschweig were connected to the CIDECT programme (Kordina & Klingsch 1983, Haß 1986). The results of those test campaigns are interesting. For example, a Round Robin study revealed that the fire resistance time of 5 nominally identical columns (produced at one site and tested by five different laboratories) ranged from 81 to 134 minutes. Eventually, those programmes led to the development of ECCS (1988) recommendations, which were further largely transferred to

Eurocode 1994-1-2 (Ibáñez 2015). As far as circular columns are concerned, Grandjean et al. (1980) reported results for 14 such columns. Kordina & Klingsch (1983) mentioned only a single circular column.

**SUMMARY:** 14 CFST columns with a length of 3.6 m, 3.7 m or 5.8 m were tested, mainly 219.1 mm in diameter and tube thickness of 3.6 mm. They were filled with ordinary concrete (up to 46 MPa), and three columns were reinforced with rebars. The CIDECT program tremendously affected the development of European calculation procedures, primarily based on square CFST columns. Unfortunately, as indicated in the research reports, there were significant problems with properly executing the boundary conditions at the supports. Hence, those results were disregarded in the validation domain for this thesis.

### 5.1.7. Summary of the historical test data

For the abovementioned reasons, tests performed in the late XIX century, tests by Ingberg et al. (1921) and in the framework of the CIDECT program are regarded as historical data. They give interesting qualitative data (given the number of experiments performed) but cannot serve as validation cases for the numerical model developed in this thesis.

## 5.2. Modern fire resistance tests of CFST columns

Later tests of CFST columns represent the modern era of fire resistance testing, and they provide data that could be used for model validation in this thesis. Hence, the fire resistance tests performed by Lie & Chabot (1992), Wainman & Toner (1992), Han et al. (2003), Kim et al. (2005), Romero et al. (2011), and Moliner et al. (2013), among others, will be described in detail in the following section. Based on the tests, it was also revealed that the calculation method in Eurocode 1994-1-2 was not safe for slender columns. This discovery strengthened the efforts towards testing and developing calculation procedures and impacted the course of this PhD thesis.

The study presented in this section is based on experimental data obtained by various researchers. The database used for validation contains the input parameters and results of full-scale CFST specimens tested under mechanical load in standard fire test conditions. The historical data from early tests by Möller & Lüthmann, Ingberg, and the CIDECT program were disregarded due to the aforementioned reasons, mainly related to the poor control of the test conditions (from today's perspective).

### 5.2.1. NRC Canada (1982-1994)

The first extensive testing programme focusing on circular CFST columns was executed in NRC Canada (Lie & Chabot 1992). The NRC Canada conducted an extensive experimental programme on the fire resistance of CFST columns. Numerous NRC reports (No. 570, 573, 611, 628, 691) present the details of the experiments. The data relevant to this thesis were presented in the report No. 611 by Lie & Chabot (1992) for plain concrete filling, and in the report No. 628 by Chabot & Lie (1992) for rebar-reinforced columns. Between 1982 and 1994, NRC tested at least 68 CFST columns. The research included varying factors, such as filling with plain or reinforced concrete, siliceous or siliceous-carbonate aggregates, NSC or HSC, and circular or square tubes. Other studied factors were the effect of concrete strength, load level, and boundary conditions. One column was loaded eccentrically. Columns were 3810 mm long (150

inches). The fire resistance time varied from 33 to 294 minutes. Subsequent research included square, fibre-reinforced, and high strength concrete filling. The study from NRC presented the largest variation of cross-sectional dimensions ever tested.

Notably, the NRC did several tests on the fire resistance of RC columns, which stemmed from replacing the working stress theory with the strength design theory in the 1971 version of the American Building Code ACI 318. The NRC study on CFST columns study was "*aimed at developing methods capable of predicting the fire resistance of concrete-filled hollow steel columns*" (Lie & Chabot 1992). Simultaneously it was underlined that CFST columns do not require external fire protection, and steel tubes act as a formwork during erection.

In all the NRC reports, the studied variables included:

- column diameter (141.3 mm to 406.4 mm),
- tube thickness (4.78 mm to 12.7 mm),
- concrete strength (23 MPa to 93 MPa),
- type of concrete aggregate (siliceous, or mix of siliceous and calcareous),
- length (3.8-meter columns with fixed or pinned boundary conditions),
- load (110 kN to almost 3800 kN),
- eccentricity (axially or eccentrically loaded).

#### **SUMMARY:**

- when considering the initial load ratio, the ratio of load to the compressive resistance of the core (instead of the compressive resistance of the whole core-tube assembly) should be used for comparing test results. This ratio was called 'the load intensity',
- for columns with larger outer diameters, the fire resistance time increases, even when subjected to the same load intensity,
- thickness of the tube had a negligible influence on the fire resistance,
- columns filled with carbonate aggregate performed better than columns filled with siliceous aggregate,
- the authors pointed out that the performance of larger columns was '*sometimes erratic, when the load was high*',
- it was found difficult to draw conclusions regarding the effect of concrete strength,
- load eccentricity influenced the fire resistance time significantly. It was therefore recommended that eccentrically loaded columns should be reinforced with rebars.

#### **5.2.2. British Steel (1991-1992)**

Wainman & Toner (1992) tested three CFST columns; all three are included in this thesis. The columns varied in diameter, tube thickness and load. The tests were carried out to validate a numerical model. Furthermore, the load was reapplied 18 hours after the fire test to find out if the load could be supported after the fire. Notably, all columns passed this additional test.

In the Wainman & Toner (1992) report, the studied variables included:

- column diameter (244.5 mm, 323.9 mm, 355.6 mm),
- tube thickness (6.3 mm, 9.5 mm),

- load (635.4 kN, 1864 kN, 900 kN).

The length of all columns was equal to 3.4 m, with pinned-pinned boundary conditions. All columns were axially loaded. Siliceous aggregate concrete was used with 49 MPa strength.

Notably, Wainman & Toner noticed a decrease in the force applied to two out of three CFST columns. It is not uncommon that the testing rig cannot follow the displacement. For column No. 1, the FRT was 58 minutes, and data were recorded for 60 minutes. For column No. 2, the respective values were 45 and 50 minutes. For column No. 3, the testing rig followed the column, and the prescribed load was kept for the 143-minute period shown in Fig. 5.5. A detailed analysis of columns after fire tests is provided in [Gaunt et al. \(1993\)](#).

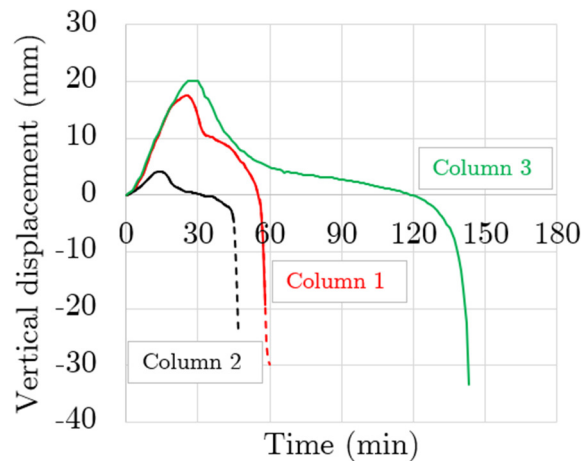


Fig. 5.5 Fire resistance time (solid line) and test time to be disregarded due to decreased force applied by the testing jack.

**SUMMARY:** due to only three columns tested, varying cross-sections and loads, no general conclusions could be drawn. Interestingly, columns loaded 18 hours after the test could carry the load applied during the test. This is a valuable observation concerning the post-fire resistance of CFST columns.

### 5.2.3. Han et al. (2003)

[Han et al. \(2003\)](#) described a test program consisting of 13 specimens. Their research focused on the effects of concrete strength, eccentricity, and thickness of fire protection. Four CFST columns were filled with NSC and did not have additional fire protection. Therefore, they are included in this study. Columns were loaded axially or eccentrically, with a constant utilisation level of 77 %. The ratio of load eccentricity to the radius was equal to 0, 0.3 or 0.6. Due to the high utilisation level, FRT varied from 17 to 32 minutes.

Variables studied by [Han et al. \(2003\)](#) included:

- column diameter (219 mm, 478 mm),
- tube thickness (5 mm, 8 mm),
- load (300 kN to 4700 kN),
- eccentricity (0 mm, 32.85 mm, 65.7 mm, 71.7 mm).

The length of all columns was equal to 3.77 m, with pinned-pinned boundary conditions. Calcareous aggregate concrete was used with 31 MPa strength. Furthermore, some columns

were filled with HSC, and some were tested with additional fire protection of varying thickness, which this thesis does not study. Due to the high load utilisation ratio, CFST columns tested by Han et al. (2003) did not experience a clear expansion phase (Fig. 5.6).

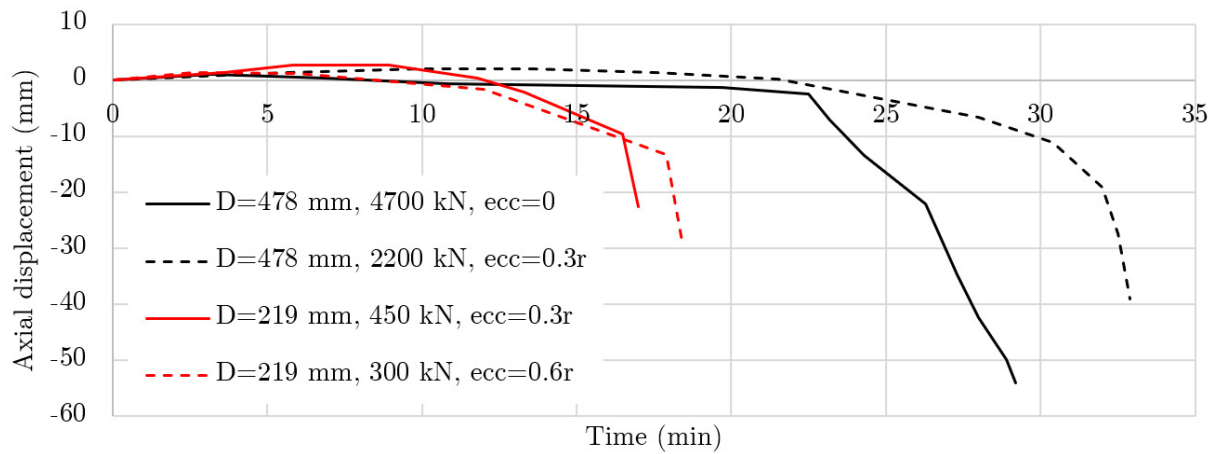


Fig. 5.6 Behaviour of CFST columns without protection (Han et al. 2003).

**SUMMARY:** Besides the conclusions regarding the positive influence of protection coating, the authors observed (1) ductile behaviour of columns and (2) insignificant effect of eccentricity when the load ratio is kept constant.

#### 5.2.4. Universitat Politècnica de València (UPV, 2009-2013)

One of the most extensive recent research programs regarding the fire behaviour of slender CFST columns is described by Romero et al. (2011) and Moliner et al. (2013) and a research report from the BIA2009\_09411 project (Espinosa et al. 2014). This program included 40 fire resistance tests with different load ratios (0.2, 0.4 or 0.6), loaded axially or eccentrically. Various fillings included: plain or reinforced concrete, normal or high strength concrete, and fibre-reinforced concrete.

Variables reported by Romero et al. (2011), Moliner et al. (2013), Espinosa et al. (2014) included:

- concrete strength (24 MPa to 42 MPa for the NSC fillings),
- concrete filling (no filling, NWC, as well as HSC, FRC – outside of scope here),
- reinforcement (no reinforcement or four 12 mm rebars),
- load (126 kN to 687 kN),
- load level (20 %, 40 %, or 60 %),
- eccentricity (axially or eccentrically loaded – 0 mm, 20 mm, 50 mm).

The length of all columns was equal to 3.18 m, with a diameter of 159 mm and 6 mm tube thickness. Mainly, fixed-pinned boundary conditions were used, and the aggregate in concrete was calcareous. HSC and FRC fillings were also investigated. However, they are outside of the scope of this thesis.

**SUMMARY:**

- Load level – the higher the load, the lower the fire resistance time

- Load eccentricity – the higher the load eccentricity, the lower the fire resistance time
- Concrete strength – for a load level of 20 %, HSC performed equally as well or better than NSC. For load level of 40 %, HSC specimens performed worse than NSC.
- Steel fibre reinforcement – columns filled with SFR presented fire behaviour similar to their NWC or HSC counterparts without steel fibre. No effect of fibre was observed.
- Rebar reinforcement – for similar load levels, the reinforcement did not affect the fire resistance time of axially loaded columns. For eccentrically loaded columns, an increase in FRT was observed.

### 5.2.5. Description of tests not included in the validation domain

One of the goals of the state-of-the-art analysis with regard to experiments on fire resistance of CFST columns, is to build an extensive and reliable database. Several other research programmes were also analysed. They provide valuable data on the phenomena observed during fire resistance tests of circular CFST columns. However, they could not be included in the validation domain for several reasons. This section intends to explain why some modern research was neglected.

#### *Kim et al. (2005)*

[Kim et al. \(2005\)](#) tested twenty columns. Ten were circular, and the other ten were square. All columns were loaded axially, with the utilisation ratio varying from 0.40 to 0.60. Five out of ten columns did not reach their load-bearing capacity because the furnace was switched off. Furthermore, three columns had their duplicates tested, and the results raise concerns about the repeatability of tests. Two columns denoted as 'CAL1' did not reach fire resistance time (>80 vs. >80 minutes). Out of two columns denoted as CBL1, one had an FRT of 59 minutes, while the other did not fail in 80 minutes. The last pair (CBH2) displayed the results of 88 and 108 minutes. Hence, no column from [Kim et al. \(2005\)](#) is included here.

**SUMMARY:** external tube size and thickness had a limited influence on recorded steel temperature; the higher the load, the lower the fire resistance time.

#### *University of Coimbra (UC, 2012-2020)*

An innovative and one-of-a-kind test setup was used in the tests at the University of Coimbra. [Pires et al. \(2012\)](#) reported several fire resistance tests using an electrical furnace and a unique frame capable of partially restraining thermal elongation and rotation at the column's end. Such boundary conditions contrast with boundary conditions in other laboratories, which are described as pinned or fixed. Several cross-sections were investigated, including hollow steel sections, plain and reinforced CFST columns, and ring sections. Two axial stiffness values were applied, each with corresponding rotational stiffnesses in two perpendicular directions. The temperature inside the furnace fell behind the ISO curve and was not uniform over the height of the column. Subsequent research included more columns ([Rodrigues et al. 2018](#), [Lopes & Rodrigues 2020](#)). Overall, it was concluded that the axial restraint reduced the critical time, and the rotational restraint increased it. However, it shall be borne in mind that the critical time was defined as the time, when the overall column axial elongation was negative (meaning load being redistributed through the frame, so that column no longer supported the same load as initially). In other words, the critical time was defined as "*the instant when the restraining forces return to the value of initial load applied*". The furnace was electrical, and the

temperature was not controlled with plate thermometers. Those tests were excluded from the validation domain mainly due to the discrepancies in the description of bottom boundary conditions (modelled as fixed, pinned, or rotationally restrained by various authors). Moreover, no researchers managed to model the response past the 'critical time', and sometimes, the thermal expansion of steel was modelled with an artificial lowering factor to fit the calculated and experimental data regarding the reaction force. Nevertheless, the studies offer several interesting conclusions that are especially valuable due to the one-of-a-kind test setup.

**SUMMARY:** Due to an interesting test setup, those tests provided comprehensive data on the effects of partial restraint on the structural fire behaviour of CFST columns. Overall, for columns filled with plain concrete, it was concluded that:

- axial restraint caused increased reaction at the top of the column,
- columns with the same load level (30 % of 70 % of the buckling load) displayed similar critical time, irrespective of their diameter,
- the level of axial and rotational restraint did not affect the critical time.

*State University of Campinas (UNICAMP, 2010-2014)*

Leite et al. (2010) presented test results of 24 circular CFST columns. They investigated two diameters (114.3 mm and 168.3 mm), two types of concrete (normal and high strength) and three loading levels (30 %, 50 %, and 70 %). A clear baseline level was established by testing eight additional columns without exposure to high temperature and additional columns with no filling (Sant'Anna et al. 2014). Moreover, this was an exemplary study regarding test repeatability. However, there are several reasons why those results were not used in the model validation: (1) boundary conditions were not clearly described, (2) engulfed length was about 1/3 of the overall column height, but precise numbers were not reported, and (3) the detailed results with respect to temperature or vertical displacement were not given. Scarce conclusions can be drawn because columns varied in length depending on their filling – 2.0, 2.34, and 2.52 m for hollow, NSC-filled, and HSC-filled columns, respectively.

**SUMMARY:** concrete compressive strength did not influence the fire resistance (columns with a similar load level were compared). Fire resistance diminished with an increase in the load level.

*Other research programmes*

An experimental investigation of the fire resistance of preloaded circular columns was carried out by Yu et al. (2019b). Geopolymer CFST columns were tested by Katwal et al. (2022). Tao et al. (2016) used stainless steel tubes. Espinos (2012) presented an extensive study on elliptical columns. Circular carbon steel tubular columns filled with ordinary concrete are the primary concern of this thesis. Therefore, tests regarding other shapes, fillings, or tube materials were not described. A review of test programs, including square and protected columns, can be found in, e.g. the PhD thesis of Rush (2013).

### **5.2.6. Summary**

Let a quote from Lie & Chabot (1992) serve as a summary for the presented description of fire resistance test programmes:

"The results of these tests can be used in two ways. First, the results can be used to assess, by interpolation, the fire resistance of columns in particular applications. Secondly and most importantly, they can be used to validate mathematical models which predict the behaviour of concrete-filled hollow steel columns exposed to fire".

A review of test programs indicates that results reported by [Lie & Chabot 1992](#), [Wainman & Toner \(1992\)](#), [Han et al. \(2003\)](#), [Romero et al. \(2011\)](#) and [Moliner et al. \(2013\)](#) can be used as a valuable source of data for the validation of the numerical model.

Table 5.1 summarises data related to the mix design and test conditions in material tests associated with full-scale CFST testing.

Table 5.1 Data related to mix design and test conditions in material tests associated with full-scale CFST testing.

	<b>Concrete mixture and Eurocode classification</b>	<b>Specimens and moisture content</b>	<b>Time of testing</b>
<a href="#">Lie &amp; Chabot (1992)</a>	Siliceous or calcareous coarse aggregate Silica-based sand Superplasticizer Retarder  Eurocode classification: Siliceous	Cylinder 150 mm 28-day, and day of testing  moisture content: 'corresponding to 85-95 % relative humidity'	2 to 4 years after casting
<a href="#">Wainman &amp; Toner (1992)</a>	Granitic aggregate Detailed mix design not reported  Eurocode classification: Siliceous	Cube, NDA 7, 28, 90-day  moisture content: NDA	110-131 days after casting
<a href="#">Han et al. (2003)</a>	Calcareous coarse aggregate Silica-based sand  Eurocode classification: Calcareous (NSC) Siliceous (HSC)	Cube 100 mm 28-day  moisture content: NDA	28 days after casting
<a href="#">Romero et al. (2011)</a> <a href="#">Moliner et al. (2013)</a> <a href="#">Espinosa et al. (2014)</a>	Calcareous aggregate Detailed mix design not reported  Eurocode classification: Calcareous	Cylinder 150 mm Day of testing  moisture content: 1.0-6.6 %, with a mean value of 3.2 % (dried at 150 °C)	NDA

### 5.3. Reliability of temperature measurement

Examination of the test data reveals that even when temperatures in the furnace are similar, the temperature measured on the steel surface and further inside the concrete core might display a large scatter.

In the next section, the influence of the TC positioning is discussed. The required tolerance class of thermocouples used in fire resistance testing according to EN 1363-1 and EGOLF recommendations is class 1, meaning they are manufactured to strict industry tolerances of up to  $\pm 5$  °C at 1200 °C ([EN 60584-1](#)). However, the analysis of temperatures measured at the same target points revealed a large scatter of results, and it is unlikely that calibrating heat transfer properties based on a single test would yield valid results. This section provides the

analysis of experimental results provided by [Wainman & Toner \(1992\)](#), [Espinosa et al. \(2014a\)](#), and [Wang et al. \(2022a\)](#).

The results provided by [Wainman & Toner \(1992\)](#) are a valuable source of data related to the variability of temperature measurement in concrete. For all three tested CFST columns, temperatures were measured at three different heights. On each height, 13 thermocouples were present: four to measure the steel temperature and nine embedded in concrete: four located at the  $D_c/8$  depth, four located at the  $D_c/4$  depth and one in the centre of the core ( $D_c/2$  depth), where  $D_c$  is the diameter of column's core (internal diameter of the tube).

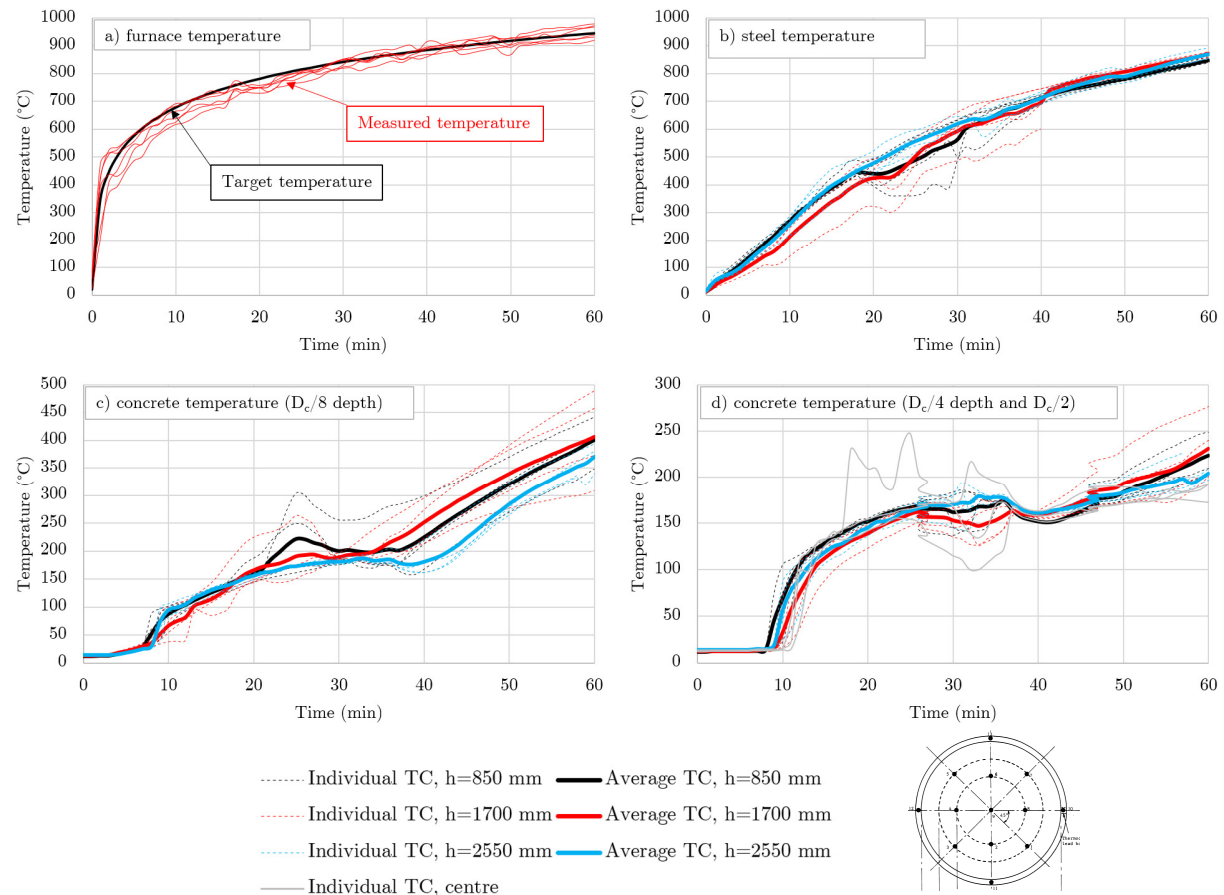


Fig. 5.7 Temperatures measured by [Wainman & Toner \(1992\)](#) during the test of one of the CFST columns. (a) temperature inside the furnace, (b) temperature of steel, (c) temperature at the  $D_c/8$  depth, (d) temperature at the  $D_c/4$  depth. A large scatter of results is evident. Black, red, and blue lines indicate measurements at three different heights. Grey lines in Fig. (d) illustrate the temperature measured in the centre of the cross-section.

In Fig. 5.7 A, B, and C denote levels above the furnace floor (850 mm, 1700 mm, and 2550 mm, respectively). Broken lines represent temperature reported by individual thermocouples, and thick solid lines illustrate average temperatures recorded by 4 TCs at each level. A large scatter of results is evident, especially regarding thermocouples located at the  $D_c/8$  depth (Fig. 5.7 c). Notably, two other columns tested by [Wainman & Toner \(1992\)](#) displayed similar scatter.

Another test programme well-equipped with temperature-measuring devices was described in detail in a report by [Espinosa et al. \(2014\)](#). They conducted 40 fire tests of columns with the same geometry, where they used concrete mixtures with two target strengths: 30 MPa or 90

MPa. Fifteen columns filled with NSC (without steel fibre) were chosen for further comparison in Fig. 5.8. Notably, the research by Espinos et al. was one of the few that used PTs to control the conditions inside a furnace. The following figures give an overview of the furnace temperature, temperature measured on the steel surface and temperature measured inside concrete at various depths. Grey lines in Fig. 5.8 indicate individual experimental data with the distinction between data deemed as plausible (grey solid lines) and rejected data (grey dashed lines, see e.g. Fig. 5.8 b). Black lines represent the average of all experimental data. Red dashed lines represent the average of experimental data deemed plausible.

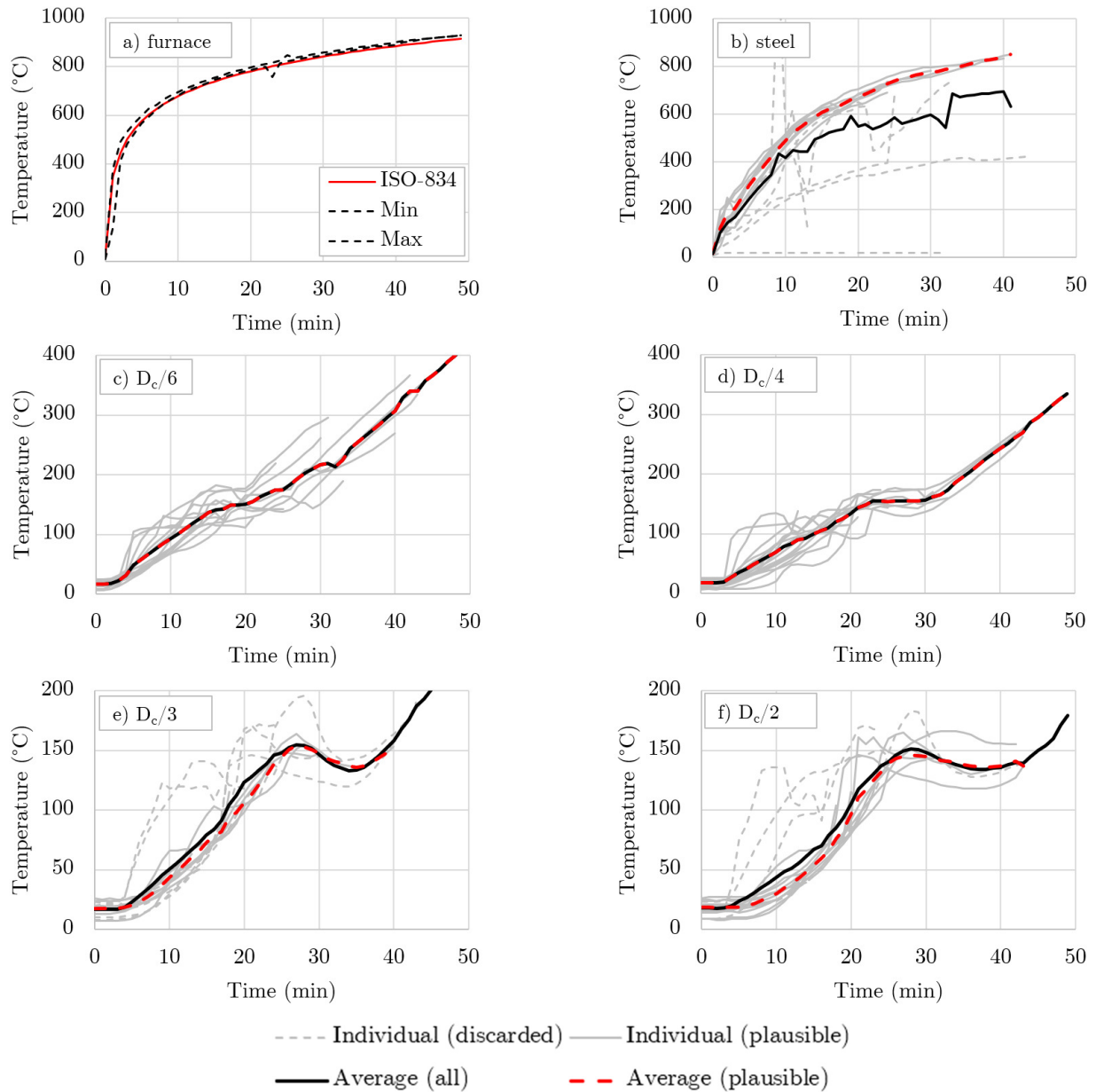


Fig. 5.8 Temperatures inside CFST columns filled with NCS (without steel fibre): (a) PT temperature, (b) steel surface temperature, (c) TC at the  $D_c/6$  depth, (d) TC at the  $D_c/4$  depth, (e) TC at the  $D_c/3$  depth, (f) TC at the  $D_c/2$  depth (centre). Raw data were extracted from a report by Espinos et al. (2014).

Further figures (Fig. 5.8 c, d, e, f) present the temperature inside the concrete core at four respective depths ( $D_c/6$ ,  $D_c/4$ ,  $D_c/3$ , and  $D_c/2$ ). A considerable scatter can be observed in Fig. 5.8 (c, d). On the other hand, most of the data in Fig. 5.8 (e, f) overlap. However, some

erroneous readings can also be observed, showing faster temperature increases in deeper parts of the cross-section compared to points closest to the surface ( $D_c/6$ ).

Fig. 5.8 (a) illustrates average PT readings inside a furnace. Based on those readings, it could be assumed that conditions in the furnace were uniform, and the furnace was well-controlled. Fig. 5.8 (b) presents the steel temperature. Most of the data overlap; however, some thermocouples showed erroneous readings. Data judged as unreliable were marked with a dashed grey line (– –) and disregarded. The black solid line presents the average temperature based on all TCs, and the red dashed line illustrates the average temperature based on data deemed plausible. Romero et al. (2011) found that the variability in steel surface temperature could be explained partially by the influence of flames from the gas burners, affecting the measurement. They used a 16-burner furnace and concluded that results from thermocouples attached to steel tubes at  $1/4$  of the length of the column were consistent with the results for additional stub columns. In comparison, the measurements at the  $1/2$  length of the column were affected by flames (they used a 5 m x 3 m furnace equipped with two horizontal rows of 8 burners each, located at the furnace mid-height). Burners at temperatures are presented in Fig. 5.9.

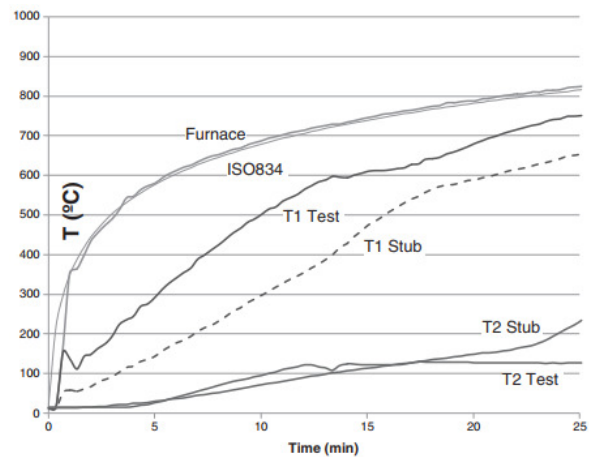


Fig. 5.9 Left: column and gas burners; Right: Temperature measurement during one of the tests (T1 Test – thermocouple attached to steel tube at mid-height of the main column, T1 Stub – thermocouple attached to steel tube of the additional stub column, 400 mm from the furnace floor. T2 Test and T2 Stub – thermocouples at the  $D_c/6$  depth of the two respective columns. Both images were reprinted from Romero et al. (2011), with permission from Elsevier.

For an easier comparison, Fig. 5.10 summarises the data, where a plateau forming at around 150 °C can be observed. The plateau also becomes longer with the increase in the depth of the measurement point.

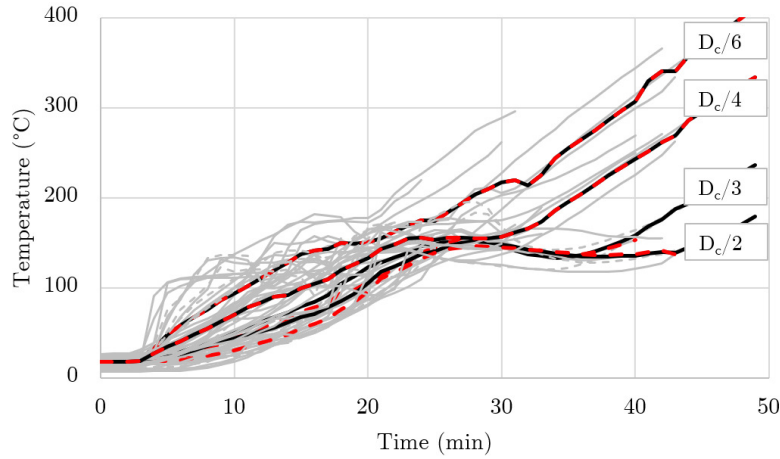


Fig. 5.10 Experimental data from *Espinos et al. (2014)*. For legend, see the caption to Fig. 5.8.

Lie & Chabot's (1992) graphs showed thermocouple readings, but a closer examination raised doubts about the accuracy of temperature measurements. One of the probable reasons might have been the questionable thermocouple placement. In more than half of the tests, the measurements by some of the thermocouples were deemed unreliable. For instance, thermocouples in different positions showed similar temperatures (e.g. TC3 and TC4 in column C06, or TC4 and TC5 in column C26). There were also instances of thermocouples being placed deeper in the concrete core, showing higher temperatures than those closer to the surface (e.g. columns C08 and C09).

Wang et al. (2022a) showed that even in well-controlled conditions, the discrepancies in recorded temperatures can be high, partially due to the influence of random distribution of aggregate particles. They used star-shaped thermocouple nets. Temperatures were measured at four depths along eight concentric lines (Fig. 5.11). One of the nets suffered from an offset (Fig. 5.11), but the other had a near-perfect alignment. Nevertheless, the measured temperatures showed considerable scatter, presented in Fig. 5.12.

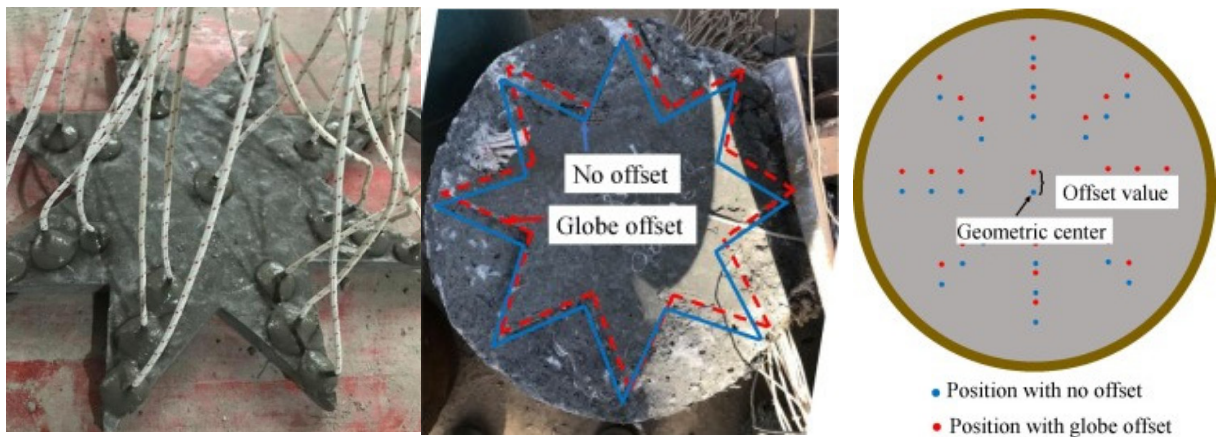


Fig. 5.11 Test setup used by *Wang et al. (2022a)* (CC license).

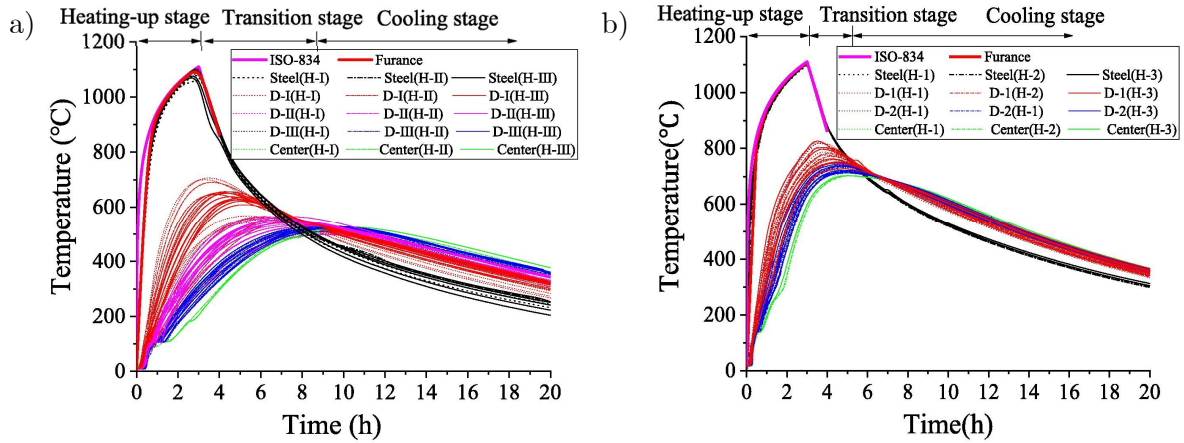


Fig. 5.12 Temperatures at different depths ( $D$ ) and heights ( $H$ ). Depths are differentiated through colours (red, purple, and blue). (a) column with globe offset, (b) column with near-perfect globe alignment (no offset). Source: Wang et al. (2022a) (CC license).

Similar results discrepancy could be seen in Yu et al. (2019b), who tested 12 pre-loaded columns of the same geometry, all filled with the same concrete mixture. Data from Wainman & Toner (1992), Espinos et al. (2014a), and Wang et al. (2022a) reinforce the view that calibrating a model based on a single test is inherently unreliable.

Moreover, it can be seen in Fig. 5.7 and Fig. 5.8, that the temperature plateau, which is attributed to the evaporation of water, formed at a level of around 150 °C. Furthermore, analysis of data presented by Espinos et al. (2014) shows the plateaus for HSC-filled columns forms at higher levels than for NSC-filling. This reinforces the view that the thermal properties of concrete are related to the internal pore pressure. Moreover, it indicates that a model of specific heat with a peak between 100 °C and 200 °C presented in Eurocode 4 may be robust enough to capture the sealed and unsealed conditions within the CFST column.

To quantify the possible differences due to thermocouple misplacement (e.g. due to shift during concrete vibration), a numerical analysis was performed for a 159 mm x 6 mm cross-section filled with concrete. Fig. 5.13 shows that a higher temperature variability might be expected closer to the surface than further inside the core. The results were obtained assuming an upper limit of thermal conductivity, 3 % moisture content with a specific heat peak at 115 °C, and thermal gap conductance of 100 W/(m<sup>2</sup>·K).

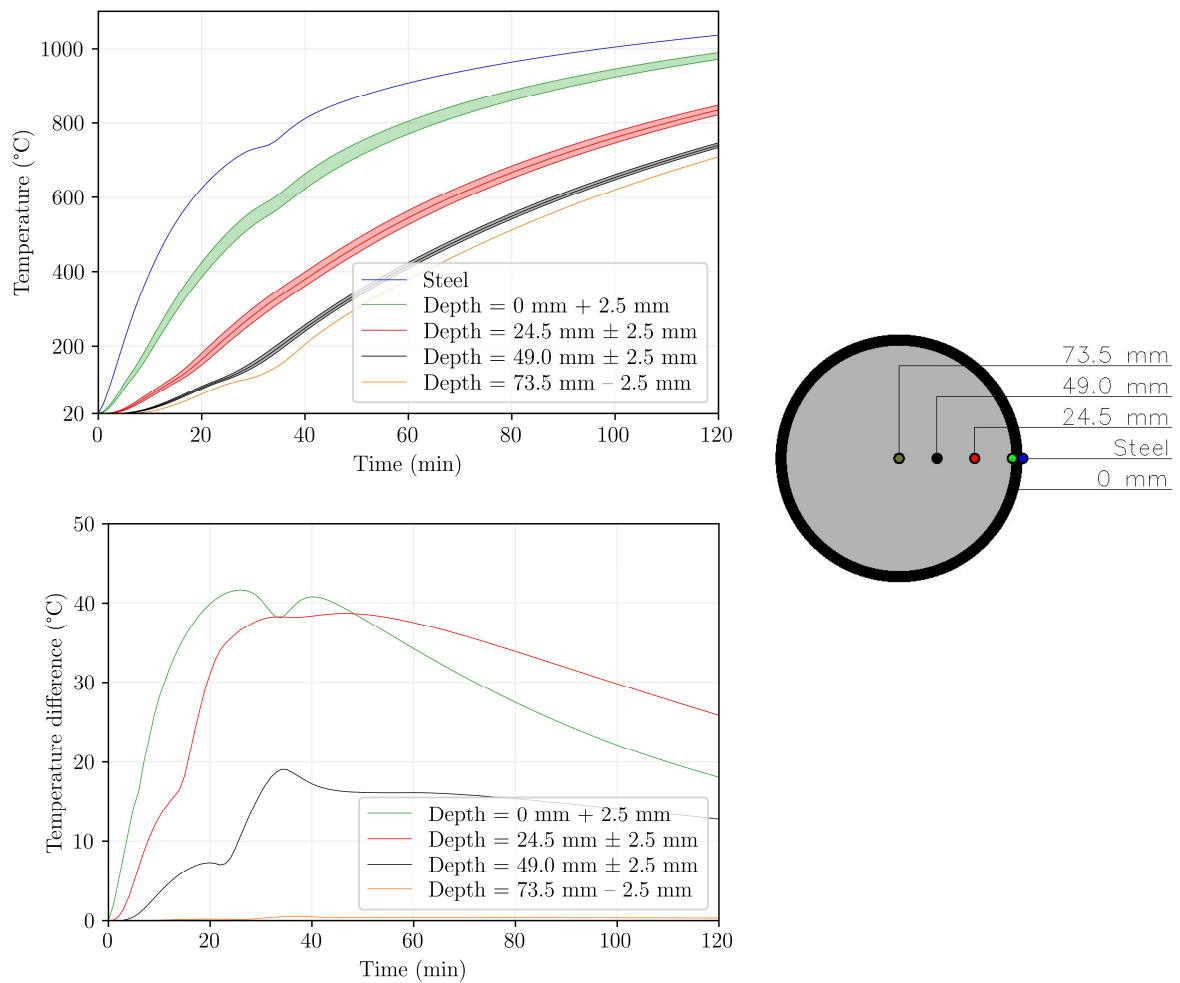


Fig. 5.13 The effect of thermocouple misplacement at various nominal depths: 0 mm, 24.5 mm, 49.0 mm, 73.5 mm, with  $\pm 2.5$  mm shifts. (a) temperature; (b) temperature difference between extreme positions (own calculations).

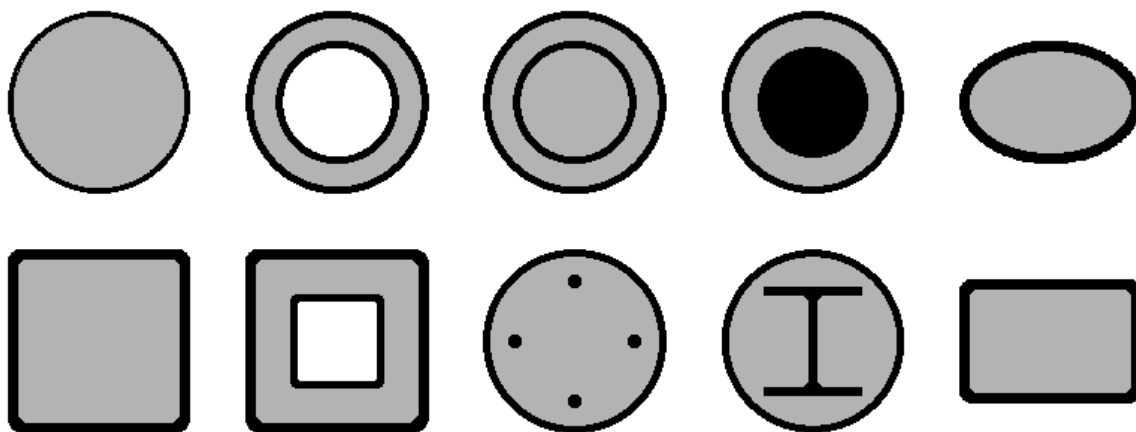
#### 5.4. Recommendations for future experimental research

Recommendations for future experimental research, based on missing or ambiguous data in currently available test reports are as follows:

- detailed concrete mix quantities and properties should be given;
- proper execution of boundary conditions is essential. Details regarding the construction of fixed or pinned supports should be given;
- details regarding the measurement of concrete compressive strength should be given (specimen size, shape, number of specimens);
- if possible, coupon tests of steel should be conducted;
- moisture content should be measured by drying specimens at 105 °C, and the conditioning details should be reported;
- the examination of the column after the test could include determination of the exact thermocouple location.

## 5.5. Design methods at ambient conditions

The data on the performance of CFST columns at ambient conditions is vast. Goode & Lam (2008) compiled a database of 1819 columns (short, long, circular, square and rectangular, loaded axially or eccentrically). The comparison of test results and calculations based on Eurocode 4 made by Goode & Lam (2008) showed the ratio of test to calculated load to be 1.11. Other authors also compared the results of codified calculation methods with experiments, e.g. Kang et al. (2015), Thai et al. (2019), Thai et al. (2020). Tao et al. (2008) compared results obtained with six different codes. Large databases were used in machine learning (Naser et al. 2021, Xuan & Le 2021). In Naser's database, 3103 columns were presented. Researchers agree that the Eurocode 4 procedure for the ambient design of CFST columns is reliable but, in some cases, overly conservative. Some researchers point out that other areas require further development, such as the effects of long-term loading, load transfer, CFRP tubes, UHPC filling, or blast loads. Examples of less popular tube materials are CFRP, aluminum, or fibreglass. There is a larger variety of materials that were used for filling the tubes, e.g. aluminum foam, rammed earth, timber, ice, or water and a variety of concretes, as indicated in Fig. 5.14. Tube might be reinforced with other steel cross-sections, such as solid, or H-sections. The variety of cross-section shapes varies from square and rectangular, through hexagonal, octagonal, multitube to circular and elliptical. However, as shapes other than circular are not relevant to this thesis, their influence will not be discussed here.



**Tube materials:** steel, CFRP, aluminum, fiberglass

**Filling materials:** ordinary concrete, lightweight concrete, aluminum foam, rammed earth, timber, ice, water and a variety of concretes: expansive, foamed, geopolymer, palm oil, recycled aggregate, reactive powder, rubberised, sea sand, steel slag concrete

*Fig. 5.14 Examples of concrete-filled cross-sections.*

## 5.6. Design methods in fire conditions

### 5.6.1. Prescriptive design

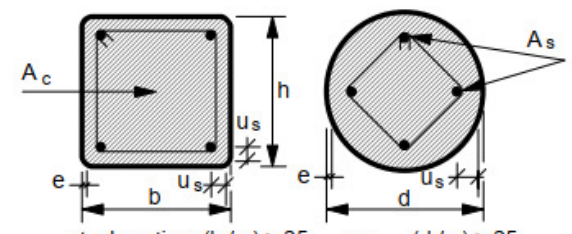
Until the 1980s, the fire design methods of CFST columns were prescriptive. That is, a CFST column filled with plain concrete was deemed to satisfy the load-bearing criterion for 25 minutes of fire. If rebar-reinforced, the CFST column was expected to withstand thermal exposure for 45 minutes. Those values originated from Ingberg's research in 1921 and did not change much

for decades. For example, the bulletin of the National Headquarters of the State Fire Service of Poland in 1975 assigned CFST columns with a fire resistance of 24 to 60 minutes, depending on their diameter and tube thickness.

**5.6.2. Tabulated data and simplified calculation methods**

Based on the efforts by, e.g. Haß (1986), tabulated data and simplified design methods were developed. The experimental programmes described earlier led to the development of tabulated and simplified design methods. Those efforts were summarised in ECCS (1988) recommendations, which were further largely transferred to Eurocode 1994-1-2 (Ibáñez 2015) in the form presented in Fig. 5.15. The same tabulated method is available in other codes, such as DIN 4102-4 (1994).

**Table 4.7: Minimum cross-sectional dimensions, minimum reinforcement ratios and minimum axis distance of the reinforcing bars of composite columns made of concrete filled hollow sections**



		Standard Fire Resistance				
		R30	R60	R90	R120	R180
1	Minimum cross-sectional dimensions for load level $\eta_{\bar{n},t} \leq 0,28$					
1.1	Minimum dimensions h and b or minimum diameter d [mm]	160	200	220	260	400
1.2	Minimum ratio of reinforcement $A_S / (A_C + A_S)$ in (%)	0	1,5	3,0	6,0	6,0
1.3	Minimum axis distance of reinforcing bars $u_S$ [mm]	-	30	40	50	60
2	Minimum cross-sectional dimensions for load level $\eta_{\bar{n},t} \leq 0,47$					
2.1	Minimum dimensions h and b or minimum diameter d [mm]	260	260	400	450	500
2.2	Minimum ratio of reinforcement $A_S / (A_C + A_S)$ in (%)	0	3,0	6,0	6,0	6,0
2.3	Minimum axis distance of reinforcing bars $u_S$ [mm]	-	30	40	50	60
3	Minimum cross-sectional dimensions for load level $\eta_{\bar{n},t} \leq 0,66$					
3.1	Minimum dimensions h and b or minimum diameter d [mm]	260	450	550	-	-
3.2	Minimum ratio of reinforcement $A_S / (A_C + A_S)$ in (%)	3,0	6,0	6,0	-	-
3.3	Minimum axis distance of reinforcing bars $u_S$ [mm]	25	30	40	-	-

Fig. 5.15 Tabulated data for CFST column design in EN 1994-1-2.

The situation with calculation methods in fire conditions is not as clear as for ambient design. The current Eurocode method (Annex H) is based on the work of CIDECT that started around 1970. Shortly before the introduction of the Eurocode, Renaud et al. (2004) hinted that the Eurocode method has a "questionable level of approximation", as the safety level depended on the slenderness of the column. Eurocode 1994-1-2 was published in 2005, and it was soon confirmed that the method in Annex H gives unsafe results for columns with high relative slenderness (Aribert et al. 2008). In 2014 range of application of this method was limited to CFST columns with relative slenderness lower than 0.5. For this reason, CEN started a project SC4.T4, 'Develop new rules for composite columns (concrete filled tubes) in fire'.

According to structural design code EN 1994-1-2, the load-bearing criterion 'R' of protected CFST columns may be assumed to be met when the temperature of the steel section is lower

than 350 °C. Without protection, this temperature is reached after about 10 minutes of furnace exposure. The test standard for applied protection to CFST columns (EN 13381-6) allows using dry sand infill as an alternative to concrete. Consequently, the performance of the CFST column's protection is assessed using steel temperature only. Such an approach neglects the concrete role in carrying mechanical loads and considers it only as a heat sink.

The problem of assessing the fire resistance time under a constant load or load-bearing capacity after a certain time of fire exposure is present in the literature (Kodur 2007, Espinos et al. 2010). This originates from the desire to assure safety and law requirements to provide sufficient fire resistance (for example, R30, R60, etc. classes).

Several meta-analyses of the Eurocode provisions exist for the fire design of CFST columns. Aribert et al. 2008 showed that the Annex H method gives results higher than their numerical model. On the other hand, Rush et al. (2012) showed that the tabular data and Annex H method yield conservative results compared to most of the experimental data. Espinos et al. (2012) showed that the results were mostly conservative for slenderness up to 0.5 and unconservative for slenderness equal to 1.0, 1.5 and 2.0. On the other hand, a study by Wang et al. (2023) showed contradictory results, where the Eurocode Annex H method yielded conservative results, with the mean ratio of predicted to experimental fire resistance time equal to 0.30. Such discrepancies show that the Eurocode Annex H method is considered unconservative by most researchers. However, significant discrepancies can be observed in the conclusions drawn from the meta-analyses. Furthermore, those discrepancies relate both to qualitative and quantitative assessment of the Annex H method.

Several simplified design methods were proposed by other researchers, including Aribert et al. 2008, Kodur (1999), Bergmann (2013), and Han et al. (2003). Their applicability is subjected to limitations, as described elsewhere by the author (Szymkuć 2016).

## 5.7. Numerical modelling

Efforts to develop calculation methods were undertaken by, e.g., Hań (1986) or Lie (1984). Later, refined numerical models were developed, e.g., Ding & Wang (2008), Espinós (2012) and Ibáñez et al. (2019). To this day, the numerical modelling of CFST columns attracts significant attention (Tao et al. 2016, Liu et al. 2019, Dai et al. 2020, Tan et al. 2020, Li et al. 2022b), and the results are published in the most renowned journals. In terms of numerical modelling, the seminal work was presented by Ding & Wang (2008). They were the first to acknowledge the influence of the thermal gap conductance. They also provided a sensitivity analysis of the column's performance regarding friction effects, mesh size, allowing or constricting movement between the tube and core, or the sensitivity to an initial eccentricity.

Hong & Varma (2009) provided another large and influential numerical study using the FE software Abaqus. To fit the numerical and experimental data better, they suggested a constant thermal expansion coefficient for concrete ( $6 \cdot 10^{-6}$  1/K), which was later used by, e.g. Espinos (2012), Yao et al. (2016), Zhang et al. (2020) or Zhou et al. (2021).

Later, a detailed numerical modelling with several sensitivity studies was presented in a PhD thesis by Espinos (2012).

In general, the properties of steel are usually adopted from the Eurocode 3 (Zhang et al. 2020, Zhou et al. 2021). For concrete, several models are explored by other researchers. Yao et al. (2016) used a model by Han et al. (2003). A model of Lie (1994), which assumes no loss of concrete strength at temperatures up to 450 °C, was used by Zhang et al. (2020) and Zhou et al. (2021). Hong & Varma (2009) explored two models of concrete stress-strain relationship in compression and concluded that a model by Lie & Irwin (1995) gave better results. Similar to the model by Lie (1984), Lie & Irwin's model assumes no loss of concrete strength at temperatures up to 450 °C. Furthermore, Hong & Varma concluded that Lie & Irwin's model was better for CFST members since it accounted for the effects of confinement. The effect of confinement of the concrete core by the steel tube is non-existent in fire conditions, as elaborated in section 6.2.1. Wang & Young (2013) also analysed models from the Eurocode, Poh (2001) and Lie & Irwin (1995) and concluded the Eurocode model gave the best results.

Tao et al. (2016) modelled the local buckling of steel tubes in the CFST columns. However, the authors did not provide a sensitivity study, and it is difficult to state to what extent the local imperfections influenced the column's response. Nevertheless, it is one of the few studies that used photogrammetry to measure the initial imperfections. Azad & Uy (2020) and Farzarian et al. (2023) reported several techniques of modelling imperfections for the analysis of CFST columns at ambient conditions. The reasons for not considering local buckling in fire conditions are explained further in chapter 6.2.5.

Tao et al. (2016) used the stress-strain model given by the Eurocodes and employed the concrete damaged plasticity model for concrete. Their sensitivity study revealed that the response of the column was not sensitive to parameters such as the ratio of the compressive strength under biaxial loading to uniaxial compressive strength ( $f_{b0}/f_c'$ ), the ratio of the second stress invariant on the tensile meridian to that on the compressive meridian ( $K_c$ ), or flow potential eccentricity ( $e$ ). However, the authors found out the dilation angle ( $\psi$ ) affected the column's response and found the value of  $\psi=40^\circ$  to give the best predictions. Contrary to those results, Tran et al. (2020) found  $\psi$  and  $K_c$  did not influence the response of stub columns, while the friction angle did.

Other aspects of numerical modelling are elaborated in, e.g. 6.2.8, or 7.3.1. What is often missing in the existing numerical studies, is the presentation of experimental background. Unfortunately, some columns are simply ignored by other researchers without a detailed explanation. This is further elaborated in chapter 6.2.2. However, from the perspective of numerical modelling, the 'controversial' C06, C15, and C16 columns (among others) were left off by, e.g. Xiong & Liew (2016), Xiong & Liew (2018), Liu et al. (2019), Yang et al. (2020) or Li et al. (2022), without explanation. A good example is the work of Espinos (2012), who identified the problem and provided a detailed analysis of boundary conditions in three tests by Lie & Chabot (1992), as explained in 6.2.2. The work of Wang & Young (2013) is an example where the experimental results were analysed in detail. Most of the researchers rely on the nominal values of yield strength given by Lie & Chabot (1992), while the measured values (unfortunately only for some of the columns) were given in an earlier report – NRC 570 by Lie & Caron (1988).



## 6. Analysis of structural behaviour of CFST columns in standard fire conditions

The analysis of the structural fire behaviour of CFST columns is presented based on:

- (1) experimental data obtained by other researchers and
- (2) own numerical model.

Unlike the review in chapter 5, the analysis provided in this chapter is the author's cross-comparison, focusing on particular factors and not on single research studies.

### 6.1. Structural fire behaviour of CFST columns

The steel tube and concrete core carry the load at ambient temperature. However, when the column is exposed to fire, the contact between the steel tube and the concrete core is lost. This is caused by the difference in temperatures of steel tube (directly exposed to environmental conditions) and concrete core (which will show a considerable temperature gradient). Hence, the steel elongates faster than the core, and consequentially, it might carry the whole load for a limited time. The structural fire behaviour of CFST columns is traditionally expressed in terms of vertical displacement-time relationship. This allows for distinguishing at least three distinct stages, as presented in Fig. 6.1.

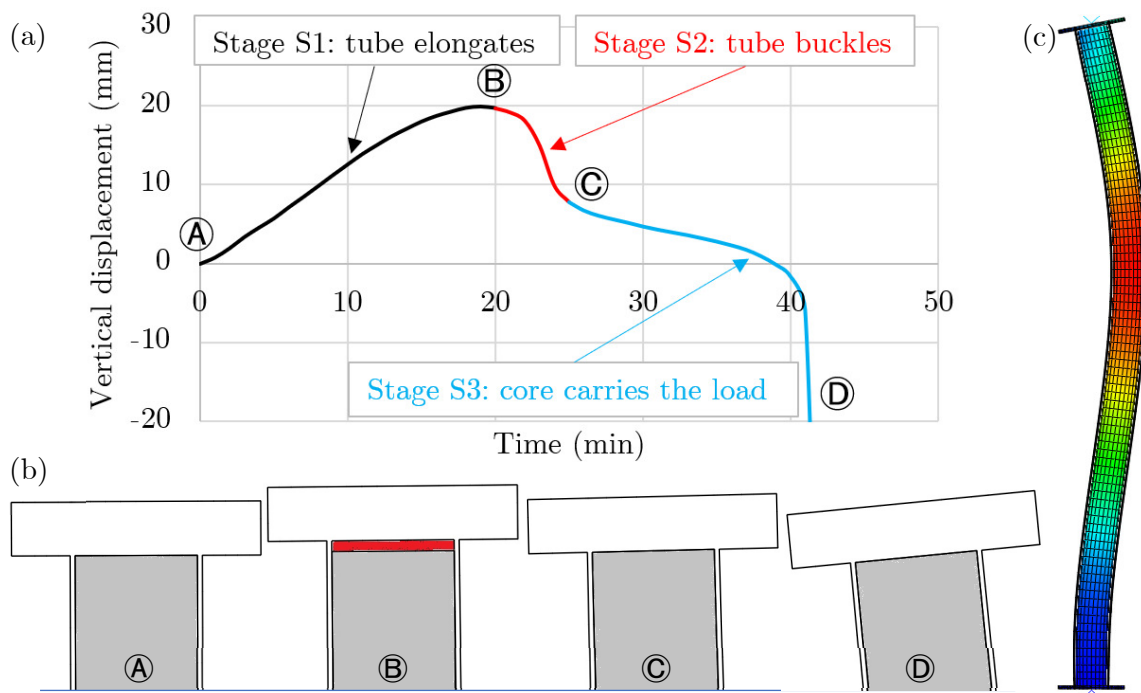


Fig. 6.1 (a) Typical relation between vertical displacement and time during a fire resistance test of CFST column. **A** Start of the test; **B** tube reaches critical temperature; **C** loading plate rests on the concrete core; **D** failure of the column; (b) column's top corresponding to time **A**, **B**, **C** and **D**; (c) column deflected shape at failure time.

- **The first stage (S1)** – it lasts until the load-bearing capacity of the tube deteriorates to the point, when it is equal to the applied load (**A**→**B**).
- **The second stage (S2)** – the tube starts to buckle, and at some point, the loading plate comes in contact with the core again (**B**→**C**).

- **The third stage (S3)** – this is the most important stage if a CFST column is to reach high fire resistance ( $\text{C} \rightarrow \text{D}$ ). The load is transferred by the core, while the mechanical properties of the steel tube degrade further. Therefore, it is a prerequisite to use a filling that can supply the desired fire resistance time. Furthermore, as the temperature of the external tube rises fast, high strength steel or steel for high-temperature applications is of limited use (Espinosa et al. 2015). During stage S3, the column continues to contract. Ultimately, it fails, and the point of failure is denoted as  $\text{D}$ .

Depending on the relation between the load and the load-bearing capacity of concrete core and steel tube, three types of behaviour can be distinguished:

- **Type A behaviour** – typical and desired behaviour of CFST column, where concrete provides fire resistance (stages S1, S2, S3) as explained above
- **Type B behaviour** – concrete fails to provide fire resistance (no stage S3) - in columns that have a filling not capable of supporting the load, only stages 1 and 2 might be distinguished, as concrete core fails upon contact with the loading plate (Fig. 6.2, type B behaviour).
- **Type C behaviour** – the tube is overloaded (stages S1 and S2 are not present) - for heavily loaded columns, where the tube is not able to carry the whole load, the stages might look like for an ordinary RC column – with an expansion stage at the beginning and contraction afterwards (Fig. 6.2, type C behaviour).

The three types of behaviour are presented in Fig. 6.2. The examples shown in Fig. 6.1 and Fig. 6.2 show that the concrete core might (i) provide no additional fire resistance to the column (Fig. 6.2, type B behaviour), (ii) provide additional 20 minutes (Fig. 6.1), or (iii) provide more than an additional hour (Fig. 6.2, type A behaviour). Therefore, the cautious design of the core or core material is of uttermost importance as far as the fire resistance time of the CFST column is concerned.

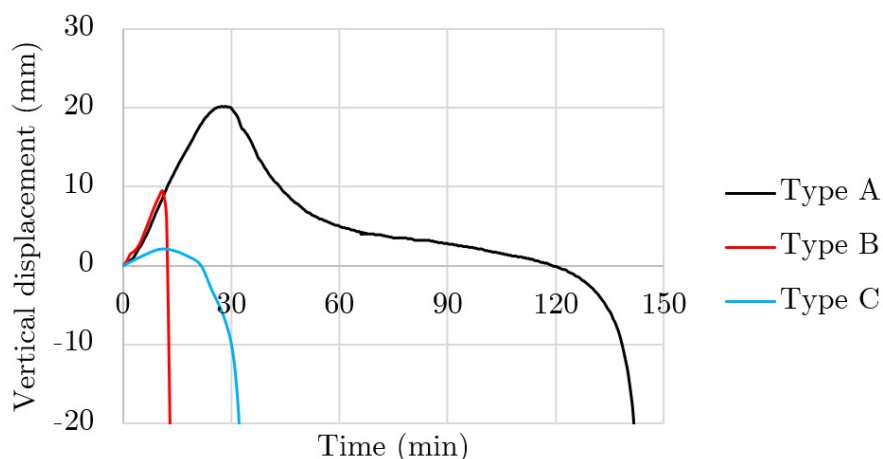


Fig. 6.2 Three types of structural fire behaviour of CFST column during a standard fire resistance test are shown as vertical displacement-time relationships.

Point D in Fig. 6.1 denotes the failure of a column. Two criteria are commonly used as indicators of specimen failure during standardised fire exposure: vertical contraction (mm) and rate of vertical contraction (mm/min). For vertically loaded elements (columns), the limits are:

- limiting vertical contraction:  $C = \frac{h}{100}$  (mm) or (6.1)

- limiting rate of vertical contraction:  $\frac{dC}{dt} = \frac{3h}{1000}$  (mm/min), (6.2)

where  $h$  is the initial height (in mm) of the test specimen once the load has been applied. The vertical displacement is expressed according to the convention defined in EN 1363-1 clause 10.4.4.2, i.e., the increased height is expressed in positive values, and a decrease below the original height is negative.

## 6.2. Analysis of influencing factors based on experimental data

### 6.2.1. The role of the interaction between steel tube and concrete core

This section discusses the role of interaction between steel tube and concrete core and the potential failure modes of CFST columns. Ideally, the concrete core and steel tube would carry the load, with the bond between them allowing for a smooth load transfer. However, several modes of unexpected CFST column failure were identified, such as:

- premature buckling of the steel tube due to improper casting or vibration ([Hanswille & Lippes 2008](#), [Espinos et al. 2015](#)),
- failure induced by the unplanned gap between the concrete core and the top loading plate ([Hanswille & Lippes 2008](#)),
- spherical-cap gaps ([Liao et al. 2011](#)) and circumferential gaps due to casting imperfections ([Liao et al. 2011](#), [Wang et al. 2022b](#)).

It had been stipulated that a concrete core might prevent the inward buckling of the tube. Such a hypothesis was proven wrong by [O'Shea & Bridge \(1997\)](#). In their test, the loading plate was attached to a steel tube and did not touch the concrete core, and the steel was greased so that the bond and friction between the steel tube and the concrete core were minimised. Their results showed that an unbonded concrete core did not increase the load-bearing capacity of the tube compared to an unfilled tube. Hence, they proved that preventing inward buckling is not the governing mechanism of the increased load-bearing capacity of CFST columns. Some codes, for example, Australian AS 4100, American AISC 360, or Chinese GB 50017 have a different limit for the slenderness of steel tube for hollow and concrete-filled steel tubes in compression ([Azad & Uy 2020](#)). In EN 1993-1-1 and EN 1994-1-1, the limit is the same,  $90/(235/f_y)$ , irrespective of the presence of concrete filling. According to [Sauerborn & Kretz \(2010\)](#), it is based on the recommendations of Roik and Bergmann. The subject was elaborated in detail by [Azad & Uy \(2020\)](#).

Confinement of concrete by steel tube leads to an increase in compressive strength. The influence of biaxial compression was thoroughly studied at ambient temperature by [Kupfer \(1973\)](#) and at elevated temperatures by [Ehm \(1986\)](#). On the structural level, the influence of confinement can be significant for axial loads. However, this influence diminishes with increasing load eccentricity, as shown by, e.g. [Godycki-Ćwirko et al. \(1999\)](#) for circular RC columns with hoop reinforcement. In fire conditions, [Serega et al. \(2015\)](#) showed that tightly spaced ties positively affected the fire resistance time of axially loaded circular RC columns, likely due to the confinement effect.

Concrete confinement can be expected in CFST columns under axial loading at ambient conditions. In such case, a steel tube might act as a hoop reinforcement and provide a triaxial stress state, thus increasing the load-bearing capacity. On the level of material modelling, many researchers implemented the stress-strain models that assumed ideal plastic behaviour, where there was no descending branch of the concrete stress-strain relationship, e.g. [Han et al. \(2005\)](#). While this approach might be correct for stub or stocky, axially loaded columns, it no longer applies to slender, eccentrically loaded columns. This phenomenon is also reflected in the guidance given by [EN 1994-1-1](#), where the confinement-induced increase in strength of concrete may be taken into account only for eccentricities up to 10 % of the column diameter, providing relative slenderness does not exceed 0.5. Moreover, in fire conditions, the steel tube detaches from the concrete. It results from the temperature difference between the steel tube and the concrete core. In consequence, the confinement effect in fire might be non-existent.

In fire conditions, the steel tube detaches from the concrete core, forming an air gap. The effect of the air gap on thermal response is further discussed in the section related to the thermal gap conductance. The detachment makes the confinement and interface bond ineffective. Quantifying such an effect in experimental fire conditions would not be possible. However, the effect of the 'circumferential gap', shown in [Fig. 6.3 \(a\)](#) at ambient conditions was studied by [Liao et al. \(2011\)](#), who showed that introducing a gap of 1 mm (equal in size to 1.1 % of the cross-section diameter) reduced the load-bearing capacity of a column by 23 %. With the gap increased to 2.2 % of the diameter, the capacity was reduced by 29 % compared to the fully-bonded CFST column. Notably, the capacity of steel tube without concrete core was just 65 % less than that of the CFST capacity. Similar conclusions were later drawn by [Wang et al. \(2022b\)](#). While this might seem contradictory to the results of [O'Shea & Bridge \(1997\)](#), it shall be noted that in [O'Shea & Bridge](#), the load was applied only to the steel tube, as opposed to uniform loading of concrete core and steel tube in [Liao et al. \(2011\)](#) and [Wang et al. \(2022\)](#).

In summary, the research of [Liao et al. \(2011\)](#) and [Wang et al. \(2022\)](#) clearly shows the importance of confinement and contact between core and tube on the load-bearing capacity of CFST columns. It shall be underlined that, in fire conditions, the influence of steel tube on concrete confinement may be neglected. [Huang et al. \(2007\)](#) indicated that even if contact is regained at higher temperatures, the steel could not supply an effective confinement due to its mechanical degradation.

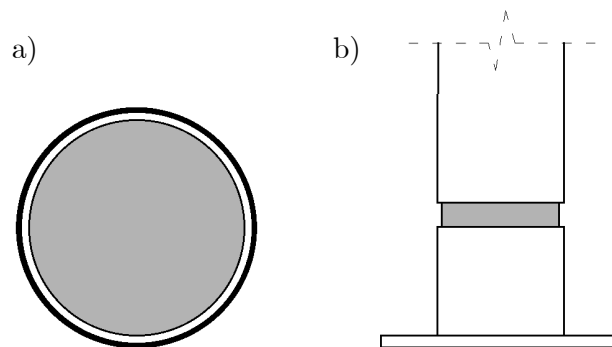


*Fig. 6.3 (a) circumferential gap between core and tube ([Liao et al. 2011](#)), (b) Intentional gap in the steel tube ([Liu et al. 2019](#)).*

Another line of research aimed at decoupling the overlapping effects of tube and core interactions was studied by [Liu et al. \(2019\)](#). They tested several columns, which had their steel tube cut near the top and bottom of the column, Fig. 6.3 (b). [Liu et al. \(2019\)](#) expected that a thin tube would (1) increase the strength and ductility of concrete, (2) prevent or delay local buckling as the load was not directly transferred to steel tube, (3) limit concrete spalling.

A simple numerical model was developed to quantify the possible size of the fire-induced gap. The model represented four cross-sections (159 mm to 355 mm in diameter). The results are presented in Fig. 6.4, which shows the development of a fire-induced gap (in mm) between the concrete core and steel tube when a perfect straightness of a column is assumed. It can be observed that the gap for a typical cross-section might vary from 0 mm to 1.5 mm during three-hour standard fire exposure. Therefore, the effect of confinement was not introduced in further numerical studies.

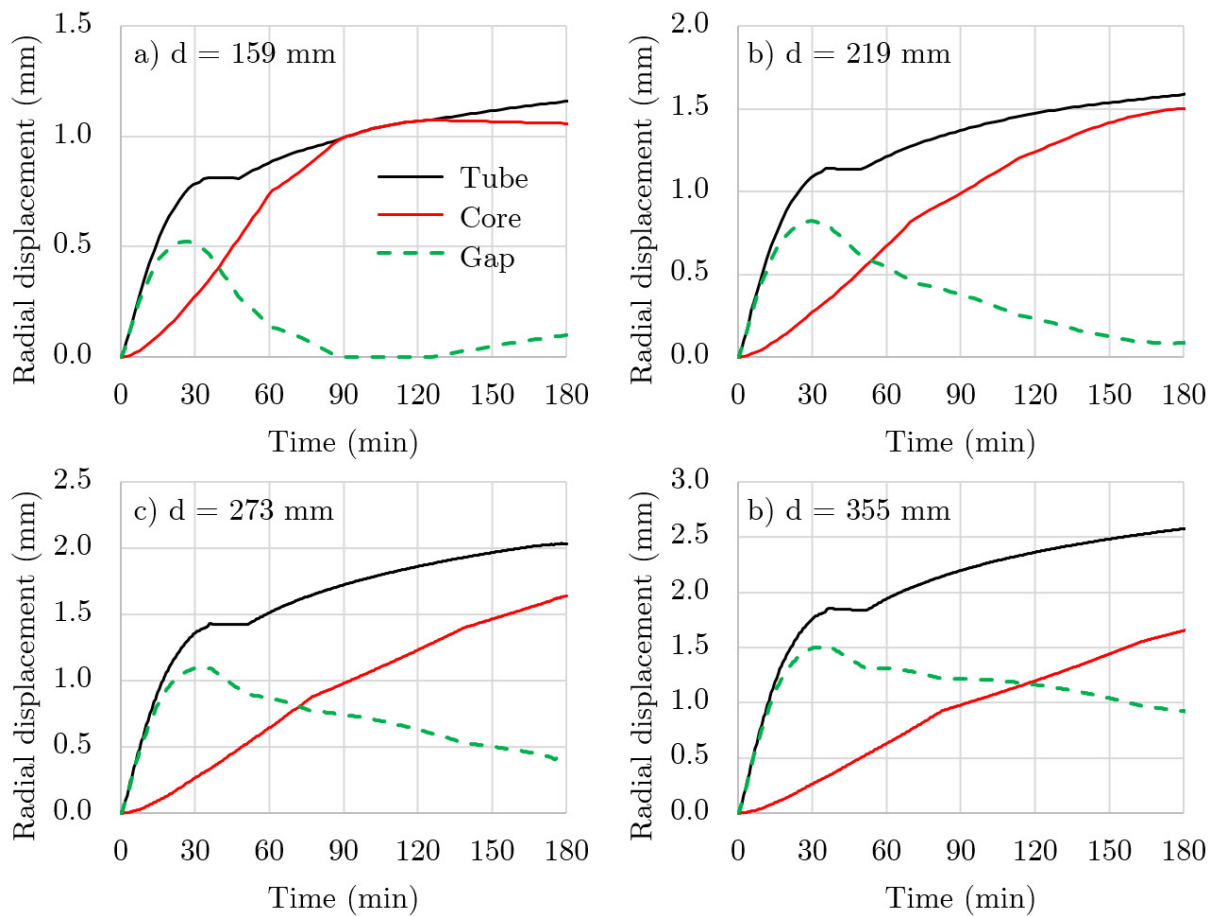


*Fig. 6.4 Development of radial displacement of the tube and concrete core during three hours of standard fire exposure. The Green dashed line (- - -) represents the gap between steel and concrete (difference between black and red line). The results for four cross-sections with different external diameters are presented: (a) 159 mm; (b) 219 mm; (c) 273 mm; (d) 355 mm (own calculations).*

Load transfer between steel and concrete is another factor worth mentioning with respect to the tube and core interaction. [Debnath et al. \(2023\)](#) discussed issues related to the load transfer mechanism between steel and concrete in CFST columns. After reviewing the CFST bond strength and slip behaviour at the steel-concrete interface, they identified two primary factors as (1) the bond strength and (2) the zone for load introduction. The cross-section dimensions

were also found to be one of the influencing factors. They also concluded that relying on bond strength is susceptible to uncertainties. The analysis of bond strength in CFST push-out tests was a primary objective of many scientific works, e.g. Starossek et al. (2008), Grzeszykowski et al. (2017), and will not be discussed here in detail. After detachment, the bond strength is non-existent, and axial load can be transferred between the tube and concrete core mainly through friction.

### 6.2.2. Effect boundary conditions, eccentricity and length

In most fire resistance tests, columns are loaded axially. The influence of eccentricity can be studied in two approaches: constant load with different eccentricities (as in Lie & Chabot 1992) or constant member utilisation level (Romero et al. 2011, Moliner et al. 2013, Han et al. 2003).

Properly executing assumed boundary conditions at the supports is a major problem in the fire testing of columns. During the comparative tests described in Kordina & Klingsch (1983) and later in more detail by Haß (1986), laboratories were asked to provide fixed-pinned boundary conditions. The examination of columns after the tests revealed that three out of five laboratories failed to provide clear pinned support. However, a subsequent test of columns with different geometry showed further inconsistencies. The Round Robin study on CFST columns showed that the fire resistance time of presumably the same columns ranged from 81 to 134 minutes for one column (square CFST 260 mm x 6.3 mm) and from 28 to 85 for the second column (square CFST 150 mm x 5.0 mm). Unfortunately, the detailed information on this exercise was not given. Hence, it is not possible to model the studied columns. Haß (1986) claimed that the discrepancy of results on CFST could be explained by boundary conditions at the supports that were not constructed according to the initial assumptions. However, this does not explain why a similar trend was not observed in the case of CFT columns for the subsequent test of columns. Fig. 6.5 presents the available axial displacement-time data from the Round Robin study. Fig. 6.7 shows the fire resistance time in different laboratories.

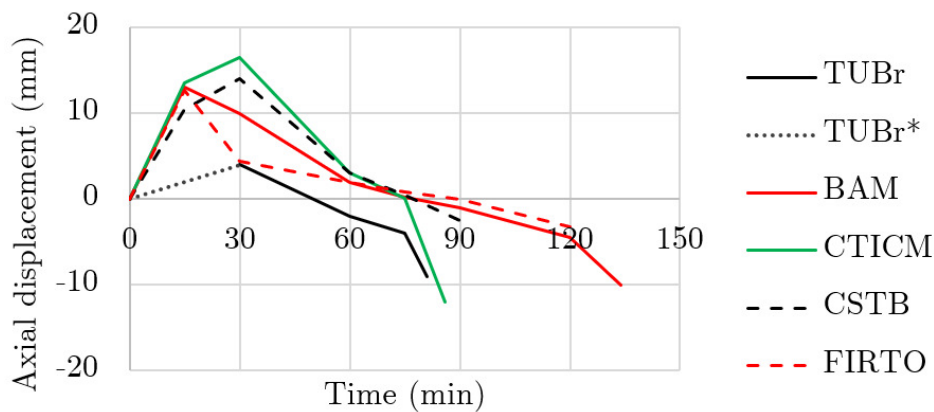


Fig. 6.5 The results of Round Robin presented in Haß (1986). Data was reported only in 15-30 minute increments.

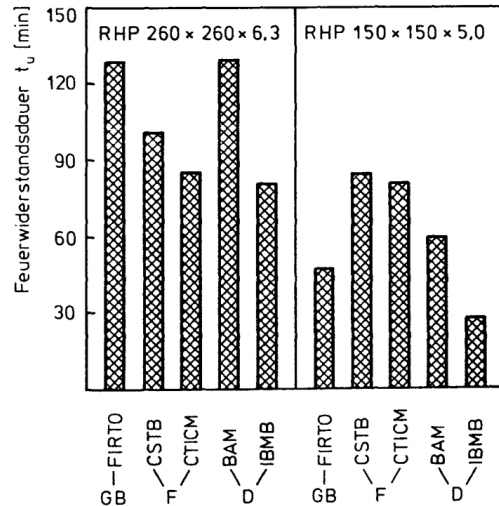


Fig. 6.6 Fire resistance time in a Round Robin study (Source: [Haß 1986](#)). The discrepancies in results for 260 x 260 x 6.3 column were explained by improper boundary conditions. But why did the results for 150 x 150 x 5.0 column not follow a similar trend?

This section highlights another problem. When validating a model, the experimental results from different laboratories should be taken into account. Otherwise, the model might be calibrated based on biased data that might have been inherently wrong. When an extensive, inter-laboratory database is used, the results can be used to identify biases. See, e.g., a study by [Gernay \(2019\)](#) on fire resistance columns, where the overall agreement between test results and numerical model is high. However, for most columns tested in NRC laboratory, the calculated FRT was higher than measured (Fig. 6.7). On the other hand, the model developed by [Jaszczak et al. \(2021\)](#) showed an opposite tendency (Fig. 6.7).

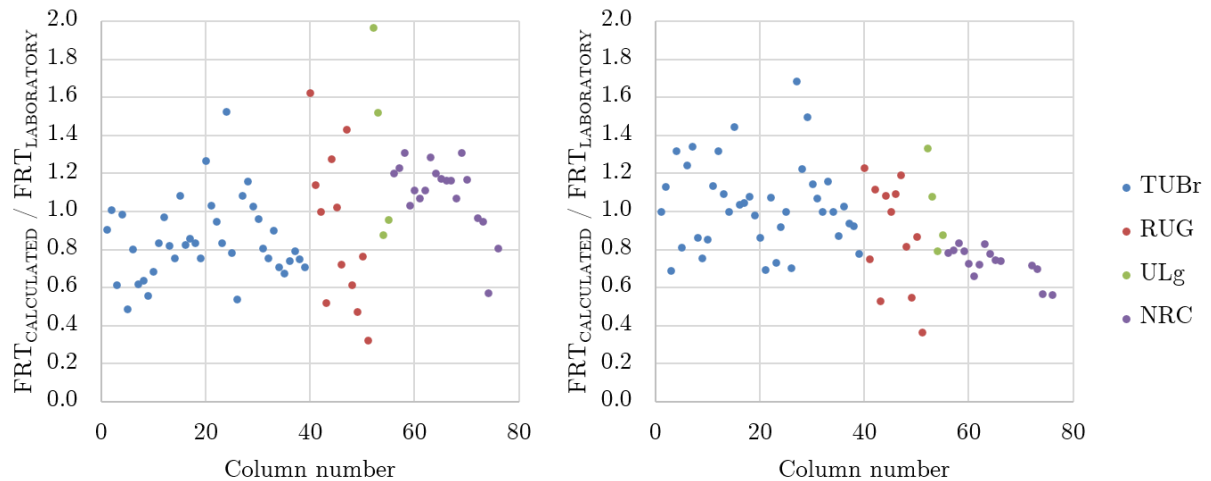


Fig. 6.7 Comparison of the ratio between calculated and measured fire resistance time according to two studies: left: [Gernay \(2019\)](#); right: [Jaszczak, Szymkuć & Kuczma \(2021\)](#).

The issues of proper boundary conditions are not specific to CFST columns. It was observed in studies of steel beams ([Dumont et al. 2015](#)) or columns ([Witteveen & Twilt 1981](#)). In the case of RC columns in fire conditions, [Achenbach \(2018\)](#) argued that NRC columns could not be included in the validation domain for his PhD thesis as welding steel rebars to the loading plates provided some degree of additional restraint. The NRC tests, however, form one of the

most extensive datasets on the fire resistance of RC columns, which was included during both the calibration of calculation methods in Eurocodes (Franssen 2000) and subsequent efforts of other authors, such as (Tan & Yao 2003, Bamonte & Lo Monte 2015, Gernay 2019, Jaszczak et al. 2021, Głowacki & Kowalski 2022). Hence, it can be concluded here that proper execution of support conditions is both essential and challenging. Visual observation of the column after the fire resistance test (see Fig. 6.8, Fig. 6.10) can help to determine whether the constructed boundary conditions were in line with what was assumed at the beginning.

Columns used in the validation domain of this thesis were tested in a full-scale. Lie & Chabot (1992) tested columns with 3810 mm length (including the loading plates), where 3200 mm was exposed to fire. Most columns were fixed at both ends (FF); however, three comparative columns with fixed boundary conditions and their pinned (PP) counterparts were also tested. The columns tested by Wainman & Toner (1992) were 3.4 meters long, with only minor parts insulated near the supports. Han et al. (2003) tested columns with 3810 mm length (including the loading plates), with a boundary condition described as pinned-pinned. However, the examination of the figures reveals that some degree of rotational restraint was present during the fire tests. The columns tested by Kim et al. (2005) were also described as pinned-pinned. Unfortunately, the available photographic material does not allow to assess whether the boundary conditions were actually pinned or restrained. Kim et al. (2005) tested 3.5-meter columns; however, up to one meter of their length near the supports was insulated during the tests (in total). The columns tested at the UPV (Romero et al. 2011, Moliner et al. 2013) were 3180 mm long, with 80 mm and 130 mm of length insulated at the bottom (fixed) and top (pinned) end, respectively. The photographic documentation of tests from Valencia shows that the BCs were well-executed.

Kodur (1999) recommended using rebar or steel-fibre reinforced concrete for eccentrically loaded columns, as he found the behaviour of plain CFST columns with eccentric loads unpredictable. The knowledge of the effect of eccentricity on FRT is limited. Han et al. (2003) tested three such columns, and only two were tested in NRC Canada. Only axially loaded columns were tested by Kim et al. (2005), Wainman & Toner (1992) and Leite et al. (2010). Several eccentrically loaded columns were presented in a report by Espinos et al. (2014). An example of constructing fixed-pinned boundary conditions with a load eccentricity is given in Fig. 6.8.

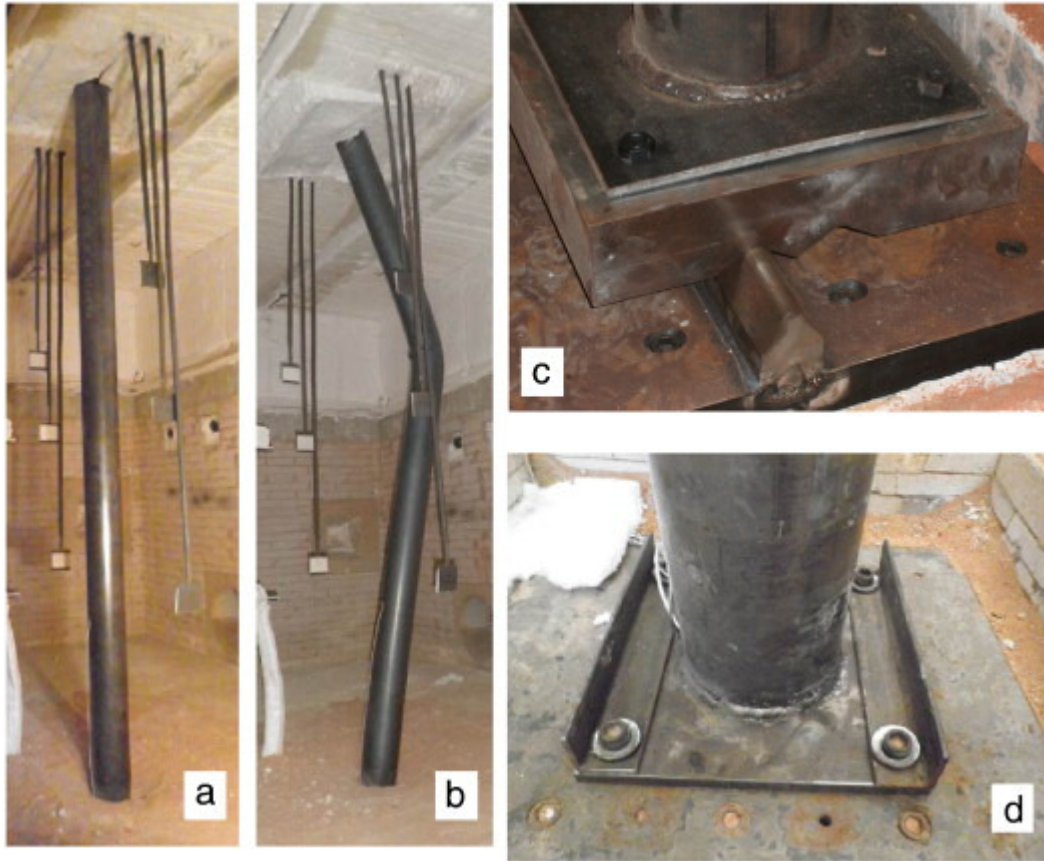


Fig. 6.8 Column inside the furnace (a) column before the test; b) column after the test; c) pinned support with eccentricity; d) fixed support. Reprinted from Moliner *et al.* (2013), with permission from Elsevier.

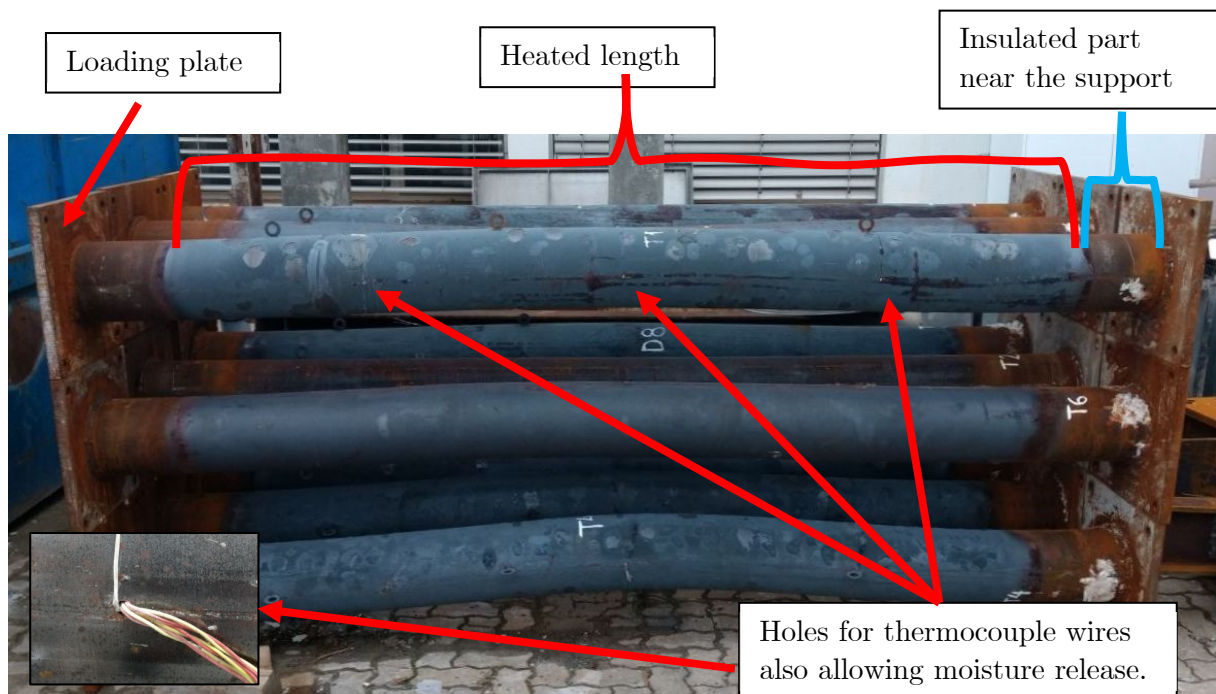


Fig. 6.9 Junkyard at the University of Coimbra (photo by the author).

Now, let us compare similar columns tested throughout different experimental campaigns. For an easier discussion, similar columns are grouped in Table 6.1.

Table 6.1 Selection of columns from NRC tests (Lie & Chabot 1992), for which direct comparisons are possible.

ID	D (mm)	t (mm)	$f_y$ (MPa)	$f_{c,test}$ (MPa)	Concrete	BC	ecc. (mm)	Load (kN)	Failure mode	FRT (min)
C05	168.3	4.78	350	32.7	S, NSC	F-F	0	150	B	76
C06	168.3	4.78	350	32.7	S, NSC	P-P	0	150	B	60
C15	219.1	8.18	350	31.9	S, NSC	P-P	0	525	B	73
C16	219.1	8.18	350	31.9	S, NSC	P-P	34	525	B	33
C17	219.1	8.18	350	31.7	S, NSC	F-F	0	525	B	82
C44	273.1	6.35	350	38.7	CS, NSC	F-F	0	715	B	178
C45	273.1	6.35	350	38.2	CS, NSC	F-F	0	712	C	144

Aggregate: S – siliceous, CS – carbonate and siliceous.

**Example of boundary conditions influence:** Two sets of columns from Lie & Chabot (1992) can be used to depict the influence of support type and eccentricity. The fire resistance time for columns C05 (fixed-fixed) and C06 (pinned-pinned) was 76 and 60 minutes, respectively (Table 6.1). The C06 column is analysed two paragraphs later, showing the pinned BC was most likely improperly executed.

**Example of boundary conditions and eccentricity influence:** Another set of columns that may serve as a direct comparison consists of columns C15, C16, and C17. The fixed-fixed column C17 presented the highest FRT (82 minutes). The time decreased to 33 minutes when the same load with an eccentricity of 34 mm ( $0.155 \cdot D$ ) was used. Changing boundary conditions from FF to PP decreased the FRT of an axially loaded column from 82 to 73 minutes.

An important point is to be made regarding the discrepancies between assumed and actual boundary conditions. Concerning numerical simulations, most researchers omitted columns C06, C15 and C16. They were not present in studies of, e.g. Xiong & Liew (2016), Xiong & Liew (2018), Liu et al. (2019), Yang et al. (2020), Li et al. (2022b). It seems that only Espinos (2012) concluded that due to the likelihood of improper support, fixed-pinned (FP) boundary conditions should be employed when simulating the fire behaviour of columns that were described as pinned-pinned (PP) by Lie & Chabot (1992). The author of this thesis arrived at similar conclusions during the numerical analysis. Pictures of columns with pinned-pinned boundary conditions and their fixed-fixed counterparts are presented in Fig. 6.10.

This leaves us with an interesting conclusion – none of the studies in the validation domain studied the effect of varying boundary conditions explicitly (and reliably). Only Espinos et al. (2014) showed the results for PP (column 02) and FP (column 03). Other than that – each study employed a single type of boundary conditions – PP (Wainman & Toner 1992, Han et al. 2003), FP (Espinos et al. 2014), or FF (Lie & Chabot 1992).

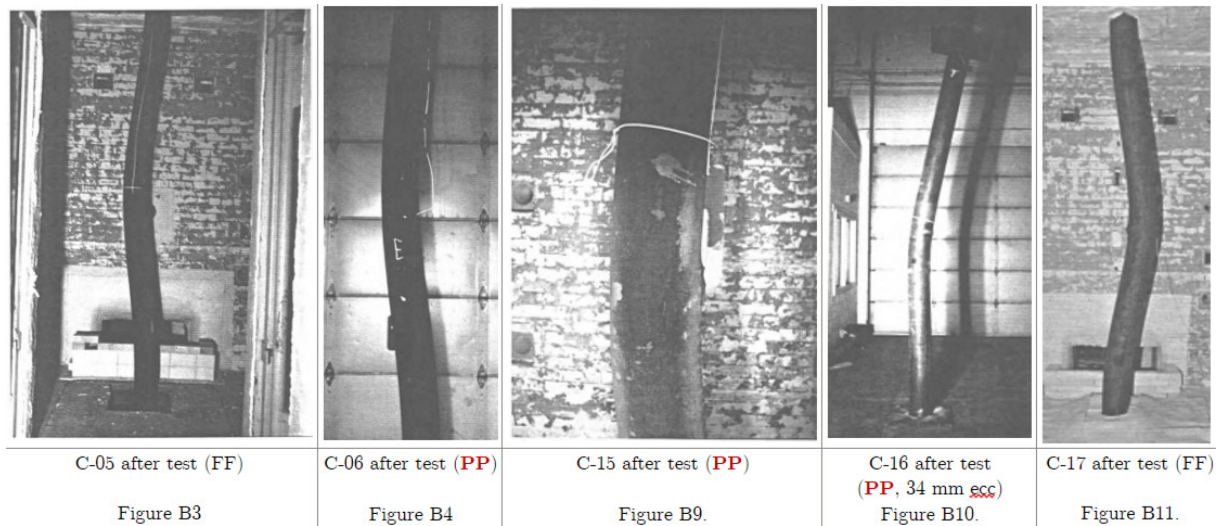


Fig. 6.10 Columns with PP boundary conditions and their FF counterparts (Lie & Chabot 1992).

**Duplicate column with different failure modes:** Lie & Chabot (1992) tested a pair of similar columns (C44 and C45), where one failed by buckling after 178 minutes, and the other failed with compression after only 144 minutes. No explanation for this behaviour was given in the report.

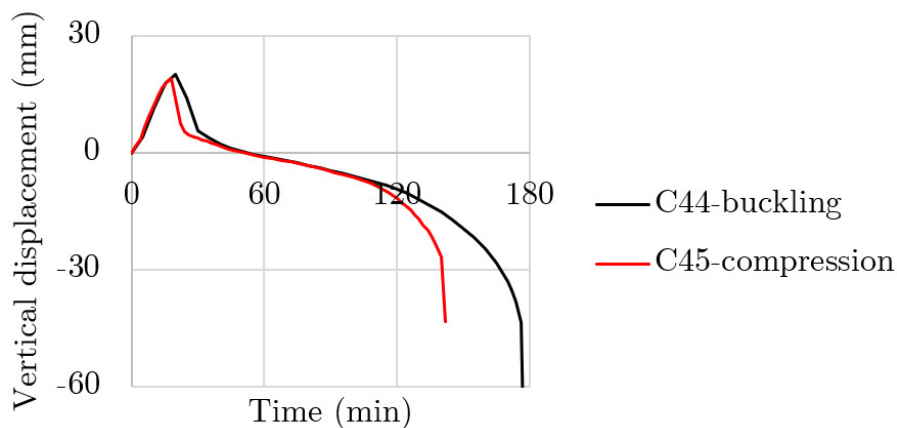


Fig. 6.11 Duplicate column with different failure modes. The two columns differed only slightly in strength (by 0.5 MPa) and load (3 kN) yet displayed two different failure modes.

### 6.2.3. Effect of load level (20, 40, 60 %)

The most exhaustive test programme in terms of the influence of load level and eccentricity was carried out at the UPV. The authors (Romero et al. 2011, Moliner et al. 2013) investigated a single geometry ( $D \times t = 156 \text{ mm} \times 6 \text{ mm}$ ), filled with three types of concrete. In terms of load, the parameters were: 20 %, 40 %, or 60 % of load utilisation, and eccentricities of 0 mm, 20 mm, or 50 mm. Their experimental results are presented in the following figures. Fig. 6.12 depicts the axial displacement – time relationship of three columns with F-P boundary conditions (under load levels equal to 20 %, 40 %, and 60 %). For comparison, a supplementary column with P-P boundary conditions was also tested. It can be observed that increasing load has an adverse effect on FRT. Furthermore, two columns displayed the type A behaviour and failed without the mechanical contribution of the core in the last phase of the test.

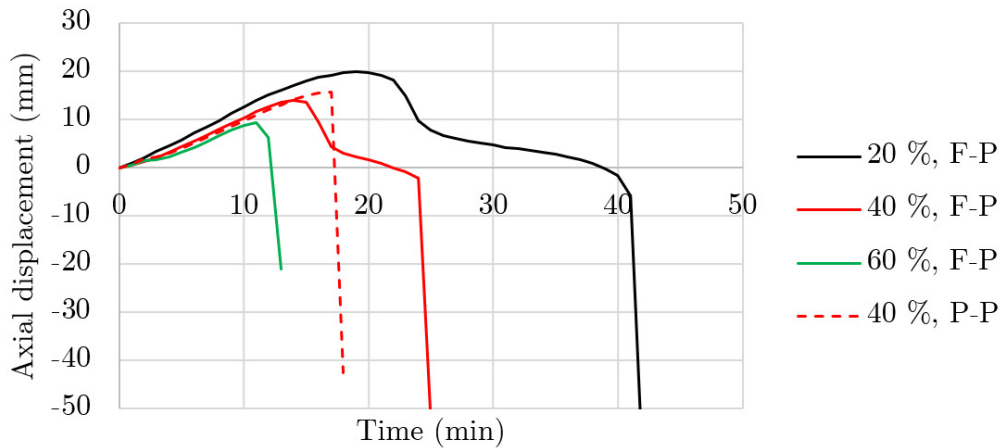


Fig. 6.12 Effect of load level (20 %, 40 % and 60 %) on the fire behaviour of CFST columns studied by Romero et al. (2011). F-P and F-F denote boundary conditions.

The effect of eccentricity (0 mm, 20 mm, 50 mm) for columns loaded at 20 % and 40 % of their load-bearing capacity is presented in figures Fig. 6.13 and Fig. 6.14, respectively. The clear effect of increasing eccentricity is visible in Fig. 6.13. Columns loaded to 40 % displayed a different behaviour (Fig. 6.14), where a 50 mm eccentricity did not influence the FRT compared to axially loaded columns. No explanation of such behaviour was found. The axial displacement during stage S1 shows that heating conditions in the two tests were similar.

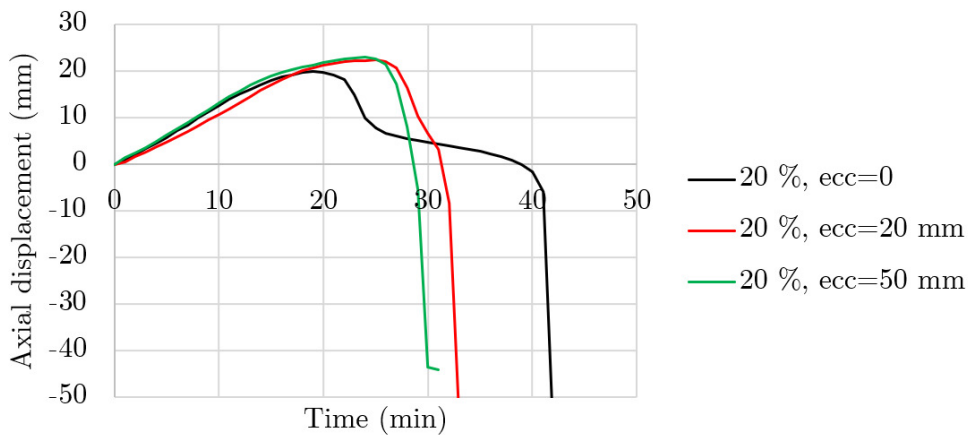


Fig. 6.13 Effect of eccentricity on columns loaded at 20 %.

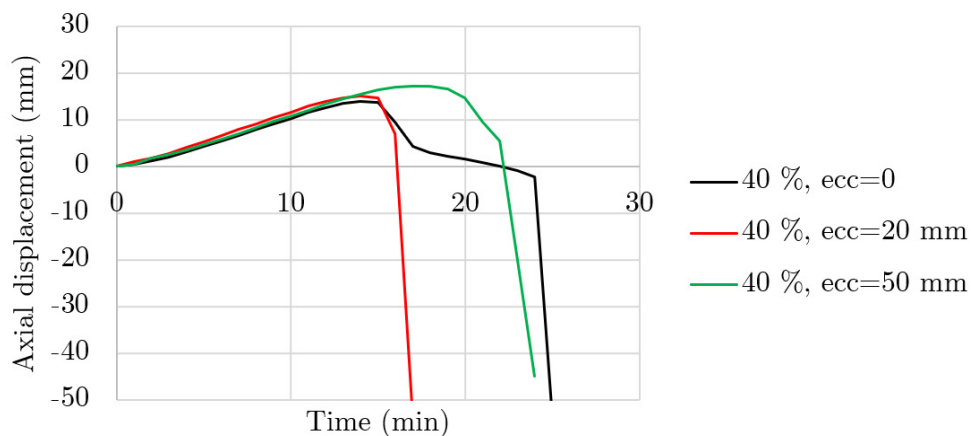


Fig. 6.14 Effect of eccentricity on columns loaded at 40 %.

Ali et al. (2016) tested 9 elliptical CFST columns. While elliptical cross-sections are not studied here, there are two reasons why those tests are mentioned. Firstly, it is the only available test of the CFST column's performance under hydrocarbon fire. Secondly, the shape of the displacement-time graphs indicates that the third stage did not develop. Fig. 6.15 depicts axial displacement-time graphs for 6 columns tested under three load levels (20 %, 40 %, and 60 %) without (solid line) or with (dashed line) concrete filling. It can be observed that (a) the lower the load, the higher the FRT and maximum displacement. For two out of three load utilisations (20 % and 40 %), concrete filling prolonged the FRT by two to five minutes. As the third stage did not develop, it is an example of columns, where concrete acted only as a heat sink and did not contribute to the load-bearing function in fire conditions.

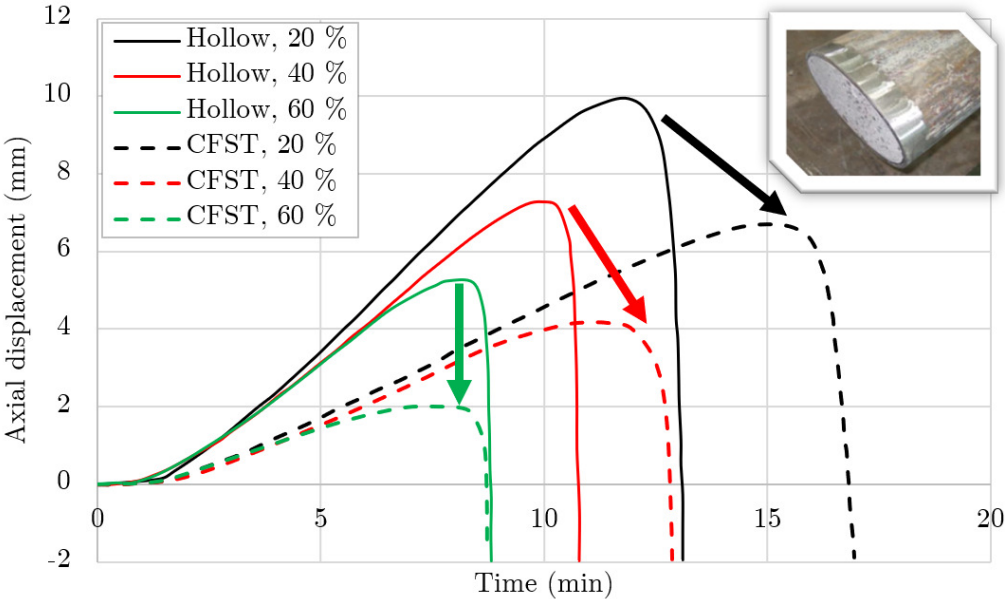


Fig. 6.15 Displacement-time graphs of 6 columns tested by Ali et al. (2016). Elliptical columns, with the same external dimensions under three load levels (20 %, 40 %, 60 %), either hollow (solid line) or filled with concrete (dashed line). The third stage did not develop (concrete core almost obsolete in fire conditions).

#### 6.2.4. The effect of infill

A set of 6 columns (C40, C41, C42, C46, C47 and C48) with similar geometry (273.1 mm x 6.35 mm tube) and load (1050 kN) but with different filling was tested by Lie & Chabot (1992). Column C47 differed in yield strength, but this is not a decisive parameter of the CFST column during fire. For ease of discussion, their selected properties are presented in Table 6.2.

Table 6.2 Selection of columns from NRC tests for which direct comparisons are possible.

ID	D (mm)	t (mm)	$f_y$ (MPa)	$f_{c,test}$ (MPa)	Concrete	BC	ecc. (mm)	Load (kN)	Failure mode	FRT (min)
C40	273.1	6.35	350	46.5	NSC	F-F	0	1050	C	106
C41	273.1	6.35	350	50.7	NSC	F-F	0	1050	C	76
C42	273.1	6.35	350	55.4	HSC	F-F	0	1050	C	90
C46	273.1	6.35	*	82.2	HSC	F-F	0	1050	C	48
C47	273.1	6.35	300	107.0	HSC	F-F	0	1050	B	51
C48	273.1	6.35	350	46.7 (RC)	NSC	F-F	0	1050	B	188
C49	273.1	6.35	350	47.0 (RC)	NSC	F-F	0	1900	B	96

Aggregate: S – siliceous, CS – carbonate and siliceous; Columns C48 and C49 were reinforced with four 19.5 mm rebars. \*There are discrepancies in the description of steel used for C46 – 350 MPa according to NRC 611, and 300 MPa according to Kodur & Latour (2005).

The vertical displacement-time relationship recorded during fire resistance test is shown in Fig. 6.16. Surprisingly, the effect of filling was not obvious, as for concrete strengths of 46.5 MPa, 50.7 MPa, 55.4 MPa, and 82.2 MPa, the respective FRTs were 106 min, 76 min, 90 min, and 48 min. A rebar-reinforced 46.7 MPa concrete-filled column with the same geometry and load (C48) failed after 188 minutes. A similar column (C49) with a higher load (1900 kN) failed after 96 minutes. Only two circular columns with rebars were tested in NRC (C48 and C49), but both clearly show the tremendous influence of rebars on the fire resistance time.

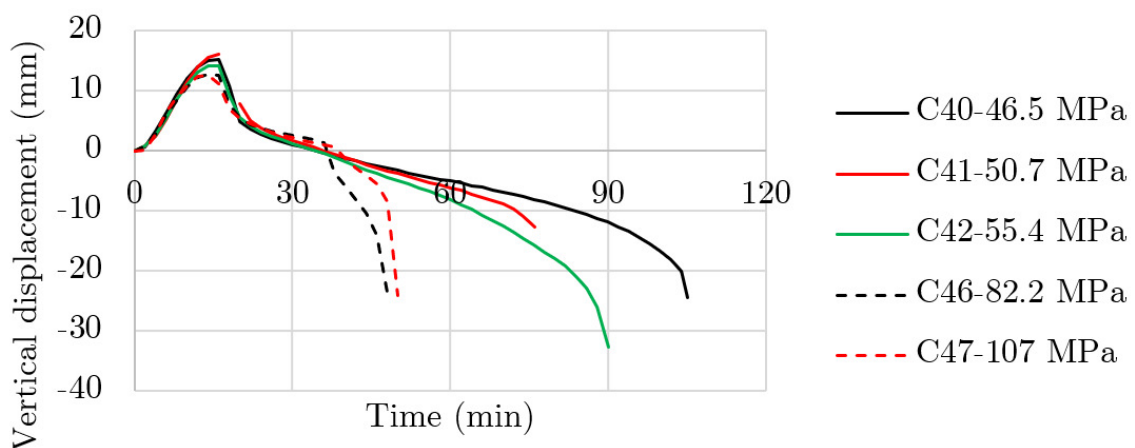


Fig. 6.16 Vertical displacement-time recorded during tests of columns that differed mainly in concrete compressive strength and/or mix design.

It is interesting to compare the fire resistance time of columns C40 and C41, as they differ only slightly by the strength of the filling material. The filling of both C40 and C41 columns was made of a single pour of concrete (pour No. 7 in the [Lie & Chabot \(1992\)](#) report) with a 28-day strength of 43.0 MPa. Contrary to the expected outcome, a column with a 50.7 MPa concrete filling failed 30 minutes earlier than a column with 46.5 MPa concrete filling (106 minutes compared to 76 minutes). In both cases, the strength on the test day is given. Column C41 was tested in October 1985, and C40 was tested in March 1986. This constitutes the erratic behaviour mentioned by [Lie & Chabot \(1990\)](#). Therefore, column C41 was excluded from further analysis. Columns C42, C46, and C47 are only mentioned here for reference, as they were made of HSC and were not included in the validation process.

**6.2.5. Local buckling**

Local buckling of steel tubes might be critical for their load-bearing capacity at ambient conditions ([Schneider 1998](#), [Kucukler 2020](#)). In fire conditions, local buckling of CFST is often observed. However, it is not the governing mechanism of failure. Local buckling might occur; however, it has not been shown as a reason for global failure during fire resistance tests. [Romero et al. \(2011\)](#) and [Moliner et al. \(2013\)](#) did not report local buckling. [Kim et al. \(2005\)](#) reported its occurrence near the supports (elephant’s foot). [Han et al. \(2003\)](#) witnessed local buckling occurring in some cases. The analysis of photographic documentation given by [Lie & Chabot \(1992\)](#) indicated cases of local buckling. However, the visual observations in the above-mentioned sources were made post-fire. The observations made by other researchers during fire tests revealed that local buckling was not the reason for failure. [Shintani et al. \(2020\)](#) observed local buckling 30 minutes into the fire test, yet the fire resistance time was between 70 and 265 minutes. Similarly, in the tests by [Wainman & Toner \(1992\)](#), local buckling occurred during the second stage of the test (as marked in Fig. 6.17) and did not influence the overall column performance. Limiting the local buckling was one of the primary reasons for introducing gaps in the steel tube ([Liu et al. 2019](#)). However, breaking the longitudinal continuity of thin steel tubes did not prevent local buckling in the late stages of fire resistance tests.

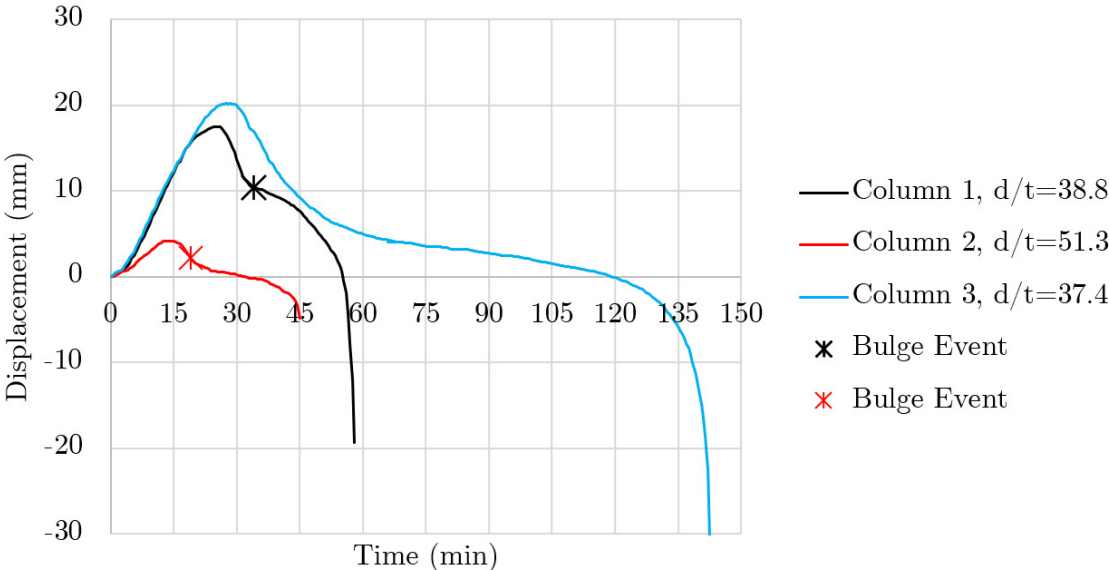


Fig. 6.17 Displacement-time relationships for three columns tested by [Wainman & Toner \(1992\)](#), with marked 'bulge events'. Evidence that local buckling might not impair the fire resistance time of CFST columns.

### 6.2.6. Effect of steel fibre

Steel fibre does not hinder spalling. However, in conjunction with PP fibres, it may be used as an effective way to mitigate spalling in UHPC (Li et al. 2019). As far as strength is concerned, steel fibre does not influence the compressive strength. However, it increases the ductility of concrete in the post-critical range (Lai et al. 2019). The effect of steel fibre is more pronounced for tensile strength (van der Merwe 2022).

Kodur & Lie (1995) were the first to experiment on fire resistance of steel fibre-reinforced CFST columns; however, they did not test comparative columns with similar geometry. Though, based on other similarities, the authors observed an increased fire resistance of fibre-reinforced concrete-filled columns, compared to column filled with plain concrete.

Regarding the influence of steel fibre on fire resistance time, Ukanwa et al. (2018) tested several square bar-reinforced and steel fibre-reinforced columns. Still, their results were inconclusive regarding the SFR influence. No effect was observed in the case of slender CFST columns (Romero et al. 2011, Moliner et al. 2013), where the difference between plain and SFR concrete did not exceed 3 minutes for most of the tested columns. In their research on slender columns, no effect of steel fibre was observed for both NSC and HSC filling.

### 6.2.7. The moisture content of concrete

The literature study reveals that measured moisture content in concrete ranges from less than 1.0 % to 6.6 %. Kim et al. (2005) reported a 6.6 % average moisture content at the time of testing (from 30 to 60 days after casting). Lie & Chabot (1992) reported the moisture content corresponding to 85-95 % relative humidity. According to EN 1363-1, a relative humidity level of 50% would result in a moisture content of 1-3 %, while a relative humidity level of 100% corresponds with 5% moisture. The moisture content in terms of water mass to the mass of dry material is a function of the porosity of concrete. Hence, precise numbers could not be derived from the statement by Lie & Chabot (1992). Detailed results are given by Espinos et al. (2014). For normal strength concrete, the moisture content established with oven-drying at 150 °C (not 105 °C) ranged from 1 % to 6.6 %, with a mean value of 3.2 %. Notably, the results reported for batches of NSC used in plain and reinforced CFST columns were inconsistent. This indicates a high variability, which, to some extent, further influences the temperatures measured with the thermocouples. What is rather unfortunate is that the details regarding curing conditions used for moisture content measurement are usually unavailable.

Various researchers used different specimens for the determination of concrete compressive strength. The compressive strength of concrete determined by testing cylinders was used for numerical modelling. If such data was not given, the following formulas recommended by a background paper to the fib Model Code 2010 (Müller et al. 2013, fib 2010) were used:

$$f_{c,cube,150} = 0.97 \cdot f_{c,cube,100} \quad (6.3)$$

$$f_{c,cyl,150} = 0.80 \cdot f_{c,cube,150} \quad (6.4)$$

where  $f_{c,cube}$  is the compressive strength of concrete determined by testing cube (150 mm or 100 mm), and  $f_{c,cyl}$  is the compressive strength of concrete determined by testing cylinders. Where detailed data regarding the specimen size was not recorded (Wainman & Toner 1992), it was assumed that standard 150 mm specimens were used.

At elevated temperatures, the free water evaporates along with the physically bound and chemically bound water. The model of the specific heat of concrete (Fig. 4.2) reflects the additional energy absorbed during the evaporation. As elaborated earlier, the Eurocode model gives the 'effective properties'. Therefore, complex thermo-hydro-mechanical analysis of moisture transport is not necessary to establish the temperature field inside the cross-section. The moisture content is related to factors such as porosity and relative humidity of the surrounding air. This can be clearly seen in the experimental results, where sorption isotherms are reported (Davie et al. 2018).

There is a large discrepancy in values adopted by various researchers in their numerical analyses. Tao & Ghannam (2013) reviewed several works and found that other researchers adopted moisture content values from 3 to 10 % (3, 4, 4.35, 5, 7, or 10 %) to fit the calculated results to those obtained experimentally. Many researchers fit their models to the experimental data. However, the previous analysis of temperatures inside concrete recorded by TCs shows that relying on a model calibrated using a single specimen is prone to errors.

### 6.2.8. Thermal gap conductance

Two important phenomena influencing heat transfer between steel tube and concrete core shall be distinguished: thermal contact conductance and air gap conductance. The former is influenced by micro- and macroscopic irregularities, described as surface roughness. For most metallic surfaces, the actual relative contact area is 1 to 2 % under contact pressure of about 10 MPa (Madhusudana 2014). This phenomenon is important in processes related to the efficient cooling or manufacturing of metallic objects (Sadowski & Stupkiewicz 2010). In general, heat transfer between bodies in contact is due to the actual contact area and air (or other substances) between bodies. At the level of pores or small gaps, radiation also plays a role. As the size of those gaps is so small that they cannot be reasonably captured in numerical models of full-scale columns, the simplification of using thermal conductance is employed.

In CFST columns, the contact between the steel tube and the concrete core is lost at the beginning of the fire exposure. As the steel tube circumference elongates, the contact is lost. That is why the phenomenon with respect CFST columns is described as air gap conductance or thermal resistance at the steel-concrete interface.

The separation of the steel tube from the concrete core, and the three stages described before were not observed until the 1970s. Ingberg et al. (1921) tracked vertical displacements at the top of the column. However, due to the extensive load, they did not record the third stage of the deformation, where the core carries the load. Notably, for a column with a reinforced core, the results were not presented in the report. The behaviour specific to CFST columns was observed years later and described by Grandjean et al. (1980). As far as numerical modelling is concerned, until the work of Ding & Wang (2008), most authors assumed the perfect contact between steel tube and concrete core - both on the thermal and mechanical level.

The air gap conductance can be macroscopically expressed in  $W/(m^2 \cdot K)$ . The values employed by different researchers in their numerical studies vary from infinite value for perfect contact to the values of the order of 100  $W/(m^2 \cdot K)$ . Usually, values of 100  $W/(m^2 \cdot K)$  (Zhou et al. 2021), 150  $W/(m^2 \cdot K)$  (Yao et al. 2016), or 200  $W/(m^2 \cdot K)$  (Ibáñez et al. 2015) are employed. A temperature-dependent relationship was proposed by Ghojel (2004), who performed a study on

small concrete-filled tubular columns filled with normal strength concrete, and suggested a temperature-dependent relationship. However, the Ghojel's calibration was based on assumed concrete thermal properties according to ENV version of the Eurocode, and the test was poorly controlled. Moreover, only one specimen was used for the model calibration, which consisted of a galvanised steel tube filled with 28-day concrete. [Espinosa \(2012\)](#), in her PhD, concluded that Ghojel formulation provided the best results; however, due to simplicity, used  $200 \text{ W}/(\text{m}^2\cdot\text{K})$  in subsequent works ([Ibáñez et al. 2015](#)).

#### **6.2.9. Concrete aggregate type**

[Wainman & Toner \(1992\)](#) used siliceous aggregates, [Romero et al. \(2011\)](#), and [Moliner et al. \(2013\)](#) used calcareous aggregates. [Han et al. \(2003\)](#) used a mix of siliceous and calcareous aggregates. Even though in [Lie & Chabot \(1992\)](#) some of the columns were described as carbonate (calcareous), the carbonate aggregate mass proportion in all aggregate was below 80 %. Hence, such concretes should be classified as siliceous in the Eurocode's nomenclature. Even though the aggregate influences the thermal conductivity of concrete, the available data does not allow to form strong relationships. Moreover, as the aggregate type is not a parameter in Eurocode's thermal conductivity models, this influence was not investigated further.

### **6.3. Summary**

In this chapter, several factors influencing the FRT were identified. Some affected the fire performance of CFST columns only slightly and could be disregarded in the subsequent numerical analysis. Other factors, such as BCs or load level, influence the fire resistance times. Sometimes, the behaviour is erratic. This should only encourage further numerical investigations aimed at studying several factors in a way more systematic than possible by full-scale testing.

## 7. Numerical model of CFST column in fire conditions

### 7.1. Description of the numerical model

A parametrical numerical model is formulated to study the behaviour of CFST columns. A parametrised computational approach is necessary to include a large number of specimens in the validation domain. A parametrised approach allows to investigate numerous parameters and to make relevant predictions based on an extensive study.

Fig. 7.1 outlines the workflow. First, the available test programmes and numerical studies are reviewed, and the key parameters are identified. Then, the relevant data are collected from papers and research reports and put into a database. Matlab is used to read the data from the database. Python scripts are created to generate Abaqus (version 6.12) input files.

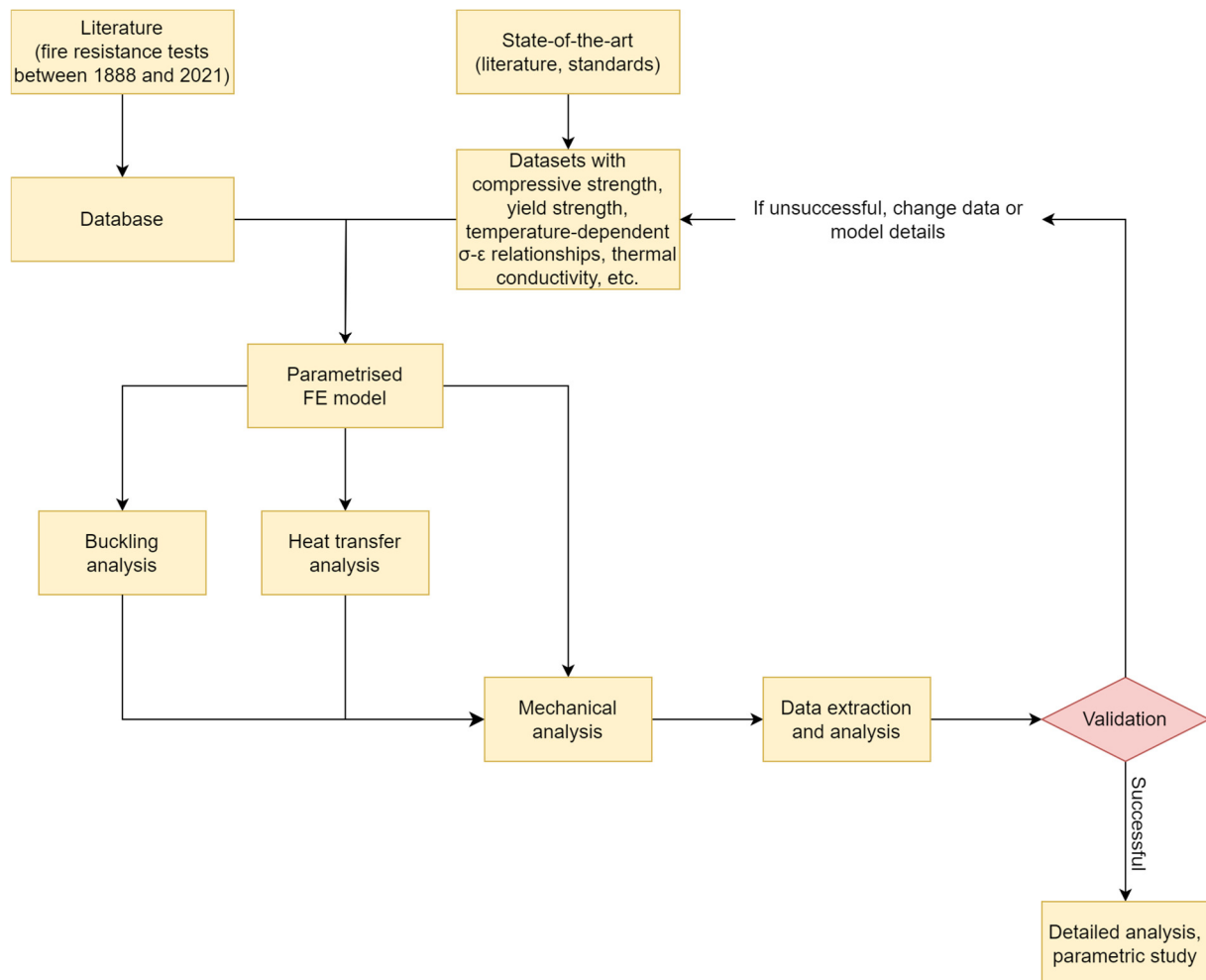


Fig. 7.1 Flowchart presenting the model development.

Two types of data are used: (1) database with a detailed description of investigated columns (numerical values of text) and (2) datasets (python tuples) containing, e.g.  $\sigma$ - $\epsilon$  relationships for steel and concrete (for ambient, fire, and post-fire conditions), and other temperature-dependent data, such as thermal conductivity (e.g., lower, and upper limit of thermal

conductivity of concrete), specific heat, density, modulus of elasticity, thermal expansion, temperature-time curves. Fig. 7.2 depicts a numerical model representing a typical column in a fire resistance test.

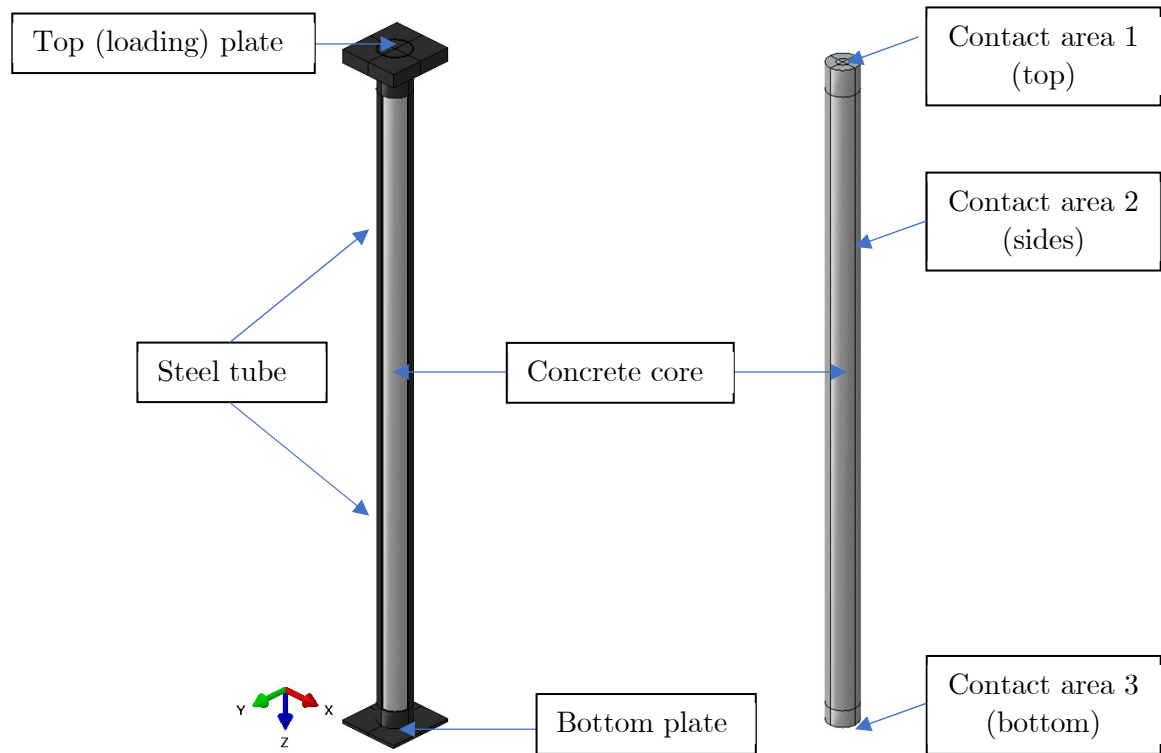


Fig. 7.2 An overview of the numerical model representing a typical column in a fire resistance test (steel tube with plates at both ends, filled with concrete).

The database includes all information relevant to building a model of a column, that is:

- (1) length of the column between loading plates –  $l$  (mm),
- (2) diameter of the tube –  $D$  (mm),
- (3) thickness of the tube –  $t$  (mm),
- (4) top loading plate dimensions – x-direction (mm),
- (5) top loading plate dimensions – y-direction (mm),
- (6) bottom loading plate dimensions – x-direction (mm),
- (7) bottom loading plate dimensions – y-direction (mm),
- (8) boundary conditions (BC) at the top – text: 'F' – fixed, 'P' – pinned,
- (9) boundary conditions (BC) at the bottom – text: 'F' – fixed, 'P' – pinned,
- (10) the degree of axial restraint if boundary conditions were other than pinned or fixed –  $K_{as}$  (N/mm),

- (11) the degree of rotational restraint if boundary conditions were other than pinned or fixed, x-direction –  $K_{rs,x}$  (N·mm/rad),
- (12) the degree of rotational restraint if boundary conditions were other than pinned or fixed, y-direction –  $K_{rs,y}$  (N·mm/rad),
- (13) loading force –  $N_{fi}$  (kN),
- (14) eccentricity in x direction –  $e_x$  (mm),
- (15) eccentricity in y direction –  $e_y$  (mm),
- (16) number of rebars –  $n$  (-),
- (17) area of each rebar –  $A_s$  (mm<sup>2</sup>),
- (18) axis distance of rebars –  $a$  (mm),
- (19) length of the fire-insulated part of the column near the top end – value (mm),
- (20) length of the fire-insulated parts of the column near the bottom end - value (mm),
- (21) temperature-time curve in the test – text, implying a data set.

And material data:

- (22) concrete aggregate type – text: 'calcareous', 'siliceous',
- (23) compressive strength of concrete –  $f_c$  (MPa),
- (24) yield strength of tube –  $f_y$  (MPa),
- (25) yield strength of rebars –  $f_s$  (MPa),

Based on the concrete aggregate type (22) and compressive strength of concrete (23), scripts refer to data stored as a 'tuple' data type. For example, when the Eurocode  $\sigma$ - $\epsilon$  model is used for a siliceous aggregate concrete with a compressive strength of 30 MPa, data is imported from two previously prepared text files: "*concrete\_young\_poisson\_02\_siliceous\_30.txt*" and '*concrete\_strength\_EC\_siliceous\_30.txt*'.

In the former, the modulus of elasticity and Poisson's ratio are defined as a function of temperature:

**(modulus of elasticity (MPa), Poisson's ratio (-), temperature (°C)):**

{((17825.9850, 0.2000, 20), (16582.3116, 0.2000, 30), (15500.8565, 0.2000, 40), ..., (4.9913, 0.2000, 1180))}

The latter file contains true plastic stress and true plastic strain as a function of temperature:

**(true plastic stress (MPa), true plastic strain (-), temperature (°C)):**

((12.008078094959824, 0.0, 20), (13.577657439478505, 2.545937038018315e-06, 20), (15.115382528989533, 7.550144211557024e-06, 20), (16.613921699199366, 1.4744269488315364e-05, 20), (18.065581301017044, 2.4559911805447287e-05, 20), (19.462484687440867, 3.74389358948526e-05, 20), (20.79676845758362, 5.382246340905031e-05, 20), (22.060789243511607, 7.413927261753182e-05, 20), (23.247332843478265, 9.879406647534533e-05, 20), (24.349816544595065, 0.00012815612274982542, 20), (25.36247518886321, 0.0001625488561103434, 20), (26.28052200294159, 0.00020224079591900086, 20), (27.100276433095306,

0.0002474384149607999, 20), (27.819253109889107, 0.00029828113871278915, 20), (28.436208436989283, 0.0003548387318109637, 20), (28.95114391998177, 0.000417111113106206, 20), (29.365267963406037, 0.0004850304897918349, 20), (29.68092021743218, 0.0005584656193506252, 20), (29.90146444493542, 0.0006372278015291408, 20), (30.031157169521578, 0.0007210782558832005, 20), (30.074999999999996, 0.000809736404266552, 20), (30.072762573750925, 0.0008347992640620901, 20), (30.06463134814753, 0.0008601921316611146, 20), (30.050729501828002, 0.0008859080970341777, 20), (30.03118215704747, 0.0009119401411188154, 20), (30.006116147420922, 0.0009382811488491192, 20), (29.97565978986003, 0.0009649239219487128, 20), (29.93994266122963, 0.0009918611914611767, 20), (29.899095380205356, 0.0010190856299864897, 20), (29.853249394770117, 0.0010465898636024685, 20), (29.80253677574303, 0.001074366483446471, 20), (29.74709001669126, 0.001102408056941246, 20), (29.687041840532316, 0.0011307071386432522, 20), (29.62252501309217, 0.001159256280702091, 20), (29.553672163844546, 0.0011880480429157716, 20), (29.480615614016408, 0.0012170750023749546, 20), (29.403487212207256, 0.0012463297626834758, 20), (29.322418177633196, 0.0012758049627524667, 20), (29.237538951071528, 0.0013054932851611597, 20), (29.14897905354966, 0.0013353874640854699, 20), (29.056866952789697, 0.001365480292789284, 20), (24.34786147277678, 0.002521308535956818, 20), (19.182671498187204, 0.003701933408287594, 20), (14.962398131820995, 0.004828757519836633, 20), (11.78785377528511, 0.005896126918716617, 20), (9.439198744294213, 0.006916375552085723, 20), (7.689407948386671, 0.007902240449422518, 20), (6.365918404742503, 0.008863403427597488, 20), (5.347429178070631, 0.00980667060748015, 20), (4.550171992440907, 0.01073674260354647, 20), (3.916063513340246, 0.011656879155772487, 20), (3.404321694451091, 0.012569369434834598, 20), (2.98586086326164, 0.013475846465947131, 20), (2.639594778093201, 0.014377494519545965, 20), (2.349989497510185, 0.015275186390142614, 20), (2.105425851894196, 0.016169575258213963, 20), (1.8970882848538102, 0.017061157023858048, 20), (1.7181994601689172, 0.01795031324373593, 20), (1.5634850228369697, 0.018837341156855866, 20), (1.4287937743190662, 0.019722474991950092, 20), ..., (0.0338261866593, 0.0, 1180), (0.0469151698229, 2.79715098126e-05, 1180), ..., (0.0566139519133, 0.035063791453, 1180))) - (.

Furthermore, other variables are used to control the values that are usually not measured:

- (26) thermal conductivity of concrete – text: 'upper', 'lower', 'EC2020',
- (27) moisture content of concrete – value (%),
- (28) location of the peak specific heat of concrete – value (°C).

Excerpt from tuple representing the upper limit of thermal conductivity:

**(thermal conductivity (mW/(mm·K)), temperature (°C)):**

((1.9514, 20.0), (1.9274, 30.0), (1.9037,40.0), (1.8801, 50.0), (1.8568, 60.0), (1.8337, 70.0), ..., (0.5996, 1200.0)) -.

Tuple representing specific heat of concrete – peak value at 115 °C corresponding to 3 % moisture content:

**(specific heat (mJ/(tonne·K)), temperature (°C)):**

((900000000.0, 20.0), (900000000.0, 100.0), (2020000000.0, 115.0), (1000000000.0, 200.0), (1100000000.0, 400.0), (1100000000.0, 1200.0))

And excerpt from a tuple representing concrete density:

**(density (tonne/mm<sup>3</sup>), temperature (°C)):**

((2.34931e-09, 20.0), (2.34696e-09, 30.0), (2.34461e-09, 40.0), (2.34227e-09, 50.0), ..., (2.07236e-09, 1200.0))

The peculiar units, such as tonne representing mass, milliwatt (mW), or millijoule (mJ), are used for consistency with the Abaqus built-in unit system.

To perform a successful numerical analysis, other parameters are required, such as thermal gap conductance, friction between tube and core, emissivity of steel surface, coefficient of convective heat transfer, and master-slave assignment for the contact pairs in the model.

Each column tested by [Wainman & Toner \(1992\)](#), [Romero et al. \(2011\)](#), [Moliner et al. \(2013\)](#), [Han et al. \(2003\)](#), [Lie & Chabot \(1992\)](#), and [Chabot & Lie \(1992\)](#) is thoroughly examined, described by the information listed above, and put into a database.

The Abaqus software (version 6.12) is used for numerical modelling. An interface between the database and Abaqus is defined to supply the software with relevant data. All relevant data, e.g.,  $\sigma$ - $\varepsilon$  relationships, were defined in separate text files and were loaded as an input to the model when necessary. Such an approach allowed to study the influence of several parameters based on a large validation domain in an automatised way.

Subsequently, Abaqus generates the input files for the solver. Input files are further modified to include factors such as imperfections. The analysis is submitted, and when the results are available, additional scripts are used to extract and analyse the results.

A sequential numerical analysis is carried out (Fig. 7.3). First, a relevant imperfection shape is determined. Second, a thermal analysis is performed. Lastly, based on the temperature field obtained from the thermal analysis, the fire-induced mechanical response of the column is calculated. Therefore, three submodels comprise the numerical model of a single column:

- (1) model used to obtain the relevant imperfection shape ('Buckling analysis'),
- (2) model used to calculate temperature field ('Heat transfer analysis'),
- (3) model used to calculate the mechanical behaviour of a column during a fire ('Mechanical analysis').

### *1. Buckling analysis*

The first analysis is used to supply the mechanical model with the relevant imperfection shape. A sinusoidal initial imperfection with a maximum value of  $l/1000$  at mid-length is used, where  $l$  is the length of each column between loading plates.

### *2. Heat transfer analysis*

The Heat transfer model considers the geometry of each column and the following factors:

- thermal actions during the relevant tests,
- temperature-dependent thermal properties of steel and concrete.

### *3. Mechanical analysis*

The mechanical response model considers the geometry of each column and the following factors:

- the geometrical imperfections (obtained from the Buckling analysis),
- the temperature field history (obtained from the Heat transfer analysis),
- temperature-dependent mechanical properties of steel and concrete,
- geometrical non-linear effects,
- non-linear material behaviour.

The main outputs from the last analysis are displacement, stress, strain, and temperature. Fig. 7.3 depicts models used for buckling, heat transfer, and mechanical analyses.

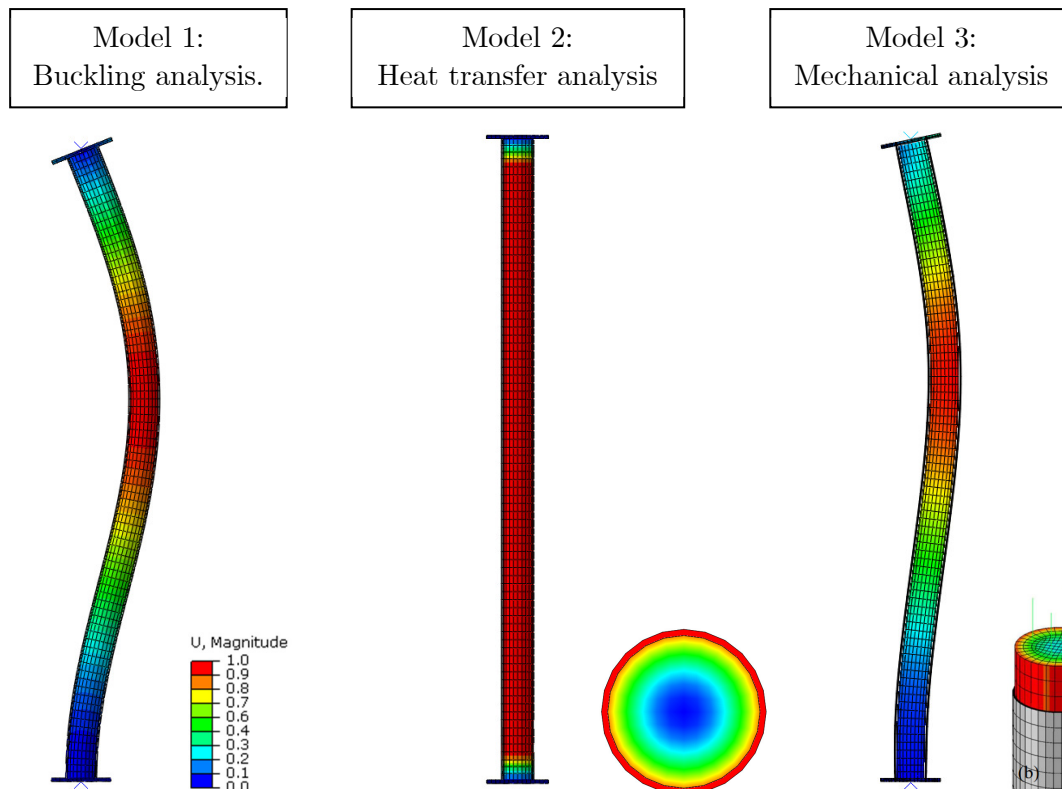


Fig. 7.3 Models used for buckling, heat transfer, and mechanical analyses.

### Postprocessing

After careful, manual examination of the initial results, it is possible to identify what data are relevant, quantify the accuracy of computations and identify any odd numerical behaviour. After the analysis is completed, another Python script is used to process the data, for example, to extract column designation, fire resistance time, and a history of vertical displacement at the top of each column. Furthermore, diagnostic data are also collected, such as a history of reactions at the bottom of the column, data regarding iterations needed for each increment of the computation, and the CPU time of each analysis. The Python script is also used to catch any errors that might have occurred during the analysis.

#### 7.1.1. Modelling of concrete and steel

The heat transfer within the column is modelled using the simple heat diffusion equation, therefore neglecting the water migration and pressure changes. Concrete thermal behaviour is modelled according to Eurocode 2 and Eurocode 4. An initial density of  $2350 \text{ kg/m}^3$  is assumed for all columns, following the relationship given in Fig. 4.1. Specific heat of concrete is modelled according to Eurocode 4, with the specific heat peak located at  $115 \text{ }^\circ\text{C}$ , corresponding to 3 % moisture content ( $2020 \text{ kJ}/(\text{kg}\cdot\text{K})$ ), see Fig. 4.2. The upper limit of thermal conductivity is chosen, as it was explicitly calibrated for composite structures (Fig. 4.3). The convective heat transfer coefficient of  $25 \text{ W}/(\text{m}^2\cdot\text{K})$  is assumed along the whole column length. The emissivity is set as a constant value equal to 0.7. Thermal expansion of steel and concrete is modelled according to the Eurocode. For the friction coefficient, thermal gap conductance, and

description of the steel-concrete interface, see chapter 7.1.2. The friction between steel and concrete is described in chapter 7.1.2 and in chapter 7.3. The finite element mesh is described in chapter 7.1.3. Strategies implemented to help the solver converge without premature failures included mesh alignment (chapter 7.1.2) and tweaking the solution controls and time incrementation rules (elaborated in detail in chapter 7.3).

A Drucker-Prager plasticity model is used for concrete. Two values of friction angle (30° and 36°) and three values of dilation angle (15°, 30°, and 36°) were initially studied. No significant changes were observed. Therefore, for all the analyses in this dissertation, the friction angle was assumed to be equal to 36°, the dilation angle equal to 36°, and the flow potential eccentricity of 0.1. Concrete is assumed to follow a linear elastic behaviour at each temperature up to a strain corresponding to  $0.4f_{c,\theta}$ . After reaching that strain, the Drucker Prager Hardening suboption is used to define the non-elastic part of the stress-strain curve – for the ascending and descending branches (see Fig. 4.10). The elasticity modulus is derived from equation (4.9) and the Poisson’s ratio is assumed to be independent of temperature and equal to 0.2.

The thermal properties of steel were modelled according to Eurocode 3 without any exceptions (chapter 4.3). Von Mises yield criterion is used with the stress-strain relationship and the reduction factors following the recommendations given in Eurocode 3 (chapter 4.4). The elasticity modulus is assumed as 210 GPa, and 200 GPa for structural and reinforcing steel, respectively. The temperature-independent value of the Poisson’s ratio is set at 0.3 for both the structural and reinforcing steel.

Stress-strain relationships presented in Fig. 4.10 (chapter 4.2.5) are used for concrete. They are defined as a function of initial concrete strength, temperature, and strain.

The linear-elliptical-linear relationships presented in Fig. 4.21 (chapter 4.4.2) are used for steel tube and rebars. Both relationships are defined by engineering strain and stress. Hence, the following expressions are used to recalculate engineering stress and strain to true stress and strain:

$$\begin{aligned}\varepsilon_{true} &= \ln(1 + \varepsilon_{eng}) \\ \sigma_{true} &= \sigma_{eng}(1 + \varepsilon_{eng})\end{aligned}\tag{7.1}$$

The influence of several other assumptions regarding material properties is further discussed in chapter 7.6.

The thermal elongation  $\varepsilon_{th}(\theta_i)$  is defined as the ratio between elongation  $\Delta l$  and initial length  $l$  (m/m). The thermal expansion coefficient  $\alpha$  at a given temperature ( $\theta_i$ ) ( $\frac{1}{^\circ\text{C}}$ ) is calculated as:

$$\alpha(\theta_i) = \frac{\varepsilon_{th}(\theta_i)}{(\theta_i - \theta_0)} = \frac{\Delta l}{l} \frac{1}{(\theta_i - \theta_0)}\tag{7.2}$$

where  $\theta_0$  is the initial temperature (usually 20 °C). The temperature-dependent thermal expansion coefficients are then used as an input to the model.

### 7.1.2. Steel-concrete interface

Several phenomena occur at the interface between concrete core and steel tube and must be modelled appropriately. This section provides details for the three models used for buckling, heat transfer and mechanical analysis.

In the buckling analysis, the nodes of the numerical model of the core and tube are tied. Consequentially, the relative movement between steel and concrete is not allowed.

In the thermal analysis, a gap thermal conductance is modelled. Four values of thermal gap conductance are studied: 10 W/(m<sup>2</sup>·K), 100 W/(m<sup>2</sup>·K), 200 W/(m<sup>2</sup>·K), and 10<sup>5</sup> W/(m<sup>2</sup>·K) (close to perfect heat transfer between bodies). A gap thermal conductance, relevant heat fluxes and their application area, are presented in Fig. 7.4.

In the mechanical analysis, the influence of friction between bodies is modelled. The Coulomb friction model is used, where the friction force is proportional to the friction coefficient ( $\mu$ ) and the contact normal pressure. The tangential behaviour contact property is used in Abaqus with the penalty friction formulation and a constant friction coefficient. In this study, two values are used:  $\mu = 0$  (frictionless) and  $\mu = 0.3$ .

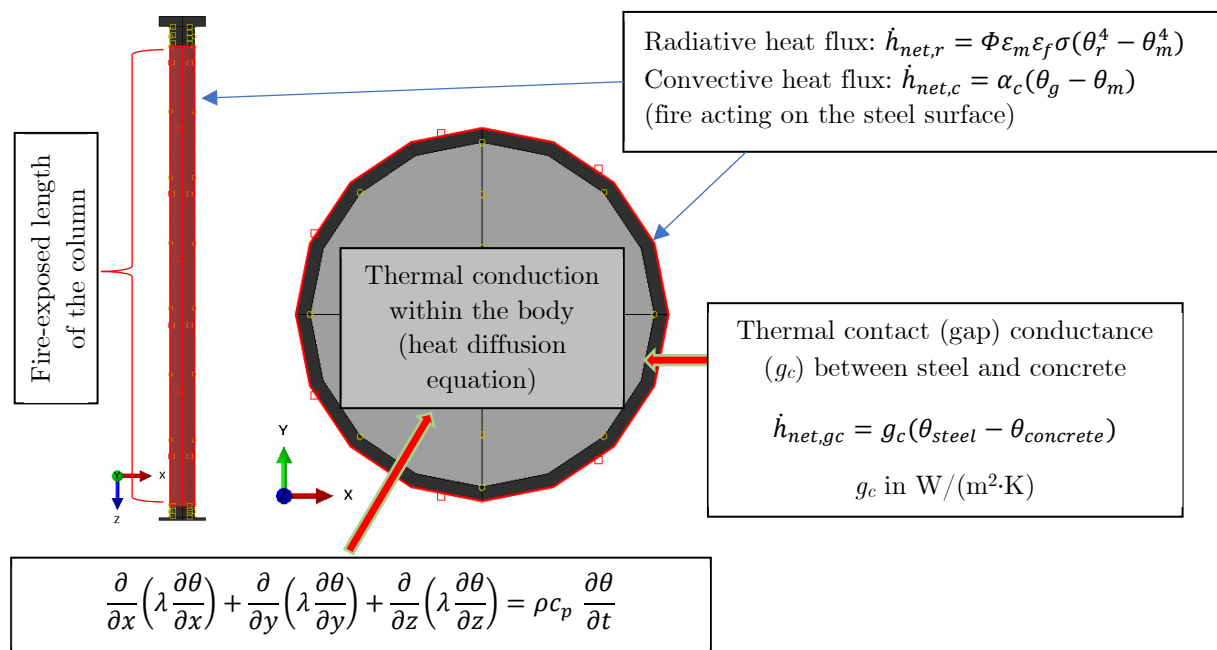


Fig. 7.4 Heat transfer within the column with a marked length of the column to which radiative and convective heat fluxes are applied directly.

For normal behaviour, contact property is used with the 'Hard' Contact utilising the classical Lagrange multiplier constraint enforcement method. Separation between tube and core after contact is allowed. Settings for the constraint enforcement method are defined to enforce constraints using a default contact pressure-overclosure relationship. The surface-to-surface contact is modelled by defining a contact pair consisting of a master and slave surface. The following contact pairs are distinguished: (i) contact between the bottom plate and concrete core, (ii) contact between the loading plate and concrete core, and (iii) contact between the side surface of the concrete core and the internal surface of the steel tube. For pair (i), the bottom plate is modelled as tied to the concrete core (relative movement is restricted). Surface-

to-surface penalty contact is modelled for contact pairs (ii) and (iii). The general recommendations for assigning master/slave surfaces require considering the mesh size and stiffness of the body. Since mesh discretisation of steel tube and concrete core is of comparable dimensions and the stiffness of both bodies changes with temperature, the preferred choice is not obvious. Hence, all possibilities for contact pairs (ii) and (iii) are investigated, revealing that the differences in the calculated fire resistance time are negligible.

### **7.1.3. Finite elements and finite element mesh**

Both core and tube are modelled as three-dimensional eight-node linear elements. In thermal analyses, continuum DC3D8 elements (a three-dimensional eight-node linear heat transfer brick) are used. To model rebars, DC1D2 elements are used. The corresponding continuum elements are used for mechanical analyses: C3D8R and T3D2. C3D8R is a three-dimensional eight-node linear brick with reduced integration and default hourglass control. Selected analyses utilised elements like modified 10-node tetrahedral C3D10M and C3D20R. However, they were computationally expensive and did not provide better results.

The initial modelling revealed that several analyses failed prematurely due to contact issues. Those issues were overcome with the following four techniques (depicted in Fig. 7.5).

- (i) Dividing the cross-section into four quarters – technique (i) enforced a more structured mesh in the tube and core, which prevented some contact issues, especially early in the analysis.
- (ii) Aligning the position of nodes at the tube-loading plates interface (top of the column) – technique (ii) prevented contact issues at the area where the load is transferred from the top plate to the concrete core.
- (iii) Aligning the position of nodes at the steel-concrete interface (sides of the column) – technique (iii) prevented contact issues during the buckling of the tube (normal pressure from the steel tube transferred to the side of the concrete core was handled better),
- (iv) Aligning the position of rebar and core nodes (inside core) so they coincide – technique (iv) improved the results for columns with rebars.

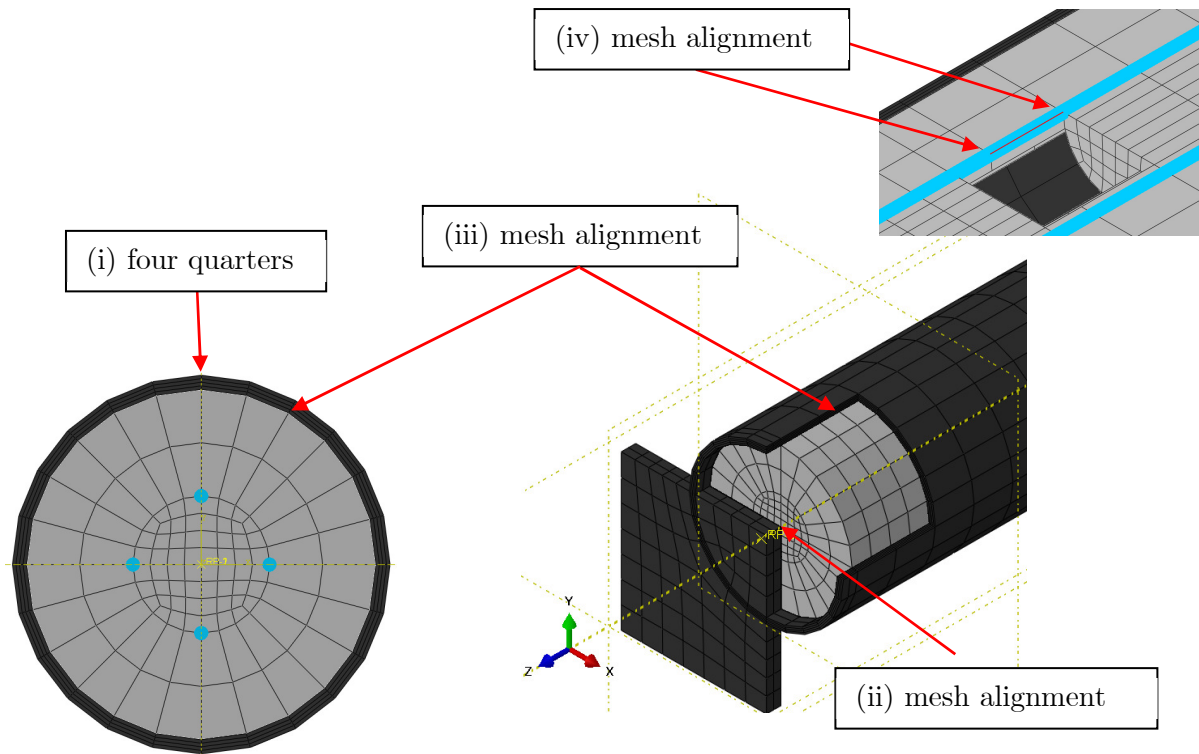


*Fig. 7.5 Visualisation of the FE mesh and four techniques (i-iv) used to improve convergence of the numerical analyses.*

A mesh sensitivity study is carried out to compare the results using FE of the following sizes:

- Mesh A: 20 mm x 20 mm x 40 mm,
- Mesh B: 20 mm x 20 mm x 20 mm,
- Mesh C: 10 mm x 10 mm x 10 mm.

The differences in the results between models with Mesh A and Mesh B are below 1 % of the fire resistance time. For the finest mesh, C, the analysis time becomes unreasonably time-consuming, even when calculations are carried out using a High-Performance Computational Cluster. Therefore, the FE size of approximately 20 x 20 x 40 millimetres is used due to its accuracy and computational efficiency.

## 7.2. Validation of the numerical model

### 7.2.1. What is fire resistance?

According to EN 1991-1-2, fire resistance is "*ability of a structure, a part of a structure or a member to fulfil its required functions (load bearing function and/or fire separating function) for a specified load level, for a specified fire exposure and for a specified period of time*".

In this dissertation, mainly the load-bearing capacity is of concern. Therefore, fire resistance is the same as the load-bearing function (R), which, according to the same standard, is the "*ability of a structure or a member to sustain specified actions during the relevant fire, according to defined criteria*".

In chapter 6.1 two criteria for reaching fire resistance were introduced:

- limiting vertical contraction, Eq. (6.1), and
- limiting rate of vertical contraction, Eq. (6.2).

For columns in the validation domain, the above criteria translate to:

- limiting vertical contraction between 31.8 mm and 37.7 mm, and
- limiting rate of vertical contraction between 9.5 mm/min and 11.3 mm/min.

The following figures (Fig. 7.6 – Fig. 7.9) present the vertical displacement at the top of four columns in time. Two solid lines present the observed (black line) and simulated (red line) behaviour. The dashed line represents the calculated rate of displacement. For details on the columns' properties, see Table 7.1. Obtaining the limiting vertical contraction or the limiting rate of vertical contraction was not always possible through the numerical model. It shall be borne in mind that the criteria were introduced to have a certain threshold that would protect the furnace during the fire resistance tests. The criteria were not developed for numerical modelling. Therefore, it was judged that if the rate of vertical displacement shows signs of abrupt changes at the end of the simulation, the fire resistance time was reached. If there were no signs of the rate of vertical displacement changing, the model was reviewed in search of numerical problems (examples of such problems are presented later, e.g. in Fig. 7.17).

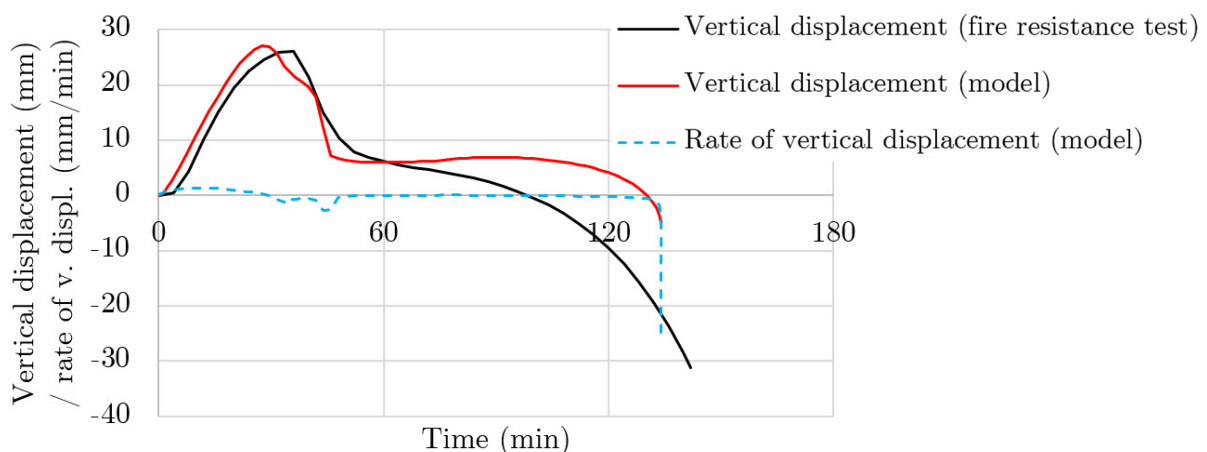


Fig. 7.6 Vertical displacement and the rate of vertical displacement of Lie & Chabot's (1992) C23 column.

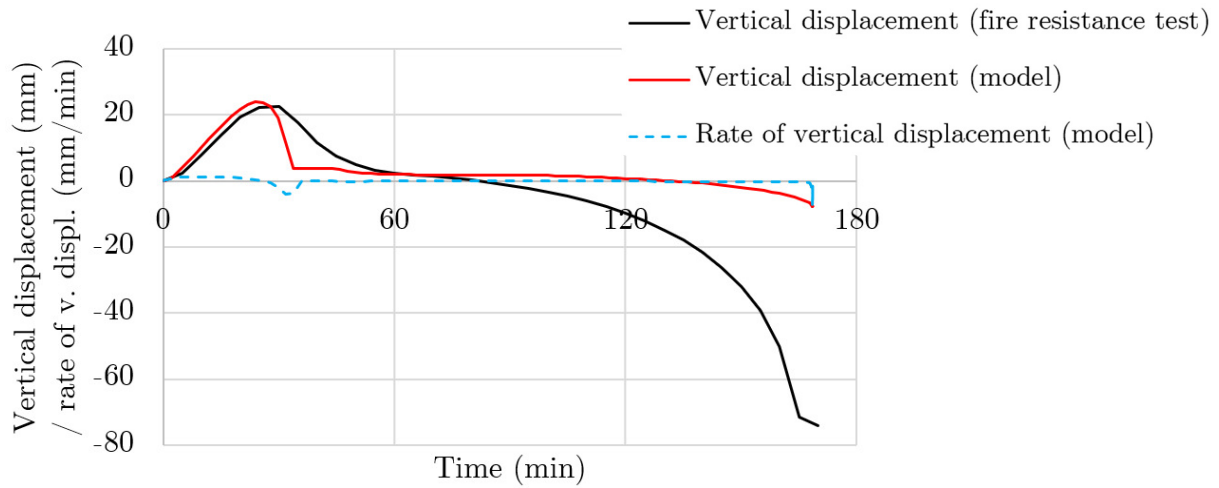


Fig. 7.7 Vertical displacement and the rate of vertical displacement of *Lie & Chabot's (1992) C29 column*.

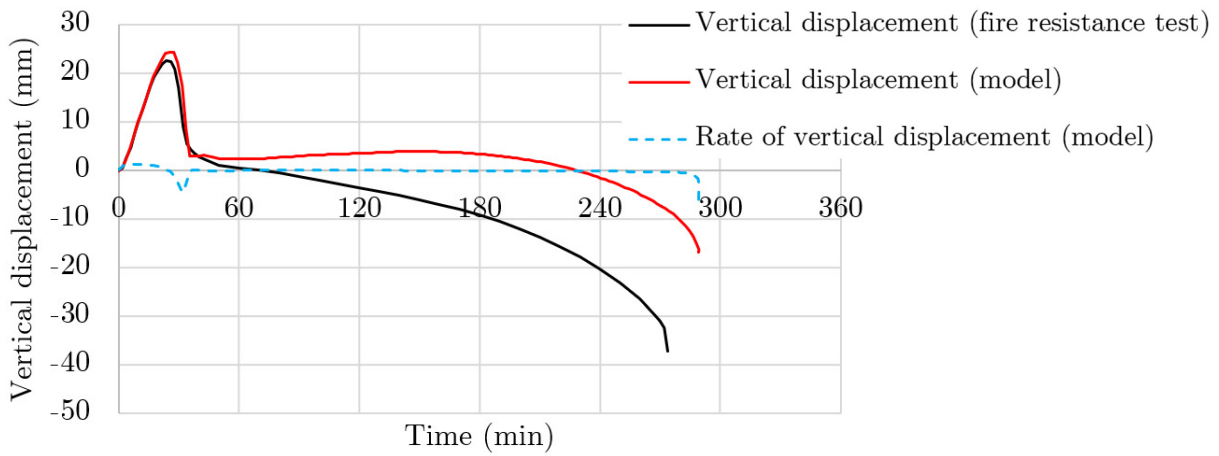


Fig. 7.8 Vertical displacement and the rate of vertical displacement of *Lie & Chabot's (1992) C55 column*.

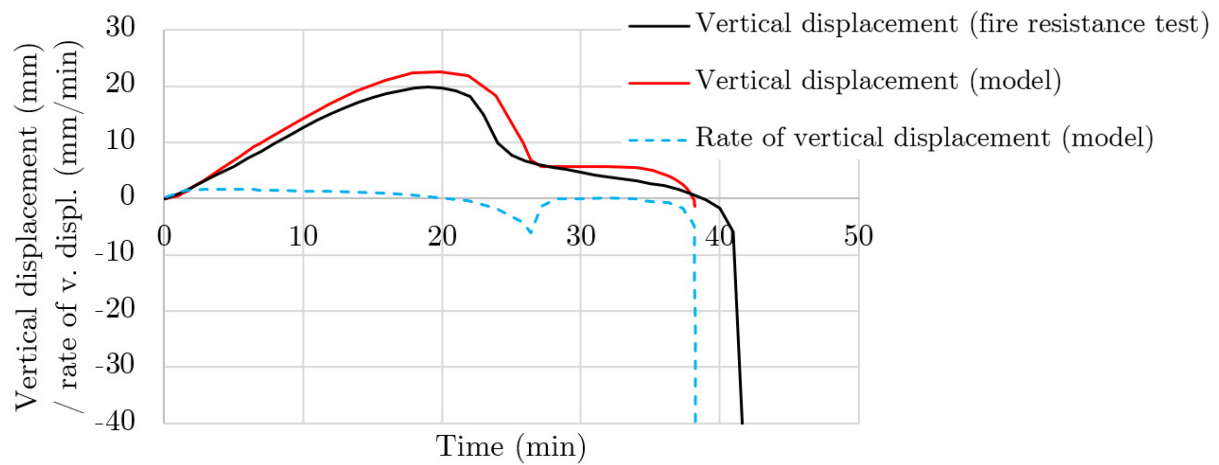


Fig. 7.9 Vertical displacement and the rate of vertical displacement of *Espinosa et al. (2014) 04 column*.

### 7.2.2. Validation domain

The numerical model is validated based on experimental data from the literature. Table 7.1 presents the essential data regarding columns used for the validation process. The data include concrete aggregate type, diameter, thickness and length of the tube, boundary conditions, load, eccentricity, concrete compressive strength, yield strength of steel tube and fire resistance time. The remainder of the collected data are omitted here for clarity.

In summary, 50 circular columns are used for the validation process:

- 41 columns filled with plain concrete, 9 reinforced with rebars,
- 8 P-P columns, 14 F-P columns, and 28 F-F columns,
- 19 columns with siliceous aggregate, 18 columns with calcareous aggregate, and 13 columns with a mix of two types of aggregate,
- 39 axially and 11 eccentrically loaded columns.

Table 7.1 Parameters of columns used for the validation (columns 2-12), calculated FRT (column 13), and the ratio between numerical and experimental results (FRTR, column 14).

Data <sup>a</sup>	ID	Agg <sup>b</sup>	D	t	L <sup>c</sup>	BC <sup>d</sup>	load	ecc.	f <sub>c</sub> <sup>e</sup>	f <sub>y</sub>	FRT <sup>f</sup>		FRTR <sup>g</sup>
											test	num	
-	-	-	mm	mm	mm	-	kN	mm	MPa	MPa	min	min	-
(1)	(2)	(3)	(4)	(5)	(6)	(7)	(8)	(9)	(10)	(11)	(12)	(13)	(14)
WT	1	S	244.5	6.3	3400	P-P	635.4	0	49	355	56	47.8	0.85
	2	S	323.9	6.3	3400	P-P	1864	0	49	354	45	55.6	1.24
	3	S	355.6	9.5	3400	P-P	900	0	49	348	142	161.8	1.14
Han	C1-1	C	478	8	3770	P-P	4700	0	31	293	29	36.3	1.25
	C1-2	C	478	8	3770	P-P	2200	71.7	31	293	32	17.2	0.54
	C2-1	C	219	5	3770	P-P	450	32.85	31	293	17	15.3	0.90
	C2-2	C	219	5	3770	P-P	300	65.7	31	293	18	19.2	1.07
NRC	C02	S	141.3	6.55	3772	F-F	110	0	33	350	55	56.3	1.02
	C04	S	141.3	6.55	3772	F-F	131	0	31	402	57	45.3	0.79
	C05	S	168.3	4.78	3772	F-F	150	0	33	350	76	76.4	1.01
	C08	S	168.3	4.78	3772	F-F	218	0	36	347	56	61.0	1.09
	C09	S	168.3	6.35	3772	F-F	150	0	35	350	81	80.9	1.00
	C11	S	219.1	4.78	3760	F-F	492	0	31	322	80	70.9	0.89
	C13	S	219.1	4.78	3760	F-F	384	0	32	322	102	89.4	0.88
	C17	S	219.1	8.18	3760	F-F	525	0	32	367	82	68.6	0.84
	C20	S	273.1	5.56	3760	F-F	574	0	29	413	112	132.4	1.18
	C21	S	273.1	5.56	3760	F-F	525	0	29	413	133	141.6	1.06
	C22	S	273.1	5.56	3760	F-F	1000	0	27	413	70	61.9	0.88
	C23	S	273.1	12.7	3760	F-F	525	0	27	350	143	133.9	0.94
	C25	S	323.9	6.35	3734	F-F	699	0	28	440	145	195.7	1.35
	C26	S	323.9	6.35	3734	F-F	1050	0	24	440	93	111.0	1.19
	C29	S	355.6	12.7	3734	F-F	1050	0	25	388	170	168.4	0.99
	C31	C+S	141.3	6.55	3772	F-F	80	0	30	350	82	69.1	0.84
	C32	C+S	141.3	6.55	3772	F-F	143	0	35	350	64	47.4	0.74
	C34	C+S	219.1	4.78	3760	F-F	500	0	35	350	111	88.4	0.80
	C35	C+S	219.1	4.78	3760	F-F	560	0	43	350	108	93.0	0.86
	C37	C+S	219.1	8.18	3760	F-F	560	0	29	350	102	65.9	0.65
C40	C+S	273.1	6.35	3760	F-F	1 050	0	47	350	106	135.0	1.27	
C44	C+S	273.1	6.35	3760	F-F	715	0	39	350	178	159.9	0.90	
C45	C+S	273.1	6.35	3760	F-F	712	0	38	350	144	157.5	1.09	
C48*	C+S	273.1	6.35	3760	F-F	1050	0	47	350	188	160.8	0.86	

Data <sup>a</sup>	ID	Agg <sup>b</sup>	D	t	L <sup>c</sup>	BC <sup>d</sup>	load	ecc.	f <sub>c</sub> <sup>e</sup>	f <sub>y</sub>	FRT <sup>f</sup>		FRTR <sup>g</sup>
											test	num	
(1)	(2)	(3)	(4)	(5)	(6)	(7)	(8)	(9)	(10)	(11)	(12)	(13)	(14)
	C49*	C+S	273.1	6.35	3760	F-F	1900	0	47	350	96	87.9	0.92
	C50	C+S	323.9	6.35	3734	F-F	820	0	42	350	234	260.3	1.11
	C55	C+S	355.6	12.7	3734	F-F	965	0	41	350	274	289.2	1.06
	C57	C+S	406.4	6.35	3734	F-F	1 400	0	44	350	294	382.0	1.30
UPV	02	C	159	6	3180	P-P	338	0	30	338	18	16.0	0.89
	03	C	159	6	3180	F-P	396	0	29	338	25	17.8	0.71
	04	C	159	6	3180	F-P	198	0	36	338	42	38.1	0.91
	05	C	159	6	3180	F-P	594	0	34	338	14	13.3	0.95
	06*	C	159	6	3180	F-P	229	0	24	338	43	38.8	0.90
	07*	C	159	6	3180	F-P	458	0	30	338	30	21.1	0.70
	08*	C	159	6	3180	F-P	687	0	34	338	13	13.7	1.06
	17	C	159	6	3180	F-P	169	20	36	332	32	33.9	1.06
	18	C	159	6	3180	F-P	337	20	42	332	16	19.9	1.24
	21	C	159	6	3180	F-P	126	50	31	344	30	34.7	1.16
	22	C	159	6	3180	F-P	253	50	38	366	23	22.4	0.98
	25*	C	159	6	3180	F-P	180	20	39	357	48	49.5	1.03
	26*	C	159	6	3180	F-P	360	20	40	357	24	23.4	0.97
	29*	C	159	6	3180	F-P	140	50	31	386	39	41.0	1.05
	30*	C	159	6	3180	F-P	280	50	40	386	20	24.3	1.21
<b>Mean:</b>												<b>0.99</b>	
<b>Standard deviation:</b>												<b>0.18</b>	
<sup>a</sup> Data sources: WT – <a href="#">Wainman &amp; Toner (1992)</a> Han – <a href="#">Han et al. (2003)</a> NRC – <a href="#">Lie &amp; Chabot (1992)</a> , <a href="#">Chabot &amp; Lie (1992)</a> UPV – <a href="#">Romero et al. 2011</a> ), <a href="#">Moliner et al. (2013)</a> , <a href="#">Espinosa et al. (2014)</a> <sup>b</sup> Agg.: Aggregate: S – siliceous or C – calcareous, C+S – mix of siliceous and calcareous. <sup>c</sup> L: length of the column between the bottom and top loading plate. <sup>d</sup> BC: Boundary conditions: P-P = pinned-pinned, F-F = fixed-fixed, F-P = fixed-pinned. <sup>e</sup> f <sub>c</sub> given in the table is the average strength of concrete determined by testing 150 mm x 300 mm cylinders. In some papers, results for 100 mm cubes were reported. In those cases, to obtain the respective 150 mm cylinder strength, the original values were modified with the following formula: f <sub>c</sub> = f <sub>c,cube(100)</sub> ·0.97/1.25. <sup>f</sup> FRT <sub>test</sub> : fire resistance time obtained in the test. FRT <sub>num</sub> fire resistance time predicted by the model. <sup>g</sup> FRTR – ratio of FRT <sub>num</sub> and FRT <sub>test</sub> . * Reinforced concrete infill Where possible, measured values from NRC tests were used (see <a href="#">Lie &amp; Caron 1988</a> ). When unavailable, the nominal yield strength was used (i.e. values reported by <a href="#">Lie &amp; Chabot 1992</a> and <a href="#">Chabot &amp; Lie 1992</a> ).													

It shall be noted that the following columns from [Lie & Chabot's \(1992\)](#) study were excluded from the validation domain: C06, C15, C16, C28, C30, C41, C51, C53, C59, C60. For the explanations, see e.g. chapters 5.2.1, 5.7, 6.2.2, and 6.2.4.

The next series of graphs presents the distribution of the input (test) data. Fig. 7.10 shows histograms of the fire resistance time of CFST columns (column 12 in Table 7.1). The experimental FRT varies from 17 to 294 minutes. The data distribution is presented in histograms, where the wide grey bars represent the whole dataset (50 columns), and coloured bars represent histograms for individual literature sources. It can be observed that all columns tested by [Han et al. \(2003\)](#) and [Espinosa et al. \(2014\)](#) failed in less than an hour. Only one

column tested by [Wainman & Toner \(1992\)](#) and most columns tested by [Lie & Chabot \(1992\)](#) reached FRT higher than 60 minutes.

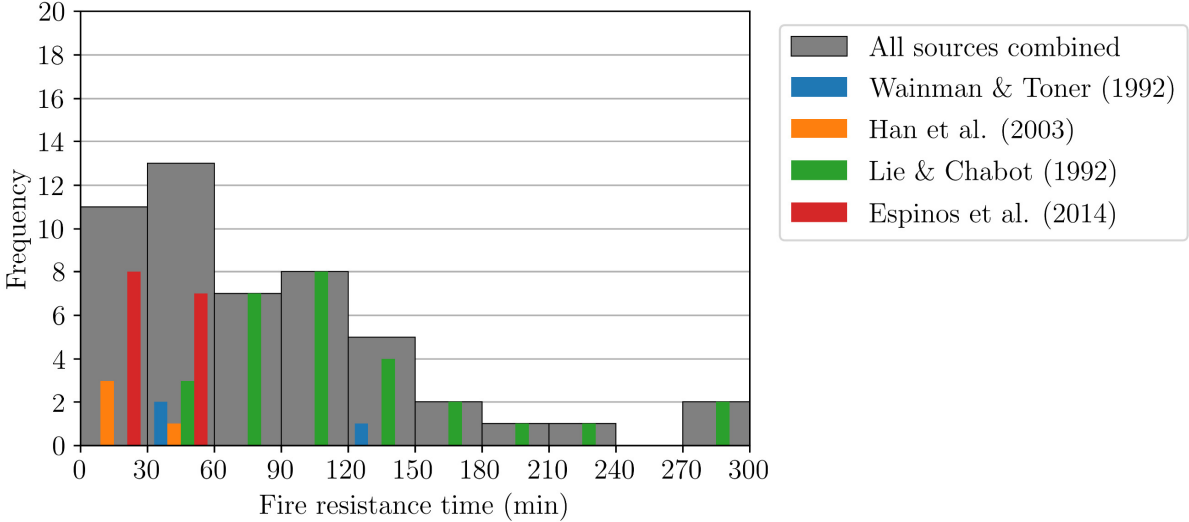


Fig. 7.10 Histogram of the fire resistance time of CFST columns in Table 7.1.

The histograms in Fig. 7.11 present the data similarly to Fig. 7.10, focusing on the compressive strength of the concrete infill.

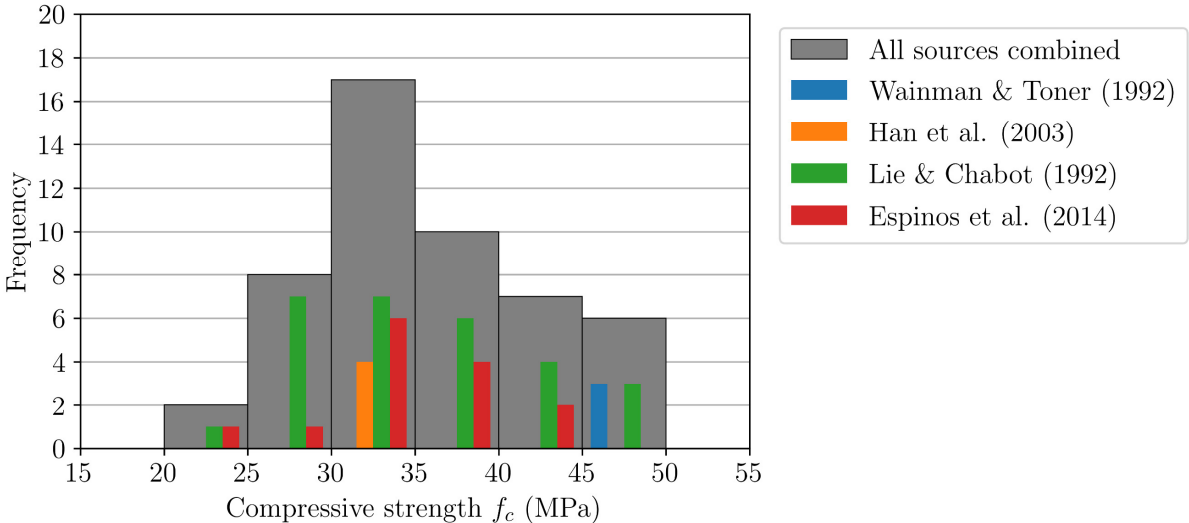


Fig. 7.11 Histogram of the compressive strength of concrete filling of CFST columns in Table 7.1.

Fig. 7.12 shows FRT against different variables included in Table 7.1. It can be observed that each laboratory used a specified effective length, while the diameter varied in most experiments (except for [Espinos et al. 2014](#), where a single diameter was used). Interestingly, 90 % of the columns were tested under a load up to 1050 kN. This percentage is worth comparing to reinforced concrete columns. According to [Jaszczak et al. \(2021\)](#), reinforced concrete columns in fire resistance tests were loaded up to 2000 kN, where 23 % of the columns were loaded between 1050 kN and 2000 kN. The following graphs in Fig. 7.12 present the eccentricities, compressive strength, and steel tube thickness.

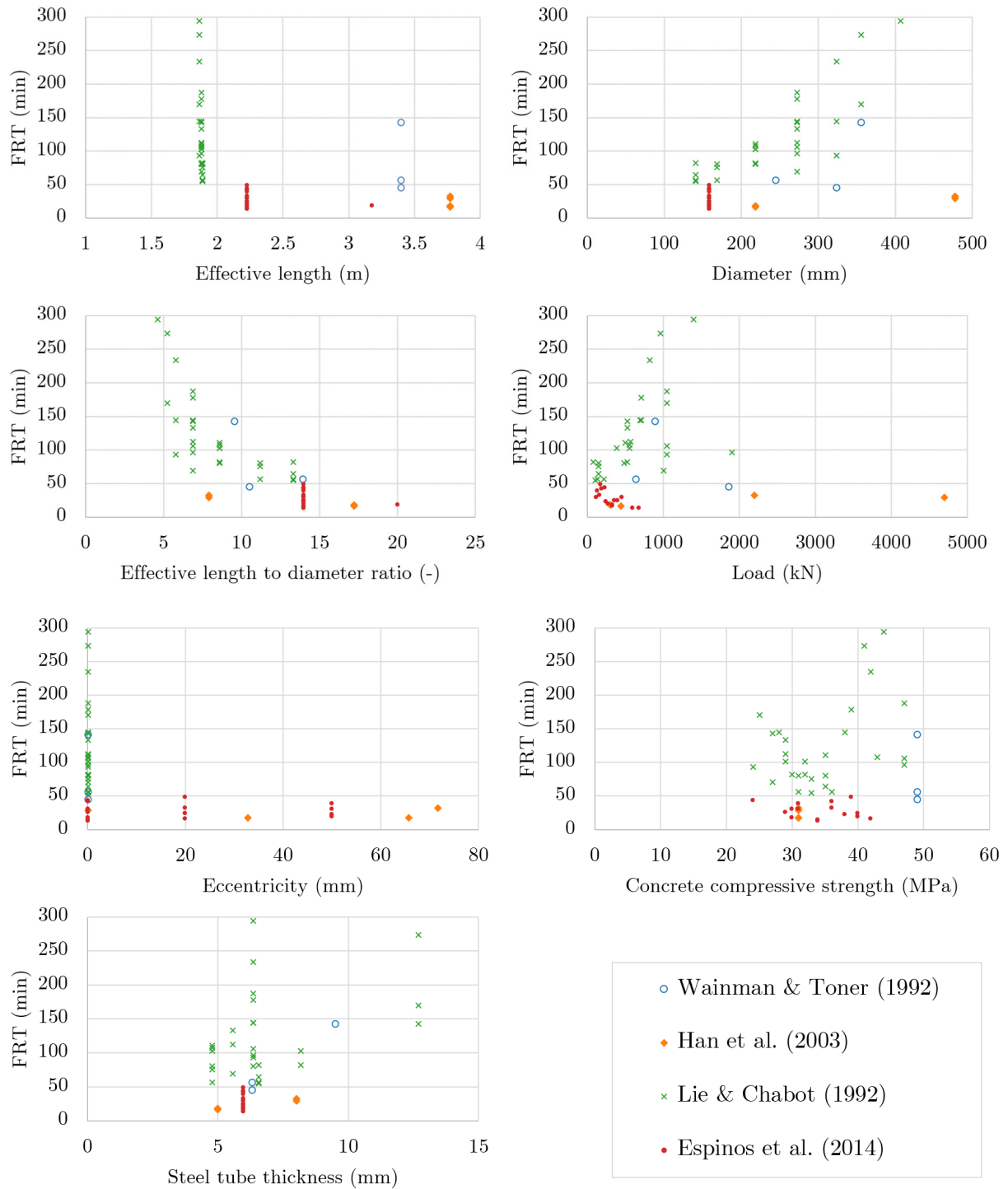


Fig. 7.12 Fire resistance time obtained in laboratory tests, plotted against various variables.

Additionally, Fig. 7.13 presents the number of columns with a given diameter and thickness.

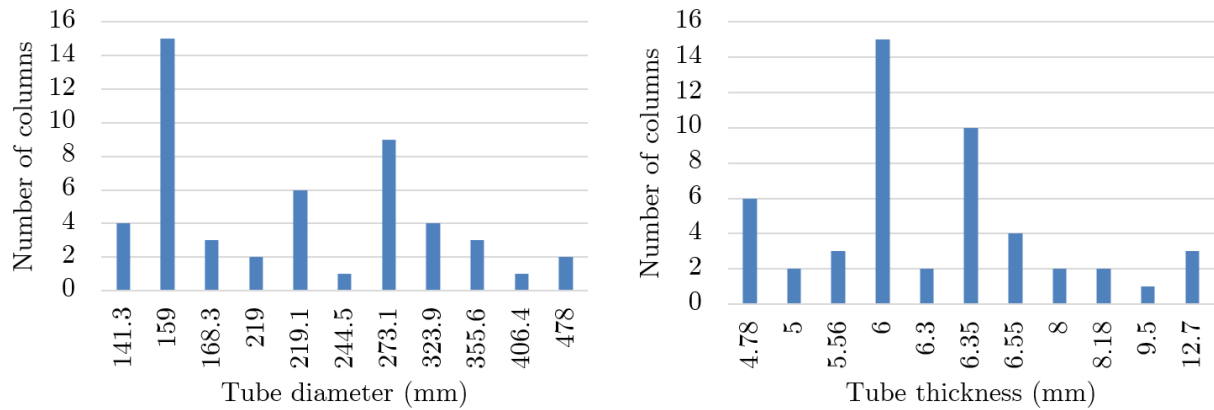


Fig. 7.13 Frequency of occurrences of specific tube diameter and thickness.

### 7.2.3. Validation results

Fig. 7.14 presents how the model performed in the validation. A good agreement between the predicted (horizontal axis) and measured (vertical axis) fire resistance time can be observed. Most data lie within the  $\pm 15\%$  of the experimentally obtained value. The shape of the graph in Fig. 7.14 follows the recommendations given by EN 1990 Annex D. However, plotting a ratio of  $FRT_{num}$  (Fire Resistance Time obtained with the numerical model) to  $FRT_{test}$  (Fire Resistance Time obtained in the test) against other variables allows to present data in a more comprehensible way. Thus, Fig. 7.15 shows the ratio for all 50 columns plotted against the  $FRT_{test}$ . The properties used in the model, for which the results are presented in Table 7.1, Fig. 7.14, and Fig. 7.15, are given in Table 7.2.

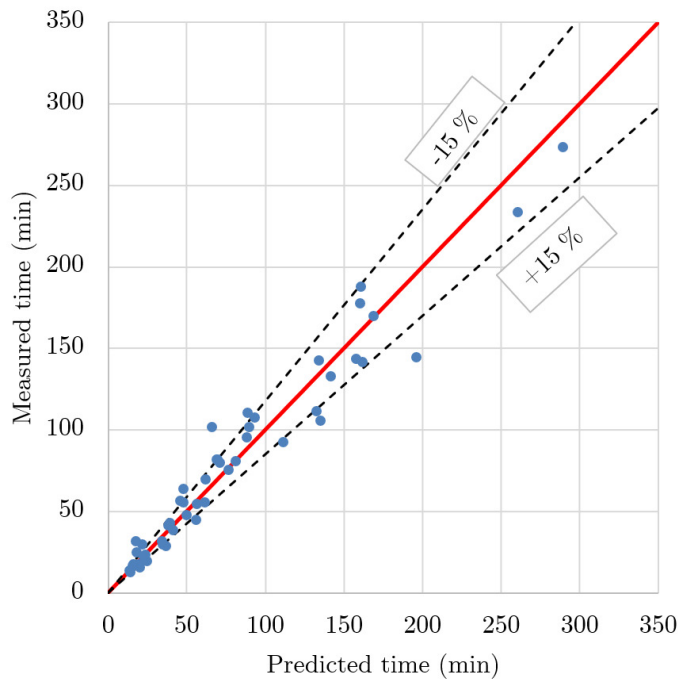


Fig. 7.14 Measured and predicted fire resistance time.

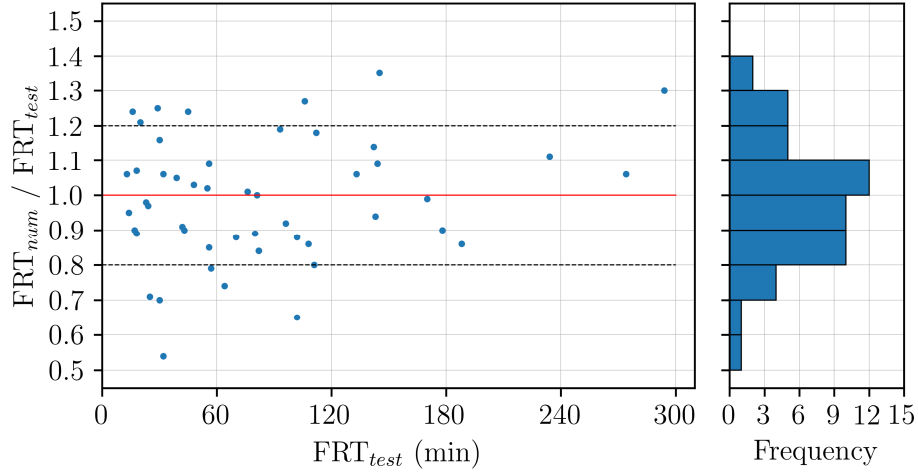


Fig. 7.15 Fire resistance time ratio against  $FRT_{test}$ .

Table 7.2 The properties used in the model, for which the results are presented in Table 7.1, Fig. 7.14, and Fig. 7.15.

Property	Value
Moisture content	3 %
Location of the specific heat peak	115 °C
Thermal conductivity limit	Upper limit
Convective heat transfer coefficient	25 W/(m <sup>2</sup> ·K)
Thermal gap conductance	100 W/(m <sup>2</sup> ·K)
Steel emissivity	0.7
Coefficient of thermal expansion	Eurocode
Friction coefficient	0.3
Mesh	20 mm x 20 mm x 40 mm
Contact	Tube side: slave, Top loading plate: master
The solution controls for displacement and rotation	$R_n^\alpha=0.01$ & $C_n^\alpha=0.1$
Time incrementation rules	$I_0=10$ & $I_R=12$

Table 7.3 presents the average ratio of calculated and measured fire resistance time based on the data in Table 7.1 (columns 12, 13) for separate research programmes.

Table 7.3 Summary of the average  $FRT_{num}/FRT_{test}$  ratio, with respect to individual data sources ( $n$  – number of columns).

Data source	n	Mean $FRT_{num}/FRT_{test}$	Standard deviation
Wainman & Toner (1992)	3	1.08	0.18
Han et al. (2003)	4	0.94	0.16
Lie & Chabot (1992)	28	0.98	0.17
Espinos et al. (2014)	15	0.99	0.15
All columns	50	0.99	0.18

Further graphs are used to determine whether selected variables have an undesirable influence on the numerical results. Fig. 7.16 presents the FRTR against column diameter. It can be seen

that the model tends to slightly overpredict the FRT of columns with larger diameters. Similar graphs are created for other parameters, such as compressive strength, effective length, and effective length-to-diameter ratio (Fig. 7.16). Fig. 7.16 (c) further distinguishes between columns with different boundary conditions. However, it shall be stressed that a specific type of BC is related to each laboratory (pinned columns in [Wainman & Toner \(1992\)](#) and [Han et al. \(2003\)](#), mainly fixed in [Lie & Chabot \(1992\)](#) and fixed-pinned (with one exception) in [Espinosa et al. \(2014\)](#)). Some of the columns tested by [Lie & Chabot \(1992\)](#) were pinned. However, the analysis of test reports indicated boundary conditions were wrongly executed. Consequently, such columns were disregarded from the validation domain. As already stated, similar conclusions were drawn by [Espinosa \(2012\)](#), while other researchers usually ignore pinned columns tested by [Lie & Chabot \(1992\)](#) without providing any explanation.

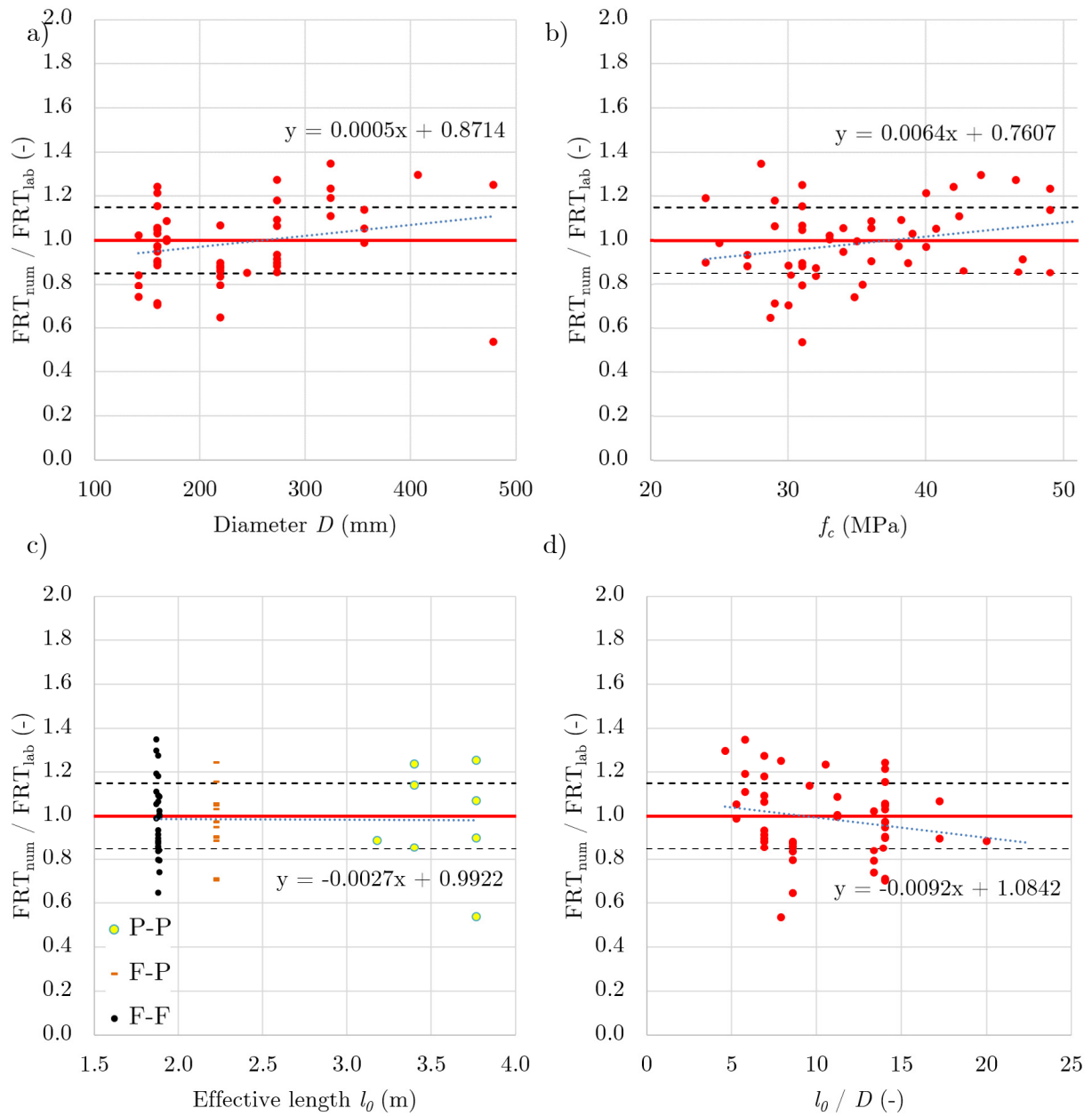


Fig. 7.16 FRTR against selected input variables.

### 7.2.4. Conclusions

This section compared the fire resistance time obtained in the test and the model predictions. The results are in good agreement. Therefore, the next step is to use the numerical model to:

1. provide insights into the structural fire behaviour of CFST columns,
2. explore the influence of factors that were not the subject of comparison in the experiments,
3. perform a parametric study to discover relationships between physical factors, model assumptions and fire resistance time.

To ensure repeatability, and reproducibility of the results, the input files will be uploaded to a dedicated open repository (Szymkuć 2023a). All the other files will be available upon request from the author ([wojciech.szymkuc@put.poznan.pl](mailto:wojciech.szymkuc@put.poznan.pl) or [wojciech.szymkuc@gmail.com](mailto:wojciech.szymkuc@gmail.com)).

## 7.3. Improving the convergence

### 7.3.1. Friction

In the test results from Espinos et al. (2014), the observed vertical displacement at the top of the column was between 0.4 mm and 1.6 mm. It is clear that the separation of steel from concrete takes place in the early stage of the fire due to the radial expansion of the tube. Therefore, formulation of shear strength (e.g.  $\tau_{Rd} = 0.55 \text{ N/mm}^2$  recommended by Eurocode 1994-1-1) does not impact the results. Similar conclusions were also drawn by other researchers (Ding & Wang 2008, Espinos 2012).

Ding & Wang (2008) showed, based on a study of a single column, that the friction coefficient in the range of 0.2-0.8 did not influence the results. Espinos (2012) also investigated the effect of friction by comparing the column's response assuming friction coefficients of 0 (frictionless), 0.3, or a full bond. The response for 0 and 0.3 was barely noticeable. Also the author (Szymkuć et al. 2015) concluded the friction might be disregarded. However, introducing friction was found to be beneficial for some of the columns, as it helped with the convergence. Adding friction can influence the time of numerical calculations (15 % on average). Hence it is not computationally expensive.

Two friction coefficient values are studied: 0 (frictionless) and 0.3. In most cases, the numerical analyses are unaffected by the friction coefficient's value. Espinos (2012) suggested that frictionless models can be adopted. However, based on a large set of simulations, it is noted that the friction coefficient has a positive effect on the calculated fire resistance time for some columns. Selected results are shown in Fig. 7.17. They show that introducing friction might be regarded as a factor that helps with the convergence. It is therefore recommended to avoid frictionless contact formulation. Furthermore, introducing friction is not computationally expensive (the analysis time increased by 15 % - from 129 to 149 hours).

Fig. 7.18 presents the effect of introducing friction on the time increment size. The response of the same column is presented, with  $\mu=0$  and with  $\mu=0.3$ . The analysis of a column with  $\mu=0$  fails prematurely (after about 54 minutes), due to reaching the minimum increment size without the solution converging. The same column analysed with  $\mu=0.3$  displays a clear decline at the end (60 minutes).

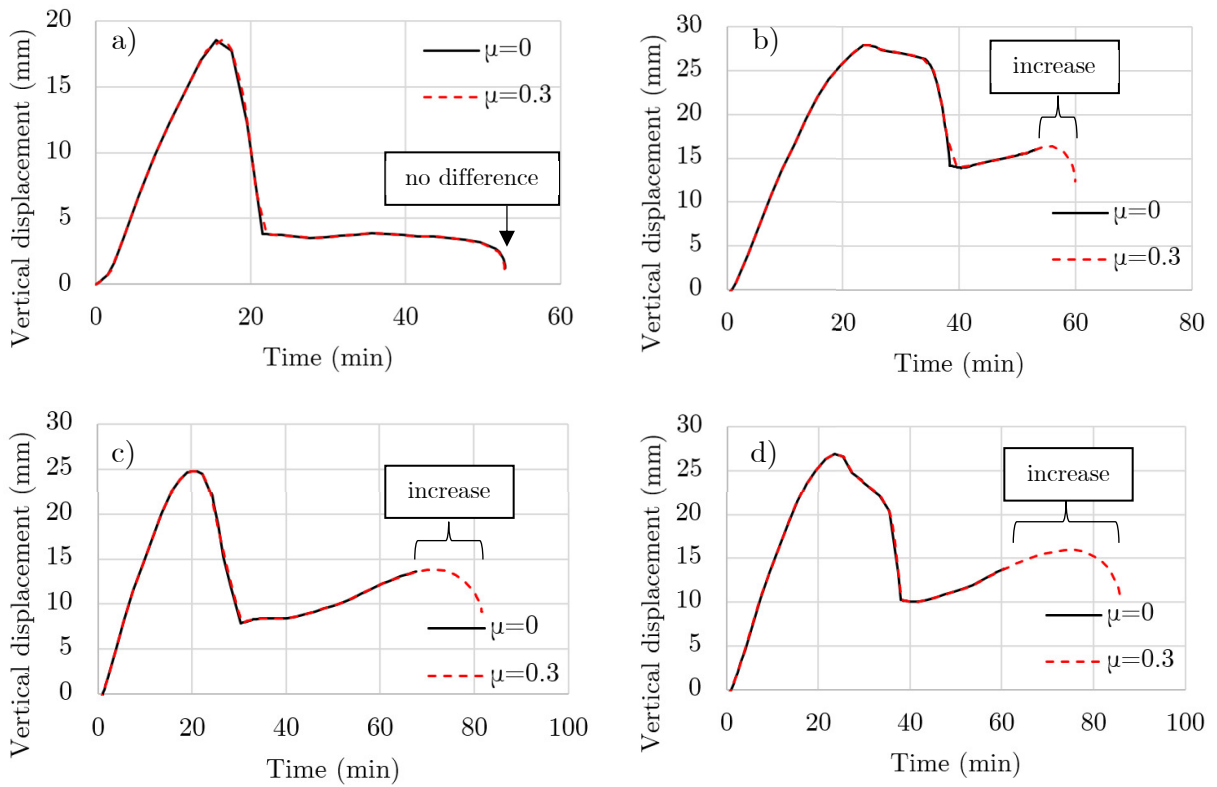


Fig. 7.17 The effects of including friction coefficient between steel and concrete. In most cases, friction does not affect the calculated response, as presented in (a). However, introducing friction helped with the analysis convergence for some columns, with the most prominent examples shown in (b), (c), and (d).

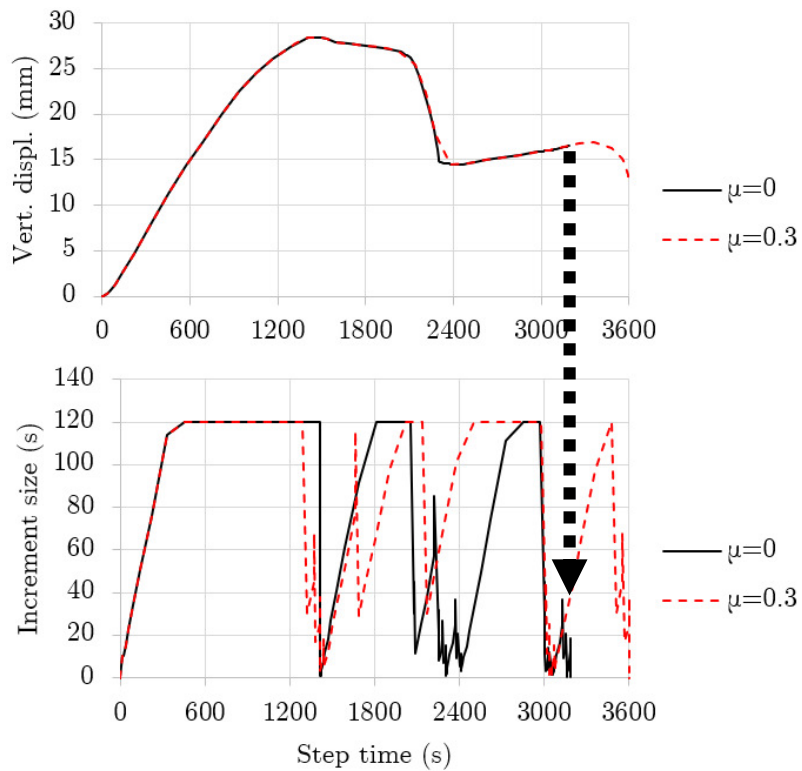


Fig. 7.18 The effect of introducing friction on time increment size. Top: columns' response, Bottom: Increment size. The analysis of a column with  $\mu=0$  fails prematurely.

### 7.3.2. Convergence criteria

When analysing the vertical displacement in time, it was noticed that some of the analyses ended without a clear sign of reaching the column's load-bearing capacity (see e.g. Fig. 7.18). In addition, it was observed that performing a sensitivity study and changing parameters that are irrelevant for the column's response (such as increasing the steel tube thickness by 0.1 % could sometimes significantly influence the results. It was observed that the axial displacement response obtained from several numerical simulations was almost identical up to a point when convergence criterion was judged unlikely in Abaqus. And for some simulations, the analysis would stop. For others, it would continue.

In Abaqus, by default, the analysis is aborted when the ratio of the largest residual to the corresponding average flux norm (0.005) is exceeded after several iterations. The default Abaqus values related to convergence criteria ( $R_n^\alpha$  and  $C_n^\alpha$ ) are given in Table 7.4.

By default, the check for increasing residuals in two consecutive iterations is made in Abaqus after 4 equilibrium iterations. If residuals are increasing, the analysis is aborted. The default value was found to be too low, and it was increased to 10 or 20, depending on the analysis. Such approach increases the computational time due to more iterations before the increment size cutback; however, it yields better results in some cases.

Table 7.4 Convergence criteria and equilibrium iterations in Abaqus.

Symbol	Definition	Default	Used
$R_n^\alpha$	convergence criterion for the ratio of the largest residual to the corresponding average flux norm for convergence	0.005	0.01
$C_n^\alpha$	convergence criterion for the ratio of the largest solution correction to the largest corresponding incremental solution value	0.01	0.1
$I_0$	number of equilibrium iterations (without severe discontinuities) after which the check is made whether the residuals are increasing in two consecutive iterations	4	10 or 20
$I_R$	number of consecutive equilibrium iterations (without severe discontinuities) at which logarithmic rate of convergence check begins	8	12 or 20

Further, it was observed that for one of the columns in one of the analysed sets, the calculated FRT was very low. The column's response did not show any sign of reaching the load-bearing capacity. Therefore, the number of equilibrium iterations was further increased to 20. This simple change increased the FRT from 1.31 minutes (unreasonable value) to 64 minutes.

### 7.4. Analysis of the behaviour of fire-exposed CFST columns

A validated FE model helps better understand the influence of several factors, as they can be studied in a comprehensive, systematised approach. For easier reference, the three stages (S1, S2, and S3), characteristic points (A, B, C, and D), and three behaviour types (type A, type B, and type C), as explained in Chapter 6.1, are presented in Fig. 7.19.

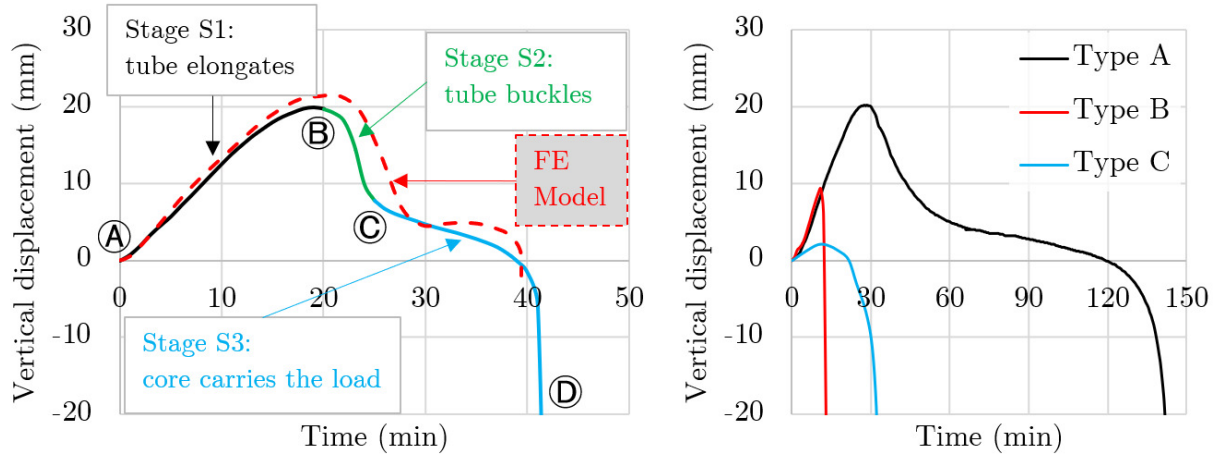


Fig. 7.19 Stages, characteristic points, and behaviour types of CFST columns.

#### 7.4.1. Contribution of core and tube to FRT

Interesting phenomena are discovered when analysing what portion of the axial force is transmitted by the concrete core and steel tube during fire. For this reason, the axial force ratio (AFR) is the ratio between the axial force carried by a column's constituents and the initial load acting on a column. Hence,  $AFR_{\text{tube}}$  (portion of the axial load carried by the tube) and  $AFR_{\text{core}}$  (part of the axial load carried by the core) are distinguished. The following sections analyse columns representing three distinct types of behaviour (Fig. 7.19).

##### *Column with type A behaviour*

The first example is based on a column similar to '04' (see Table 7.1). Fig. 7.20 shows that initially (before fire), the tube carries 62 % of the load, and the core carries the remaining 38 % of the load. When the fire starts, the tube elongates faster than the core, as presented in Fig. 7.20 (a). This corresponds with the rise of  $AFR_{\text{tube}}$  from 0.62 to 1.00. The tube carries the load until the loading plate is in contact with the core again (see Fig. 7.19, point ©). From that point, the load carried by the tube gradually decreases. Consequently, the  $AFR_{\text{core}}$  rises. At failure, the  $FRT_{\text{tube}}$  and  $FRT_{\text{core}}$  are 0.30 and 0.70, respectively. All three stages (S1, S2, S3, as explained in Fig. 6.1, and Fig. 7.19) develop. This behaviour is defined as type A, as illustrated in Fig. 6.2 and Fig. 7.19.

The failure of the column is defined as a time when the column is no longer capable of carrying the imposed load. This is related to the increase in vertical displacement. Fig. 7.20 (a) presents both the vertical displacement (mm) and the rate of displacement (mm/min) as a function of time. The increasing rate of displacement at the end of the simulation lets clearly identify the column's failure time (40.9 minutes).

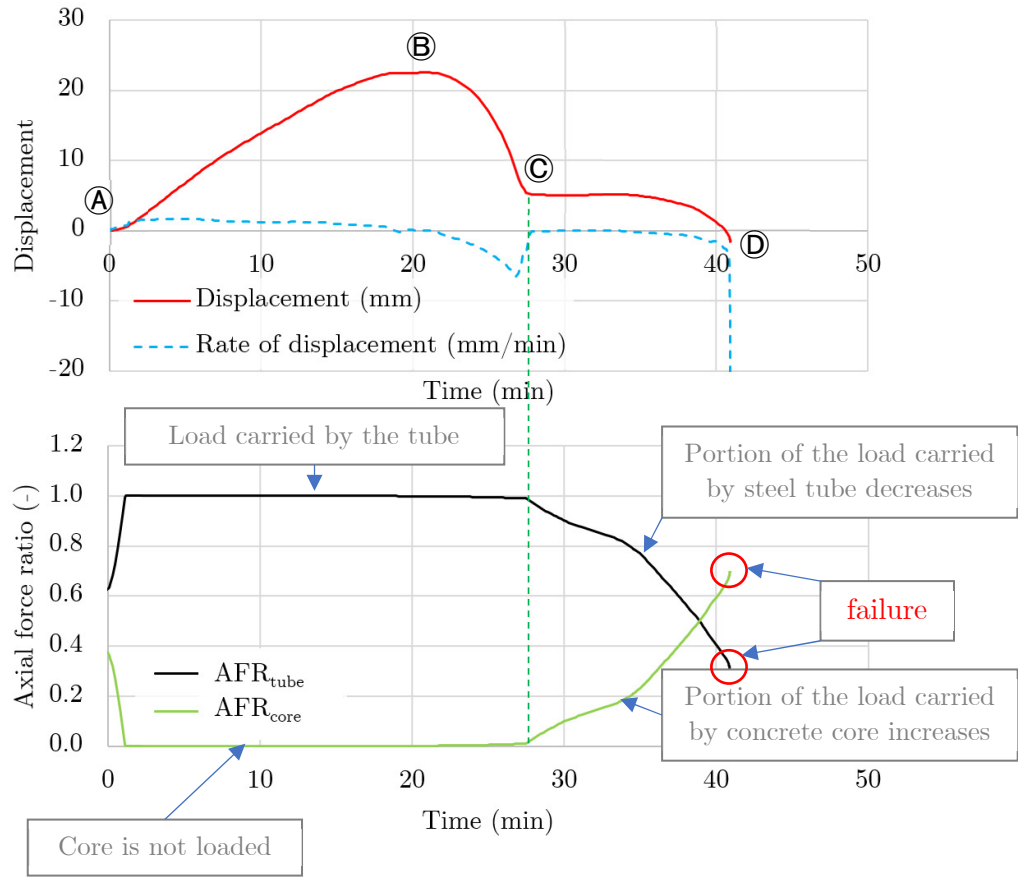


Fig. 7.20 Structural behaviour of CFST column (similar to '04' column). Load: 198 kN (a) Displacement and rate of displacement; (b) Axial force ratio of the steel tube and concrete core. In the early stage of fire, the load is carried by the steel tube. Then it is gradually transferred to the concrete core until the column fails.

A second example is based on a column with a different geometry (larger diameter) and longer fire resistance time. The behaviour in Fig. 7.21 is similar to the one presented in Fig. 7.20. However, a substantial decrease of  $AFR_{\text{tube}}$  can be observed. The temperature-induced degradation of steel mechanical parameters causes the  $AFR_{\text{tube}}$  to decrease.

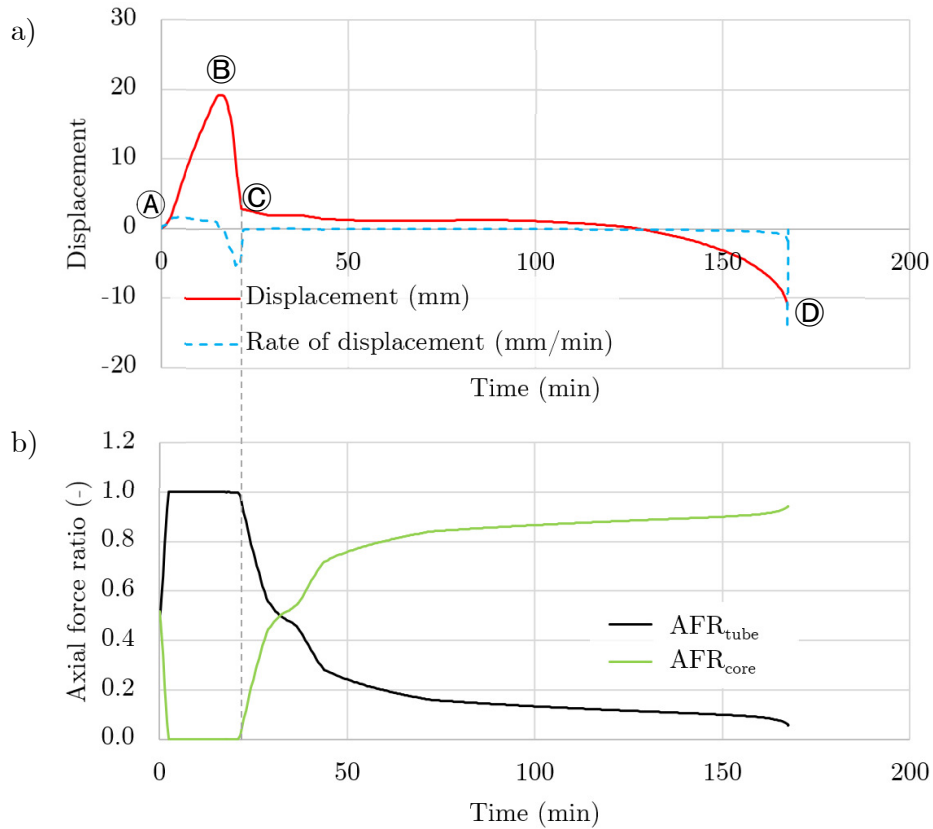


Fig. 7.21 Structural behaviour of CFST column (similar to 'C45' column). Load: 712 kN (a) Displacement and rate of displacement; (b) Axial force ratio of the steel tube and concrete core. In the early stage of fire, the load is carried by the steel tube, which is then gradually transferred to the concrete core until the column fails.

The case presented in Fig. 7.21 is similar to that in Fig. 7.20. However, due to the lower initial utilisation level of the column's capacity, the FRT exceeds 2.5 hours. Consequently, a longer exposure time leads to higher temperature and lower force transmitted by the steel tube. At the end of the analysis, the steel tube carries 6 % of the load, and the core carries the remaining 94 % of the axial load.

### Column with type B behaviour

A different type of behaviour is presented in Fig. 7.22. For a given column, the tube carries 62 % of the load, and the core carries 38 % of the load. When a fire starts, the tube elongates faster than the core, as presented in Fig. 7.22 (a). This is also related to the rise of  $AFR_{\text{tube}}$  from 0.62 to 1.00. The tube carries the load until the loading plate is in contact with the core again (see Fig. 7.19, point ©). However, stage S3 (see Fig. 6.1) does not develop. Due to extensive load, that point denotes failure of the column. This behaviour is similar to type B behaviour, as explained in Fig. 6.2.

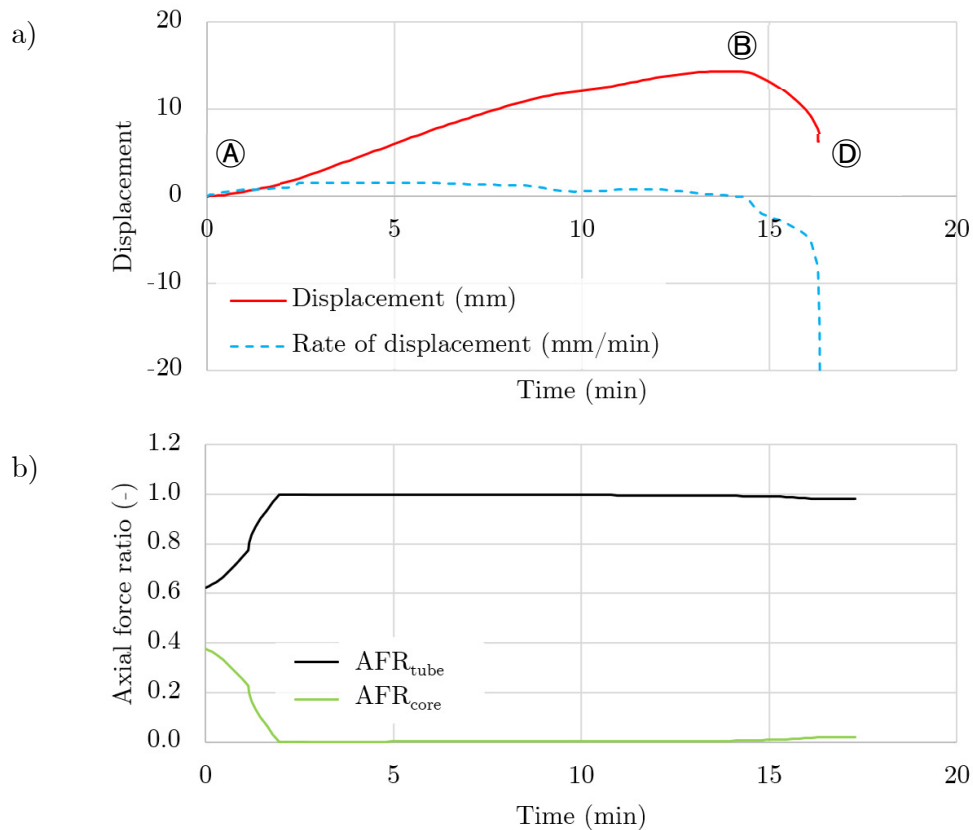


Fig. 7.22 Structural behaviour of CFST column (geometry as in '04' column). Load: 500 kN (a) Displacement and rate of displacement; (b) Axial force ratio of the steel tube and concrete core. In the early stage of fire, load is carried by the steel tube, then tube buckles and concrete core is not able to support the load. Column fails.

### Column with type C behaviour

A column representative of the type C behaviour is presented in Fig. 7.23. Initially, for a given load (950 kN), the tube carries 63 % of the load. The steel tube tries to elongate; however, the concrete core is only partially unloaded. This behaviour is similar to type C behaviour, as explained in Fig. 6.2.

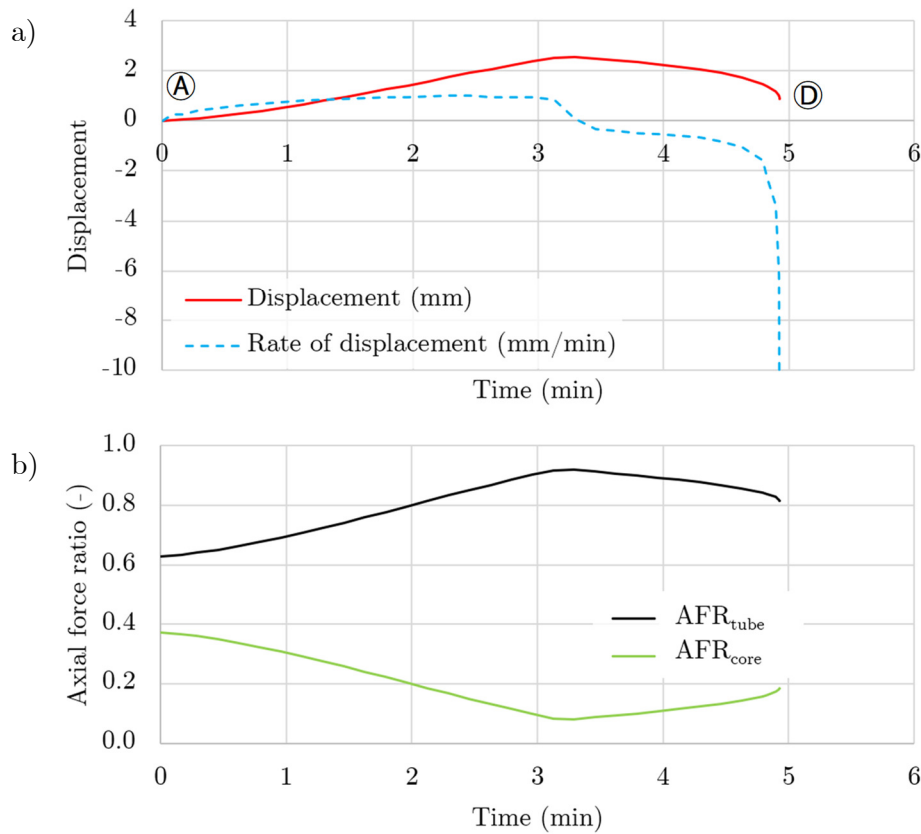


Fig. 7.23 Structural behaviour of CFST column (geometry as in '04' column). Load: 950 kN.

Additionally, Fig. 7.24 presents the horizontal deflection of the analysed column with three different loads and respective behaviour types.

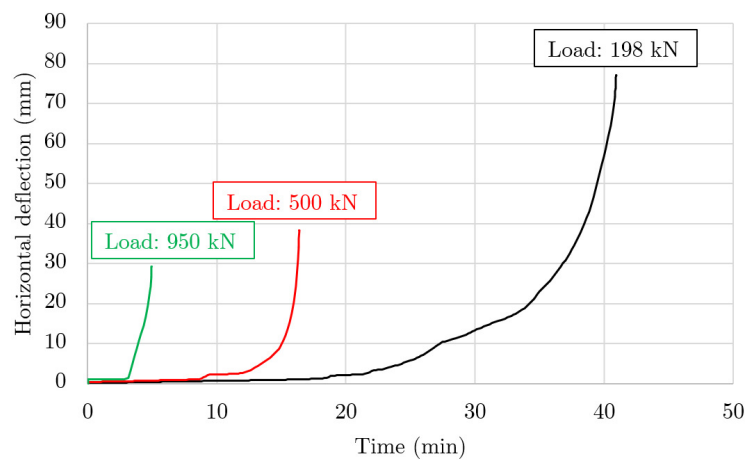


Fig. 7.24 Horizontal deflection of columns presented in Figs. AFR1 (198 kN), AFR3 (500 kN), and AFR4 (950 kN).

### 7.4.2. Contact pressure

One of the previous sections emphasised the gap, which forms due to the temperature difference between the tube and core. Consequentially, the steel no longer provides confinement to the concrete core. To investigate the interaction between steel tube and concrete core in the later stages of fire, a column is chosen to present the location and magnitude of contact pressure exerted by the buckled steel tube on the concrete core. The results are presented in Fig. 7.25. The results show that the tube comes in contact with concrete at the time denoted as © in Fig. 6.1. During stage S3, the contact pressure is exerted near the inflexion points of the column (see points marked with arrows). However, the magnitude of the side surface contact pressure is below 1 MPa for the whole fire duration. Those results further reinforce the view that the confinement effect in CFST columns is lost in fire.

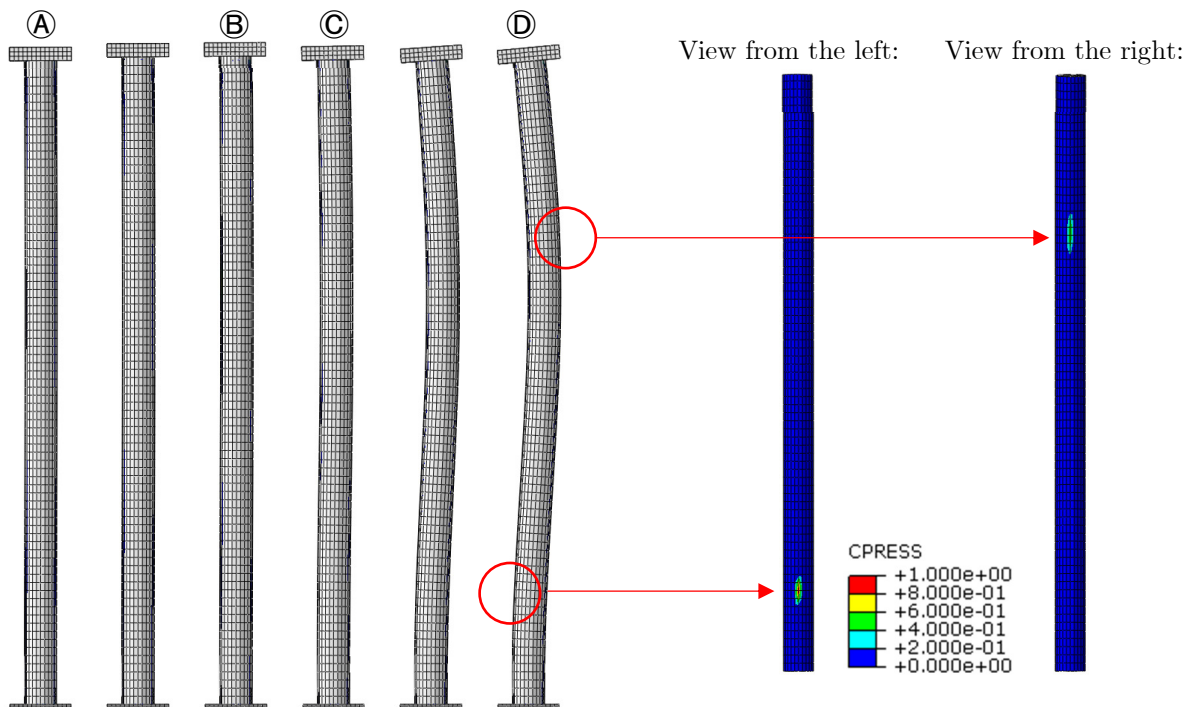


Fig. 7.25 Column displacement at time: 0 min, 10 min, 20 min, 30 min, 40 min and at failure (41 min).  
Colour figures in the right show the side surface of concrete core, with areas near supports truncated.  
Contact pressure appears only locally and is not higher than 1 MPa (column as in Fig. 7.20).

## 7.5. The effect of boundary conditions and partial restraint

The boundary conditions influence the structural fire behaviour of a column. Standard fire resistance tests give data for isolated columns where the rotational restraint is either non-existent (pinned) or infinite (fixed). Within a structure, a partial restraint is present. This concerns both the axial and rotational restraints adjacent members might provide. Therefore, studying the effects of axial and rotational restraints on composite columns is critical for future understanding of their response in structures.

### 7.5.1. The effect of rotational restraint

First, the effect of partial rotational restraint is presented and analysed. Table 7.5 presents the fire resistance time of columns with boundary conditions that are either pinned or fixed. Columns filled with concrete with 30 MPa and 50 MPa compressive strength are analysed. The

FRT for 30 MPa filling ranges from 22.9 to 55 minutes, and for 50 MPa, it ranges from 25.2 to 69.6 minutes. Fig. 7.26 presents the vertical displacement for columns in Table 7.5.

Table 7.5 Fire resistance time (min) of 159 mm x 6 mm x 3180 mm column filled with 30 MPa or 50 MPa concrete. Load: 198 kN.

Boundary conditions	FRT (min)	
	30 MPa	50 MPa
P-P	22.9 minutes	25.2 minutes
F-P	36.2 minutes	47.7 minutes
F-F	55.0 minutes	69.6 minutes

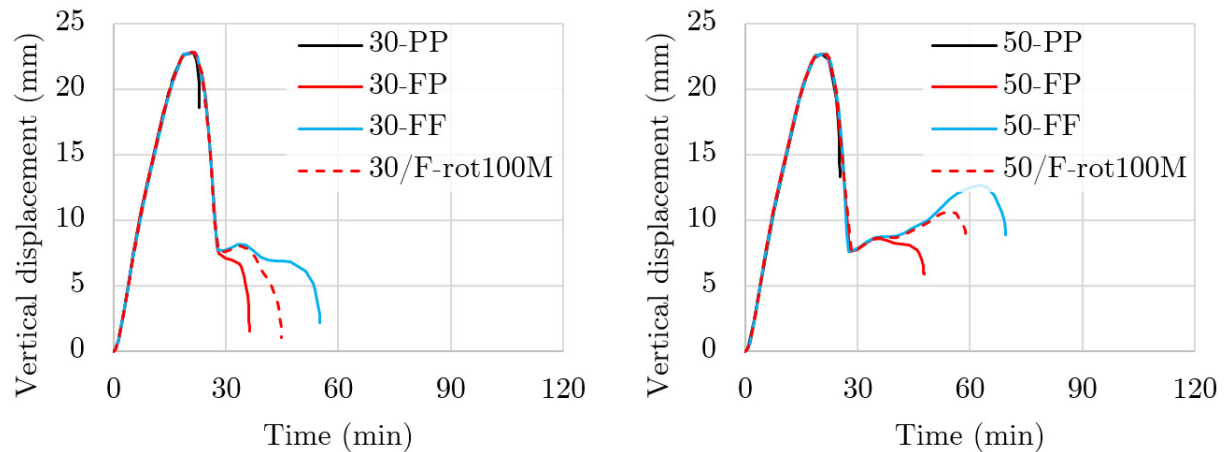


Fig. 7.26 Vertical displacement – time relationship for 159 mm x 6 mm x 3180 mm column, filled with 30 MPa or 50 MPa concrete. Load: 198 kN. Boundary conditions: pinned, fixed, fixed-pinned or partially restrained rotation ( $10^8$  N·mm/rad) at the top.

The rotational restraint has a positive effect, as shown in Fig. 7.26. The lowest FRT is observed for P-P columns and the highest for F-F columns. The effect of various levels of rotational restraint is presented in Fig. 7.27, where the results for a column with a fixed bottom and partially restrained rotation at the top are presented. A gradual rise of FRT can be observed as the rotational stiffness increases from  $10^7$  N·mm/rad to  $10^9$  N·mm/rad.

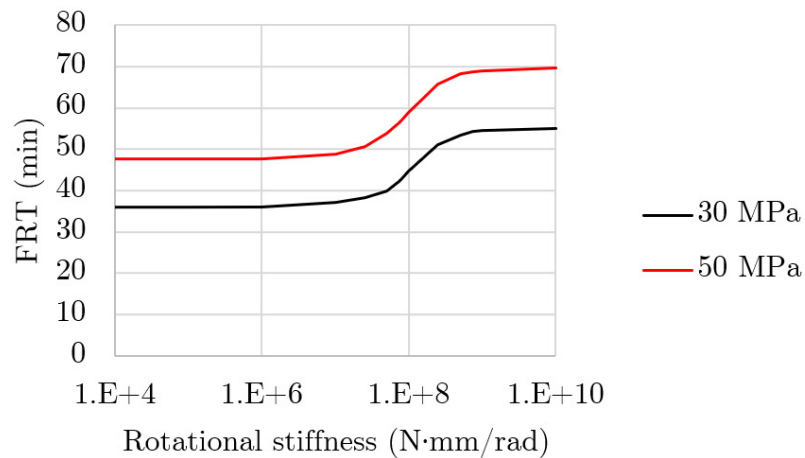


Fig. 7.27 The effect of partial rotational restraint at the top of the 159x6x3180 column, filled with 30 MPa or 50 MPa concrete. Load: 198 kN, bottom: fixed.

The effect of partial rotational restraint is noticeable, and any partial restraint will result in the column's behaviour between the boundaries set by pinned (zero rotational restraint) and fixed (infinite rotational restraint) support.

### 7.5.2. The effect of axial restraint

As concluded in the previous section, the effect of partial rotational restraint is qualitatively straightforward. The bigger the rotational restraint, the higher the FRT. However, the effect of axial restraint is not as obvious. Depending on the restraint level and column's properties, the axial restraint might positively or negatively affect the fire resistance time.

An additional metric is used to analyse the behaviour of the axially restrained CFST column – a relative reaction force (RRF). If a vertical displacement of a given column is fully restrained at the bottom, and the surrounding structure partially restrains the top, the reaction at the bottom is a sum of the initial load and forces caused by the restraint. The bottom reaction divided by the initial load (applied before fire) is the RRF. To visualise it, the effect of partial axial restraint is presented in Fig. 7.28, where the 'critical time' is an instant when the restraining forces return to the value of the initial load applied (and the vertical displacement changes from positive to negative values).

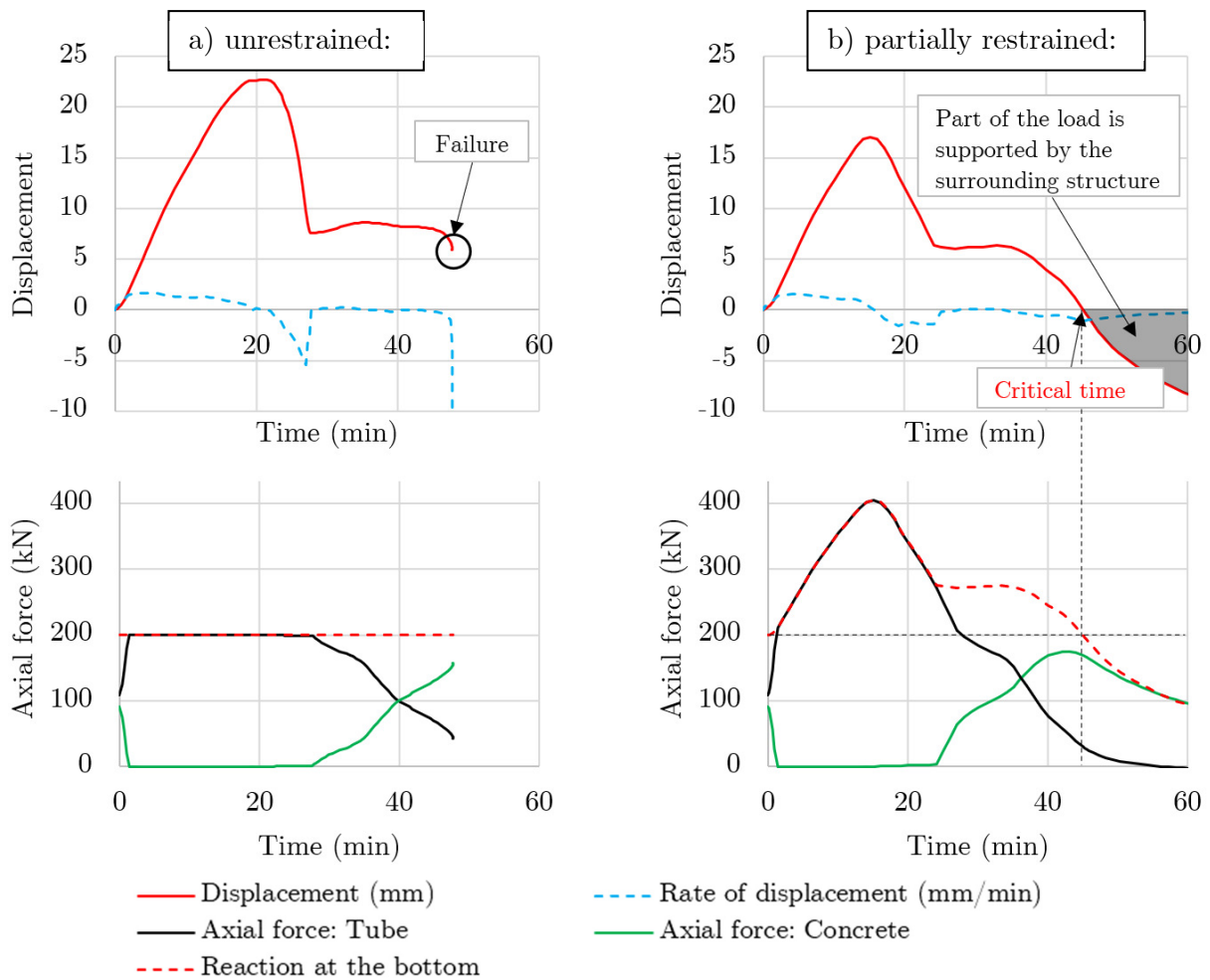


Fig. 7.28 Behaviour of (a) unrestrained; (b) partially axially restrained CFST column.

Fig. 7.28 depicts the structural behaviour of CFST column in two variants: unrestrained (pinned-fixed) and partially axially restrained (12 kN/mm). It can be observed that:

1. unrestrained column fails after approximately 48 minutes,
2. partially axially restrained column does not fail after 60 minutes,
3. the critical time of a partially axially restrained column is 45 minutes,
4. reaction at the bottom support remains constant for an unrestrained column and varies for the restrained column,
5. the axial restraint hinders the column elongation (23 mm vs. 17 mm),
6. the surrounding structure exerts additional normal force, peaking at around 400 kN (double the initial load value). Consequentially, the tube buckles faster (compare time when concrete is loaded in the lower part of Fig. 7.28 a and b),
7. after the critical time, the load action on a column gradually decreases (red dashed line), which prolongs the fire resistance time of the analysed member.

It can also be observed in Fig. 7.28 that as the vertical displacement graph passes 0, the axial force falls below the initial value. If the restraint level is sufficient, more and more load might be carried by the surrounding structure. However, such behaviour is not always the case. To explain it further, the behaviour of two columns is presented. The filling is 30 MPa (Fig. 7.29 a) or 50 MPa (Fig. 7.29 b). The upper part shows the vertical displacement and the lower depicts the relative reaction force.

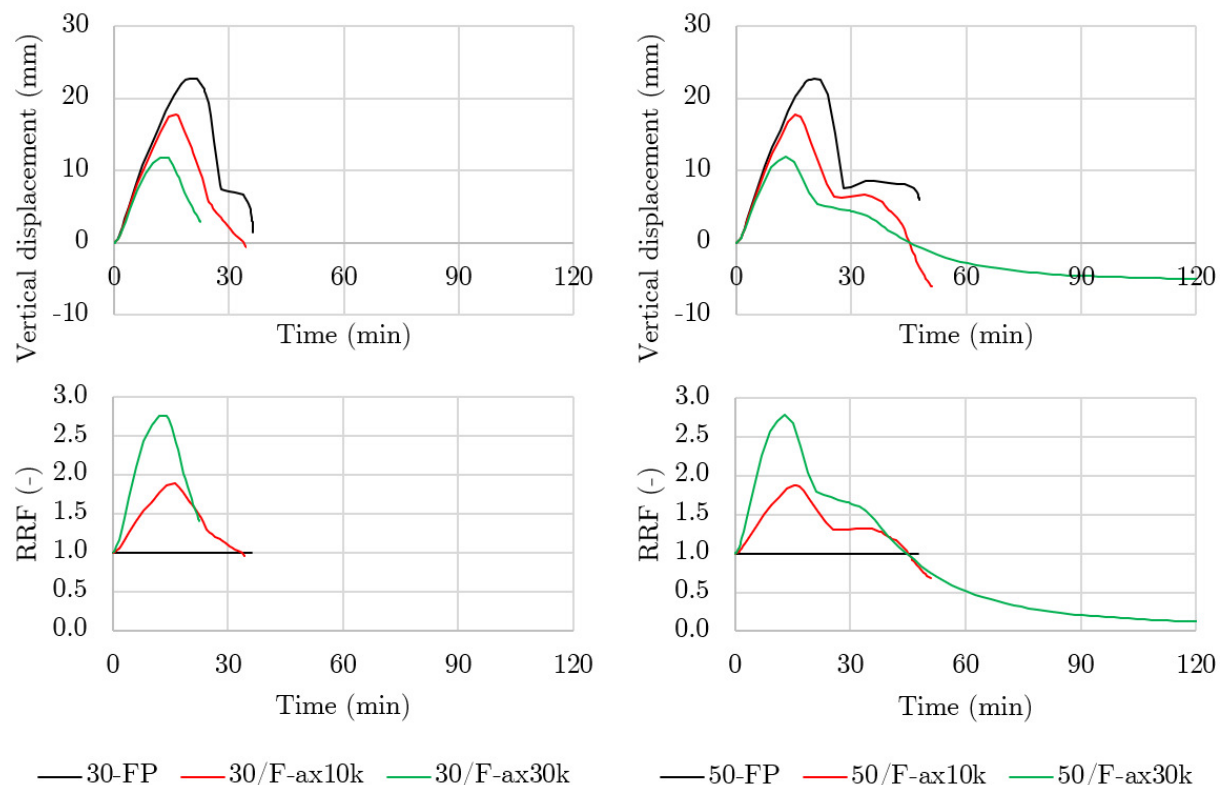


Fig. 7.29 Vertical displacement and RRF of two columns (filled with 30 MPa or 50 MPa concrete) under the three restraint levels at the top: 'FP' - 0 kN/mm, 'ax10k' - 10 kN/mm, and 'ax30k' - 30 kN/mm.

The columns presented in Fig. 7.29 are fixed at the bottom end. At the top end, they are (i) free to elongate, (ii) restrained 10 kN/mm, and (iii) restrained 30 kN/mm. In the case of the

30 MPa filling, the increase of axial restraint causes the column to fail earlier. However, in the case of 50 MPa filling, the 10 kN/mm restraint increases the fire resistance time slightly, and the 30 kN/mm restraint results in a fire resistance time of more than 120 minutes. Contrary to a column with a 50 MPa filling, a column with a 30 MPa filling cannot sustain the load increase due to axial restraint.

## 7.6. Parametric study

This section provides the results of a numerical parametric study. A validated numerical model allows the analysis of various parameters, including material inside the tube and its properties, thermal gap conductance, and emissivity of the steel surface.

Table 7.6 gives an overview of the studied parameters. Some are related to the physical properties of the materials, and others are related to the numerical modelling. The first column in Table 7.6 contains the property (parameter name). The second column gives the property value used in the 'Reference' set (e.g., 6 % moisture content). The third column lists the values studied for a given parameter (e.g., two values were investigated for moisture content, i.e. 3 % and 6 %). The whole set of 50 columns is calculated for each set of parameters. The results summary for each set is presented in

Table 7.7. The total computational time for each set (for all three types of analysis: buckling, heat transfer, and mechanical) is about 170 hours (four cores of an Intel Xeon E5-2620v3 2.40GHz processor).

Table 7.6 Table with the investigated parameters.

Property	Reference	Studied
Moisture content (%)	6	3, 6
Location of the specific heat peak (°C)	115	115, 165
Thermal conductivity	Upper limit	Lower limit, Upper limit, prEN 1992-1-2
Convective heat transfer coefficient (W/(m <sup>2</sup> ·K))	25	25
Thermal gap conductance (W/(m <sup>2</sup> ·K))	100	10, 100, 200, ∞
Steel emissivity (-)	0.7	0.7, 0.8
Coefficient of thermal expansion (1/K)	Eurocode	Eurocode, Hong & Varma (2009)
Friction coefficient (-)	0.3	0, 0.3
Max mesh size (mm)	20 x 20 x 40	20 x 20 x 40 20 x 20 x 20 10 x 10 x 10
Contact	Tube side: slave Top loading plate: master	All possible combinations for contact pairs: core-tube (side) and core-loading plate (top)
Solution controls for displacement and rotation	$R_n^\alpha=0.01$ & $C_n^\alpha=0.1$	$R_n^\alpha=0.01$ & $C_n^\alpha=0.1$ $R_n^\alpha=0.005$ & $C_n^\alpha=0.01$
Time incrementation rules	$I_0=10$ & $I_R=12$	$I_0=4$ & $I_R=8$ $I_0=10$ & $I_R=12$

Table 7.7 Sets used for the parametric analysis of columns in the validation domain. The parameters subjected to change in relation to the 'Reference' set are distinguished with a light blue filling.

Set name:	Reference	Moisture 115-3	Moisture 165-3	Moisture 165-6	Th.cond. lower	Th.cond. EC2020a	Th.cond. EC2020b	Th. gap conduct.	Th. gap conduct.	Th. gap conduct.	Emissivity	Th. exp	Frictionless
Set number:	1	2	3	4	5	6	7	8	9	10	11	12	13
Specific heat peak location (°C)	115	115	165	165	115	115	115	115	115	115	115	115	115
Moisture content (%)	6	3	3	6	6	6	3	6	6	6	6	6	6
Thermal conductivity limit	Upper	Upper	Upper	Upper	Lower	prEN 1992-1-2	prEN 1992-1-2	Upper	Upper	Upper	Upper	Upper	Upper
Convective heat transfer coefficient	25	25	25	25	25	25	25	25	25	25	25	25	25
Thermal gap conductance W/(m <sup>2</sup> ·K)	100	100	100	100	100	100	100	10	200	10 <sup>5</sup>	100	100	100
Steel emissivity	0.7	0.7	0.7	0.7	0.7	0.7	0.7	0.7	0.7	0.7	0.8	0.7	0.7
Coefficient of thermal expansion (concrete)	Eurocode (EC)	EC	EC	EC	EC	EC	EC	EC	EC	EC	EC	6·10 <sup>-6</sup> 1/K	EC
Friction coefficient $\mu$	0.3	0.3	0.3	0.3	0.3	0.3	0.3	0.3	0.3	0.3	0.3	0.3	0
Imperfection L - column length	L/1000	L/1000	L/1000	L/1000	L/1000	L/1000	L/1000	L/1000	L/1000	L/1000	L/1000	L/1000	L/1000
Mesh size: Concrete (mm)	20x20 x40	20x20 x40	20x20 x40	20x20 x40	20x20 x40	20x20 x40	20x20 x40	20x20 x40	20x20 x40	20x20 x40	20x20 x40	20x20 x40	20x20 x40
Steel (elements per tube thickness)	4	4	4	4	4	4	4	4	4	4	4	4	4
	FRT <sub>num</sub> / FRT <sub>test</sub> for each set:												
All columns	1.05	0.99	0.99	1.05	1.11	1.11	1.05	1.47	0.99	0.94	1.02	1.02	1.03
<a href="#">Wainman &amp; Toner (1992)</a>	1.18	1.08	1.08	1.17	1.28	1.27	1.16	1.77	1.08	0.98	1.16	1.19	1.18
<a href="#">Han et al. (2003)</a>	0.99	0.94	0.94	0.98	0.84	0.98	0.94	0.98	0.98	1.01	0.97	0.96	0.96
<a href="#">Lie &amp; Chabot (1992)</a>	1.05	0.99	0.98	0.98	1.16	1.14	1.07	1.58	0.97	0.89	1.00	1.01	1.03
<a href="#">Espinosa et al. (2014)</a>	1.04	0.99	0.99	1.04	1.05	1.05	1.03	1.34	1.01	0.99	1.00	1.04	1.03

The exemplary graph (Fig. 7.30) illustrates that the FRT predicted by the model for a given set ('Set name' in the header) is 20 minutes higher than for the 'Reference' set. Graphs presented in Fig. 7.31 follow the same convention and are described in further paragraphs.

To enable easier comparison by the reader, all graphs are grouped here. Their description is given later in the text.

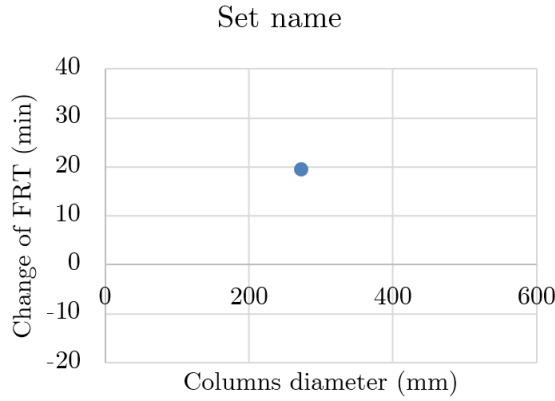


Fig. 7.30 Change of FRT (in minutes, vertical axes) against the external diameter of columns (horizontal axes) for various sets of parameters.

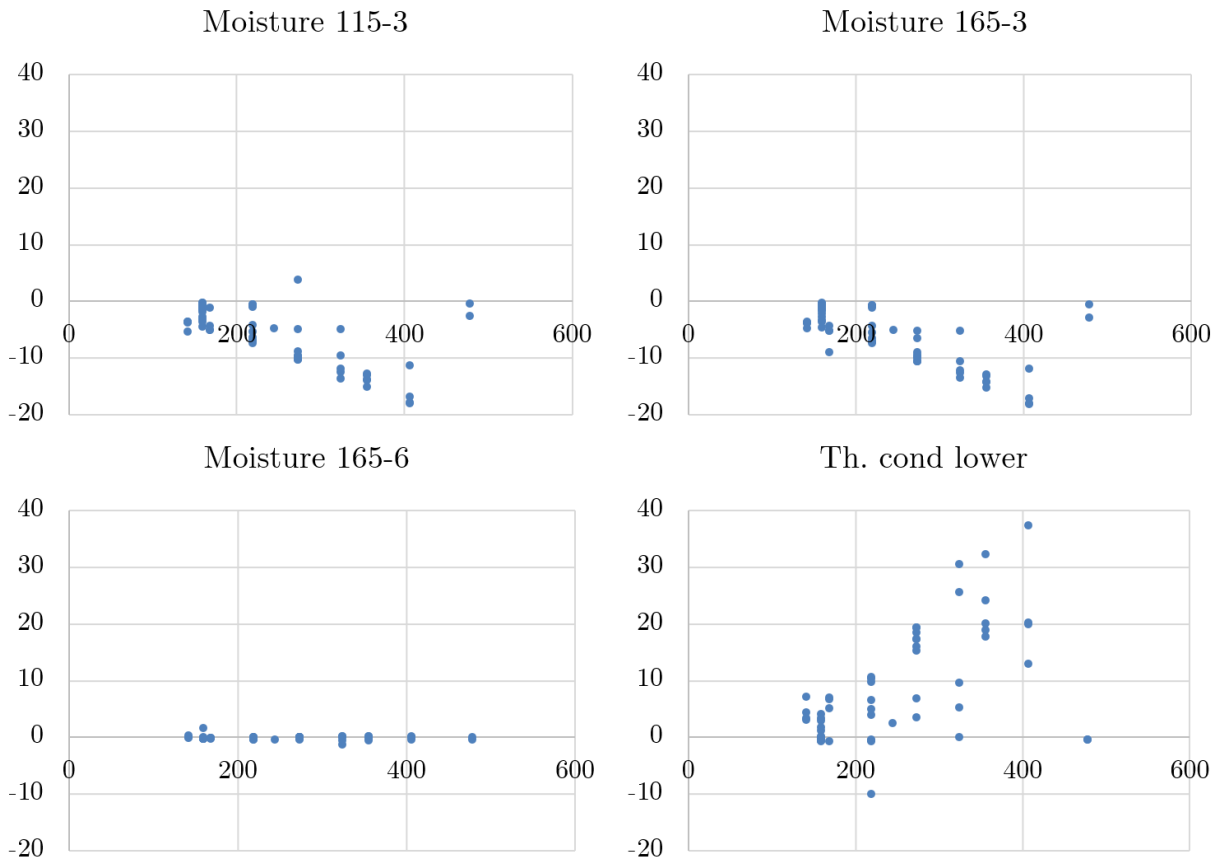


Fig. 7.31 Change of FRT (in minutes, vertical axes) against the external diameter of columns (horizontal axes), for various sets of parameters, compared to the Reference set (see

Table 7.7, and Fig. 7.30).

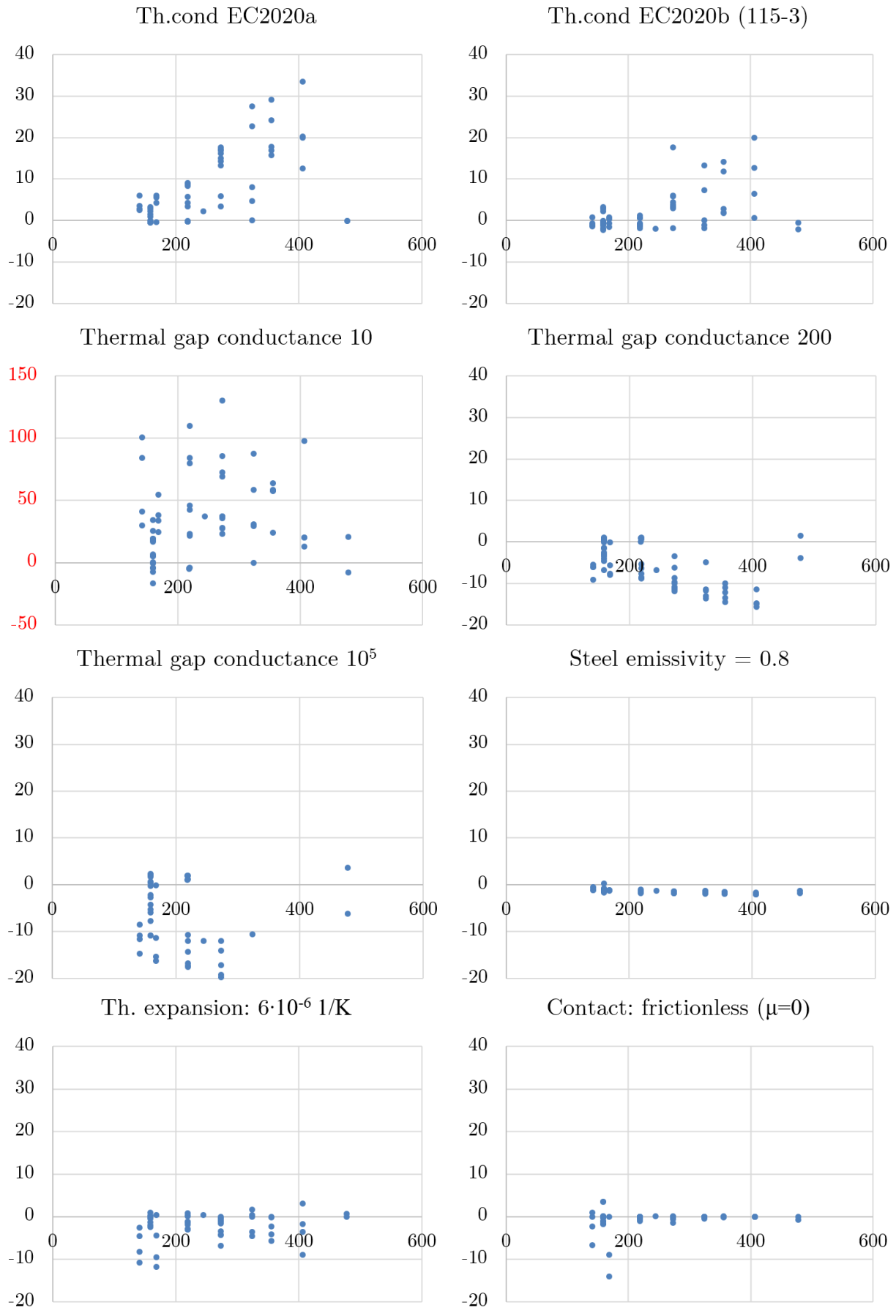


Fig. (continued) . Note changed vertical scale for 'Gap thermal conductance 10'.

### 7.6.1. The diameter and thickness of the steel tube

To investigate the influence of cross-section diameter and thickness of the steel tube on its temperatures, a 2-D thermal analysis is carried out. Temperatures are calculated for columns with three diameters (219.1 mm, 300 mm, and 350 mm) and various thicknesses (1 mm, 5 mm, 10 mm, 15 mm, and 20 mm).

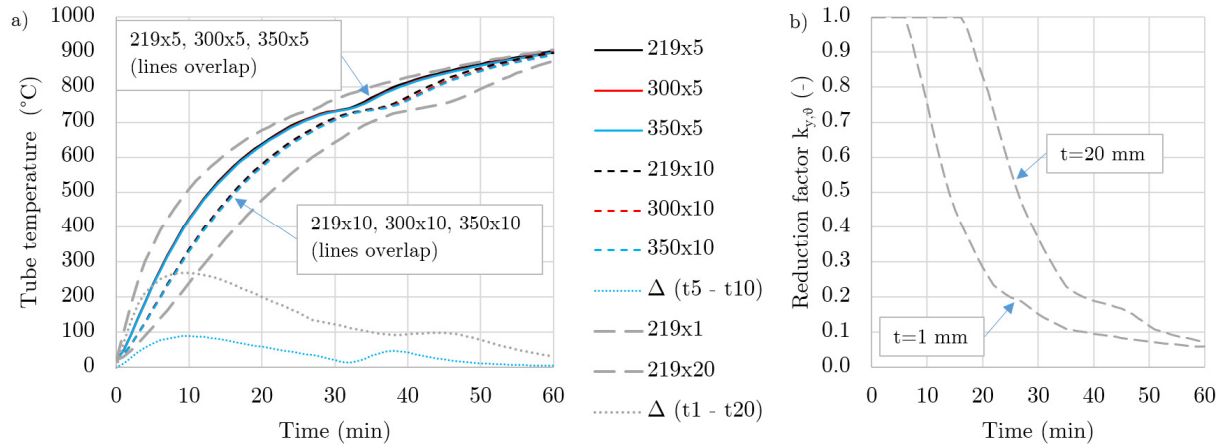


Fig. 7.32 The influence of tube thickness (5 mm, 10 mm) and tube diameter (219 mm, 300 mm, 350 mm) on tube temperature in CFST cross-section. Temperatures for 1 mm and 20 mm thickness are plotted for reference as a boundary; (b) boundaries of reduction factor  $k_{y,\theta}$ , corresponding to tube thickness of 1 mm and 20 mm.

The results presented in Fig. 7.32 (a) show that the diameter of the column (consequently the diameter of the concrete core) does not influence the tube's temperature. This is not a new finding; however, it will be shown later that the column's diameter influences the tube's temperature during cooling. With respect to the influence of thickness, a straightforward dependency can be observed – the higher the thickness, the lower the steel temperature. Two thicknesses are analysed to establish boundaries: 1 mm and 20 mm. Fig. 7.32 (b) might serve to estimate the mechanical parameters of the tube during the first 60 minutes of fire exposure.

### 7.6.2. The moisture content of concrete (sets 1, 2, 3, 4)

Two variables are studied with respect to modelling the specific heat of concrete: location and height of the peak related to water evaporation (see Fig. 7.33).

**Location of the specific heat peak** – the results summary in the lower part of

Table 7.7 shows that the location of the specific heat peak (set 1 and set 4) did not influence the FRT. For the specific heat model, see Fig. 4.2. Even for columns of smaller diameters, the effect is negligible (Fig. 7.31) This can be explained based on Fig. 7.33, which shows a negligible influence of two studied locations (115 °C and 165 °C) on the temperature inside the cross-section.

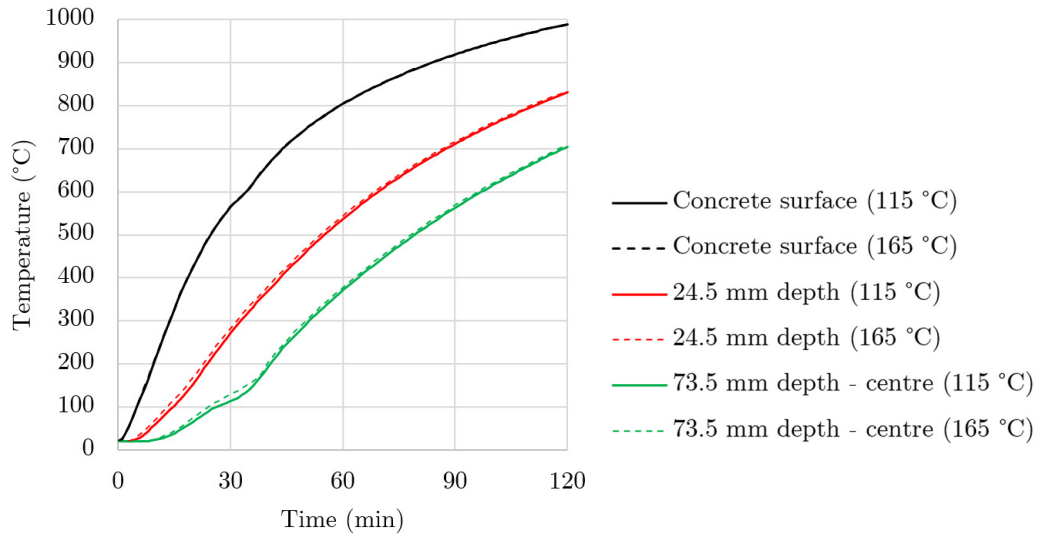


Fig. 7.33 The influence of location of the specific heat peak (115 °C, 165 °C) on temperature of concrete core (steel tube 159 mm x 6 mm).

**Moisture content** – the height of the specific heat peak (related to 3 % and 6 % moisture content) influences the results. For the specific heat model see Fig. 4.2. The overall  $FRT_{num}/FRT_{test}$  decreases from 1.05 to 0.99, when a moisture content of 3 % is assumed instead of 6 %. Fig. 7.31 shows clearly that the effect of moisture content is more pronounced for columns with larger diameters. Fig. 7.34, which additionally presents data for 10 % moisture content, shows the temperatures inside the cross-section for the three mentioned moisture contents. It can be observed that the effect of moisture content is more pronounced deeper in the cross-section.

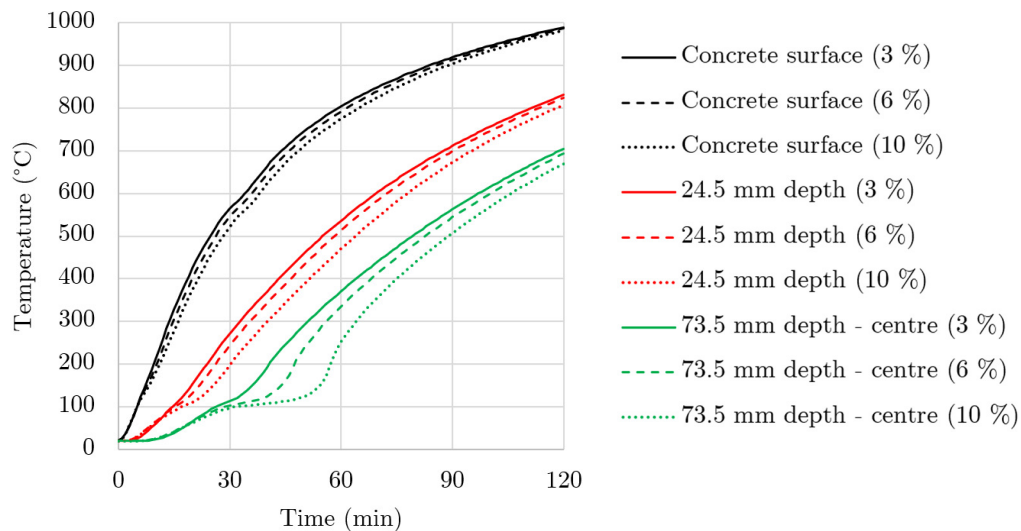


Fig. 7.34 The influence of moisture content (3 %, 6 %, 10 %) on the concrete core temperature (steel tube 159 mm x 6 mm).

### 7.6.3. Thermal conductivity of concrete (sets 1, 5, 6, 7)

**The upper limit of thermal conductivity** – the upper limit of thermal conductivity is assumed for the Reference set, as this limit was calibrated for composite structures analysed according to EN 1994-1-2, as indicated by Anderberg et al. (2004). For the thermal conductivity model see Fig. 4.3.

**The lower limit of thermal conductivity** – when the lower, instead of the upper limit of thermal conductivity is used, on average, the FRTR increases from 1.05 to 1.11. Fig. 7.31 shows a clear influence of the change – the higher the diameter, the higher the FRT change.

**The thermal conductivity from prEN 1992-1-2** – the new relationship for concrete thermal conductivity was studied for 3 % and 6 % moisture content. The difference between the lower limit of EN 1992-1-2 and prEN 1992-1-2 is negligible.

Lastly, Fig. 7.35 presents the influence of the assumed thermal conductivity model on temperature development at three depths previously referred to in Fig. 7.33 and Fig. 7.34. It can be observed that the difference between results for the lower limit of EN 1992-1-2 and formulation in prEN 1992-1-2 is negligible.

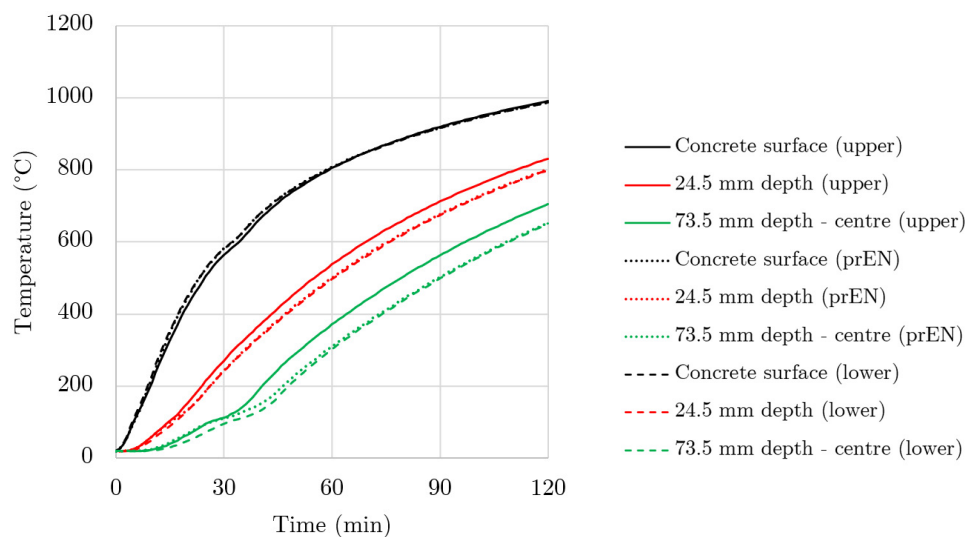


Fig. 7.35 The influence of thermal conductivity (upper and lower limit defined in EN 1992-1-2, and relationship given in prEN 1992-1-2) on the concrete core temperature (steel tube 159 mm x 6 mm).

### 7.6.4. Thermal gap conductance (sets 1, 8, 9, 10)

The study concerning thermal gap conductance served two purposes. First, different values were employed by various researchers. Furthermore, the lowest investigated value represents a possible additional highly insulating material that could be used as an internal lining of the steel tube. This was done to determine whether, if feasible, such an approach would be beneficial. Therefore, four values were investigated: 10 W/(m<sup>2</sup>·K), 100 W/(m<sup>2</sup>·K), 200 W/(m<sup>2</sup>·K) and 10<sup>5</sup> W/(m<sup>2</sup>·K). For the description of thermal gap conductance, see section 6.2.8 on page 119. Compared to the gap conductance of 100 W/(m<sup>2</sup>·K):

**Thermal gap conductance 10 W/(m<sup>2</sup>·K)** – a significant increase of FRT is observed for most analysed columns. A decrease is observed for columns relying on the steel tube and not on the concrete core (Behaviour type C). This is because a thermal barrier hinders heat transfer from steel to core. Consequentially, steel temperature is higher.

**Thermal gap conductance 200 W/(m<sup>2</sup>·K)** – an overall decrease of FRT was observed, caused by more efficient heat transfer towards the concrete core (Table 7.7, Fig. 7.31)

**Thermal gap conductance 10<sup>5</sup> W/(m<sup>2</sup>·K)** – due to more efficient heat transfer from the steel tube to the concrete core, a decrease of FRT was observed for most cases. If the column relies mainly on core load-bearing capacity – FRT decreases. If the steel tube is more important (e.g., behaviour type B or C), the FRT increases as the heat is transferred away from the tube, making the tube temperature lower than in the Reference set.

#### **7.6.5. The emissivity of the steel surface (sets 1, 11)**

A minor decrease of FRT was observed for an increased steel emissivity from 0.7 (recommended by EN 1993-1-2) to 0.8 (recommended by EN 1991-1-2). Overall, the 11<sup>th</sup> set showed the  $FRT_{num}/FRT_{test}$  mean ratio of 1.03.

#### **7.6.6. Thermal expansion of concrete (sets 1, 12)**

A constant thermal expansion coefficient of  $6 \cdot 10^{-6}$  1/K, proposed by Hong & Varma (2009) has a minor influence on the results.

#### **7.6.7. Friction between concrete and steel (sets 1, 13)**

A friction coefficient of 0.3 helps to obtain the numerical convergence. The effects of introducing a friction coefficient were further discussed in section 7.3.1.

#### **7.6.8. Engulfed and insulated length**

In both natural and test conditions, parts of columns near the supports are not directly exposed to fire. The length of a column exposed to fire (engulfed length) in standard fire resistance tests depends on the furnace's construction. In natural conditions, slabs, beams, or other types of protection might protect part of the column.

In tests described in this thesis, the protected length varied from 80 mm (Romero et al. 2011), through about 280 mm (Lie & Chabot 1992) to 500 mm (Kim et al. 2005). In the numerical model, columns are modelled as they were constructed, e.g. for specimens described by Romero et al. (2011), the total length of the column is 3180 mm, with additional load plates (300 mm x 300 mm x 15 mm each). The load is applied in the place where a knife bearing was used (Fig. 7.36 b). Furthermore, the fire exposure (modelled as radiative and convective heat fluxes) is applied to the length of the column, decreased by the protected length at the top (130 mm in case of described tests) and the protected length at the bottom (80 mm in case of described tests, see details in Romero et al. (2011) and Fig. 7.36).

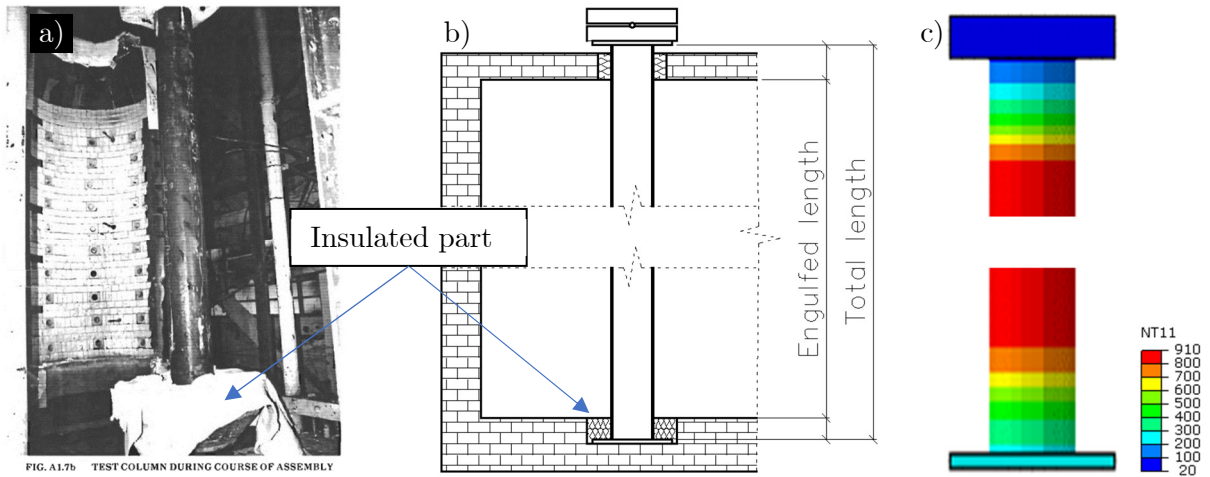


Fig. 7.36 (a) an overview of a column in a furnace (Wainman & Toner 1992), (b) areas near supports that are protected from fire (Espinosa et al. 2014), (c) temperature near the supports calculated after a 1-hour exposure. Furnace setup reproduced from Espinosa et al. (2012).

With the validated model, it is possible to investigate the effect of the protected length of the column. As an example, a column with a single geometry (159 mm x 6 mm x 3180 mm) is investigated. The results in Table 7.8 (30 MPa filling) and Table 7.9 (50 MPa filling) are given for four different loads (100 kN, 200 kN, 300 kN, and 400 kN), assuming the protected length of the column at each end of 50 mm, 100 mm, 200 mm, 300 mm, 400 mm, and 500 mm. Since the total length of the column is 3180 mm, the respective engulfed lengths are 3080 mm, 2980 mm, 2780 mm, 2580 mm, 2380, and 2180 mm. The results in Table 7.8, and Table 7.9 indicate that for the case with 300 mm protected length, the fire resistance time might increase by 8 % to 15 %. This is not to suggest such length of the column might be protected by, e.g. slabs. Instead, this study aims to investigate the potential gains resulting from, e.g. partial passive protection applied on the column.

Fig. 7.37 shows that the maximum elongation of the column is related to the insulated length. Furthermore, the higher the insulated length, the longer the fire resistance time.

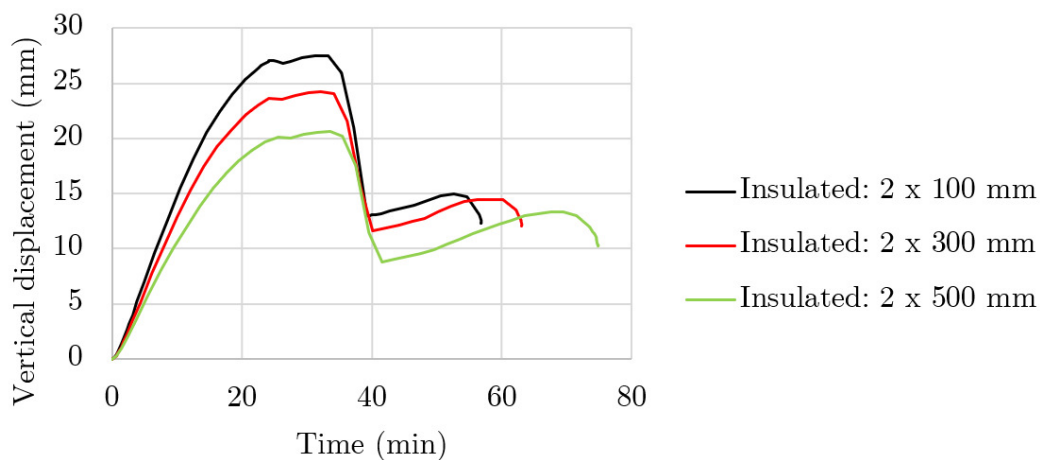


Fig. 7.37 The influence of insulated length on the vertical displacement – time relationship of a CFST column.

Table 7.8 The influence of the protected length on fire resistance time of a 159 mm x 6 mm x 3180 mm column filled with 30 MPa concrete.

Insulted length	Relative FRT for a given load			
	100 kN	200 kN	300 kN	400 kN
2 x 50 mm	55.8 minutes (100 %)	33.5 minutes (100 %)	22.2 minutes (100 %)	18.1 minutes (100 %)
2 x 100 mm	102 %	102 %	102 %	101 %
2 x 200 mm	106 %	106 %	108 %	105 %
2 x 300 mm	113 %	110 %	115 %	113 %
2 x 400 mm	128 %	121 %	132 %	128 %
2 x 500 mm	134 %	130 %	144 %	136 %

Table 7.9 The influence of the protected length on fire resistance time of a 159 mm x 6 mm x 3180 mm column filled with 50 MPa concrete.

Insulted length	Relative FRT for a given load			
	100 kN	200 kN	300 kN	400 kN
2 x 50 mm	81.1 minutes (100 %)	43.5 minutes (100 %)	33.4 minutes (100 %)	25.5 minutes (100 %)
2 x 100 mm	100 %	102 %	102 %	101 %
2 x 200 mm	105 %	105 %	105 %	105 %
2 x 300 mm	108 %	111 %	109 %	110 %
2 x 400 mm	118 %	125 %	120 %	128 %
2 x 500 mm	121 %	132 %	127 %	137 %

In conclusion, partial column insulation can increase the FRT.

## 7.7. Conclusions

The numerical model is able to capture the behaviour of CFST columns during standard fire exposure. The fire resistance time obtained in the test and the model predictions are in good agreement.

A set of reliable experimental data on standard fire resistance tests of 50 full-scale columns was presented. The collected data were put into a database – each column was described by 28 unique parameters. A fully parametrised numerical model was created, that allowed to study the influence of several modelling assumptions, that are necessary in the absence of detailed data in terms of, e.g. moisture content of concrete. Since the thermal properties are the effective properties, such a study is necessary.

A numerical study identified which factors are important and which can probably be neglected in future analyses. It also allowed to determine what properties of concrete are in demand as far as FRT is concerned. Some of the specific conclusions are as follows:

1. the confinement effect in CFST columns is lost in fire,
2. contact pairs assignment (master-slave) does not influence the results,
3. introducing friction and setting specific convergence criteria in the numerical model helps with the results convergence.

The results of the numerical studies allow to proceed to other areas that are worth exploring and will help answer the following questions:

1. What is the post-fire performance of CFST columns?
2. How could the fire performance of CFST columns be improved?

In the absence of experimental data on full-scale CFST columns after fire exposure, the model validated in standard fire conditions, enriched by reasonable assumptions, will allow for answering the 1<sup>st</sup> question.

## 8. Burnout resistance of CFST columns

### 8.1. The concept of burnout resistance and PDB analyses

This chapter analyses the response of CFST columns exposed to realistic fire. This area of research connects the recognition of the problem (Braidwood 1866), early appeals for considering actual conditions (Reed 1896), the 'full' protection of (Sachs 1903), and modern understanding of burnout resistance (Gernay et al. 2022), all of which were introduced in Chapter 2.

To achieve that, this chapter presents the necessary assumptions for the numerical model of fire-exposed CFST columns during heating and cooling. In other words, the columns are analysed until burnout, and their residual load-bearing capacity is assessed after cooling. The column is analysed assuming it is part of an open car park to address the 'realistic' fire conditions.

The EU regulation CPR 305/2011 requires that safety in case of fire is provided. One of the specific requirements to achieve this safety is to "*design and built in a way that in the event of an outbreak of fire, the load-bearing capacity of the construction can be assumed for a specific period of time*". However, this might not be enough in some cases, as avoiding demolishing the buildings as well as efficient and timely retrofitting are of utmost importance in case of fire.

The idea is to look at a building holistically – to consider events such as fire and conditions that follow the fire. That is, to design load-bearing members for burnout (a fire that ends) and to design them in a way that requires minimum refurbishment after a fire.

Burnout resistance is related to fire resistance but implies that a member or an entire structure can survive fire for the whole fire duration. The term burnout resistance was present in the earliest version of the ASTM standard. The term was later used by Thomas (1970) and was recently re-introduced by Gernay (2019).

The general objective of the research is to effectively challenge the current paradigm of the structural fire design of structures. Since the time of Ira H. Woolson, we base our evaluation of structures on the standard temperature-time curve. It hasn't changed much since then. One peculiar thing is that the temperature in such a 'standard fire' is assumed to rise indefinitely.

This chapter postulates that the existing framework can be extended using a new metric called **residual load-bearing capacity (RLBC)**, Fig. 8.1). This new metric promotes structural members that do not have their load-bearing capacity significantly reduced and are not permanently impaired by a fire. RLBC helps assess the fire resistance (or perhaps more appropriately, fire endurance) of structures.

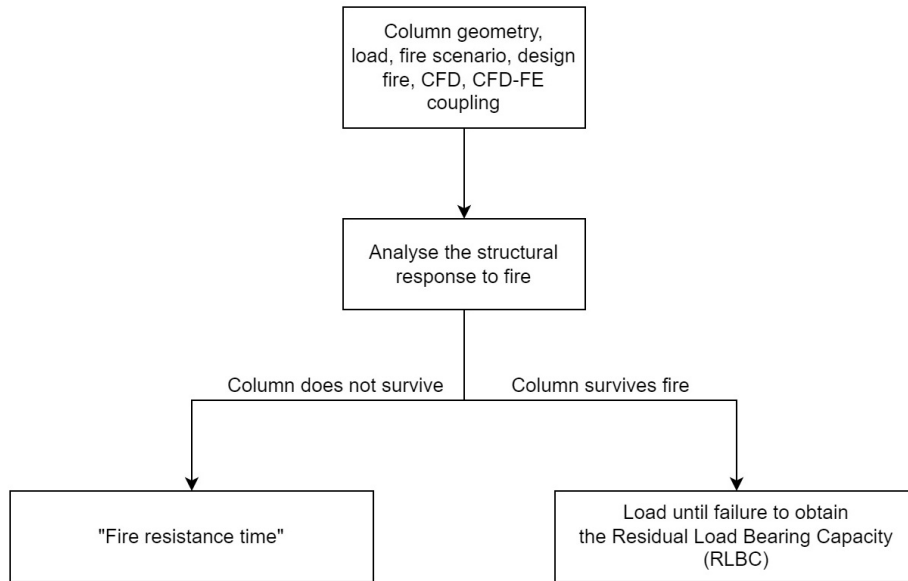


Fig. 8.1 Flowchart showing the difference between fire resistance time and RLBC.

This work also builds upon the achievements of Polish scholars, e.g. Prof. Kosiorek, who defined fire endurance as "*the time it takes for a structure to fail under actual fire conditions*". Therefore, those actual and probable fire conditions are central to this research. However, the concepts laid by Kosiorek are extended to include the possibility of the survivability of a structure under fire conditions, which is expressed by residual load-bearing capacity.

The proposed approach extends the current framework of standard fire resistance. It builds upon and extends the framework set by ISO standards such as ISO 24679-1:2019, where a step-wise procedure is recommended:

- **Step 1 - identification of FSO** – fire safety objectives – such as "*safety of life*".
- **Step 2 - identification of FR** – functional requirements (qualitative) – such as "*stability maintained for a reasonable period*".
- **Step 3 - Select Risk Analysis Approach** – Credible Worst Case (CWC), Probabilistic Approach (PA) or Semi-Probabilistic Approach (SPA).
- **Step 4 - definition of PC** – performance criteria (quantitative) - for example, if deflection is below a certain threshold, the design is considered to meet the corresponding qualitative FR.

First, the performance criteria shall be established as this study focuses on the PBD approach. The column may **(1)** fail during heating, **(2)** fail during cooling, or **(3)** not fail. The failure of the column can usually be assessed based on **(1)** the current load-bearing capacity dropping below the level of the applied load, **(2)** maximum vertical displacement, and **(3)** maximum rate of vertical displacement. The first criterion is usually used in the calculations, while the latter are adopted for fire resistance testing to protect the furnace during testing. In this work, the criterion of residual load-bearing capacity is applied, which shall be higher than the applied load during the whole duration of the fire. Notably, there are some similarities between the

chosen approach and an early ASTM E119 standard (ASTM 1918), which required members to sustain additional load after completing the fire test, or required a fire and water test.

**8.2. Numerical model**

**8.2.1. Accounting for non-reversibility in numerical analysis**

The non-reversibility of selected material properties is modelled using the USDFLD and UVARM used subroutines (Fig. 8.3). The subroutines are written in Fortran and are used to assign the material properties relevant to the maximum temperature reached during the heat transfer analysis. The non-reversibility during and after cooling is schematically shown in Fig. 8.2. The changes in concrete thermal conductivity are mainly related to the loss of all forms of water, microcracking, and increasing porosity. Thus, when concrete is heated to a specific temperature (e.g. 600 °C, Fig. 8.2), it can be assumed that conductivity maintains the same level during and after cooling (Table 8.1).

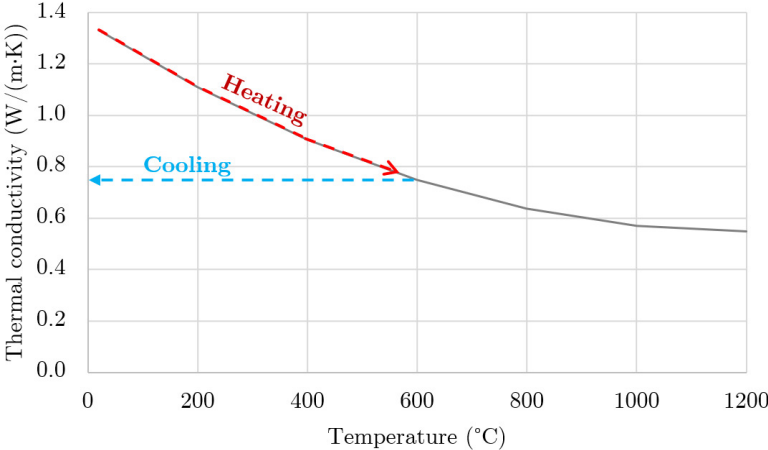


Fig. 8.2 Thermal conductivity of concrete during a heating and cooling cycle (irreversible changes occur, and the thermal conductivity is a function of the maximum temperature reached at a given point).

Table 8.1 Thermal conductivity values used in Abaqus for analyses with the lower limit of thermal conductivity (for clarity, a limited number of intermediate values in a range from 20 to 600 °C are presented).

Thermal conductivity	Current temperature	Field Variable 'Field 1', representing maximum temperature
(1)	(2)	(3)
1.333	20	20
1.111	200	20
0.907	400	20
0.749	600	20
0.637	800	20
0.570	1000	20
0.549	1200	20
<b>1.111</b>	20	200
<b>1.111</b>	200	200
0.907	400	200
0.749	600	200
0.637	800	200
0.570	1000	200
0.549	1200	200

0.907	20	400
0.907	200	400
0.907	400	400
0.749	600	400
0.637	800	400
0.570	1000	400
0.549	1200	400
0.749	20	600
0.749	200	600
0.749	400	600
0.749	600	600
0.637	800	600
0.570	1000	600
0.549	1200	600

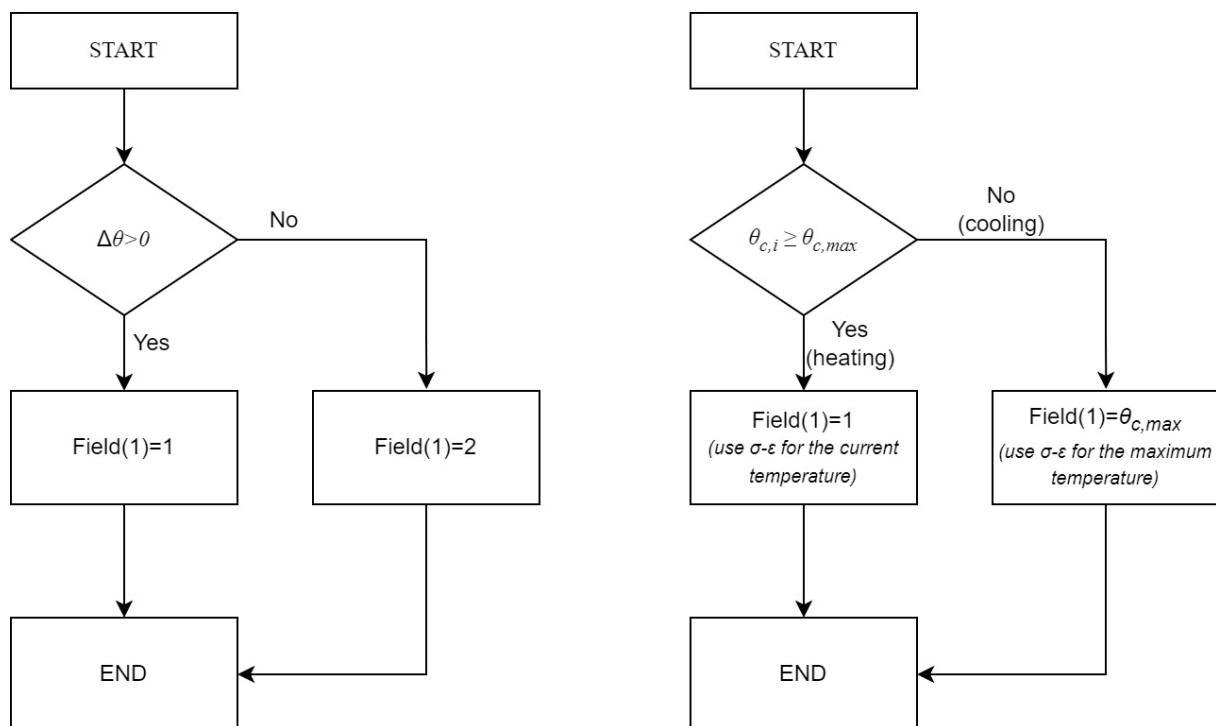


Fig. 8.3 User subroutine flowchart for an automatic selection of thermal properties in heating and cooling phases: (a) subroutine proposed by Tan et al. (2020); (b) subroutine used to consider the possibility of many heating and cooling cycles.

A clear distinction between heating and cooling can be made in idealised fire conditions, such as parametric fire. Due to thermal inertia, the temperature of parts deeper in the cross-section increases. After reaching a peak value, the temperature gradually decreases. However, the temperature change during heating and cooling might not be monotonic for real fires.

### 8.2.2. Temperature within cross-section during heating and cooling

This section presents temperatures within two cross-section in an idealised fire with a decay phase, where the temperature-time curve follows the standard fire exposure for 60 or 120 minutes, followed by a linear decay. Two cross-sections are chosen to illustrate the temperatures at various depths over time:  $d \times t = 159 \text{ mm} \times 6 \text{ mm}$  and  $d \times t = 219.1 \text{ mm} \times 6 \text{ mm}$ .

*159 mm x 6 mm cross-section after one-hour and two-hour exposure followed by linear decay*

Fig. 8.4 presents the temperature development in a 159 mm x 6 mm cross-section filled with concrete. An upper limit of thermal conductivity is assumed, with non-reversible changes in thermal properties during cooling. The left hand side graphs (a, c, e) present the results for a 60-minute exposure followed by decay. The right hand side graphs (b, d, f) present the results for a 120-minute exposure followed by decay. Fig. 8.4 (a, b) show the exposure temperature (assuming gas temperature and effective radiation temperature are equal, as argued in Chapter 3.1.2). Fig. 8.4 (a, b) present temperature at the concrete face (73.5 mm), and at various distances from the centre (60 mm, 45 mm, 30 mm, 15 mm, and 0 mm). Fig. 8.4 (c, d) present the temperature profile along the radius of the cross-section after selected times (from 30 to 600 minutes).

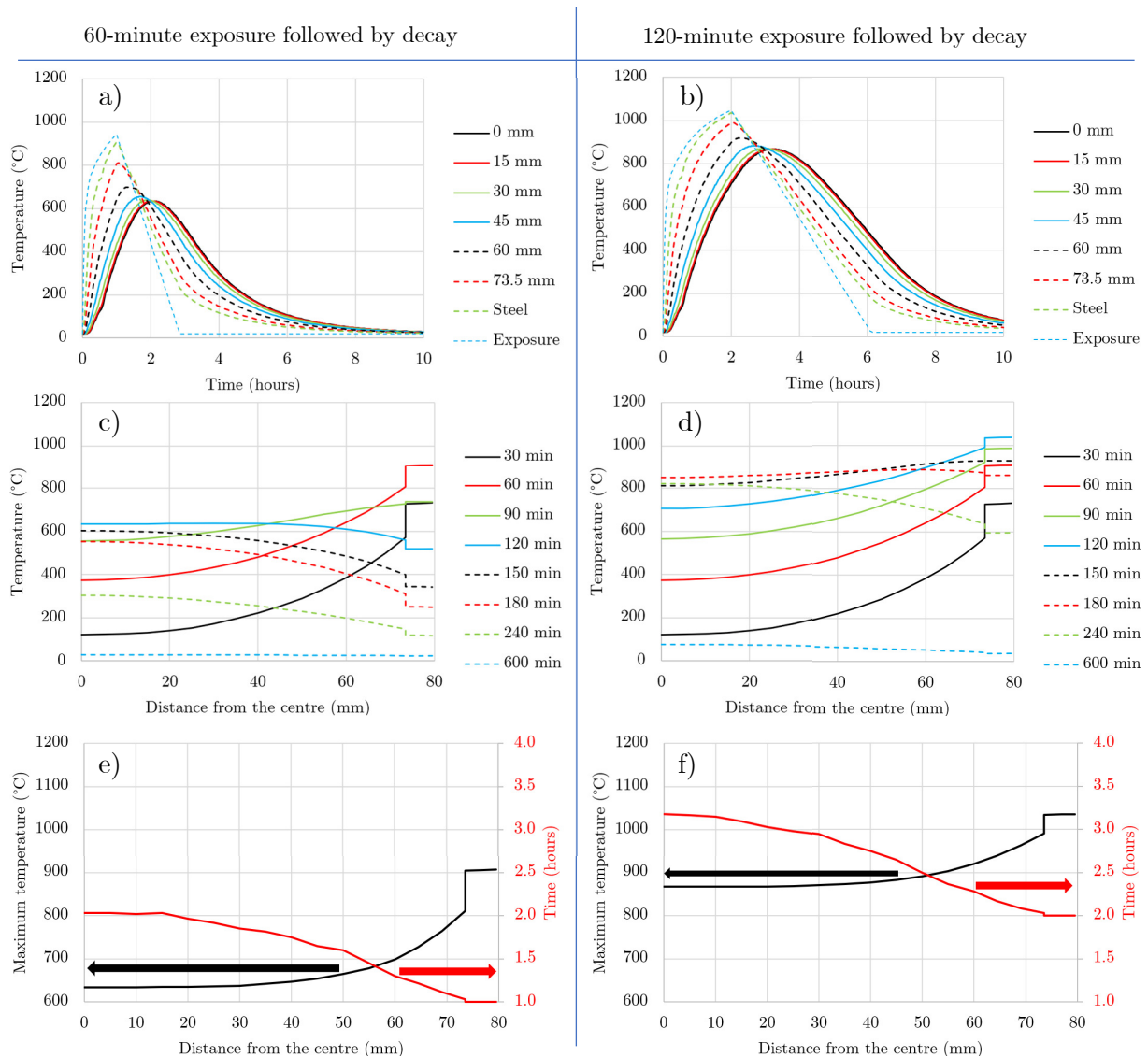


*Fig. 8.4 Temperature development in a 159x6 cross-section filled with concrete. An upper limit of thermal conductivity is assumed, with non-reversible changes in thermal properties during cooling. Left: 60-minute exposure followed by cooling. Right: 120-minute exposure followed by cooling.*

The lower part of Fig. 8.4 (e, f) illustrates when the maximum temperature is reached at a given distance from the cross-section centre. As expected, the highest temperature of the steel

tube is reached at the end of fire exposure. However, the highest temperature in the centre is reached after two hours for a 60-minute heating phase (Fig. 8.4 e) and after more than three hours for a 120-minute heating phase (Fig. 8.4 f). This means that the lowest load-bearing capacity will occur not within the heating phases, but later – during or after the decay phase.

*219 mm x 6 mm cross-section after one-hour and two-hour exposure followed by linear decay*

Fig. 8.5 presents the temperature development in a 219 mm x 6 mm cross-section filled with concrete. An upper limit of thermal conductivity is assumed, with non-reversible changes in thermal properties during cooling. The left hand side graphs (a, c, e) present the results for a 60-minute exposure followed by decay. The right hand side graphs (b, d, f) present the results for a 120-minute exposure followed by decay.

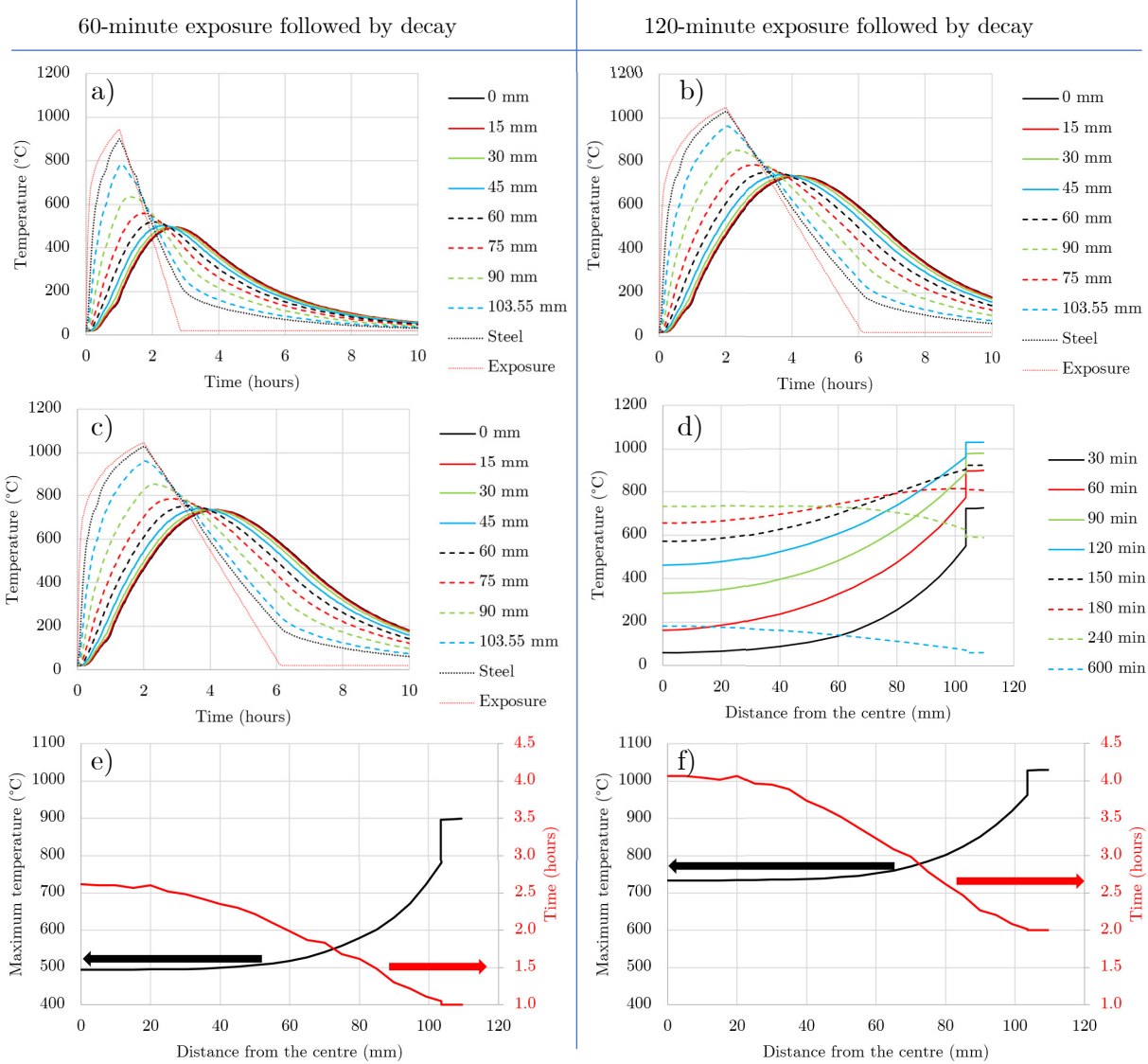


Fig. 8.5 Temperature development in a 219.1x6 cross section filled with concrete. Upper limit of thermal conductivity is assumed, with non-reversible changes in thermal properties during cooling. Left: 60-minute exposure followed by cooling; right: 120-minute exposure followed by cooling.

Fig. 8.5 (a, b) show the exposure temperature, temperature at concrete face (103.55 mm), and at various distance from the centre (90 mm, 75 mm, 60 mm, 45 mm, 30 mm, 15 mm, and

0 mm). Fig. 8.5 (c, d) present the temperature profile along the radius of the cross-section after selected times (from 30 to 600 minutes).

The lower part of Fig. 8.5 (e, f) illustrates when the maximum temperature is reached at a given distance from the cross-section centre. Similar to Fig. 8.4, the highest temperature of the steel tube is reached at the end of fire exposure. However, the highest temperature in the centre is reached after two and a half hours for a 60-minute heating phase (Fig. 8.5 e), and after four hours for a 120-minute heating phase (Fig. 8.5 f). This means that the lowest load-bearing capacity will occur not within the heating phases, but later - during or after the decay phase. Furthermore, it will occur later than in the case of smaller cross-section (Fig. 8.4). Column's diameter only slightly affects the temperature of the steel tube during cooling. When graphs in Fig. 8.4 (d) and Fig. 8.5 (d) are compared, the difference is visible at the 180<sup>th</sup> minute.

Fig. 8.6 (a) and Fig. 8.7 (a) present the reduction factors for concrete strength after 30, 60, 90, and 120-minute exposure. The graphs on the right (b) present the retention factors for concrete after 60-minute exposure and decay (red dashed line), and after 120-minute exposure and decay (blue dashed line). By comparing those lines, it can be observed, how the thermal inertia of the concrete core influences the strength retained by concrete.

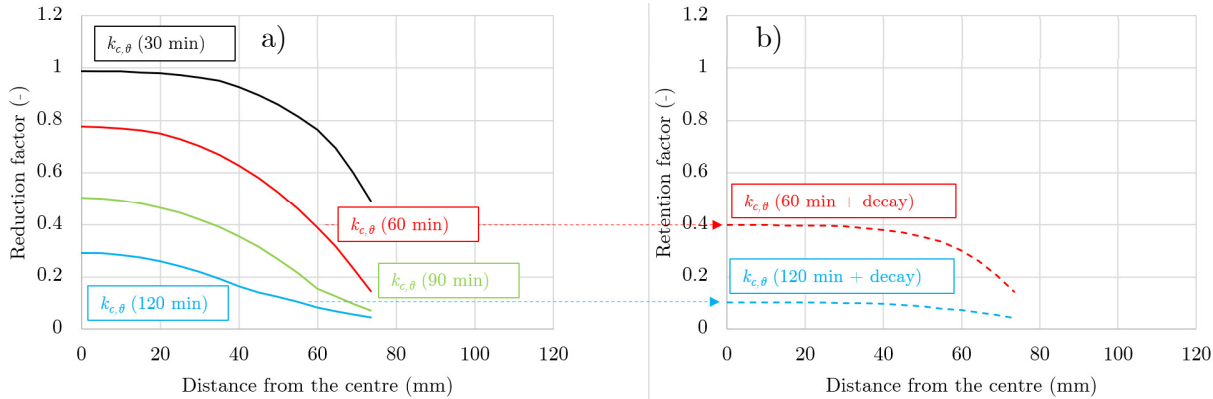


Fig. 8.6 Reduction and retention factors for a 219.1x6 cross-section filled with siliceous concrete. Left: Reduction factors after 30-, 60-, 90- and 120-minute exposure. Right: Retention factors after 60- and 120-minute exposure followed by cooling. Reduction and retention factors correspond to temperatures in Fig. 8.4.

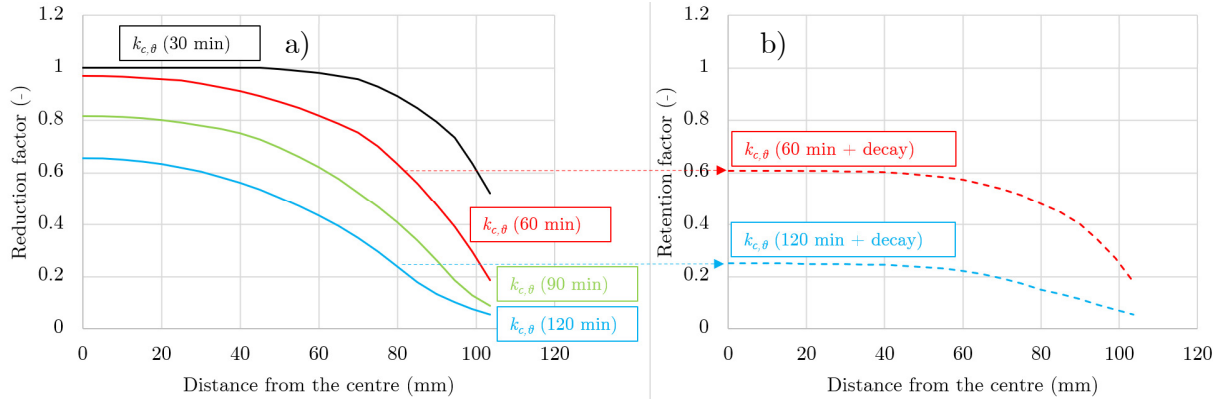


Fig. 8.7 Reduction and retention factors for a 219.1x6 cross-section filled with siliceous concrete. Left: Reduction factors after 30-, 60-, 90- and 120-minute exposure. Right: Retention factors after 60- and 120-minute exposure followed by cooling. Reduction and retention factors correspond to temperatures in Fig. 8.5.

### 8.3. Case study (car park)

Thermal analysis is required to analyse the structural fire behaviour of structural members exposed to high temperatures caused by fires. Typically, a standard temperature-time curve is used. However, the localised fire methodology can be applied in large compartments where a fully developed fire is less likely to occur. For realistic fires, the analysis should be based on qualitative fire scenarios and a quantitative description of appropriate design fires.

The investigation is based on the thermo-mechanical analyses of structures in fire, where the thermal exposure is obtained from the computational fluid dynamics (CFD) analyses performed in FDS. Coupled analyses have been around for some time (Welch et al. 2008). The Adiabatic Surface Temperature was introduced by Wickström et al. (2007), and since then, several tools have been developed to transfer data from FDS to FE codes. For instance, FDS2FEM (Paajanen et al., 2013) and FDS2FTMI (Silva et al., 2016). Malendowski & Glema (2017) used the radiation intensities approach. However, they later preferred the AST approach (Malendowski 2018, Malendowski et al. 2021) due to its computational efficiency, which allowed analysis of large steel structures under fire. While some early efforts focused on radiation intensities (Tondini et al., 2016), recent papers frequently favour the AST approach (Khan et al., 2021; Yan & Gernay, 2021; Yan et al., 2022).

In a previous paper (Szymkuć et al. 2018b), we presented the methodology of CFD-FEM coupling (FDS-Abaqus), where we investigated the fire of four cars around the column, a common scenario at that time. However, recent fires involving more cars indicate such a scenario might not be safe, as seen in car park fires in Liverpool, Stavanger, or Warsaw.

Metrics used by other researchers to assess the post-fire resistance of columns are, e.g. residual strength index (RSI) or the duration of the heating phase (DHP). The RSI is the residual load-bearing capacity of a column after heating and cooling. It was used by, e.g. Huo et al. (2009) and Rush et al. (2015) to help describe the experimental results. Tan et al. (2020) used the RSI in numerical analyses of full-scale columns under standard temperature-time conditions followed by cooling. Gernay (2019) proposed the DHP metric, and defined it as "*the shortest duration of the heating phase that leads to eventual failure of the structural member*".

The state-of-the-art analysis indicates that available metrics were used only for standardized fire conditions and did not account for realistic fire conditions also referred to as natural fire, physically-based fire exposure, or a realistic fire. That is why, in this chapter, the burnout resistance of CFST columns is investigated under realistic fire conditions. The novelty of this research is two-fold: the type of columns investigated and the design fire.

It is common to use a fire scenario with a number of cars limited to three or four, sometimes with one larger car representing a utility vehicle. However, until now, it has not been shown how different design fires might affect the columns' structural fire behaviour, including its **residual load-bearing capacity (RLBC)**. The RLBC considers fire and normal conditions that follow a realistic fire that ends. Such a metric might promote structural members that do not have their load-bearing capacity significantly impaired due to a whole course of fire.

There is limited research on the behaviour of CFST columns under realistic fire scenarios. Previous studies, such as those conducted by Yang et al. (2013) and Guo et al. (2017), examined

square CFST columns exposed to fire on less than four sides, while [Chen et al. \(2019\)](#) did experiments on CFST columns subjected to a parametric fire followed by a blast load. [Wang et al. \(2015\)](#) investigated the localised fire model and proposed a simple approach using an equivalent fire severity concept but did not account for non-uniform exposure. Other studies, such as those by [Fike & Kodur \(2009\)](#), [Dimia et al. \(2017\)](#), and [Ibáñez et al. \(2018, 2019\)](#), investigated the effect of fire with a decay phase. Still, none considered localized or travelling fires with non-uniform exposure along the length of a member. The study presented in this chapter fills this gap and demonstrates the capabilities of advanced coupled CFD and FEM analyses.

### 8.3.1. Geometry of the building

A multi-storey open car park with a flat deck is under consideration. This structure comprises four levels, each 32.0 m wide and 55.0 m long. The minimum clearance height is 2.4 m, and the storey height of the car park is 3.0 m. Columns are positioned at all nodes of the 16.0 m x 5.0 m rectangular parking module grid. The floor structure is made of concrete slabs supported by 16.0 m long beams positioned every 5.0 m. The parking levels can be accessed by a lengthwise ramp and two staircases for internal communication and means of escape. Each parking space measures 2.5 m x 5.0 m. Spandrels prevent vertical fire spread. The parking geometry is shown in Fig. 8.8.

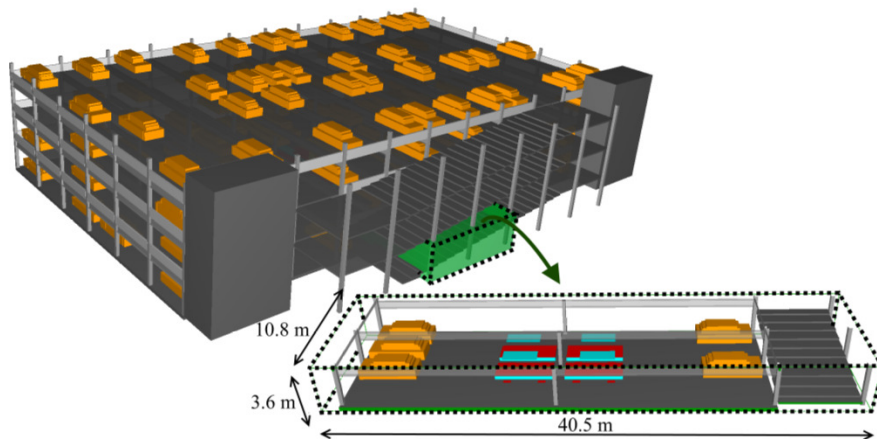


*Fig. 8.8 Numerical model in FDS and boundaries of the computational domain used for the 4-car fire scenario (Szymkuć et al. 2018b).*

### 8.3.2. Fire scenario and the design fire

The fire scenario assumes that cars are arranged in two rows, and that fire can spread from the first car to the second one in 12 minutes. The fire starts in car ① and, after 12 minutes, spreads to cars marked as ②. After another 10 minutes, the fire propagates to cars marked with ④, it takes another 10 minutes for cars marked with ⑤, and another 10 minutes for cars marked with ⑥ to start burning.

The base fire scenario involves a four cars around the column on one of the decks. The fire scenario and the design fire are presented in Fig. 8.9 (a). Further parts of Fig. 8.9 present scenarios for 8, 12, and 16 cars. It is important to note that vertical propagation of fire from one storey to another has been observed in several large open car park fires.

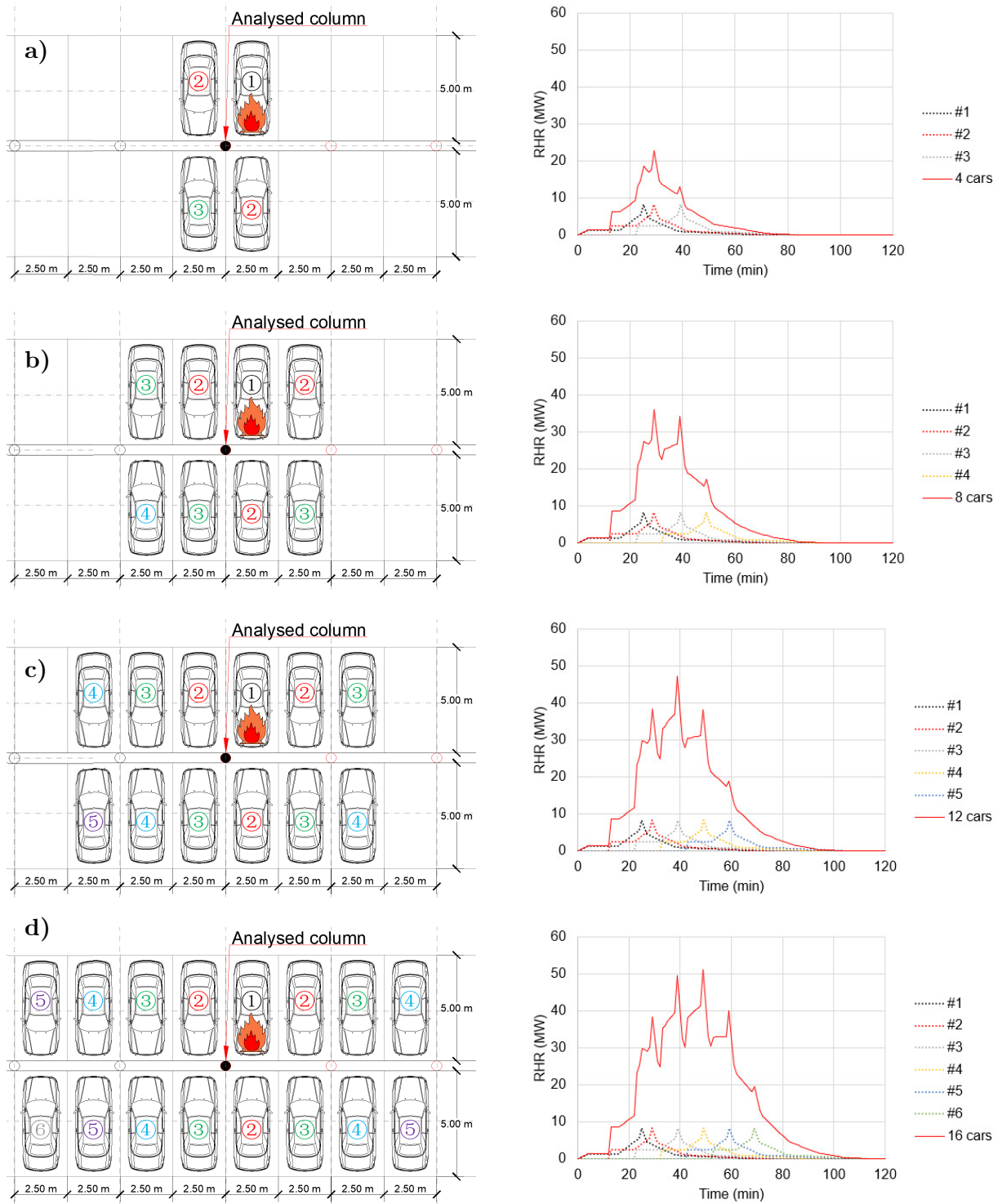


Fig. 8.9 Layout of the cars in car park and total HRR for a given scenario: a) four cars; b) eight cars; c) twelve cars; d) sixteen cars.

The heat release rate curve of one burning car is based on the work of [Schleich \(1999\)](#), and includes both the fire growth and decay phases (Fig. 8.10).

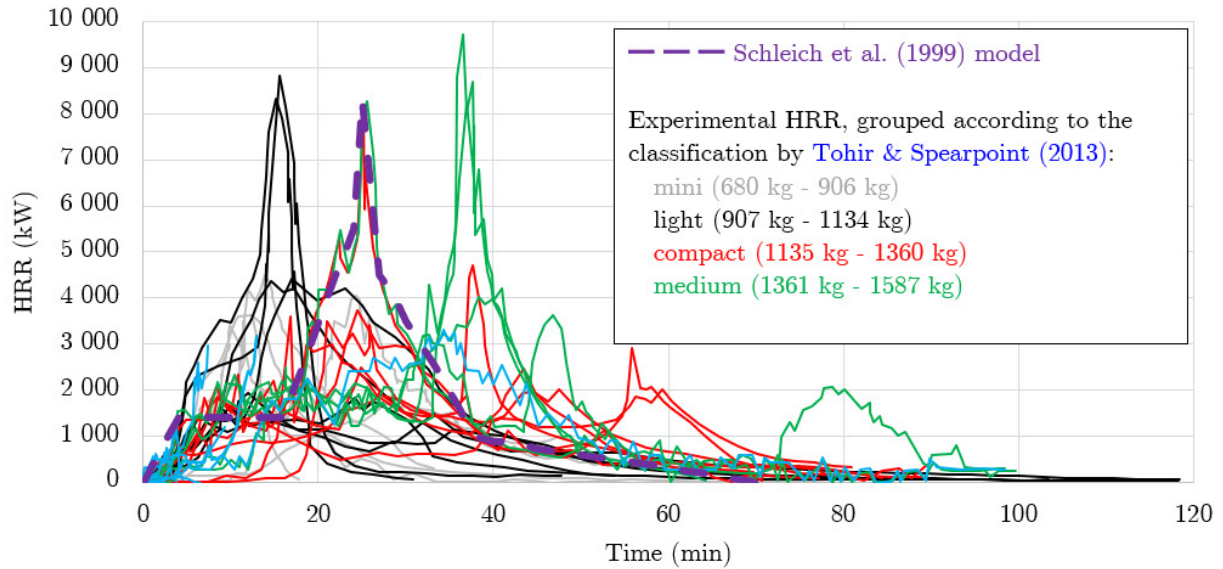


Fig. 8.10 Heat release rates from various experiments. Colours are used to distinguish the classification by *Tohir and Spearpoint (2013)*. The Schleich model, adopted in this chapter is also marked.

### 8.3.3. Fire

It shall be stressed that the CFD simulation presented here is performed only to have reasonable heating and cooling conditions for the CFST column. Therefore, the unnecessary details are omitted for clarity.

A simulation of a fire was conducted using FDS 6.7.5 software. The computational domain was limited to the area where the fire had the most impact. The dimensions of the computational domain were 40.5 m x width x 3.6 m, where width depended on the fire scenario. A sensitivity study was conducted for grid resolutions of 0.075m, 0.100m, 0.125m, 0.150m, 0.200m, and 0.300m, with the cell aspect ratio set to 1.0. Based on the obtained results, their convergence and run times, the grid size of 0.15 m x 0.15 m x 0.15 m was chosen.

For the simulation, a car was modelled as a cuboid platform with a burning top surface. The Heat Release Rate Per Unit Area (HRRPUA) was assigned to the surfaces using a simple pyrolysis model (*McGrattan et al. 2020*). The heat release rate was assigned to the top of the cuboid platform, a rectangular surface measuring 4.5 m x 1.8 m at a height of 0.6 m, which resulted in  $HRRPUA = 1024.7 \text{ kW/m}^2$ . The simulation did not consider the influence of weather conditions or ventilation systems. The computational domain boundaries were set as OPEN, allowing free heat and smoke outflow, and fresh air inflow. Other relevant parameters like fuel species ( $C_{1.0}H_{1.8}O_{0.17}N_{0.17}$ ), soot yield (0.1 kg/kg), radiative fraction (0.35) are listed in Table 8.2. The distances between the cars were 0.6 m or 0.75 m. The temperature-dependent materials properties were taken from the available guidelines (*McGrattan et al. 2020; Hurley 2016; Eurocode 2; Eurocode 3*).

Table 8.2 CFD model details.

<b>Software</b>	FDS 6.7.5
<b>Maximum number of burning cars</b>	4, 8, 12 or 16
<b>Computational domain</b>	Four-car scenario: 40.5 m x 10.8 m x 3.6 m Eight-car scenario: 40.5 m x 22.8 m x 3.6 m Twelve-car scenario: 40.5 m x 28.8 m x 3.6 m Sixteen-car scenario: 40.5 m x 28.8 m x 3.6 m
<b>Mesh size</b>	0.15 m
<b>Total fire load from a single car</b>	6.8 GJ
<b>Peak HRR from single car</b>	8.3 MW
<b>Car geometry and HRR</b>	Cuboid platform 4.5 x 1.8 x 0.6 m, max 1024.7 kW/m <sup>2</sup>
<b>Boundaries</b>	OPEN, without wind
<b>Fuel</b>	C <sub>1.0</sub> H <sub>1.8</sub> O <sub>0.17</sub> N <sub>0.17</sub>
<b>Soot yield</b>	0.1 kg/kg
<b>Radiative fraction</b>	0.35

### 8.3.4. CFD-FE coupling

FDS can be used to calculate temperatures within a solid only in limited cases. The limitations concern, e.g. (i) circular members that cannot be precisely modelled in FDS, (ii) thermal gap conductance, or (iii) non-reversibility of the material properties during cooling, which cannot be modelled in FDS. Furthermore, each CFD simulation took from two to four weeks to finish (depending on the computational domain size). Modelling the column in an FE code allows to consider various cross-sections and materials based on a single time-consuming CFD analysis. This has another advantage: the AST data can be reused for other types of columns, such as reinforced concrete or steel columns.

Therefore, a dedicated interface to extract the AST from CFD and use it as a thermal boundary condition in FE software is necessary. In such a way, CFD code can be used to simulate fire, and a FE code can be used for thermal and subsequent mechanical analysis of a column.

The temperature from those points is then mapped on an auxiliary circular surface (a concept similar to the envelope of receiving surfaces, see EN 1991-1-2, Annex G) to calculate convective and radiative heat fluxes (see sections 3.1.1, 3.1.2 and 3.2). The AST is used to provide complementary information about the heat exposure of the structure. It is a single quantity used to describe the convection and radiation influences. The heat flux between the surrounding fire environment and the surface of the CFST column is described by a formula which takes into account the steel emissivity, the Stefan-Boltzmann constant, the convective heat transfer coefficient, the adiabatic surface temperature (FDS output), and the temperature of the external surface of the CFST column (calculated in Abaqus). Therefore, the heat fluxes can be expressed as:

$$\begin{aligned} \dot{h}_{net,c} &= \alpha_c(\theta_{AST} - \theta_m) \\ \dot{h}_{net,r} &= \Phi \varepsilon_m \varepsilon_f \sigma (\theta_{AST}^4 - \theta_m^4) \end{aligned} \quad (8.1)$$

where the symbols were explained in section 3.1. In Abaqus, the heat-transfer finite elements were used (DC3D8).

This auxiliary surface is present only in heat transfer analyses and does not contribute to the mechanical analyses. Heat transfer analyses in the solid phase are carried out in the FE software Abaqus, considering thermal contact (gap) conductance between steel and concrete equal to  $100 \text{ W}/(\text{m}^2 \cdot \text{K})$ .

Eight measuring points are distributed along the circumference on each selected height at twenty equally distributed levels, resulting in 160 measurement points. The data were stored every 2 seconds. Each AST device in FDS faced the direction normal to the steel tube (see Fig. 8.11). Fig. 8.11 depicts a column with the AST measuring points (marked as small red squares, making an analogy to ideal plate thermometers). The three charts in Fig. 8.11 show the Adiabatic Surface Temperature (black) and gas temperature (light red) at three different heights (52.5 cm, 157.5 cm, and 292.5 cm). The two lower charts clearly show the importance of radiation in the lower part of the column.

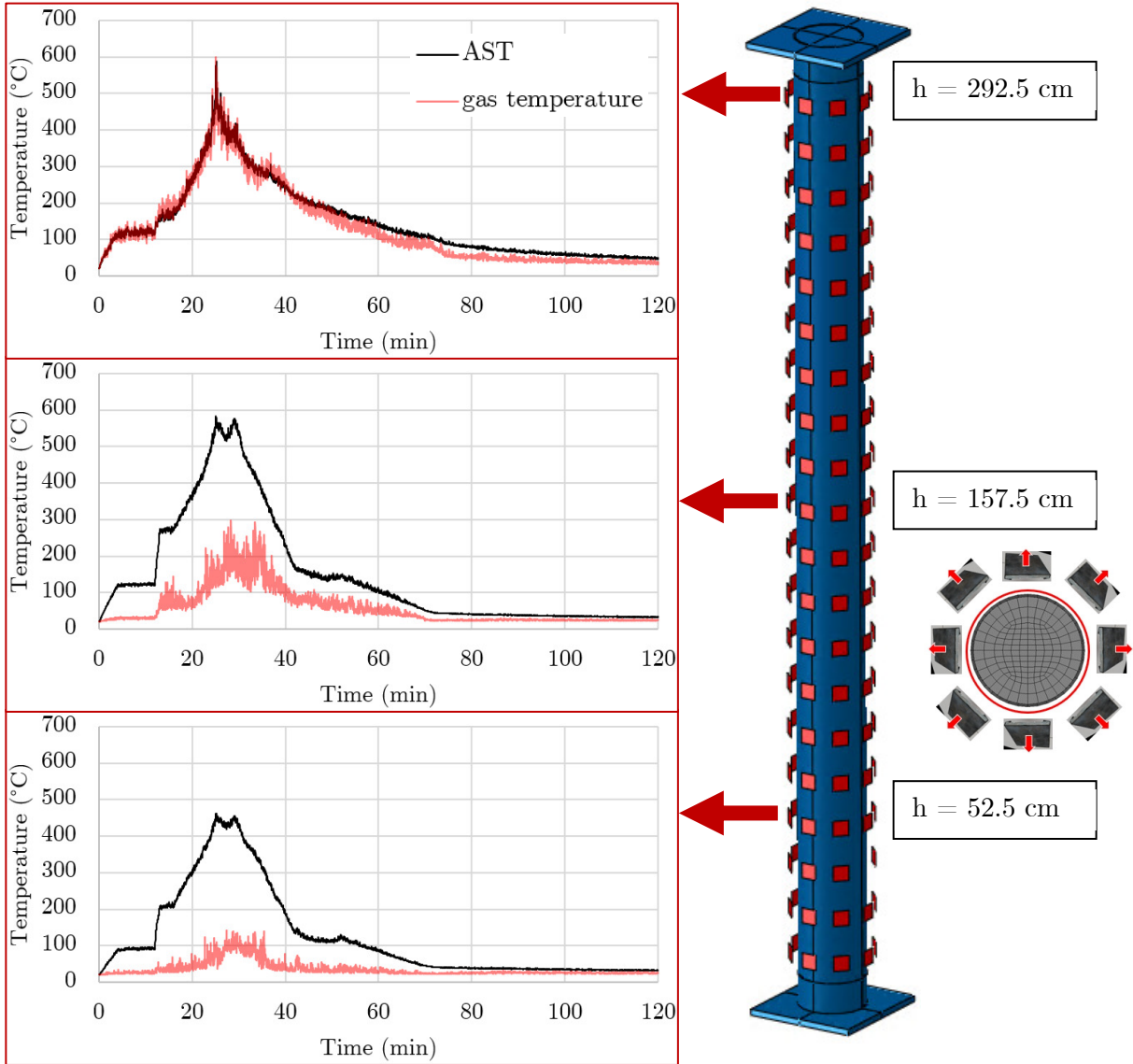


Fig. 8.11 Visualisation of the column, with the AST measuring points (marked as small red squares) and AST and gas temperature corresponding to three points at three different heights (for a four-car fire scenario). Right: the cross-section of a CFST column, with the auxiliary envelope (red circle), and eight AST measuring points distributed along the circumference.

Fig. 8.12 shows the maximum AST and maximum gas temperature at the height of the column, for a four-car fire scenario. It can be observed that the AST is higher in the lower parts of the column (where radiation is dominant). In the upper part of the column, the gas temperature is higher than the AST. Note, that AST is the measure of the effective exposure; therefore, it is always between effective radiation temperature and gas temperature.

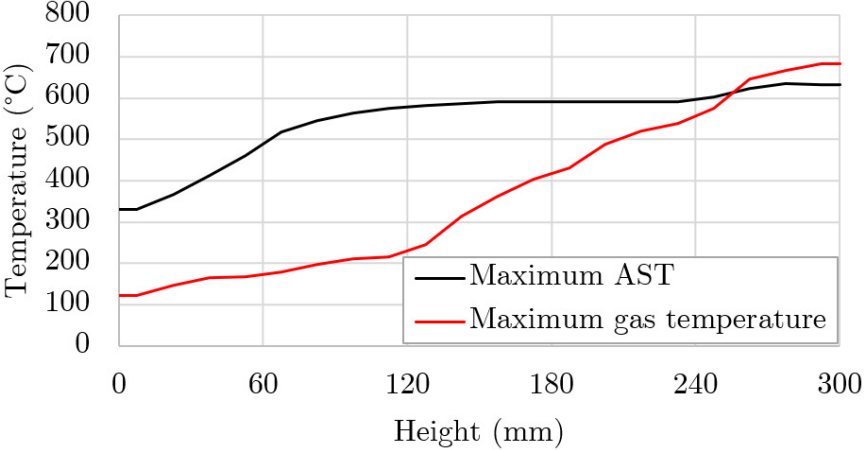


Fig. 8.12 Graph showing maximum AST and maximum gas temperature at height of the column, for a four-car fire scenario.

This section presented the exposure conditions for a column. The boundary conditions in terms of the AST are prescribed to Abaqus. Three stages of the FE analysis can be distinguished:

- heat transfer (section 8.3.5),
- column behaviour during heating and cooling (section 8.3.6),
- determination of the RLBC, if the column survived the whole fire (section 8.3.6).

**8.3.5. Results of the thermal analysis**

Quantifying the thermal effects of a localized fire and presenting it graphically can be challenging, as the exposure changes over time and space. For each of the points marked in Fig. 8.11, a separate graph could be made showing the exposure conditions. Even more graphs could be used to show temperature-time data inside the column. For the sake of clarity and to omit multiple figures showing temperatures at the boundaries or inside the cross-section (at different levels), the histograms of AST were created (Fig. 8.13). Histograms present the AST at the perimeter of the column during fire scenarios involving a varying number of burning cars. Data for the histogram in Fig. 8.13 were gathered for 7200 seconds of each fire simulation, the relative frequency of all bins sums to 1, and the bin with temperature between 20 °C and 100 °C was omitted for clarity. The data presented in Fig. 8.13 show that increasing the number of cars from four to eight results in a higher frequency of temperatures in the range of 200 °C to 700 °C. The difference is pronounced for temperatures between 500 °C and 600 °C. Increasing the number of cars to twelve or sixteen does not change the results significantly.

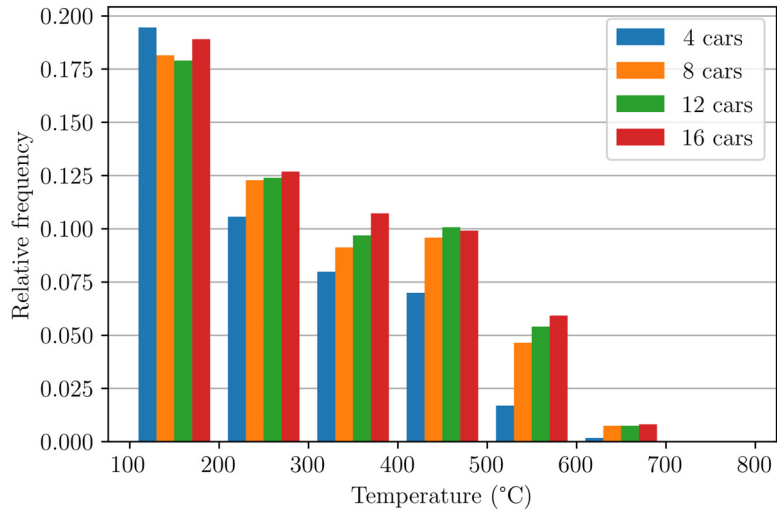


Fig. 8.13 Histogram of AST for the four investigated fire scenarios.

Fig. 8.14 shows one side of the steel tube temperature after 40 minutes of four presented fire scenarios. Fig. 8.15 presents temperature field within a concrete core cross-section (about 30 cm below the column's top).

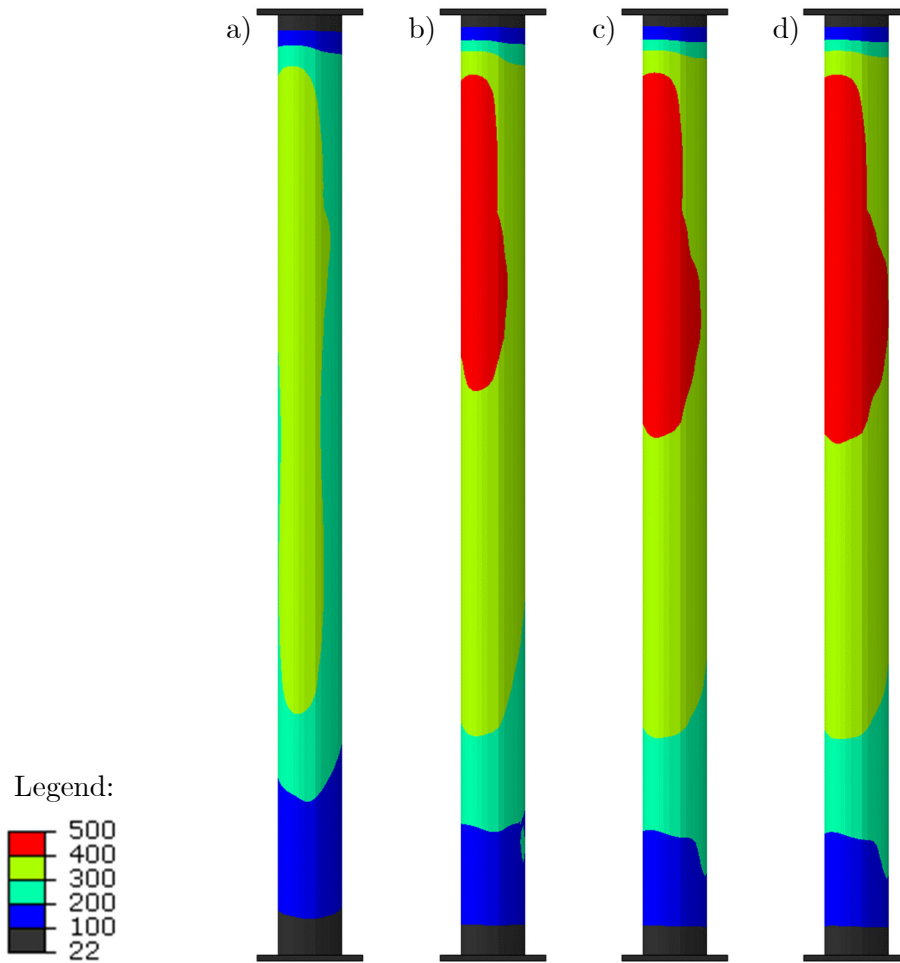


Fig. 8.14 Steel temperature (in °C) after 40 minutes (a) four-car, (b) eight-car, (c) twelve-car, (d) sixteen-car fire scenario.

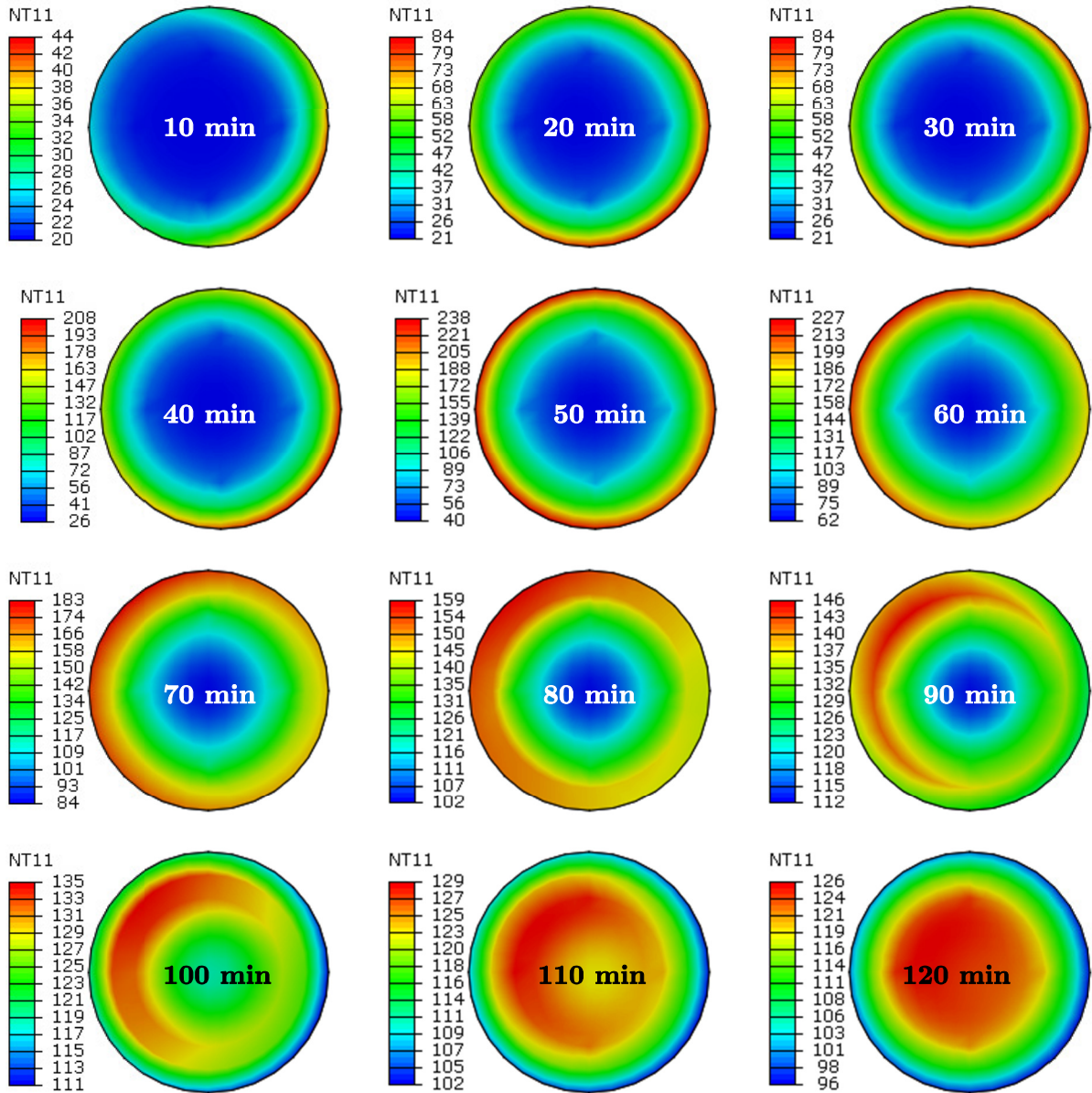


Fig. 8.15 Temperature field (in °C) in one of the upper cross-sections of the column (after 10 – 120 minutes).

It can be clearly seen that no number of Figures can help assess the severity of fire exposure. Therefore, ultimately the fire resistance time, or the residual load-bearing capacity, will be used to assess the column's performance.

### 8.3.6. Results of the mechanical analysis

For subsequent mechanical analysis, the same FE model was utilized, but with the FE type C3D8R. The temperature history of each FE node was based on data obtained from thermal analysis. Material properties during the heating process were taken from Eurocodes. For cooling Fortran user subroutines were used (USDFLD and UVARM), as explained in section 8.2. Steel and concrete were modeled using Mises and Drucker-Prager yield criteria, respectively. Thermal properties of concrete, such as specific heat, thermal conductivity, and density were considered non-reversible. The specific heat peak was modelled with for a moisture content of 3%. Stress-

strain relationships for concrete at elevated temperatures were modeled as a function of current and maximum temperature. Additional compressive strength loss during or after cooling was not considered.

The investigated column is a concrete-filled steel tube (219.1 mm x 5 mm, steel S235), filled with normal weight concrete with an initial compressive strength of 40 MPa. The column length is 3200 mm, with a fixed bottom and pinned top. The restraints by the surrounding structure are not considered.

The burnout resistance is affected by the field of the highest temperatures reached inside the column. The compressive strength of concrete is permanently lost when it is exposed to high temperatures. Additionally, the pre-existing load can influence the post-fire behaviour of the column by affecting its deformation during heating.

The analysis is conducted in multiple steps. Firstly, the data from the CFD model is extracted and mapped properly. Then, the heat transfer analysis between fire and solid is performed, and the resulting temperature history of the CFST column is calculated. Next, a mechanical analysis is conducted where the column is loaded, and its structural behaviour is analysed. If the column survives burnout, it is loaded until failure (with a displacement-controlled procedure at the 20-hour mark) in the last step.

The behaviour of a CFST column was investigated under three different initial loads (1100 kN, 1500 kN, and 2000 kN). Fig. 8.16 shows that when the initial load is 1100 kN, the column survives the fire, and the residual load-bearing capacity is 1957 kN. When the initial load is increased to 1500 kN, the column also survives the fire. However, the residual load-bearing capacity is lower – 1761 kN. When the initial load is 2000 kN, the column fails during cooling. The failure occurs in the cooling phase: less than three hours after the fire started.

Even though the fire ended in less than two hours, the heat was accumulated for a longer time. As a result, a column was exposed to elevated temperatures for a time longer than what would appear from scenarios presented in Fig. 8.9. Furthermore, due to the thermal inertia, the temperature inside the concrete core rises after the peak of the RHR and the exposure. Consequently, it takes several hours until the temperature of the whole column returns to the initial ambient temperature (20 °C).

It is common to express the structural fire behaviour of CFST columns by presenting the vertical displacement at their top throughout fire exposure (Fig. 6.1). Fig. 8.16 illustrates such behaviour. The initial vertical displacement (starting point at time = 0 h) represents the column contraction due to the load at ambient temperature, which is about 2 mm to 4 mm, depending on the initial load. Then, the tube elongates due to its increasing temperature and thermal expansion of steel. After some time, the tube starts to shrink (either due to reaching its load-bearing capacity or due to the decay of fire).

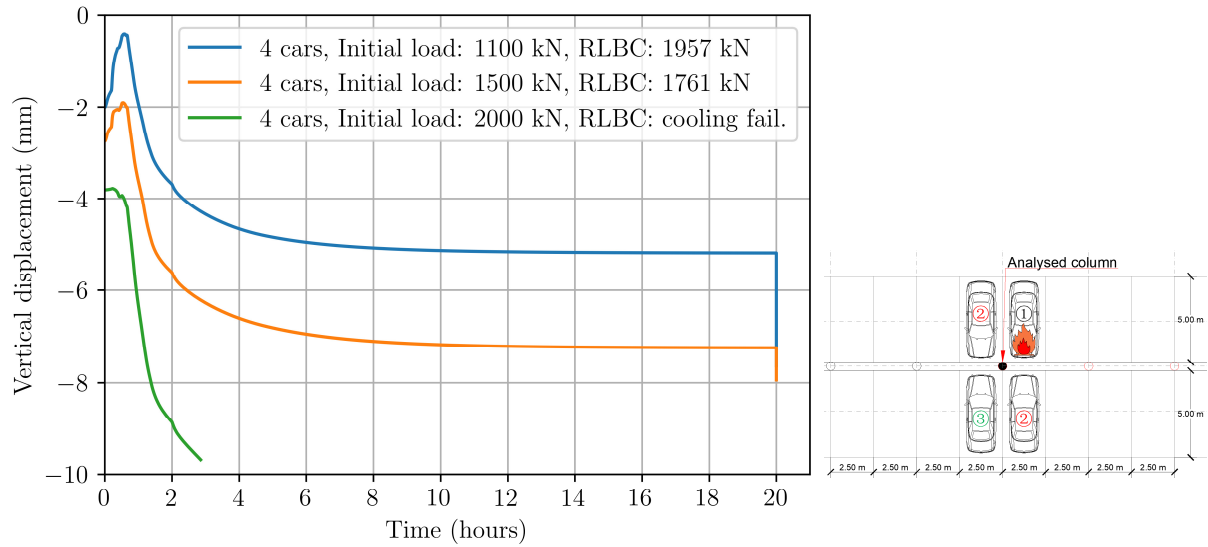


Fig. 8.16 Vertical displacement at the top of the column in a four-car fire scenario and three initial loads: 1100 kN, 1500 kN, and 2000 kN. The residual load-bearing capacity (RLBC) is given in the legend.

The next figure (Fig. 8.17) presents the results for the same column, but the fire scenario involves eight cars. Interestingly, only the column loaded to 1100 kN was able to survive the fire. Columns preloaded at 1500 kN and 2000 kN failed after six hours and 90 minutes, respectively.

Interestingly, only the column loaded to 1100 kN survived the fire, unlike in the four-car fire scenario. Columns preloaded at 1500 kN and 2000 kN failed during the cooling stage. In the case of a 1500 kN load, the failure occurred during the exposure; however, the RHR was near zero at that time (Fig. 8.9). For the highest load, the failure occurred when the cars were no longer burning.

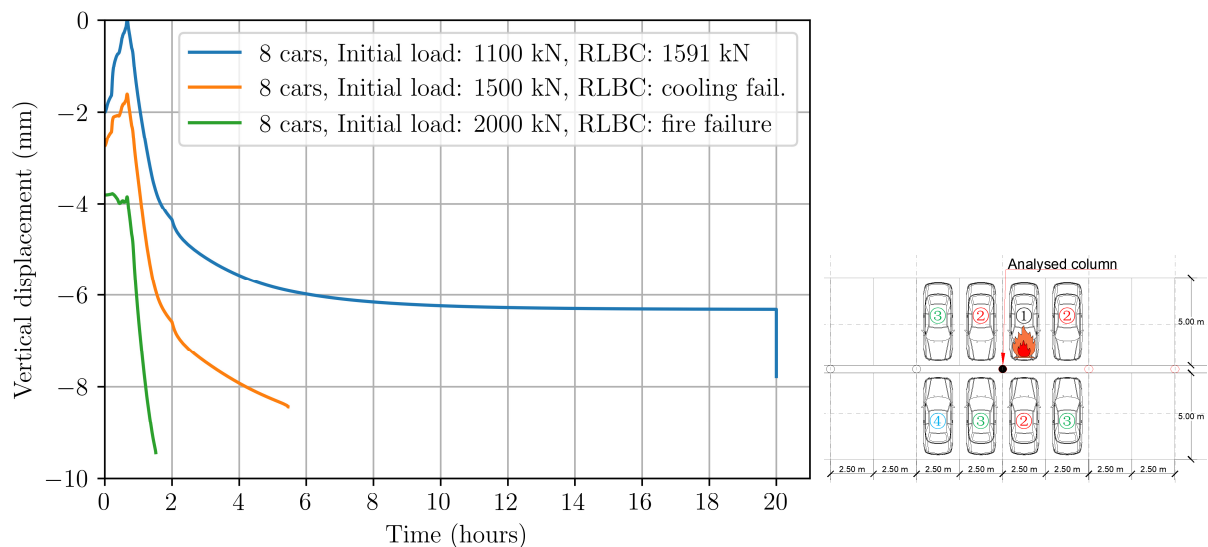


Fig. 8.17 Vertical displacement at the top of the column in an eight-car fire scenario and three initial loads: 1100 kN, 1500 kN, and 2000 kN. The residual load-bearing capacity (RLBC) is given in the legend.

Importantly, the comparison of the RLBC for a load of 1100 kN shows a significant difference when the effect of a four-car fire, and eight-car fire are considered (decrease of the RLBC from 1957 kN to 1591 kN).

Increasing the number of cars to twelve or sixteen did not change the results significantly (the respective RLBC is 1468 kN, and 1408 kN for an initial load of 1100 kN).

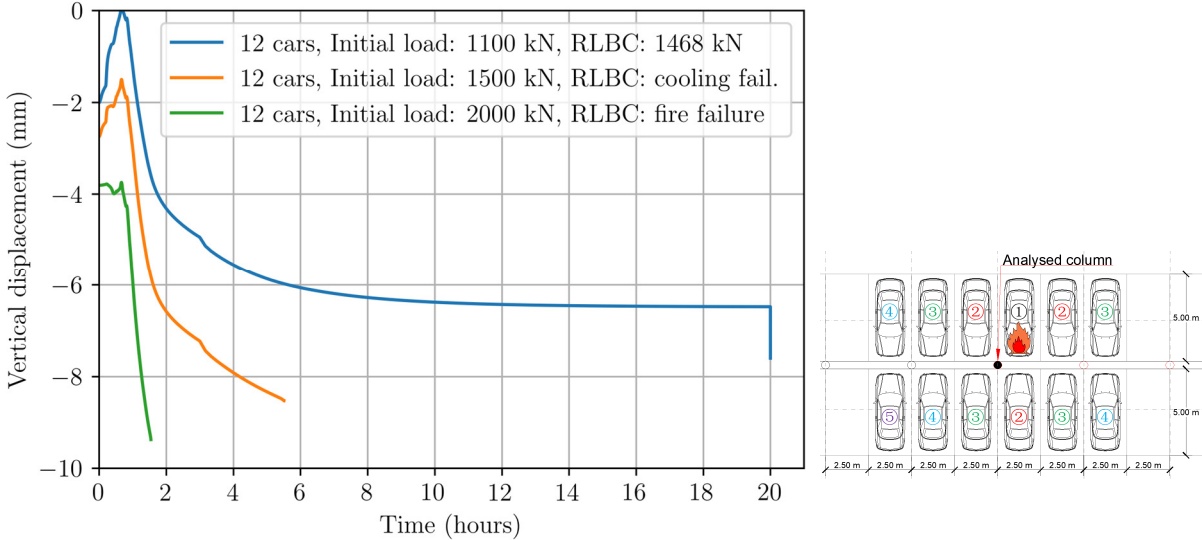


Fig. 8.18 Vertical displacement at the top of the column in a twelve-car fire scenario and three initial loads: 1100 kN, 1500 kN, and 2000 kN. The residual load-bearing capacity (RLBC) is given in the legend.

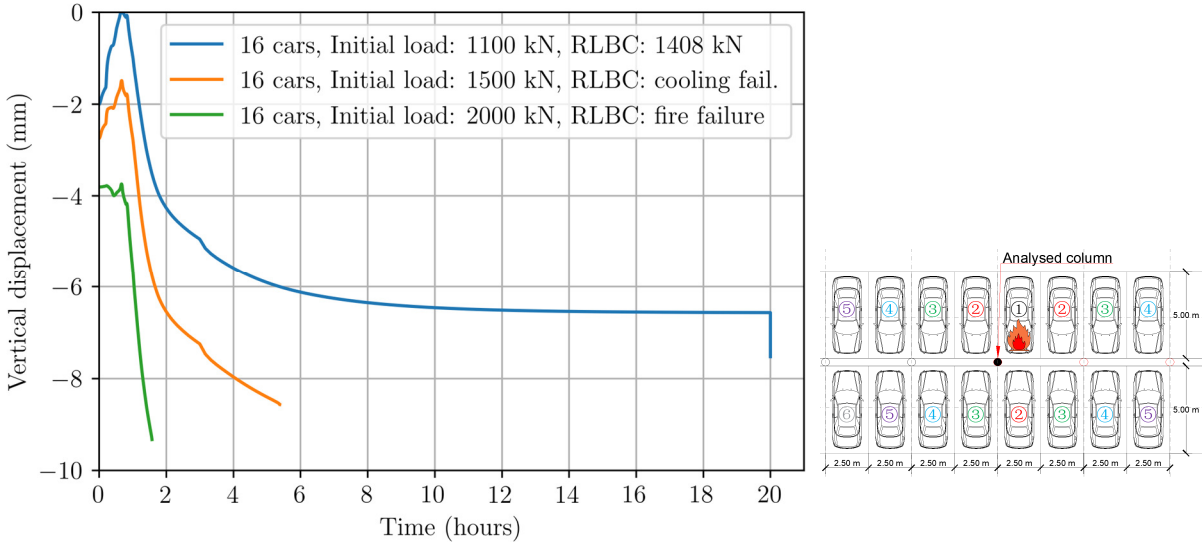


Fig. 8.19 Vertical displacement at the top of the column in a sixteen-car fire scenario and three initial loads: 1100 kN, 1500 kN, and 2000 kN. The residual load-bearing capacity (RLBC) is given in the legend.

### **8.3.7. Conclusions**

The CFD-FEM interface was successfully used to investigate the influence of the initial load and four fire scenarios on the burnout resistance and residual load-bearing capacity of the CFST column. The study showed that limiting the number of cars in fire to just four is questionable. It was demonstrated that an increased number of vehicles could significantly alter the fire response of a column.

For the investigated cases, various types of fire behaviour were observed, including (i) failure during the heating stage, (ii) failure during the cooling phase, and (iii) the burnout resistance. In the future, the deterministic approach, could be enriched by the probabilistic approach.

To better quantify the burnout resistance, the columns that survived the entire fire were loaded until failure, and the results were expressed in terms of the maximum sustained load. The study showed that the residual load-bearing capacity (RLBC) could be significantly affected by the fire exposure and by the initial load level.

## 9. CFST with lightweight cementitious composites

The parametric study presented in the previous chapter identified factors important when considering an improvement of the fire performance of CFST columns. Those factors are:

- (1) an increase of the compressive strength of concrete,
- (2) a decrease of the thermal conductivity of the filling,

Factor (1) can be realised by designing concrete with higher compressive strength. However, a high strength concrete is known to be more prone to the effects of elevated temperature. A positive effect may be achieved by using a concrete (cementitious composite) not as prone to elevated temperature as ordinary concrete. Factor (2) can be realised by using a low-density filling (ergo: low thermal conductivity). Other factors can be helpful, for example change of steel surface emissivity (achievable through using e.g., galvanised, or stainless steel), providing thermal barrier on the core-tube interface. However, it seems that the most significant improvement can be made through the modification of the filling of CFST column. Moreover, the filling can be designed to have specific properties, which are in demand.

With the aim to develop a material with an enhanced resistance to elevated temperatures, a theoretical-experimental study is conducted.

It is known that elevated temperature caused by fire has a detrimental effect on the mechanical properties of concrete. This effect is attributed to various physio-chemical processes, including dehydration of cement paste, weakening of the interfacial transition zone (ITZ), and growth of microcracks. Propagation of microcracks results from differences in thermal expansion (thermal incompatibility) between cement paste and aggregate (Pimienta et al. 2017). Consequentially, aggregates with a low coefficient of thermal expansion positively affect strength during and after exposure to elevated temperatures (Halicka et al. 2013; Khoury et al. 2007). Several studies underlined the influence of aggregate composition (Qureshi et al. 2020; Schneider 1982) and the physicochemical properties, such as a porous outer shell of lightweight aggregates, on the compressive strength of concrete (Lu et al. 2021).

Fly Ash Cenosphere (FAC) might be a material suitable for diminishing the negative effects fire has on concrete and cementitious composites. FAC (Fig. 9.1) is a silica and alumina sphere usually smaller than 0.5 mm in diameter. Like fly ash, it is a by-product of coal combustion in thermal power plants (Hanif et al. 2016). According to Kolay and Singh (2001), FAC particles are filled with inert gases (mainly CO<sub>2</sub> and N<sub>2</sub>); however, the presence of other gases and water was also reported (Bradło 2016). From the perspective of this study, the essential properties of FAC are its bulk density (400 kg/m<sup>3</sup>), thermal conductivity (0.1 W/(m·K)), and low coefficient of thermal expansion (Arizmendi-Morquecho et al. 2012; Losiewicz et al. 1996). Compared to ordinary concrete, those properties provide reduced self-weight and better thermal insulation of FAC-based cementitious composites. The thermal expansion coefficient of cenosphere was reported as about 6·10<sup>-6</sup> 1/K (Arizmendi-Morquecho et al. 2012; Shen et al. 2021). It is lower than the thermal expansion of common aggregates used for concrete (see Fig. 9.4). Consequentially, low thermal expansion might result in improved thermal compatibility between cement paste and aggregate (i.e., cenosphere).



*Fig. 9.1 A bowl of loose cenosphere and a cylinder.*

Materials consisting of cement and FAC were mentioned for the first time in patents in the 1970s (Biederman Jr. 1970; Gebhardt 1971). In 1984, Montgomery & Diamond (Montgomery & Diamond 1984) published a paper on the influence of FAC on the cracking of cement pastes, though without referring to their density or strength properties. The use of FAC in cementitious cenospheres is usually associated with the potential to reduce weight. Hence, the resultant composites will be referred to as **LCCC – Lightweight Cementitious Composites with fly ash Cenosphere**. In 1996 Losiewicz et al. (1996) developed low strength (up to 3 MPa), insulating LCCC with thermal conductivity between 0.1 W/(m·K) and 0.15 W/(m·K). The first LCCC suited for structural applications were developed by Lilkov et al. (1999), who designed several composites with densities around 1550 kg/m<sup>3</sup> and compressive strength up to 41 MPa. Three years later, McBride et al. (2002) pioneered using FAC with coarse aggregate. They were also the first to combine FAC with silica fume (SF), significantly improving compressive strength. In the following years, LCCC did not attract much attention until Chia et al. (2011) developed the LCCC with the strength to density ratio reaching almost 45 MPa/(kg/dm<sup>3</sup>). In the following years, several researchers studied LCCC at ambient temperatures, as indicated in a review by Danish et al. (2022). However, data on the influence of elevated temperatures on LCCC is scarce. Fig. 9.2 depicts the yearly number of scientific papers with experimental data on LCCC, published each year since 1999. Moreover, the appearance of papers related to the influence of elevated temperatures on LCCC can be observed in 2017.

Studies published prior to 2017 indicated the benefits of using FAC in heat-resistant materials other than cementitious composites (Chávez-Valdez et al. 2011; Puri and Khanna 2016). However, those studies did not report the effect of elevated temperatures on mechanical strength. Chávez-Valdez et al. (Chávez-Valdez et al. 2011) attributed FAC with high thermal stability, high thermal shock resistance, and low thermal expansion due to mullite. Ranjbar & Kuenzel 2017 drew similar conclusions. Wang et al. (2012) attributed the growth of mullite from FAC to the silica-based matrix to the increased flexural strength after sintering at temperatures up to 1300 °C. In addition to mullite, the presence of gehlenite was confirmed by (Huang et al. 2017), which was reported to fill cracks after high-temperature exposure (Ma et al. 2015; Sobia et al. 2015).

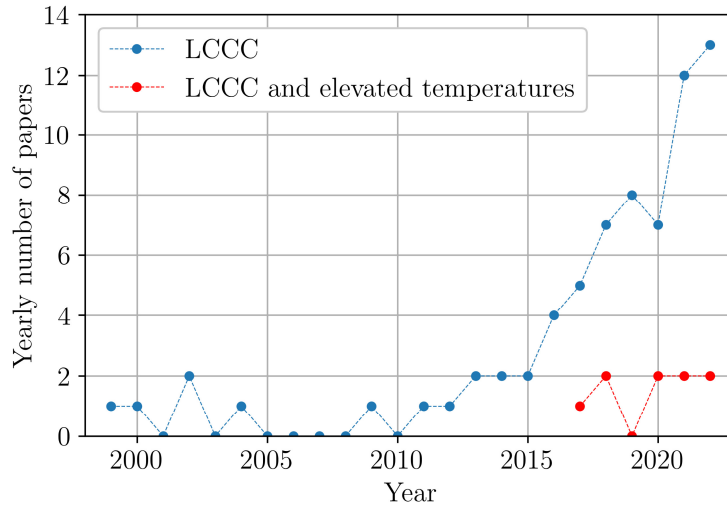


Fig. 9.2 The yearly number of experimental papers on LCCC since 1999. The first paper on the influence of elevated temperatures was published in 2017.

The low thermal conductivity, low coefficient of thermal expansion and presence of mullite were exploited by various researchers to develop heat-resistant materials. For example, thermal barrier coatings (Arizmendi-Morquecho et al. 2012; Chávez-Valdez et al. 2011), refractories (Pundiené et al. 2018), intumescent coatings (Puri and Khanna 2016) and FAC/mullite composites (Ren et al. 2018). However, there is a lack of research regarding the influence of elevated temperatures on the properties and microstructure of cementitious composites with cenospheres. Huang et al. (Huang et al. 2017, 2018) reported that the residual compressive strength of LCCC was better than that of ordinary concrete. They studied mixes with a constant amount of FAC, focusing on the effect of different kinds and amounts of fibres and two fly ash replacement levels. Szymkuć et al. (Szymkuc et al. 2018a) investigated a single mix and reported thermal conductivity at ambient temperature and strength properties after high-temperature exposure. Other researchers did not explore the impact of high temperatures on the mechanical properties of cement pastes with FAC. Instead, they turned their attention to the effect of limited range temperatures (up to 450 °C, 600 °C or 800 °C) on composites, where FAC was used with other aggregates (Danish & Mosaberpanah 2021; Gupta & Kua 2020; Shen et al. 2021).

The motivation of this research is to investigate the properties of a material that, in the future, could be used in structural applications, such as filling of steel tubular columns (Espinosa et al. 2015; Szymkuc et al. 2018a) or other composite members (Liew et al. 2017), preferably providing them with enhanced fire resistance. Composites with fly ash cenosphere might fulfil those demands. The existing research indicates that cenosphere was primarily used for high temperature applications in various types of coatings, and the knowledge of the performance of cementitious composites with FAC after exposure to high temperatures is limited. This study provides results regarding LCCC tested after exposure to temperatures up to 1200 °C, obtained on mixes with varying FAC to binder ratios, with or without polypropylene fibre. The experimental results are compared with the standard mortar. The main differences are found in density, residual strength and microstructure after heating and cooling. Compared to ordinary concrete, LCCC possess superior strength to density ratio, which might cause a decrease in material consumption due to reduced self-weight.

Most of the research on composites with cenospheres focuses on material properties. Data on the performance of members or structures are limited.

Fig. 9.3 presents the compressive strength and thermal conductivity in relation to the density of FAC composites. In Fig. 9.3 and in subsequent sections, there is a distinction between FAC-pastes (cement paste with FAC as the only aggregate), FAC-mortars (FAC and fine aggregate) and FAC-concretes (FAC and coarse aggregates, sometimes with other fine aggregates). The authors of 57 papers analysed the influence of FAC on the properties of cement paste, 10 articles describe mortars and 9 deal with concretes. Only [Sahmenko et al. \(2018\)](#) examined both pastes and mortars in one paper, and only the PhD thesis of Mohaine (2018) contains data on both mortars and concretes. Values of thermal conductivity of 149 FAC-composites were found in 20 references.

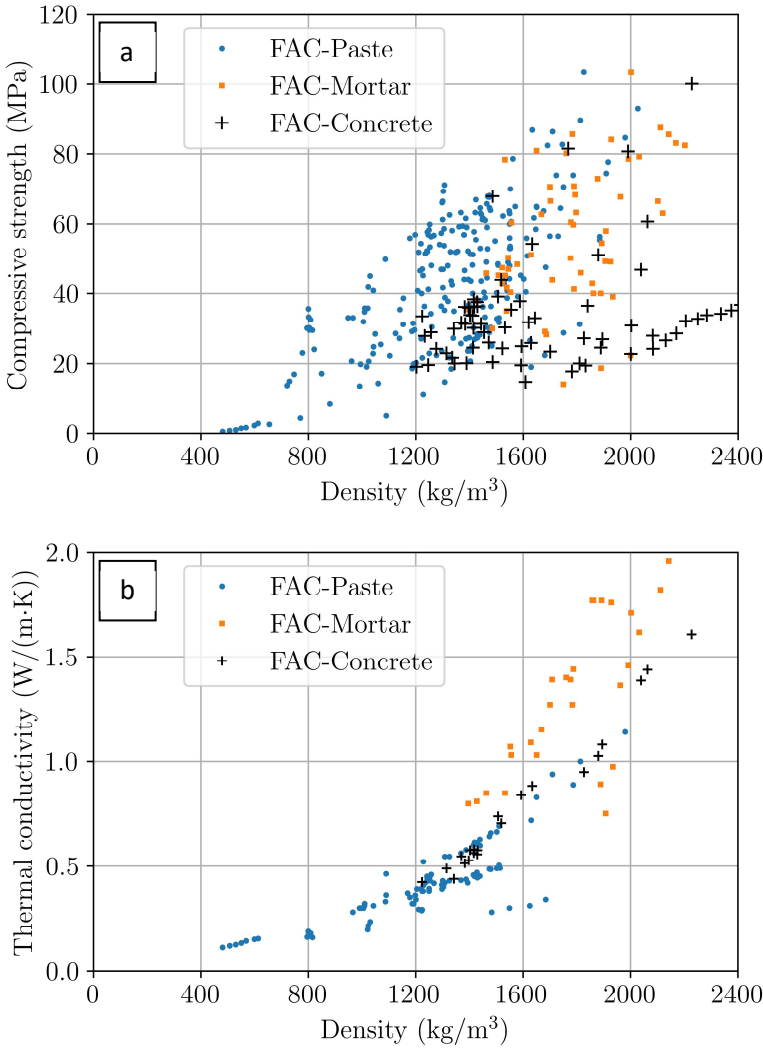


Fig. 9.3 Relationship between density and (a) compressive strength (365 data points); (b) thermal conductivity (149 data points) of FAC-composites; Note that compressive strength values were not available for some of the mixes.

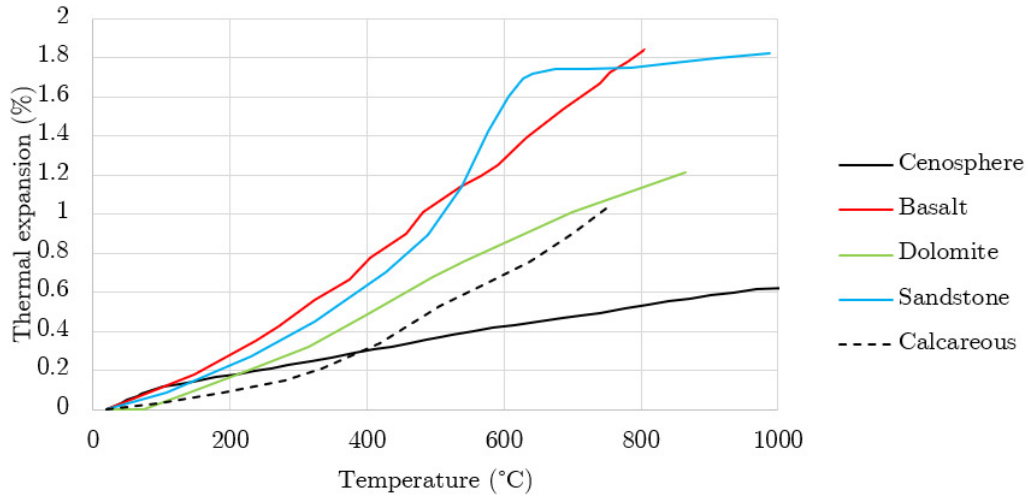


Fig. 9.4 Thermal expansion of selected aggregates: cenosphere (Arizmendi-Morquecho et al. 2012); calcareous (Niry Razafinjato et al. 2016); sandstone R 5 (Keppert et al. 2017); dolomite (Cruz & Gillen 1980); basalt (Kong & Sanjayan 2010).

### 9.1. Materials and methods

Fly Ash Cenosphere (Cenospheres Trade & Engineering, Poland) with a loose bulk density of 410 kg/m<sup>3</sup> is used as an aggregate. The particle size distribution indicates that only 4 % of FAC by mass has a diameter lower than 0.125 mm, 83 % has a diameter between 0.125 mm and 0.25 mm, and 13 % has a diameter higher than 0.25 mm. No particles are bigger than 0.5 mm. Fig. 9.5 depicts SEM images of loose cenosphere. Table 9.1 shows the chemical composition of cenosphere determined with X-ray fluorescence (XRF).

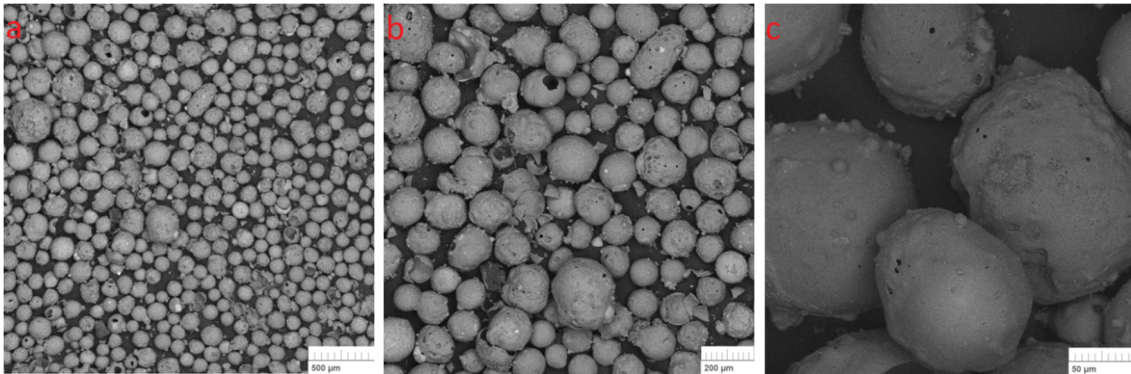


Fig. 9.5 SEM images of cenosphere (before heating).

Table 9.1 Chemical composition (test method: XRF).

Chemical composition	SiO <sub>2</sub>	Al <sub>2</sub> O <sub>3</sub>	Fe <sub>2</sub> O <sub>3</sub>	K <sub>2</sub> O	CaO	MgO	SO <sub>3</sub>	TiO <sub>2</sub>	P <sub>2</sub> O <sub>5</sub>
FAC	52.93	37.50	2.50	0.84	2.31	-	-	1.75	1.68
Cement	16.40	4.42	2.89	1.05	69.67	1.12	3.77	0.27	-
Silica fume	95.28	-	1.21	0.98	0.40	1.04	0.37	-	0.48

Two binders are used: Ordinary Portland Cement (OPC) CEM 42.5 R (Góraźdźe Heidelberg Cement Group, Poland) and silica fume (SF) (SILIMIC, Poland). Siliceous sand is used to

produce standard mortar conforming to the requirements of EN 196-1. The superplasticizer (SP) is Sika Viscocrete-3 (Sika, Poland). Polypropylene fibre (PP) Astra Belmix (Astra, Poland), with a nominal length and diameter equal to 6 mm and 34  $\mu\text{m}$ , respectively, is used in one mix to mitigate spalling.

For the initial mix design, a variety of materials are used, including cenosphere from two different suppliers, five superplasticizers, inclusion of fly ash, presence of varying amount of PP fibres, and varying FAC content. Mixes ranged from pure cement paste, cement paste with partial substitution of cement with silica fume, and/or fly ash, to LCCC with varying FAC content. The FAC to binder (binder = cement + silica fume + fly ash) ratio of 0.15, 0.35, 0.42, 0.45, 0.50, and 0.60 by mass was investigated. The selection of mixes for more detailed research is based on the following criteria: (1) flow of at least 12 cm, (2) composite's density below 1400  $\text{kg}/\text{m}^3$ , (3) favourable strength to density ratio at ambient temperature, (4) feasibility for high-temperature applications assessed after heating to two temperatures (600 °C and 800 °C).

Cenosphere composites might retain about 10 % of free water by mass. At elevated temperature, the high moisture content might cause spalling. Preliminary tests confirmed the propensity of non-oven-dried LCCC to spalling, even at a relatively low heating rate (Szymkuć et al. 2018a). During those tests, one out of four specimens spalled explosively (Fig. 9.6). For this reason, two means of spalling mitigation were employed: (1) drying in an oven at  $105 \pm 5$  °C until the mass changes were less than 0.2 % in 24 hours (EN 12390-7) or (2) the addition of polypropylene fibres.



Fig. 9.6 The results of preliminary tests. Specimens without PP fibres and oven drying: (a) before and (b) after heating to 600 °C at a rate of 5 °C/min (Szymkuć et al. 2018a).

Table 9.2 presents the mass proportions of the studied mixes. The mixtures are named according to the following pattern: FAC to binder ratio / water to binder ratio / other additions. For example, 0.45/0.30/1.8PP is a mix with FAC to binder ratio equal to 0.45 by mass (binder = OPC + SF = 1.0) and 0.30 water (including superplasticizer) to binder ratio. 1.8PP symbolises 1.8 kg of PP fibre per cubic meter of the hardened composite. A standard mortar is prepared for comparative purposes.

Table 9.2 Mix proportions (by mass).

	<b>FAC</b>	<b>OPC</b>	<b>SF</b>	<b>water+SP</b>	<b>SP</b>	<b>PP</b>	<b>sand</b>
					(% of OPC)	(kg/m <sup>3</sup> )	
0.30/0.25	0.30	0.92	0.08	0.25	2.5	-	-
0.45/0.30	0.45	0.92	0.08	0.30	2.5	-	-
0.45/0.30/1.8PP	0.45	0.92	0.08	0.30	2.5	1.8	-
Standard mortar	-	1	-	0.50	-	-	3

Abbreviations used in the table: FAC - fly ash cenosphere, OPC – Ordinary Portland Cement, SF – Silica Fume, SP – Superplasticizer, PP – Polypropylene fibre. Note that OPC+SF=1.0.

### 9.1.1. Mixing procedure

Mixes with cenosphere are prepared using a two-step procedure. First, OPC and SF are mixed in a barrel. They are put into a compulsory mixer (Diem-Werke DZ 120VS), where a solution of water and the superplasticizer is added, and the mixer starts. FAC is gradually added during the next two to three minutes. Cenosphere is not pre-wetted, so it first soaks water from cement paste and progressively releases it. The release of water is visible as a change of consistence, which stabilizes after about 20 minutes of mixing. Standard mortar specimens are prepared according to EN 196-1. Mixtures are cast into 160 mm x 40 mm x 40 mm moulds.

### 9.1.2. Conditioning

After casting, specimens are kept in the moulds covered with wet fabric for the first 24 hours. Specimens are then demoulded and put in water (22 °C ± 2 °C) for the next 27 days. All specimens, including control specimens tested without heat exposure, are then removed from water, and are kept in laboratory conditions for 24 months. To mitigate spalling, mixes 0.35/0.25 and 0.45/0.30 are dried in an oven at 105 °C until they reach constant mass. Mixes 0.45/0.30/1.8PP and standard mortar are not dried prior to heating; however, additional specimens are dried to determine their oven-dried density.

### 9.1.3. Heating regime for mechanical tests

The specimens are placed in an electric furnace and heated to desired temperature (up to 400 °C, 600 °C, 800 °C, 1000 °C or 1200 °C) at a target rate of 5 °C/min. Samples are kept at the target temperature for one hour. Then the furnace is shut down, and specimens are kept inside until they cool to ambient temperature. The residual flexural and compressive strengths are tested one day after heating.

### 9.1.4. Density

Density is reported in three states before exposure: saturated-surface-dry ( $\rho_{\text{ssd}}$ ), air-dry ( $\rho_{\text{air dry}}$ ) and dried at 105 °C ( $\rho_{\text{oven-dried}}$ ). Each result is based on the mean mass of three prismatic specimens.

### 9.1.5. Flexural and compressive strength

Flexural and compressive strength before and after heating are determined following the procedure described in EN 196-1 (load rates 50 N/s and 2400 N/s for flexural and compressive tests, respectively). Specimens are tested after cooling. The flexural strength is determined on

three specimens for each temperature. Then, six halves of the prisms are used to determine the residual compressive strength.

### 9.1.6. Scanning electron microscopy (SEM)

A scanning electron microscope (TESCAN Vega 3) is used to observe microstructural changes caused by heating. SEM allows studying the temperature-induced propagation of microcracks and the interface between cement paste and siliceous aggregate or cenosphere.

## 9.2. Results and discussion of material tests

### 9.2.1. Density under ambient conditions and mass loss after heating

Table 9.3 presents the density of studied mixes. The density of mixes with FAC to binder ratio equal to 0.45 is 40 % lower than the density of standard mortar (2329 kg/m<sup>3</sup>). Fig. 9.7 depicts the temperature-induced mass loss (in per cent) relative to the SSD state. Error bars in Fig. 9.7, Fig. 9.8, and Fig. 9.9 represent two standard deviations. The mass loss at 105 °C can be attributed mainly to the evaporation of free and physically bounded water (Chen et al. 2021). Exposure to higher temperatures causes the dehydration of cement paste and further mass loss (Castellote et al. 2004). The relative mass loss of FAC specimens is higher than that of standard mortar. This is because siliceous aggregate occupies a large volume of standard mortar.

Table 9.3 Density in various states.

Mix ID	$\rho_{SSD}$ (kg/m <sup>3</sup> )	$\rho_{air-dry}$ (kg/m <sup>3</sup> )	$\rho_{oven-dried}$ (kg/m <sup>3</sup> )
0.30/0.25	1572	1502	1432
0.45/0.30	1353	1306	1222
0.45/0.30/PP	1348	1305	1213
Standard mortar	2329	2212	2146

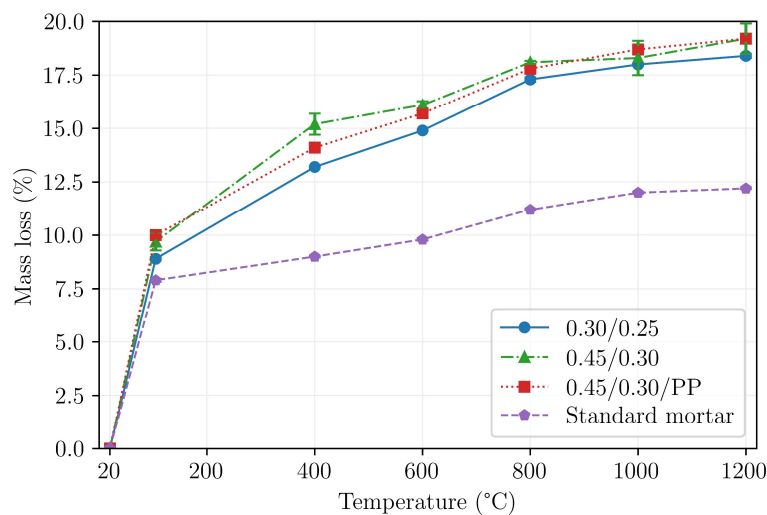


Fig. 9.7 Mass loss after exposure to high temperatures, relative to mass at the SSD condition.

### 9.2.2. Flexural and compressive strength

This section presents the results of flexural and compressive tests of four mixes, tested after exposure to 400 °C, 600 °C, 800 °C, 1000 °C or 1200 °C. The ambient flexural and compressive strengths before heating are presented in Table 9.4. Prior to heating, the compressive strength of mix 0.30/0.25 and standard mortar is similar, with the respective values of 71.7 MPa, and 70.5 MPa. With the increase of cenosphere to binder content to 0.45, the compressive strength decreases to 55.2 MPa. Adding PP fibres decreases compressive strength from 55.2 MPa to 53.8 MPa. In terms of strength to oven-dried density ratio, the respective values for 0.30/0.25, 0.45/0.30, 0.45/0.30/PP and standard mortar are 50 MPa/(kg/dm<sup>3</sup>), 45 MPa/(kg/dm<sup>3</sup>), 44 MPa/(kg/dm<sup>3</sup>), and 33 MPa/(kg/dm<sup>3</sup>).

Table 9.4 Flexural and compressive strength before heating.

	Flexural strength (MPa)	Compressive strength (MPa)
0.30/0.25	5.9	71.7
0.45/0.30	5.3	55.2
0.45/0.30/PP	6.0	53.8
Standard mortar	8.0	70.5

It is worth noting that all three mixes with cenosphere exhibit a similar strength loss after high temperature exposure (Fig. 9.8). The flexural strength of LCCC specimens is about 6 MPa, and it decreases to 50-70 % after exposure to 400 °C. It seems that exposure to higher temperatures has a moderate effect on the flexural strength – most of the time, between 40 % and 60 % of the original strength is retained, except for mixes with FAC/b=0.45, where an increase is observed after exposure to 1200 °C. On the other hand, standard mortar suffers a gradual decrease in flexural strength, reaching its minimum after exposure to 1000 °C, when the relative residual strength is only 6.2 %. Exposure to 1200 °C increases flexural strength, which was also observed by other researchers (Cao et al. 2019; Vyšvařil et al. 2014) and is usually attributed to the sintering effect (Chan et al. 1996; Thomas et al. 2019). The sintering effect in relation to FAC in silica-based composites was observed by Wang et al. (2012) and is attributed to the creation of heat-resistant phases, such as gehlenite.

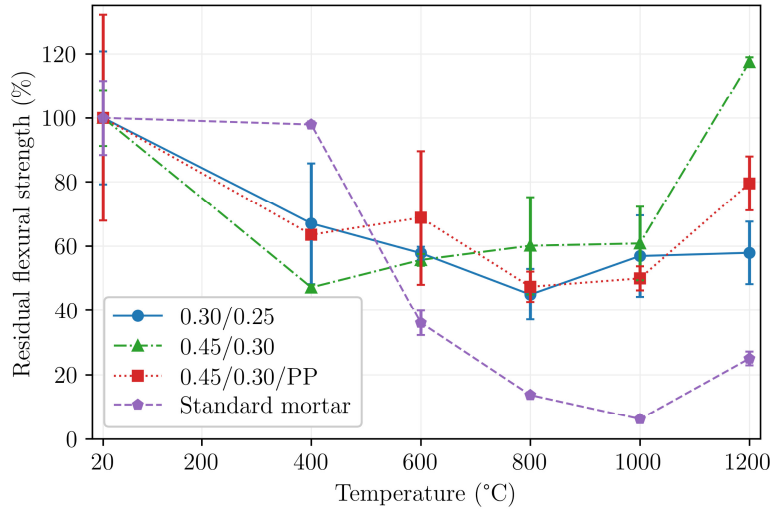


Fig. 9.8 Flexural strength of specimens before and after heating.

The residual compressive strength is presented in Fig. 9.9, which clearly illustrates a similar trend for all LCCC mixes contrasting with the residual behaviour of mortar. All mixes suffer a similar loss of strength after exposure to 400 °C. Up to this temperature, strength loss is usually attributed to several inter-related factors, including water transport, vaporisation, the start of C-S-H dehydration (Jiang et al. 2020), and microcracking (Pimienta et al. 2017).

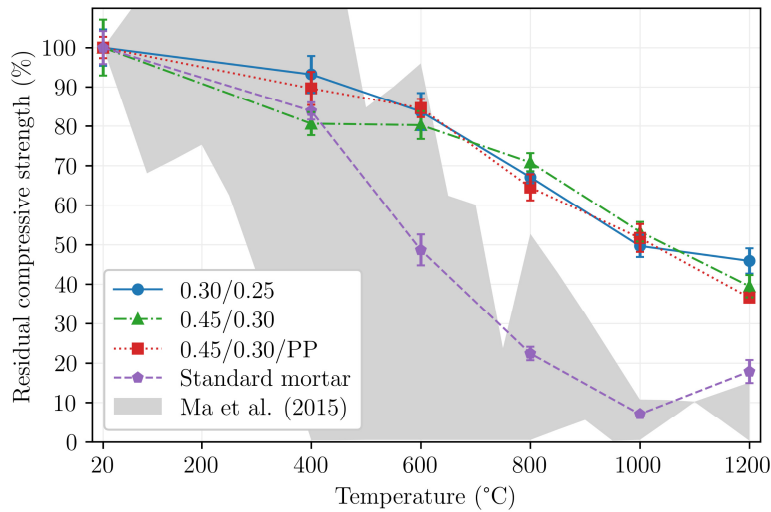


Fig. 9.9 Residual compressive strength of standard mortar and three LCCC mixes. Shaded area represents the outline of an extensive review by Ma et al. (2015) that covered 46 references.

From 600 °C and above, the difference between LCCC and standard mortar becomes more pronounced. After heating to 600 °C, portlandite is decomposed completely (Castellote et al. 2004), and the residual compressive strength of standard mortar falls below 50 %, while for LCCC, it maintains a level above 80 %. This difference can be partially attributed to the influence of silica fume and FAC on the hydration products, which facilitate C-S-H formation.

The C-S-H is present up to higher temperatures than  $\text{Ca}(\text{OH})_2$  (Tajuelo Rodriguez et al. 2017; Yim et al. 2019).

Other researchers found evidence of reactivity between FAC and cement paste (Danish et al. 2022; Hanif et al. 2017; Haustein & Kuryłowicz-Cudowska 2022), which might enhance the ITZ between FAC particles and cement paste. Pichór (2006) suggested densification of the ITZ may result from a pozzolanic reaction between portlandite and FAC. On the other hand, standard mortar experienced a significant loss of strength after 600 °C that can be partially attributed to thermal incompatibility and the expansive phase transformation of siliceous aggregate at 573 °C (Meloni et al. 2019). When exposed to 800 °C, the residual strength of standard mortar is 22 %, and for LCCC it lies between 64 % and 71 %. No significant difference is found between the performance of mix with and without fibres. After exposure to 1000 °C, the compressive strength of LCCC is still about half its initial value, while for the standard mortar, it is about 8 %. Up to this temperature, the results for standard mortar are close to those previously reported, e.g., by (Ratajczak et al. 2019). Heating to 1200 °C further influences the degradation of strength properties of LCCC mixes. Interestingly, LCCC retain about 40 % of their initial strength. The level of residual compressive strength after heating to 1000 °C and 1200 °C is higher compared to the data reported in the existing reviews (Elsanadedy 2019; Ma et al. 2015; Rawat et al. 2021). The residual compressive strength of standard mortar is 18 % after heating to 1200 °C, which is nine percentage points higher than after exposure to 1000 °C and indicates a sintering effect. As discussed earlier, such a phenomenon has already been reported concerning an observed increase in residual flexural strength. However, unlike for the flexural strength, the increase of compressive strength is observed only for the standard mortar and not LCCC.

### 9.2.3. Thermal analysis

A thermogravimetric analyser (TA Instruments Q50) was used for TGA. Approximately 20 mg samples were heated from 20 °C to 1000 °C at a heating rate of 10 °C/min in an oxygen atmosphere.

This section describes the TG analysis of FAC and one of the LCCC (0.45/0.30 mix). TG curves in Fig. 9.10 (a) show the weight loss of two FAC samples (about 20 mg each). The curves illustrate that FAC is thermally stable up to 300 °C when an abrupt mass loss occurs. At 400 °C, the samples lose about 8 % or 18 % of their initial weight. The mass loss is likely caused by violate cracking of the FAC shell, the expulsion of gases trapped inside and the evaporation of water inside pores in the cenosphere walls or inside FAC particles. From 500 to 1000 °C, the mass of FAC remains constant. Similar behaviour was reported by (Kolay and Singh 2001; Puri and Khanna 2016).

Fig. 9.10 (b) illustrates TG and DTG of two samples representing the 0.45/0.30 mix. The same mix as for XRD analysis was selected to help understand the response of LCCC to high temperature. Samples were tested in two conditions: non-dried and dried at 105 °C. Fig. 9.10 (b) shows four and three distinct peaks (b) on the DTG curves for non-dried and dried samples, respectively. The peak at around 100 °C represents the loss of free water and the C-S-H interlayer water (L'Hôpital et al. 2016). The next peak, which is more pronounced, can be attributed to the decomposition of portlandite (Pimienta et al. 2017). The main mass loss of the C-S-H occurs between 50 °C and 600 °C, followed by the decomposition of C-S-H to wollastonite, as reported by (Khoury et al. 2007; Tajuelo Rodriguez et al. 2017). The third

major peak occurs above 650 °C and is likely caused by the decarbonation of  $\text{CaCO}_3$  (Fares et al. 2010; Meloni et al. 2019). The last peak on the DTG curve occurs at around 900 °C.

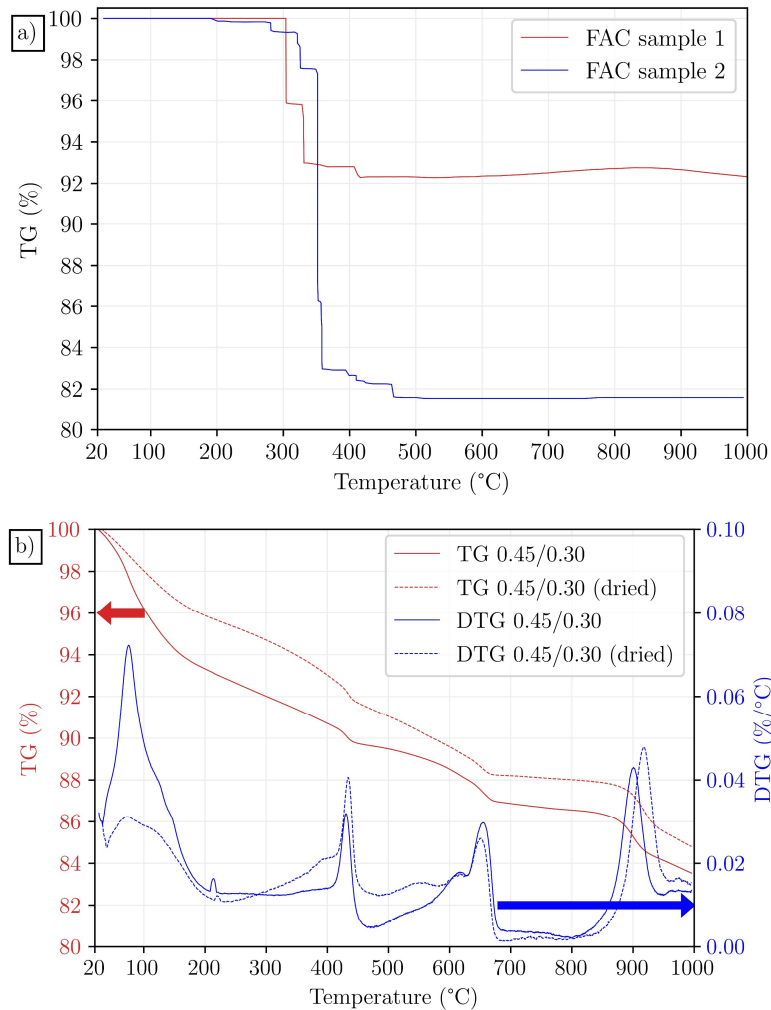


Fig. 9.10 TG analysis; (a) mass loss of two FAC samples; (b) TG and DTG curves of two LCCC samples.

A differential scanning calorimeter (Mettler Toledo DSC 1) was used to measure the specific heat. Approximately 15 mg samples were heated from 20 °C to 500 °C at a heating rate of 10 °C/min in a nitrogen atmosphere.

Fig. 9.11 presents the specific heat of FAC and LCCC (0.45/0.30 mix, same as for XRD and TGA), measured with the Differential Scanning Calorimeter (DSC). The specific heat at room temperature is about 1200 J/(kg·K). The clear endothermic peak is reached around 120 °C, representing the energy needed to remove the free and interlayer water. Then, the specific heat decreases gradually and flattens at about 1600 J/(kg·K) to increase at 460 °C to the local maximum of 2138 J/(kg·K). The last peak is caused by  $\text{Ca}(\text{OH})_2$  decomposition. The specific heat of FAC is plotted for reference. In contrast to LCCC, FAC does not show prominent endothermic peaks. However, a couple of abrupt changes can probably be explained by FAC cracking and the release of its interior products.

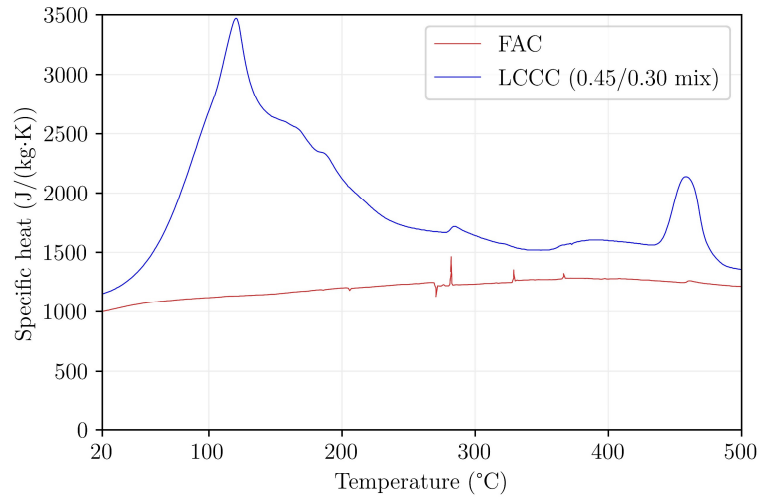


Fig. 9.11 Specific heat measured with DSC: LCCC (0.45/0.30 mix), and FAC sample.

### 9.2.4. Microstructure analysis

The microstructure of cenosphere and LCCC is analysed using SEM. SEM pictures are provided by the courtesy of Dr Maria Ratajczak. Fig. 9.5 and Fig. 9.12 depict cenosphere before and after heating to 1200 °C, respectively. There are no distinct differences between heated and non-heated FAC. Therefore, images after heating to intermediate temperatures are not presented.

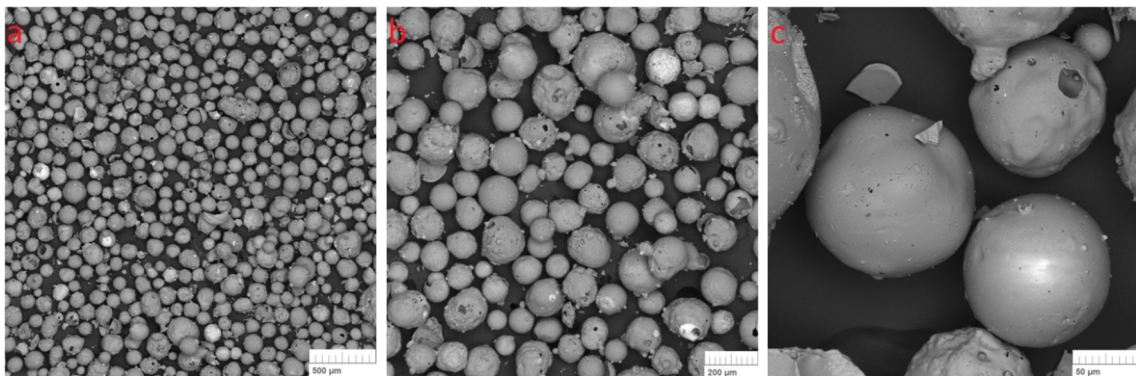
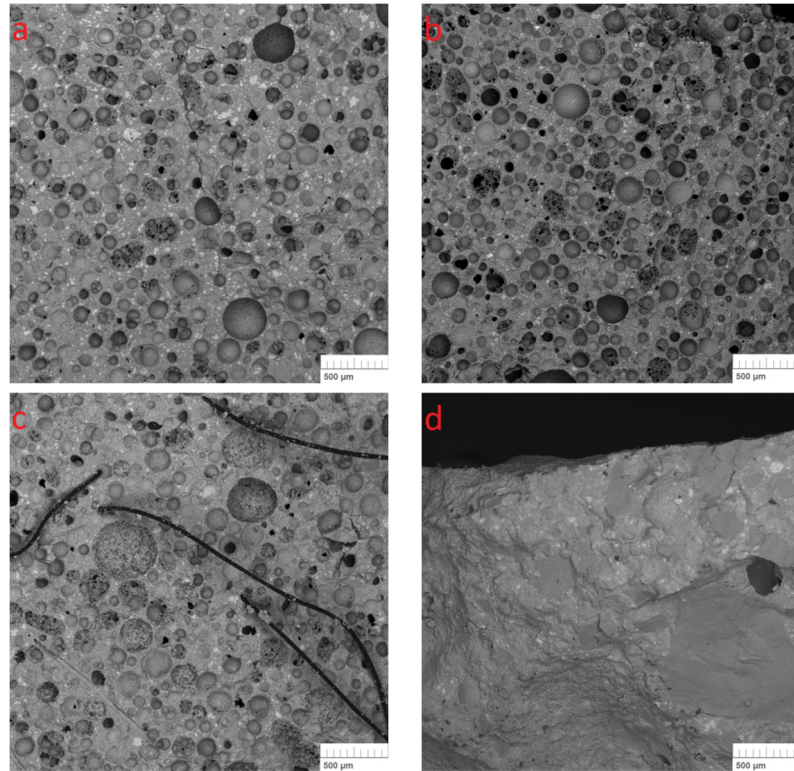


Fig. 9.12 SEM images of FAC after heating to 1200 °C (a – MAG100, b – MAG200, c – MAG1.0k). See also Fig. 9.5 for SEM images before heating.

The microstructure of LCCC is analysed before and after exposure to a range of temperatures (Fig. 9.13 and Fig. 9.14). Fig. 9.13 illustrates the overview of samples before heating. The difference in the amount of FAC is easily visible (Fig. 9.13, micrographs a and b), showing lower content of FAC in the 0.30/0.25 mix. Fig. 9.13 (c) depicts PP fibres embedded in the 0.45/0.30/PP mix. In Fig. 9.13 (d) siliceous aggregates can be distinguished from cement paste.



*Fig. 9.13 SEM images with the overview of the samples before heating (a – 0.30/0.25, b – 0.45/0.30, c – 0.45/0.30/PP, d – standard mortar; MAG100).*

To give an overview of the effect of high temperatures on different samples, Fig. 9.14 depicts SEM micrographs before and after heating to various temperatures. FAC particles can be observed, broken during strength tests and partially embedded in the cement matrix. Furthermore, the inside of FAC is exposed along with the thickness of FAC shells, which displays a small number of pores. Compared with standard mortar (Fig. 9.14 d), LCCC (Fig. 9.14 a, b, c) shows a dense and compact microstructure both before and after high temperature exposure. Fig. 9.14 (a, b) do not reveal major cracks. In line with the expectations, PP fibres are no longer present after heating to 400 °C (Fig. 9.14 c). Instead, the channels after fibre vapourisation are observed. A representative region with either fibre (20 °C) or a channel left after fibre evaporation (400 °C and above) is chosen (Fig. 9.14 c) to illustrate the cracks that intensify near the fibre channels. This observation corresponds well with the previous findings (Li et al. 2019). Propagation of these microcracks increases along with the exposure temperature. However, judging by the compressive strength results presented in Fig. 9.9, those cracks do not diminish the strength performance of LCCC. Fig. 9.14 (d) shows that temperatures of 600 °C and above significantly affect the ITZ between cement paste and aggregates in standard mortar.

A porous structure of cement matrix is observed after heating to 1000 °C. Notably, standard mortar after 1000 °C was the only sample to visually deteriorate with time. After exposure to temperatures from 400 °C to 1000 °C, the cenosphere can be easily distinguished from the cement paste in SEM images. Although no changes in FAC samples were detected after heating to 1200 °C (compare Fig. 9.5 and Fig. 9.12), FAC shells are no longer easily distinguishable in the LCCC after exposure to 1200 °C (Fig. 9.14).

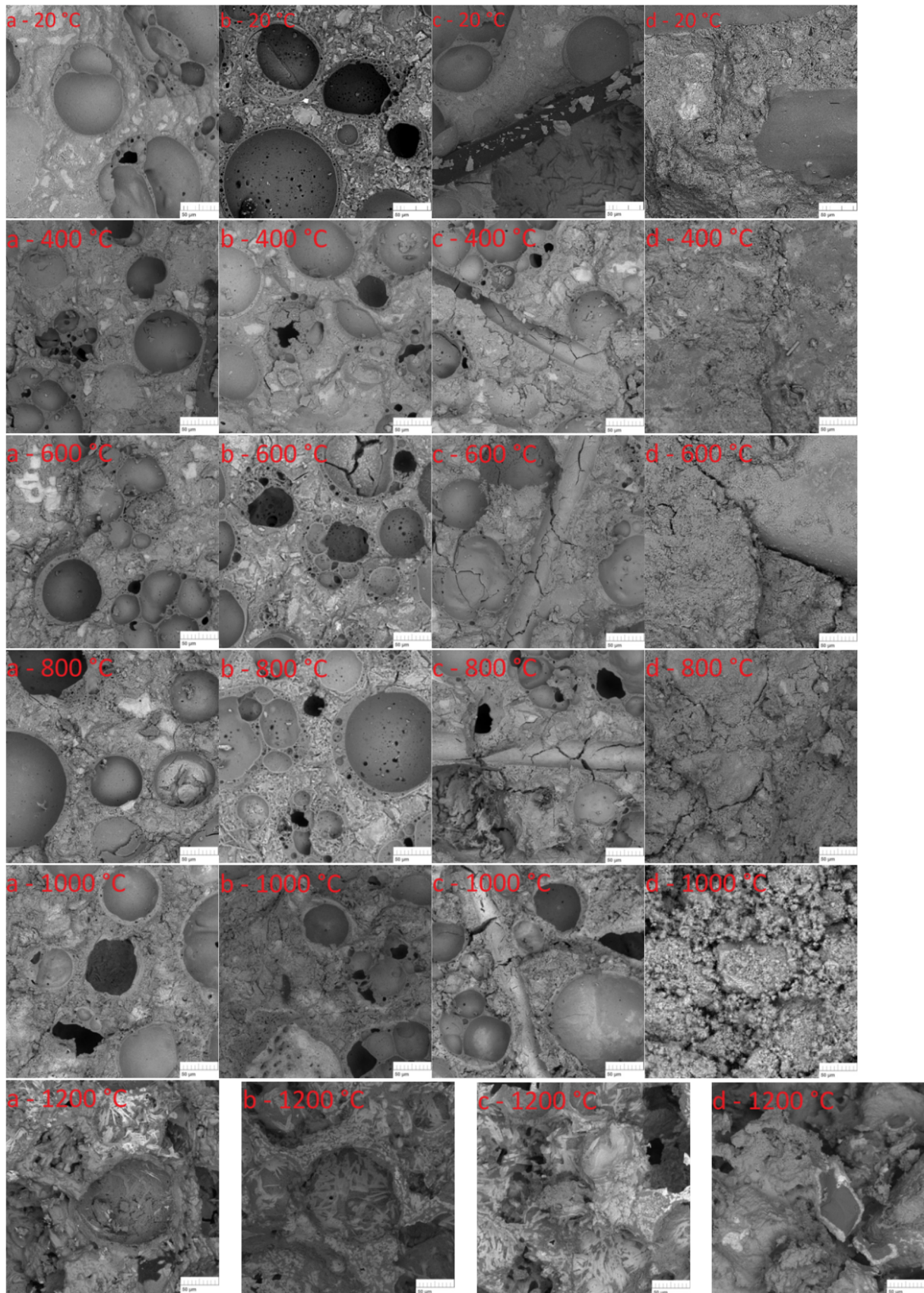
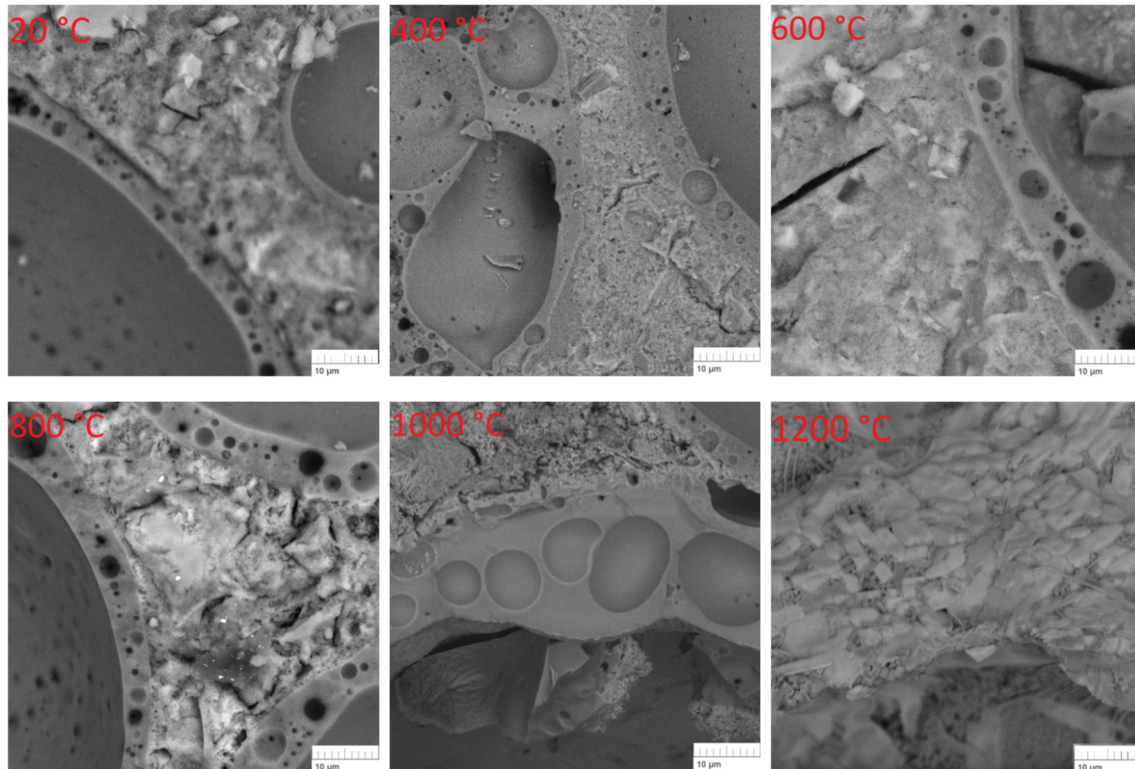


Fig. 9.14 SEM images of LCCC samples before and after heating to 400 °C, 600 °C, 800 °C, 1000 °C, and 1200 °C (a - 0.30/0.25, b - 0.45/0.30, c - 0.45/0.30/PP, d - standard mortar; MAG1.0k).

To further study the ITZ between FAC and cement paste, Fig. 9.15 presents the ITZ between FAC particles and cement paste before and after heating. Exposure to 600 °C is usually associated with pronounced microcracks propagating from ITZ to cement matrix, as presented in Fig. 9.14 (d). Notably, in the case of the LCCC, the ITZ appears unaffected by high temperature, as no major cracks appear in this region. Thus, it is likely that the primary mechanism leading to high residual compressive strength presented in Fig. 9.9 is hindering the growth of interconnected cracks.



*Fig. 9.15 ITZ microstructure in 0.45/0.30 mix before and after heating to 400 °C, 600 °C, 800 °C, 1000 °C, and 1200 °C (MAG5.0k).*

More information on the effect of elevated temperatures on LCCC can be found in [Szymkuc et al. \(2023\)](#), where the results of XRD, TGA, DSC, and temperature-induced colour changes of the composite are reported.

In the research described so far, a heating rate of 5 °C/min was used. Low heating rates (about 5 °C/min and less) allow for decoupling structural from material effects. However, building members may be subjected to more severe conditions during exposure to real fires. To address this problem, additional specimens are placed inside a furnace and heated according to the standard temperature-time curve ([EN 1363-1](#)) until 800 °C and kept at constant temperature for 60 minutes. The help of Professor Paweł Ogrodnik from the Main School of Fire Service in Poland, is here kindly acknowledged.

After exposure to conditions described by the standard temperature-time curve, the residual strength of 0.45/0.30 is 84 %, while the residual strength of standard mortar is 27 %. The level of reduction corresponds well with results for the 5 °C/min heating rate, where residual compressive strength after 800 °C is 71 % and 22 % for respective mixes. However, the time needed to reach 800 °C in the slow-heating furnace is 156 minutes, compared to 23 minutes for

the standard temperature-time curve. This evidence supports the statement that the heating rate does not affect the residual strength of the specimens heated to 800 °C. Other researchers drew similar conclusions for ordinary concrete (Mohamedbhai 1986, Pimienta et al. 2019) and ultra-high performance concrete (Xiong & Liew 2015) unless spalling is involved. After specimens are removed from the furnace, they are assessed visually. Fig. 9.16 shows the surface of specimens representing two mixes. The standard mortar cracked extensively, while visible cracks did not develop on the 0.45/0.30 surface.

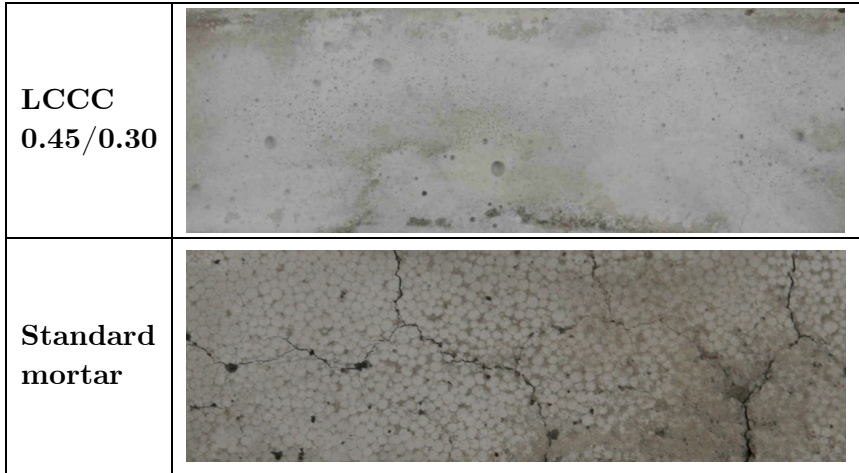


Fig. 9.16 Surface of specimens subjected to heating according to standard temperature/time curve. Photos taken before strength tests.

Fig. 9.17 presents the colour change of all four mixes. The colour changes of cement composites are attributed to the dehydration of the cement paste and transformations within the aggregate (Hager 2014; Meloni et al. 2019). Before heating, the specimens' colour can generally be described as dark grey (Fig. 9.17). The colour difference between standard mortar and FAC specimens is not distinct due to two effects: the whitish colour of FAC makes the specimen lighter. At the same time, the silica fume darkens the specimens. After heating to 600 °C, the dark grey becomes lighter, and a pinkish colouration appears, attributed to the oxidation of iron compounds (Annerel & Taerwe 2009; Hager et al. 2021a).

Further heating to 800 °C reveals a more pinkish colour. The samples with cenosphere turn buff with accents of pink and orange when heated to 1000 °C. Huang et al. (2018) attribute those changes to the cenosphere itself. It might explain why standard mortar's colour is lighter than the colour of LCCC samples after 1000 °C. Standard mortar heated up to 1000 °C was the only sample to degrade with time, as presented in Fig. 9.17. After heating to 1200 °C, the colour is similar for all samples as it becomes orange. The distinct colour change between 1000 °C and 1200 °C is interesting and could be used to assess the highest temperature during fires based on the extension of colour changes over depth. Sophisticated methods, such as XRD, TGA, or SEM, provide more detailed results (Alarcon-Ruiz et al. 2005). However, rehydration makes their interpretation difficult (Iwama & Maekawa 2022; Sabeur et al. 2019). The knowledge of colour changes helps determine the potential location for drilling when a post-fire assessment is required (Wróblewska & Kowalski 2020).

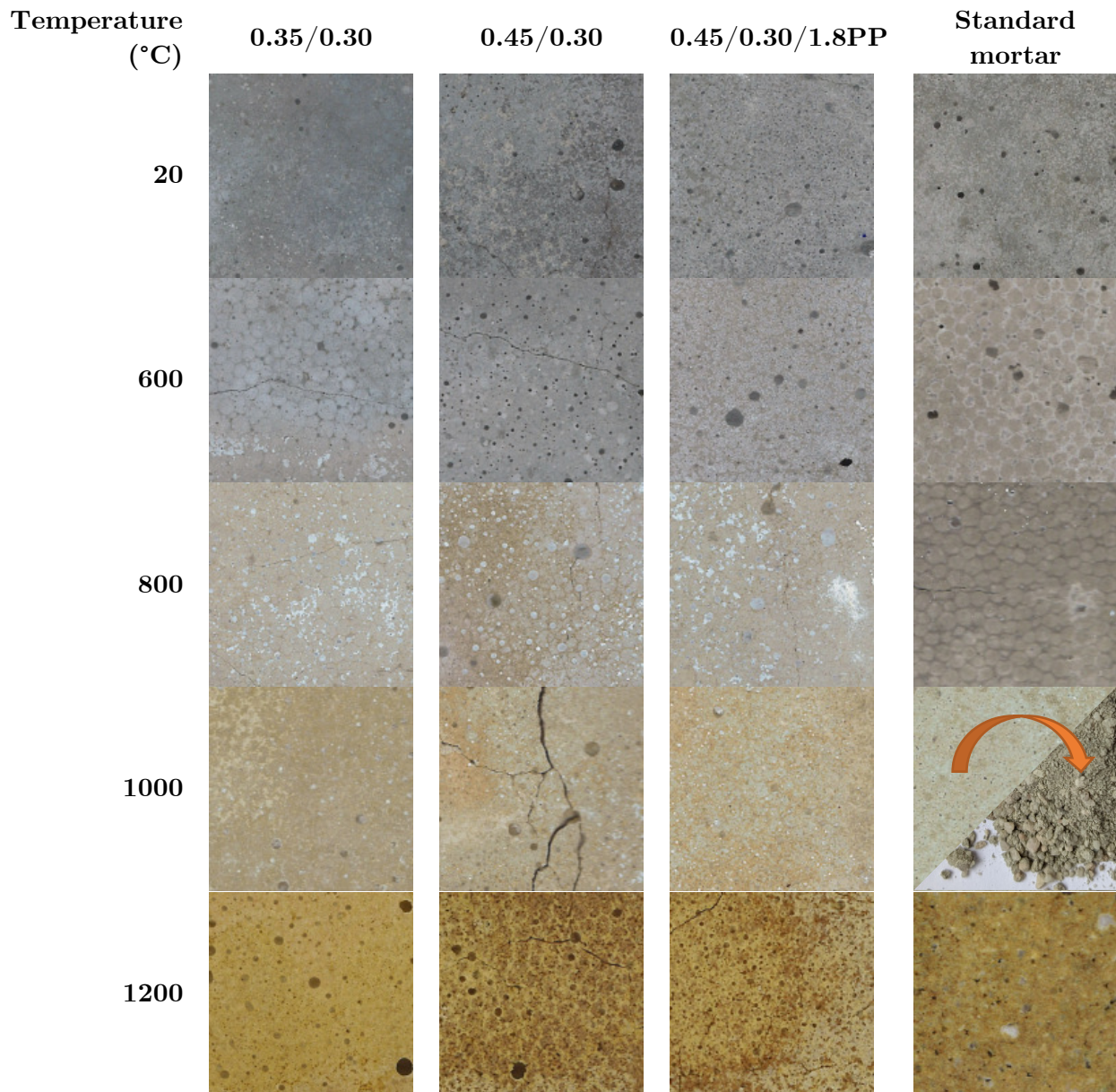


Fig. 9.17 Colour changes of specimens after heating (scanned after strength tests). Additional picture is presented for standard mortar after exposure to 1000 °C, as it was the only specimen to visually degrade with time.

### 9.2.5. Conclusions of the experimental research on LCCC

The lightweight cementitious composites with fly ash cenosphere have superior residual compressive strength compared to standard mortar. LCCC shows a potential for utilisation as a material that could positively affect the post-fire load-bearing capacity of structural members, especially considering its compressive strength above 50 MPa and a density below 1600 kg/m<sup>3</sup>. The conclusions of the experimental study are:

- (1) The residual strength of all LCCC composites is higher compared to the standard mortar. The average residual compressive strength of LCCC after exposure to 400 °C, 600 °C, 800 °C, 1000 °C and 1200 °C is 88 %, 83 %, 67 %, 52 %, and 41 %, respectively. The respective values obtained for standard mortar are 84 %, 49 %, 22 %, 7 %, and 18 %. LCCC shows superior behaviour in temperatures between 600 °C and 1200 °C.

- (2) SEM analysis indicates that cenosphere accommodates thermal strains of cement paste, and most of the ITZ is found intact. The presence of FAC hinders heat-induced crack propagation. In the LCCC with PP fibres composites, cracks concentrate near the channels left by vapourised fibres. However, they do not diminish the composite mechanical performance.

Having the promising data obtained for small prismatic specimens (Fig. 9.9), the numerical model developed in this PhD might be used to simulate the structural fire behaviour of LCCC-filled CFST columns. The following Sections give an overview of the material parameters used in the numerical model. No researcher tested LCCC-filled CFST columns. Therefore, the subsequent analyses are based on reasonable assumptions supported by the experimental data, wherever possible. As such, the following analyses can be considered a feasibility study.

### 9.3. Determination of LCCC properties for the numerical model

After a successful series of lightweight composites were developed and tested, it is necessary to establish the parameters that could be used in numerical modelling. This section documents how the specific heat, density, thermal conductivity, the resultsnt thermal diffusivity, and stress-strain response of the LCCC were determined.

#### 9.3.1. Specific heat

The specific heat was determined using two methods: DSC and TPS. The DSC shows that the specific heat of FAC-composite follows a similar trend as ordinary concrete in the temperature range of 20 °C to 500 °C (Fig. 9.11). The TPS method was used to establish the initial value, which is 1013 J/(kg·K). The experimentally obtained values are higher than those proposed by the Eurocode for concrete. Ultimately, to be conservative, a similar relationship as the one proposed in Eurocode 2 is used: a peak of specific heat is modelled at 115 °C, with a linear decrease to 1000 J/(kg·K) at 200 °C. Between 200 °C and 400 °C specific heat is assumed to increase linearly up to 1100 J/(kg·K) at 400 °C, and it is assumed to remain constant. Table 9.5 presents the specific heat values as a function of temperature. Those assumptions are verified in chapter 9.3.4.

*Table 9.5 Specific heat–temperature relationship used for predicting performance of LCCC-filled steel tubular columns.*

Temperature (°C)	Specific heat (J/(kg·K))
20	1013
100	1013
115	3554
200	1000
400	1100
1200	1100

### 9.3.2. Density

The measured density of the 0.45/0.30/PP mix in used in the model (air dry state and after heating to various temperatures). Table 9.6 reports the density as a function of temperature.

Table 9.6 Density–temperature relationship used in the model for the performance predictions of LCCC-filled steel tubular columns.

Temperature (°C)	Density (kg/m <sup>3</sup> )
20	1305
100	1305
200	1213
400	1156
600	1134
800	1105
1000	1096
1200	1088

### 9.3.3. Thermal conductivity

Thermal conductivity at room temperature was measured using Transient Plane Source (TPS) method at the University of Coimbra. The mean thermal conductivity value is 0.60 W/(m·K), without pre-drying in an oven. There is no experimental data for the thermal conductivity of LCCC at elevated temperatures. However, based on a review study (Fig. 7, Szymkuć 2023b), the following linear relationship was proposed for oven-dried cement paste with FAC (named FAC-pastes in Fig. 9.18):

$$\lambda_{FAC-paste} = 0.00039 \cdot \rho - 0.08 \quad (9.1)$$

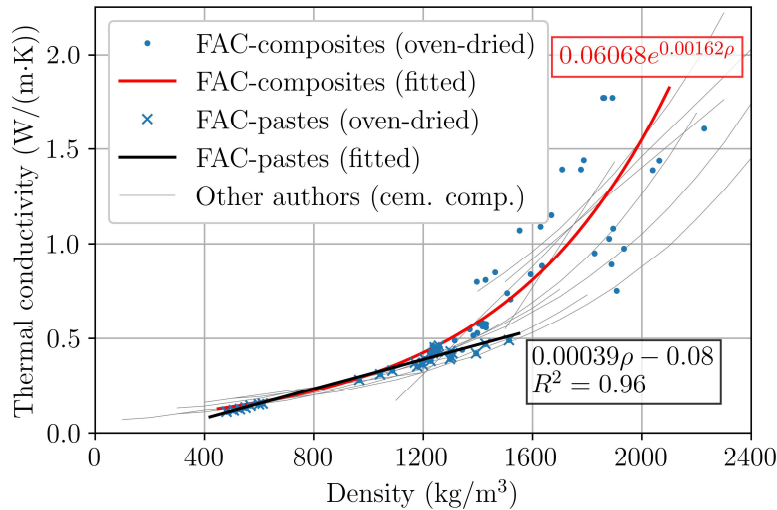


Fig. 9.18 Thermal conductivity as a function of oven-dried density of FAC-pastes and FAC-composites; grey lines in the background represent models in the literature (Szymkuć 2023b).

Therefore, a measured value of 0.60 W/(m·K) obtained for an air-dried composite is assumed between 20 °C and 100 °C. The thermal conductivity for temperatures between 200 °C and 1200 °C is assumed to be a function of composite's density, e.g. at 400 °C, eq. (9.1) yields:

$$\lambda_{FAC-paste} = 0.00039 \cdot 1156 - 0.08 = 0.37 \text{ W/(m·K)}$$

Table 9.7 presents the thermal conductivity values as a function of temperature.

Table 9.7 Thermal conductivity – temperature relationship used for the predictions of the performance of LCCC-filled steel tubular columns.

Temperature (°C)	Thermal conductivity (W/(m·K))
20	0.60
100	0.60
200	0.39
400	0.37
600	0.36
800	0.35
1000	0.35
1200	0.34

### 9.3.4. Thermal diffusivity

To check the correctness of some of the assumptions related to thermal properties of LCCC at elevated temperatures, an additional test was carried out. The methodology followed the procedure given by, e.g. Felicetti et al. (2012), Khoury et al. (1984), or Hager et al. (2021a). A cylinder was grinded, then holes were drilled (Fig. 9.19 a). The specimen was insulated with several layers of insulation material on both sides (bottom and top) to ensure radial heat transfer. Thermocouples were put through the insulation layer into the drilled holes (Fig. 9.19 b). Then the whole specimen was put into the furnace (Fig. 9.19 c), and heated at a constant rate (Keramikos furnace was used for that purpose, as it offers better control of the temperature in the early stages of heating, compared to the Carbolite furnace). Temperatures were recorded, and the thermal diffusivity was calculated as:

$$\alpha = \frac{v_h^* R_c^2}{4\Delta\theta} \quad (9.2)$$

where  $v_h^*$  is the heating rate in the representative point of the thermal field,  $R_c$  is the radius of the ideal cylindrical surface containing the thermocouple #1, and  $\Delta\theta$  is the temperature difference between temperature measured in the centre of the specimen (thermocouple #3) and thermocouple # 1. The location of the thermocouples is presented in Fig. 9.19.

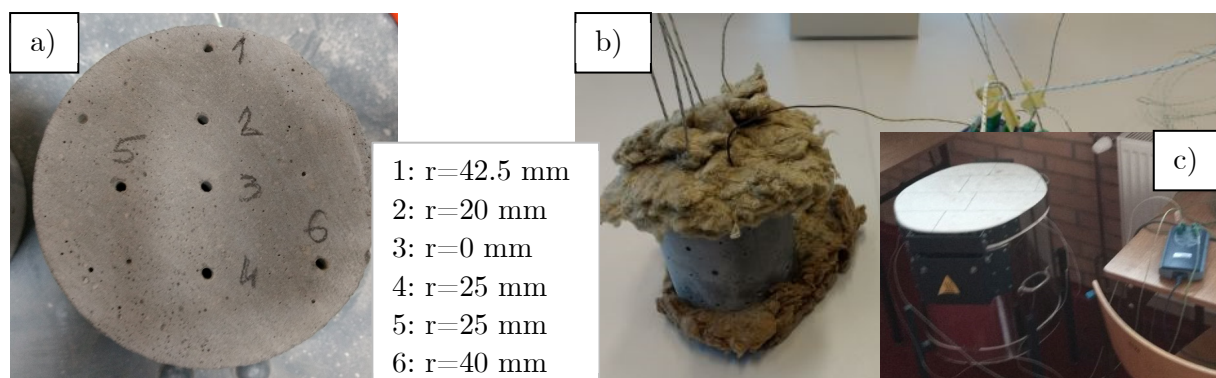


Fig. 9.19 Setup for experimental determination of thermal diffusivity.

The thermal diffusivity obtained experimentally, and the model based on the assumptions presented previously, are compared in Fig. 9.20. It can be observed that the results are in a good agreement. There is no drop of diffusivity related to water evaporation in the experiment, as the test was run on dried specimen. For reference, the same graph shows thermal diffusivity calculated based on the Eurocode 2 model.

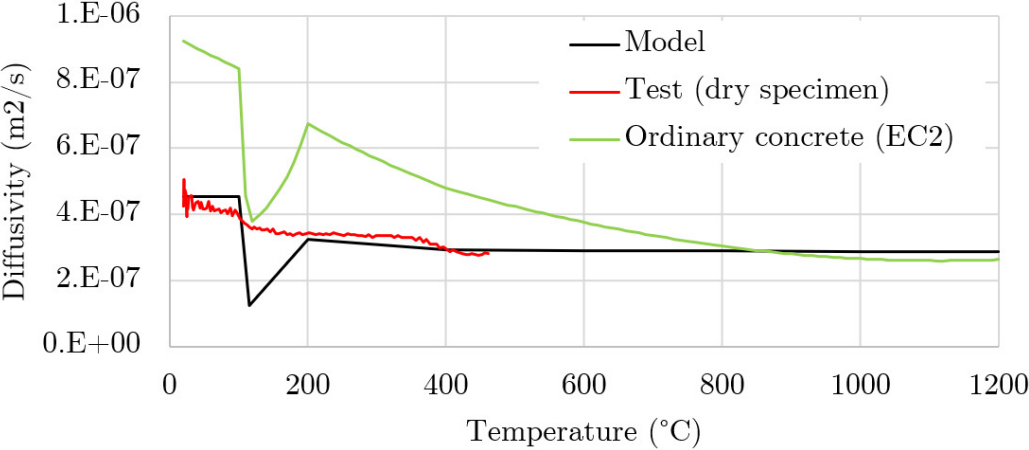


Fig. 9.20 Thermal diffusivity. Curves represent (1) model based on data in Table 9.5, Table 9.6, Table 9.7; (2) test data; (3) model based on Eurocode 2 with upper limit of conductivity.

To further validate the proposed formulations of specific heat, thermal conductivity, and density, the results of a numerical simulation of a heat transfer inside a cylinder (100 mm in diameter) are compared with the experiment. Since the specimen was previously heated, the effects of free water presence on thermal properties are not considered in this model. Fig. 9.21 presents a good agreement between experimental and calculated results. Therefore, the effective thermal properties of the LCCC mix are established correctly.

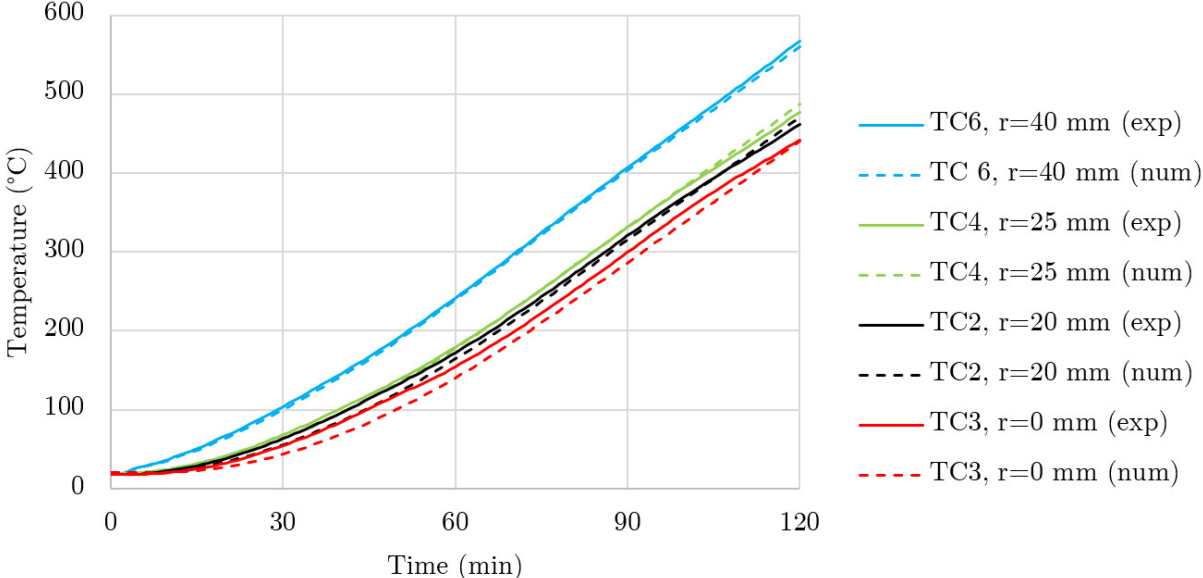


Fig. 9.21 Validation of the thermal properties used in the numerical model. Cylindrical specimen heated at 5 °C/min, with thermocouples in positions described in Fig. 9.19, where  $r$  is the distance from the centre of the specimen.

### 9.3.5. Strength reduction factors at elevated temperatures

As elaborated earlier, residual tests are considered a good proxy for high-temperature properties since the hot strength is usually higher than the residual strength (hence, the results might be regarded as conservative). However, it is likely that the results after heating to 1200 °C might not be representative for hot strength (judged by the appearance of large quantities of gehlenite formed during cooling from 1200 °C). Therefore, in the numerical simulations a linear decrease between values obtained for 1000 °C and  $k_{c,\vartheta} = 0.001$  at 1200 °C is assumed. Table 9.8 presents the strength reduction factors as a function of temperature, based on the strength test results of the 0.45/0.30/PP composite. The increase of compressive strength of dried specimens was observed in previous research (Szymkuć et al. 2018a), however it was not considered and the reduction factor  $k_{c,\vartheta}$  at 100 °C was assumed equal to 1. For intermediate values, a linear interpolation was used.

Table 9.8 Strength reduction factors of LCCC at elevated temperatures, as measured for halves of the prisms.

Temperature (°C)	$k_{c,\vartheta,measured}$ (-)	$k_{c,\vartheta,assumed}$ (-)
20	1	1
100		1
200		0.965
300		0.931
400	0.896	0.896
500		0.871
600	0.846	0.846
700		0.745
800	0.645	0.645
900		0.581
1000	0.517	0.517
1100		0.259
1200	0.366	0.001

### 9.3.6. Stress-strain relationship for cylindrical specimens

Due to a lack of experimental data regarding stress-strain relationships of LCCC at elevated temperatures, it was assumed that the relationship recommended by the Eurocode is applicable to LCCC. Tests at elevated temperatures are challenging, expensive, and time-consuming. Furthermore, currently, they are beyond the testing capabilities of any facility in Poland. Therefore, the analysis provided in the later sections can be considered a feasibility study, and hopefully, the results will encourage detailed material-focused research in the future.

The results presented so far were obtained on standard prisms, which allowed to test the residual compressive strength of several mixes after heating. However, small prismatic specimens cannot provide data on the stress-strain behaviour of the material. To address this issue, a batch of cylinders (100 mm x 200 mm) was cast for a mechanical characterisation of the material. The same mix design was used, as for 0.45/0.30 mix (Table 9.2, Table 9.9).

Table 9.10 summarises the geometrical properties of grinded cylindrical specimens before and after heating.

Table 9.9 Mix proportions (by mass).

Mix ID	FAC	OPC	SF	Water & SP	SP
	(mass ratio)				(mass % of OPC)
0.45/0.30	0.45	0.92	0.08	0.30	2.5

Table 9.10 Geometry and mass of cylindrical specimens.

ID	m (g)	h (mm)	d (mm)	Area (mm <sup>2</sup> )	m <sub>post-heat</sub> (g)	h (mm)	d (mm)	Area (mm <sup>2</sup> )
20-Cyl1	1937.2	197.68	99.89	7837.24	-	-	-	-
20-Cyl2	1941.6	197.86	99.96	7847.70	-	-	-	-
20-Cyl3	1983.6	195.29	99.88	7835.14	-	-	-	-
20-Cyl4	1993.0	196.44	99.96	7848.22	-	-	-	-
600-Cyl1	1842.6	197.47	99.88	7835.67	1687.6	196.03	99.12	7715.84
600-Cyl2	1896.2	195.59	99.82	7825.73	1725.6	194.46	99.09	7711.69
600-Cyl3	1889.0	195.18	99.91	7840.37	1720.2	193.65	99.17	7724.67
800-Cyl1	1928.4	197.21	99.89	7837.24	1636.6	195.00	98.78	7663.00
800-Cyl2	1931.2	196.67	99.94	7844.56	1639.6	194.68	98.89	7680.07
800-Cyl3	1853.6	198.76	99.86	7831.48	1654.0	196.80	98.90	7681.63
1000-Cyl1	1848.4	197.62	99.93	7842.99	1633.8	195.78	98.93	7686.29
1000-Cyl2	1991.0	195.99	99.95	7846.65	1676.6	194.06	98.96	7691.99
1000-Cyl3	1891.6	195.55	99.87	7833.57	1671.0	193.80	98.93	7687.32

The LCCC cylinders were heated at a rate of 1 °C/min (following RILEM TC 200-HTC recommendations: Schneider et al. 2007), kept at the target temperature for 120 minutes and then cooled at a rate not exceeding 2 °C/min. Specimens were tested the next day after cooling. The uniaxial compression tests are performed using a universal testing machine (Instron 8505) with a capacity of 2400 kN. Two extensometers (Instron, 50 mm measurement base) were used to monitor the strains at two opposite sides of each specimen. Fig. 9.22 and Fig. 9.23 depict equipping specimens with extensometers (Fig. 9.22) and specimens ready for the compressive test. Additionally, the DIC measurement system ARAMIS (Fig. 9.23) was used to determine the strain field and validate the use of extensometers with a limited length. Data was acquired with MGC Plus system (Hottinger Baldwin Messtechnik). A displacement-controlled procedure was used. Selected experiments were carried out to study the suitability of displacement rates between 0.5 µm/s and 3.33 µm/s (2 mm/min).

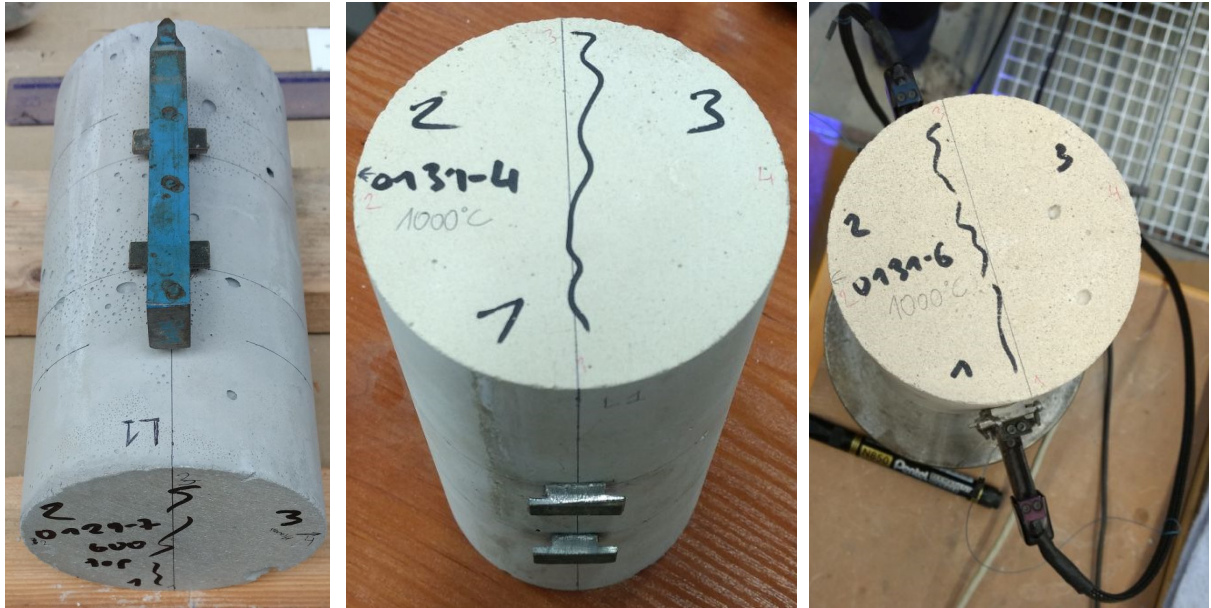


Fig. 9.22 Equipping specimens with extensometers.

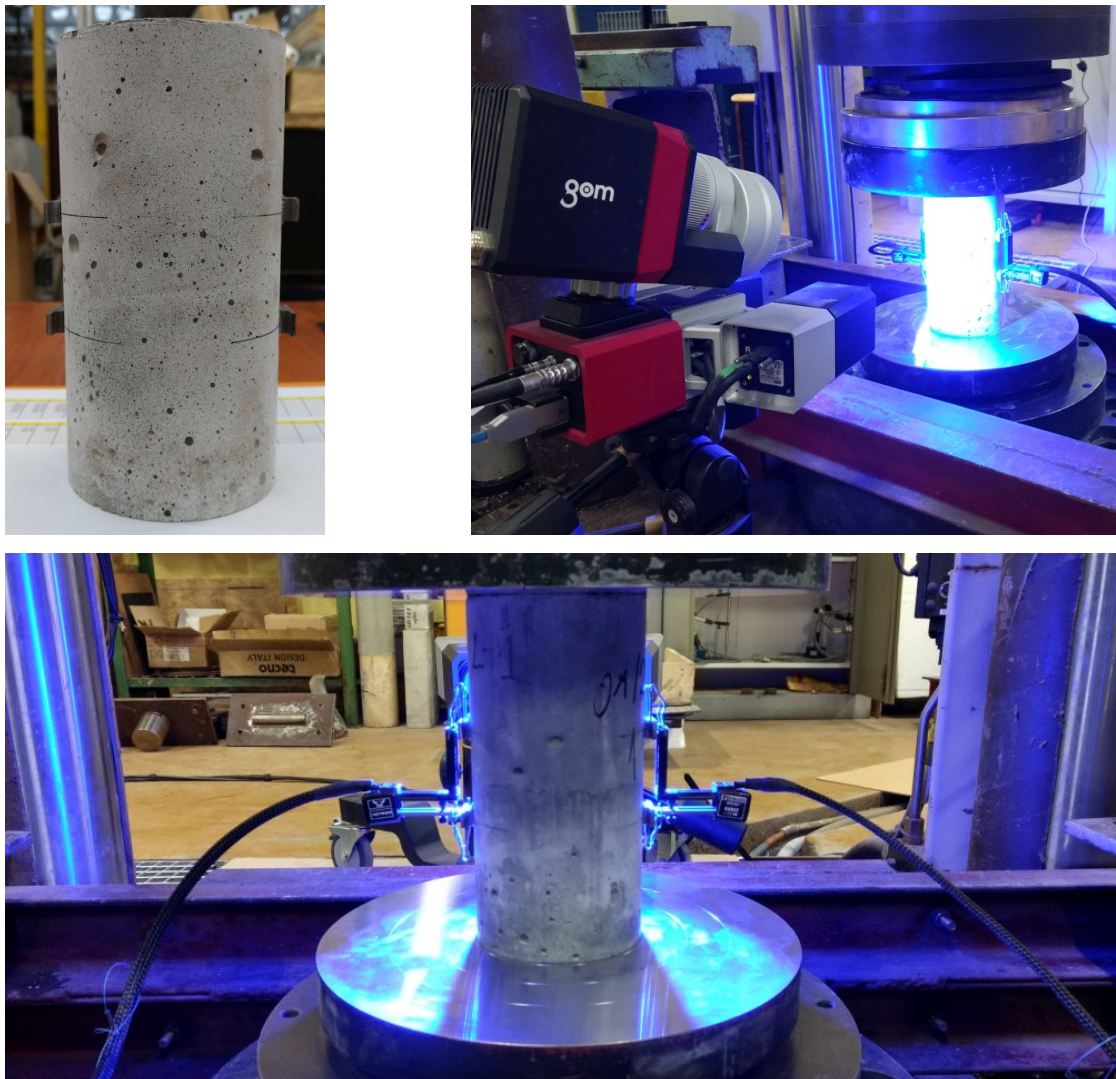


Fig. 9.23 Specimen with applied speckle pattern before and during testing.

The specimens were placed centrally in the testing rig. The test method was based on [EN 12390-13](#) (Determination of secant modulus of elasticity in compression) and RILEM recommendations ([Schneider et al. 2007](#)).

The goals of the tests on cylindrical specimens are prioritised in the following order:

1. measure the compressive strength before and after heating,
2. measure the stress-strain response during compressive tests,

and, if possible:

3. obtain the post-peak response,
4. obtain the elastic degradation by performing several loading-unloading cycles.

[EN 12390-13](#) requires extensometers base of at least two-thirds of the specimen diameter. The extensometers used in the test have a base of 50 mm. However, the DIC measurements indicated the limited length of extensometer's base did not influence the results, likely because of the homogeneity of the material and lack of coarse aggregate.

First, specimens were preloaded to 0.5 MPa. Then, checks for the variation of strain in second and third cycle, and strain difference on two measuring lines at the third cycle were performed ([EN 12390-13](#)). If the limit was not achieved, the specimen was re-centred and the test was restarted.

Fig. 9.24 presents surface of specimens before (20 °C) and after heating (600 °C, 800 °C, and 1000 °C). Surface cracks are visible on the specimen heated to 1000 °C. For reference, surface of cylindrical specimens heated by other researchers is depicted in Fig. 9.25.

[Mendes et al. \(2009\)](#) observed a significant degradation of cement paste, when they visually compared specimens (i) immediately and (ii) two days after heating to 800 °C and cooling (Fig. 9.25 a, b). [Bednarek et al. \(2009\)](#) did experiments on C30/37 concrete after heating. Up to 800 °C specimens survived the heating and it was possible to determine their strength. However, when heated to 1000 °C, specimens degraded significantly. [Halicka et al. \(2013\)](#) investigated two cement types (Portland and alumina) and three aggregate types (gravel, granite, and ceramic). They observed visual degradation of specimens made of Portland cement immediately after opening the furnace, and degradation of specimens made of high alumina cement with gravel aggregate 30 days after exposure (Fig. 9.25 c). Fig. 9.25 shows the specimens investigated by the author, where the cracking pattern on a cement paste (w/c=0.3) is shown immediately after heating and cooling (Fig. 9.25 d), and three months later (Fig. 9.25 e). Last image (Fig. 9.25 f) shows remains of the standard mortar specimen three months after heating to 1000 °C. It is worth noting, that the standard mortar heated to 1000 °C showed the lowest strength among all investigated mixes and temperatures (Fig. 9.9). The time might influence the results. Therefore, it is important to keep the time regime between cooling and testing.

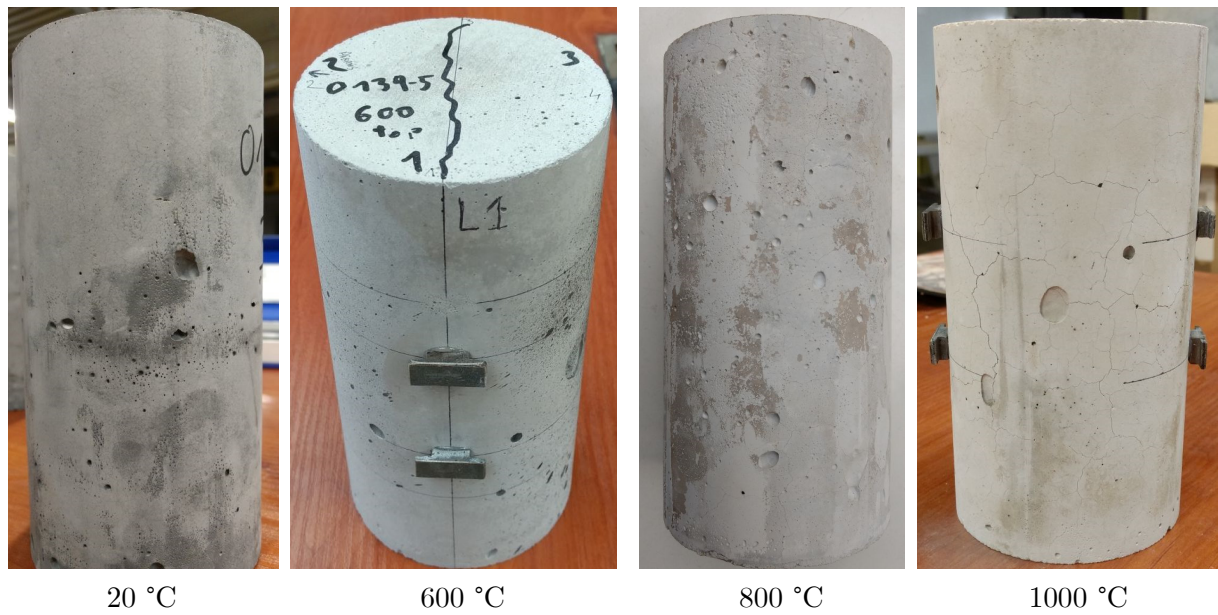


Fig. 9.24 Surface of the specimens before and after heating.

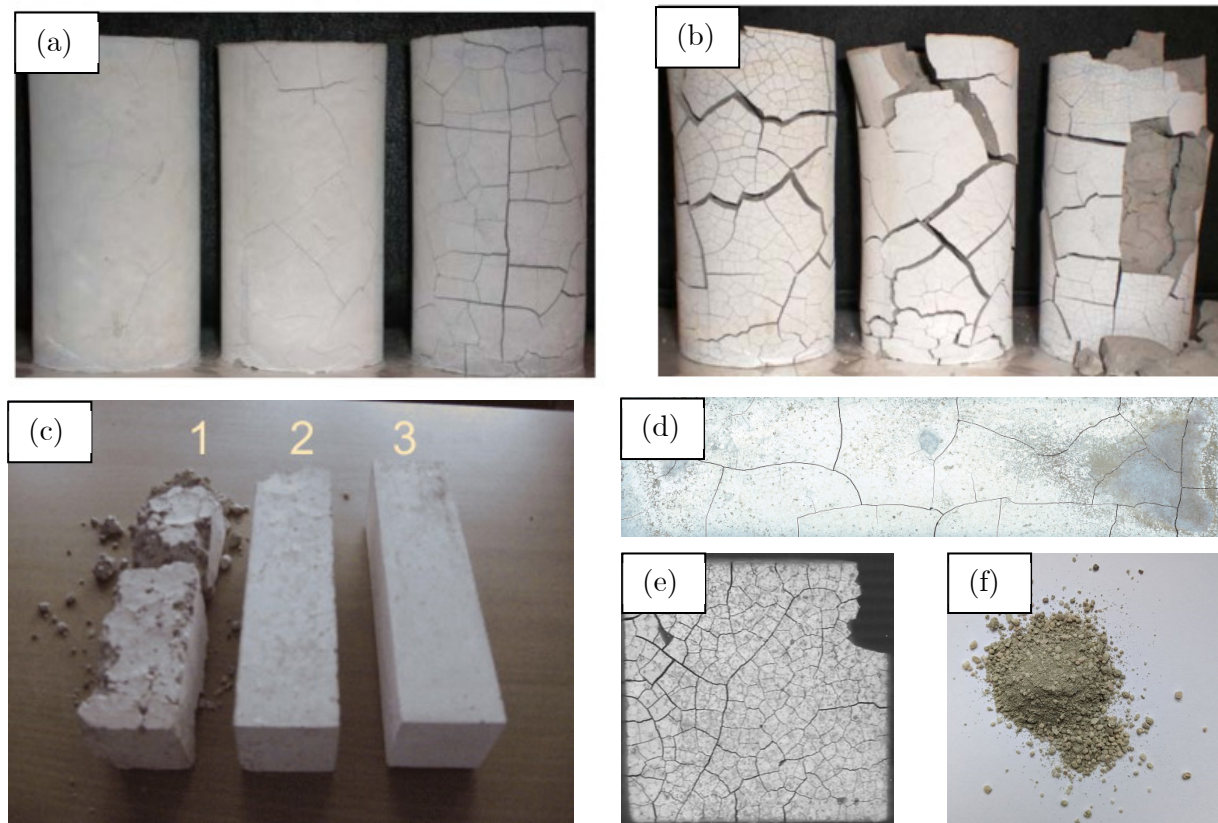
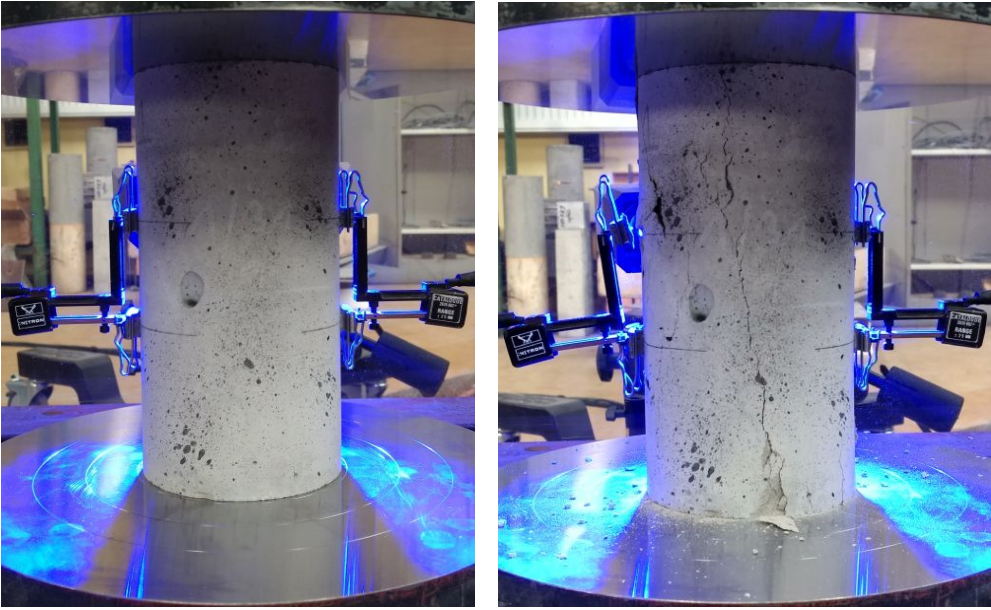


Fig. 9.25 Degradation of cement paste and concrete after heating. (a) cement paste immediately after heating to 800 °C and cooling, and (b) two days after heating to 800 °C and cooling (a, b reprinted from [Mendes et al. 2009](#), with permission from Elsevier); (c) specimen with different aggregate 1–gravel, 2–granite, 3–ceramic 30 days after heating (reprinted from [Halicka et al. 2013](#), with permission from Elsevier); (d) cement paste one day after heating to 800 °C; (e) cement paste three months after heating to 800 °C; (f) standard mortar three months after heating (own research).

Fig. 9.26 and Fig. 9.27 present specimens during and after testing.



*Fig. 9.26 One of the specimens before and after failure (after heating to 600 °C).*



*Fig. 9.27 One of the specimens after several loading-unloading cycles.*

Before tests, the universal testing machine was tuned to the stiffness of the specimen to be able to follow the prescribed displacement rate. Fig. 9.28 shows the displacement-time and strain-time curves before tuning (left) and after tuning (right).

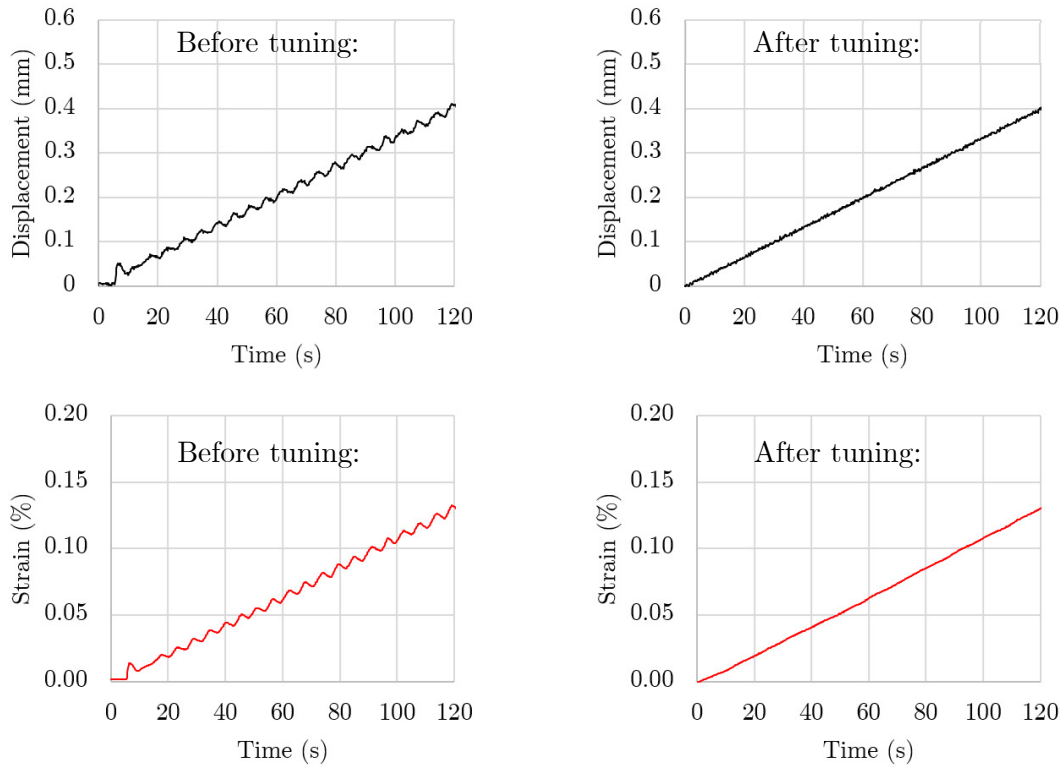


Fig. 9.28 Ability of the universal testing machine to follow prescribed displacement rate before and after tuning and its influence on the strain measurement.

### 9.3.7. Behaviour of cylindrical specimens

#### 9.3.6.1 Pre-peak response

Fig. 9.29 depicts the compressive stress-strain response of LCCC specimens without heating. Non-heated specimens exhibit a near-linear behaviour. The average compressive strength is 63.16 MPa. The average strain at failure ( $\epsilon_{c1,20^\circ C}$ ) is 0.46 %. The average modulus of elasticity between  $0.1 f_c$  and  $0.333 f_c$  is 14.39 GPa. A linear stress-strain relationship is common for cement pastes. The response becomes curved for mortars, and the curvature might increase for concretes (Popovics 1973, see Fig. 9.30).

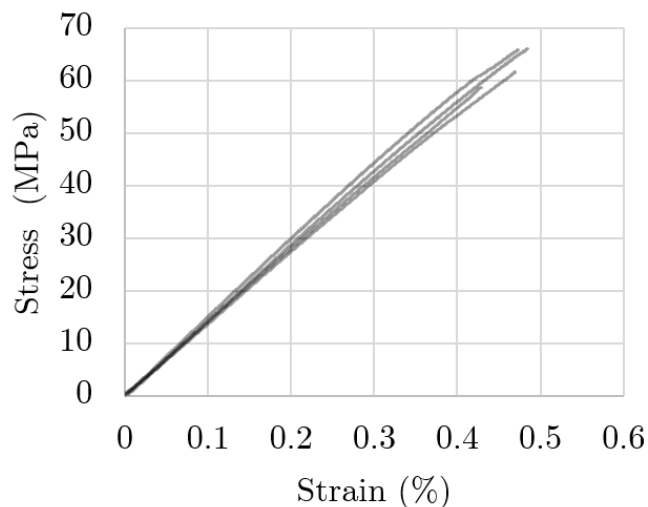


Fig. 9.29 Stress-strain response of LCCC without heating.

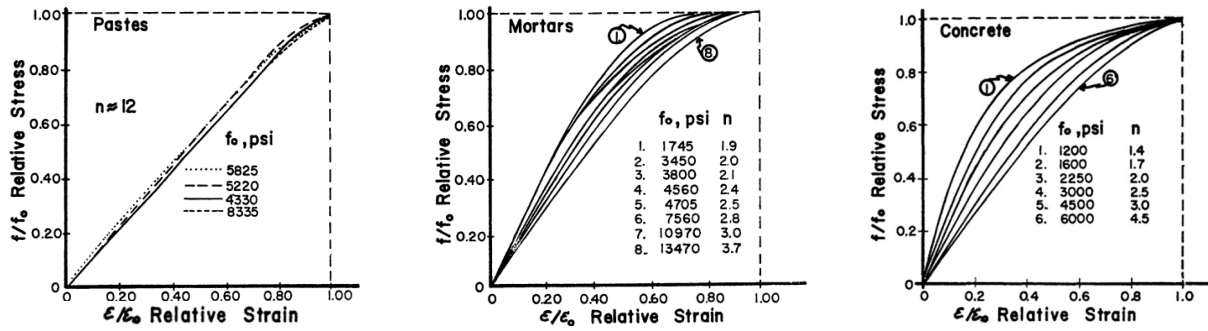


Fig. 9.30 Relative stress-relative strain response for pastes, mortars, and concrete (Reprinted from Popovics 1973, with permission from Elsevier).

Furthermore, Fig. 9.31 illustrates an excellent agreement between the results obtained with extensometers and DIC, which validated the use of a 50-mm base length extensometer.

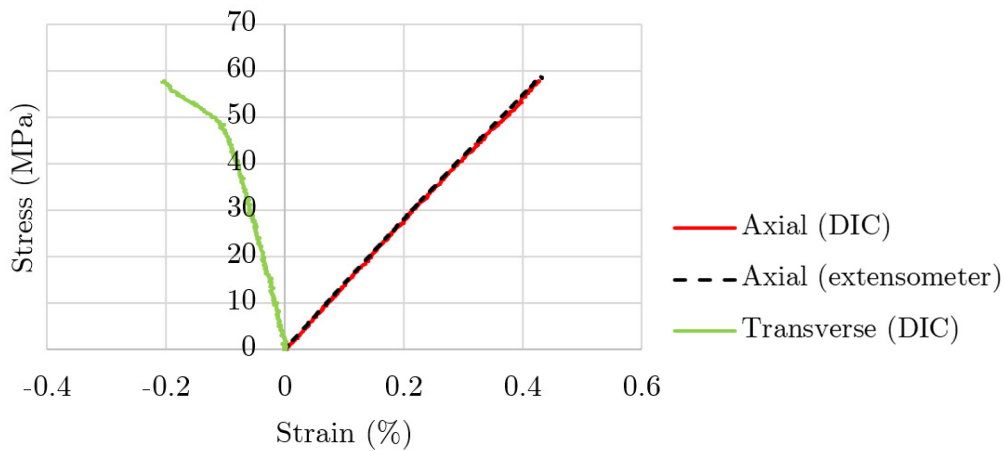


Fig. 9.31 Axial and transverse strain of an unheated specimen. The axial strain was measured using two extensometers and a DIC system; a near-perfect alignment between extensometers and DIC is visible. The agreement between the two measuring methods validated the use of a limited, 50-mm base length extensometer.

Table 9.11 summarises the experimental data obtained for cylindrical specimens before and after heating.

Table 9.11 Mechanical properties of cylindrical specimens.

Temperature (°C)	Compressive strength (MPa)	Modulus of elasticity (GPa)	Strain at peak stress (‰)	$k_{c,\theta}$ (-)	$k_{E,\theta}$ (-)
	Mean (standard deviation)				
20	63.16 (3.10)	14.39 (0.49)	4.63 (0.02)	1	1
600	43.78 (1.86)	7.68 (0.45)	4.96 (0.02)	0.693	0.534
800	29.67 (2.25)	5.78 (0.17)	5.21 (0.01)	0.470	0.402
1000	18.69 (1.09)	4.09 (0.39)	4.39 (0.05)	0.296	0.285

It can be observed in Table 9.11 that the reduction factors  $k_{c,\theta}$  obtained on cylindrical specimens are more favourable than the factors proposed in the Eurocode, and more favourable than the values obtained by most of the other researchers (see Fig. 9.9 and the results reported by [Ma et al. 2015](#)). However, the reduction factors for cylinders are less favourable than those obtained on standard prisms. Halves of standard prisms were primarily used to evaluate the compressive strength of LCCC in this investigation. Such samples were commonly used by other researchers to assess the performance of:

- pastes and mortars ([Horszczaruk et al. 2017](#), [Plechawski & Fic 2018](#), [Cao et al. 2019](#), [Koksal et al. 2021](#)),
- concrete ([Halicka et al. 2013](#)),
- ultra-high-performance composites ([Huang et al. 2019](#)),
- or geopolymers ([Zhang et al. 2014](#), [Hager et al. 2021a](#)).

Some researchers used small cuboid specimens, such as 20 mm ([Jiang et al. 2018](#)), 50 mm ([Ashkezari & Razmara 2020](#)), or 70 mm ([Arioz 2007](#)).

Mechanical loading causes the development of microcracks related to the direction of principal stress. This process is non-reversible and eventually leads to material failure ([Litewka et al. 2003](#)). Additionally, in thermal loads, the cracking patterns might be influenced by the specimen's shape and size ([Szeląg 2018](#)). Hence, the cracks developed due to heating and their orientation might affect the compressive strength results. Thus far, surprisingly, the research on the effect of the shape of heated specimens is scarce. A more common line of research is studying the effect of size, which, according to most researchers, is negligible as far as the residual strength (in per cent) is concerned ([Arioz 2009](#), [Erdem 2014](#)). Regarding the direct comparisons between cuboid and cylindrical specimens, differences up to 13 percentage points were found by [Bamonte & Gambarova \(2010\)](#). A more pronounced effect was reported by [Gulsan et al. \(2018\)](#) after the cuboid, and cylindrical specimens were heated to 750 °C. Therefore, investigation of the specimen's shape and size influence on the relative compressive strength and its causes might form one of the future research studies.

Fig. 9.32 presents the stress-strain curves for LCCC without heating (20 °C), and after heating and cooling 600 °C, 800 °C, 1000 °C. Each line represents an average of the readings from two extensometers. It can be observed in Fig. 9.32, that the stress-strain response appears to be concave at low stress values. This behaviour is consistent with the results presented by other researchers, e.g. [Chang et al. \(2006\)](#), who attribute it to closing of thermally-induced cracks.

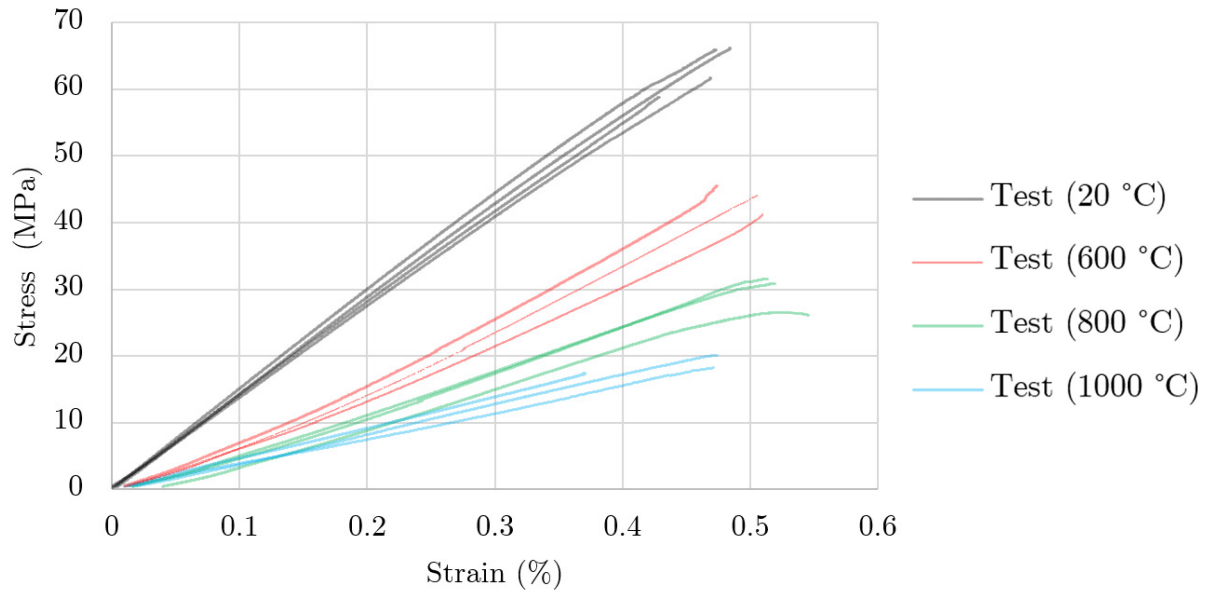


Fig. 9.32 Measured stress-strain curves for LCCC without heating (20 °C) and after heating and cooling (600 °C, 800 °C, 1000 °C).

Fig. 9.33 presents the relationship between LCCC compressive strength and elasticity modulus (before and after exposure to elevated temperatures).

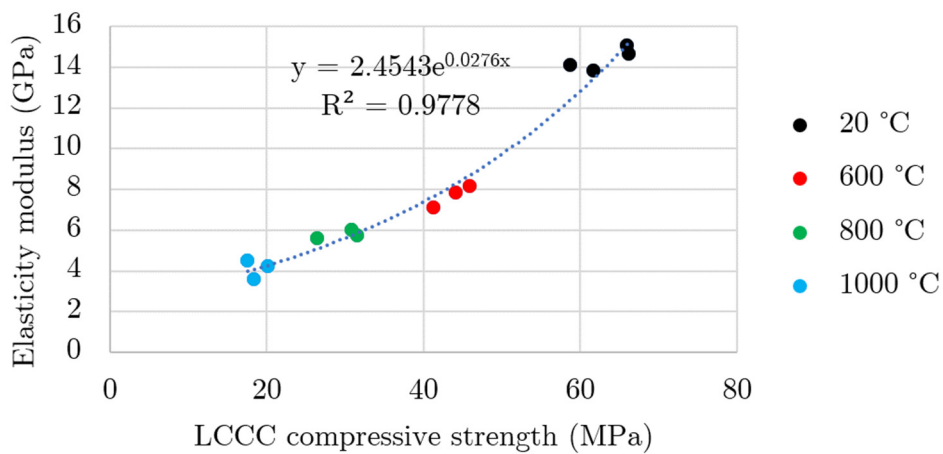


Fig. 9.33 Measured stress-strain curves for LCCC without heating (20 °C) and after heating and cooling (600 °C, 800 °C, 1000 °C).

The prediction of stress-strain relationship for a variety of concretes that could be based on limited data, was a subject of research for decades. One such model was proposed by [Popovics 1973](#). In 1985 the RILEM Committee PHT 44 recommended the Popovics model to be implemented in the Eurocode to describe the stress-strain relationship at elevated temperatures. Currently, the RILEM Technical Committee 306-CFR "Concrete during Fire - Reassessment of the framework" is working on the revision of this model, and the author of the proposal is participating in the efforts of this group.

The Popivics model (for elevated temperature) in general form is expressed as:

$$\sigma(\theta) = \frac{f_{c,\theta}}{\varepsilon_{c1,\theta}} \cdot \frac{n\varepsilon}{(n-1) + \left(\frac{\varepsilon}{\varepsilon_{c1,\theta}}\right)^n} \quad (9.3)$$

In the form implemented in the Eurocode 1992-1-2,  $n=3$ , therefore:

$$\sigma(\theta) = \frac{f_{c,\theta}}{\varepsilon_{c1,\theta}} \cdot \frac{3\varepsilon}{2 + \left(\frac{\varepsilon}{\varepsilon_{c1,\theta}}\right)^3} \quad (9.4)$$

Thus, the tangent modulus of elasticity is equal to the first derivative of Eq. (9.3):

$$\begin{aligned} E_{\theta,tangent} &= \frac{f_{c,\theta}}{\varepsilon_{c1,\theta}} \cdot \frac{n \left[ (n-1) + \left(\frac{\varepsilon}{\varepsilon_{c1,\theta}}\right)^n \right] - n\varepsilon n \frac{\varepsilon^{n-1}}{\varepsilon_{c1,\theta}^n}}{\left[ (n-1) + \left(\frac{\varepsilon}{\varepsilon_{c1,\theta}}\right)^n \right]^2} = \\ &= n \frac{f_{c,\theta}}{\varepsilon_{c1,\theta}} \cdot \frac{n-1 + \left(\frac{\varepsilon}{\varepsilon_{c1,\theta}}\right)^n - n \left(\frac{\varepsilon}{\varepsilon_{c1,\theta}}\right)^n}{\left[ (n-1) + \left(\frac{\varepsilon}{\varepsilon_{c1,\theta}}\right)^n \right]} = \\ &= n(n-1) \cdot \frac{f_{c,\theta}}{\varepsilon_{c1,\theta}} \cdot \frac{1 - \left(\frac{\varepsilon}{\varepsilon_{c1,\theta}}\right)^n}{\left[ (n-1) + \left(\frac{\varepsilon}{\varepsilon_{c1,\theta}}\right)^n \right]} \end{aligned} \quad (9.5)$$

For  $\varepsilon=0$  (initial tangent modulus of elasticity):

$$E_{\theta,tangent}(\varepsilon = 0) = \frac{n}{n-1} \cdot \frac{f_{c,\theta}}{\varepsilon_{c1,\theta}} \quad (9.6)$$

If the secant modulus of elasticity is expressed between  $(0, 0)$  and  $(\varepsilon_{c1,\theta}, f_{c,\theta})$ , there is a relationship:

$$\frac{E_{sec,f_{c,\theta}}}{E_{\theta,tangent}(\varepsilon = 0)} = \frac{n}{n-1} \quad (9.7)$$

In ordinary concrete, it is usually assumed that the linear range of the stress-stain relationship reaches up to 30-40 % of the compressive strength. As the microcracks propagate, the stiffness

of concrete decreases, and the stress-strain response becomes non-linear (Litewka & Dębiński 2003). For numerical modelling, a linear elastic response was assumed up to 40 % of the strength at each temperature. After the corresponding strain is reached, the behaviour is assumed to be plastic and to follow the curve given by Eq. (9.3).

Assuming the linear response up to  $\frac{\sigma(\theta)}{f_{c,\theta}} = 0.4$ , and  $\frac{\varepsilon}{\varepsilon_{c1,\theta}} = x$ , and substituting Eq. (9.3):

$$0.4 = \frac{nx}{n-1+(x)^n} \quad (9.8)$$

Which becomes:

$$0.4x^n - nx + 0.4n - 0.4 = 0 \quad (9.9)$$

When solved for  $n=3$ , there are three solutions to Eq. (9.9):

$$x_1 = -2.8633$$

$$x_2 = 0.26927$$

$$x_3 = 2.59403$$

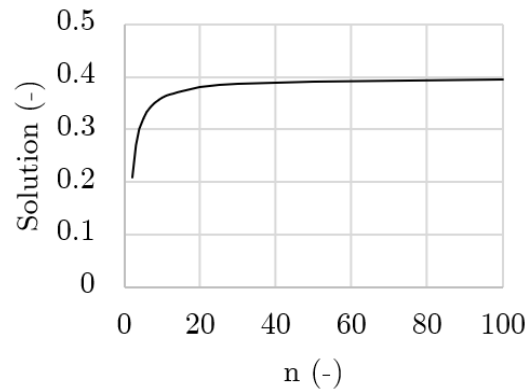
Only the solution in the range (0, 0.4) is physical, therefore for a linear response up to 40 % of the compressive strength, followed by plastic response, the secant elastic modulus is

$$E_{c,\theta,secant(0.4f_{c,\theta})} = \frac{0.4f_{c,\theta}}{0.26927\varepsilon_{c1,\theta}} \quad (9.10)$$

The solutions for  $\frac{\sigma(\theta)}{f_{c,\theta}} = 0.4$  and other values of  $n$  are given in Fig. 9.34.

Fig. 9.34 Solutions to eq. 10.7 for the  $\frac{\sigma(\theta)}{f_{c,\theta}} = 0.4$  and various  $n$  values.

<b>n</b>	<b>x</b>
2	0.20871
3	0.26927
4	0.30082
5	0.32027
6	0.33343
7	0.34289
8	0.35001
<b>9</b>	<b>0.35556</b>
10	0.36000



Finally, the implementation of the stress-strain model, fitted to the experimental data ( $n=9$ ), gives the strain corresponding to  $0.4f_{c,\theta}$  equal to  $0.35556\varepsilon_{c1,\theta}$ .

Therefore, the numerical implementation is based on a linear stress-strain relationship in the range  $0 \leq \varepsilon \leq 0.35556\varepsilon_{c1,\theta}$ , with  $n=9$ :

$$\sigma = \varepsilon \cdot \frac{0.4f_{c,\theta}}{0.35556\varepsilon_{c1,\theta}}$$

and Popovics model for  $0.35556\varepsilon_{c1,\theta} < \varepsilon \leq \varepsilon_{c1,\theta}$ :

$$\sigma = \frac{f_{c,\theta}}{\varepsilon_{c1,\theta}} \cdot \frac{9\varepsilon}{(9-1) + \left(\frac{\varepsilon}{\varepsilon_{c1,\theta}}\right)^9}$$

For  $\varepsilon > \varepsilon_{c1,\theta}$ , a descending branch should be adopted, which is elaborated next.

Bear in mind that stress and strain are converted to true values, Eq. (7.1). The measured stress-strain response of specimens after heating to various temperatures and a variation of the Popovics model ( $n=9$ ) is presented in Fig. 9.35.

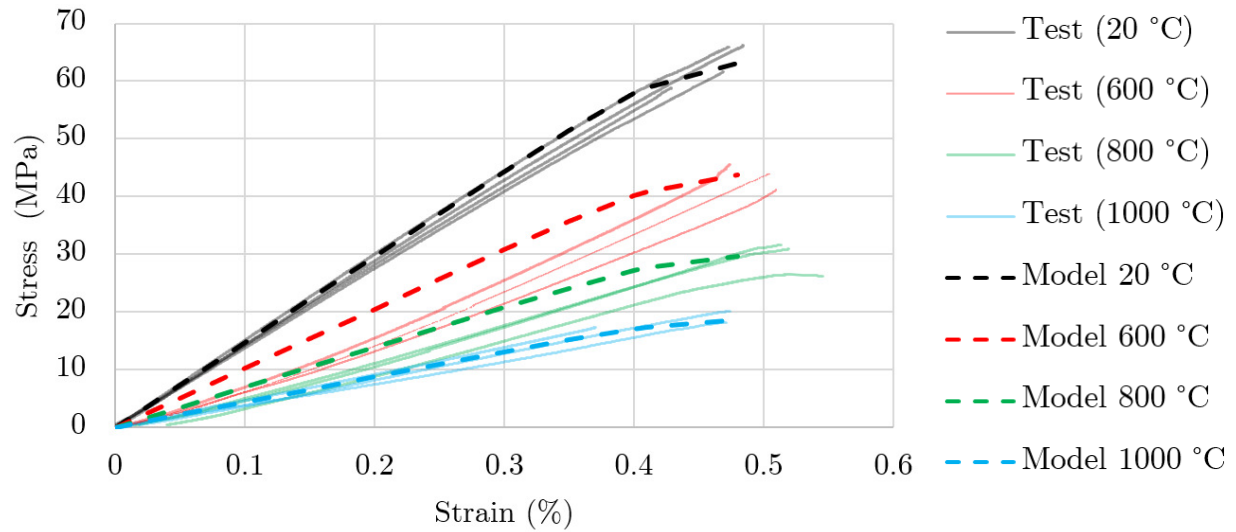


Fig. 9.35 Stress-strain curves measured during the test for individual specimens and the Popovics model ( $n=9$ , ascending branch only).

### 9.3.6.2 Post-peak response

Fig. 9.36 and Fig. 9.37 show the stress-displacement response of a heated specimen during several load-unload sequences. Gradual damage of the material is visible.

Fig. 9.37 shows the same data, but stress and displacement are normalised and expressed as relative values (relative displacement equal to 1 is reached for the peak stress).

The presented results finalise the experimental part of this dissertation.

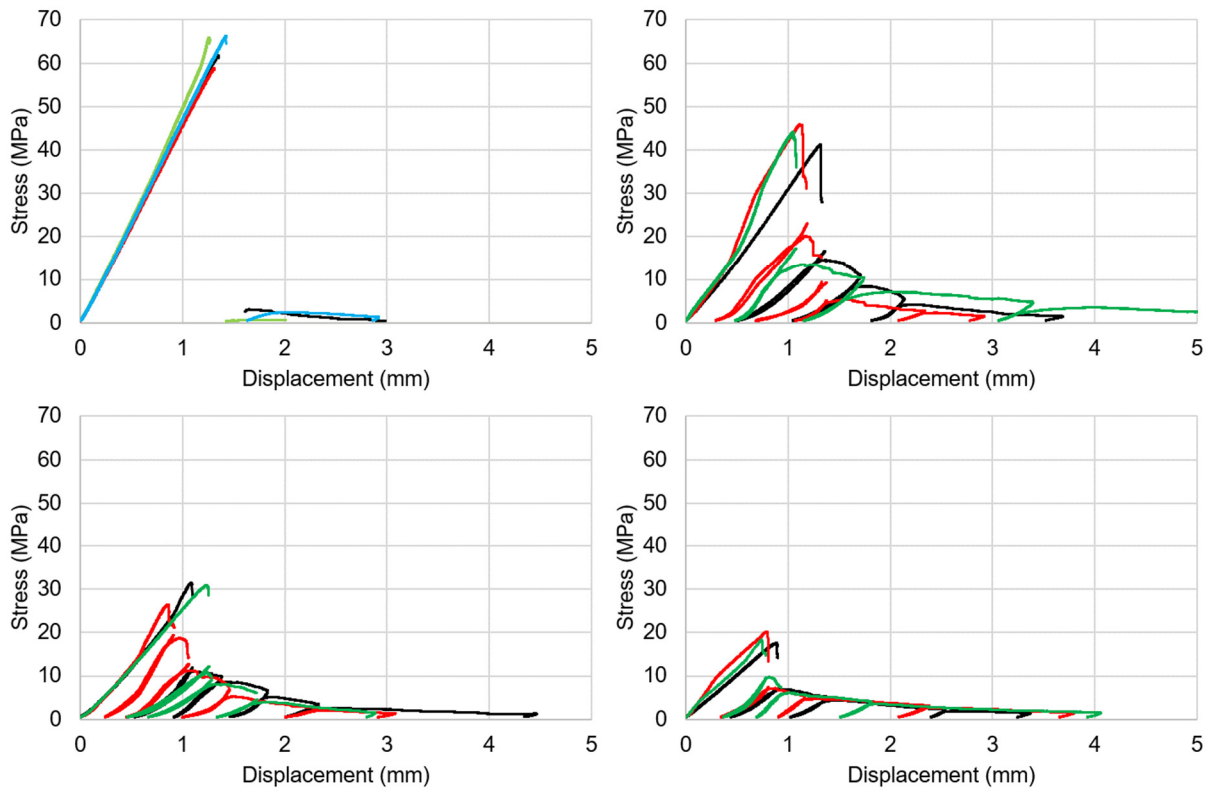


Fig. 9.36 Stress-displacement relationship obtained in the preliminary investigation for a specimen after heating and cooling. The displacement was read from the testing rig; the proper test should have included LVDTs, which were unavailable during the testing period.

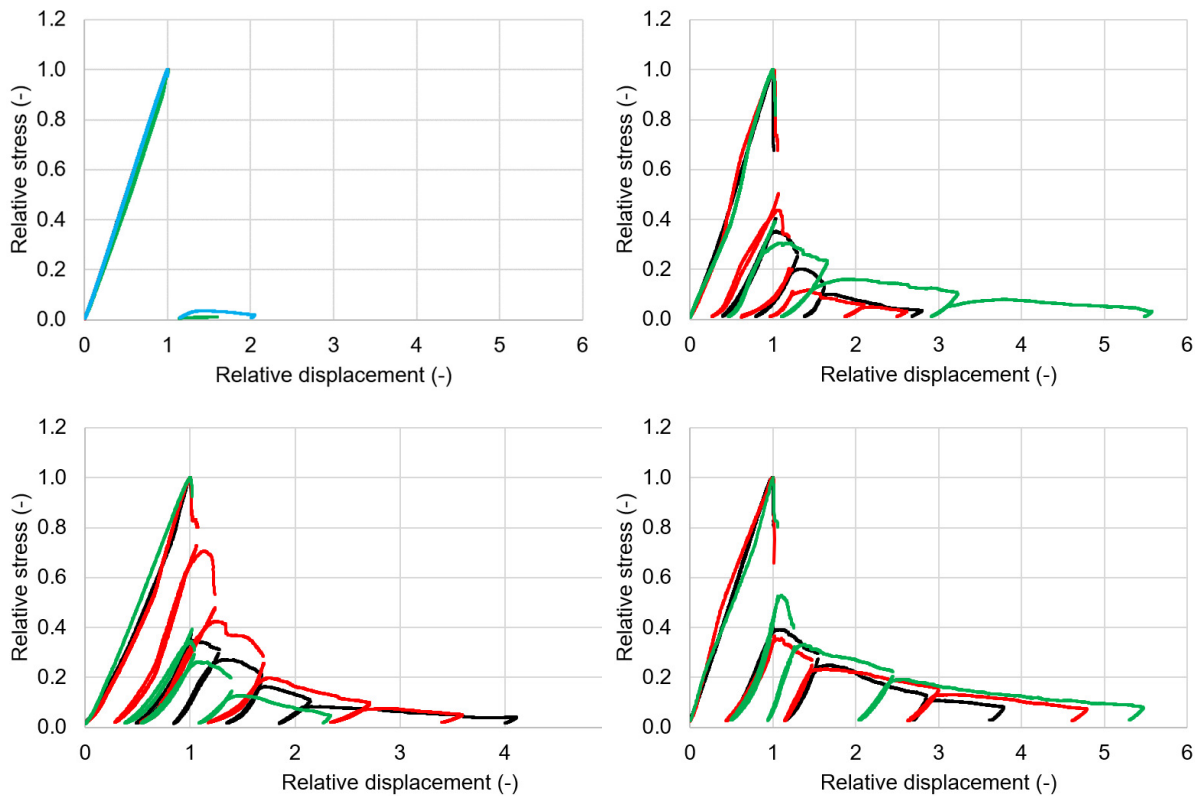


Fig. 9.37 Relative stress-displacement relationships.

#### 9.4. Fire performance of LCCC-filled steel tubular columns

The numerical model described in the earlier sections is used for the feasibility study of LCCC-filled steel tubular columns (LCFST). The same set of 50 columns used for validation is used here to enable easier comparisons between the previously presented numerical results.

In the absence of comprehensive experimental data (for example stressed tests at elevated temperature), several variants are studied and compared to the results presented in Table 7.1. For example, three primary mechanisms might influence the fire resistance of LCCC-filled steel tubular columns: (i) increased compressive strength, (ii) favourable strength reduction factors, (iii) better insulation properties compared to ordinary concrete. Therefore, the influence of those three mechanisms is studied separately. Such an analysis might benefit future work on the filling material, as it shows a promising research direction.

The promising results show that fire resistance time might increase if LCCC is used instead of ordinary concrete. Fig. 9.38 depicts the behaviour of a 3.8-meter-long column made of a steel tube filled with concrete. The fire resistance time in the test was 143 minutes (black line), and the time obtained with the numerical model is 134 minutes (red line). When compressive strength reduction factors presented in Fig. 9.9 are assumed along with the original concrete strength (27 MPa), the calculated fire resistance time is 287 minutes (2.14 times longer than calculated for NWC filling). In the remainder of this chapter, the feasibility of LCCC filling is assessed, by presenting and discussing several sets of assumptions, backed-up by available test data. Such approach allows decoupling effects of individual parameters and provides detailed insight into the increased performance that LCCC might introduce to the structural fire resistance of steel tubular columns.

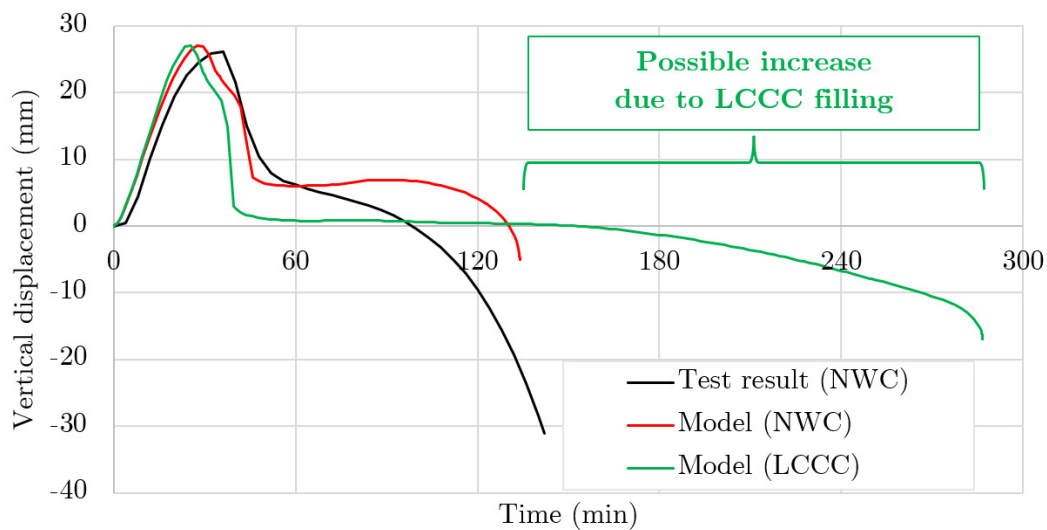


Fig. 9.38 Behaviour of the C23 column (tested by Lie & Chabot 1992) during a fire resistance test: test result, simulations assuming original NWC filling, and a prediction with LCCC filling.

The remainder of the results are organised as follows:

1. A certain set of properties (e.g. measured reduction factors of LCCC instead of reduction factors from the Eurocode) are assumed.
2. A fire resistance time is calculated based on the model presented in chapter 7, substituted with material properties presented in chapter 9.3.

- For each analysed column, the time obtained with the numerical model is compared, giving an expected change in fire resistance time in terms of minutes and per cent.

For example, the results for three columns are presented in Fig. 9.39. Those are the first three columns in Table 7.1, and they are shown in Table 9.12 using a similar layout.

When assuming a certain set of properties (e.g. measured reduction factors of LCCC instead of reduction factors from the Eurocode), the fire resistance time of each column changes. Each column is represented by two bars in Fig. 9.39 (red with solid filling represents the FRT change in minutes (compared to the numerical results in Table 7.1), and the empty black bar expresses the relative FRT change (in per cent). For easier reference, a part of Table 7.1 is repeated in Table 9.13.

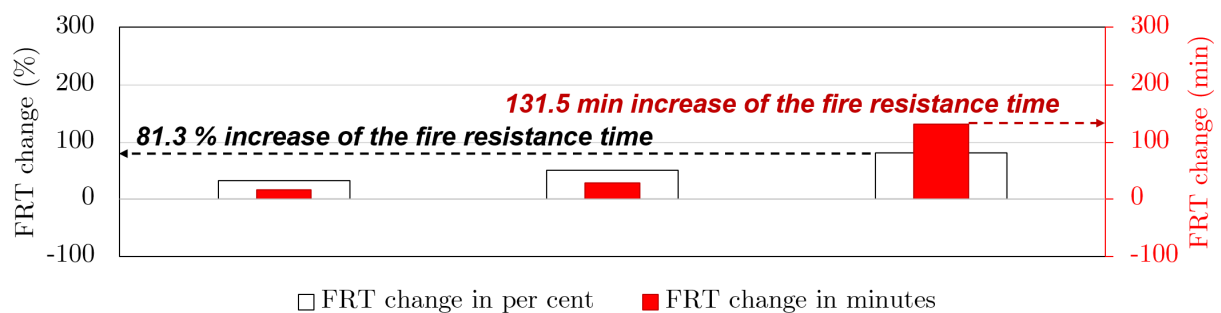


Fig. 9.39 The explanatory graph on how to read the results for the following sets.

Table 9.12 Table with data used to produce the explanatory graph above (Fig. 9.39).

Data	No.	ID	FRT		FRTR	FRT (predicted)	FRT change	FRT change
			test	num				
	-	-	min	min	-	min	min	%
(1)	(2)	(3)	(4)	(5)	(6)	(7)	(8)	(9)
WT	1	1	56	47.8	0.85	63.0	15.3	31.9
	2	2	45	55.6	1.24	83.2	27.6	49.7
	3	3	142	161.8	1.14	293.3	131.5	81.3

In Fig. 9.39 and Table 9.12 it can be seen, that for a certain set of assumptions, the fire resistance time increased by 15.3 minutes (31.9 %), 27.6 minutes (49.7 %), and 131.5 minutes (81.3 %), for columns 1, 2, and 3, respectively.

Table 9.13 Set of 50 columns used in validation and feasibility study.

Data	No.	ID	D	t	L	BC	load	ecc.	f <sub>c</sub>	f <sub>y</sub>	FRT	
											test	num
		-	mm	mm	mm	-	kN	mm	MPa	MPa	min	min
(1)	(2)	(3)	(4)	(5)	(6)	(7)	(8)	(9)	(10)	(11)	(12)	(13)
WT	1	1	244.5	6.3	3400	P-P	635.4	0	49	355	56	47.8
	2	2	323.9	6.3	3400	P-P	1864	0	49	354	45	55.6
	3	3	355.6	9.5	3400	P-P	900	0	49	348	142	161.8
Han	4	C1-1	478	8	3770	P-P	4700	0	31	293	29	36.3
	5	C1-2	478	8	3770	P-P	2200	71.7	31	293	32	17.2
	6	C2-1	219	5	3770	P-P	450	32.85	31	293	17	15.3
	7	C2-2	219	5	3770	P-P	300	65.7	31	293	18	19.2
NRC	8	C02	141.3	6.55	3772	F-F	110	0	33	350	55	56.3
	9	C04	141.3	6.55	3772	F-F	131	0	31	350	57	45.3
	10	C05	168.3	4.78	3772	F-F	150	0	33	350	76	76.4
	11	C08	168.3	4.78	3772	F-F	218	0	36	350	56	61.0
	12	C09	168.3	6.35	3772	F-F	150	0	35	350	81	80.9
	13	C11	219.1	4.78	3760	F-F	492	0	31	350	80	70.9
	14	C13	219.1	4.78	3760	F-F	384	0	32	350	102	89.4
	15	C17	219.1	8.18	3760	F-F	525	0	32	350	82	68.6
	16	C20	273.1	5.56	3760	F-F	574	0	29	350	112	132.4
	17	C21	273.1	5.56	3760	F-F	525	0	29	350	133	141.6
	18	C22	273.1	5.56	3760	F-F	1000	0	27	350	70	61.9
	19	C23	273.1	12.7	3760	F-F	525	0	27	350	143	133.9
	20	C25	323.9	6.35	3734	F-F	699	0	28	350	145	195.7
	21	C26	323.9	6.35	3734	F-F	1050	0	24	350	93	111.0
	22	C29	355.6	12.7	3734	F-F	1050	0	25	350	170	168.4
	23	C31	141.3	6.55	3772	F-F	80	0	30	350	82	69.1
	24	C32	141.3	6.55	3772	F-F	143	0	35	350	64	47.4
	25	C34	219.1	4.78	3760	F-F	500	0	35	350	111	88.4
	26	C35	219.1	4.78	3760	F-F	560	0	43	350	108	93.0
	27	C37	219.1	8.18	3760	F-F	560	0	29	350	102	65.9
	28	C40	273.1	6.35	3760	F-F	1 050	0	47	350	106	135.0
	29	C44	273.1	6.35	3760	F-F	715	0	39	350	178	159.9
	30	C45	273.1	6.35	3760	F-F	712	0	38	350	144	157.5
	31	C48*	273.1	6.35	3760	F-F	1050	0	47	350	188	160.8
	32	C49*	273.1	6.35	3760	F-F	1900	0	47	350	96	87.9
	33	C50	323.9	6.35	3734	F-F	820	0	42	350	234	260.3
	34	C55	355.6	12.7	3734	F-F	965	0	41	350	274	289.2
	35	C57	406.4	6.35	3734	F-F	1 400	0	44	350	294	382.0
UPV	36	02	159	6	3180	P-P	338	0	30	338	18	16.0
	37	03	159	6	3180	F-P	396	0	29	338	25	17.8
	38	04	159	6	3180	F-P	198	0	36	338	42	38.1
	39	05	159	6	3180	F-P	594	0	34	338	14	13.3
	40	06	159	6	3180	F-P	229	0	24	338	43	38.8
	41	07	159	6	3180	F-P	458	0	30	338	30	21.1
	42	08	159	6	3180	F-P	687	0	34	338	13	13.7
	43	17	159	6	3180	F-P	169	20	36	332	32	33.9
	44	18	159	6	3180	F-P	337	20	42	332	16	19.9
	45	21	159	6	3180	F-P	126	50	31	344	30	34.7
	46	22	159	6	3180	F-P	253	50	38	366	23	22.4
	47	25	159	6	3180	F-P	180	20	39	357	48	49.5
	48	26	159	6	3180	F-P	360	20	40	357	24	23.4
	49	29	159	6	3180	F-P	140	50	31	386	39	41.0
	50	30	159	6	3180	F-P	280	50	40	386	20	24.3

The following figures (Fig. 9.40-SLUPx) present the change in fire resistance time (FRT) in minutes and % for 50 analysed columns. Change is caused by using different assumptions related to the potential LCCC instead of NSC filling.

The results are presented for several sets of assumptions described above each graph. The order of the columns in Fig. 9.40-SLUPx is the same as in Table 7.1 and Table 9.13.

Therefore, the first column is Wainman & Toner (1992) column No. 1, followed by two other columns tested by these researchers. Next, four columns are from Han et al. (2003), followed by columns tested by Lie & Chabot (1992), and Espinos et al. (2014).

**Set 1:**

- Strength: original
- $\sigma$ - $\epsilon$ : Eurocode 2
- Reduction factors Eurocode 2
- Thermal properties: LCCC (Table 9.5, Table 9.6, Table 9.7)
- Average FRT increase: 8.5 min (3.1 %)

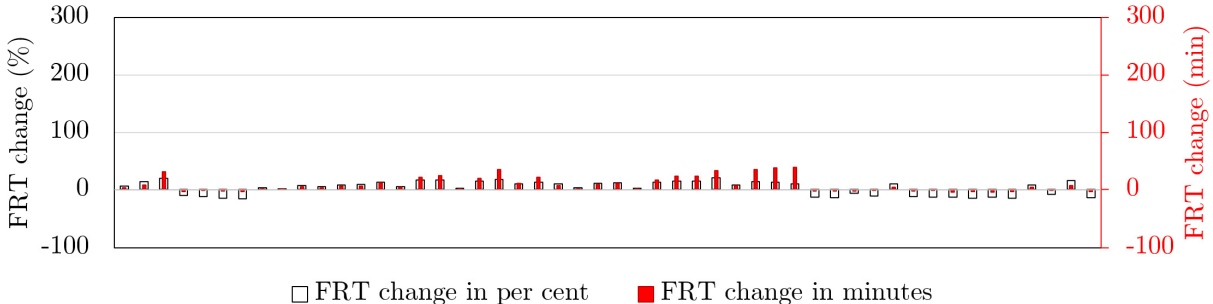


Fig. 9.40 Results for Set 1 (vertical scale consistent with graphs for sets 1-5).

Set 1 explores the effects of changing the thermal properties only. Strength, reduction factors, and stress-strain relationships of the filling were assumed as in chapter 7. The results are far from spectacular. It can be observed that columns with the highest diameter tend to benefit from the insulating properties of the filling. On the contrary, columns with a higher contribution of the steel tube show an FRT decrease due to limited heat transfer towards the core and the resultant increase of steel tube temperature. The average FRT increase for the whole set is 8.5 minutes (which corresponds to 3.1 %).

Sets 2, 3 and 4 are used to explore the potential of the filling compressive strength. In Set 2, strength was increased by 10 % from the reference value (given in Table 7.1). In Set 3, strength was increased by 20 %, and in Set 4, strength was assumed to be 54 MPa (Table 9.4).

**Set 2:**

- Strength: increased by 10 %
- $\sigma$ - $\varepsilon$ : Eurocode 2
- Reduction factors: Eurocode 2
- Thermal properties: Eurocode 2
- Average FRT increase: 11.5 min (13.7 %)

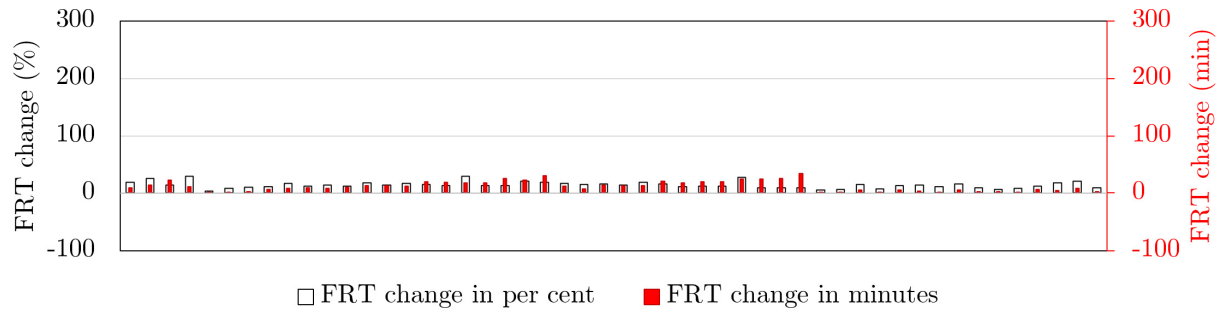


*Fig. 9.41 Results for Set 2 (vertical scale consistent with graphs for sets 1-5).*

**Set 3:**

- Strength: increased by 20 %
- $\sigma$ - $\varepsilon$ : Eurocode 2
- Reduction factors: Eurocode 2
- Thermal properties: Eurocode 2
- Average FRT increase: 16.7 min (20.5 %)

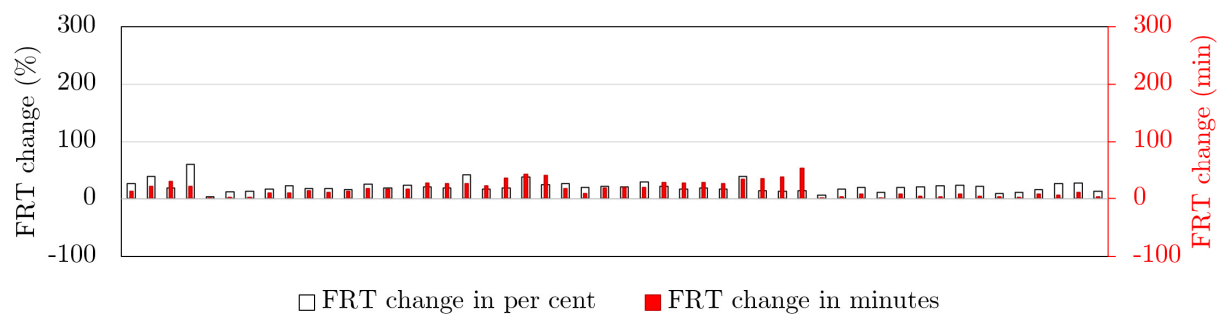


*Fig. 9.42 Results for Set 3 (vertical scale consistent with graphs for sets 1-5).*

**Set 4:**

- Strength: 54 MPa
- $\sigma$ - $\varepsilon$ : Eurocode 2
- Reduction factors: Eurocode 2
- Thermal properties: Eurocode 2
- Average FRT increase: 32.1 min (44.9 %)

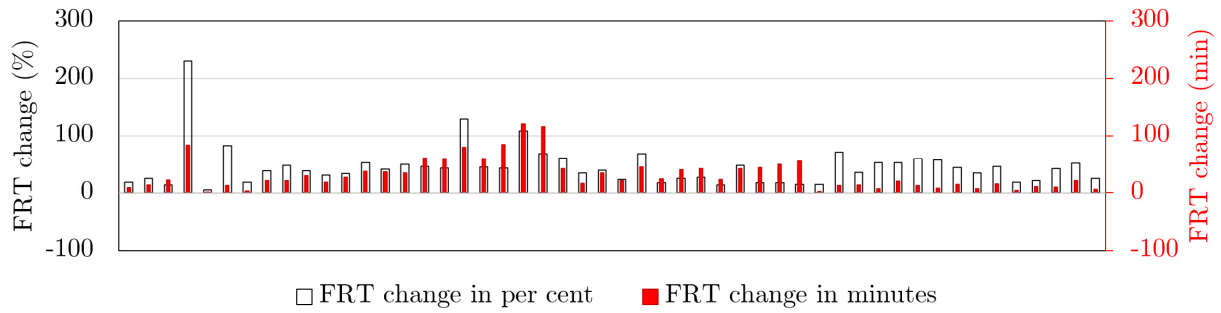


Fig. 9.43 Results for Set 4 (vertical scale consistent with graphs for sets 1-5).

### Summary of sets 1-4:

Based on the results presented for sets 1-4, it can be observed that the insulating properties of LCCC do not have a major influence on the performance of CFST columns. Likely, the effect of low thermal conductivity is countered by low density. Consequently, the effect of lower thermal diffusivity is not as pronounced.

The following two sets (#2, #3) form a sensitivity of FRT to the compressive strength of concrete. An increase of 10 %, or 20 % (relative to the original values in Table 7.1), increases the fire resistance time of all columns. The increase is more pronounced for stocky columns. The increase becomes more pronounced when the compressive strength is assumed to be 54 MPa (value measured for LCCC).

### Set 5:

- Strength: original
- $\sigma$ - $\varepsilon$ : Eurocode 2
- Reduction factors:  $k_{c,y}$  for halves of prisms (Fig. 9.9, Table 9.8)
- Thermal properties: LCCC (Table 9.5, Table 9.6, Table 9.7)
- Average FRT increase: 61.8 min (46.6 %)

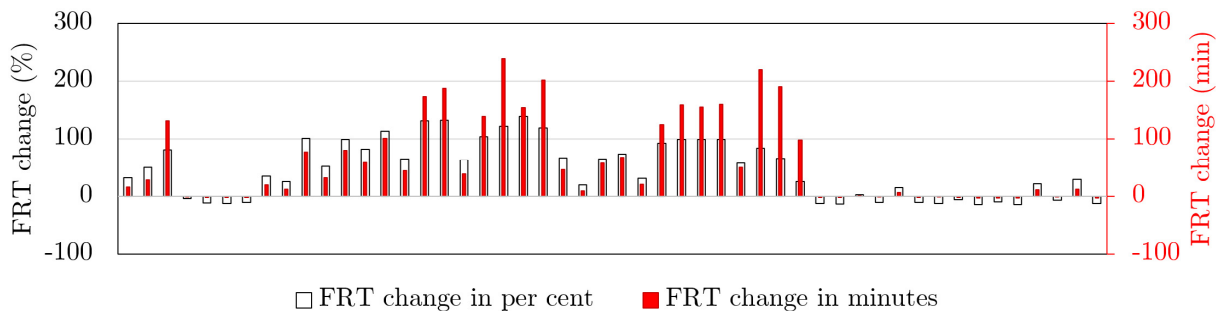


Fig. 9.44 Results for Set 5 (vertical scale consistent with graphs for sets 1-5).

Results are calculated using the original initial strength (reported by researchers) but assuming strength reduction factors from own experiments on LCCC (Fig. 9.9, Table 9.8). Set 5 answers the question: "What would happen if ordinary concrete displayed the same reduction factors, as reported for LCCC?" It can be observed that for some columns, the FRT decreases due to the prevailing effect of thermal properties (again, highly insulating concrete prevents heat from dissipating towards the core and increases the steel tube temperature). Therefore, it can be

concluded that the favourable reduction factors obtained for LCCC have a higher influence, than the change in compressive strength.

For the remainder of the sets, note the change in the vertical scale.

**Set 6:**

- Strength: 54 MPa
- $\sigma$ - $\varepsilon$ : Eurocode 2
- Reduction factors:  $k_{c,\theta}$  for halves of prisms (Fig. 9.9, Table 9.8)
- Thermal properties: LCCC (Table 9.5, Table 9.6, Table 9.7)
- Average FRT increase: 120.6 min (120.3 %)

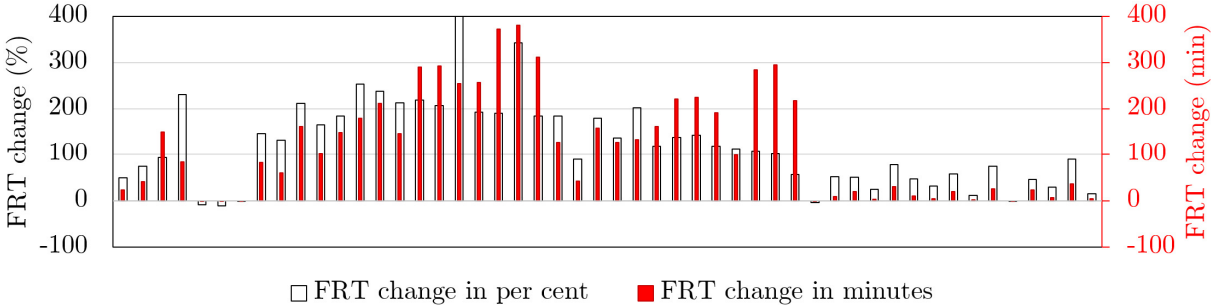


Fig. 9.45 Results for Set 6 (vertical scale consistent with graphs for sets 6-9).

Set 6 answers the question: 'What would happen, if ordinary concrete displayed the same reduction factors, as reported for LCCC, and the initial compressive strength would be 54 MPa?'

**Set 7:**

- Strength: 63 MPa
- $\sigma$ - $\varepsilon$ : Eurocode 2
- Reduction factors:  $k_{c,\theta}$  for cylinders (Table 9.11)
- Thermal properties: LCCC (Table 9.5, Table 9.6, Table 9.7)
- Average FRT increase: 92.1 min (92.6 %)

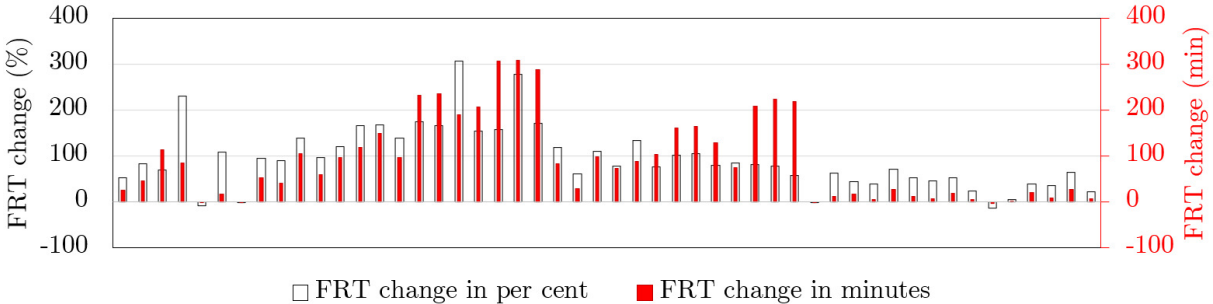


Fig. 9.46 Results for Set 7 (vertical scale consistent with graphs for sets 6-9).

In Set 7, the reduction factors obtained for cylindrical specimens are used. The initial compressive strength is assumed to be 63 MPa. Most researchers indicate a conversion factor between 150 mm and 100 mm cylinders in the range of 0.97-1.0.

When Sets 6 and 7 are compared, the influence of the input values obtained on halves of standard prisms and 100 mm x 200 mm cylinders is visible.

The simulations presented above for Sets 6-7 are based on the Eurocode adoption of Popovics model (with  $n=9$  in Eq. (9.3)). However, as noted earlier in the experimental part, LCCC displayed more linear stress-strain behaviour. Therefore, the following Sets are based on the Popovics model with different values of  $n$ . (see Fig. 9.47).

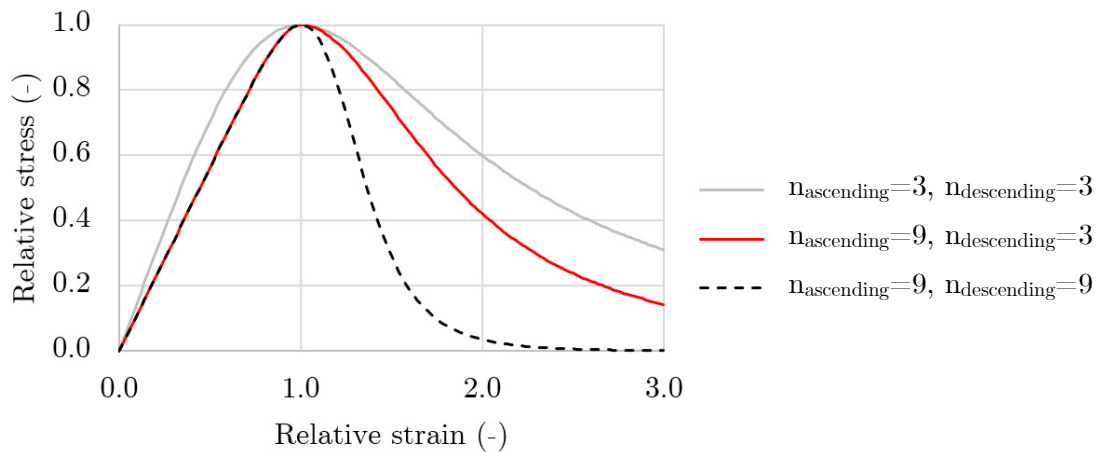


Fig. 9.47 Popovics model with.

Chronologically, during the work on this thesis, results for sets 1-6 were obtained after testing halves of the prisms (chapter 9.2). Since the results were promising, additional experiments were conducted to obtain more information – especially with regard to cylindrical specimens. The results for Sets 1-7 are presented to explain track of thought during the research.

**Set 8:**

- Strength: 63 MPa
- $\sigma$ - $\varepsilon$ : Popovics, ascending:  $n=9$ , descending:  $n=9$
- Reduction factors:  $k_{c,\theta}$  for cylinders (Table 9.11)
- Thermal properties: LCCC (Table 9.5, Table 9.6, Table 9.7)
- Average FRT change: -32.6 min (1.9 %)

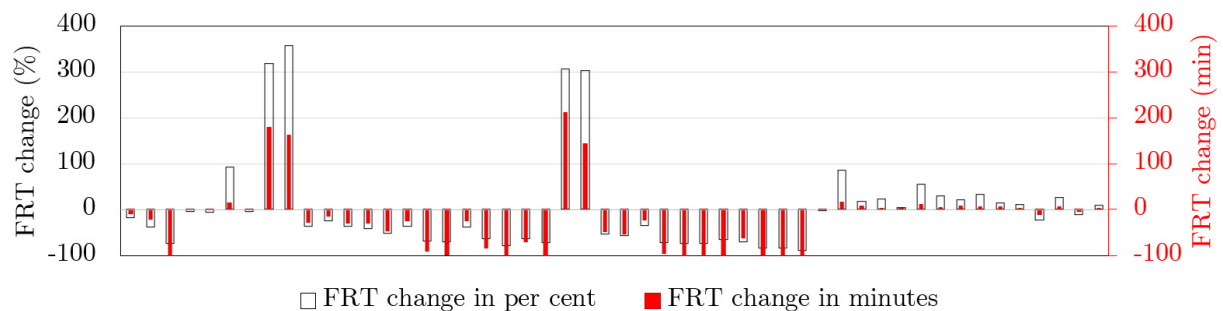


Fig. 9.48 Results for Set 8 (vertical scale consistent with graphs for sets 6-9).

As seen in Fig. 9.48, the model showed an improvement of FRT only for a handful of columns.

More sets were explored, including a Popovics model with  $n=9$  and  $n=5$  for the ascending and descending branches. What was found, was a significant influence of the descending branch. Therefore, other values were explored numerically, to see what the intended performance of the material should be to satisfy the need of increasing the fire resistance of CFST columns. In the end, it is found that, a modified LCCC, with a more ductile response ( $n=4$  in the descending branch), could satisfy the needs of an increased fire resistance of CFST columns. The results are presented in Fig. 9.49.

**Set 9:**

- Strength: 63 MPa
- $\sigma$ - $\varepsilon$ : Popovics, ascending:  $n=9$ , descending:  $n=4$
- Reduction factors:  $k_{c,\theta}$  for cylinders (Table 9.11)
- Thermal properties: LCCC (Table 9.5, Table 9.6, Table 9.7)
- Average FRT change: 181.7 min (107 %)

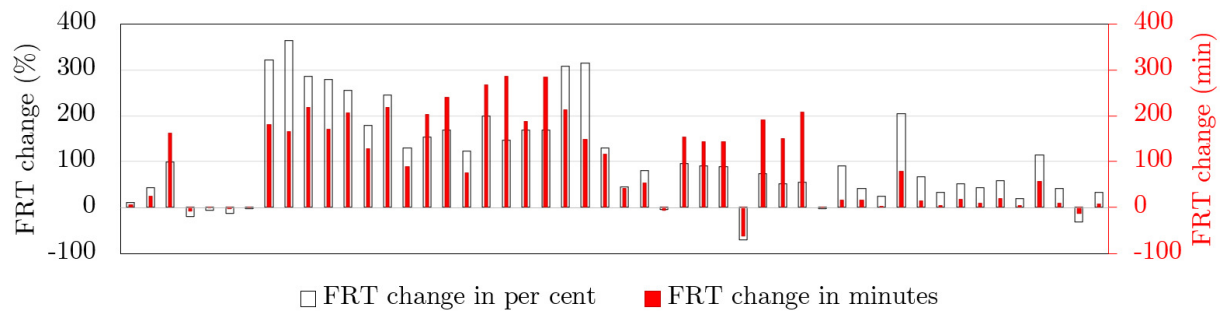


Fig. 9.49 Results for Set 9 (vertical scale consistent with graphs for sets 6-9).

Moreover, increases similar to those presented in Fig. 9.49 could be reached, if thermal expansion was lower than the one assumed here. The low thermal expansion of LCCC might be anywhere between values reported for concrete and cement paste, compare Fig. 4.5 and Fig. 9.4.

With an effort put into a design of a more ductile concrete, the LCCC might be a way to improve the fire resistance of composite columns significantly. Furthermore, even though stress-strain of the hot unstressed specimens and residual stress-strain curves are similar, the transient strain developing in hot stressed specimens will account for a more ductile response. Such investigations require a good justification, and, hopefully, the last part of chapter 9 offered exactly that: a good justification. The link between the results presented in Fig. 9.48, and in Fig. 9.49 is discussed as an area of future improvement in the next section.

## 9.5. Conclusions and future work

The results presented in this chapter show that the fire resistance of Concrete-Filled Steel Tubular columns can be improved by tailored core composites.

The developed composite offers outstanding mechanical performance, including high compressive strength and favourable reduction factors after exposure to elevated temperature.

There is an area of improvement, which can be gained by, e.g. sacrificing the initial strength in favour of a more ductile response. Even ordinary high strength concrete shows an abrupt failure. Yet, steel tubular columns filled with high strength concrete show a similar performance (in terms of fire resistance time) as those filled with normal strength concrete. This was confirmed by [Espinosa et al. \(2014\)](#) for several columns tested under the same load utilisation levels.

In the future, more comprehensive research on the mechanical performance of LCCC is planned to uncover the effect of elevated temperatures on the stress-strain response after and preferably during exposure. Unfortunately, most of the specimens show an abrupt failure, and it was not possible to obtain a smooth post-peak response. One of the primary goals related to mix design will be to obtain a more ductile response (Fig. 9.50). One of the possible areas worth exploring is the steel fibre reinforced concrete, which improved the performance of columns investigated by [Kodur & Lie \(1995\)](#), as discussed in chapters on infill (6.2.4) and steel fibre reinforced concrete – (6.2.6). Furthermore, the propensity to spalling shall be assessed.

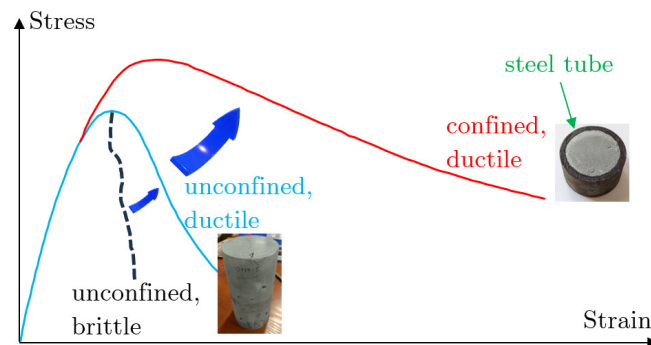


*Fig. 9.50 The desired ductility increase – from brittle to ductile behaviour. Due to lack of external confinement in fire, the increase should rely on the core composite properties, not on the external steel tube.*

Of course, ultimately, full-scale testing will answer the question of the LCCC feasibility. However, small-scale tests prove to be good enough to formulate initial hypotheses. From then, further experimental, or numerical analyses can identify factors that could be worked upon.

The presented experimental and numerical results complement each other. On the one hand, the numerical model allowed determining the properties in demand regarding the filling material. On the other hand, experimental research supplied numerical models with the necessary data for the feasibility study of LCCC-filled steel tubular columns.

Therefore, it is confirmed here that even at a smaller scale, the placement of well-thought-out instrumentation generates valuable data that eventually leads to a meaningful understanding.

## **10. Summary**

This chapter presents the general and specific conclusions that can be derived from the presented work. They are also complemented by recommendations for the future tests, as some gaps that could be filled were identified.

### **10.1. General**

Various aspects of the structural fire behaviour of circular CFST columns were investigated in this dissertation. A historical background and its connections to the current state-of-the-art were presented. The available experimental data were analysed and described, and a detailed analysis allowed to identify areas worth improving in the future.

A fully parametrised, non-linear, three-dimensional finite element model was formulated. The parametrisation allowed to study 50 columns with unique properties (length ranging from 3 to 4 meters, varying material properties, loads, etc.). The numerical model captured the behaviour of CFST columns during standard fire exposure. The fire resistance time obtained in the test and the model predictions were in good agreement.

Then, the validated numerical model was used to perform studies on the burnout resistance of CFST columns. In this dissertation, the burnout resistance was assessed with a reasonable fire scenario (unlike in existing research, where a linear decay phase is usually assumed).

The last part of this dissertation explored the possibilities of improving the structural fire performance of CFST columns by filling them with a material less prone to the adverse effects of high temperature. To that end, a literature study was provided, and several stages of experimental research were conducted. In the end, the test results on the material, supported by a numerical modelling of LCCC-filled steel tubular columns, showed that reaching higher fire resistance is feasible.

### **10.2. Specific conclusions and recommendations**

Several factors influencing the FRT were identified in Chapter 6. During the analysis of CFST columns' fire performance, certain factors were discovered to have little impact and could be ignored in the subsequent numerical investigation. Other factors, such as boundary conditions or load levels, can affect fire resistance time significantly.

Eurocode's material properties, with the upper limit of thermal conductivity, specific heat peak at 115 % corresponding to 3 % moisture content, and a thermal gap conductance of 100 W/(m<sup>2</sup>·K), allowed to achieve a mean ratio of the calculated to measured fire resistance time of 0.99, with a standard deviation of 0.18 (chapter 7.2).

For the numerical model to converge, it was recommended to use the friction coefficient of 0.3 (instead of a frictionless approach) and to increase the number of equilibrium iterations, as the default values provided by the software were found to be inefficient for several columns.

Three types of column behaviour were identified. The preferable, type A, utilises the concrete core load-bearing capacity in the last stage of the column's behaviour.

The effect of partial axial and rotational restraints was analysed. While the effect of partial rotational restraints is straightforward, the axial restraint might have a positive or an adverse effect on the column's fire performance.

A parametric study identified the influence of several model assumptions. Some of them are controllable, and the results might be used to enhance the column's performance. To some extent, partial protection near the ends could improve columns' performance.

It is essential to consider the experimental results from various laboratories while validating a model. If not taken into account, the model may be calibrated based on biased data, which could be fundamentally incorrect. An extensive inter-laboratory database can help identify any biases in the results and improve the model's accuracy. It shall be stressed that one of the biggest problems lies in the boundary conditions. Most existing experimental studies use the same boundary conditions at the supports for all studied columns.

It seems that introducing plate thermometers successfully harmonised fire thermal exposure resistance in fire resistance furnaces. However, plate thermometers are still not being used in some modern furnaces at the research centres. For researchers doing the modelling, actual fire exposure conditions would be of great benefit. As presented in Chapter 8, analyses considering non-uniform exposure are possible. Still, data for individual plate thermometers shall be made available instead of reducing their output to an average furnace temperature.

We cannot expect the ideal conditions in any furnace. After all, the conditions in a real fire are far from uniform, controllable, and even predictable. Nevertheless, the knowledge generated from fire resistance tests is of great value. Any drawbacks should motivate more systematic numerical investigations that could study multiple factors more comprehensively than full-scale testing allows.

Recommendations for future experimental research based on missing or ambiguous data in currently available test reports are as follows:

- (1) detailed concrete mix quantities and properties should be given;
- (2) proper execution of boundary conditions is essential. Details regarding construction of fixed or pinned supports should be given;
- (3) details regarding the measurement of concrete compressive strength should be given (specimen size, shape, number of specimens);
- (4) if possible, coupon tests of steel should be conducted;
- (5) moisture content should be measured by drying specimens at 105 °C, and the conditioning details should be reported;
- (6) the load exerted by the testing rig should be reported, as in the late stage of the fire resistance test, the rig might not follow the specimen;
- (7) the examination of a column after the test should include the determination of the exact thermocouple location.

The conclusions of the experimental study are:

- (1) The residual strength of all LCCC composites is higher compared to the standard mortar. The average residual compressive strength of LCCC after exposure to 400 °C, 600 °C, 800 °C, 1000 °C and 1200 °C is 88 %, 83 %, 67 %, 52 %, and 41 %, respectively. The respective values obtained for standard mortar are 84 %, 49 %, 22 %, 7 %, and 18 %. LCCC shows superior behaviour in temperatures between 600 °C and 1200 °C.
- (2) SEM analysis indicates that cenosphere accommodates thermal strains of cement paste, and most of the ITZ is found intact. The presence of FAC hinders heat-induced crack propagation. In the LCCC with PP fibres composites, cracks concentrate near the channels left by vapourised fibres. However, they do not diminish the composite mechanical performance.
- (3) The stress-strain relationship measured on cylindrical specimens showed a linear response. Obtaining the descending (post-peak) branch of the stress-strain curve proved to be challenging and it was highlighted as the area of future improvement.

### **10.3. Future work**

In this thesis, two filling types were investigated: normal strength concrete and lightweight cementitious composites with cenospheres. As pointed out in chapter 5.5, several other fillings exist. Furthermore, other materials are used for tubes, e.g. stainless steel or carbon fibre-reinforced polymer. For some of them, the implementation of the relevant constitutive models should be relatively straightforward. With the successfully developed numerical model, it will be possible to cover other materials, including high strength concrete, geopolymer concrete and stainless steel, which seem to be the most utilised, at least by researchers doing the full-scale fire resistance tests.

The advent of new tests has always been driven by change. For instance, the extensive fire resistance program for RC in NRC Canada in the 1980s was motivated by a change in calculation methods. The new methods of design at ambient conditions raised questions regarding the reliability of the then-existing fire design methods, which were largely prescriptive.

Another critical driving force is the emergence of new materials, a trend that has gained momentum recently due to the need to achieve sustainability goals. The use of new materials often poses challenges when employing existing calculation methods. As such, the development of new materials, new material constitutive models, and the assessment of structures and fire conditions will be of great importance.

In terms of the numerical model, a more refined model, taking into account the transient thermal strain, could be developed. Thus far, no material tests were performed on concrete that would be, just as in the case of CFST columns, unloaded during the first 20-30 minutes and then loaded while being heated. Furthermore, with regard to post-fire studies, a study focusing on the local buckling of steel tubes, and the restraints induced by the surrounding structure (see chapter 7.5) would be beneficial.

The development of LCCC proved to be successful. A lightweight composite was developed and tested. LCCC will not solve all the problems of fire resistance and will not substitute concrete. But, by studying the material properties and material performance in full-scale structures, we might be able to generate valuable data that eventually will lead to a meaningful understanding.

In the future, more comprehensive research on the mechanical performance of LCCC is planned to uncover the effect of elevated temperatures on stress-strain response after and preferably during high-temperature exposure. One of the primary goals related to mix design will be to obtain a more ductile response. Furthermore, the propensity to spalling shall be assessed.

With that being said, let us now reconnect with Sir William Fairbairn, whose scientific curiosity made him the first to conduct experiments on the strength of iron at elevated temperatures (mentioned in chapter 2.1):

*"an engineer is, according to the strict derivation of the term, not necessarily a person who has to do with engines, but anyone who seeks in his mind, who sets his mental powers in action, in order to discover or devise some means of succeeding in a difficult task he may have to perform".*

Fairbairn & Pole (1877)

## **Bibliography**

- Ablaoui, E.M., Malendowski, M., Szymkuc, W., Pozorski, Z. (2023) Determination of Thermal Properties of Mineral Wool Required for the Safety Analysis of Sandwich Panels Subjected to Fire Loads. *Materials* 16(17), 5852. <https://doi.org/10.3390/ma16175852>
- Abramowicz, M., Kowalski, R. (2005) The influence of short time water cooling on the mechanical properties of concrete heated up to high temperature. *Journal of Civil Engineering and Management* 11(2), pp. 85-90. <https://doi.org/10.1080/13923730.2005.9636336>
- Abrams, M.S. (1971) Compressive Strength of Concrete at Temperatures to 1600 F. ACI Symposium Publication 25, pp. 33-58. <https://doi.org/10.14359/17331>
- Abramski, M. (2018) Load-carrying capacity of axially loaded concrete-filled steel tubular columns made of thin tubes. *Archives of Civil and Mechanical Engineering* 18(3), pp. 902-913. <https://doi.org/10.1016/j.acme.2018.01.002>
- Achenbach, M. (2018) Weiterentwicklung der Zonenmethode für den Nachweis der Feuerwiderstandsdauer von rechteckigen Stahlbetondruckgliedern. PhD Thesis. Bauhaus-Universität Weimar. Germany.
- ACI 216.1 (2014) Code Requirements for Determining Fire Resistance of Concrete and Masonry Construction Assemblies. ACI, USA.
- Addis, B. (2007) Engineering design in the time of Thomas Telford. *Proceedings of the Institution of Civil Engineers* 160(4), pp. 176-183. <https://doi.org/10.1680/cien.2007.160.4.176>
- Alarcon-Ruiz, A., Platret, G., Massieu, E., Ehrlicher, A. (2005) The use of thermal analysis in assessing the effect of temperature on a cement paste. *Cement and Concrete Research* 35(3), pp. 609-613. <https://doi.org/10.1016/j.cemconres.2004.06.015>
- Albero, V., Espinós, A., Romero, M.L., Wang, Y.C., Renaud, C., Schaumann, P., Nigro, E. (2018) Interaction diagram based method for fire resistance design of eccentrically loaded concrete-filled steel tubular columns, *Thin-Walled Structures* 130, pp. 641-651. <https://doi.org/10.1016/j.tws.2018.06.017>
- Ali, F., Nadjai, A., Goodfellow, N. (2016) Experimental and numerical study on the performance of hollow and concrete-filled elliptical steel columns subjected to severe fire. *Fire and Materials* 40, pp. 635-652. <https://doi.org/10.1002/fam.2316>
- Anderberg Y., Forsen, N.E., Hietanen, T., Izquierdo, J.M., Le Duff, A., Richter, E., Whittle, R.T., Bossenmayer, H., Litzner, H-U., Kruppa, J. (2004) Background documents to EN 1992-1-2 Eurocode 2: Design of concrete structures – Part 1-2: General rules – Structural fire design. 239 pages.
- Anderberg Y., Magnusson S. E., Pettersson O., Thelandersson S., Wickström U. (1978) An analytical approach to fire engineering design of concrete structures. ACI Special Publication SP 55-16, pp. 409-438
- Anderberg, Y. (1988) Modelling steel behaviour. *Fire Safety Journal* 13, pp. 17-26. [https://doi.org/10.1016/0379-7112\(88\)90029-X](https://doi.org/10.1016/0379-7112(88)90029-X)
- Anderberg, Y. Thelandersson, S. (1976) Stress and Deformation Characteristics of Concrete at High Temperatures. 2. Experimental Investigation and Material Behaviour Model. Lund Institute of Technology, Lund, Sweden.
- Andres, B., Livkiss, K., Bhargava, A. van Hees, P. (2021) Using Micro-Scale and Solid Material Data for Modelling Heat Transfer in Stone Wool Composites Under Heat Exposures. *Fire Technology* 57, pp 1541-1567. <https://doi.org/10.1007/s10694-021-01122-0>
- Andrews, R.D., Jacques, H., Rantoul, A.N. (1891) Tests of fireproof arches. *The American Architect and Building News* 31(796), March 28, 1891, pp. 195-201.
- Annerel, E., Taerwe, L. (2009) Revealing the temperature history in concrete after fire exposure by microscopic analysis. *Cement and Concrete Research* 39(12), pp. 1239-1249. <https://doi.org/10.1016/j.cemconres.2009.08.017>
- Aribert, J-M., Renaud, C., Zhao, B. (2008) Simplified fire design for composite hollow-section columns. *Proceedings of the Institution of Civil Engineers. Structures & Buildings* 161 Issue SB6, pp. 325-336. <https://doi.org/10.1680/stbu.2008.161.6.325>

- Arioz, O. (2007) Effects of elevated temperatures on properties of concrete. *Fire Safety Journal* 42(8), pp. 516-522. <https://doi.org/10.1016/j.firesaf.2007.01.003>
- Arioz, O. (2009) Retained properties of concrete exposed to high temperatures: Size effect. *Fire and Materials* 33(5), pp. 211-222. <https://doi.org/10.1002/fam.996>
- Arizmendi-Morquecho, A., Chávez-Valdez, A., Alvarez-Quintana, J., (2012) High temperature thermal barrier coatings from recycled fly ash cenospheres, *Applied Thermal Engineering* 48, pp. 117-121. <https://doi.org/10.1016/j.applthermaleng.2012.05.004>
- Ashkezari, G.D., Razmara, M. (2020) Thermal and mechanical evaluation of ultra-high performance fiber-reinforced concrete and conventional concrete subjected to high temperatures. *Journal of Building Engineering* (2020) <https://doi.org/10.1016/j.jobbe.2020.101621>
- Askeland, D.R., Wright, W.J. (2016) *The Science and Engineering of Materials*. 7th Edition. Cengage Learning.
- Associated Architects, Resolutions of the Associated Architects with the Report of a Committee by Them Appointed to Consider the Causes of the Frequent Fires and the Best Means of Preventing the like in the Future, 1793
- ASTM (1918) Standard specifications for fire tests of materials and construction
- Atreya, A., (2016) Convection Heat Transfer. In: *SFPE Handbook of Fire Protection Engineering*, pp. 53-101. Edited by: Hurley, M.J. Springer. 5th Edition.
- Azad, S.K. Uy, B. (2020) Effect of concrete infill on local buckling capacity of circular tubes. *Journal of Constructional Steel Research* 165, 105899. <https://doi.org/10.1016/j.jcsr.2019.105899>
- Babrauskas, V. (2009) Unexposed-face temperature criteria in fire resistance tests: A reappraisal. *Fire Safety Journal* 44(6), pp. 813-818. <https://doi.org/10.1016/j.firesaf.2009.03.003>
- Babrauskas, V., Williamson, R.B. (1978a) The historical basis of fire resistance testing — Part I. *Fire Technology* 14, pp. 184-194. <https://doi.org/10.1007/BF01983053>
- Babrauskas, V., Williamson, R.B. (1978b) The historical basis of fire resistance testing — Part II. *Fire Technology* 14, pp. 304-316. <https://doi.org/10.1007/BF01998390>
- Bahr, O., Schaumann, P., Bollen, B., Bracke, J. (2013) Young's modulus and Poisson's ratio of concrete at high temperatures: Experimental investigations. *Materials and Design* 45, pp. 421-429. <https://doi.org/10.1016/j.matdes.2012.07.070>
- Bamonte, P., Gambarova, P.G. (2010) Thermal and mechanical properties at high temperature of a very high-strength durable concrete. *Journal of Materials in Civil Engineering* 22 (6). <https://ascelibrary.org/doi/abs/10.1061/%28ASCE%29MT.1943-5533.0000058>
- Bamonte, P., Gambarova, P.G. (2012) A study on the mechanical properties of self-compacting concrete at high temperature and after cooling. *Materials and Structures* 45, 1375-1387. <https://doi.org/10.1617/s11527-012-9839-9>
- Bamonte, P., Lo Monte, F. (2015) Reinforced concrete columns exposed to standard fire: Comparison among different constitutive models for concrete at high temperature. *Fire Safety Journal* 71, pp. 310-323. <https://doi.org/10.1016/j.firesaf.2014.11.014>
- Bednarek, Z., Krzywobłocka-Laurów, R., Drzymała, T. (2009) Wpływ wysokiej temperatury na strukturę, skład fazowy i wytrzymałość betonu. *Zeszyty Naukowe SGSP* 38, pp. 5-27.
- Bergman, T.L., Lavine, A.S. (2017) *Fundamentals of Heat and Mass Transfer*. Wiley. 8th Edition.
- Bergmann, M.: *Zur Bemessung von Hohlprofilverbundstützen im Brandfall*, Institut für Konstruktiven Ingenieurbau, Bergische Universität Wuppertal, PhD Dissertation, 2013.
- Bhadeshia, H., Honeycombe, R. (2017) *Steels: Microstructure and Properties*. 4th Edition. Elsevier.
- Biederman Jr., E.W. (1970) Lightweight cements for oil wells. US Patent Office, Patent No. 3669701. <https://patents.google.com/patent/US3669701A/en>
- Both, C. Twilt, L. (1990) Report No. BI-89-208. TNO Building and Construction Research, The Netherlands.
- Bradło, D. (2016) *Uszlachetnione mikrosfery glinokrzemianowe jako napelniacz kompozytów polimerowych*. PhD thesis (in Polish). Cracow University of Technology.
- Braidwood, J. (1866) *Fire Prevention and Fire Extinction*. Bell and Daldy, London. 197 pages.

- Brooks, A. L., Zhou, H., Hanna, D. (2018) Comparative study of the mechanical and thermal properties of lightweight cementitious composites. *Construction and Building Materials* 159, pp. 316-328. <https://doi.org/10.1016/j.conbuildmat.2017.10.102>
- BS 476-1 (1953) Fire tests on building materials and structures. BSI, UK.
- Buchanan, A.H., Abu, A.K. (2017) *Structural Design for Fire Safety*. 2nd Edition. Wiley, UK.
- Byström, A. (2017) *Compartment Fire Temperature: Calculations and Measurements*. PhD thesis. Luleå University of Technology. 219 pages.
- Byström, A., Sjöström, J., Wickström, U., Lange, D., Veljkovic, M. (2015) Large Scale Test on a Steel Column Exposed to Localized Fire. *Journal of Structural Fire Engineering* 5(2), pp. 147-160. <https://doi.org/10.1260/2040-2317.5.2.147>
- Byström, A., Wickström, U., Veljkovic, M. (2011) Use of plate thermometers for better estimate of fire development. *Applied Mechanics and Materials* 82, pp 362-367. <https://doi.org/10.4028/www.scientific.net/AMM.82.362>
- Cao, M., Ming, X., Yin, H., Li, L. (2019) Influence of high temperature on strength, ultrasonic velocity and mass loss of calcium carbonate whisker reinforced cement paste. *Composites Part B: Engineering* 163, pp. 438-446. <https://doi.org/10.1016/j.compositesb.2019.01.030>
- Cao, W.X. (1998) *Analysis of fire behaviour of steel frames considering the damage accumulation*. PhD thesis, Tongji University, Shanghai, China (in Chinese).
- Casaroli, A., Boniardi, M., Gerosa, R., Rivolta, B. (2022) How to Use Metallurgical Analysis for Fire Investigation: The Case of AISI 316 Stainless Steel. *Fire Technology* 58, pp. 2641-2660. <https://doi.org/10.1007/s10694-022-01230-5>
- Castellote, M., Alonso, C., Andrade, C., Turrillas, X., Campo, J. (2004) Composition and microstructural changes of cement pastes upon heating, as studied by neutron diffraction. *Cement and Concrete Research* 34(9), pp. 1633-1644. [https://doi.org/10.1016/S0008-8846\(03\)00229-1](https://doi.org/10.1016/S0008-8846(03)00229-1)
- Castillo, C., Durrani, A.J. (1990) Effect of transient high temperature on high-strength concrete. *ACI Materials Journal* 87(1), pp. 47-53. <https://doi.org/10.14359/2356>
- CEN (2001) Background document on Parametric temperature—time curves according to Annex A of prEN1991-1-2 (24-08-2001). CEN/TC250/SC1/N298A. Document EC1-1-2/72.
- CEN (2019) Background document for section 5 - material properties (2<sup>nd</sup> draft – April 2019). CEN TC250/SC2/WG1/SC2.T2
- Chabot, M., Lie, T.T., (1992) *Experimental studies on the fire resistance of hollow steel columns filled with bar-reinforced concrete*. National Research Council of Canada. Internal Report No. 628. <https://doi.org/10.4224/20358523>
- Chan, S.Y.N., Peng, G-f., Chan, J.K.W. (1996) Comparison between high strength concrete and normal strength concrete subjected to high temperature. *Materials and Structures* 29, 616-619. <https://doi.org/10.1007/BF02485969>
- Chang, Y.F., Chen, Y.H., Sheu, M.S., Yao, G.C. (2005) Residual stress–strain relationship for concrete after exposure to high temperatures. *Cement and Concrete Research* 36(10), pp. 1999-2005. <https://doi.org/10.1016/j.cemconres.2006.05.029>
- Chávez-Valdez, A., Arizmendi-Morquecho, A., Vargas, G., Almanza, J. M., Alvarez-Quintana, J. (2011) Ultra-low thermal conductivity thermal barrier coatings from recycled fly-ash cenospheres. *Acta Materialia* 59(6), pp. 2556-2562. <https://doi.org/10.1016/j.actamat.2011.01.011>
- Chen, M., Sun, Z., Tu, W., Yan, X., Zhang, M. (2021) Behaviour of recycled tyre polymer fibre reinforced concrete at elevated temperatures. *Cement and Concrete Composites* 124, 104257. <https://doi.org/10.1016/j.cemconcomp.2021.104257>
- Chen, W., Zhou, Z., Zou, H., Guo, Z. (2018) Predictions of residual carrying-capacities for fire and near-field blast-damaged reactive powder concrete-filled steel tube columns. *International Journal of Protective Structures* 9(4), pp. 525-553. <https://doi.org/10.1177/2041419618784738>
- Chia, K.S., Zhang, M.H., Liew, J.Y.R. (2011) High-strength ultra lightweight cement composite — material properties. *Proceedings of the 9th International Symposium on High Performance Concrete design, Verification and Utilization*, pp. 1-8. 9-11 Aug 2011, Rotorua, New Zealand.
- Childs, P.R.N. (2013) *Temperature measurement*. In: *Handbook of Measurement in Science and Engineering*, Kutz, M. (Ed). Wiley.

- Cooper L.Y., Steckler, K.D. (1996) Methodology for Developing and Implementing Alternative Temperature-Time Curves for Testing the Fire Resistance of Barriers for Nuclear Power Plant Applications. NISTIR 5842. National Institute of Technology. Gaithersburg, U.S.
- Crook, R.N. (1980) The elevated temperature properties of reinforced concrete. PhD thesis, University of Aston, Birmingham, UK. <https://research.aston.ac.uk/en/studentTheses/the-elevated-temperature-properties-of-reinforced-concrete>
- Cruz, C.R., Gillen, M. (1980) Thermal Expansion of Portland Cement Paste, Mortar and Concrete at High Temperatures. *Fire and Materials* 4(2), pp. 66-70. <https://doi.org/10.1002/fam.810040203>
- Czarniawski, T. (2016) Nośność konstrukcji zespolonych powłokowych na przykładzie elementów rurobetonowych CFST. *Budownictwo* 22. <https://doi.org/10.17512/znb.2016.1.03>
- Dai, P., Yang, L., Wang, J., Zhou, Y. (2020) Compressive strength of concrete-filled stainless steel tube stub columns. *Engineering Structures* 205:110106. <https://doi.org/10.1016/j.engstruct.2019.110106>
- Danish, A., Mosaberpanah, M.A. (2021) Influence of cenospheres and fly ash on the mechanical and durability properties of high-performance cement mortar under different curing regimes. *Construction and Building Materials* 279, 122458. <https://doi.org/10.1016/j.conbuildmat.2021.122458>
- Danish, A., Mosaberpanah, M.A., Tuladhar, R., Salim, M.U., Yaqub, M.A., Ahmad, N. (2022) Effect of cenospheres on the engineering properties of lightweight cementitious composites: A comprehensive review. *Journal of Building Engineering* 49, 104016. <https://doi.org/10.1016/j.jobbe.2022.104016>
- Davie, C.T., Pearce, C.J., Kukla, K., Bicanic, N. (2018) Modelling of transport process in concrete exposed to elevated temperatures - An alternative formulation for sorption isotherms, *Cement and Concrete Research* 106, pp. 144-154. <https://doi.org/10.1016/j.cemconres.2018.01.012>
- Debnath, P.P., Xu, F., Chan, T-M. (2023) Load transfer mechanism in concrete-filled steel tubular columns: Developments, challenges and opportunities. *Journal of Constructional Steel Research* 203, 107781. <https://doi.org/10.1016/j.jcsr.2023.107781>
- Deutsche Bauzeitung (1891) Mitteilungen aus Vereinen. *Deutsche Bauzeitung* 83 (17.10.1891), pp. 507-508.
- Dias, W.P.S., Khoury, G.A., Sullivan, P.J.E. (1990) Mechanical Properties of Hardened Cement Paste Exposed to Temperatures up to 700 C (1292 F). *ACI Materials Journal* 87(2), pp. 160-166. <https://doi.org/10.14359/1981>
- Dimia, M.S., Sekkiou, S., Baghdadi, M., Guenfoud, M. (2017) Structural behaviour of concrete filled hollow steel sections exposed to parametric fire. *Challenge Journal of Structural Mechanics* 3(4), pp. 160-165. <https://doi.org/10.20528/cjsmec.2017.02.004>
- DIN 4102 (1965) Brandverhalten von Baustoffen und Bauteilen. DIN. Germany.
- DIN 4102-4 (1994) Brandverhalten von Baustoffen und Bauteilen. Zusammenstellung und Anwendung klassifizierter Baustoffe, Bauteile und Sonderbauteile. DIN. Germany.
- Ding, F., Zhang, C., Yu, Y., Lan, L., Man, M. (2019) Hysteretic behavior of post fire structural steels under cyclic loading. *Journal of Constructional Steel Research* 105847. <https://doi.org/10.1016/j.jcsr.2019.105847>
- Ding, J., Wang, Y.C. (2008) Realistic modelling of thermal and structural behaviour of unprotected concrete filled tubular columns in fire *Journal of Constructional Steel Research* 64, pp. 1086-1102. <https://doi.org/10.1016/j.jcsr.2007.09.014>
- Dumont, F., Boström, L., Łukowski, M., van den Berg, G. (2015) Summary report of the EGOLF Round-Robin nr. TC2 14-1 in fire resistance testing. EGOLF (European Group of Organisations for Fire Testing, Inspection and Certification). <https://orbi.uliege.be/handle/2268/181017>
- ECCS (1988) Calculation of the fire resistance of centrally loaded composite steel-concrete columns exposed to the standard fire, Technical Note, ECCS Technical Committee 3, 55, Brussels, Belgium.
- Eekhout, M. (2011) Tubular Structures in Architecture. Cidect & TU Delft. 225 pages.

- Eggemann, H. (2003) Vereinfachte Bemessung von Verbundstützen im Hochbau. Entwicklung, historische Bemessung und Herleitung eines Näherungsverfahrens. RWTH Aachen. PhD thesis. 123 pages.
- Ehm, C. (1986) Versuch zur Festigkeit und Verformung von Beton unter zweiachsialer Beanspruchung und hohen Temperaturen. PhD thesis. Technische Universität Braunschweig. 133 pages.  
<https://doi.org/10.24355/dbbs.084-201409031506-0>
- Elsanadedy, H.M. (2019) Residual Compressive Strength of High-Strength Concrete Exposed to Elevated Temperatures. *Advances in Materials Science and Engineering* 2019, 6039571.  
<https://doi.org/10.1155/2019/6039571>
- EN 10052:1993 Vocabulary of heat treatment terms for ferrous products
- EN 12390-13:2021 Testing hardened concrete - Part 13: Determination of secant modulus of elasticity in compression
- EN 12390-7:2009 Testing hardened concrete - Part 7: Density of hardened concrete
- EN 13381-6:2012 Test methods for determining the contribution to the fire resistance of structural members - Part 6: Applied protection to concrete filled hollow steel columns
- EN 13501-2:2016 Fire classification of construction products and building elements - Part 2: Classification using data from fire resistance and/or smoke control tests, excluding ventilation services
- EN 1363-1:1999 Fire Resistance Tests - Part 1: General Requirements
- EN 1363-1:2012 Fire Resistance Tests - Part 1: General Requirements
- EN 1363-2:1999 Fire Resistance Tests - Part 2: Alternative and additional procedures
- EN 1365-1:2012 Fire resistance tests for loadbearing elements - Part 1: Walls
- EN 1365-4:1999 Fire resistance tests for loadbearing elements - Part 4: Columns
- EN 196-1:2016 Methods of testing cement - Part 1: Determination of strength
- EN 1991-1-2:2002 Eurocode 1: Actions on structures - Part 1-2
- EN 1992-1-1:2004 Eurocode 2: Design of concrete structures - Part 1-1: General rules and rules for buildings
- EN 1992-1-2:2004 Eurocode 2: Design of concrete structures - Part 1-2: General rules - Structural fire design
- EN 1994-1-2:2005+A1:2014 Eurocode 4 - Design of composite steel and concrete structures - Part 1-2: General rules - Structural fire design
- EN 60584-1:2013 Thermocouples - Part 1: EMF specifications and tolerances
- ENV 1992-1-2:1996 Eurocode 2: Design of concrete structures - Part 1-2: General rules - Structural fire design
- Erdem, T.K. (2014) Specimen size effect on the residual properties of engineered cementitious composites subjected to high temperatures. *Cement and Concrete Composites* 45, pp. 1-8.  
<https://doi.org/10.1016/j.cemconcomp.2013.09.019>
- Espinos, A. (2012) Numerical analysis of the fire resistance of circular and elliptical slender concrete filled tubular columns. PhD thesis. Universitat Politècnica de València. 402 pages
- Espinos, A., Romero, M.L., Hospitaler, A. (2010) Advanced model for predicting the fire response of concrete filled tubular columns. *Journal of Constructional Steel Research* 66(8-9), pp. 1030-1046.  
<https://doi.org/10.1016/j.jcsr.2010.03.002>
- Espinos, A., Romero, M.L., Hospitaler, A. (2012) Simple calculation model for evaluating the fire resistance of unreinforced concrete filled tubular columns. *Engineering Structures* 42, pp. 231-244.  
<http://doi.org/10.1016/j.engstruct.2012.04.022>
- Espinos, A., Romero, M.L., Hospitaler, A. (2014) Experimental investigation on the fire behaviour of axially loaded slender concrete filled tubular columns. Research report from the experimental investigation was carried out in the framework of the research project BIA2009\_09411, funded by the Spanish Ministry of Science and Innovation.
- Espinos, A., Romero, M.L., Hospitaler, A., Pascual, A.M., Albero, V. (2015) Advanced materials for concrete-filled tubular columns and connections, *Structures* 4, pp. 105-113.  
<https://doi.org/10.1016/j.istruc.2015.08.006>

- FABIG (2014) Design Guidance for Hydrocarbon Fires (FABIG Technical Note 13). Steel Construction Institute (SCI)
- Fairbairn, W. (1837) On the strength and other properties of iron obtained from the hot and cold blast. In: Report of the seventh meeting of The British Association for the Advancement of Science. Volume 6. Printed by John Murray, London.
- Fairbairn, W., Pole, W. (1877) The life of Sir William Fairbairn, Bart. Longmans, Green, and Co. London. 507 pages.
- Fang, H., Wong, M.B., Bai, Y. (2017) Heating rate effect on the thermophysical properties of steel in fire. *Journal of Constructional Steel Research* 128, pp. 611-617.  
<http://doi.org/10.1016/j.jcsr.2016.09.016>
- Fares, H. Remond, S., Noumowe, A., Cousture, A. (2010) High temperature behaviour of self-consolidating concrete. Microstructure and physicochemical properties. *Cement and Concrete Research* 40(3), pp. 488-496. <https://doi.org/10.1016/j.cemconres.2009.10.006>
- Farzarian, S., Louhghalam, A., Schafer, B.W., Tootkaboni, M. (2023) Geometric imperfections in CFS structural members: Part I: A review of the basics and some modeling strategies. *Thin-Walled Structures* 186, 110619. <https://doi.org/10.1016/j.tws.2023.110619>
- Felicetti, R., Gambarova, P. G., & Bamonte, P. (2012). Thermal and mechanical properties of light-weight concrete exposed to high temperature. *Fire and Materials*, 37(3), 200–216.  
<https://doi.org/10.1002/fam.2125>
- fib (2013) fib Model Code for Concrete Structures 2010. fédération internationale du béton / International Federation for Structural Concrete (fib). Wilhelm Ernst & Sohn, Berlin, Germany.
- Figuli, L., Horváth, L.I., Kubíková, Z., Magdolenová, P., Malendowski, M., Mózer, V., Spremić, M., Szikra, C., Szymkuć, W., Takács, L., Wald, F. (2021) V4 guidelines on advanced structural fire safety design with Eurocodes. Czech Technical University in Prague, 116 pages.  
<https://sin.put.poznan.pl/publications/details/i41158>
- Fike, R.S., Kodur, V.K.R. (2009) An Approach for Evaluating the Fire Resistance of CFHSS Columns under Design Fire Scenarios. *Journal of Fire Protection Engineering* 19, pp. 239-259.  
<https://doi.org/10.1177/1042391509105597>
- Flaga, K., Furtak, K. (2015) Examples of Solutions for Steel-Concrete Composite Structures in Bridge Engineering. *Civil and Environmental Engineering Reports* 16(1), pp. 51-68.  
<https://doi.org/10.1515/ceer-2015-0004>
- Franssen, J-M. (2000) Design of concrete columns based on EC2 tabulated data - a critical review. First International Workshop "Structures in Fire", pp. 323-340, Copenhagen, Denmark
- Franssen, J-M. (2006) Calculation of temperature in fire-exposed bare steel structures: Comparison between ENV 1993-1-2 and EN 1993-1-2. *Fire Safety Journal* 41(2), pp. 139-143.  
<https://doi.org/10.1016/j.firesaf.2005.11.007>
- Franssen, J-M., Schleich, J-B., Cajot, L-G., Azpiazu, W. (1996) A Simple Model for the Fire Resistance of Axially Loaded Members - Comparison with Experimental Results. *Journal of Constructional Steel Research* 37(3), pp. 175-204. [https://doi.org/10.1016/0143-974X\(96\)00008-9](https://doi.org/10.1016/0143-974X(96)00008-9)
- Freitag, J.K. (1899) The Fireproofing of Steel Buildings. John Wiley & Sons. New York, USA.
- Frycz Modrzewski, A. (1551) O poprawie Rzeczypospolitej (De Republica emendanda).
- Gale, W.F., Totemeier, T.C. (2004) *Smithells Metals Reference Book*. Eight Edition, Elsevier.
- Gales, J., Chorlton, B., Jeanneret, C. (2020) The Historical Narrative of the Standard Temperature–Time Heating Curve for Structures. *Fire Technology* 57, pp. 529-558.  
<https://doi.org/10.1007/s10694-020-01040-7>
- Gales, J., Chorlton, B., Jeanneret, C. (2021) Response to Vytenis Babrauskas "Comments on “The Historical Narrative of the Standard Temperature–Time Heating Curve for Structures” by Gales, et al. *Fire Technology*. <https://doi.org/10.1007/s10694-021-01165-3>
- Gambarova, P.G. (2005) Opening Address on Some Key Issues Concerning R/C Fire Design. Proceedings of the Workshop "Fire Design of Concrete Structures: What now? What next?" Eds.: Gambarova, P.G., Felicetti, R., Meda, A., Riva, P. Milan University of Technology, Milan, Italy, December 2-3, 2004. Printed by Starrylink.

- Gary, M. (1911) Brandproben an Eisenbetonbauten. Deutscher Ausschuss für Eisenbeton. Verlag von Wilhelm Ernst & Sohn. Berlin.
- Gaunt, I.M., Latham, D.J., Chapman, J.A. (1993) The evaluation of two fire tested concrete filled hollow circular sections. British Steel Technical Report No. SL/LP/R/S2348/1/93/D. Swinden Laboratories, Rotherham, UK.
- Gawin, D., Pesavento, F., Schrefler, B.A. (2011) What physical phenomena can be neglected when modelling concrete at high temperature? A comparative study. Part 1: Physical phenomena and mathematical model. *International Journal of Solids and Structures* 48, pp. 1927-1944. <https://doi.org/10.1016/j.ijsolstr.2011.03.004>
- Gebhardt, J.C. (1971) Lightweight, high strength concrete and method for manufacturing the same. US Patent Office, Patent No. 3782985. <https://patents.google.com/patent/US3782985A/en>
- Gernay, T. (2019) Fire resistance and burnout resistance of reinforced concrete columns. *Fire Safety Journal* 104, pp. 67-78. <https://doi.org/10.1016/j.firesaf.2019.01.007>
- Gernay, T., Franssen, J-M. (2015) A performance indicator for structures under natural fire. *Engineering Structures* 100, pp. 94-103. <http://doi.org/10.1016/j.engstruct.2015.06.005>
- Gernay, T., Franssen, J-M., Robert, F., McNamee, R., Felicetti, R., Bamonte, P., Brunkhorst, S., Mohaine, S., Zehfuß, J. (2022) Experimental investigation of structural failure during the cooling phase of a fire: Concrete columns. *Fire Safety Journal* 134, 103691. <https://doi.org/10.1016/j.firesaf.2022.103691>
- Ghannam, M. (2019) Proposed models for concrete thermal expansion with different aggregate types and saturation conditions. *SN Applied Sciences* 1, 425. <https://doi.org/10.1007/s42452-019-0452-1>
- Ghojel J. (2004) Experimental and analytical technique for estimating interface thermal conductance in composite structural elements under simulated fire conditions. *Experimental Thermal and Fluid Science* 28, pp. 347-354. [https://doi.org/10.1016/S0894-1777\(03\)00113-4](https://doi.org/10.1016/S0894-1777(03)00113-4)
- Głowacki, M., Kowalski, R. (2022) Simple consideration of second-order effects in the calculation of RC column fire resistance. *Fire Safety Journal* 133, 103650. <https://doi.org/10.1016/j.firesaf.2022.103650>
- Godycki-Ćwirko T., Korzeniowski P., Nagrodzka-Godycka K. (1999) O skuteczności uzwojenia w słupach żelbetowych. *Inżynieria i Budownictwo* nr 12/1999
- Goode, C.D., Lam, D. (2008) Concrete-Filled Steel Tube Columns-Tests Compared with Eurocode 4. *International Conference on Composite Construction in Steel and Concrete 2008*. [https://doi.org/10.1061/41142\(396\)26](https://doi.org/10.1061/41142(396)26)
- Grandjean, G., Grimault, J.P., Petit, L. (1980) Détermination de la durée au feu des profils creux remplis de béton. Final Report. 280 Pages.
- Grzeszykowski, B., Szadkowska, M., Szmigiera, E. (2017) Analysis of stress in steel and concrete in CFST push-out test samples. *Civil And Environmental Engineering Reports* 26(3), pp. 145-159. <https://doi.org/10.1515/Ceer-2017-0042>
- Gulsan, M. E., Abdulhaleem, K.N., Kurtoglu, A.E., Cevik, A. (2018) Size effect on strength of Fiber-Reinforced Self-Compacting Concrete (SCC) after exposure to high temperatures. *Computers and Concrete* 21(6), pp. 681-695. <https://doi.org/10.12989/cac.2018.21.6.681>
- Guo, H. Long, X., Yao, Y. (2017) Fire resistance of concrete filled steel tube columns subjected to non-uniform heating. *Journal of Constructional Steel Research* 128, pp. 542-554. <https://doi.org/10.1016/j.jcsr.2016.09.014>
- Gupta, S., Kua, H. W. (2020) Application of rice husk biochar as filler in cenosphere modified mortar: Preparation, characterization and performance under elevated temperature. *Construction and Building Materials* 253, 119083. <https://doi.org/10.1016/j.conbuildmat.2020.119083>
- Hager, I. (2013) Behaviour of cement concrete at high temperature. *Bulletin of the Polish Academy of Sciences* 61(1), pp. 145-154. <https://doi.org/10.2478/bpasts-2013-0013>
- Hager, I. (2014) Colour Change in Heated Concrete. *Fire Technology* 50, pp. 945-958. <https://doi.org/10.1007/s10694-012-0320-7>
- Hager, I., Kaňka, S. Mašlak, M. (2021b) Properties of quenched and self-tempered reinforcing steel subjected to high temperature and different cooling conditions. *Journal of Structural Fire Engineering* 12(2), pp. 141-152. <https://doi.org/10.1108/JSFE-08-2019-0030>

- Hager, I., Pimienta, P. (2004) The impact of the addition of polypropylene fibres on the mechanical properties of high performance concretes exposed to high temperatures. In 6th RILEM Symposium on Fibre-Reinforced Concretes (FRC) (pp. 575–582). Varenna, Italy.
- Hager, I., Sitarz, M., Mróz, M. (2021a) Fly-ash based geopolymer mortar for high-temperature application – Effect of slag addition. *Journal of Cleaner Production* 316, 128168. <https://doi.org/10.1016/j.jclepro.2021.128168>
- Hagn, H. (1891) Zum Speicherbrand in Hamburg. *Deutsche Bauzeitung* 52 (30.06.1891), pp. 313-314.
- Hagn, H. (1904) *Schutz von Eisenkonstruktionen gegen Feuer*. Verlag von Julius Springer
- Hajmohammadian Baghban, M., Hovde, P.J., Jacobsen, S. (2013) Analytical and experimental study on thermal conductivity of hardened cement pastes. *Materials and Structures* 46, pp. 1537-1546. <https://doi.org/10.1617/s11527-012-9995-y>
- Halicka, A., Ogrodnik, P., Zegardlo, B. (2013) Using ceramic sanitary ware waste as concrete aggregate. *Construction and Building Materials* 48, pp. 295-305. <https://doi.org/10.1016/j.conbuildmat.2013.06.063>
- Han, L.H., Zhao, X.L., Yang, Y.F., Feng, J.B. (2003) Experimental study and calculation of fire resistance of concrete-filled hollow steel columns. *Journal of Structural Engineering* 129(3), pp. 346-356, 2003. [https://doi.org/10.1061/\(ASCE\)0733-9445\(2003\)129:3\(346\)](https://doi.org/10.1061/(ASCE)0733-9445(2003)129:3(346))
- Han, L-H., Chen, F., Liao, F-Y., Tao, Z., Uy, B. (2013) Fire performance of concrete filled stainless steel tubular columns. *Engineering Structures* 56, pp. 165-181. <http://doi.org/10.1016/j.engstruct.2013.05.005>
- Han, L-H., Yang, Y-F., Yang, H., Huo, J-s. (2002) Residual strength of concrete-filled RHS columns after exposure to the ISO-834 standard fire. *Thin-Walled Structures* 40, pp. 991-1012. [https://doi.org/10.1016/S0263-8231\(02\)00044-7](https://doi.org/10.1016/S0263-8231(02)00044-7)
- Han, L-H., Yao, G-H., Zhao, X-L. (2005) Tests and calculations for hollow structural steel (HSS) stub columns filled with self-consolidating concrete (SCC). *Journal of Constructional Steel Research* 61, pp. 1241-1269. <https://doi.org/10.1016/j.jcsr.2005.01.004>
- Hanif, A., Diao, S., Lu, Z., Fan, T., Li, Z. (2016) Green lightweight cementitious composite incorporating aero-gels and fly ash cenospheres - Mechanical and thermal insulating properties. *Construction and Building Materials* 116, pp. 422-430. <https://doi.org/10.1016/j.conbuildmat.2016.04.134>
- Hanswille, G., Lippes, M. (2008) Einsatz von hochfesten Stählen und Betonen bei Hohlprofil-Verbundstützen. *Stahlbau* 77(4), pp. 296-307. <https://doi.org/10.1002/stab.200810041>
- Hanus, F., Vassart, O., Caillet, N., Franssen, J-M. (2017) High temperature full-scale tests performed on S500M steel grade beams. *Journal of Constructional Steel Research* 133, pp. 448-458. <https://doi.org/10.1016/j.jcsr.2017.03.001>
- Harmathy, T.Z., Lie, T.T. (1970) Fire test standard in the light of fire research. *ASTM Special Technical Publication* 464, pp. 85-97. <https://doi.org/10.4224/40001469>
- Harmathy, T.Z., Sultan, M.A. (1988) Correlation between the severities of the ASTM E119 and ISO 834 fire exposures. *Fire Safety Journal* 13(2-3), pp. 163-168. [https://doi.org/10.1016/0379-7112\(88\)90011-2](https://doi.org/10.1016/0379-7112(88)90011-2)
- Harmathy, T.Z., Sultan, M.A., MacLaurin, J.W. (1987) Comparison of severity of exposure in ASTM E 119 and ISO 834 fire resistance tests. *Journal of Testing and Evaluation* 15(6), pp. 371-375. <https://doi.org/10.1520/jte11036j>
- Hartley, D. (1773) Patent No. 1037, Securing Buildings and Ships from Fire
- Haß (Hass), R. (1986) Zur praxisgerechten brandschutztechnischen Beurteilung von Stützen aus Stahl und Beton. Heft 69. T Braunschweig. Report/PhD thesis, 190 pages. <https://doi.org/10.24355/dbbs.084-201310181517-0>
- Haustein, E., Kuryłowicz-Cudowska, A. (2022) Effect of Particle Size of Fly Ash Microspheres (FAMs) on the Selected Properties of Concrete. *Minerals* 12, 847. <https://doi.org/10.3390/min12070847>
- Holan, J., Novák, J., Müller, P., Štefan, R. (2020) Experimental investigation of the compressive strength of normal-strength air-entrained concrete at high temperatures. *Construction and Building Materials* 248, 118662. <https://doi.org/10.1016/j.conbuildmat.2020.118662>
- Holman, J.P. (2010) *Heat Transfer*. McGraw-Hill, New York, 10th edition.

- Hong, S., Varma, A.H. (2009) Analytical modeling of the standard fire behavior of loaded CFT columns. *Journal of Constructional Steel Research* 65, pp. 54-69.  
<https://doi.org/10.1016/j.jcsr.2008.04.008>
- Horszczaruk, E., Sikora, P., Cendrowski, K., Mijowska, E. (2017) The effect of elevated temperature on the properties of cement mortars containing nanosilica and heavyweight aggregates. *Construction and Building Materials* 137, pp. 420-431.  
<https://doi.org/10.1016/j.conbuildmat.2017.02.003>
- Howell, J.R., Siegel, R., Mengüç, M.P. (2013) *Thermal Radiation Heat Transfer*. 5th Edition. CRC press.
- Hu, Y., Zhao, P., Yang, B., Dai, G. (2016) Numerical study on temperature distribution of high-strength concrete-filled steel tubes subjected to a fire. *International Journal of Steel Structures* 16(4), pp. 1057-1069. <https://doi.org/10.1007/s13296-016-0021-z>
- Hua, N., Khorasani, N.E., Tessari, A. (2022) Numerical modeling of the fire behavior of reinforced concrete tunnel slabs during heating and cooling. *Engineering Structures* 258, 114135.  
<https://doi.org/10.1016/j.engstruct.2022.114135>
- Huang, S-S, Burgess I.W., Huang Z-H., Plank R.J (2007) The Buckling of Slender Concrete and Concrete-Filled Columns in Fire. *Proceedings of the fib Workshop: Fire Design of Concrete Structures - from Materials Modelling to Structural Performance*, Coimbra 2007, 12 pages.
- Huang, H., Wang, R., Gao, X. (2019) Improvement effect of fiber alignment on resistance to elevated temperature of ultra-high performance concrete. *Composites Part B: Engineering*, 177.  
<https://doi.org/10.1016/j.compositesb.2019.107454>
- Huang, Z., Liew, J.Y.R Li, W. (2017) Evaluation of compressive behavior of ultra-lightweight cement composite after elevated temperature exposure. *Construction and Building Materials* 148, pp. 579-589. <https://doi.org/10.1016/j.conbuildmat.2017.04.121>
- Huang, Z., Padmaja, K., Li, S., Liew, J.Y.R. (2018) Mechanical properties and microstructure of ultra-lightweight cement composites with fly ash cenospheres after exposure to high temperatures. *Construction and Building Materials* 164, pp. 760-774.  
<https://doi.org/10.1016/j.conbuildmat.2018.01.009>
- Hull, W.A., Ingberg, S.H. (1925) Fire resistance of concrete columns. *Technologic papers of the bureau of standards* Np. 272. Government Printing Office, Washington.
- Huo, J., Huang, G., Xiao, Y. (2009) Effects of sustained axial load and cooling phase on post-fire behaviour of concrete-filled steel tubular stub columns. *Journal of Constructional Steel Research* 65(8), pp. 1664-1676. <https://doi.org/10.1016/j.jcsr.2009.04.022>
- Hurley, M.J. (2016) *SFPE handbook of Fire Protection Engineering*, 5th Edition. Springer
- Hutton, N.H. (1876) Fire-proof construction. *The American Architect and Building News* 1 (Feb. 5), pp. 43-44.
- Hyatt, T. (1873) Improvement in fire-proof columns. US patent No. 145180.  
<https://patents.google.com/patent/US145180A/en>
- Ibáñez, C. (2015) Fire response analysis of circular concrete filled tubular columns and the effects of axial and rotational restraints. PhD thesis. Universitat Politècnica de València. 376 pages
- Ibáñez, C., Aguado, J.V., Romero, M.L., Espinos, A., Hospitaler, A. (2015) Fire design method for concrete filled tubular columns based on equivalent concrete core cross-section. *Fire Safety Journal* 78, pp. 10-23. <http://doi.org/10.1016/j.firesaf.2015.07.009>
- Ibáñez, C., Bisby, L., Rush, D., Romero, M.L., Hospitaler, A. (2019) Post-heating response of concrete-filled steel tubular columns under sustained loads. *Structures* 21, pp. 90-102.  
<https://doi.org/10.1016/j.istruc.2019.04.003>
- ID2 (1994) Interpretative document No. 2 - Safety in case of fire. *Official Journal of the European Communities* No. C62, Vol. 37, pp. 23-72.
- Ingberg, S. H., Griffin, H. K., Robinson, W. C., Wilson, R. E. (1921) Fire tests of building columns. An experimental investigation of the resistance of column loaded and exposed to fire or fire and water, with record of characteristic effects. *Technologic Papers of the Bureau of Standards* No. 184. Washington Government Printing Office.
- ISO 24679-1 (2019) Fire safety engineering — Performance of structures in fire — Part 1: General

- ISO 834 (1975) Fire-resistance tests – Elements of building construction. ISO. Switzerland.
- ISO 834-1 (1999) Fire-resistance tests – Elements of building construction – Part 1: General requirements. ISO. Switzerland.
- ISO TR-3956 (1975) Principles of structural fire-engineering design with special regard to the connection between real fire exposure and the heating conditions of the standard fire-resistance test (ISO 834). Technical Report 3956. ISO - International Organization for Standardization.
- Iwama, K., Maekawa, K. (2022) Modeling of carbonation, de-carbonation and re-carbonation processes of structural concrete subjected to high temperature heating. *Cement and Concrete Composites* 129, 104493. <https://doi.org/10.1016/j.cemconcomp.2022.104493>
- Jansen, D.C., Shah, S.P. (1997) Effect of length on compressive strain softening of concrete. *Journal of Engineering Mechanics* 123, pp. 25-35. [https://doi.org/10.1061/\(ASCE\)0733-9399\(1997\)123:1\(25\)](https://doi.org/10.1061/(ASCE)0733-9399(1997)123:1(25))
- Jansson, R., Boström, L. (2013) Fire spalling in concrete – The moisture effect, part II. 3rd International RILEM Workshop on Concrete Spalling due to Fire Exposure. Paris, France.
- Jaszczak, B., Kuczma, M., Szymkuć, W. (2021) Comparison of the load-bearing capacity of reinforced concrete columns under fire conditions using the method A, zone method and isotherm 500 method. *Fire Safety Journal* 124, 103396. <https://doi.org/10.1016/j.firesaf.2021.103396>
- Jelčić Rukavina, M., Gabrijel, I., Netinger Grubeša, I., Mladenović, A. (2022) Residual Compressive Behavior of Self-Compacting Concrete after High Temperature Exposure—Influence of Binder Materials. *Materials* 15(6), 2222. <https://doi.org/10.3390/ma15062222>
- Jiang, C., Fang, J., Chen, J-Y., Gu, X-L. (2020) Modeling the instantaneous phase composition of cement pastes under elevated temperatures. *Cement and Concrete Research* 130, 105987. <https://doi.org/10.1016/j.cemconres.2020.105987>
- Jiang, C., Lu, D., Lu, C. (2018) The effect of nanoparticles on the properties of calcium aluminate cement pastes at high temperatures. *Advances in Cement Research* 30(5), pp. 195-203. <https://doi.org/10.1680/jadcr.17.00039>
- Johann, M.A., Albano, L.D., Fitzgerald, R.W., Meacham, B.J. (2006) Performance-Based Structural Fire Safety. *Journal of Performance of Constructed Facilities* 20(1), pp. 45-53. [https://doi.org/10.1061/\(asce\)0887-3828\(2006\)](https://doi.org/10.1061/(asce)0887-3828(2006))
- Johnson, J.B. (1898) *The materials of construction. A treatise for engineers on the strength of engineering materials.* Wiley & Sons. New York, USA.
- Kang, W-H., Uy, B., Tao, Z., Hicks, S. (2015) Design strength of concrete-filled steel columns. *Advanced Steel Construction* 11(2), pp. 165-184. <https://doi.org/10.18057/IJASC.2015.11.2.3>
- Karlsson, B., Quintiere, J.G. (2022) *Enclosure fire dynamics. Second Edition.* CRC Press. <https://doi.org/10.1201/b22214>
- Katwal, U., Aziz, T., Tao, Z., Uy, B., Rahme, D. (2022) Tests of circular geopolymers concrete-filled steel columns under ambient and fire conditions. *Journal of Constructional Steel Research* 196, 107393. <https://doi.org/10.1016/j.jcsr.2022.107393>
- Kawagoe (1958) *Fire Behaviour in Rooms.* Report 27 of the Building Research Institute of Japan.
- Kay, T.R., Kirby, B.R., Preston, R.R. (1996) Calculation of the heating rate of an unprotected steel member in a standard fire resistance test. *Fire Safety Journal* 26(4), pp. 327-350. [https://doi.org/10.1016/S0379-7112\(96\)00016-1](https://doi.org/10.1016/S0379-7112(96)00016-1)
- Keerthan, P., Mahendran, M. (2013) Thermal Performance of Composite Panels Under Fire Conditions Using Numerical Studies: Plasterboards, Rockwool, Glass Fibre and Cellulose Insulations. *Fire Technology* 49, pp. 329-356. <https://doi.org/10.1007/s10694-012-0269-6>
- Keppert, M., Fořt, J., Trník, A., Koňáková, D., Vejmelková, E., Pokorný, J., Svora, P., Pavlík, Z., Černý, R. (2017). Behavior of Sandstones Under Heat Treatment. *International Journal of Thermophysics*, 38(4). <https://doi.org/10.1007/s10765-017-2191-0>
- Khan, A.A., Usmani, A., Torero, J.L. (2021) Evolution of fire models for estimating structural fire-resistance. *Fire Safety Journal* 124, 103367. <https://doi.org/10.1016/j.firesaf.2021.103367>
- Khoury, G.A. (1992) Compressive strength of concrete at high temperatures: a reassessment. *Magazine of Concrete Research* 44(161), pp. 291-309. <https://doi.org/10.1680/mac.1992.44.161.291>

- Khoury, G.A., Anderberg, Y., Both, K., Fellingner, J, Høj, N.P., Majorana, C. (2007) fib Bulletin 38: Fire design of concrete structures - materials, structures and modelling. State-of-art report. International Federation for Structural Concrete (fib). Lausanne, Switzerland.
- Khoury, G.A., Sullivan, P.J.E., Grainger, B.N. (1984) Radial temperature distributions within solid concrete cylinders under transient thermal states. Magazine of Concrete Research 36(128), pp. 146-156. <https://doi.org/10.1680/mac.1984.36.128.146>
- Kim, D.K., Choi, S.M. Kim, J.H., Chung K.S., Park, S.H. (2005) Experimental study on fire resistance of concrete-filled steel tube column under constant axial loads. International Journal of Steel Structures, 5(4), pp. 305-313.
- Kim, K. H., Jeon, S. E., Kim, J. K., Yang, S. (2003) An experimental study on thermal conductivity of concrete. Cement and Concrete Research 33(3), pp. 363-371. [https://doi.org/10.1016/S0008-8846\(02\)00965-1](https://doi.org/10.1016/S0008-8846(02)00965-1)
- Kirby, B.R., Lapwood, D.G., Thomson, G. (1986) The Reinstatement of Fire Damaged Steel and Iron Framed Structures. British Steel Swinden Laboratories, ISBN 0900206462, 84 pages. Reprinted in 1993.
- Kirby, B.R., Preston, R.R. (1988) High temperature properties of hot-rolled, structural steels for use in fire engineering design studies. Fire Safety Journal 13(1), pp. 27-37. [https://doi.org/10.1016/0379-7112\(88\)90030-6](https://doi.org/10.1016/0379-7112(88)90030-6)
- Knaack, A.M., Kurama, Y.C., Kirkner, D.J. (2010) Compressive strength relationships for concrete under elevated temperatures. ACI Materials Journal 107(2), pp. 164-175. <https://doi.org/10.14359/51682492>
- Knobloch, M., Pauli, J., Fontana, M. (2013) Influence of the strain-rate on the mechanical properties of mild carbon steel at elevated temperatures. Materials and Design 49, pp. 553-565. <https://doi.org/10.1016/j.matdes.2013.01.021>
- Kodur, V.K.R. (1999) Performance-based fire resistance design of concrete-filled steel columns. Journal of Constructional Steel Research 51(1), pp. 21-36. [https://doi.org/10.1016/S0143-974X\(99\)00003-6](https://doi.org/10.1016/S0143-974X(99)00003-6)
- Kodur, V.K.R. (2007) Guidelines for Fire Resistant Design of Concrete-Filled Steel HSS columns - State-of-the-Art and Research Needs. Steel Structures 7:173-182.
- Kodur, V.K.R., Harmathy, T.Z. (2016) Properties of Building Materials. In: SFPE Handbook of Fire Protection Engineering. Edited by: M.J. Hurley. Springer, New York, NY. [https://doi.org/10.1007/978-1-4939-2565-0\\_9](https://doi.org/10.1007/978-1-4939-2565-0_9)
- Kodur, V.K.R., Lie, T.T. (1995) Experimental Studies on the Fire Resistance of Circular Hollow Steel Columns Filled with Steel-Fibre-Reinforced Concrete. National Research Council of Canada. Internal Report No. 691. <https://doi.org/10.4224/20375221>
- Kodur, V.K.R., Venkatachari, S. (2020) Effect of transient creep on stability of steel columns exposed to fire. The 11th International Conference on Structures in Fire. The University of Queensland, Brisbane, Australia, 30th November - 2nd December, 2020.
- Koksal, F., Kocabeyoglu, E.T., Gencil, O., Benli, A. (2021) The effects of high temperature and cooling regimes on the mechanical and durability properties of basalt fiber reinforced mortars with silica fume. Cement and Concrete Composites 121, 104107. <https://doi.org/10.1016/j.cemconcomp.2021.104107>
- Kolay, P.K., Singh, D.N. (2001) Physical, chemical, mineralogical, and thermal properties of cenospheres from an ash lagoon. Cement and Concrete Research 31(4), pp. 539-542. [https://doi.org/10.1016/S0008-8846\(01\)00457-4](https://doi.org/10.1016/S0008-8846(01)00457-4)
- Kong, D.L.Y., Sanjayan, J.G. (2010) Effect of elevated temperatures on geopolymers paste, mortar and concrete. Cement and Concrete Research 40(2), pp. 334-339. <https://doi.org/10.1016/j.cemconres.2009.10.017>
- Kordina, K., Klingsch, W. (1983) Brandverhalten von Stahlstützen im Verbund mit Beton und von massiven Stahlstützen ohne Beton. Report. TU Braunschweig. 567 pages. <https://op.europa.eu/pl/publication-detail/-/publication/995b97fe-bbf0-4e65-98cb-774afb16098f>
- Kowalski, R., Kisielinski, R. (2019) Experimental approach to strength reduction and elongation of self-tempered reinforcing bars tensioned at a steady and an increasing temperature. Structural Concrete 20(2), pp. 823-835. <https://doi.org/10.1002/suco.201800076>

- Krasuski, A. (2019) Multisimulation: Stochastic simulations for the assessment of building fire safety. The Main School of Fire Service. Masovian Printing Center, Warsaw, Poland. 218 pages.
- Król, P.A. (2015) Źródła niepewności w ocenie bezpieczeństwa pożarowego konstrukcji stalowych. *BiTP* 37(1), pp. 65-86. <https://doi.org/10.12845/bitp.37.1.2015.6>
- Kucukler, M. (2020) Compressive resistance of high-strength and normal-strength steel CHS members at elevated temperatures. *Thin-Walled Structures* 152, 106753. <https://doi.org/10.1016/j.tws.2020.106753>
- Kumar, S., Mukhopadhyay, T., Waseem, S. A., Singh, B., Iqbal M. A. (2016) Effect of Platen Restraint on Stress–Strain Behavior of Concrete Under Uniaxial Compression a Comparative Study. *Strength of Materials* 48(4), pp. 592-602. <https://doi.org/10.1007/s11223-016-9802-z>
- Kupfer, H. (1973) Das Verhalten des Betons unter mehrachsiger Kurzzeitbelastung unter besonderer Berücksichtigung der zweiachsigen Beanspruchung. Deutscher Ausschuss für Stahlbeton (DAfStb) Heft 229. Ernst & Sohn. Berlin 1973.
- Kupina, M. (2015) Nośność krępych osiowo ściskanych słupów stalowo – betonowych w postaci kwadratowych rur wypełnionych betonem zwykłym. PhD thesis. Opole University of Technology
- L'Hôpital, E., Lothenbach, B., Kulik, D.A., Scrivener, K. (2016) Influence of calcium to silica ratio on aluminium uptake in calcium silicate hydrate. *Cement and Concrete Research* 85, pp. 111-121. <https://doi.org/10.1016/j.cemconres.2016.01.014>
- Lai, B., Liew, J.Y.R., Xiong, M. (2019) Experimental study on high strength concrete encased steel composite short columns. *Construction and Building Materials* 228, 116640. <https://doi.org/10.1016/j.conbuildmat.2019.08.021>
- Lange, D., Sjostrom, J. (2014) Mechanical response of a partially restrained column exposed to localised fires. *Fire Safety Journal* 67, pp. 82-95. <http://doi.org/10.1016/j.firesaf.2014.05.013>
- Langley, B. (1749) The London prices of bricklayers materials and works, both of new buildings and repairs, justly ascertained
- Lapuebla-Ferri, A., Pons, D., Romero, M.L. (2021) Load and temperature influence on the post-fire mechanical properties of steel reinforcements. *Journal of Constructional Steel Research* 185, 106866. <https://doi.org/10.1016/j.jcsr.2021.106866>
- Lattimer, B. (2016) Heat transfer from fires to surfaces. In: *SFPE Handbook of Fire Protection Engineering*, pp. 745-798. Edited by: Hurley, M.J. Springer. 5th Edition.
- Lautenberger, C., Tien, C.L., Lee, K.Y., Stretton, A.J. (2016) Radiation Heat Transfer. In: *SFPE Handbook of Fire Protection Engineering*, pp. 102-137. Edited by: Hurley, M.J. Springer. 5th Edition.
- Law, A., Bisby, L. (2020) The rise and rise of fire resistance. *Fire Safety Journal* 116, 103188. <https://doi.org/10.1016/j.firesaf.2020.103188>
- Le, X.L., Torero, J.L., Dao, V.T.N. (2019) Understanding the effects of stress on the coefficient of thermal expansion. *International Journal of Engineering Science* 141, pp. 83-94. <https://doi.org/10.1016/j.ijengsci.2019.05.016>
- Leite Jr, G.S., Gomide, K.A., Moreno Jr, A.L., Silva, V.P. (2010) Fire Resistance of Axially Loaded Slender Concrete Filled Steel Tubular Columns. *Proceedings of the Sixth International Conference on Structures in Fire*, pp. 433-440. DESTech Publications, Inc., Lancaster, U.S.A.
- Li, L., Shi, L., Wang, Q., Liu, Y., Dong, J., Zhang, H., Zhang, G. (2020). A review on the recovery of fire-damaged concrete with post-fire-curing. *Construction and Building Materials* 237, 117564. <https://doi.org/10.1016/j.conbuildmat.2019.117564>
- Li, L-y., Purkiss, J. (2005) Stress–strain constitutive equations of concrete material at elevated temperatures. *Fire Safety Journal* 40, pp. 669-686. <https://doi.org/10.1016/j.firesaf.2005.06.003>
- Li, P., Hu, J., Xing, F., Sui, L., Zhou, Y., Chen, C. (2021a) Behavior and modeling of double-skin tubular columns filled by ultra-lightweight cement composites (ULCCs). *Composite Structures* 263, 113709. <https://doi.org/10.1016/j.compstruct.2021.113709>
- Li, Q., Sun, H., Wang, M., Liu, P. (2022) Effects of moisture content and heating temperature on the thermal expansion deformation of concrete. *Structural Concrete* 23(4), pp. 2301-2312. <https://doi.org/10.1002/suco.202100088/>

- Li, Y., Mi, T., Liu, W., Dong, Z., Dong, B., Tang, L., Xing, F. (2021b) Chemical and mineralogical characteristics of carbonated and uncarbonated cement pastes subjected to high temperatures. *Composites Part B: Engineering* 216, 108861. <https://doi.org/10.1016/j.compositesb.2021.108861>
- Li, Y., Tan, K. H., Yang, E.-H. (2019) Synergistic effects of hybrid polypropylene and steel fibers on explosive spalling prevention of ultra-high performance concrete at elevated temperature. *Cement and Concrete Composites* 96, pp. 174-181. <https://doi.org/10.1016/j.cemconcomp.2018.11.009>
- Li, Y., Wang, M., Li, G., Jiang, B. (2021c) Mechanical properties of hot-rolled structural steels at elevated Temperatures: A review. *Fire Safety Journal* 119, 103237. <https://doi.org/10.1016/j.firesaf.2020.103237>
- Li, Z., Ding, F., Cheng, S., Lyu, F. (2022b) Mechanical behavior of steel-concrete interface and composite column for circular CFST in fire. *Journal of Constructional Steel Research* 196:107424. <https://doi.org/10.1016/j.jcsr.2022.107424>
- Liao, F.-Y., Han, L.-H., He, S.-H. (2011) Behavior of CFST short column and beam with initial concrete imperfection: Experiments. *Journal of Constructional Steel Research* 67(12), pp. 1922-1935. <https://doi.org/10.1016/j.jcsr.2011.06.009>
- Lie, T.T. (1984) A procedure to calculate the fire resistance of structural members. *Fire and Materials* 8(1), pp. 40-48. <https://doi.org/10.1002/fam.810080108>
- Lie, T.T. (1994) Fire resistance of circular steel columns filled with bar-reinforced concrete. *Journal of Structural Engineering* 120 (5), pp. 1489-1509. [https://doi.org/10.1061/\(ASCE\)0733-9445\(1994\)120:5\(1489\)](https://doi.org/10.1061/(ASCE)0733-9445(1994)120:5(1489))
- Lie, T.T., Caron, S.E. (1988) Fire Resistance of Circular Hollow Steel Columns Filled with Silicious Aggregate Concrete: Test Results. National Research Council of Canada. Internal Report No. 570. <https://doi.org/10.4224/20358588>
- Lie, T.T., Chabot, M. (1992) Experimental Studies on the Fire Resistance of Hollow Steel Columns Filled with Plain Concrete. National Research Council of Canada. Internal Report No. 611. <https://doi.org/10.4224/20358480>
- Lie, T.T., Irwin, R.J. (1995) Fire resistance of rectangular steel columns filled with bar-reinforced concrete. *Journal of Structural Engineering*, 121(5), pp. 797-805. [https://doi.org/10.1061/\(ASCE\)0733-9445\(1995\)121:5\(797\)](https://doi.org/10.1061/(ASCE)0733-9445(1995)121:5(797))
- Liew, J.Y.R., Yan, J.-B., Huang, Z.Y. (2017) Steel-concrete-steel sandwich composite structures-recent innovations. *Journal of Constructional Steel Research* 130, pp. 202-221. <http://doi.org/10.1016/j.jcsr.2016.12.007>
- Lilkov, V., Djabarov, N., Bechev, G., Kolev, K. (1999) Properties and hydration products of lightweight and expansive cements Part I: Physical and mechanical properties. *Cement and Concrete Research* 29(10), pp. 1635-1640. [https://doi.org/10.1016/S0008-8846\(99\)00150-7](https://doi.org/10.1016/S0008-8846(99)00150-7)
- Litewka A., Bogucka J., Dębiński J. (2003) Anisotropic Behaviour of Damaged Concrete and Fiber Reinforced Concrete. In: Skrzypek J.J., Ganczarski A.W. (eds) *Anisotropic Behaviour of Damaged Materials. Lecture Notes in Applied and Computational Mechanics*, vol 9. Springer, Berlin, Heidelberg. [https://doi.org/10.1007/978-3-540-36418-4\\_6](https://doi.org/10.1007/978-3-540-36418-4_6)
- Litewka, A., Dębiński, J. (2002) Damage-induced Anisotropy and Deformability of Brittle Rock-like Materials. *Key Engineering Materials Vols 230-232* pp. 505-508. <https://doi.org/10.4028/www.scientific.net/KEM.230-232.505>
- Liu, F., Wang, Y., Gardner, L., Varma, A.H. (2019) Experimental and Numerical Studies of Reinforced Concrete Columns Confined by Circular Steel Tubes Exposed to Fire. *Journal of Structural Engineering* 145(11), 04019130. [https://doi.org/10.1061/\(ASCE\)ST.1943-541X.0002416](https://doi.org/10.1061/(ASCE)ST.1943-541X.0002416)
- Liu, Q., Park, H., Shen, R., Jayathunga-Mudiyanselage, L. (2021) A New Method to Calculate Incident Radiant Heat Flux by Using Plate Thermometer. *Fire Technology* 57, pp. 341-359. <https://doi.org/10.1007/s10694-020-01006-9>
- Lopes, R.F.R., Rodrigues, J.P.C. (2020) Behaviour of restrained concrete filled square double-skin and double-tube hollow columns in case of fire. *Engineering Structures*, 216, 110736. <https://doi.org/10.1016/j.engstruct.2020.110736>

- Losiewicz, M., Halsey, D. P., Dews, S. J., Olomaiye, P., Harris, F. C. (1996) An investigation into the properties of micro-sphere insulating concrete. *Construction and Building Materials* 10(8), pp. 583-588. [https://doi.org/10.1016/S0950-0618\(96\)00022-0](https://doi.org/10.1016/S0950-0618(96)00022-0)
- Lu, J-X., Shen, P., Ali, H.A., Poon, C.S. (2021) Development of high performance lightweight concrete using ultra high performance cementitious composite and different lightweight aggregates. *Cement and Concrete Composites* 124, 104277. <https://doi.org/10.1016/j.cemconcomp.2021.104277>
- Lucherini, A., Jovanović, B., Van Coile, R., Merci, B. (2021) Background and limitations of the Eurocode parametric fire curves, including the fire decay phase. *Application of Structural Fire Engineering*. Pages. Ljubljana, Slovenia.
- Lucio-Martin, T., Roig-Flores, M., Izquierdo, M., Alonso, M.C. (2021) Thermal conductivity of concrete at high temperatures for thermal energy storage applications: Experimental analysis. *Solar Energy* 214, pp. 430-442. <https://doi.org/10.1016/j.solener.2020.12.005>
- Luo, X., Wang, B. (2008) Structural and elastic properties of LaAlO<sub>3</sub> from first-principles calculations. *Journal of Applied Physics* 104, 073518. <https://doi.org/10.1063/1.2990068>
- Madhusudana, C.V. (2014) *Thermal Contact Conductance*. Second Edition. Springer. <https://doi.org/10.1007/978-3-319-01276-6>
- Magnusson, S.E., Thelandersson, S. (1970) Temperature-time curves for the complete process of fire development. *Acta Polytechnica Scandinavica. Civil Engineering and Building Construction Series No. 65. Bulletin of Division of Structural Mechanics and Concrete Construction, Bulletin 16*. Lund Institute of Technology. Subtitle: Theoretical study of wood fuel fires in enclosed spaces. <https://portal.research.lu.se/en/publications/temperature-time-curves-of-complete-process-of-fire-development>
- Mahon, C. (1778) Description of a most effectual method of securing buildings against fire, Invented by Charles Lord Viscount Mahon, F. R. S. *Philosophical Transactions of the Royal Society of London* 68, pp. 884-894. <https://www.jstor.org/stable/106351>
- Malaska, M., Alanen, M., Cábová, K., Lišková, N., Mela, K., Pajunen, S., Wald, F. (2019) Experimental study on temperature distribution of sandwich panel joints in fire. *ce/papers* 3(3-4). Special Issue: Proceedings of Nordic Steel 2019. <https://doi.org/10.1002/cepa.1123>
- Malendowski M., Glema, A. (2017) Development and Implementation of Coupling Method for CFD-FEM Analyses of Steel Structures in Natural Fire. *Procedia Engineering* 172, pp. 692-700. <https://doi.org/10.1016/j.proeng.2017.02.082>
- Malendowski, M. (2017) Analytical Solution for Adiabatic Surface Temperature (AST), *Fire Technology* 53(1), pp. 413-420. <https://doi.org/10.1007/s10694-016-0585-3>
- Malendowski, M., (2018) Performance-based fire engineering for civil engineering structural design. PhD Thesis. 303 pages. Poznan University of Technology, Poland.
- Malendowski, M., Szymkuć, W., Daszkiewicz, T., Turkowski, P., Węgrzyński, W. (2023) Fire exposure measurements using plate thermometers. *ce/papers* 6(3-4), pp. 2157-2160. <https://doi.org/10.1002/cepa.2690>
- Malendowski, M., Szymkuć, W., Turkowski, P., Glema, A., Węgrzyński, W. (2021) Heat transfer model for calculation of the temperature field inside thin-walled sections in fire. *Thin-Walled Structures* 169, 108416-1 - 108416-26. <http://doi.org/10.1016/j.tws.2021.108416>
- Malhotra, H.L. (1956) The effect of temperature on the compressive strength of concrete. *Magazine of Concrete Research* 8(23), pp. 85-94. <https://doi.org/10.1680/mac.1956.8.23.85>
- Malhotra, H.L., Pearce, N.S. (1987) Revision of ISO 834 — 1975. Fire resistance tests — Elements of building construction. Part 3 — Guidance on test method and test data application. Third Draft. CEN document ISO TC 92/SC4/WG1 N270
- Maluk, C., Bisby, L., Terrasi, G., Krajcovic, M., Torero, J.L. (2012) Novel Fire Testing Methodology: Why, how and what now? Proceedings of the Mini Symposium on Performance-based Fire Safety Engineering of Structures as part of the 1st International Conference on Performance Based Land Life Cycle Structural Engineering, 5-7 December, 2012, Hong Kong, pp. 448-458.
- Maraveas, C., Fasoulakis, Z., Tsavdaridis, K.D. (2017) Post-fire assessment and reinstatement of steel structures. *Journal of Structural Fire Engineering* 8(2), pp. 181-201. <https://doi.org/10.1108/JSFE-03-2017-0028>

- Martens, A. (1888) Ueber das Verhalten von Eisen und Eisenconstructions im Feuer. *Stahl und Eisen* 8(2), pp. 76-82.
- Maślak, M. (2008) Trwałość pożarowa stalowych konstrukcji prętowych. Monografia 370, Politechnika Krakowska. Kraków, Poland.
- McBride, S. P., Shukla, A., Bose, A. (2002) Processing and characterization of a lightweight concrete using cenospheres. *Journal of Materials Science* 37(19), pp. 4217-4225. <https://doi.org/10.1023/A:1020056407402>
- McGrattan, K., Hostikka, S., Floyd, J., McDermott, R., Vanella, M. (2020) Fire Dynamics Simulator User's Guide. NIST Special Publication 1019 Sixth Edition. <http://doi.org/10.6028/NIST.SP.1019> (version 6.7.5)
- McGuire, J.H. (1978) A method of achieving positive pressure in a fire resistance furnace. *Fire Technology* 14, pp. 195-205. <https://doi.org/10.1007/BF01983054>
- Meacham, B.J., Custer, R.L.P. (1995) Performance-Based Fire Safety Engineering: An Introduction of Basic Concepts. *Journal of Fire Protection Engineering* 7(2), pp. 35-54. <https://doi.org/10.1177/104239159500700201>
- Meloni, P., Mistretta, F., Stochino, F., Carcangiu, G. (2019) Thermal Path Reconstruction for Reinforced Concrete Under Fire. *Fire Technology* 55, pp. 1451-1475. <https://doi.org/10.1007/s10694-019-00835-7>
- Mendes, A., Sanjayan, J., Collins, F. (2008). Phase transformations and mechanical strength of OPC/Slag pastes submitted to high temperatures. *Materials and Structures/Materiaux et Constructions*, 41(2), pp. 345-350. <https://doi.org/10.1617/s11527-007-9247-8>
- Mendes, A., Sanjayan, J.G., Collins, F. (2009) Long-term progressive deterioration following fire exposure of OPC versus slag blended cement pastes. *Materials and Structures* 42, pp. 95-101. <https://doi.org/10.1617/s11527-008-9369-7>
- Merwe, van der, J.E. (2022) Evaluation of concrete tensile strength as a function of temperature. *Construction and Building Materials* 329, 127179. <https://doi.org/10.1016/j.conbuildmat.2022.127179>
- Mohamedbhai, G. T. G. (1986). Effect of exposure time and rates of heating and cooling on residual strength of heated concrete. *Magazine of Concrete Research*, 38(136), 151–158. <https://doi.org/10.1680/mac.1986.38.136.151>
- Moliner, V., Espinos, A., Romero, M., Hospitaler, A. (2013) Fire behavior of eccentrically loaded slender high strength concrete-filled tubular columns. *Journal of Constructional Steel Research* 83, pp. 137-146. <https://doi.org/10.1016/j.jcsr.2013.01.011>
- Molkens, T., Cashell, K.A., Rossia, B. (2021) Post-fire mechanical properties of carbon steel and safety factors for the reinstatement of steel structures. *Engineering Structures* 234, 111975. <https://doi.org/10.1016/j.engstruct.2021.111975>
- Molkens, T., Rossi, B. (2022) The Post-fire Assessment of Steel Structures, a Reliability-Based Semi-probabilistic Approach. *Fire Technol.* <https://doi.org/10.1007/s10694-022-01293-4>
- Möller, M. (1885) Zur Frage des Verhaltens gussieserner und schmiedeiserner Stützen bei Feuersbrünsten. *Deutsche Bauzeitung* No. 53 (3.07.1886), pp. 314.
- Möller, M., Lühmann, R. (1888) Über die Widerstandsfähigkeit auf Druck beanspruchter eiserner Baukonstruktionsteile bei erhöhter Temperatur. Verlag von Leonhard Simion. Berlin
- Montgomery, D., Diamond, S. (1984) The influence of fly ash cenospheres on the details of cracking in flyash-bearing cement pastes. *Cement and Concrete Research* 14(6), pp. 767-775. [https://doi.org/10.1016/0008-8846\(84\)90001-2](https://doi.org/10.1016/0008-8846(84)90001-2)
- Morino, S., Uchikoshi, M., Yamaguchi, I. (2001) Concrete-Filled Steel Tube Column System-Its Advantages. *International Journal of Steel Structures* 1, pp. 33-44.
- Morovat, M.A., Engelhardt, M.D. (2020) Critical Review of Test Methods for Mechanical Characterization of Steel for Structural-Fire Engineering Applications. *Journal of Structural Engineering* 146(11), 04020228. [https://doi.org/10.1061/\(asce\)st.1943-541x.0002787](https://doi.org/10.1061/(asce)st.1943-541x.0002787)
- Müller, H.S., Anders, I. Breiner, R., Vogel, M. (2013) Concrete: treatment of types and properties in fib Model Code 2010. *Structural Concrete* 14(4), 320-334. <https://doi.org/10.1002/suco.201200048>
- Müller, M. (1891a) Zum Speicherbrand in Hamburg. *Deutsche Bauzeitung* 35 (2.05.1891), pp. 212-214.

- Müller, M. (1891b) Noch einmal über die Bedeutung empirischer Forschung im Bauwesen. Deutsche Bauzeitung 93 (21.11.1891), pp. 564-565.
- Mushahary, S.K., Singh, K.D., Jayachandran, S.A. (2021) Mechanical properties of E350 steel during heating and cooling. Thin-Walled Structures 160, 107351. <https://doi.org/10.1016/j.tws.2020.107351>
- Naser, M.Z., Thai, S., Thai, H-T. (2021) Evaluating structural response of concrete-filled steel tubular columns through machine learning. Journal of Building Engineering 34, 101888. <https://doi.org/10.1016/j.jobbe.2020.101888>
- Naser, M.Z., Uppala, V.A. (2020) Properties and material models for construction materials post exposure to elevated temperatures. Mechanics of Materials 142, 103293. <https://doi.org/10.1016/j.mechmat.2019.103293>
- NBC (1953) National Building Code of Canada. Associate Committee on the National Building Code. National Research Council. Ottawa, Canada.
- NBS (1942) Fire-Resistance Classifications of Building Constructions. NBS Building and Materials Structures. Report BMS92. National Bureau of Standards.
- Neuenschwander, M., Knobloch, M., Fontana, M. (2016) Suitability of the damage-plasticity modelling concept for concrete at elevated temperatures: Experimental validation with uniaxial cyclic compression tests. Cement and Concrete Research 79, pp. 57-75. <https://doi.org/10.1016/j.cemconres.2015.07.013>
- NFPA (1917) Report of Committee on Fire Resistive Construction. In: Proceedings of the twenty-first annual meeting, pp. 391-413. Washington, D.C. <https://babel.hathitrust.org/cgi/pt?id=hvd.hb17v0&view=1up&seq=399&skin=2021>
- NFPA (1918) Report of Committee on Fire Resistive Construction. In: Proceedings of the twenty-second annual meeting, pp. 170-221. 7-9 May, Chicago. <https://babel.hathitrust.org/cgi/pt?id=hvd.hb17v0&view=1up&seq=658&skin=2021>
- NFPA Quarterly (1916) Fire Tests of Building Columns At Underwriters' Laboratories, Chicago. Prospectus. NFPA Quarterly 9(3), pp. 253-260.
- Niry Razafinjato, R., Beaucour, A-L., Hebert, R.L., Ledesert, B., Bodet, R. Noumowe, A. (2016) High temperature behaviour of a wide petrographic range of siliceous and calcareous aggregates for concretes. Construction and Building Materials 123, pp. 261-273. <https://doi.org/10.1016/j.conbuildmat.2016.06.097>
- Ogrodnik, P., Szulej, J. (2017) The impact of aeration of concrete based on ceramic aggregate, exposed to high temperatures, on its strength parameters. Construction and Building Materials 157, pp. 909-916. <https://doi.org/10.1016/j.conbuildmat.2017.09.155>
- O'Shea, M.D., Bridge, R.Q. (1997) Local buckling of thin-walled circular steel sections with or without internal restraint. Journal of Constructional Steel Research 41(2-3), pp. 137-157. [https://doi.org/10.1016/S0143-974X\(97\)80891-7](https://doi.org/10.1016/S0143-974X(97)80891-7)
- Outinen, J. (2007) Mechanical Properties of Structural Steels at High Temperatures and After Cooling Down. PhD thesis. Helsinki University of Technology Laboratory of Steel Structures Publications 32.
- Paaajanen, A., Korhonen, T., Sippola, M., Hostikka, S., Malendowski, M., Gutkin, R. (2013) FDS2FEM a tool for coupling fire and structural analyses. In Proceedings of the IABSE Workshop: Safety, Failures and Robustness of Large Structures, Volume 100, pp. 218–224. International Association for Bridge and Structural Engineering. <https://github.com/atpaaajan/fds2fem>
- Pacheco, J., de Brito, J., Chastre, C., Evangelista, L. (2019) Probabilistic Conversion of the Compressive Strength of Cubes to Cylinders of Natural and Recycled Aggregate Concrete Specimens. Materials 2019, 12(2), 280. <https://doi.org/10.3390/ma12020280>
- Paloposki, T., Liedquist, L. (2006) Steel emissivity at high temperatures. VTT Tiedotteita – Research Notes 2299. 81 pages, Espoo, Finland.
- Paudel, D., Rinta-Paavola, A., Mattila, H-P., Hostikka, S. (2021) Multiphysics Modelling of Stone Wool Fire Resistance. Fire Technology 57, pp. 1283-1312. <https://doi.org/10.1007/s10694-020-01050-5>

- Peet, M.J., Hasan, H.S. Bhadeshia, H.K.D.H. (2011) Prediction of thermal conductivity of steel. *International Journal of Heat and Mass Transfer* 54(11-12), pp. 2602-2608. <https://doi.org/10.1016/j.ijheatmasstransfer.2011.01.025>
- Phan, L. T., Carino, N. J. (2002) Effects of Test Conditions and Mixture Proportions on Behavior of High - Strength Concrete Exposed to High Temperatures. *ACI Materials Journal* 99(1), pp. 54-66. <https://doi.org/10.14359/11317>
- Pichór, W. (2006) The interfacial transition zone between filler and matrix in cement based composites with cenospheres. *Kompozyty (Composites)* 6(3), pp. 71-77.
- Pichór, W. (2009) Properties of fiber reinforced cement composites with cenospheres from coal ash. In *Proceedings of an International Symposium Brittle Matrix Composites 9*, pp. 245-254. Eds.: A.M. Brandt, J. Olek. <https://doi.org/10.1533/9781845697754.245>
- Pimienta, P., Alonso, M.C., Jansson McNamee, R., Mindeguia, J-C. (2017) Behaviour of High-Performance Concrete at High Temperatures: Some Highlights. *RILEM Technical Letters* 2, pp. 45-52. <https://doi.org/10.21809/rilemtechlett.2017.53>
- Pimienta, P., Jansson McNamee, R., Mindeguia, J-C. (2019) Physical Properties and Behaviour of High-Performance Concrete at High Temperature. State-of-the-Art Report of the RILEM Technical Committee 227-HPB. Springer, Switzerland. <https://doi.org/10.1007/978-3-319-95432-5>
- Pires, T.A.C., Rodrigues, J.P.C., Rêgo Silva, J.J. (2012) Fire resistance of concrete filled circular hollow columns with restrained thermal elongation. *Journal of Constructional Steel Research* 77, pp. 82-94. <https://doi.org/10.1016/j.jcsr.2012.03.028>
- Plechawski, S., Fic, S.B. (2018) Wpływ wysokiej temperatury na charakterystykę pęknięcia zaczynu, zaprawy i betonu. *Przegląd Budowlany* 89 (9), pp. 16-21.
- PN-B 02851 (1964) Ochrona przeciwpożarowa w budownictwie. Metoda badania odporności ogniowej elementów konstrukcji budowlanych. PKN. Poland.
- Poh, K.W. (2001) Stress-strain-temperature relationships for structural steel. *Journal of Materials in Civil Engineering* 13(5), pp. 371-379. [https://doi.org/10.1061/\(ASCE\)0899-1561\(2001\)13:5\(371\)](https://doi.org/10.1061/(ASCE)0899-1561(2001)13:5(371))
- Poh, K.W. (2014) Erratum for "Stress-Strain-Temperature Relationship for Structural Steel" by K. W. Poh. *Journal of Materials in Civil Engineering* 26(2), pp. 388-389. [https://doi.org/10.1061/\(asce\)mt.1943-5533.0000902](https://doi.org/10.1061/(asce)mt.1943-5533.0000902)
- Pons, D., Lapuebla-Ferri, A., Romero, M.L. (2022) Post-fire Residual Strength and Ductility of Structural Steels from Hollow Sections. *ce/papers* 5(4), pp. 458-466. The International Colloquium on Stability and Ductility of Structures (SDSS). <https://doi.org/10.1002/cepa.1777>
- Popovics, S. (1973) A numerical approach to the complete stress-strain curve of concrete. *Cement and Concrete Research* 3(5), pp. 583-599. [https://doi.org/10.1016/0008-8846\(73\)90096-3](https://doi.org/10.1016/0008-8846(73)90096-3)
- prEN 13501-2:2022 Fire classification of construction products and building elements - Part 2: Classification using data from fire resistance and/or smoke control tests, excluding ventilation services
- prEN 1991-1-2:2021 Eurocode 1: Actions on structures - Part 1-2: General actions - Actions on structures exposed to fire
- prEN 1992-1-2:2021 Eurocode 2: Design of concrete structures - Part 1-2: General rules - Structural fire design
- Prince, R.E. (1915) Tests on the inflammability of untreated wood and of wood treated with fire-retarding compounds. *Proc. NFPA* 19, pp. 108-158.
- Prša, A., Harmanec, P., Torres, G., Mamajek, E., Asplund, M., Capitaine, N., Christensen-Dalsgaard, J., Depagne, É., Haberreiter, M., Hekker, S., Hilton, J., Kopp, G., Kostov, V., Kurtz, D.W., Laskar, J., Mason, B.D., Milone, E.F., Montgomery, M., Richards, M., Schmutz, W., Schou, J., Stewart, S.G. (2016) Nominal values for selected solar and planetary quantities: IAU 2015 Resolution B3. *The Astronomical Journal* 152(2), pp. 1-7. <http://doi.org/10.3847/0004-6256/152/2/41>
- Pundienė, I., Korjakins, A., Pranckevičienė, J., Kligys, M. (2018) Effect of silicon carbide aggregate, prepared by different methods, on the properties of refractory concrete with cenospheres. *Ceramics International* 44(13), pp. 15944-15953. <https://doi.org/10.1016/j.ceramint.2018.06.015>

- Puri, R.G., Khanna, A.S. (2016) Effect of cenospheres on the char formation and fire protective performance of water-based intumescent coatings on structural steel. *Progress in Organic Coatings* 92, pp. 8-15. <https://doi.org/10.1016/j.porgcoat.2015.11.016>
- Qureshi, R., Ni, S., Elhami Khorasani, N., Van Coile, R., Hopkin, D., Gernay, T. (2020) Probabilistic Models for Temperature Dependent Strength of Steel and Concrete. *Journal of Structural Engineering* 146(6), 04020102. [https://doi.org/10.1061/\(asce\)st.1943-541x.0002621](https://doi.org/10.1061/(asce)st.1943-541x.0002621)
- Ramberg, W., Osgood, W.R. (1943) Description of stress-strain curves by three parameters. National Advisory Committee for Aeronautics (NACA) Technical Note No. 902. <https://ntrs.nasa.gov/citations/19930081614>
- Ranjbar, N., Kuenzel, C. (2017) Cenospheres: A review. *Fuel* 207, pp. 1-12. <https://doi.org/10.1016/j.fuel.2017.06.059>
- Ratajczak, M., Babiak, M., Kulczewski, P. (2019) Changes in the Crystal Structure of Cement Mortars Subjected to a High Temperature. *Key Engineering Materials* 808, pp. 165-171. <https://doi.org/10.4028/www.scientific.net/KEM.808.165>
- Rawat, S., Lee, C.K., Zhang, Y.X. (2021) Performance of fibre-reinforced cementitious composites at elevated temperatures: A review. *Construction and Building Materials* 292, 123382. <https://doi.org/10.1016/j.conbuildmat.2021.123382>
- Reed, S.A. (1896) Work of the committee on fire-proofing tests. *Journal of the Franklin Institute* 142(5), pp. 321-335. [https://doi.org/10.1016/S0016-0032\(96\)90220-3](https://doi.org/10.1016/S0016-0032(96)90220-3)
- Ren, C., Dai, L., Huang, Y., He, W. (2020) Experimental investigation of post-fire mechanical properties of Q235 cold-formed steel. *Thin-Walled Structures* 150, 106651. <https://doi.org/10.1016/j.tws.2020.106651>
- Ren, S., Tao, X., Xu, X., Guo, A., Liu, J., Fan, J., Ge, J. Fang, D., Liang, J. (2018) Preparation and characteristic of the fly ash cenospheres/mullite composite for high-temperature application. *Fuel* 233, pp. 336-345. <https://doi.org/10.1016/j.fuel.2018.06.058>
- Renaud, C., Joyeux, D., Kruppa, J. (2004) Improvement and extension of the simple calculation method for fire resistance of unprotected concrete filled hollow columns. CIDECT Research project 15Q. Final report. 101 pages.
- Ríos, J. D., Cifuentes, H., Leiva, C., García, C., Alba, M. D. (2018) Behavior of high-strength polypropylene fiber-reinforced self-compacting concrete exposed to high temperatures. *Journal of Materials in Civil Engineering (ASCE)* 30(11), 04018271. [https://doi.org/10.1061/\(ASCE\)MT.1943-5533.0002491](https://doi.org/10.1061/(ASCE)MT.1943-5533.0002491)
- Robertson, A.F. (1955) Fire research work in Britain and France. U.S. Department of Commerce. National Bureau of Standards.
- Rodrigues, J.P.C., Correia, A.J.M., Kodur, V. (2018) Boundary Conditions and Fire Behavior of Concrete Filled Tubular Composite Columns. *International Journal of High-Rise Buildings* 7(4), pp. 313-325. <https://doi.org/10.21022/IJHRB.2018.7.4.313>
- Rodrigues, J.P.C., Laím, L. (2017b) Fire response of restrained composite columns made with concrete filled hollow sections under different end-support conditions. *Engineering Structures* 141, pp. 83-96. <https://doi.org/10.1016/j.engstruct.2017.02.073>
- Rodrigues, J.P.C., Santos, dos, C.C., Pires, T.A. (2012) Fire resistance tests on concrete columns. 15th International Conference on Experimental Mechanics. Paper ID 3153, 12 pages.
- Romero, M. L., Espinós, A., Lapuebla-Ferri, A., Albero, V., Hospitaler, A. (2020). Recent developments and fire design provisions for CFST columns and slim-floor beams. *Journal of Constructional Steel Research*, 172, 106159. <https://doi.org/10.1016/j.jcsr.2020.106159>
- Romero, M., Moliner, V., Espinos, A., Ibáñez, C., Hospitaler, A. (2011) Fire behavior of axially loaded slender high strength concrete-filled tubular columns. *Journal of Constructional Steel Research* 67, pp. 1953-1965. <https://doi.org/10.1016/j.jcsr.2011.06.012>
- Romero, M.L., Espinós, A., Renaud, C., Bihina, G., Schaumann, P., Kleiboemer, I., Gardner, L., Rodrigues, J.P., Laim, L., Lozano, C., Iglesias, G. (2016) Fire resistance of innovative and slender concrete filled tubular composite columns. RFCS FRISCC project, grant RFSR-CT-2012-00025. Final report.

- Rostásy, F. S., Budelmann, H. (1986) Strength and deformation of concrete with variable content of moisture at elevated temperature up to 90°C. *Cement and Concrete Research* 16(3), pp. 353-362. [https://doi.org/10.1016/0008-8846\(86\)90111-0](https://doi.org/10.1016/0008-8846(86)90111-0)
- Rozzkowski, P., Sulik, P. (2016) Sandwich panels – behavior in fire based on fire resistance tests. *Applications of Structural Fire Engineering - Proceedings of the International Conference in Dubrovnik*, 15 - 16 October, 2015. <https://doi.org/10.14311/asfe.2015.065>
- Rubert, A., Schaumann, P. (1985) Temperaturabhängige Werkstoffeigenschaften von Baustahl bei Brandbeanspruchung. *Stahlbau*, 54 (3), pp. 81-86.
- Rubert, A., Schaumann, P. (1986) Structural steel and plane frame assemblies under fire action. *Fire Safety Journal* 10(3), pp. 173-184. [https://doi.org/10.1016/0379-7112\(86\)90014-7](https://doi.org/10.1016/0379-7112(86)90014-7)
- Rush, D. (2013) Fire performance of unprotected and protected concrete filled steel hollow structural sections. PhD thesis, 380 pages. The University of Edinburgh.
- Rush, D., Bisby, L., Melandinos, A., Lane, B. (2012) Fire Resistance Design of Unprotected Concrete Filled Steel Hollow Sections: Meta-Analysis of Available Furnace Test Data. *Fire Safety Science - Proceedings of the Tenth International Symposium*, pp. 1549-1562. <https://doi.org/10.3801/Iafss.Fss.10-1549>
- Sabeur, H., Saillio, M., Vincent, J. (2019) Thermal stability and microstructural changes in 5 years aged cement paste subjected to high temperature plateaus up to 1000 °C as studied by thermal analysis and X-ray diffraction. *Heat and Mass Transfer* 55, pp. 2483-2501. <https://doi.org/10.1007/s00231-019-02599-w>
- Sachs, E.O. (1902a) Facts on fire prevention. The results of fire tests conducted by the British Fire Prevention Committee (BFPC). Volume 1. Printed by B.T. Batsford, London.
- Sachs, E.O. (1902b) Facts on fire prevention. The results of fire tests conducted by the British Fire Prevention Committee (BFPC). Volume 2. Printed by B.T. Batsford, London.
- Sachs, E.O. (1903) Suggested standards of fire resistance. Report of proceedings of the International fire prevention congress, convened in London. Edited by Woolson, I.H. New York.
- Sadiq, H., Wong, M. B., Tashan, J., Al-Mahaidi, R., Zhao, X.-L. (2013) Determination of Steel Emissivity for the Temperature Prediction of Structural Steel Members in Fire. *Journal of Materials in Civil Engineering*, 25(2), pp. 167-173. [https://doi.org/10.1061/\(asce\)mt.1943-5533.0000607](https://doi.org/10.1061/(asce)mt.1943-5533.0000607)
- Sadowski, P., Stupkiewicz, S. (2010) A model of thermal contact conductance at high real contact area fractions. *Wear* 268(1-2), pp. 77-85. <https://doi.org/10.1016/j.wear.2009.06.040>
- Safuta, A. (1975) Odporność ogniowa konstrukcji budowlanych. Komenda Główna Straży Pożarnych. Instytut Wydawniczy ORZZ, Warszawa, Poland.
- Sahmenko, G., Namsone, E., Rubenis, K., Dubnika, A., Niparts, G. (2018) Effect of Various Additives and Aeration on the Properties of Lightweight Concrete. *Key Engineering Materials* 762, pp. 351-355. <https://doi.org/10.4028/www.scientific.net/kem.762.351>
- Sajid, H.U., Kiran, R. (2018) Influence of stress concentration and cooling methods on post-fire mechanical behavior of ASTM A36 steels. *Construction and Building Materials* 186, pp. 920-945. <https://doi.org/10.1016/j.conbuildmat.2018.08.006>
- Sandström, J. (2008) Thermal Boundary Conditions Based on Field Modelling of Fires. *Heat Transfer Calculations in CFD and FE Models With Special Regards to Fire Exposure Represented With Adiabatic Surface Temperatures*. Licentiate Thesis. Luleå University of Technology. 110 pages.
- Sant'Anna, M.S., Moreno Jr, A.L., Gomide, K.A. (2014) Slender Mixed Concrete Filled Steel Columns, in Fire Condition. *Advanced Materials Research* 875-877, pp. 490-495. <https://doi.org/10.4028/www.scientific.net/AMR.875-877.490>
- Sauerborn & Kretz (2010) Verbundstützen. In: *Stahlbau Kalender 2010*, Eds.: U. Kuhlmann, pp. 432 Ernst & Sohn, Berlin, Germany.
- Schaumann, P., Bahr, O., Zhao, B., Renaud, C., Viridi, K., Chica, J.A., Barcenilla, S.P., Dürr, A., Hemker, A. (2013) Unbraced composite structures in fire. RFCS UCoSiF project RFSR-CT-2007-00044. Final report.

- Schaumann, P., Kleibömer, I. (2018) Experimental and numerical investigations of the composite behaviour in concrete-filled tubular columns with massive steel core at high temperatures. *Journal of Structural Fire Engineering* 9(2), pp. 147-160. <https://doi.org/10.1108/JSFE-01-2017-0010>
- Schleich, J.B., Cajot, L.G., Pierre, M., Brasseur, M., Franssen, J.M., Kruppa, J., Joyeux, D., Twilt, L., Van Oerle, J., Aurtinetxe, G. (1999) Development of design rules for steel structures subjected to natural fires in closed car parks, Report of the European Commission.
- Schneider, S.P. (1998) Axially Loaded Concrete-Filled Steel Tubes. *Journal of Structural Engineering* 124(10), pp. 1125-1138. [https://doi.org/10.1061/\(ASCE\)0733-9445\(1998\)124:10\(1125\)](https://doi.org/10.1061/(ASCE)0733-9445(1998)124:10(1125))
- Schneider, U. (1982) Behavior of concrete at high temperatures. *Deutscher Ausschluß für Stahlbeton*, Heft 337. <https://doi.org/10.24355/dbbs.084-201705161117-0>
- Schneider, U., Felicetti, R., Debicki, G., Diederichs, U., Franssen, J.-M., Jumppanen, U.-M., Morris, W.A., Leonovich, S., Millard, A., Phan, L.T., Pimienta, P., Rodrigues, J.P.C., Schlangen, E., Zaytsev, Y. (2007) Recommendation of RILEM TC 200-HTC: mechanical concrete properties at high temperatures—modelling and applications. Part 2: Stress–strain relation. *Materials and Structures* 40, pp. 855-864. <https://doi.org/10.1617/s11527-007-9286-1>
- Schulze, F., Wedler, B. (1939) Brandversuche mit belasteten Eisenbetonbauteilen und Steineisendecken. Teil 2. Säulen. *Deutscher Ausschluß für Eisenbeton*. Heft 92.
- Scrivener, K., Ouzia, A., Juilland, P., Kunhi Mohamed, A. (2019) Advances in understanding cement hydration mechanisms. *Cement and Concrete Research* 124, 105823. <https://doi.org/10.1016/j.cemconres.2019.105823>
- Serega, S. (2015) Effect of transverse reinforcement spacing on fire resistance of high strength concrete columns. *Fire Safety Journal* 71, pp. 150-161. <https://doi.org/10.1016/j.firesaf.2014.11.017>
- Shah, S.P., Choi, S., Jansen, D.C. (1995) Strain softening of concrete in compression. *Proceedings of FraMCoS-2 Vol. 3*, pp. 1827-1841. Zurich, Switzerland. <http://www.framcos.org/FraMCoS-2/3-4-1.pdf>
- Shahraki, M., Hua, N., Elhami-Khorasani, N., Tessari, A., Garlock, M. (2022) Residual compressive strength of concrete after exposure to high temperatures: A review and probabilistic models. *Fire Safety Journal* 135, 103698. <https://doi.org/10.1016/j.firesaf.2022.103698>
- Shen, J., Xu, Q. (2019) Effect of moisture content and porosity on compressive strength of concrete during drying at 105 °C. *Construction and Building Materials* 195, pp. 19-27. <https://doi.org/10.1016/j.conbuildmat.2018.11.046>
- Shen, Z., Zhou, H., Brooks, A., Hanna, D. (2021) Evolution of elastic and thermal properties of cementitious composites containing micro-size lightweight fillers after exposure to elevated temperature. *Cement and Concrete Composites* 118, 103931. <https://doi.org/10.1016/j.cemconcomp.2021.103931>
- Shi, G., Wang, S., Rong, C. (2022) Experimental investigation into mechanical properties of Q345 steel after fire. *Journal of Constructional Steel Research* 199, 107582. <https://doi.org/10.1016/j.jcsr.2022.107582>
- Shintani, Y., Nishimura, T., Okazaki, T., Kinoshita, T., Ito, H., Liew, J.Y.R. (2020) Experimental study on the fire resistance of unprotected concrete-filled steel tubular columns under multi-loading. *Fire Safety Journal*, 103174. <https://doi.org/10.1016/j.firesaf.2020.103174>
- Silva, J.C.G., Landesmann, A., Ribeiro, F.L.B. (2016) Fire-thermomechanical interface model for performance-based analysis of structures exposed to fire. *Fire Safety Journal* 83, pp. 66-78. <http://doi.org/10.1016/j.firesaf.2016.04.007>
- Sjöström, J., Jansson, R. (2012) Measuring thermal material properties for structural fire engineering. 15th International Conference on Experimental Mechanics. Paper ID 2846, 10 pages
- Skowroński, W. (1988) A study of the steel beam deformation during fire. *Building and Environment* 23(2), pp. 159-167. [https://doi.org/10.1016/0360-1323\(88\)90030-3](https://doi.org/10.1016/0360-1323(88)90030-3)
- Skowroński, W. (1993) Buckling fire endurance of steel columns. *Journal of Structural Engineering* 119(6). [https://doi.org/10.1061/\(ASCE\)0733-9445\(1993\)119:6\(1712\)](https://doi.org/10.1061/(ASCE)0733-9445(1993)119:6(1712))
- Sobia, A.Q., Hamidah, M.S., Azmi, I., Rafeeqi S.F.A. (2015) Elevated Temperature Resistance of Ultra-High-Performance Fibre-Reinforced Cementitious Composites. *Magazine of Concrete Research* 67(17), pp. 923-937. <https://doi.org/10.1680/mac.14.00134>

- Starossek, U., Falah, N., Loehning, T. (2008) Numerical-analyses-of-force-transfer-in concrete-filled steel tube columns. The 4th International Conference on Advances in Structural Engineering and Mechanics (ASEM'08) Jeju, Korea, pp. 2651-2666.
- Stefan, M.J. (1879) Über die Beziehung zwischen der Wärmestrahlung und der Temperatur. Sitzungsberichte der Mathematisch-Naturwissenschaftlichen Classe. Vienna.
- Stewart, P.M. (1902) Making Buildings safe. Fireproof Materials and methods of construction. New York Tribune, October 19, 1902.
- Su, S., Li, X., Wang, T., Zhu, Y. (2016) A comparative study of environmental performance between CFST and RC columns under combinations of compression and bending. Journal of Cleaner Production 137, pp. 10-20. <https://doi.org/10.1016/j.jclepro.2016.07.043>
- Sultan, M.A. (2004) A Comparison of heat exposure in fire resistance test furnaces controlled by plate thermometers and by shielded thermocouples. INTERFLAM 2004, pp. 219-229.
- Sultan, M.A., Harmathy, T.Z., Mehaffey, J.R. (1986) Heat transmission in fire test furnaces. Fire and Materials 10(2), pp. 47-55. <https://doi.org/10.1002/fam.810100202>
- Sylvester, C. (1819) The Philosophy of Domestic Economy. Printed by H. Barnett. London, UK.
- Szeląg, M. (2018) Influence of specimen's shape and size on the thermal cracks' geometry of cement paste. Construction and Building Materials 189, pp. 1155-1172. <https://doi.org/10.1016/j.conbuildmat.2018.09.078>
- Szopa (2007) Współpraca betonu i stali na różnych poziomach obciążenia w osiowo ściskanych elementach zespolonych stalowo-betonowych. PhD thesis. Cracow University of Technology.
- Szymkuć, W. (2016) Odporność ogniowa słupów zespolonych stalowo-betonowych z rur wypełnionych betonem – dostępne metody obliczeń. Przegląd Budowlany 2016(12), pp. 43-48.
- Szymkuć, W. (2023a) Concrete-filled tubular columns exposed to fire Dataverse. [https://dataverse.harvard.edu/dataverse/CFT\\_szymkuc](https://dataverse.harvard.edu/dataverse/CFT_szymkuc)
- Szymkuć, W. (2023b) The effect of fly ash cenospheres on compressive strength, density, and thermal conductivity of lightweight cementitious composites – a systematic review. Under review.
- Szymkuć, W., Glema, A., Malendowski, M. (2015) Fire performance of steel tubular columns filled with normal strength concrete. Proceedings of 5th International Workshop PROTECT 2015, Michigan State University, East Lansing, USA, pp. 865-872.
- Szymkuć, W., Glema, A., Malendowski, M., Mielcarek, A., Smardz, P., Poteralski, A. (2018b) Numerical investigation of fire and post-fire performance of CFT columns in an open car park fire. 10th International Conference on Structures in Fire, pp. 407-414, Ulster University, Belfast, UK.
- Szymkuć, W., Malendowski, M., Glema, A. (2023) Burnout resistance of concrete-filled steel tubular (CFST) columns under realistic fire conditions. ce/papers 6(3-4), pp. 2184-2188. <https://doi.org/10.1002/cepa.2685>
- Szymkuć, W., Tokłowicz, P., Glema, A., Craveiro, H. (2018a) Study on the use of ultra-lightweight cement composite for enhancing fire performance of concrete filled tubular columns. 10th International Conference on Structures in Fire, pp. 585–592, Ulster University, Belfast, UK.
- Szymkuć, W., Tokłowicz, P., Ratajczak, M. (2023) The Effect of High Temperature on Lightweight Cementitious Composites with Fly Ash Cenosphere. Preprint: <http://doi.org/10.2139/ssrn.4463651>
- Taylor, A., Dalal, S.P., Desai, A.K. (2017) Comparative Performance Evaluation of Steel Column Building & Concrete Filled Tube Column Building under Static and Dynamic Loading - Procedia Engineering 173, 1847-1853. <https://doi.org/10.1016/j.proeng.2016.12.233>
- Tajuelo Rodriguez, E., Garbev, K., Merz, D., Black, L., Richardson, I.G. (2017) Thermal stability of C-S-H phases and applicability of Richardson and Groves' and Richardson C-(A)-S-H(I) models to synthetic C-S-H. Cement and Concrete Research 93, pp. 45-56. <https://doi.org/10.1016/j.cemconres.2016.12.005>
- Tan, K.H., Yao, Y. (2003) Fire Resistance of Four-Face Heated Reinforced Concrete Columns. Journal of Structural Engineering 129(9), pp. 1220-1229. [https://doi.org/10.1061/\(ASCE\)0733-9445\(2003\)129:9\(1220\)](https://doi.org/10.1061/(ASCE)0733-9445(2003)129:9(1220))

- Tan, Q-H., Gardner, L., Han, L-H., Song T-Y. (2020) Performance of concrete-filled stainless steel tubular (CFSSST) columns after exposure to fire. *Thin-Walled Structures* 149:106629. <https://doi.org/10.1016/j.tws.2020.106629>
- Tao, Z., Ghannam, M. (2013) Heat transfer in concrete-filled carbon and stainless steel tubes exposed to fire. *Fire Safety Journal* 61, pp. 1-11. <https://doi.org/10.1016/j.firesaf.2013.07.004>
- Tao, Z., Ghannam, M., Song, T-Y., Han, L-H. (2016) Experimental and numerical investigation of concrete-filled stainless steel columns exposed to fire. *Journal of Constructional Steel Research* 118, pp. 120-134. <http://doi.org/10.1016/j.jcsr.2015.11.003>
- Tao, Z., Uy, B., Han, L-H., He, S-H. (2008) Design of concrete-filled steel tubular members according to the Australian Standard AS 5100 model and calibration. *Australian Journal of Structural Engineering* 8(3), pp. 197-214. <https://doi.org/10.1080/13287982.2008.11464998>
- Tao, Z., Wang, X.-Q., Uy, B. (2013) Stress-Strain Curves of Structural and Reinforcing Steels after Exposure to Elevated Temperatures. *Journal of Materials in Civil Engineering* 25(9), pp. 1306-1316. [https://doi.org/10.1061/\(asce\)mt.1943-5533.0000676](https://doi.org/10.1061/(asce)mt.1943-5533.0000676)
- Tatro, S.B. (2006) Thermal Properties. ASTM report No. STP169D: Significance of Tests and Properties of Concrete and Concrete-Making Materials. Edited by: Lamond, Pielert, pp. 226-237.
- Thai H.T., Thai S. (2020) Reliability Evaluation of Eurocode 4 for Concrete-Filled Steel Tubular Columns. In: *Innovation for Sustainable Infrastructure. Lecture Notes in Civil Engineering*, vol 54. Springer, Singapore. [https://doi.org/10.1007/978-981-15-0802-8\\_49](https://doi.org/10.1007/978-981-15-0802-8_49)
- Thai S., Thai H.-T., Uy B., Ngo T. (2019) Concrete-filled steel tubular columns: Test database, design and calibration. *Journal of Constructional Steel Research* 157, pp. 161-81. <https://doi.org/10.1016/j.jcsr.2019.02.024>
- The Building News (1861). Fireproof construction. *The Building News* 7 (5 July 1861), pp. 557-558.
- Thomas, C., Rico, J., Tamayo, P., Ballester, F., Setién, J., Polanco, J.A. (2019) Effect of elevated temperature on the mechanical properties and microstructure of heavy-weight magnetite concrete with steel fibers, *Cement and Concrete Composites* 103, pp. 80-88, <https://doi.org/10.1016/j.cemconcomp.2019.04.029>
- Thomas, F.G., Webster, C.T. (1953) National Building Studies Research Paper No. 18. Investigation on Building Fires. Part VI. The Fire Resistance of Reinforced Concrete Columns.
- Thomas, P.H. (1970) The fire resistance required to survive a burn out. *Fire Research Note* No. 901, Borehamwood.
- Timoshenko, S.P. (1953) *History of Strength of Materials*. McGraw-Hill Book Company, Inc. USA
- Tohir, M.Z.M., Spearpoint, M. (2013) Distribution analysis of the fire severity characteristics of single passenger road vehicles using heat release rate data. *Fire Science Reviews* 2, article number 5. <https://doi.org/10.1186/2193-0414-2-5>
- Tondini, N., Morbioli, A., Vassart, O., Lechêne, S., Franssen, J-M. (2016) An integrated modelling strategy between a CFD and an FE software Methodology and application to compartment fires. *Journal of Structural Fire Engineering* 7(3), pp. 217-233. <https://doi.org/10.1108/JSFE-09-2016-015>
- Torić, N., Burgess, I.W. (2016) A unified rheological model for modelling steel behaviour in fire conditions. *Journal of Constructional Steel Research* 127, pp. 221-230. <https://doi.org/10.1016/j.jcsr.2016.07.031>
- Torić, N., Harapin, A., Boko, I. (2013) Experimental verification of a newly developed implicit creep model for steel structures exposed to fire. *Engineering Structures* 57, pp. 116-124. <https://doi.org/10.1016/j.engstruct.2013.09.024>
- Turkowski, P., Węgrzyński, W. (2022) Comparison of a Standard Fire-Resistance Test of a Combustible Wall Assembly with Experiments Employing Pre-defined Heat Release Curves. *Fire Technology* 58, pp. 1767-1787. <https://doi.org/10.1007/s10694-022-01226-1>
- Ukanwa, K.U., Clifton, G.C., Lim, J.B.P., Hicks, S.J., Sharma, U., Abu, A. (2018) Design of a continuous concrete filled steel tubular column in fire. *Thin-Walled Structures* 131, pp. 192-204. <https://doi.org/10.1016/j.tws.2018.07.001>

- US Geological Survey (1907) Bulletin No. 324 of the United States Geological Survey. The San Francisco Earthquake and Fire of April 18, 1906 and their effects on structures and structural materials. <https://archive.org/details/bulletinofunited324gilb>
- Uszball, S., Knobloch, M. (2022) Material characterization tests and advanced modeling of high- and ultra-high-strength steels under natural fire conditions. SiF 2022– The 12th International Conference on Structures in Fire. The Hong Kong Polytechnic University, Nov 30 - Dec 2, 2022
- Van De Leur, P.H.E. and Twiit, L. (2000) Thermal Exposure In Fire Resistance Furnaces. Fire Safety Science 6, pp. 1087-1098. <https://doi.org/10.3801/IAFSS.FSS.6-1087>
- Venkatachari, S., Kodur, V.K.R. (2021) Effect of transient creep on fire induced instability in steel framed structures. Journal of Constructional Steel Research 181, 106618. <https://doi.org/10.1016/j.jcsr.2021.106618>
- Vitruvius (27 BC) De architectura (Ten Books on Architecture). The translation by M.H. Morgan. Harvard University Press 1914.
- Vyšvařil, M., Bayer, P., Chromá, M., Rovnaníková, P. (2014) Physico-mechanical and microstructural properties of rehydrated blended cement pastes. Construction and Building Materials 54, pp. 413-420. <https://doi.org/10.1016/j.conbuildmat.2013.12.021>
- Wainman, D.E., Toner, R.P. (1992) BS476: Part 21 Fire Resistance Tests. The construction and testing of three loaded CHS columns filled with concrete. British Steel Technical Report No. SL/HED/R/S2139/1/92/D. Swinden Laboratories, Rotherham, UK.
- Waite, G.B., Goodrich, E.P. (1908) The reinforced concrete work of the McGraw building. American Society of Civil Engineering, Proceedings 34(1).
- Wang, C., Liu, J., Du, H., Guo, A. (2012) Effect of fly ash cenospheres on the microstructure and properties of silica-based composites. Ceramics International 38(5), pp. 4395-4400. <https://doi.org/10.1016/j.ceramint.2012.01.044>
- Wang, J., Liu, W., Shen, Q., Li, J., Han, Z. (2022b) Experimental investigation and theoretical analysis of axially-loaded concrete-filled elliptical tubes with circumferential gaps. Thin-Walled Structures 181, 110100. <https://doi.org/10.1016/j.tws.2022.110100>
- Wang, J.H., He, J., Xiao, Y. (2023) Fire behavior and performance of concrete-filled steel tubular columns: Review and discussion. Journal of Constructional Steel Research 157, pp. 19-31. <https://doi.org/10.1016/j.jcsr.2019.02.012>
- Wang, J.Y., Chia, K.S., Liew, J.Y.R., Zhang, M. H. (2013) Flexural performance of fiber-reinforced ultra lightweight cement composites with low fiber content. Cement and Concrete Composites 43, pp. 39-47. <https://doi.org/10.1016/j.cemconcomp.2013.06.006>
- Wang, K., Young, B. (2013) Fire resistance of concrete-filled high strength steel tubular columns. Thin-Walled Structures 71, pp. 46-56. <https://doi.org/10.1016/j.tws.2013.05.005>
- Wang, M.R., Jia, D.C., He, P.G., Zhou, Y. (2011) Microstructural and mechanical characterization of fly ash cenosphere/metakaolin-based geopolymeric composites. Ceramics International 37(5), pp. 1661-1666. <https://doi.org/10.1016/j.ceramint.2011.02.010>
- Wang, R., Zhang, C., Li, G-Q. (2016) Simple approach for performance-based fire safety design of circular CFT columns in large enclosure. Advanced Steel Construction 12(1), pp. 32-43, <https://doi.org/10.18057/IJASC.2016.12.1.3>
- Wang, T., Yu, M., Zhang, X., Ye, J. (2022a) Experimental Study on Random Temperature Field of Ultra-High Performance Concrete Filled Steel Tube Columns under Elevated Temperature. Composite Structures 289, 115445. <https://doi.org/10.1016/j.compstruct.2022.115445>
- Wang, X-Q., Tao, Z., Hassan, M.K. (2020) Post-fire behaviour of high-strength quenched and tempered steel under various heating conditions. Journal of Constructional Steel Research 164, 105785. <https://doi.org/10.1016/j.jcsr.2019.105785>
- Wang, Y.C., Kodur, V.K.R. (2000) Research toward use of unprotected steel structures. Journal of Structural Engineering 126(12), pp. 1442-1450. [https://doi.org/10.1061/\(ASCE\)0733-9445\(2000\)126:12\(1442\)](https://doi.org/10.1061/(ASCE)0733-9445(2000)126:12(1442))
- Wardenier, J., Packer, J.A., Zhao, X.-L., van der Vegte, G.J. (2011) Hollow Sections in Structural Applications. 2nd Edition. CIDECT, Geneva, Switzerland. Printed by Bouwen met Staal.

- Warunki techniczne (1961) Rozporządzenie Przewodniczącego Komitetu Budownictwa, Urbanistyki i Architektury z dnia 21 lipca 1961 r. w sprawie warunków technicznych, jakim powinny odpowiadać obiekty budowlane budownictwa powszechnego
- Webster, C.T., Wraight, H.G. and Thomas, P.H. (1959) The burning of fires in rooms part I - small scale tests with cribs and high ventilation. *Fire Research Notes* 398.  
<https://publications.iafss.org/publications/frn/398/-1>
- Webster, J.G., Eren, H. (2014) *Measurement, Instrumentation, and Sensors Handbook. Spatial, Mechanical, Thermal, and Radiation Measurement*. 2nd Edition. CRC Press.
- Welch, S., Miles, S., Kumar, S., Lemaire, T., Chan, A. (2008) FIRESTRUC – Integrating Advanced Three-dimensional Modelling Methodologies for Predicting Thermo-mechanical Behaviour of Steel and Composite Structures Subjected to Natural Fires. *Fire Safety Science – Proceedings of the Ninth International Symposium*, pp. 1315-1326. <https://doi.org/10.3801/iafss.fss.9-1315>
- Wermiel, S. (1993) The Development of Fireproof Construction in Great Britain and the United States in the Nineteenth Century. *Construction History* 9, pp. 3-26.  
<http://www.jstor.org/stable/41613713>
- Wickström, Anderson, J., Sjöström, J. (2018b) Measuring incident heat flux and adiabatic surface temperature with plate thermometers in ambient and high temperatures. *Fire and Materials* 43(1), pp. 51-56. <https://doi.org/10.1002/fam.2667>
- Wickström, U. (1986) A proposal regarding temperature measurements in fire tests furnaces. SP Report, 18 pages. <http://www.diva-portal.org/smash/record.jsf?pid=diva2%3A961621&dswid=-3888>
- Wickström, U. (2005) Comments on calculation of temperature in fire-exposed bare steel structures in prEN 1993-1-2: Eurocode 3—design of steel structures—Part 1-2: general rules—structural fire design. *Fire Safety Journal* 40(2), pp. 191-192. <https://doi.org/10.1016/j.firesaf.2004.09.002>
- Wickström, U. (2006) Comments on Franssen's article on calculation of temperature in fire-exposed bare steel structures. *Fire Safety Journal* 41(6), pp. 491.  
<https://doi.org/10.1016/j.firesaf.2006.03.009>
- Wickström, U. (2016a) *Temperature Calculation in Fire Safety Engineering*. Springer.  
<https://doi.org/10.1007/978-3-319-30172-3>
- Wickström, U. (2016b) The term 'heat flux' is used ambiguously. Clear definitions are needed on how to express thermal exposure. *Fire and Materials* 40, pp. 507-510.  
<https://doi.org/10.1002/fam.2286>
- Wickström, U., Duthinh, D., McGrattan, K. (2007) Adiabatic surface temperature for calculating heat transfer to fire exposed structures, *Interflam 2007: Vol. 2, Proceedings of the 11th International Interflam Conference, London, England, Vol. 2*, pp. 943-953.
- Wickström, U., Hermodsson, T. (1997) Comments on Paper by Kay, Kirby and Preston 'Calculation of the Heating Rate of an Unprotected Steel Member in a Standard Fire Resistance Test'. *Fire Safety Journal* 29, pp. 337-343. [https://doi.org/10.1016/S0379-7112\(97\)00034-9](https://doi.org/10.1016/S0379-7112(97)00034-9)
- Wickström, U., Hunt, S., Lattimer, B., Barnett, J., Beyler, C. (2018a) Technical comment—Ten fundamental principles on defining and expressing thermal exposure as boundary conditions in fire safety engineering. *Fire and Materials* 42(8), pp. 985-988. <https://doi.org/10.1002/fam.2660>
- Witteveen, J., Twilt, L. (1981) A critical view on the results of standard fire resistance tests on steel columns. *Fire Safety Journal* 4(4), pp. 259-270. [https://doi.org/10.1016/0379-7112\(81\)90029-1](https://doi.org/10.1016/0379-7112(81)90029-1)
- Wróblewska, J., Kowalski, R. (2020) Assessing concrete strength in fire-damaged structures. *Construction and Building Materials* 254, 119122.  
<https://doi.org/10.1016/j.conbuildmat.2020.119122>
- Wróblewski, B., Pogorzelski, J.A. (1979) 221 - Wytyczne oceny odporności ogniowej elementów konstrukcji budowlanych. Warszawa.
- Xiong, M.-X., Liew, J.Y.R. (2015) Spalling behavior and residual resistance of fibre reinforced Ultra-High performance concrete after exposure to high temperatures. *Materiales de Construcción* 65(320), e071. <https://doi.org/10.3989/mc.2015.00715>

- Xiong, M.-X., Liew, J.Y.R. (2016) Mechanical behaviour of ultra-high strength concrete at elevated temperatures and fire resistance of ultra-high strength concrete filled steel tubes. *Materials & Design* 104, pp. 414–427. <https://doi.org/10.1016/j.matdes.2016.05.050>
- Xiong, M.-X., Liew, J.Y.R. (2018) Discussion on the applicability of the M-N interaction curve for the fire resistance design of CFT members. *Thin-Walled Structures* 125, pp. 172-186. <https://doi.org/10.1016/j.tws.2018.01.013>
- Xuan, N-H., Le, T-T. (2021) Effects of variability in experimental database on machine-learning-based prediction of ultimate load of circular concrete-filled steel tubes. *Measurement*, 109198. <https://doi.org/10.1016/j.measurement.2021.109198>
- Yan, X., Charlier, M., Gernay, T. (2022) Thermal response of steel framing members in open car park fires. *Frontiers of Structural and Civil Engineering*. <https://doi.org/10.1007/s11709-022-0879-0>
- Yan, X., Gernay, T. (2021) Numerical modeling of localized fire exposures on structures using FDS-FEM and simple models. *Engineering Structures* 246, pp. 112997. <https://doi.org/10.1016/j.engstruct.2021.112997>
- Yang, D., Liu, F., Huang, S-S., Yang, H. (2020) ISO 834 standard fire test and mechanism analysis of square tubed-reinforced-concrete columns. *Journal of Constructional Steel Research* 175, 106316. <https://doi.org/10.1016/j.jcsr.2020.106316>
- Yang, H., Liu, F., Zhang, S., Lv, X. (2013) Experimental investigation of concrete-filled square hollow section columns subjected to non-uniform exposure. *Engineering Structures* 48, pp. 292-312. <https://doi.org/10.1016/j.engstruct.2012.09.011>
- Yao, Y., Li, H., Guo, H., Tan, K-H. (2016) Fire resistance of eccentrically loaded slender concrete-filled steel tubular columns. *Thin-Walled Structures* 106, pp. 102-112. <https://doi.org/10.1016/j.tws.2016.04.025>
- Yim, H.J, Park, S-J., Jun, Y. (2019) Physicochemical and mechanical changes of thermally damaged cement pastes and concrete for re-curing conditions. *Cement and Concrete Research* 125, pp. 105831. <https://doi.org/10.1016/j.cemconres.2019.105831>
- Yin, Y., Zha, X-x., Li, L-y. (2006) Fire resistance of axially loaded concrete filled steel tube columns. *Journal of Constructional Steel Research* 62, pp. 723-729. <https://doi.org/10.1016/j.jcsr.2005.11.011>
- Yu, M., Wang, T., Huang, W., Yuan, H., Ye, J. (2019b) Fire resistance of concrete-filled steel tube columns with preload. Part I: Experimental investigation. *Composite Structures* 223, 110994. <https://doi.org/10.1016/j.compstruct.2019.110994>
- Yu, Y., Lan, L., Ding, F., Wang, L. (2019a) Mechanical properties of hot-rolled and cold-formed steels after exposure to elevated temperature: A review. *Construction and Building Materials* 213, pp. 360-376. <https://doi.org/10.1016/j.conbuildmat.2019.04.062>
- Yun, H.-S., Han, H.-S., Hwang, C.-H. (2020) Development and calibration of reduced-size plate thermometer for measuring incident heat flux. *Journal of Fire Sciences*, 073490412095860. <https://doi.org/10.1177/0734904120958602>
- Zehfuß, J., Robert, F., Spille, J., Razafinjato, R.N. (2020) Evaluation of Eurocode 2 approaches for thermal conductivity of concrete in case of fire. *Civil engineering design* 2(3), pp. 58-71. <https://doi.org/10.1002/cend.202000001>
- Zhang, C., Jia, B., Wang, J. (2020) Influence of artificial cooling methods on post-fire mechanical properties of Q355 structural steel. *Construction and Building Materials*, 252, 119092. <https://doi.org/10.1016/j.conbuildmat.2020.119092>
- Zhang, C., Wang, G-Y., Xue, S-D., Yu, H-X (2016) Experimental research on the behaviour of eccentrically loaded SRC columns subjected to the ISO-834 standard fire including a cooling phase. *International Journal of Steel Structures* 16, pp. 425-439. <https://doi.org/10.1007/s13296-016-6014-0>
- Zhang, C., Zhang, Z., Li, G-Q. (2016) Simple vs. sophisticated fire models to predict performance of SHS column in localized fire. *Journal of Constructional Steel Research* 120, pp. 62-69. <http://doi.org/10.1016/j.jcsr.2015.12.026>

- Zhang, H.Y., Kodur, V., Qi, S. L., Cao, L., Wu, B. (2014) Development of metakaolin-fly ash based geopolymers for fire resistance applications. *Construction and Building Materials* 55, pp. 38-45. <http://doi.org/10.1016/j.conbuildmat.2014.01.040>
- Zhang, R., Liu, J., Wang, W., Chen, Y.F. (2020) Fire behaviour of thin-walled steel tube confined reinforced concrete stub columns under axial compression. *Journal of Constructional Steel Research* 172, 106180. <http://doi.org/10.1016/j.jcsr.2020.106180>
- Zhou, H., Brooks, A. L. (2019) Thermal and mechanical properties of structural lightweight concrete containing lightweight aggregates and fly-ash cenospheres. *Construction and Building Materials* 198, pp. 512-526. <https://doi.org/10.1016/j.conbuildmat.2018.11.074>
- Zhou, X., Yang, J., Liu, J., Wang, S., Wang, W. (2021) Fire resistance of thin-walled steel tube confined reinforced concrete middle-length columns: Test and numerical simulation. *Structures* 34, pp. 339-355. <https://doi.org/10.1016/j.istruc.2021.07.078>
- Zhu, H., Zhang, C., Chen, S., Wu, J. (2022) A modified Johnson-Cook constitutive model for structural steel after cooling from high temperature. *Construction and Building Materials* 340, 127746. <https://doi.org/10.1016/j.conbuildmat.2022.127746>